

ADJ NO. **AD A049712**
DDC FILE COPY



CEEDO



CEEDO-TR-77-19

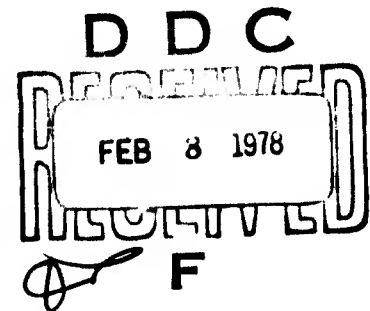
12

**THE ROLE OF IRON SULFIDES IN
CONTROLLING TRACE HEAVY METALS IN
ANAEROBIC SEDIMENTS: OXIDATIVE
DISSOLUTION OF FERROUS MONOSULFIDES
AND THE BEHAVIOR OF ASSOCIATED
TRACE METALS**

**ENVIRONMENTAL ENGINEERING AND SCIENCE
DEPARTMENT OF CIVIL ENGINEERING
STANFORD UNIVERSITY
STANFORD, CALIFORNIA 94305**

FEBRUARY 1977

**FINAL REPORT FOR PERIOD
DECEMBER 1974-DECEMBER 1976**



Approved for public release; distribution unlimited

**CIVIL AND ENVIRONMENTAL
ENGINEERING DEVELOPMENT OFFICE**

(AIR FORCE SYSTEMS COMMAND)

**TYNDALL AIR FORCE BASE
FLORIDA 32403**

UNCLASSIFIED

SECURITY CLASSIFICATION OF THIS PAGE (When Data Entered)

REPORT DOCUMENTATION PAGE		READ INSTRUCTIONS BEFORE COMPLETING FORM
1. REPORT NUMBER (18) CEEDO-TR-77-13	2. GOVT ACCESSION NO.	3. RECIPIENT'S CATALOG NUMBER (9)
4. TITLE (and Subtitle) (6) THE ROLE OF IRON SULFIDES IN CONTROLLING TRACE HEAVY METALS IN ANAEROBIC SEDIMENTS: Oxidative dissolution of ferrous monosulfides and the behavior of associated trace metals.	5. TYPE OF REPORT & PERIOD COVERED Final Report. 5 Dec 74-4 Dec 76,	
7. AUTHOR(s) (14) Michael B. Nelson, James A. Davis, III, Mark M. Benjamin, James O. Leckie	8. CONTRACT OR GRANT NUMBER(s) (15) F29601-75-C-0028 new 63-28	
9. PERFORMING ORGANIZATION NAME AND ADDRESS Environmental Engineering and Science Department of Civil Engineering, Stanford University, Stanford, California 94305	10. PROGRAM ELEMENT, PROJECT, TASK AREA & WORK UNIT NUMBERS Project 2103 (17) 4C	
11. CONTROLLING OFFICE NAME AND ADDRESS Det 1 (Civil & Environmental Engr Dev Office) HQ ADTC Tyndall Air Force Base, Florida 32403	12. REPORT DATE (10) Feb 77	
14. MONITORING AGENCY NAME & ADDRESS (if different from Controlling Office) Det 1 (Civil & Environmental Engr Dev Office) HQ ADTC Tyndall Air Force Base, Florida 32403	13. NUMBER OF PAGES (12) 416p.	
	15. SECURITY CLASS. (of this report) Unclassified	
15a. DECLASSIFICATION DOWNGRADING SCHEDULE		
16. DISTRIBUTION STATEMENT (of this Report) Approved for public release; distribution unlimited.		
17. DISTRIBUTION STATEMENT (of the abstract entered in Block 20, if different from Report) DDC FEB 8 1978 RESOLVED F		
18. SUPPLEMENTARY NOTES Available in DDC		
19. KEY WORDS (Continue on reverse side if necessary and identify by block number) Oxidation kinetics Heterogeneous systems Cadmium Ferrous monosulfides Water pollution Environics Heavy metals Ligand Effects Environmental Adsorption Silver quality Environmental chemistry		
20. ABSTRACT (Continue on reverse side if necessary and identify by block number) The study of the kinetics of oxidation of the ferrous monosulfide mackinawite and the fate of the associated heavy metals are important to a better understanding of the processes and mechanisms controlling the release, transport and retention of heavy metals in natural aquatic systems. This project undertook a detailed study of several selected aspects of the aqueous chemistry of heavy metals and of the oxidative dissolution of FeS(s)		

DD FORM 1 JAN 73 1473

EDITION OF 1 NOV 65 IS OBSOLETE

UNCLASSIFIED

SECURITY CLASSIFICATION OF THIS PAGE (When Data Entered)

400117

The rate of oxidative dissolution of FeS(s) (mackinawite) has first-order dependence on the dissolved oxygen concentration and the total available surface of FeS(s). The rate of oxidation has a fractional (1/4) dependence on the hydronium ion concentration. The empirical rate expression is

$$-\frac{d[\text{FeS}]}{dt} = k(\text{area}) P_{\text{O}_2} [\text{H}^+]^{1/4}$$

The rate of oxidation is retarded by increasing concentrations of chloride ion at pH < 9 and is not affected by chloride at pH > 9. Trace concentrations of nickel ($> 1 \times 10^{-5}\text{M}$) markedly catalyze the oxidation reaction, increasing the rate ten-fold at pH 7 and total nickel of $1 \times 10^{-4}\text{M}$. On the other hand, the presence of similar concentrations of Cu(II), Ag(I), and Cd(II) had no observable effect on either the rate of oxidation or reaction products.

The iron reaction product was always $\gamma\text{-FeOOH}$ (lepidocrocite) while the sulfur oxidation products varied as a function of pH and solution composition. At pH < 9 the major sulfur oxidation product was elemental sulfur, while at pH > 9 the fraction of dissolved sulfur oxyanions (thiosulfate and polythionates) increases markedly (> 50%). Chloride has the effect of stopping the oxidation at elemental sulfur. Thus, the oxidation of FeS at pH 8.5 in the presence of seawater concentrations of chloride results in elemental sulfur being the only detectable sulfur reaction species.

Studies on the adsorptive behavior of Ag(I), Cu(II), and Cd(II) on SiO_2 , $\gamma\text{-FeOOH}$ and amorphous $\text{Fe}(\text{OH})_3$ in the presence and absence of competing ligands indicates that solution ligands or chelons can have the effect of either increasing, decreasing or not affecting the adsorption of the trace metal. The ligand effect is very specific and depends both on the relative stability of the complex, and the ability of the ligand or chelon or the metal-ligand complex to adsorb. Chloride reduces the adsorption of Ag(I) and Cd(II) at fixed pH, while thiosulfate enhances the adsorption of Ag(I) over the low pH range but may reduce adsorption at pH > 6. On the other hand, thiosulfate only reduces the adsorption of Cd(II). Thiosulfate adsorbs on $\gamma\text{-FeOOH}$ and $\text{Fe}(\text{OH})_3(\text{am})$ in the pH range 3 to 7. Apparently the $\text{Ag}(\text{S}_2\text{O}_3)_2^{-3}$ specie and $\text{AgS}_2\text{O}_3^{-}$ specie both adsorb at pH < 8, thus enhancing the silver adsorption reaction. Thus, silver thiosulfate solutions introduced into natural aquatic systems can be expected to allow concentration of silver on suspended and bed sediments, hence resulting in the concentration of silver in the sediment material.

Organic chelons (e.g., glutamic acid, syringic acid, picolinic acid, salicylic acid, protocatechuic acid, and others) behave similar to inorganic ligands with the specific exception that complex organic chelons have greater stereochemical flexibility and, sometime, multiple ligand atoms available for coordination to both the solid surface and the heavy metal ions. Further work is clearly needed in this area.

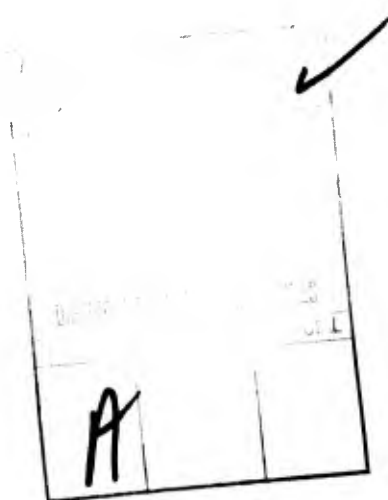
Trace metals associated with sulfidic materials (FeS) may be mobilized as is indicated by the release of cadmium associated with FeS(s) during the oxidative dissolution of FeS(s) in the presence of high concentrations of chloride. Further work needs to be done on the effect of the type of association (co-precipitation vs adsorption) of the heavy metals with the iron monosulfides.

UNCLASSIFIED

UNCLASSIFIED

SECURITY CLASSIFICATION OF THIS PAGE (When Data Entered)

Oxidation of natural sulfidic estuarine sediments gives results predicted by the laboratory rate studies. Both the relative rate of oxidation at pH 8.5 in seawater chloride concentrations and the sulfur reaction products (elemental sulfur) correspond to expected outcomes. Additional work needs to be done on several different natural sediments to explore the limits of application of the experimental work achieved in this project.



(The reverse of this page is blank)

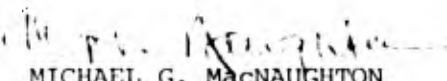
UNCLASSIFIED

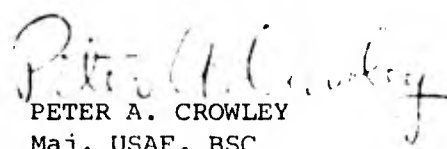
SECURITY CLASSIFICATION OF THIS PAGE (When Data Entered)

PREFACE

This study was performed under program element 63723F JON 21034C46. The project officer was Maj Michael G. MacNaughton of the Environmental Sciences Research Division, Civil and Environmental Engineering Office HQ ADTC, Tyndall AFB Florida 32403.

This report has been reviewed by the Information Office (OI) and is releasable to the National Technical Information Service (NTIS). At NTIS it will be available to the general public, including foreign nationals.


MICHAEL G. MACNAUGHTON
Maj, USAF, BSC
Chief, Env Sciences Research Div


PETER A. CROWLEY
Maj, USAF, BSC
Director of Environics

JOSEPH S. PIZZUTO
Col, USAF, BSC
Commander

TABLE OF CONTENTS

Section	Title	Page
I.	INTRODUCTION	1
II.	AQUEOUS GEOCHEMISTRY OF IRON AND SULFUR	5
	Some Thermodynamic Considerations: A Gibbsian Approach to Sediments	5
	Aspects of Sulfur Chemistry	12
	Aspects of Iron Chemistry	20
	Inorganic Ligands	23
	Metal Sulfides	29
III.	EXPERIMENTAL PROCEDURES FOR KINETIC OXIDATION STUDIES	37
	Experimental Procedure and Apparatus	37
	Analytical Procedures and Methodology	39
IV.	OXIDATIVE DISSOLUTION OF FERROUS SULFIDE	47
	Effect of Hydrogen Ion Concentration	47
	Effect of Dissolved Oxygen	47
	Temperature Effects	53
	Effect of Surface Area	60
	Effect of Ionic Strength and Chloride	65
	Effect of Catalytic Agents	69
	Effect of Mixing Rate	72
	Summary of Parametric Studies	74
	Iron Oxidation Products	74
	Sulfur Oxidation Products	83
	Discussion of Sulfur Speciation	116
	Summary and Conclusion	123
	Release of Cadmium during Oxidation of FeS	124
	Oxidation Kinetics of Natural Sediments	126
	Discussion of Kinetic Results and Models	129

TABLE OF CONTENTS (CONTINUED)

Section	Title	Page
V.	AQUEOUS CHEMISTRY OF SILVER	168
	Electronic Structure and Oxidation States	168
	Bonding and Structure of Silver(I) Complexes	169
	Photochemistry of Silver	183
	Silver(I) in Natural Aquatic Systems	186
VI.	AQUEOUS CHEMISTRY OF CADMIUM	196
	Electronic Structure and Oxidation States	196
	Cadmium Compounds	196
	Sources and Uses of Cadmium	202
	Transport of Cadmium through the Environment	207
	Cadmium in Natural Water Systems	208
	Ecological Aspects of Cadmium	213
	Summary	216
VII.	MODELS FOR ADSORPTION AT THE SOLID/SOLUTION INTERFACE	217
	Hydrolytic Behavior of Metal Ions	217
	Phenomenological Models for Adsorption of Hydrolyzable Metal Ions	219
VIII.	EXPERIMENTAL METHODS AND MATERIALS FOR ADSORPTION STUDIES	224
	Reagents	224
	Preparation of Amorphous Iron Oxide	224
	Preparation of α -Quartz	228
	pH Measurement and Adjustment	229
	Adsorption Experiments in Silver(I)/Amorphous Iron Oxide Systems	232
	Adsorption Experiments in Silver(I)/ α -Quartz Systems	236
	Adsorption Experiments in Copper(II)/Amorphous Iron Oxide and Copper(II)/ α -Quartz Systems	238
	Adsorption Experiments in Systems Containing Complexing Ligands	241
	Sampling and Analysis	243
	Container Adsorption and Cleaning Techniques	246
	Adsorption Experiments in Cadmium(II)/ α -Quartz and Cadmium(II)/ γ -FeOOH Systems	247
	Batch Adsorption Experiments	250

TABLE OF CONTENTS (CONCLUDED)

Section	Title	Page
IX.	ADSORPTION OF TRACE METALS ON HYDROUS OXIDES	254
	Surface Characteristics of Hydrous Oxides	254
	Adsorption of Silver on Hydrous Oxides	264
	Adsorption of Copper on Hydrous Oxides	276
	Adsorption of Cadmium on Hydrous Oxides	277
X.	EFFECT OF LIGANDS ON TRACE METAL ADSORPTION	310
	Ligand Adsorption on Hydrous Oxides	310
	Adsorption of Silver on Amorphous Iron Oxide and α -Quartz in Systems Containing Ligands	325
	Adsorption of Copper on Amorphous Iron Oxide and α -Quartz in Systems Containing Ligands	337
	Adsorption of Cadmium on γ -FeOOH and α -Quartz in Systems Containing Ligands	340
XI.	CONCLUSIONS	350
XII.	RECOMMENDATIONS	352
	REFERENCES	353
APPENDICES		
	Appendix A. Liquid Scintillation Counting	365
	Appendix B. Adsorption of Silver by Ferrous Monosulfide . . .	368
	Appendix C. Kinetic Data for Oxidation Reactions	369
	Appendix D. Selected Data for Adsorption Reactions	395

LIST OF FIGURES

Figure	Title	Page
1.	Schematic diagram of the complex transformation processes and mechanisms controlling release, transport, and retention of trace metals in natural aquatic systems. -----	2
2.	Stability field diagram of solid Fe phases as a function of pE and pH at 25°C and 1 atm total pressure. Diagram is computed for conditions of 1×10^{-4} M total sulfur species and 1×10^{-2} M total carbonate species in aqueous solution. Solubilities used for pyrite (FeS_2), pyrrhotite (FeS_α), hematite (Fe_2O_3), and magnetite (Fe_3O_4). -----	8
3.	Stability diagram of solid Fe phases as a function of pE and pH at 25°C and 1 atm total pressure. Diagram is calculated for conditions of 1×10^{-6} M total iron, 1×10^{-4} M total sulfur species and 1×10^{-2} M total carbonate species in aqueous solution. Solubilities used for pyrite (FeS_2), mackinawite (FeS), lepidocrocite ($\gamma\text{-FeOOH}$), siderite (FeCO_3), and ferrous hydroxide ($\text{Fe}(\text{OH})_2$). -----	9
4.	Equilibrium aqueous concentrations of iron and sulfur species as a function of pE. Note that a phase transition occurs at about pE -4 between $\text{FeS}(\text{s})$ and $\text{FeCO}_3(\text{s})$. Solution composition is typical of estuarine sediment interstitial waters. -----	10
5.	Experimental apparatus used for oxidation studies. Water jacketed vessel with top and appropriate ports for electrodes and experimental equipment. -----	38
6.	$\text{FeS}(\text{s})$ remaining as a function of time at pH 9 and 16.6 mg/l O_2 . -----	40
7.	The rate of oxidation of FeS , determined at 6 mg/l and 8 mg/l O_2 , 20°C, as a function of pH of solution during oxidation. The rate is independent of pH above pH 9. -----	48
8.	Logarithm of dissolved oxygen concentration as a function of time for reaction at pH 7. -----	51
9.	Logarithm of dissolved oxygen concentration as a function of time for reaction at pH 9.4. -----	52
10.	Oxidation rate as a function of the partial pressure of oxygen at pH 7 and 10°C. -----	54
11.	Oxidation rate as a function of the partial pressure of oxygen at pH 7 and 15°C. -----	55
12.	Arrhenius plots for sequential and parallel reactions. -----	57

LIST OF FIGURES (CONTINUED)

Figure	Title	Page
13.	Arrhenius plot of overall oxidation rate at pH 7 and 4 mg/l O ₂ . -----	58
14.	Arrhenius plot of overall oxidation rate at pH 9 and 10 mg/l O ₂ . -----	59
15.	Concentration of FeS(s) remaining as a function of time during oxidative dissolution at pH 7. -----	63
16.	Concentration of FeS(s) remaining as a function of time during oxidative dissolution at pH 9. -----	64
17.	Influence of sulfate on oxidation rate at pH 7, 20°C, and 8 mg/l O ₂ . -----	66
18.	Influence of chloride on oxidation rate at pH 7, 20°C, and 8 mg/l O ₂ . -----	67
19.	Oxidation of FeS(s) in presence and absence of chloride at pH 9. -----	68
20.	Catalytic effect of Ni on oxidation of FeS(s) at pH 7. -----	70
21.	Oxidation of FeS(s) in the presence of Cu and Ag at pH 7. ---	71
22.	Oxidation of FeS(s) in the presence of phenol at pH 7. -----	73
23.	X-ray diffraction patterns of solid iron oxyhydroxide produced during oxidation of FeS(s). -----	76
24.	Electron micrographs of γ-FeOOH (lepidocrocite). -----	77
25.	Equivalents of soluble iodine-consuming species formed as a function of moles/l FeS(s) oxidized at 20°C and 10 mg/l O ₂ . -----	87
26.	Ratio of equivalents of iodine-consuming species formed per mole of FeS(s) oxidized as a function of pH during oxidation, indicating the extent of oxidation of sulfur. -----	88
27.	The relationship between hydrogen ions and soluble iodine-consuming species produced during FeS(s) oxidation. The extent of oxidation of soluble sulfur species is indicated. The similarity between results at pH 9 and 10 indicates the distribution of soluble sulfur species is similar at both pH values. -----	89
28.	Effect of oxygen concentration during FeS oxidation on the extent of oxidation of sulfur species, as indicated by hydrogen ion formation. -----	97
29.	Effect of oxygen concentration during FeS oxidation on the extent of oxidation of sulfur species, as indicated by the soluble iodine-consuming species produced. -----	98

LIST OF FIGURES (CONTINUED)

Figure	Title	Page
30.	Relationship between hydrogen ions and soluble iodine-consuming species produced for the oxidation of FeS(s) at 10 and 43 mg/l O ₂ . -----	99
31.	Relationship between soluble sulfur species and iodine-consuming species produced during the oxidation of FeS(s) at 10 and 43 mg/l O ₂ . -----	100
32.	Hydrogen ions produced, indicating the extent of oxidation of sulfur species as a function of FeS(s) oxidized over the temperature range 5 to 44.5°C. -----	102
33.	Hydrogen ions produced as a function of the equivalents of iodine-consuming species produced over the temperature range 5 to 44.5°C. -----	103
34.	The relationship between soluble sulfur species and equivalents of iodine-consuming species produced for the oxidation of FeS(s) between 5 and 44.5°C. -----	105
35.	Formation of hydrogen ions as a function of the concentration of FeS(s) oxidized in both the presence and absence of nickel. -----	107
36.	Equivalents of hydrogen ions liberated as a function of iodine-consuming species formed during the oxidation of FeS(s) at pH 9 in the presence and absence of nickel. -----	108
37.	Equivalents of hydrogen ions liberated as a function of FeS(s) oxidized during oxidation at pH 9 in 2 x 10 ⁻⁴ M Na ₂ SO ₄ and 0.10M NaCl. -----	110
38.	Equivalents of hydrogen ions liberated as a function of the equivalents of iodine-consuming species produced during oxidation at pH 9 in 2 x 10 ⁻⁴ M Na ₂ SO ₄ and 0.1M NaCl. -----	112
39.	Thiocyanate formed as a function of total soluble iodine-consuming species including polythionates and S ₂ O ₃ ²⁻ . -----	113
40.	Relationship between the concentrations of polythionates, thiosulfate, and iodine-consuming species as a function of time of oxidation at pH 9. -----	119
41.	Relationship between the concentrations of polythionates, thiosulfate, and iodine-consuming species as a function of time of oxidation at pH 10. -----	120
42.	Oxidation of natural estuarine sulfidic sediments as a function of time. Fe(II) and S(-II) disappear with time. ---	128
43.	Oxidation data for natural estuarine sulfidic sediments corrected for Fe(II) from FeCO ₃ (s). -----	130

LIST OF FIGURES (CONTINUED)

Figure	Title	Page
44.	Oxidation rate vs partial pressure of oxygen at pH 7 and 20°C. Solid line represents theoretical relationship predicted by kinetic model using data at 10°C and 15°C. -----	135
45.	Oxidation rate vs concentration of nickel in system at pH 7 and 20°C. -----	161
46.	Complex-formation curves for silver(I) with unidentate ligands containing various coordinating atoms. Group V and VI curves are for p-phenyl (atom) benzenesulphonic acid with the appropriate atom in the ligand. Additional curves are shown for Cl ⁻ , I ⁻ , HS ⁻ , and NH ₃ . -----	182
47.	Stability field diagram showing dominance regions for solid silver phases in equilibrium with aqueous solution at 25°C and 1 atm total pressure. pE-pH diagram is computed for conditions of total sulfur of 10 ⁻³ M, total chloride of 10 ⁻⁴ M and total carbonate of 10 ⁻¹ M. -----	188
48.	Equilibrium aqueous concentrations of silver species as a function of pE. Note that a phase transition occurs at about pE of -3.7 between Ag ₂ S(s) and Ag ⁰ (s). Solution composition is typical of estuarine sediment interstitial waters. -----	189
49.	Log concentration diagrams for silver at 25°C and 1 atm total pressure. The upper diagram shows the stability field of silver oxide and the major hydrolytic species. The hash-marked curve represents the sum of all dissolved silver species. The lower diagram shows the speciation of silver computed for total silver of 10 ⁻⁶ M. -----	190
50.	Log concentration-pH diagram for silver at 25°C and 1 atm total pressure. Computed for total silver of 10 ⁻⁶ M, total chloride of 10 ⁻³ M, and total ammonia of 10 ⁻² M. The dashed region represents the formation of AgCl(s) at equilibrium conditions. The lower boundary of the dashed region shows the sum of all dissolved silver species. -----	192
51.	Log concentration diagram showing the major thiosulfate species at 25°C and 1 atm total pressure as a function of the total thiosulfate concentration. Computed for total silver of 10 ⁻⁶ M at pH 7. -----	193
52.	Log concentration diagram for AgCl(s) showing stability fields for solid silver chloride and major argentous chloride complexes at 25°C and 1 atm total pressure. The hash-marked curve represents the sum of all dissolved silver species. An additional concentration relationship is shown for a total thiosulfate concentration of 10 ⁻⁶ M. -----	194

LIST OF FIGURES (CONTINUED)

Figure	Title	Page
53.	Cd-CO ₂ -H ₂ O system. Above and to the left of the solid line CdCO ₃ (s) is the solubility-limiting phase at equilibrium. Below and to the right Cd(OH) ₂ (s) predominates. Dashes (---) indicate Cd ⁺² solubility. Dotted line (---) indicates the case of water in equilibrium with atmospheric CO ₂ . Note that CdCO ₃ (s) is the equilibrium solid in all systems equilibrated with air. $C_T^* = CO_2(aq) + HCO_3^- + CO_3^{2-}$. -----	200
54.	Stability field diagram showing dominance regions for solid cadmium phases in equilibrium with aqueous solution at 25°C and 1 atm total pressure. Total dissolved sulfur is 0.1M.---	201
55.	Relative strengths of cadmium bonds with bidentate ligands. The tendency of cadmium ion to displace other metal ions from bidentate ligands involving oxygen (O), nitrogen (N), and sulfur(s) donating ligands is shown. -----	203
56.	Equilibrium aqueous concentrations of cadmium species as a function of pE. Note that a phase transition occurs at about a pE of -3.5 between CdS(s) and CdCO ₃ (s). Solution composition is typical of estuarine sediment interstitial waters. -----	214
57.	pH dependence of the difference between experimental pH measurement techniques in amorphous iron oxide systems at 25°C and 10 ⁻¹ M ionic strength. -----	231
58.	Kinetics of silver adsorption on amorphous iron oxide. Solution conditions of 25°C, 10 ⁻¹ M ionic strength and 5 x 10 ⁻⁶ M initial silver. -----	234
59.	The adsorption of silver(I) on amorphous iron oxide as a function of pH under darkroom and laboratory lighting conditions. Data shown are for short-term 4-hr equilibria; ionic strength of 10 ⁻¹ M, and 25°C. -----	237
60.	Rate of silver(I) removal from solution by α-quartz under darkroom and laboratory lighting conditions. Container adsorption is significant in laboratory lighting but absent in the dark. Ionic strength = 10 ⁻¹ M NaNO ₃ , 25°C. -----	239
61.	Rate of copper(II) adsorption on amorphous iron oxide at pH 4.9, 25°C, and ionic strength = 10 ⁻¹ M. -----	240
62.	Rate of copper(II) adsorption on α-quartz at pH 7.2, 25°C, and ionic strength of 10 ⁻¹ M. -----	242
63.	Kinetics of adsorption of Cd onto SiO ₂ . -----	251
64.	Kinetics of adsorption of Cd onto γ-FeOOH in the presence of dissolved CO ₂ . -----	252
65.	Kinetics of adsorption of Cd onto γ-FeOOH in the absence of dissolved CO ₂ . -----	253

LIST OF FIGURES (CONTINUED)

Figure	Title	Page
66.	Change in pH (Δ pH) upon addition of sodium nitrate to amorphous iron oxide suspensions as a function of pH at low ionic strength. PZC = 7.9. -----	255
67.	Surface charge of amorphous iron oxide as a function of pH at various ionic strengths. BET surface area of 182 m ² /gm and PZC of 7.9 assumed. -----	256
68.	Surface charge curves for goethite, hematite, and amorphous iron oxide in 0.1M KNO ₃ . After Yates (1975).-----	257
69.	Determination of $pK_{a1}^{(int)}$ for amorphous iron oxide. -----	259
70.	Determination of $pK_{a2}^{(int)}$ for amorphous iron oxide. -----	260
71.	Change in pH upon addition of solid NaNO ₃ to a suspension of γ -FeOOH as a function of final pH. -----	263
72.	Adsorption of silver on amorphous iron oxide as a function of pH and surface area. -----	267
73.	Freundlich adsorption isotherm plot for silver on amorphous iron oxide at pH 6.5. -----	269
74.	Freundlich adsorption isotherm plot for silver on amorphous iron oxide at pH 10.0. -----	270
75.	Adsorption density of silver on amorphous iron oxide as a function of pH at constant Ag_{equil}^+ of $2 \times 10^{-7}M$. -----	273
76.	Adsorption-desorption data for silver on amorphous iron oxide. Experimental data denoted by squares is for adsorption equilibria in the presence of $9.4 \times 10^{-2}M$ chloride. -----	274
77.	Adsorption of silver(I) on α -quartz under darkroom conditions as a function of pH and surface area available. -----	275
78.	Adsorption of copper(II) on amorphous iron oxide as a function of pH. -----	278
79.	Adsorption of copper(II) on α -quartz as a function of pH. ---	279
80.	Fractional adsorption of Cd onto SiO ₂ as a function of pH and Cd concentration. -----	280
81.	Fractional adsorption of Cd onto SiO ₂ as a function of pH, Cd concentration, and SiO ₂ concentration. -----	281
82.	Fractional adsorption of Cd onto γ -FeOOH as a function of pH and Cd concentration. -----	282
83.	Fractional adsorption of Cd onto γ -FeOOH as a function of pH and Cd concentration. -----	283

LIST OF FIGURES (CONTINUED)

Figure	Title	Page
84.	Adsorption isotherms for the system Cd/SiO ₂ at two pH values.	284
85.	Adsorption isotherms for the system Cd/γ-FeOOH at three pH values. -----	285
86.	Adsorption of Cd onto SiO ₂ as a function of pH and ionic strength. -----	287
87.	Adsorption of Cd onto γ-FeOOH as a function of pH and ionic strength. -----	288
88.	Adsorption of Cd onto SiO ₂ as a function of pH. Effect of dissolved CO ₂ (g). -----	290
89.	Acid-base titration of the system Cd/CO ₂ /H ₂ O. -----	291
90.	Acid-base titration of the system Cd/γ-FeOOH/H ₂ O. -----	292
91.	Acid-base titration of the system Cd/γ-FeOOH/CO ₂ /H ₂ O. -----	293
92.	Acid-base titration of the system Cd/SiO ₂ /H ₂ O. -----	294
93.	Short-term adsorption of Cd onto γ-FeOOH as a function of pH and CO ₂ concentration. -----	296
94.	Release of protons as a function of Cd adsorption in the system Cd/γ-FeOOH/H ₂ O. -----	297
95.	Interaction of γ-FeOOH and CO ₃ . For no interaction, the effect of addition of CO ₃ to the system Cd/H ₂ O and Cd/γ-FeOOH/H ₂ O would be identical. System A: Cd/CO ₃ /H ₂ O. System B: Cd/H ₂ O. System C: Fe/Cd/CO ₃ /H ₂ O. System D: Fe/Cd/H ₂ O. -----	299
96.	Release of protons as a function of Cd adsorption in the system Cd/γ-FeOOH/CO ₂ /H ₂ O. -----	300
97.	Release of protons as a function of Cd adsorption in the system Cd/SiO ₂ /H ₂ O. -----	302
98.	Degree of protonation of surface sites on γ-FeOOH as a function of pH, assuming a PZC of 7.16. -----	305
99.	Ratio of doubly- to singly-protonated surface sites on γ-FeOOH as a function of pH, assuming a PZC of 7.30. -----	306
100.	Ratio of singly-protonated to deprotonated surface sites on γ-FeOOH as a function of pH. -----	307
101.	Adsorption of sulfate on amorphous iron oxide as a function of pH and total sulfate concentration. -----	313

LIST OF FIGURES (CONTINUED)

Figure	Title	Page
102.	Adsorption of thiosulfate on amorphous iron oxide as a function of pH and total thiosulfate concentration. -----	314
103.	Adsorption of glutamic acid on amorphous iron oxide as a function of pH and total glutamic acid concentration. -----	316
104.	Adsorption of syringic acid on amorphous iron oxide as a function of pH. -----	317
105.	Adsorption of salicylic acid on amorphous iron oxide as a function of pH and total salicylic acid concentration. -----	319
106.	Adsorption of protocatechuic acid on amorphous iron oxide as a function of pH. -----	321
107.	Adsorption of picolinic acid on amorphous iron oxide as a function of pH. -----	322
108.	Adsorption of 2,3-pyrazinedicarboxylic acid on amorphous iron oxide as a function of pH. -----	324
109.	Adsorption of silver on amorphous iron oxide as a function of silver and chloride concentration. -----	326
110.	Adsorption of silver on amorphous iron oxide as a function of pH in the presence of glutamic acid, salicylic acid, and cyanide. -----	327
111.	Adsorption of silver on amorphous iron oxide as a function of pH in the presence of sulfate and tellurate. -----	329
112.	Adsorption of silver on amorphous iron oxide as a function of pH and total thiosulfate concentration. -----	331
113.	Adsorption of silver and thiosulfate from an equimolar solution ($4 \times 10^{-7}M$) on amorphous iron oxide as a function of pH. -----	333
114.	Removal of silver from solution as a function of pH in the presence of thiourea and amorphous iron oxide. -----	334
115.	Adsorption of silver on α -quartz as a function of pH in the presence of ethylenediamine. -----	336
116.	Adsorption of copper on amorphous iron oxide as a function of pH in the presence of salicylic acid, protocatechuic acid, and sulfate. -----	338
117.	Adsorption of copper on amorphous iron oxide as a function of pH in the presence of glutamic acid and 2,3-pyrazinedicarboxylic acid. -----	339

LIST OF FIGURES (CONCLUDED)

Figure	Title	Page
118.	Adsorption of copper on amorphous iron oxide as a function of pH in the presence of picolinic acid and 2,3-pyrazinedicarboxylic acid. -----	341
119.	Copper adsorption on α -quartz as a function of pH in the presence of histidine and ethylenediamine. -----	342
120.	Adsorption of Cd onto SiO_2 as a function of pH and concentration of complexing ligands (Cl or SO_4) at 0.1M ionic strength. -----	344
121.	Adsorption of Cd onto SiO_2 as a function of pH and concentration of complexing ligands (Cl or SO_4) at 0.7M ionic strength. -----	345
122.	Adsorption of Cd onto SiO_2 as a function of pH and concentration of dissolved thiosulfate. -----	346
123.	Adsorption of Cd onto $\gamma\text{-FeOOH}$ as a function of pH and concentration of complexing ligands (Cl or SO_4) at 0.1M ionic strength. -----	347
124.	Adsorption of Cd onto $\gamma\text{-FeOOH}$ as a function of pH and concentration of complexing ligands (Cl or SO_4) at high ionic strength. -----	348
125.	Adsorption of Cd onto $\gamma\text{-FeOOH}$ as a function of pH and concentration of dissolved thiosulfate. -----	349

LIST OF TABLES

Table	Title	Page
1	Major Iron Sulfide Minerals -----	11
2	Major Oxyanions of Sulfur -----	13
3	Iron Sulfide Phases Formed from Aqueous Iron Species -----	32
4	Iron Sulfide Phases Formed from Solid Iron Reactants -----	33
5	Cyanolysis Reactions with Sulfoxyanions -----	42
6	Some Possible Oxidation Products of FeS -----	84
7	Mass Balance and Distribution of Sulfur Species before and after Aerial Oxidation at pH 10 -----	91
8	Mass Balance and Distribution of Sulfur Species before and after Aerial Oxidation at pH 9 -----	94
9	Sulfur Mass Balance Assuming Thiocyanate from Slow Cyanolysis of (1) $S_3O_6^{2-}$, (2) Colloidal S^0 -----	114
10	Release of Cadmium after Oxidation of Cd-Enriched Ferrous Sulfide -----	125
11	Characterization of India Basin Sediments -----	127
12	Values of (k_2K_2/k_1K_1) Computed by Iterative Method Assuming Values of K_a -----	146
13	Calculated Activity Coefficients for Solution and Surface Species -----	153
14	Calculated Values of k_1K_1 and k_2K_2 at 10° and 15°C -----	166
15	Classification of Lewis Acids and Bases -----	171
16	Solubility and Complex Formation Equilibria for Silver -----	173
17	Stability Constants for Cadmium Inorganic Ligand Complexes -----	196
18	Stability Constants for Cadmium Organic Ligand Complexes -----	204
19	Speciation of Cadmium in Natural Waters -----	211
20	Kinetic Adsorption Experiments -----	233
21	Long-Term Kinetic Adsorption Experiment -----	235

SECTION I

INTRODUCTION

Assessment, management and beneficial control of man's impact on the environment and the environment's impact on man through release and dispersal of toxic substances are among the high-priority objectives of our day. Success depends on our ability to describe and predict release and flow of contaminants through the environment to man and other organisms and their effects upon those organisms. The environment, of course, is the immensely complex mélange of lithosphere, hydrosphere, atmosphere and biosphere we live in and contaminants are everywhere in it. In order to adequately describe and predict release, transport and entrapment of trace metals, a sound understanding of the controlling processes and mechanisms must be in hand. This project addressed itself to one set of questions concerning processes and mechanisms controlling heavy-metal behavior in sediments.

This research project was concerned with the role sulfidic sedimentary environments play in trapping, storing and releasing heavy metals in natural aquatic systems. The information produced by this project is of interest because of the large quantities of cadmium and silver utilized by the U.S. Air Force in its metal-handling and plating operations, and photographic processing operations. The past and present operation of these processes has undoubtedly leaked some trace heavy metals to the environment at specific locations and hence a better understanding and enhanced insight into the behavior of cadmium and silver in aquatic systems should lead to better disposition of appropriate related environmental problems should they arise.

Sediments are known to concentrate the major fraction of heavy metals released to aquatic environments. Heavy metals may be transported into a sedimentary basin and deposited in the sediment phase by a number of different mechanisms. Most heavy metals entering the sediment are probably transported in association with particulate matter in some way (Figure 1). The heavy metal-particulate association may include: Their adsorption on the surface of particulates, bound in humic materials, on oxide coatings on particles, on exchange sites on clay minerals, or incorporated into detrital organic or mineral phases. These modes of transport are important because the form in which heavy metals enter the sediment will largely determine the rate and extent to which the heavy metals are redistributed in the surficial sedimentary materials. Under localized

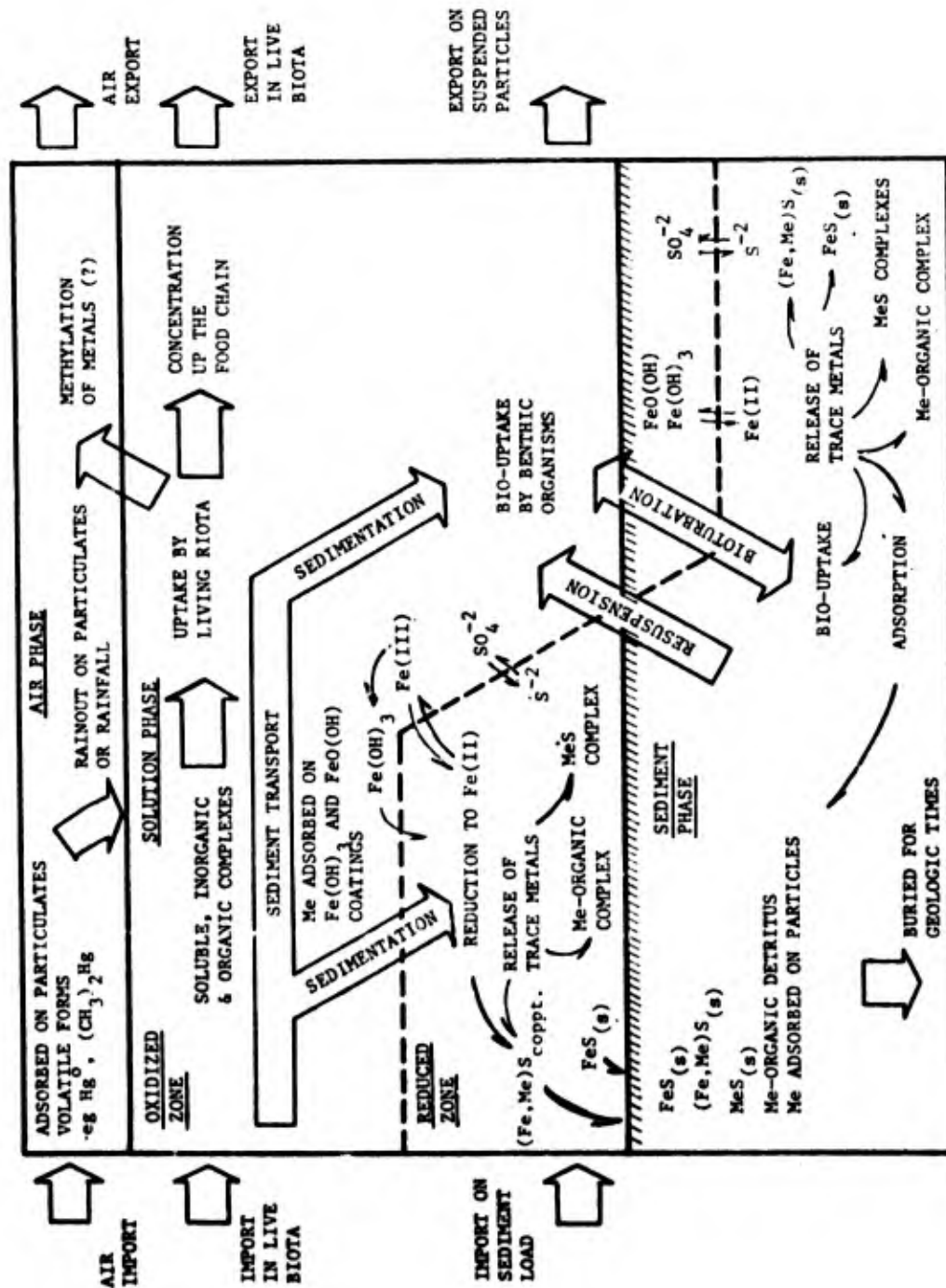


Figure 1. Schematic diagram of the complex transformation processes and mechanisms controlling release, transport, and retention of trace metals in natural aquatic systems.

anaerobic conditions, heavy metal concentrations in natural aquatic environments may be largely controlled by the solubility of their solid-sulfide phase, by the solubility of a sulfide-solid solution or by surface exchange with a ferrous sulfide mineral.

Chemical environments in anaerobic sediments are significantly different from the typically oxygenated overlying waters. Decomposition of organic matter results in the depletion of dissolved oxygen. In the absence of dissolved oxygen, sulfate becomes the dominant electron acceptor in the oxidation of organic matter. The required sulfate is usually obtained by diffusion from the water column and is reduced to sulfide by the metabolic activities of microorganisms. Reduction of sulfate during microbiological reactions often results in interstitial sulfide concentrations in the millimolar range in estuaries. A review of the literature indicates that we still lack insight into how sulfides generated in situ will affect the redistribution of heavy metals deposited in the sediments. Heavy metals typically form quite insoluble sulfide precipitates and some sulfide-solid solutions are also known to occur. The speciation of heavy metals in high sulfide environments is not well understood but most heavy metals are probably strongly complexed.

There are a number of competing factors which make anaerobic sediment environments complex. The breakdown of organic matter under anaerobic conditions results in the production of a large variety of soluble organic compounds such as fatty acids, amino acids, and aromatic alcohols and acids. In particular a wide variety of aromatic compounds are known to be metabolic products from the anaerobic degradation of the complex cellulose structure (e.g., syringic, vanillic, catechuic and protocatechuic acids). Many of these organic solutes are capable of forming stable, soluble complexes with heavy metals. Their production should tend to aid in the redistribution of heavy metals during the reductive dissolution of host iron-oxide coatings and particles (Figure 1).

The formation of complex ions can interfere with the precipitation of many metals which would otherwise normally form insoluble sulfide precipitates. Under strongly reducing conditions sulfate is reduced to sulfide and an iron-sulfide precipitate results if iron is present. The formation of iron sulfide is inhibited or prevented in the presence of humic acids, such as in organic-rich peat bogs. In addition, other heavy metals which form insoluble sulfide precipitates will form soluble complex ions with both sulfide and humic substances.

The flux and form of heavy metals released from both undisturbed and perturbed sediments will depend upon a number of complex factors. The prevalence of dissolved sulfides and iron sulfide precipitates in anaerobic sediments suggests that they may play a significant role in determining the availability of heavy metals to the water column and ultimately to aquatic organisms. Concern about the distribution and pathways of heavy metals in the environment attests to the importance and usefulness of acquiring a better understanding of the fundamental processes at work at the sediment-water interface. Sedimentary sulfides appear to be involved in one of the important mechanisms determining the availability of heavy metals in anaerobic sediments.

The research reported here has focused on questions concerned with the oxidative dissolution of ferrous sulfides and the fate of associated heavy metals both during and after the oxidation reaction. The material is organized into sections dealing with the basic aqueous chemistry of iron and sulfur, ~~(Section II)~~, silver, ~~(Section V)~~, and cadmium, ~~(Section VI)~~ followed by material on adsorption models, ~~(Section VII)~~. Section III presents experimental methodology, used in the oxidation study, and this is followed by a presentation of results and discussion of the oxidation studies (Section IV). Section VIII gives the experimental methodology used in the adsorption studies and is followed by experimental results and discussion presented in Sections IX and X. The report conclusions are summarized in Section XI with recommendations given in Section XII.

SECTION II

AQUEOUS GEOCHEMISTRY OF IRON AND SULFUR

Microorganisms are particularly important in influencing the rates of many geochemically significant reactions. For example, thermodynamically the sulfate ion should be reduced to sulfide by organic matter in the absence of oxygen. However, this reaction is not known to take place at ambient surficial conditions except when mediated biologically (Goldhaber and Kaplan, 1974). The microorganisms responsible for the transformation of iron and sulfur compounds are among the most ubiquitous in the aqueous environment. Their metabolic activities have both short- and long-term geochemical consequences.

Microbial sulfate reduction is an anoxic process. It can occur in the water column as a result of high oxygen consumption or poor oxygen replenishment. Beneath the water column, however, anoxic conditions are frequently established at, or just beneath, the sediment-water interface, again as the consequence of the accumulation of organic matter and restrictions imposed on the rate of transport of oxygen. The metabolic products of the sulfate-reducing bacteria (CO_2 , H_2S , NH_3 , PO_4 , etc.) are chemically reactive and therefore influence diagenetic processes. Metal sulfide precipitation, carbonate precipitation, pH modification, and gas generation (CO_2 , CH_4 , H_2S) are associated with the bacterial activity.

This section examines some chemical and geochemical aspects of the sedimentary iron and sulfur cycles. The material briefly summarized here was selected to provide the requisite background for the subsequent discussion of results of studies on the oxidative dissolution of ferrous monosulfides and possible mechanisms involved in the oxidation reactions.

Some Thermodynamic Considerations: A Gibbsian Approach to Sediments

Natural aquatic systems are highly dynamic redox environments. All surficial estuarine sediments are far from an equilibrium state. For example, in an estuary there may be a marked difference in redox environment between the surface in contact with oxygen in the atmosphere and the bottom waters at the sediment-water interface. The region in between may also reflect large redox gradients depending upon mixing, diffusion, and the extent of biological activity. In the sediment there will typically be a very large

redox gradient, with increasing reducing conditions moving from the sediment-water interface into the sediment depth. Exact definition of redox environments in natural sediments is not possible and in any case is less important than an understanding of the redox gradients and transport processes acting within the system.

Changing redox conditions can affect heavy metals in natural sediments in two ways: 1) by direct changes in the oxidative state of the metal ion, and/or 2) by redox changes in available and competing ligands or chelates. Fe, Mn, Hg, Ag, and Cu are examples of metals which change oxidation state within the redox range of natural sediment environments. The sulfur system is an example of changing ligands as a function of pE. Primary concern in natural systems is with environments having a pE in the range 0 to -6 and pH values in the range 6 to 9. This generally describes anoxic sedimentary environments in estuary systems (Leckie and James, 1974).

Stability Fields and Meta-Stability. Heterogeneous oxidation-reduction reactions occurring in natural aquatic systems typically have time or kinetic frameworks quite different from homogeneous interactions. Nevertheless it is useful to consider the thermodynamics of these heterogeneous reactions in order to put bounds on the possible and to aid in understanding the occurrence of kinetically inhibited meta-stable phases which frequently are found under thermodynamically impossible conditions. The purpose of this section is to briefly examine the relative stability of the major iron and sulfur species and phases found or expected under sedimentary conditions. This is important since iron phases are likely hosts for trace metals in sedimentary environments.

Sedimentary Iron Minerals. The most common iron minerals found in modern or recent surficial sediments include siderite, goethite, hematite, glauconite, and magnetite in oxidizing environments, and mackinawite, greigite, marcasite, and pyrite in reducing environments. The major source of detrital iron in sediments comes from the oxidation products of weathering: hematite and goethite. On the other hand, iron sulfides, siderite and glauconite are diagenetic minerals and are typically formed from iron released upon the reductive dissolution of hematite, goethite and amorphous iron hydroxide.

Hematite, magnetite, pyrite, and pyrrhotite are the thermodynamically most stable phases to be expected in sedimentary environments. The pE/pH stability fields for these phases are shown in Figure 2 for typical conditions under which these phases might exist. Pyrrhotite, of course, is not a sedimentary phase. Its formation is usually associated with conditions of high temperature and pressure. Under conditions typical of anaerobic sedimentary environments, the ferrous sulfide usually precipitated is the tetragonal FeS mackinawite. Similarly, hematite is not usually observed to precipitate from solution but rather is formed by the dehydration of amorphous ferric oxyhydroxide. Limonite and goethite are typical phases in which iron is introduced into sedimentary environments while lepidocrocite is the phase formed upon oxidation of ferrous solid phases. The phases typically present in surficial sediments are mackinawite, lepidocrocite, pyrite and elemental sulfur (Figure 3). Figure 3 is based on the assumption of meta-stability of the mackinawite and lepidocrocite solid phases. Pyrite is included in Figure 3 because the formation of pyrite in sulfidic estuarine sediments appears to occur relatively rapidly (Williamson, 1976). The formation of pyrite is dependent upon a dynamic sediment system which is overturned periodically causing the materials to be alternately oxidized and reduced. The consequence of the abrupt reintroduction of sulfidic materials into oxygenated environments deserves to be studied in more detail. Greater insight into the kinetics and mechanisms of the oxidation of ferrous sulfides and the resultant reaction products should contribute to a better understanding of the process leading to the formation of pyrite in recent sediments and to the control of free sulfide concentrations in sediments by available iron. The major iron sulfide minerals are summarized in Table 1.

Soluble Aqueous Species. Figure 4 presents a pC/pE diagram for an iron/sulfur system over the pE range -2.5 to -5.5, where major redox changes occur for the sulfur system. Although no major soluble iron species are given for $pE < -4.5$, experimental evidence suggests the presence of soluble ferrous iron on the order of 1 mg/l. These calculations have been made assuming typical concentrations of total soluble iron, sulfur, ammonia, and carbonate found in interstitial waters of anoxic estuarine sediments (Troup et al., 1974; Presley et al., 1972).

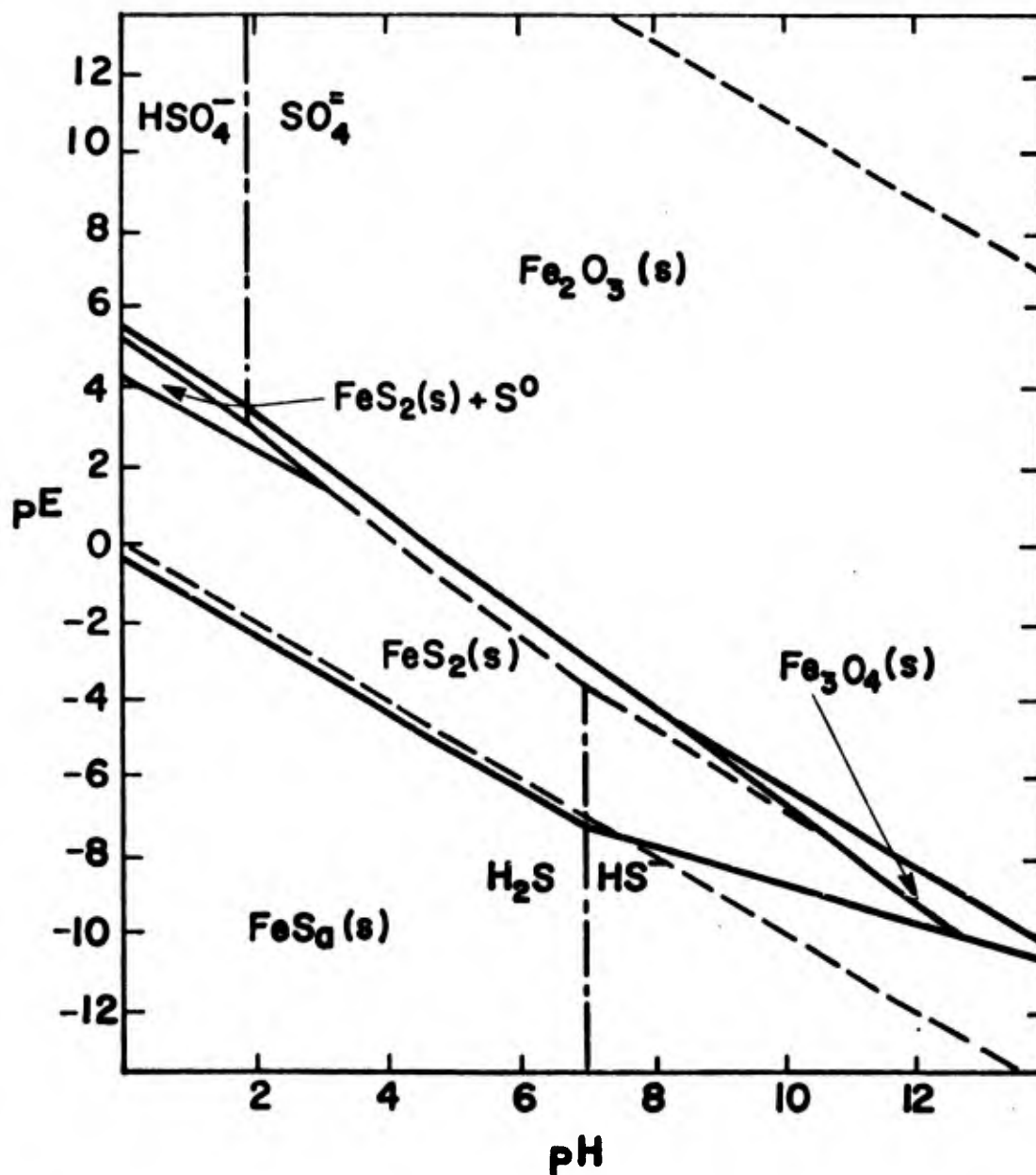


Figure 2. Stability field diagram of solid Fe phases as a function of pE and pH at 25°C and 1 atm total pressure. Diagram is computed for conditions of $1 \times 10^{-4}\text{M}$ total sulfur species and $1 \times 10^{-2}\text{M}$ total carbonate species in aqueous solution. Solubilities used for pyrite (FeS_2), pyrrhotite (FeS_q), hematite (Fe_2O_3), and magnetite (Fe_3O_4).

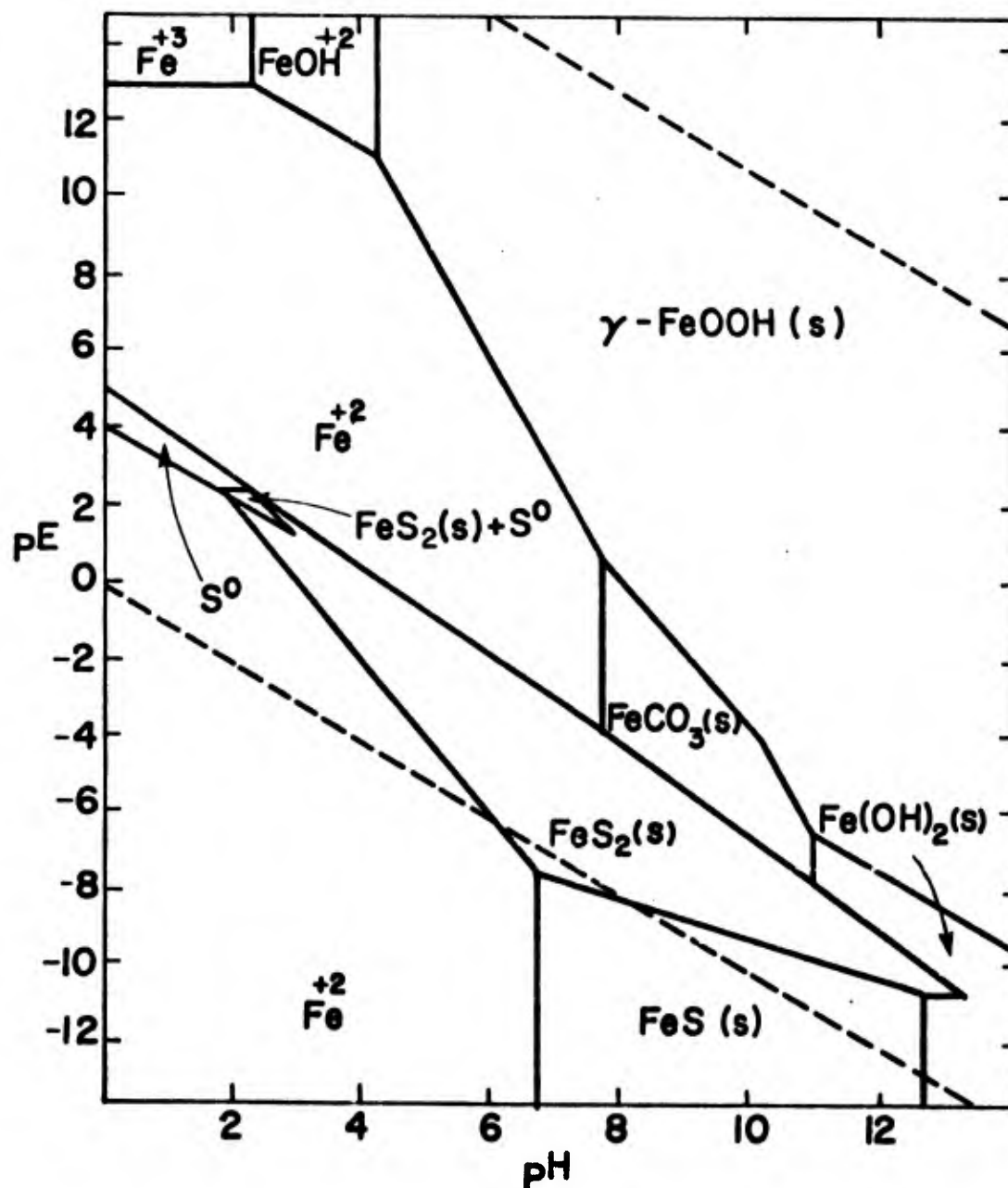


Figure 3. Stability diagram of solid Fe phases as a function of pE and pH at 25°C and 1 atm total pressure. Diagram is calculated for conditions of $1 \times 10^{-6}\text{M}$ total iron, $1 \times 10^{-4}\text{M}$ total sulfur species and $1 \times 10^{-2}\text{M}$ total carbonate species in aqueous solution. Solubilities used for pyrite (FeS_2), mackinawite (FeS), lepidocrocite ($\gamma\text{-FeOOH}$), siderite (FeCO_3), and ferrous hydroxide (Fe(OH)_2).

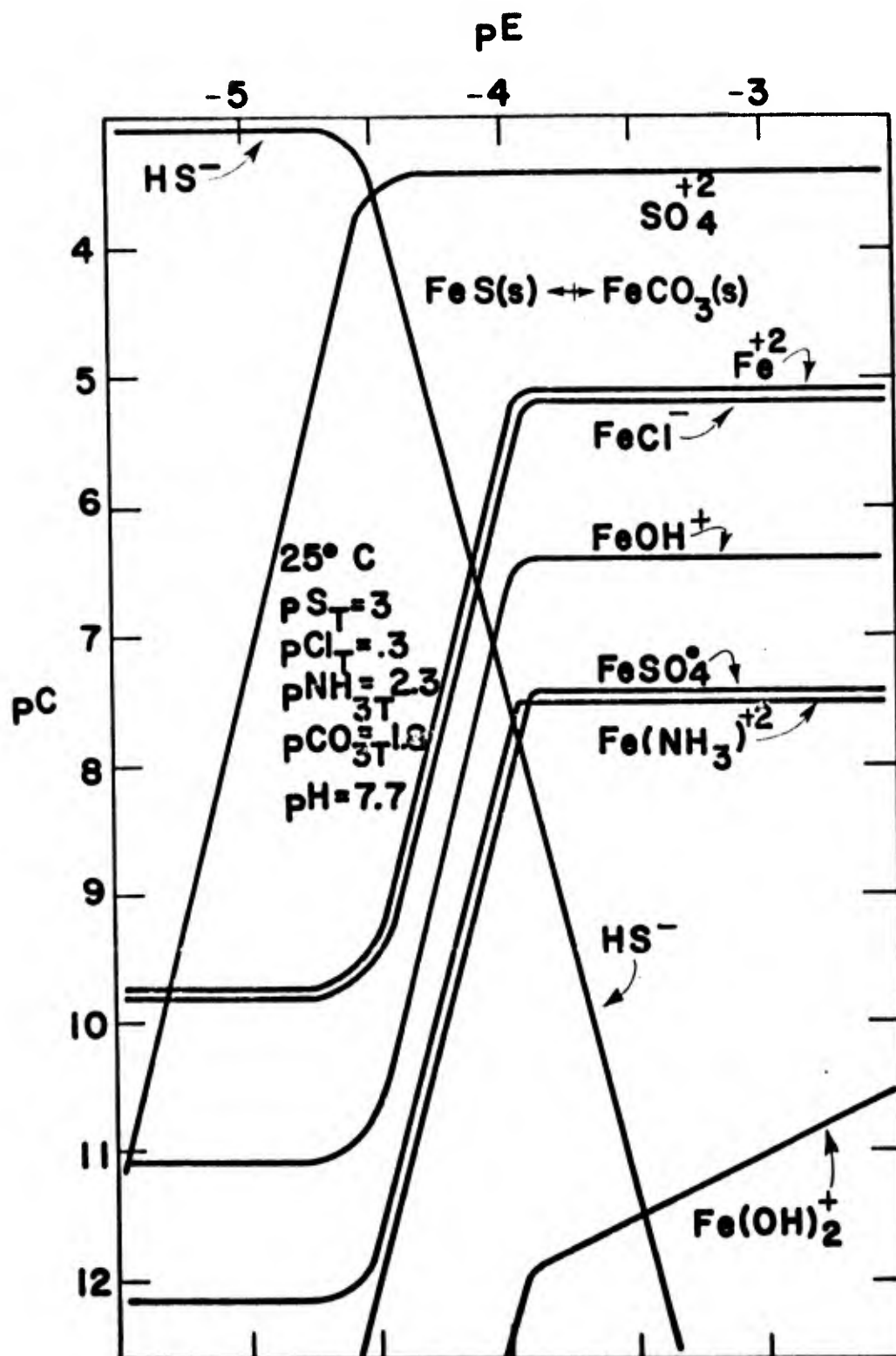


Figure 4. Equilibrium aqueous concentrations of iron and sulfur species as a function of pE. Note that a phase transition occurs at about pE -4 between FeS(s) and $\text{FeCO}_3\text{(s)}$. Solution composition is typical of estuarine sediment interstitial waters.

TABLE 1. MAJOR IRON SULFIDE MINERALS

	Alternate Names	Composition	Crystal Structure	Magnetic Susceptibility	Acid Solubility	Occurrence
MACKINAWITE	Hydrotroilite Melnikovite* Tetragonal FeS Kansite Amorphous FeS	Fe_{1+x}S , where $x = 0-0.25$. Laboratory $x = \pm 0.1$.	Tetragonal	Non-Magnetic	Yes	Recent sediments. Sulfide corrosion product of iron. Vein mineral.
GREIGITE	Melnikovite*	Fe_3S_4	Cubic	Ferromagnetic	Yes	Recent sediments. Sedimentary iron ores.
SMYTHITE		Fe_3S_4	Rhombohedral	Ferromagnetic	Yes	Sedimentary iron ores, and only in association with rhombohedral carbonates.
PYRRHOTITE	Troilite Monoclinic pyrrhotite	Fe_{1-x}S where $x = 0-0.2$.	Hexagonal and monoclinic	Magnetic, variable	Yes	Igneous rocks. Metamorphic rocks.
PYRITE		FeS_2	Cubic	Paramagnetic	No	Sedimentary deposits. Igneous rocks. Metamorphic rocks.
MARCASITE		FeS_2	Orthorhombic		No	Sedimentary deposits from near surface acidic solutions. Sedimentary rocks, limestone and clays.

Mixtures of mackinawite and greigite.

Aspects of Sulfur Chemistry

Sulfur is a member of the group VI elements (O, S, Se, Te, and Po) and the electronic structure of their valence orbitals in the elemental form is two electrons short of the noble gas configuration. The chemistry of Se, Te, and Po is basically similar to that of sulfur; however, a discussion of their chemistry is not appropriate here.

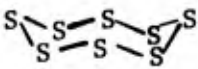
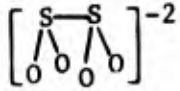
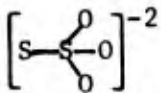
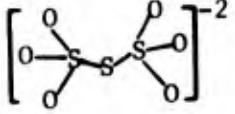
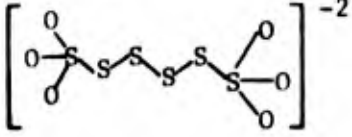
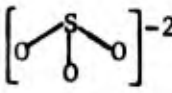
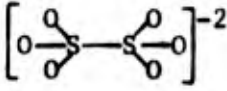
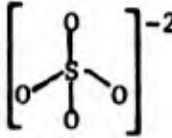
Sulfur is much larger and less electronegative than oxygen. Oxygen is found naturally in the oxidation states between 0 and -2 while sulfur exhibits formal oxidation states from -2 to +6 over the range of redox environments encountered naturally. The valence shell of sulfur has a principle quantum number of 3. The 3d-orbitals are available for bonding in addition to the 3s- and 3p-orbitals. Calculations indicate that the energies of sulfur d-orbitals are weak. The presence of ligands causes a contraction of the d-orbitals such that the radii of maximum electron density is appropriate for bonding (Nickless, 1968). Explorations of increased stability of bonding due to sulfur d-orbitals splitting typical of transition metal bonding is reported to be unimportant in sulfur bonding (Nickless, 1968).

The formation of octahedral hybrid sp^3d^2 -orbitals is normally proposed to explain bonding when sulfur has a formal oxidation number of +4 or +6 such as in sulfite or sulfate.

Some of the more common sulfoxy anions and their structures are tabulated in Table 2. The variety of combinations which sulfur enters into with oxygen, the halogens, and organic molecules is immense. The limited selection presented in Table 1 includes the species which are expected to form as transition species during the oxygenation of sulfide to sulfate. A few additional species are also included for comparative purposes.

While sulfur is capable of existing in numerous valence states, as both singular and polynuclear species, relatively few of these are observed in natural environments. Calculations of the thermodynamic stability of various species agree with observations of the distribution of species in nature. The stability of various sulfur species is plotted as a function of pE and pH in Figure 2. The most striking aspect of the diagram is the absence of a number of sulfur species which are observed to exist for extended time periods both in the laboratory and in the field. Thermodynamic calculations only describe equilibrium conditions; they say nothing about the

TABLE 2. MAJOR OXYANIONS OF SULFUR

Name	Formula	Structure	Average Oxidation State of Sulfur	Oxidation State of Individual Sulfur Atoms
Sulfide	S^{2-}	$[S]^{-2}$	-2	-2
Polysulfide	S_n^{2-}	$[S-S-S-S]^{-2}$	$-2/n$	-2, 0
Elemental Sulfur	S^0		0	0
Dithionite	$S_2O_4^{2-}$		+3	+3
Thiosulfate	$S_2O_3^{2-}$		+2	0, +4
Trithionate	$S_3O_6^{2-}$		+3.33	0, +4
Hexathionate	$S_6O_6^{2-}$		+0.83	0, +4
Sulfite	SO_3^{2-}		+4	+4
Dithionite	$S_2O_6^{2-}$		+5	+4, +6
Sulfate	SO_4^{2-}		+6	+6

kinetics of the reactions. Meta-stable products tend to accumulate when one step in the reaction process has a high activation energy. In such a case, even though there may be a substantial decrease in free energy for the overall reaction, there may not be a sufficient amount of energy or excited species present for the reaction to proceed at a detectable rate. Thus, the reactants will appear as meta-stable species and may exist for extended periods of time, despite thermodynamic predictions of their demise.

The production and distribution of meta-stable intermediates observed during sulfide oxidation are quite different from the thermodynamically predicted species. The oxidation of aqueous sulfides and their products have been observed or measured by numerous researchers. The products resulting from the homogeneous oxidation is a complex function of a number of factors, including: the initial sulfide concentration, pH, catalysts, inhibitors, dissolved oxygen concentration, and relative reaction rates.

The initial concentration of sulfide has been reported to have an effect upon the products of their oxidation. Only the general trends observed are really important, because of the different techniques of the respective researchers, and the sensitivity of the results to trace catalysts. Thus, direct comparisons are questionable. The general trend is to go from the formation of sulfur oxyanions at higher initial sulfide concentrations, through polysulfide complexes to the formation of elemental sulfur at the lower initial concentrations. The position of the polysulfide formation might be expected since their stability and the solubility of elemental sulfur are both increased by increasing sulfide concentrations.

The pH of the medium affects both the rates of reaction and the distribution of species produced. The formation of elemental sulfur is thermodynamically more favorable in the lower pH range. This is demonstrated to some extent by the observation of elemental sulfur and polysulfide formation in the neutral to slightly acidic range, and an increasing percentage of thiosulfate formed with increasing pH.

The most dramatic impact on the oxidation process is effected by trace metal catalysis. The catalytic effect of some transition metals was observed by Krebs in 1928. These observations were investigated in much greater detail by Chen (1970, 1972) and by Snively (1969), who studied the oxidation process under a variety of conditions. The catalytic effects of

transition metals is found to be so great, that special glassware-cleaning procedures must be adopted before reproducible results can be achieved. Of the metals studied, their catalytic effects were found to descend in the order: Ni^{+2} , Co^{+2} , Mn^{+2} , Fe^{+2} , Ca^{+2} ~ Mg^{+2} . In the absence of any known catalysts, the half-life of sulfide was observed to be around 50 hours in one study. The addition of 10^{-4}M Ni^{+2} solution to a sulfide solution under similar conditions reduced the half-life to a few minutes. These effects have implications in the study of natural systems, where catalysts are present, and in the use of analytical techniques, such as using specific ion electrodes to monitor changes in concentration. It has been proposed that these electrodes may actually catalyze the reactions, which would account for the wide range of reaction rates observed when different analytical techniques are employed. The action and effectiveness of catalysts can often be explained either by a lowering of the required activation energy or providing an alternate pathway with a lower activation energy. Bacteria are quite adept at catalyzing thermodynamically favorable reactions and utilizing the released energy, when otherwise the reactions would not normally occur at any appreciable rate at ambient temperatures. The reduction of sulfate in anaerobic environments is a good example. The redox conditions under which the reduction of sulfate to sulfide is thermodynamically favorable is quite broad. However, this reaction does not occur at ambient temperatures at any detectable rate in the absence of bacterial mediation.

In addition to enhancing reaction rates, transition metals also alter the stoichiometry of the oxidation reactions, and the end products observed. In the absence of catalysts, the predominant species formed in the pH range 7.5-9.4 is thiosulfate (Chen, 1972a). Chen found that when $5 \times 10^{-5}\text{M}$ Ni^{+2} was added to a sulfide solution, the oxidation products after 12 hours were 40% elemental sulfur, and 60% thiosulfate. When the experiment is repeated with a 10^{-4}M Ni^{+2} , the ratio shifts to 80% elemental sulfur, and 20% thiosulfate. In other studies, ferrous iron was also found to increase the oxidation rate, and caused a shift in product species from 50% sulfate and 35% thiosulfate in the absence of Fe^{+2} , to 82% thiosulfate when Fe^{+2} was added (Cline, 1969). The mechanism is not at all clear.

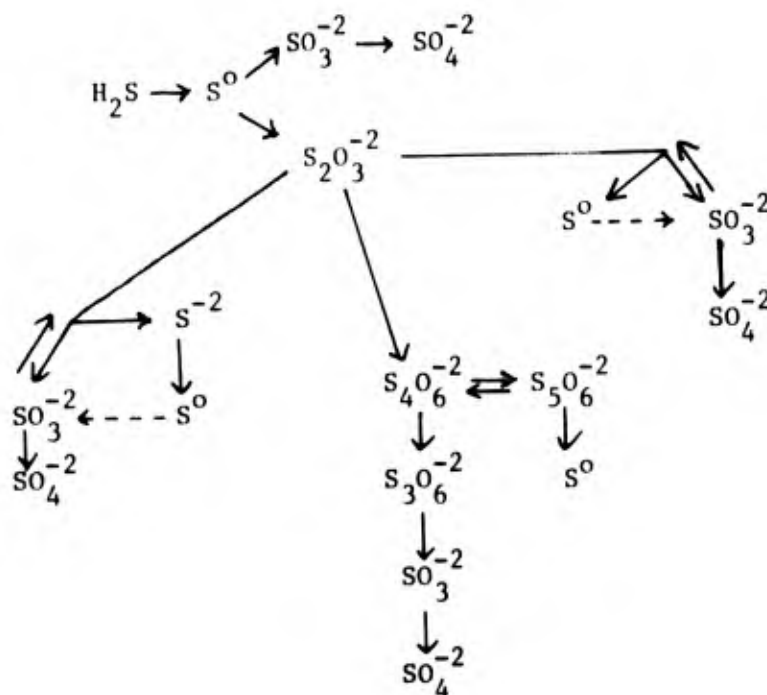
One common trait shared by all the metals showing a high efficiency of catalysis is the ability to participate in one-electron exchanges. The

production of radical chains also requires this ability (Chen, 1970). The addition of elemental sulfur was also found to catalyze the oxidation. This was interpreted as a result of the formation of the more reactive polysulfide complexes (Chen, 1973).

A number of organic compounds, including EDTA, were found to act as inhibitors to the oxidation process. This action did not appear to be related to the chelating ability of the organics, but rather to the presence of basic nitrogen groups. The free electron pair on the nitrogen presumably serves as a site for chain breaking of the free radical chains (Chen, 1970). Trace amounts of sugar or glycerin have been reported to greatly inhibit the oxidation of sulfite to sulfate by oxygen, so the causes of inhibition are undoubtedly numerous and complex.

The oxidation of sulfite has also been reported to be catalyzed by transition metals (Schroeter, 1963) and to proceed via a free radical mechanism. Both organic compounds, and inorganic ions including CN^- and NH_4^+ , are reported to serve as effective inhibitors. Sulfide also inhibits the oxidation of sulfite, possibly because it is a more effective scavenger of free radicals than sulfite (Chen, 1970). This points out the complexity and multiplicity of pathways involved in the oxidation of sulfides. The most popularly accepted mechanisms for the reactions involve the formation of free radicals.

Sulfide species, elemental sulfur and sulfate were identified earlier as the only thermodynamically stable species predicted for naturally occurring redox environments. The formation of intermediates is necessary in the sequence of reactions leading from sulfide to sulfate. The exact pathways are still unknown for both the abiogenic oxidation reaction and the microbologically mediated chemolithotrophic oxidation carried out by the thiobacilli species (Goldhaber and Kaplan, 1974). The intermediates which have been identified and the similarities between them can be compared and contrasted with the sulfoxyanions which are not observed during the oxidation of sulfide. The sulfur species identified as intermediates include: the polysulfides, elemental sulfur, thiosulfate, polythionates other than dithionate, and sulfate. Sulfite is not listed, but is undoubtedly an intermediate. Its propensity for reacting with other intermediates and relative rapidity of sulfite oxidation by oxygen under the same experimental conditions leading to the oxidation of sulfide keep its concentration low.

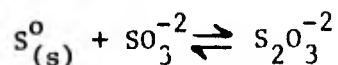


Schematic pathways for the oxidation reactions

The average formal oxidation state of sulfur in each species is shown in Table 2. The oxidation state predicted from the chemical environment surrounding individual sulfur atoms in the polymeric species is often quite different than the average oxidation state of the sulfur in the overall molecule. When the formal oxidation state of the individual sulfur atom is considered, the number of oxidation states observed is reduced to only four: -2, 0, +4, and +6. In the case of the polythionates, the average oxidation states of the two sulfite groups is +5. This is probably more accurately considered a resonance structure where the oxidation state varies from +4 to +6. When the structure is participating in a chemical reaction, the opposing groups act as if the sulfur in one is in the +4 state and is +6 in the other. The reaction of the higher polythionates with cyanide is discussed in detail in the analytical section. Cyanide attacks the sulfur atoms in the backbone of the chain forming SCN^- and liberating SO_4^{-2} and $\text{S}_2\text{O}_3^{-2}$. Further cyanolysis of $\text{S}_2\text{O}_3^{-2}$ is catalyzed with copper to yield SCN^- and SO_3^{-2} . Therefore the two $-\text{SO}_3$ groups do react as if their respective sulfur oxidation states are +4 and +6 rather than an average of +5.

The sulfur atoms in thiosulfate have very different characters and do not change their respective oxidation states while bound together. A number

of experimental approaches have been applied to demonstrate this. Thiosulfate can be formed by reacting sulfite with elemental sulfur according to the relationship:



Thiosulfate decomposes readily into sulfite and elemental sulfur when acidified. Thiosulfate prepared by boiling sulfite and a tagged elemental sulfur decomposed into sulfite and elemental sulfur with all of the radioactivity being recovered as elemental sulfur (Sienki and Plane, 1961). This demonstrates that the $-SO_3$ group is stable and that the oxygens do not change positions.

From the observed intermediates and their respective structures, it is implied that an individual sulfur atom is relatively stable with respect to oxidation by oxygen when it is in either the 0, +4, or +6 oxidation state. The oxidation state of sulfur in the various combinations of sulfur and oxygen seen in the intermediates can all be considered combinations of these three oxidation states.

Many of the intermediates readily participate in exchange reactions between themselves which do not involve redox reactions. For example, the reaction of elemental sulfur and sulfite to form thiosulfate. Elemental sulfur also dissolves in sulfide solutions forming polysulfides of the general form S_n^{-2} . Polysulfides with small sulfur chains ($n = 2-3$) apparently are less stable than the larger chains ($n = 4-5$) and disproportionate to give free HS^- and the higher polysulfides (Cotton and Wilkinson, 1972).

Solutions of higher polythionates are not stable. They gradually disproportionate to trithionate. Depending upon conditions, the trithionate decays further through thiosulfate and sulfite to sulfate. Polythionates are most stable under acidic conditions.

Solutions containing a single polythionate species also undergo disproportionation reactions leading to the formation of other polythionate species. The presence of thiosulfate and sulfite in polythionate solutions also results in a change in the distribution of polythionate species present. Therefore, if the presence of a specific higher polythionate is determined, other unidentified species will undoubtedly be present to some extent.

Thiosulfate is oxidized by mild oxidizing agents, including iodine and ferric iron, to tetrathionate. During the oxidation of ferrous sulfide under alkaline conditions the formation of both ferric iron and thiosulfate is reported (Cline, 1969). This provides a basis for anticipating the formation of tetrathionate and other polythionates as reaction products.

The fact that the oxidation of sulfide to sulfate necessarily involves a sequence of simple reactions where sulfide is oxidized to successively higher intermediate oxidation states was discussed. The only formal oxidation states for individual sulfur atoms in meta-stable sulfur species are 0, +4, and +6. The initial oxidation of sulfide by oxygen probably results in the formation of a sulfur species with an electronic population of elemental sulfur. In this form, it should be quite reactive with its unfilled orbitals. The tendency of elemental sulfur or sulfur atoms to polymerize is demonstrated by the ring and chain structures evident in elemental sulfur, polysulfides and higher polythionates. The unpolymerized sulfur is a reactive transient species which should rapidly oxidize further or associate with other sulfur species. The possible oxidation of sulfide to elemental sulfur while still in contact with other sulfide atoms in the iron sulfide lattice adds another complexity to the oxidation process which must be considered. The formation of these unpolymerized, reactive sulfur atoms provides a convenient explanation for the formation of the species identified under experimental conditions.

The list of sulfur oxyanions is fairly extensive. However, its formation of only a few species is anticipated from a knowledge of the chemistry of the various species. Molecules containing S - O - S bonds are not expected. The oxidation state of sulfur in these compounds is +4 or +6. The structure of sulfite and sulfate do not favor condensation reactions in aqueous media. Similarly the formation of an S - O - S bond would not occur during an oxidation-reduction reaction and would only serve to make the reactive intermediate less stable in any case.

The formation of elemental sulfur, thiosulfate and higher polythionates is anticipated from the similarity in structure and knowledge of their respective chemistries. Both elemental sulfur and thiosulfate have been identified as oxidation products of aqueous sulfide. The formation of tetrathionate during the oxidation of thiosulfate with ferric iron and

the formation of other polythionates in the presence of thiosulfate and elemental sulfur provide strong reasons to anticipate the formation of all of the polythionates (except dithionate) during the oxidation of FeS(s). Based upon this discussion, the sulfur species which are anticipated to be formed during the oxidation of sulfide to sulfate are elemental sulfur, polysulfides, thiosulfate, polythionates with three or more sulfur atoms, and sulfate. Polysulfide formation would be limited to situations where the free sulfide concentration is high enough to keep the sulfur in solution as polysulfides. The experimental conditions present during the oxidation of ferrous sulfide are therefore not conducive to polysulfide formation.

Aspects of Iron Chemistry

Iron occurs naturally in only two formal oxidation states (+2 and +3) in aqueous environments. The ferrous-ferric redox couple is electrochemically very active, and the distribution of dissolved iron between these two oxidation states is a good indicator of the pE of the environment. Iron species participate in electron exchange reactions easily. Aqueous ferric iron is capable of acting as an oxidizing agent, being reduced to ferrous iron in the process. In the presence of strong oxidizing agents, ferrous iron is oxidized to ferric.

Whether iron will be oxidized or act as an oxidizing agent can be readily calculated from thermodynamic data and the composition of the system since the iron couple is quite reversible. The expression describing the relationship between aqueous ferrous and ferric iron, oxygen and the hydrogen ion concentration is given by

$$10^{+7.75} = \frac{[\text{Fe}^{3+}]}{[\text{Fe}^{2+}][\text{H}^+](\text{P}_{\text{O}_2})^{1/4}}$$

The oxidation of ferrous iron is extremely favorable over a wide pH range even for very low partial pressures of oxygen. Stability field diagrams describing the conditions under which various iron and sulfur species are stable are discussed below.

Kinetics of Oxidation. The oxidation and reduction of iron species are of interest to investigators in a variety of disciplines. As a result, a

large body of literature exists describing factors which influence the rate of oxidation. The rate of oxidation of ferrous iron has a first-order dependence on the concentration of ferrous iron and the partial pressure of dissolved oxygen. Singer and Stumm (1970) investigated the influence of OH^- on the oxidation rate. They found that at pH 3, the rate is independent of pH, while at pH 4.5 the rate has a second-order dependence on OH^- concentration, suggesting that there might be two mechanisms operating in the oxidation of ferrous iron. At pH 3 the rate expression is given as

$$\frac{-d[\text{Fe(II)}]}{dt} = k[\text{Fe}^{2+}](\text{P}_{\text{O}_2})$$

At pH 4.5 the rate expression is described by

$$\frac{-d[\text{Fe(II)}]}{dt} = k[\text{Fe}^{2+}](\text{P}_{\text{O}_2})[\text{OH}^-]^2$$

The rate of oxygenation has also been observed to be influenced by the alkalinity of the solution. The rate of oxygenation at higher pHs is a function of $[\text{OH}^-]$. Stumm and Singer (1966) observed that bicarbonate appears to catalyze the oxidation. The reduced rates in poorly buffered solutions is attributed to the slower response of the $\text{HCO}_3^- - \text{H}_2\text{CO}_3$ buffer to localized shifts in pH caused by hydrolysis of the ferric iron produced in the oxidation reaction.

The influence of the buffering capacity of the solution on the oxidation rate was evaluated by Ghosh (1974) in much greater detail. His results agree well with earlier results under most conditions. At higher alkalinities, he found that the oxidation rate has a 1/2-order dependence on the buffering capacity of the solution, when the buffering capacity was greater than 4 millieq/pH. The rate can then be described by

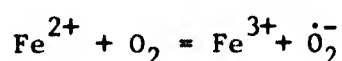
$$\frac{-d[\text{Fe(II)}]}{dt} = k[\text{Fe}^{2+}] \text{P}_{\text{O}_2} [\text{OH}^-]^2 \beta^{1/2}$$

Since the buffering capacity only affects the rate expression at $\beta \geq 4$ millieq/pH, or an alkalinity of 340 mg/l as CaCO_3 at pH 6.8, it is probably not too important in most natural waters and can be neglected in the rate expression (Ghosh, 1974). It is interesting to speculate about analogies between buffering capacities and catalysis by hydrated Si-OH and Al-OH surfaces which are discussed later.

Catalytic Agents. Wide discrepancies between the oxidation rates in the laboratory on simple, pure systems and the rates in natural samples have been observed. Depending upon the constituents in the water the effects may range from catalysis to a dramatic inhibition of the oxidation reaction. Singer and Stumm (1970) found that light catalyzed the reaction by a factor of 3 to 4 at low pHs.

Heavy metals are reported as capable of catalyzing the oxidation of ferrous iron. Stumm and Lee (1961) found that cupric ions were an effective catalyst at concentrations as low as $3 \times 10^{-7} \text{M}$. They also found that the catalytic effect was dependent upon both the Fe^{2+} and Fe^{3+} concentrations. The concentration of Fe(III) in uncatalyzed solutions had no effect upon the rate of oxidation of Fe^{2+} . When chelating agents, including E.D.T.A., tetramine, and glycine, were added to solutions of Fe^{2+} alone, they inhibited the rate of oxidation. Chelating agents did not affect the ability of the copper to catalyze the oxidation reaction.

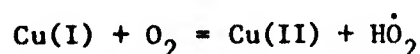
According to the mechanism proposed by Weiss (1935), the initial step in the oxidation of Fe^{2+} by O_2 is the rate-limiting step,



Here the initial reaction of the molecular oxygen and the production of the HO_2 ($\dot{\text{O}}_2^-$) free radical is rate limiting. Once the free radical is formed, it is involved in a chain of reactions where ultimately 3 more Fe^{2+} ions are oxidized to Fe^{3+} . Singer and Stumm (1970) proposed a mechanism to explain the catalytic effect of the copper where



then



The free radical is then available to participate in the remaining oxidation sequence. This bypasses the rate-limiting step in the uncatalyzed reaction. Stumm and Lee (1961) also observed this but were unable to incorporate the Cu(II) into the rate expression. They did show that the rate increased with increasing Cu(II) concentration. Also the mechanism appeared to operate in both low and neutral pH ranges.

Both Mn^{2+} and Co^{2+} were mentioned as capable of catalyzing the oxidation of Fe^{2+} .

It is not clear whether the catalytic metal must be capable of participating in one electron exchanges, and the oxidation-reduction cycle between Fe^{+2} and O_2 to function as an effective catalyst. Heavy metals which are capable of participating in one-electron exchanges have also been observed to catalyze the oxidation of aqueous sulfide species.

Surface Catalysis. The oxidation of ferrous iron in acid mine drainage, natural aquatic systems, and water-treatment processes may potentially occur in the presence of surfaces of different properties. Since clays are such ubiquitous components of a wide variety of environments, Singer and Stumm (1970) simulated clay surfaced using silica (SiO_2) and alumina (Al_2O_3).

In the pH range between 3.5 and 4.0, high surface areas of alumina ($8000 \text{ m}^2/\text{l}$) increased the oxidation rate from 10 to 30 times. Catalysis was explained by drawing an analogy of the high density of aluminol (Al-OH) groups on the surface and a condition of localized high OH^- concentration.

Orthosilicic acid (H_4SiO_4) also increased the rate of oxidation of Fe^{2+} at pH values greater than 5 (Shenck and Weber, 1968).

Colloidal $\text{Fe}(\text{OH})_3$ does not appear to catalyze the reaction (Singer and Stumm, 1970).

Inorganic Ligands

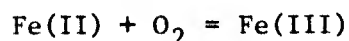
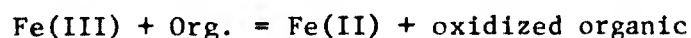
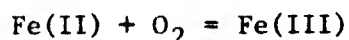
Stumm and Lee (1961) stated that H_2PO_4^- and metaphosphate increased the rate of oxygenation of ferrous iron, and it was suggested that this was due to the formation of complexes with $\text{Fe}(\text{III})$. Presumably, the effect can be interpreted as reducing the free $\text{Fe}(\text{III})$ available to participate in the reverse reactions in Weiss's mechanism.

Concentrations of Cl^- and $\text{SO}_4^{=}$ of 10 mg/l were not observed to have any effect on the oxidation rate (Singer and Stumm, 1970). Concentrations of 100 mg/l and 1 gm/l of sulfate did catalyze the reaction rate though (Singer and Stumm, 1970).

Organics. In sedimentary environments, conditions resulting in the depletion of dissolved oxygen and the reduction of iron also generally result in the production of soluble organics and humic materials. Humic materials have

been reported to comprise up to 50% of the organic content in conventional secondary effluent (Rebhun and Manka, 1971).

Ferrous iron often persists in oxygenated environments far longer than is predicted using the kinetic data available from pure, uncatalyzed systems. Stumm and Morgan (1970) suggest that the concentrations of ferrous iron observed in oxygenated surface waters are in a dynamic equilibrium between oxidation by dissolved oxygen and reduction by the organic matter present. The apparent steady-state concentration of ferrous iron observed is reached when the rate of oxidation by dissolved oxygen just equals the rate of reduction by organic matter. Presumably, the iron merely acts as an electron transfer catalyst in the oxidation of the organic matter and persists while the organic matter is being oxidized. Equations describing this are:



If step 2 is more rapid than step 1, then Fe(II) will persist in the presence of dissolved oxygen.

Theis and Singer (1973) chose a series of organic compounds with structures similar to segments of humic materials to simulate the effects of humic materials upon the oxygenation of ferrous iron in a well-defined system. They found that a few organic components, including tannic acid, gallic acid and pyrogallol, completely inhibited the oxidation of a 10^{-4}M Fe(II) solution (at 25°C , pH 6.3, and P_{O_2} 0.5 atm. with an organic concentration of 10^{-4}M) for the entire 2-hour period observed. The ferrous-tannic acid solution was found to be stable for several weeks under these conditions.

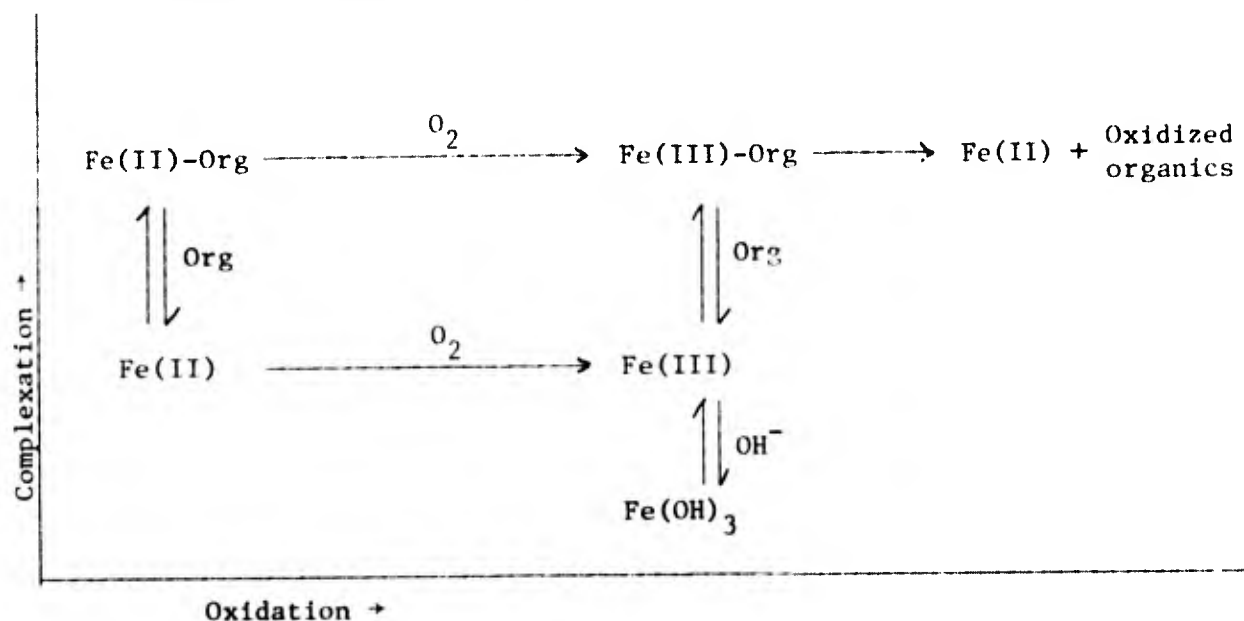
Manometric studies of a 10^{-4}M Fe(II) and 10^{-3}M tannic acid solution at pH 10 indicate that the ferrous iron is stable for 100 hours while the tannic acid is being oxidized after which the Fe(II) is oxidized and precipitated as Fe(OH)_3 . The ferrous-tannate complex is more stable to oxidation than either the ferrous iron or tannic acid alone (Theis and Singer, 1974).

Apparently iron does not play the role of an electron transfer catalyst as in the Stumm-Morgan model mentioned earlier. Theis and Singer also investigated the reduction of ferric iron by organics. Generally, they found that

many of the organics which inhibit the oxidation of ferrous iron are, in turn, oxidized by ferric iron. Because of the experimental methodology used it is not clear how far (if at all) these latter results can be extrapolated to natural waters.

Citric acid accelerates the rate of oxidation of ferrous iron, yet is also apparently rapidly reduced by ferric iron. This acceleration is explained by the formation of a ferrous-citrate complex which is much more rapidly oxidized than ferrous iron alone. Considering the stability of the ferric-citrate complex, a mechanism involving the complexation of Fe(III) by citrate, such as proposed for inorganic ligands, appears more plausible.

The overall schematic proposed by Singer is:



Stumm and Lee (1961) mention that, in the absence of organics, the oxidation reaction may be the controlling factor in removal at pH values of 7 or below. That is, oxidation is much slower than flocculation at this pH range. At pH values above 7 the rate of oxidation in uncatalyzed systems is faster than the rate of flocculation. At pH greater than 8 oxygen diffusion is probably the rate-limiting step. Therefore, if organics reduce the rate of oxidation of ferrous iron, then since the rate of hydrolysis and flocculation of any free ferric iron formed should be much faster than the rate of oxidation, the oxidation step would be the limiting factor in Fe(II) removal.

Ferric Oxide and Oxyhydroxide Phases. There are a number of ferric oxide and oxyhydroxide phases which are observed to exist in natural environments or to form in the laboratory. The most common pedological ferric oxide and hydrated phases found naturally include: limonite (ferric oxide gel), goethite (α -FeOOH), lepidocrocite (γ -FeOOH), hematite (α -Fe₂O₃), and maghemite (γ -Fe₂O₃).

Ferric oxyhydroxides are produced synthetically in the laboratory routinely. Conditions under which a solid phase is generated dictate the final product. Conditions leading to the formation of some of the phases of interest in sediments and soils are described by phase.

Ferric oxide gels. X-ray amorphous ferric oxide gels result from rapid increase in pH of ferric solutions and subsequent hydrolysis of ferric iron. Colloidal suspensions form when low concentrations of ferric iron are hydrolyzed in weakly acidic solutions (pH 3). When hydrolysis occurs in less acidic solutions or the iron concentration is higher, a brown precipitate forms. Fresh gel is reported to yield a weak electron diffraction pattern identified as goethite (Mackenzie et al., 1971). Similarly fresh gels which are powdered by freeze drying yield a number of broad weak lines after 12 hours exposure to MoK α radiation. The material is reported to have cell dimensions similar to γ -Fe₂O₃. Crystallites have been observed in the gel with transmission electron microscopy (van der Geissen, 1966).

Goethite. Goethite (α -FeOOH) is the iron oxyhydroxide phase formed under a variety of starting conditions. Goethite is typically formed during the hydrolysis of ferric iron solutions in the pH range 1 to 3. The presence of carbon dioxide enhances this formation (Atkinson et al., 1968; Hsu and Ragone, 1972). When an amorphous gel is aged at ambient temperature, it is gradually converted to goethite and hematite. Conditions under which the suspension is aged determine the final product. Lower temperatures and higher pH favor formation of goethite over hematite (Schwertmann, 1959). The presence of Mg(II), Ca(II), Al(III), Fe(II), CO₃²⁻, and SO₄²⁻ ions also favor the conversion of amorphous gels to goethite (Landra and Gast, 1973). The presence of excess ferrous iron, dissolved or adsorbed, particularly enhances the rate of conversion of amorphous gel to goethite (Langmuir, 1969b).

Adsorption of organic matter (in soils) and other materials such as phosphate and silicate may inhibit or prevent the conversion of gels to

goethite even under extreme conditions such as boiling at pH 13 for hours (Schwertmann, 1966). The apparent stability of amorphous gels in natural systems is attributed to this mechanism.

Goethite is also formed during the oxidation of both solid and aqueous ferrous iron at ambient temperatures. In neutral pH range the formation of α -FeOOH was observed during both rapid and slow oxidation (Baudisch and Albrecht, 1932; Langmuir, 1969b; 1969c).

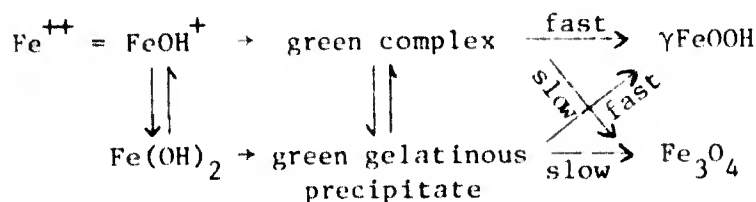
Hematite. Thermodynamically hematite is the most stable of all of the ferric oxides under oxidizing conditions. It is not believed to form directly from solution but rather by exclusion of water from existing oxide phases. Atkinson et al (1968) identified hematite after aging amorphous gels at pH 11. Others (Schwertmann, 1959; Feitrecht and Michaelis, 1962; Landra and Gast, 1973) found that aging gels at neutral or acidic conditions, particularly at elevated temperatures, favor conversion to hematite.

Lepidocrocite. Lepidocrocite is rarely the solid phase which forms from aqueous solution at ambient temperature (Langmuir, 1969b). This is because it is only formed over a relatively limited range of conditions.

The preparation of γ -FeOOH from aqueous solution is described by Baudisch and Albrecht (1932). They found that when slightly acidic ferrous bicarbonate solutions are oxidized over a period of weeks or months by air, the iron oxyhydroxide phases formed are a mixture of α - and γ -FeOOH. Baudisch and Albrecht (1932) also report that the formation of γ -FeOOH did not occur until after a portion of the solution is already oxidized. This observation is confirmed by Schickor (1930) who observed that the formation of a labile green ferrous-ferric complex is a necessary intermediate in the formation of γ -FeOOH. The oxidation of ferrous ammonium sulfate by iodate in the presence of thiosulfate also results in the precipitation of γ -FeOOH (Hahn and Hertrich, 1923). The presence of ligands, particularly nitrogen-containing compounds (pyridine, sodium azide), greatly enhance the formation of γ -FeOOH (Baudisch and Albrecht, 1932; Welo and Baudisch, 1934).

The function of the ligands is not clear. The partial oxidation of ferrous sulfate and ferrous chloride solutions under neutral to slightly alkaline conditions results in the formation of a green solution or green gelatinous precipitate. The existence of ferrous-ferric complexes was established by Misawa (Misawa et al., 1973b). The complexes form as intermediate species during the oxidation of ferrous sulfate solutions. The

rapid aerial oxidation of both greenish solution and the suspension of ferrous iron at pH 8 leads to the formation of γ -FeOOH, while after slow aerial oxidation Fe_3O_4 was identified (Misawa et al., 1973b). Pathways proposed are



The pH of the solution is quite important in determining the oxide phase formed. The pH ranged between 2 and 6.5 in all of the above experiments. Lepidocrocite has been synthesized during the oxidation of ferrous hydroxide outside this pH range. Schwertmann (1959) found a mixture of poorly crystallized γ -FeOOH and X-ray amorphous gel after the slow oxidation of ferrous hydroxide at pH 4 to 5. A similar experiment conducted between 5 and 8 in the absence of carbon dioxide yielded predominantly γ -FeOOH. The greenish color in ferrous hydroxide, which is a white solid, is caused by a ferrous-ferric complex formed due to slight oxidation of the iron. The introduction of carbon dioxide shifts the ferric oxyhydroxide phase formed to α -FeOOH.

The formation of lepidocrocite has also been observed during the hydrolysis of ferric perchlorate solutions. Hsu and Ragone (1972) aged two identical batches of 0.01M ferric perchlorate at 25°C and pH 2.4 for five weeks. A portion of the iron in each batch hydrolyzed and precipitated. The solid in one was identified as γ -FeOOH and as α -FeOOH in the second. The authors offered no explanation for this differentiation. The precipitate formed from hydrolysis of ferric perchlorate solutions aged at pH 2-3 in the presence of $\text{HCO}_3^-/\text{Fe(III)}$ molar ratios of 1:1 and 2:1 for two years was identified as mixture of α - and γ -FeOOH.

In summary, the formation of γ -FeOOH from ferrous iron requires that the pH of the solution be between 2 and 6.5, and the oxidation occurs slowly over a period of weeks. The presence of ferrous complexes enhances the crystallization process and may be necessary intermediate species in the formation of γ -FeOOH.

Lepidocrocite in Natural Environments. The most extensive investigations and identifications of lepidocrocite ($\gamma\text{-FeOOH}$) have been done by soil scientists. Ferric oxyhydroxides are common in the aerobic zone of most soils and sediments. Lepidocrocite is typically found in soils with impeded drainage, particularly those with high organic content (Schwertmann, 1972, 1973; Marel, 1951; Brown, 1953, 1954). It has not been identified in samples from well-drained soils (Brown, 1953). Marel (1951) identified lepidocrocite as the iron oxide phase present in peats and humic iron concretions in Rodooen soils in the Netherlands. The orange-brown mottling of soils with poor drainage has been identified as lepidocrocite (Schwertmann, 1973; Brown, 1953, 1954). The $\gamma\text{-FeOOH}$ is formed in situ. No lepidocrocite was found in Millstone Grit shale from which soils containing lepidocrocite were derived (Brown, 1953). Lepidocrocite is believed to be formed from the oxidation of reduced ferrous iron precipitates. Reduced iron compounds are formed under anaerobic conditions which result from decomposition of organic matter. Lepidocrocite then forms when oxygen is reintroduced into these anaerobic regions. Brown (1954) feels that the rate of oxidation determines whether $\alpha\text{-}$ or $\gamma\text{-FeOOH}$ are formed, $\alpha\text{-FeOOH}$ being favored by rapid oxidation. This was based upon the occurrence of $\alpha\text{-FeOOH}$ near the surface. Since $\gamma\text{-FeOOH}$ is less stable than $\alpha\text{-FeOOH}$ and can be converted fairly easily to the α form (among others), this conclusion is unsupported. The form of the reduced iron preceding $\gamma\text{-FeOOH}$ was not identified.

The lepidocrocite crystals in soils have been observed under the electron microscope. The $\gamma\text{-FeOOH}$ crystals are not associated with the surface of other minerals as are other iron oxides. The particles also exhibit a high degree of crystallinity which allows them to be examined by XRD even at fairly low concentration. Two crystal forms are found; laths both single and twined, and serrated plates. The plate lengths vary from $< 0.1 \mu\text{m}$ to $1 \mu\text{m}$. Since synthetic lepidocrocite of similar morphology can be produced by oxygenation of ferrous solutions at pH 6-7 at ambient temperature, Schwertmann (1973) suggests that a similar mechanism may be operating in nature.

Metal Sulfides

Transition metals have a strong affinity for sulfide, as is demonstrated by the extremely insoluble solid phases and strong aqueous metal sulfide

complexes formed. The explanation for the highly covalent transition metal-sulfide bond is the strong d-orbital backdonation to sulfur on the part of the transition metals. The difference in the strength of similar bonds between oxygen and transition metals lies in the ability of sulfide to utilize its d-orbitals. Transition metal oxides and sulfides have very different characteristics. Because of the difference in ionic radii between oxygen and sulfide, and the ability of sulfide to utilize its d-orbitals, the bonding in metal oxides has a much more ionic character than in metal sulfides due to the smaller ionic radius and higher negative charge density on the oxygen atom. Sulfur atoms have a much larger ionic radius, and d-orbitals for bonding. The strong covalent nature of the transition metal-sulfide bond is demonstrated by the relative close proximity of the metal ions in metal sulfide crystal lattices. This close approach would not be permitted in solids with ionic characteristics due to electrostatic repulsion. The distances between iron atoms in tetragonal iron sulfide (mackinawite) is relatively short (2.602 \AA) and the atoms are not distributed to maximize the distance between them. This proximity indicates metal-metal bonding. Each iron appears to have 4 metal-metal bonds in addition to the tetrahedrally coordinated sulfur atoms surrounding each iron. Tetragonal iron sulfide is reported to have certain metallic properties including metallic conduction and temperature-independent paramagnetism which can be explained in terms of metal-metal bonding. The exact nature of this bonding and its relationship to the iron-sulfur bond is not fully understood (Ribbe, 1974).

Mackinawite and greigite are iron monosulfides commonly identified in sulfidic sediments. Tetragonal iron sulfide, mackinawite, is the least stable, most reactive and probably predominant of the two in recent estuarine sulfidic sediments. One of the principle objectives of this work is to determine the response of iron sulfides in sediments upon resuspension in oxygenated environments. Mackinawite is the most important sulfide phase which must be considered in the study of oxidation kinetics of natural sulfidic sediments.

Mackinawite is a jet black, non-magnetic, tetragonal iron sulfide of the general formula Fe_{1-x}S (see Table 1). A review of the properties of many reported iron sulfides indicates that they are incorrectly identified

and are in fact tetragonal FeS. Naturally occurring mackinawite is slightly sulfur-deficient, with an iron:sulfur ratio of about 1.05:1. The formula for tetragonal iron sulfide is typically written Fe_{1+x}S where $0.07 \geq x \geq 0.04$ which implies there is an excess of iron in the structure. Crystallographic studies indicate, however, that there is actually a deficiency of sulfur in the structure rather than an excess of iron (Ribbe, 1974). Natural mackinawite reportedly always contains some nickel and cobalt (Ribbe, 1974), and the presence of substitutions stabilizes its crystal structure inhibiting its transformation to more stable phases.

Berner (1964a) found that when a solution of Na_2S is titrated with a dilute solution of FeSO_4 , the resultant solid has an iron:sulfur ratio of 1.1:1. When a solution of FeSO_4 is titrated with Na_2S to an excess of sulfide, the FeS formed has an iron:sulfur ratio of 0.9:1. Rickard (1969) synthesized tetragonal FeS in the laboratory from aqueous solutions with an iron:sulfur ratio of 1:2. This yields an iron sulfide precipitate with an iron:sulfur ratio of 0.91:1. The excess sulfur is presumed to be adsorbed or co-precipitated. These observations are also in agreement with other researchers who found that tetragonal iron sulfide formed by precipitation from a solution with an excess of sulfide has compositions with iron to sulfur ratios of 0.94:1 and 0.95:1 (Grönvold and Haraldson, 1952; Arnold, 1962). Since the FeS formed in all of the above cases was identified as tetragonal, the relative concentration of reactants apparently only affects the stoichiometry of the solid formed, not the crystal structure or phase formed.

Tetragonal iron sulfides are formed naturally and in the laboratory under a variety of conditions and from a variety of different iron sources (Tables 3 and 4). Berner (1964a) observed the formation of tetragonal FeS from a variety of starting materials, and over a wide pH range. Rickard also found that mackinawite was always the initial species formed upon the precipitation of iron sulfide from aqueous solutions of ferrous iron and sulfide over the pH range from 2.3 to 11.7. From Tables 3 and 4, it is not evident how important the mackinawite phase is. In some ways these results understate the importance of this phase, because tetragonal FeS is the initial transition phase formed before the final product which is reported in Tables 3 and 4. The formation of some of the other iron sulfide phases appears to be dependent upon subsequent transformation of mackinawite.

TABLE 3. IRON SULFIDE PHASES FORMED FROM AQUEOUS IRON SPECIES

Reactants	pH	Temperature	Time	Products	Source
$\text{FeSO}_4 + \text{H}_2\text{S}$	3	20-25 °C	2 hrs	Amorphous FeS	1
$\text{FeSO}_4 + \text{Na}_2\text{S}$	3.4-6.5	25 °C		Greigite	2
$\text{FeSO}_4 + \text{H}_2\text{S}$	3	60-65 °C	2 days	Greigite + S^0	1
$\text{FeSO}_4 + \text{H}_2\text{S}$	3	85-90 °C	30 min.	TETR. FeS	1
$\text{FeSO}_4 + \text{H}_2\text{S} + \text{O}_2$	3	85-90 °C	15 min.	Greigite, pyrite and marcasite	1
$\text{FeSO}_4 + \text{H}_2\text{S} + \text{O}_2$	3	60-65 °C	2 days	Pyrite and marcasite	1
$\text{FeSO}_4 + \text{H}_2\text{S} + \text{O}_2$	3	40-42 °C	25 days	Pyrite + marcasite	1
$\text{FeSO}_4 + \text{S}_n^{=}$	< 4.4	25 °C		Elemental sulfur	2
$\text{FeSO}_4 + \text{H}_2\text{S} +$ Acetic Acid	7	20-25 °C	5 days	Amorphous FeS	1
$\text{FeSO}_4 + \text{H}_2\text{S} +$ Beckman Buffer	7	40-42 °C	7 days	TETR. FeS + S^0	1
$\text{FeSO}_4 + \text{Na}_2\text{S}$	6.5-11.7	25 °C		TETR. FeS	2
$\text{FeSO}_4 + \text{S}_n^{=}$	4.4-9.5	25 °C		Pyrite, marca- site and S^0	2
$\text{FeSO}_4 + \text{Na}_2\text{S} +$ Beckman Buffer	9	20-25 °C	7 days	Amorphous FeS	1
$\text{FeSO}_4 + \text{Na}_2\text{S} +$ Beckman Buffer	9	40-42 °C	200 days	TETR. FeS + S^0	1
$\text{FeSO}_4 + \text{S}_2\text{O}_3^{=}$	5.4-11.2	25 °C		No reaction	2

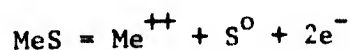
TABLE 4. IRON SULFIDE PHASES FORMED FROM SOLID IRON REACTANTS

Reactants	pH	Temperature	Time	Products	Source
Nat'l Goethite + H_2S	4	20-25 °C	14 hrs	Pyrite + FeS_{tetr} + goethite	1
Synth. Goethite + H_2S	4	20-25 °C	2 days	Pyrite + FeS_{tetr}	1
Synth. Goethite + Na_2S	4.4-7	25 °C		S^0 , marcasite and pyrite	2
Synth. Goethite + H_2S	7	20-25 °C	2 days	Amorphous FeS	1
Synth. Goethite + H_2S + NH_4OH	6.5	20-25 °C	22 days	TETR FeS + S^0	1
Synth. Goethite + H_2S + NH_4OH	6	60-65 °C	20 hrs	TETR FeS	1
Synth. Goethite + Na_2S	7-9	25 °C		TETR FeS	2
Synth. Goethite + Na_2S + Acetic Acid	8	20-25 °C	11 days	Broad band at ~ 5A° + S^0	1
Synth. Goethite + Polysulfide	4-11	25 °C		Sulfur	2
Synth. Goethite + Thiosulfate	4-11	25 °C		Sulfur	2
$FeCO_3$ + Na_2S	6.5-10.3	25 °C		Smythite, FeS_{tetr} + siderite	2
Fe^0 + H_2S	4-9	25-85 °C	3hr-6days	TETR FeS + <u>minor</u> amounts of pyrrhotite, pyrite, + S^0	1
FeS_{tetr} + $S_2O_3^{=}$	6-8	25 °C		No reaction	2
FeS_{tetr} + $S_n^{=}$	7	25 °C		Pyrite, marcasite and sulfur	2
References: (1) Berner, R. A. (1964a); (2) Rickard, D. T. (1969).					

The oxidation of ferrous iron, sulfide and ferrous sulfide by oxygen is predicted thermodynamically. Ferrous sulfide exists in a number of crystal structures, and the reactivity of the various phases varies considerably. The kinetics of the oxidation of homogeneous solutions of ferrous iron and sulfide and possible mechanisms to explain the observed rates have been discussed.

Neither the kinetics nor mechanisms of the oxidation of ferrous sulfide in aqueous solution at ambient temperature have been given much attention. High temperature oxidation of metal sulfide ores of commercial interest has been studied extensively, but these results give little insight into processes occurring under surficial conditions. The task of identifying the initial step in the oxidation of a number of metal sulfides at ambient conditions was undertaken by Sato (1960).

The initial step in the oxidative dissolution of metal sulfides has been singled out by Sato (1960) as the most important step. After the metal-sulfide bonds are broken, the metal and sulfur species can presumably be treated independently (Sato, 1960). Operating on this premise Sato attempted to determine the initial oxidation step in the dissolution of metal sulfides using electrochemical techniques. Selected metal sulfide ores were placed in solutions of known composition, and the potential at the surface of the solid was measured versus a standard reference electrode. The half-cell potentials for possible reactions were calculated from thermodynamic data and the composition of the solution using the Nernst Equation. These theoretical potentials were then compared with the experimental values to determine which theoretical relationships best fit the experimental data. The potential of all divalent metal-monosulfides studied was best predicted by a general half-cell reaction of the form



The proposed mechanism has the metal ions moving into solution, while the sulfide loses two electrons and remains behind in the solid, resulting in an increasing sulfur-to-metal ratio. The oxidation of the elemental S^0 then commences at the completion of the oxidation of the sulfide present. This mechanism is derived from comparisons of electrode potentials with theoretical thermodynamic calculations and is not supported experimentally by Sato.

The proposed mechanism for the disulfides, pyrite and marcasite, is slightly different. The $S_2^{=}$ group is oxidized to S_2^0 and released into solution concurrently with the Fe^{2+} . It was further stated that, since both Fe^{2+} and S_2^0 are unstable, they are rapidly oxidized further. Unfortunately, this is not supported by any experimental evidence.

The generally proposed reaction of Sato does receive substantial support from the work of Chen and others. As discussed earlier, transition metals catalyze the oxidation of aqueous sulfides and influence the end products--favoring the production of elemental sulfur. Chen (1972) found that when heavy metals are added to sulfide solutions, colored solutions or colloidal suspensions result. Upon subjection to dissolved oxygen, these solutions usually clear gradually, and colloidal elemental sulfur is left in solution (Chen, 1972). The reaction was believed to proceed through polymerized heavy metal-sulfide complexes. Studies on the oxidation of marcasite (FeS_2), on the other hand, indicate that elemental sulfur is produced (Gottschalk, 1912). The experimental conditions of Gottschalk were rather poorly controlled, but the results nevertheless do bring up some questions about Sato's proposed mechanisms for metal disulfides.

Gottschalk also ran some rather novel experiments to determine the possibility of electrolytic action influencing oxidation rates when two different metal sulfides are placed in contact. First, the potentials of various sulfides and oxides were determined versus copper wire and listed in order of potentials generated. Pyrite and galena were then placed in a solution and connected with a copper wire (the copper was not in contact with the solution). The same emf as predicted by the table of potentials was generated through the copper wire. The lead sulfide was rapidly coated with lead sulfate in a matter of days, while a similar piece of galena in the same solution but not in contact with the pyrite remained shiny. A similar experiment, replacing galena with sphalerite, yielded similar results except that the initial oxidation was even more rapid. An oxide coating formed on the sphalerite which caused the emf to drop off rapidly. Cleaning the oxide coating off the surface restored the original emf. Preliminary tests substituting hematite for pyrite suggest that hematite may also electrolytically enhance the oxidation rates of metal sulfides with a lower half-cell potential.

Leaching experiments conducted on ZnS , PbS , CuS , and FeS_2 separately and in various combinations demonstrated that electrolytic action does

substantially increase the extent and rate of oxidation of the sulfide with the lower emf, while offering considerable protection to the sulfide with the higher half-cell potential. This is completely analogous to the use of sacrificial metals to provide cathodic protection for metals which are more noble.

It is not clear how far these results can be extrapolated to the interaction of trace metals co-precipitated with iron sulfides, or what the fate of the trace metals in FeS is upon the conversion of FeS to pyrite FeS₂. It is interesting to note, however, that a number of metal sulfides including ZnS, CdS, PbS, and Cu₂S fall in between the potentials of FeS and FeS₂.

From the discussion it is evident that neither the chemical bonding in tetragonal ferrous sulfide nor the processes leading to its oxidation have been well established. This brief review of the chemistry of iron and sulfur should provide an adequate framework within which to discuss the experimental results.

SECTION III

EXPERIMENTAL PROCEDURES FOR KINETIC OXIDATION STUDIES

Experimental kinetic studies have been conducted to determine the effect of pH, dissolved oxygen concentration, solid concentration, chloride concentration, ionic strength and temperature on the rate of oxidation of FeS, and on the products formed. This chapter is organized into two sections. The first section discusses experimental apparatus while the second section covers the analytical methodology used in the rate study investigation.

Experimental Procedure and Apparatus

The oxidation experiments are conducted in the following manner in one-liter water-jacketed vessels. The top of the vessel is covered with a plastic top which can be raised and lowered over the solution (Fig. 5). The top contains ports for a dissolved oxygen probe, glass pH electrode, calomel reference electrode, and a burett tip for introduction of sodium hydroxide. There are also ports for taking samples and introducing gas streams. Gas mixtures are introduced through porous glass spargers. The solution is stirred with a 2-1/2-inch teflon-coated magnetic stirring bar.

The temperature is held constant to $\pm 0.2^\circ\text{C}$ with a Lauda K2/R circulating constant-temperature water bath. Solution pH is monitored and held constant with a Sargent Model D titrimeter. Dissolved oxygen is monitored with a YSI dissolved oxygen probe and meter, and the concentration-time curve is recorded on a Linear Instrument recorder. Gas mixtures of compressed air, nitrogen and oxygen are manually combined and regulated to achieve the desired dissolved oxygen concentration, as measured by the D.O. meter.

The reaction vessel is filled with the reaction medium and brought to the appropriate temperature. The dissolved oxygen probe and the pH electrodes are then calibrated. The solution is then purged with nitrogen. An aliquot of stock ferrous sulfide is added to the reaction vessel, and the system is kept under nitrogen by bubbling N_2 through the suspension. The pH is then adjusted to the desired starting value and the titrimeter is set to maintain the pH. A sample is taken prior to the start of each experiment.

Air or oxygen flow is then turned on and the dissolved oxygen concentration is brought up to the desired level. When the dissolved oxygen

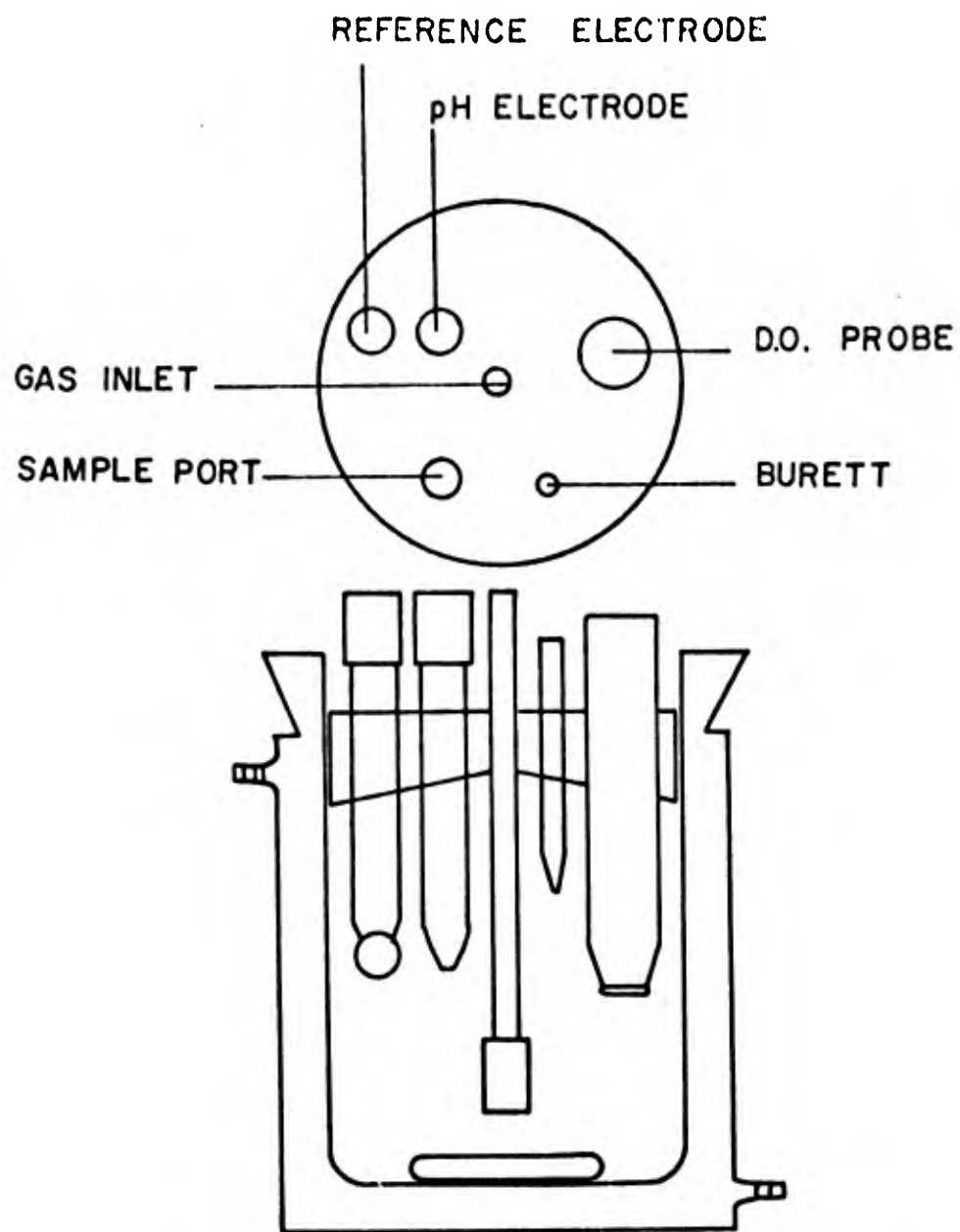


Figure 5. Experimental apparatus used for oxidation studies. Water jacketed vessel with top and appropriate ports for electrodes and experimental equipment.

level becomes constant, the first sample is taken and the experiment is initiated. Samples are then taken at periodic intervals until the end of the experiment. The volume of sodium hydroxide added is recorded as a function of time on a strip-chart recorder.

Analytical Procedures and Methodology

Iodimetric Determination of FeS. The determination of ferrous sulfide is based on an oxidation reaction with iodine acting as the oxidant. Under acidic conditions ferrous sulfide readily dissolves. Iodine quantitatively oxidizes the released sulfide to elemental sulfur. Under these conditions ferrous iron is not oxidized by iodine. Ferric iron should not be present to any significant extent since ferric iron will oxidize iodide to iodine. This analysis is based upon determination of the amount of iodine consumed by the reaction with sulfide. The ferric oxyhydroxide formed as a reaction product does not interfere with the iodimetric reaction when the iron phase is precipitated as a well-crystallized material.

When the experimental oxidation of ferrous sulfide is carried out around pH 7, the oxidation products are elemental sulfur and a well-crystallized ferric oxyhydroxide, γ -FeOOH. None of the products react with iodine. Experimental oxidation of FeS under more alkaline conditions results in oxidation products of soluble sulfur oxyanions, some of which are iodine reactive (e.g., thiosulfate). Corrections must be made for the iodine reactive species. This is accomplished by taking two samples of the FeS suspension. One sample is filtered and the filtrate is analyzed for iodine-consuming species, and the other sample is analyzed for total iodine consumption. FeS is determined by difference.

Determination of Ferrous Iron and Total Iron. A modified analytical method using ferrozine was used to determine the concentration of ferrous iron remaining in the suspension as the reaction proceeded, as reported by Nelson in private communication. Remaining ferrous sulfide was determined during reactions using both the iodine titration method and the ferrozine method. Typical results for both methods are given in Figure 6 showing good agreement between the two methods.

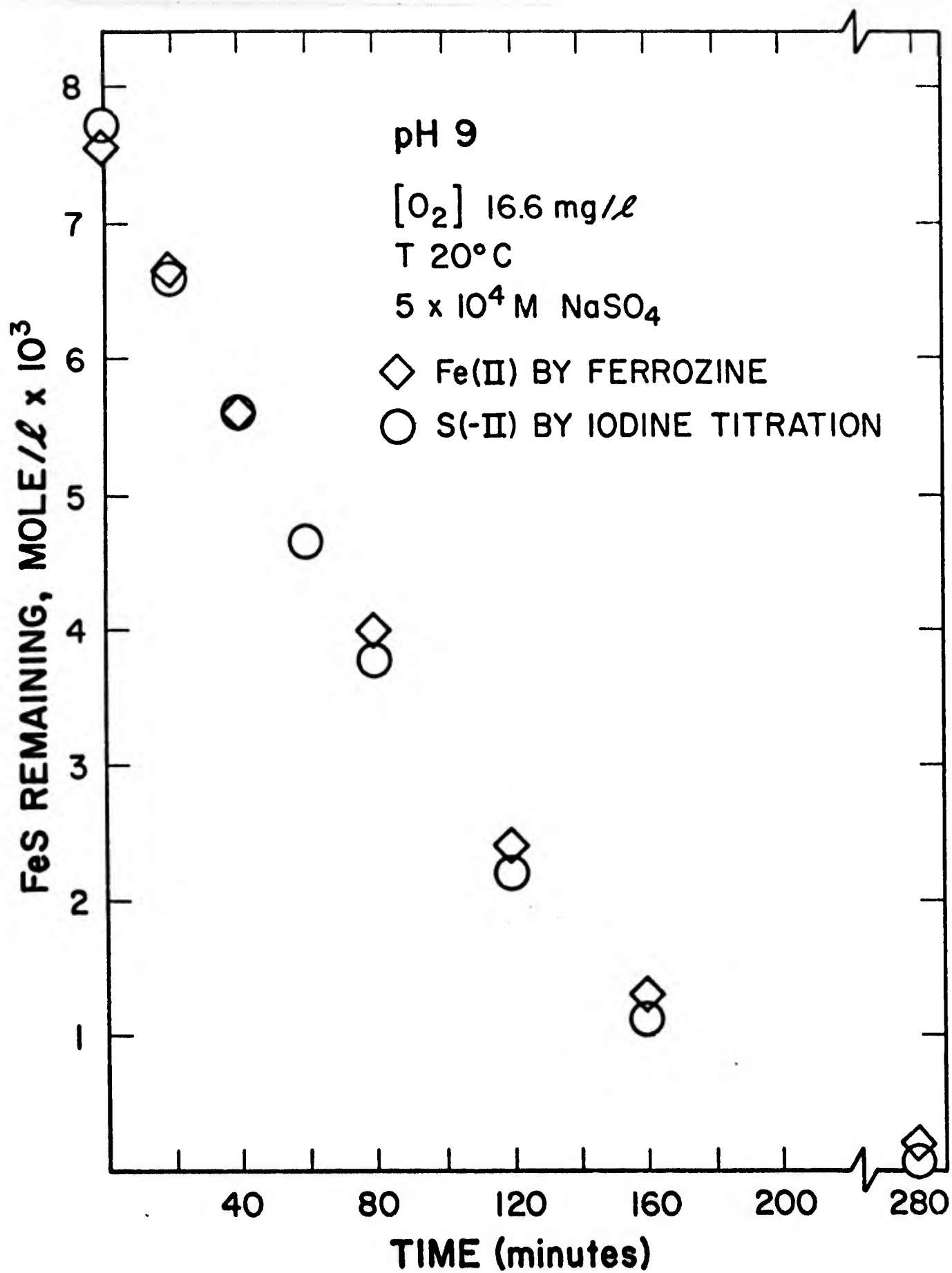


Figure 6. FeS(s) remaining as a function of time at pH 9 and 16.6 mg/l O₂.

Sulfide Determination Using Methylene Blue. The analytical method for sulfide is modified from method 228C, 13th edition of Standard Methods (APHA, 1971). This method is principally used as a secondary check on the results of other analytical techniques.

Determination of Elemental Sulfur. The experimental oxidation of FeS gives elemental sulfur as one typical end product. The elemental sulfur is typically co-mixed with the solid ferric oxyhydroxide solid. Elemental sulfur is hydrophobic and tends to concentrate at air/water and water/glass interfaces, thus causing sampling problems. The sampling problem is especially acute during the course of a reaction because the bubbling gas causes accumulation of the sulfur at or on the surface of the liquid and glass reaction vessel, electrodes and plastic cover.

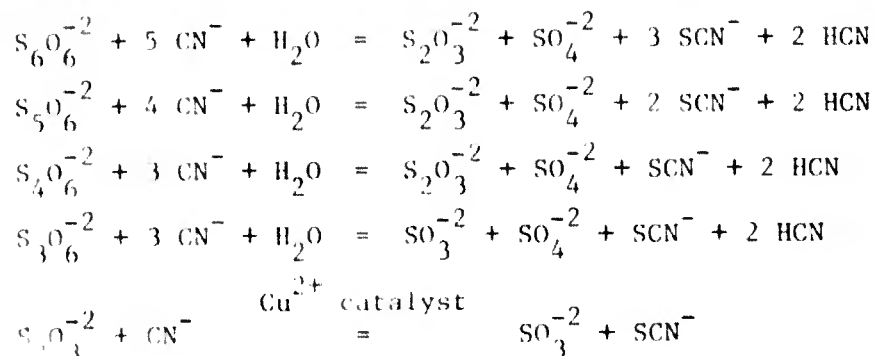
Samples are pipetted from the suspension and filtered through 0.05 μ m millipore filters. Use of 0.45 μ m filters passes significant quantities of colloidal sulfur. The membrane filter bearing the elemental sulfur and ferric oxyhydroxide is transferred to a 35-ml screw-top centrifuge tube. Final analysis involves conversion of elemental sulfur to thiocyanate in 95% acetone (Bartlett and Skoog, 1954).

Determination of Sulfur Oxyanions. The quantitative measurement and identification of sulfur oxyanions is based upon their rate and extent of reaction with cyanide. The reaction of cyanide with thiosulfate and polythionates (other than dithionate) occurs at significantly different rates, thus allowing identification and quantification of mixtures of sulfoxyanions.

Cyanolysis of polythionates in weakly alkaline solutions is described by reactions given in Table 5. The cyanolysis of tetra and higher polythionates is very rapid, going to completion in less than two minutes at $\geq 20^{\circ}\text{C}$ and 10 to 15 minutes at 15°C (Kolthoff and Belcher, 1957). The cyanolysis of trithionate is much slower, requiring > 9 hours for 99.9% completion of the reaction at 25°C (Urban, 1961b). The cyanolysis reaction of trithionate can be accelerated by heating the solution to near 100°C for 45 minutes, cooling and adding Cu(II) to convert all thiosulfate formed to thiocyanate (Kelly et al., 1969).

The concentrations of the individual polythionates are calculated from the stoichiometry of the reactions and the known quantity of thiocyanate released by the treatment of samples under the various conditions. The specific

TABLE 5. CYANOLYSIS REACTIONS WITH SULFOXYANIONS



analytical approach used in this study to determine thiosulfate, trithionate and higher polythionates follows the method developed by Urban (1961a, 1961b).

Elemental sulfur also reacts slowly with cyanide under alkaline conditions to form thiocyanate. The suspension is filtered through a 0.05- μm filter which removes non-colloidal sulfur. However, any colloidal elemental sulfur which passes through the filter will react with cyanide forming thiocyanate and interfere with the determination of trithionate. The results of the analysis for trithionate are ambiguous as either trithionate or elemental sulfur will give rise to thiocyanate, which is the species measured. The ambiguity in interpretation can be resolved using indirect measurements including total mass balance of sulfur in solution and a mass balance of the formation of hydronium ions during the reaction.

Sulfate Analysis. Sulfate was determined colorimetrically using the method developed by Bertolacini and Barney (1957). Solid barium chloranilate is added to the sample containing sulfate and allowed to react at pH 4 in 50% ethanol. Barium chloranilate is relatively insoluble; however, barium sulfate is less soluble. In the presence of sulfate, barium is released from the chloranilate and reprecipitated as barium sulfate. The acid-chloranilate ion is highly colored and exhibits a broad absorption band at 530 nm. Ethyl alcohol decreases the solubility of both barium sulfate and barium chloranilate, and increases the sensitivity of the method.

Total Soluble Sulfur. Total soluble sulfur is operationally defined as all sulfur which passes through a 0.05 μm filter. This includes all of the

sulfoxyanions and colloidal elemental sulfur. A measured aliquot of filtered solution is placed in a 150-ml beaker. Ten ml of 37% hydrogen peroxide are added and the pH adjusted to 11-12 with sodium hydroxide. The solution is then brought to a very gentle boil. After 20 minutes an additional 10 ml of hydrogen peroxide is added and the solution cooled. The pH is readjusted to 11-12 with NaOH and brought to a gentle boil again for a total of 45 minutes. The solution is then diluted to a known volume. This procedure converts all sulfur species present to sulfate. The sulfate present is analyzed.

Determination of Iodine Reactive Species. The procedure consists of filtering a sample of the suspension through 0.05 μ m membrane filter, acidifying and adding an aliquot of iodine solution. Excess iodine is then titrated with standardized thiosulfate solution. The procedure is repeated using a deionized water blank. The difference represents the amount of iodine consumed by the iodine reactive species.

The oxidation of sulfide past elemental sulfur results in a suite of soluble oxyanions of sulfur. Measurement of soluble iodine reactive species provides an empirical methodology for monitoring reaction products as a function of time and correlates consistently with the analysis for specific oxyanion speciation.

Reactions describing the oxidation of FeS to ferric oxyhydroxide and various sulfox anions is discussed in Section II. Reactions lead to various end products, including hydronium ion. There is a correlation between the amount of base consumed (in pH-started reactions) and the production of soluble sulfoxyanions. Comparison of the quantity of hydrogen ions produced and iodine reactive species indicates whether or not there is a shift in the proportion of reactants over the course of the experiment. A linear relationship indicates no change in proportion of products. Data on specific sulfox anions, iodine reactive species, and hydrogen ion production during experimental oxidation studies is discussed in detail in Section IV.

Dissolved Oxygen Concentration. The concentration of dissolved oxygen is monitored using a YSI oxygen meter and probe. The probe is mounted in the reaction vessel cover (Figure 5) and is calibrated using at least two known concentrations of dissolved oxygen before the start of each experiment. The probe measures the partial pressure of dissolved oxygen in solution rather than concentration. The meter and probe demonstrated linear response over

the range 0 to 20 mg/l O_2 . The solubility of oxygen at a given partial pressure, ionic strength, and temperature must be known in order to calibrate the meter-probe system. Tabulated data relating dissolved oxygen with ambient partial pressures at one atm total pressure over 0 to 50°C and NaCl concentrations from 0 to 20,000 mg/l (0 to 0.563M) are available (APHA, 1971). Dissolved oxygen dependency in Na_2SO_4 solutions are given by Linke (1965).

Determination of Cadmium. Cadmium analyses were conducted using a Perkin-Elmer atomic absorption spectrophotometer Model 403 with an HGA Model 2100 graphite furnace. This instrumentation provides an extremely sensitive method for determination of total cadmium at concentrations below 1 μ g/l.

X-Ray Diffraction Analysis (XRD). Identification of the crystalline structure of both the ferrous sulfide and ferric oxyhydroxide phases were done using XRD analysis. Actual sample preparation of the two solids differed because of the extreme sensitivity of the ferrous sulfide to oxidation by oxygen.

Ferrous Sulfide. Preparation of samples for identification appears to be the critical step in the identification of the iron sulfide phase. Both Berner (1964a) and Rickard (1969) emphasize the extreme sensitivity of tetragonal iron sulfide to oxidation by oxygen. Rickard reports that attempts to mount dried samples on a slide and analyze by X-ray diffraction failed due to rapid oxidation of the sample and high background-to-signal ratios.

Berner (1962a, 1964a) prepared his samples by washing to remove excess sulfide, then drying rapidly with acetone. The dried solid was then mounted in a powder camera, but the method of preparation is not stated. Unfiltered $FeK\alpha$ radiation for periods of 20 to 40 hours is required. For freshly precipitated samples, Berner did not get a pattern adequate for positive identification. Rickard (1969) reviewed Berner's data on amorphous FeS and notes that the broad weak peaks are adequate to positively identify the samples as tetragonal. He also found a broad peak at around 5 Å on all of the samples reported by Berner. This peak is the dominant and characteristic line of tetragonal iron sulfide.

Rickard drew his samples up into a 0.3 mm bore Lindemann glass capillary tube which was then heat sealed. These were then mounted in a powder camera and analyzed with $CoK\alpha$ radiation. Rickard's technique is preferred because it allows analysis of a sample with properties close to the properties of the

bulk precipitate in suspension. Drying the sample first increases the probability that the material ultimately analyzed is not representative of the material initially present. The more radical the sample preparation, the stronger this argument becomes.

Based upon a review of the literature and experimental observations, tetragonal iron sulfide is the first identifiable phase to form in a suspension precipitated from homogeneous solution. A recognizable diffraction pattern should be attainable after a week of aging, if sufficient care is taken to prevent exposure to atmospheric oxygen during preparation of samples for X-ray analysis.

The sample preparation used here is similar to that described by Rickard (1969). The iron sulfide suspension is first filtered or centrifuged under nitrogen to concentrate the solids. The paste produced is transferred under nitrogen to a plastic 3 cc syringe and forced from the syringe into a 0.3 mm Lindemann glass capillary tube. After heat sealing the ends of the capillary tube, it is mounted in a Debye Scherrer camera and irradiated with $\text{FeK}\alpha$ radiation for four to twelve hours. The use of iron radiation reduces the problem of fluorescence encountered with copper radiation.

Glass capillary tubes appear to provide the optimum method of preparing samples. Sample preparation requires far less time with this method, and it is also much easier to avoid exposure to oxygen and prevent oxidation of the sample. Most important, it allows analysis of the suspension with a minimum of alteration and in a form as close as possible to the original state. This provides a degree of assurance that the material finally analyzed is representative of the original material.

Ferric Oxyhydroxide. Sample preparation and analysis of ferric oxyhydroxide phases formed is much simpler than that for ferrous sulfide. The samples can be prepared and analyzed in the presence of oxygen which simplifies the procedures. It also allows analysis by diffractometer by mounting the sample on a petrographic slide. Fluorescence of the sample in the X-ray beam is not a problem. This allows a greater choice in source and wavelength of X-rays.

Samples of the oxidized suspension are withdrawn at the conclusion of the oxidation experiment and filtered through a $0.45\mu\text{m}$ membrane filter. The filter cake is washed repeatedly with deionized water, scraped into a beaker, and resuspended in 5 ml of acetone or deionized water. The suspension is

spread onto a petrographic slide, partially air dried, and placed in a diffractometer. X-ray diffraction was done using Cu, Mo, or FeK α radiation. The XRD analysis is performed within two hours of the conclusion of the oxidation experiment. The diffraction patterns obtained from ferric oxyhydroxide suspensions formed by oxidizing ferrous sulfide suspensions at different pHs are presented in Section IV.

Transmission Electron Microscopy. Samples of both the ferrous sulfide phase and the ferric oxyhydroxide phase have been examined using a transmission electron microscope. Emphasis was placed on observing the particle morphology and estimating particle size.

Analysis of Natural Sediment Materials. Sediment samples were taken from the anoxic layer of sediments below the low tide line. The sediment samples were transferred to a one-gallon polypropylene wide-mouth jar and stored at 4°C. Acid-soluble sulfide and total acid-soluble iron were determined using the methylene-blue technique and the ferrozine technique, respectively.

For the oxidation-rate studies the reaction vessel is prepared in the normal manner, adding 980 ml water and deaerating. A core of the sediment material is taken using a plastic 20-ml syringe which has the end of the barrel cut off. The barrel of the syringe is forced down into the sediment as the end of the plunger is held at the surface of the sediment. Once loaded in this manner the syringe is withdrawn, the exterior wiped clean and weighed. This method of sampling minimizes exposure of the material to oxygen. The sediment is transferred into the deaerated water in the reaction vessel. The empty syringe is then reweighed and the weight of sediment calculated.

The sediment is resuspended in deaerated water under nitrogen using a mechanical teflon stirring propeller and magnetic stirring bar. The oxidation of the suspension is performed in the manner used for synthetic ferrous sulfide suspensions.

SECTION IV

OXIDATIVE DISSOLUTION OF FERROUS SULFIDE

Ferrous iron and sulfide form a number of solid phases of varying composition and crystal structure. The susceptibility of the different phases to different biological, chemical, and physical perturbations ranges from highly reactive to almost inert. In order to draw meaningful conclusions from laboratory observations and extrapolate the results to natural systems, it is critical that the phase being modeled is the same as the phase observed in natural sediments. The necessity of using solids of known composition and characteristics is self-evident.

Mackinawite is the ferrous monosulfide predominant in surficial sulfidic-sediment environments and studies of the oxidative dissolution of mackinawite are presented in this section. Results of parametric studies on the effect of pH, dissolved-oxygen concentration, temperature, surface area, ionic strength, chloride concentration, and catalysts on the oxidation of mackinawite are presented first. This is followed by a discussion of the results of studies on the variation of iron and sulfur reaction products as a function of experimental conditions. Discussion of the kinetic studies including appropriate kinetic models concludes the section.

Effect of Hydrogen Ion Concentration

The rate of oxidation of ferrous sulfide exhibits very little pH dependence over the pH range studied (6.5 to 11). The pH dependence of the rate of oxidation is shown in Figure 7. Between pH 9 and 11 the rate of oxidation is essentially independent of the hydrogen ion concentration. As pH decreases from 9 to 6.5, the rate of oxidation increases with increasing pH. However, the magnitude of increase is rather small. The hydrogen ion concentration increases by a factor of 316 times, while the rate of oxidation of ferrous sulfide only increases by approximately a factor of 4.

Effect of Dissolved Oxygen

Molecular oxygen acts as the oxidant in the oxidation of both ferrous iron and sulfide to a variety of end products. Dependence of the rate of oxidation and the end products formed upon reaction conditions indicates the oxidation of ferrous sulfide may consist of a number of interdependent reactions occurring both in sequence and in parallel. The response of the

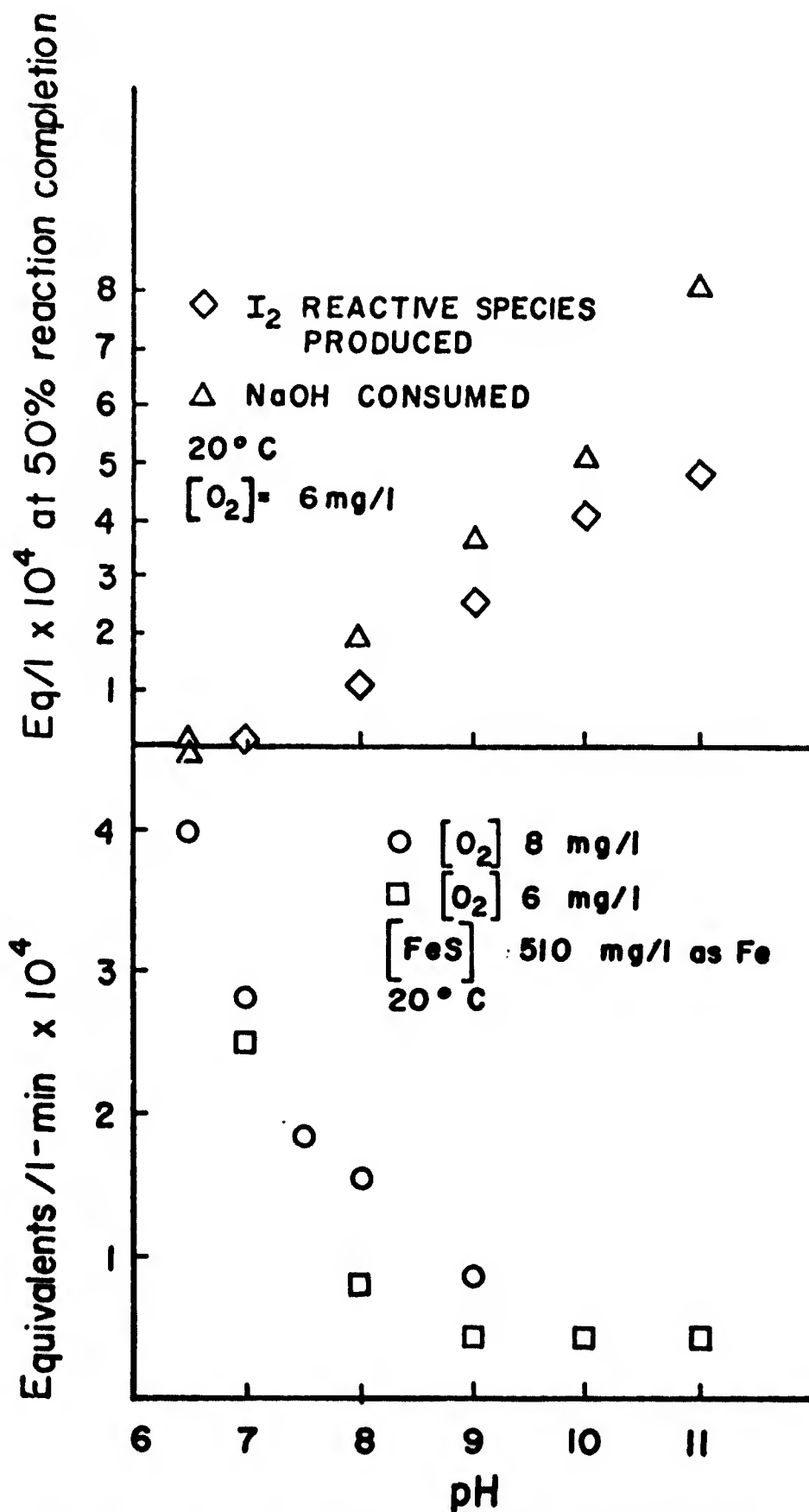
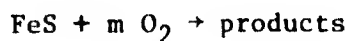


Figure 7. The rate of oxidation of FeS, determined at 6 mg/l and 8 mg/l O₂, 20°C, as a function of pH of solution during oxidation. The rate is independent of pH above pH 9.

rate of oxidation to oxygen concentration provides insight into the mechanisms involved in the oxidation.

The stoichiometry of the reaction between oxygen and ferrous sulfide depends upon the sulfur products. The general reaction can be written



when sulfide is only oxidized as far as elemental sulfur $m = 0.75$, and when the oxidation proceeds all the way to sulfate $m = 2.25$. However for any given set of solution conditions, the stoichiometry remains constant and the rate of oxygen consumption is directly proportional to the rate of oxidation of ferrous sulfide. This can be expressed as

$$\frac{d[\text{FeS}]}{dt} = \frac{1}{m} \frac{d[\text{O}_2]}{dt}$$

Monitoring the dissolved oxygen concentration remaining as a function of time provides useful data for evaluating the effect of oxygen concentration upon the rate of reaction. The experimental apparatus, design, and procedure are described in Section III. In summary, the reactor is prepared by establishing a predetermined concentration of dissolved oxygen in a fixed volume of water. All gas phases are eliminated from the reaction vessel and the vessel sealed to prevent the introduction of atmospheric oxygen. A sufficiently large amount of ferrous sulfide is introduced into the reaction vessel such that insignificant changes in surface area occur during the experiment. The dissolved oxygen concentration is monitored as a function of time, all other parameters being constant.

The rate of oxygen consumption, when all other parameters including surface area are held constant, is given by

$$\frac{d[\text{O}_2]}{dt} = -k_c [\text{O}_2]^n$$

where k_c is a composite constant for the specific conditions of temperature, pH, surface area, etc. When the rate of oxidation has a first order dependence upon oxygen concentration, $n = 1$. The rate expression can be integrated to yield a linear relationship between the logarithm of the remaining oxygen concentration and time,

$$\log[\text{O}_2]_o - \log[\text{O}_2]_c = \log[\text{O}_2]_r = -\frac{k_c}{2.303} t$$

where

$[O_2]_0$ = initial oxygen concentration,

$[O_2]_c$ = concentration of O_2 consumed at t ,

$[O_2]_r$ = concentration of O_2 remaining at t .

Experimental results obtained at pH 7 and 9.4 are reduced according to the relationship above and are presented graphically in Figures 8 and 9. The linear relationship between the log of the concentration remaining and time demonstrates that the rate of oxygen consumption, and therefore the rate of ferrous sulfide oxidation, do have a first-order dependence upon the dissolved oxygen concentration over the range investigated. The range of oxygen concentrations which could be investigated with this approach was limited to relatively low concentrations due to the solubility of oxygen and response time of the dissolved oxygen probe. There is also a lower limit to the levels of oxygen which can be evaluated reliably. Below concentrations of 0.3 mg/l, experimental difficulties including slight reaeration by diffusion of atmospheric oxygen through leaks in the physical apparatus, shifts in the baseline of the recorder, and non-linearity in the oxygen probe make quantitative measurements of the rate of change of oxygen concentration by reaction with ferrous sulfide impossible.

As mentioned, the rate at which oxygen is consumed provides an indirect means of determining the rate of oxidation of ferrous sulfide. The stoichiometry of the reaction between FeS and O_2 depends upon such solution parameters as pH, temperature, and the ionic composition as is discussed below. For example, at neutral pH sulfide is oxidized to elemental sulfur, while in alkaline solutions the oxidation proceeds as far as the polythionates which requires more oxygen per mole of ferrous sulfide oxidized. In order to relate the rate of oxidation of FeS to the rate of O_2 consumption, the exact stoichiometry of the overall reaction products must be known. Thus, to eliminate any ambiguity, it is more expedient to measure the FeS remaining as a function of time as well as the specific reaction products. Most of the oxidation kinetic studies were monitored for both unreacted FeS and specific reaction products.

In a majority of experiments the parameters monitored over time included FeS remaining, iodine reactive species, pH, and specific sulfur oxidation products. During the oxidation experiments, the concentration of dissolved oxygen was held constant and monitored with a dissolved oxygen meter and probe. The concentration of ferrous sulfide remaining was measured as a

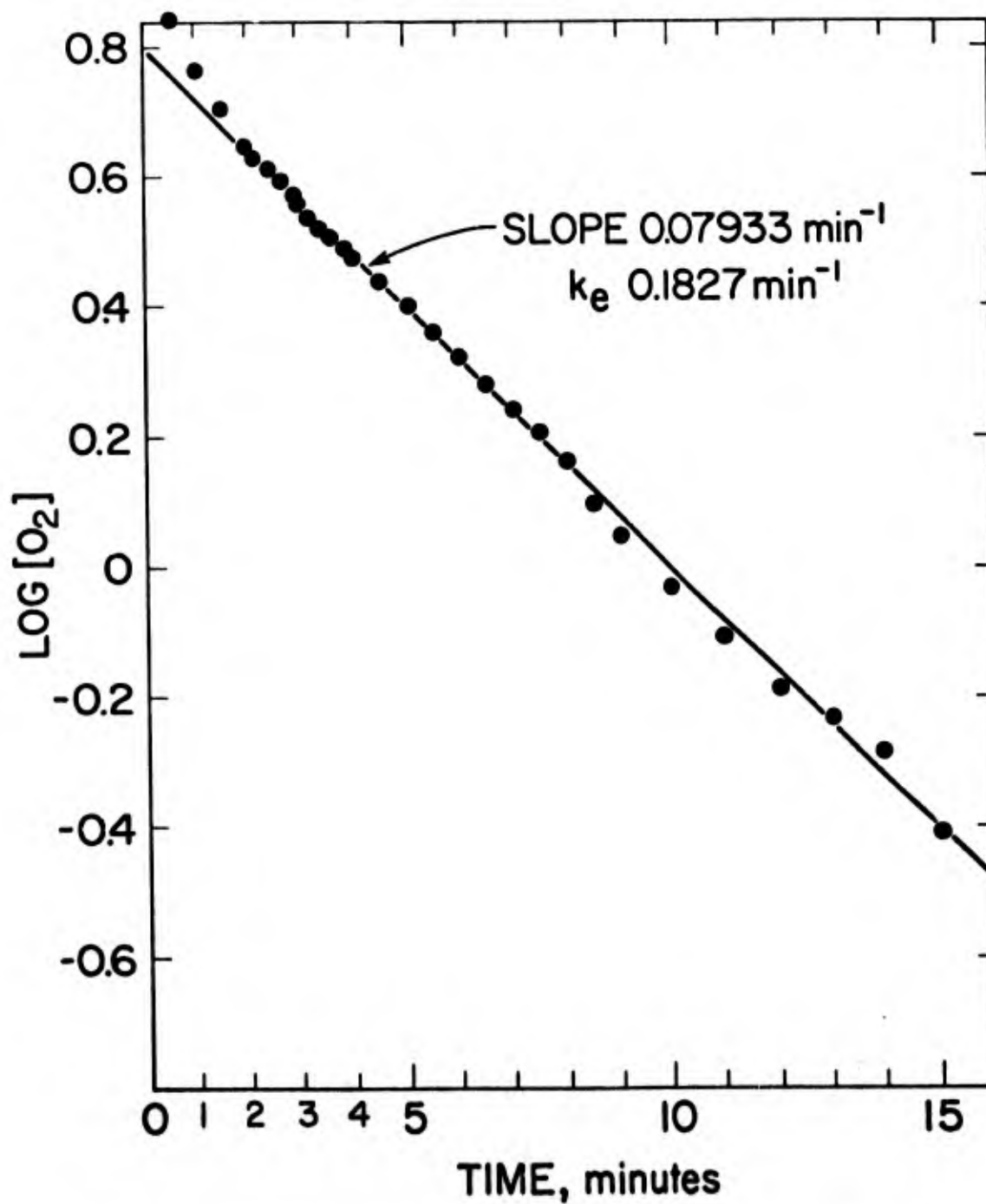


Figure 8. Logarithm of dissolved oxygen concentration as a function of time for reaction at pH 7.

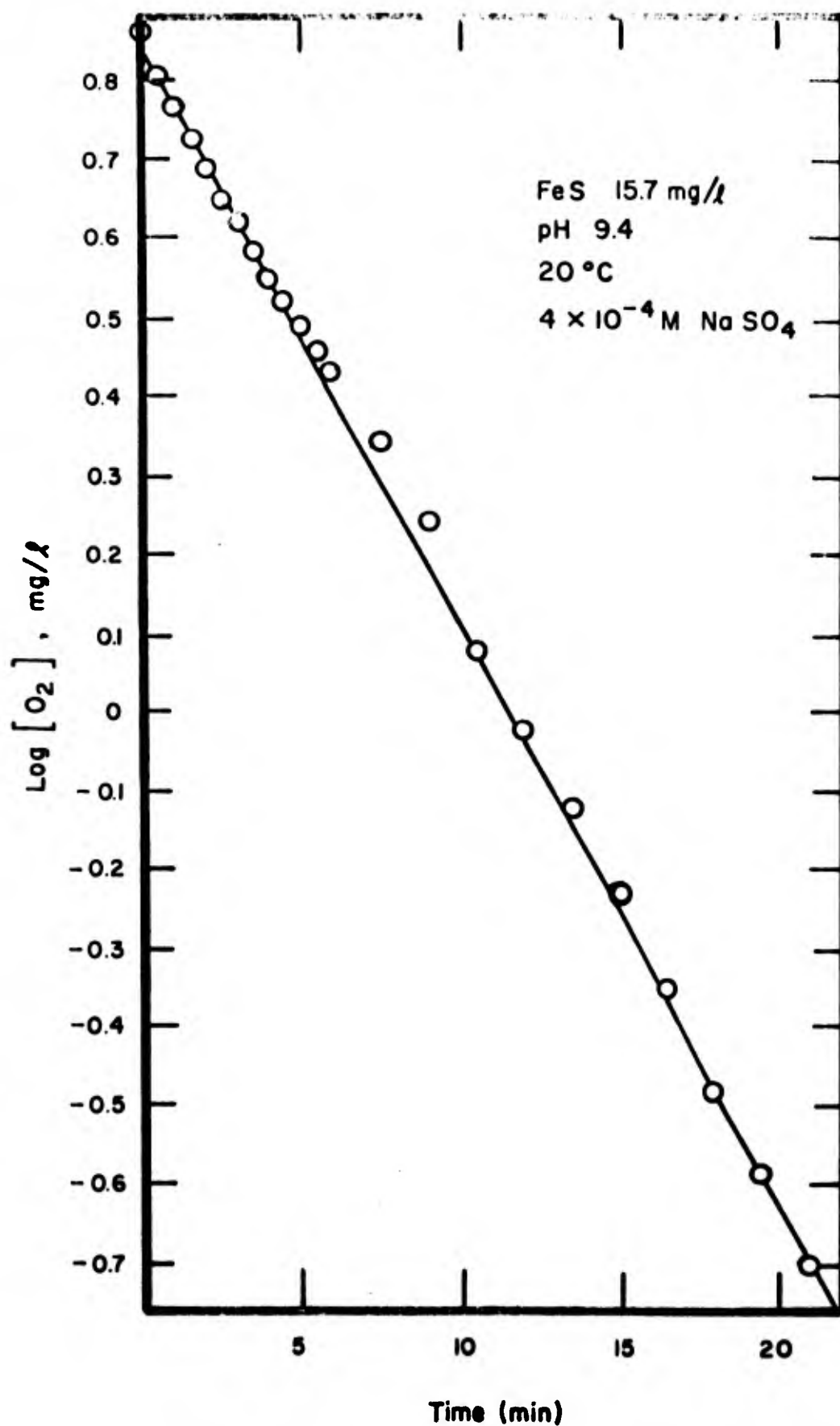


Figure 9. Logarithm of dissolved oxygen concentration as a function of time for reaction at pH 9.4.

function of time throughout the experiment. This experimental approach allows the rate of oxidation to be determined at significantly greater oxygen concentrations. The range of oxygen concentrations which can be used is limited by a number of factors. The design of the reactor limits the maximum partial pressure of oxygen to one atmosphere. The rate of oxidation increases very rapidly with temperature. Inability to operate the system under steady-state conditions and take samples rapidly limits the investigation of the rate of oxidation at higher temperatures to lower oxygen concentrations. At lower oxygen concentrations, the rate of oxidation exhibits essentially first-order dependence upon the concentration of dissolved oxygen. This is manifested in a linear relationship between the rate of oxidation and dissolved oxygen concentration. At 15°C and below, the rate of oxidation is slow enough that partial pressures of one atmosphere oxygen could be used to adjust the oxygen concentration in solution. The actual concentration of oxygen in solution in the reactor was monitored with a specially modified dissolved oxygen probe which expanded the range of concentrations which could be measured by approximately 250%. The rate of oxidation was determined over a range of dissolved oxygen concentrations at 10°C and 15°C. The results are shown in Figures 10 and 11. In both cases there is a noticeable deviation from linearity with increasing oxygen concentration. This indicates that the rate of oxidation is a complex function of oxygen concentration which merely reduces to a pseudo first-order dependence at low oxygen concentrations. The significance of the observed deviation is discussed in terms of reaction mechanisms below.

Temperature Effects

The oxidation of FeS is very complex, undoubtedly involving a number of reactions occurring both in parallel and in series. The dependency of reaction rate on temperature can provide insight into the nature of parallel or sequential reactions. By reducing data on a semi-logarithmic plot of log-rate constant against the inverse of absolute temperature, a linear relationship yields information on the energy of activation (slope) and the frequency factor A (intercept).

When a complex reaction proceeds along a pathway comprised of a series of reactions, the overall rate is determined by the slowest step in the sequence. If this step also has the lowest activation energy of all steps

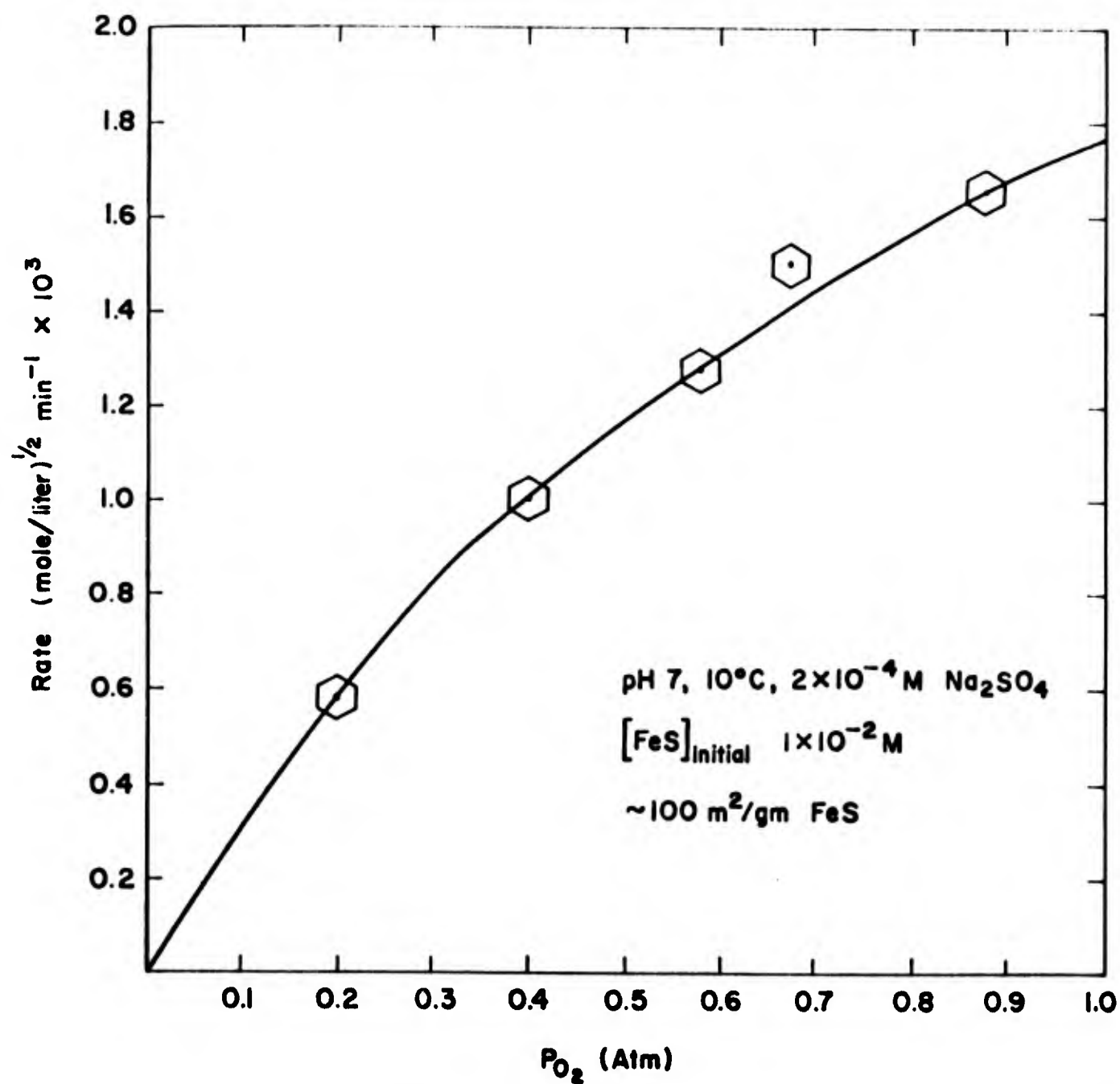


Figure 10. Oxidation rate as a function of the partial pressure of oxygen at pH 7 and 10°C.

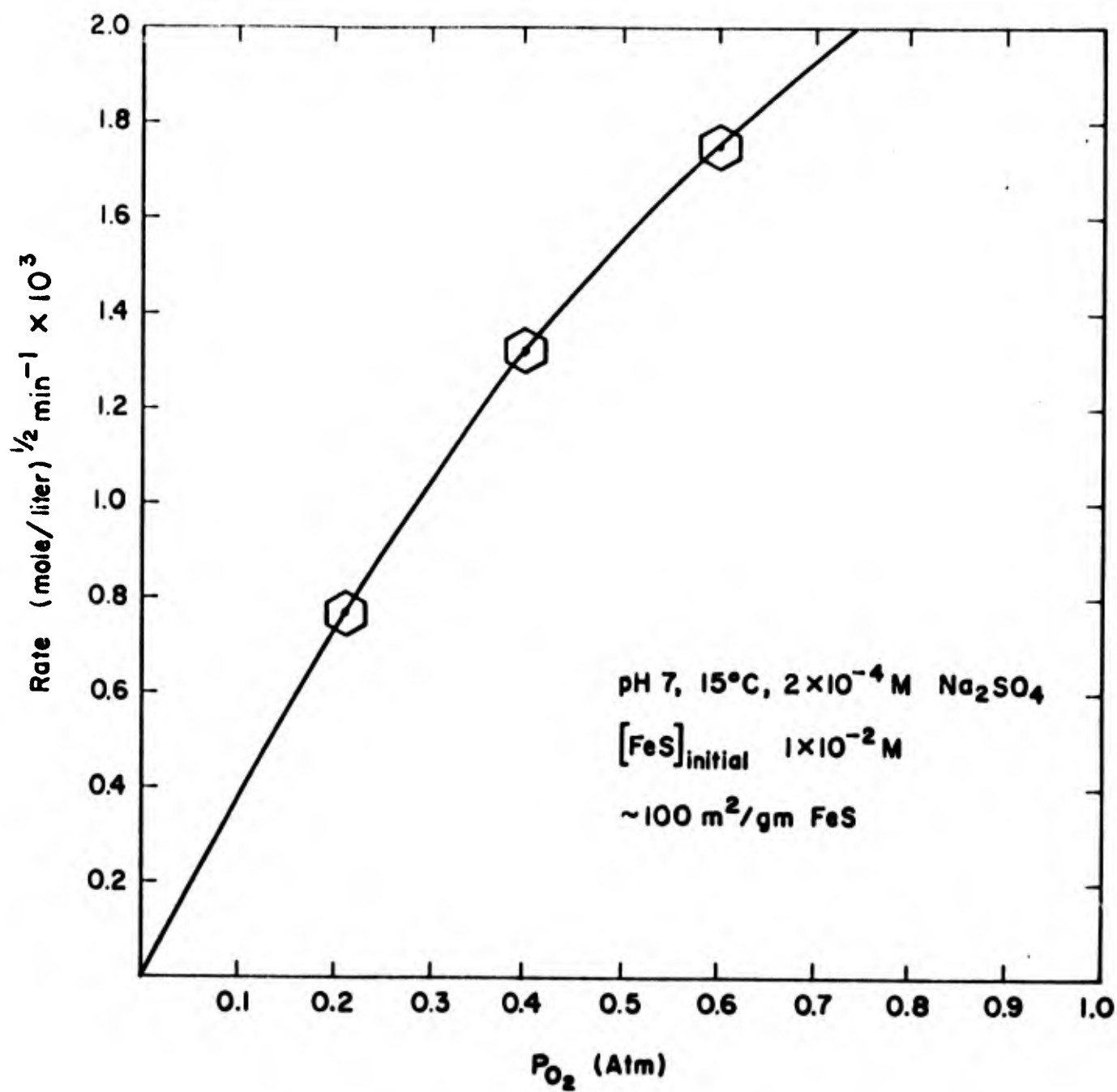


Figure 11. Oxidation rate as a function of the partial pressure of oxygen at pH 7 and 15°C.

in the series of reactions, it will always be the slowest and therefore the rate-controlling step in the overall reaction. If the rate-controlling step changes more rapidly with temperature than a second step in the sequence, then as temperature increases, at some temperature the second step will become the rate-controlling step in the overall sequence (Figure 12).

When the overall reaction proceeds by several pathways, the rate of consumption of reactants is the sum of the rate of all individual reaction pathways. Figure 12 shows the effect of different activation energies for the rate-controlling steps of the two alternate pathways. Notice that the direction of changing slope of $\log k$ vs $1/T$ differs for parallel and sequential reactions.

The rate of oxidation of ferrous sulfide is quite sensitive to changes in temperature; the rate approximately doubles for every 10°C increase in temperature. The activation energy for the oxidation of fresh FeS aged 8 days at pH 7 was determined on two different batches of ferrous sulfide. The data from both experiments were comparable, and Figure 13 presents a semilog Arrhenius plot of the data. The change in slope is obvious giving an activation energy of 10.45 Kcal for the reaction in the low-temperature range and 15.2 Kcal in the high-temperature range ($5-20^{\circ}\text{C}$). The increased slope (increased activation energy) at higher temperatures ($20-35^{\circ}\text{C}$) is consistent with two parallel reactions (Figure 12).

The activation energy for the oxidation reaction at pH 9 was determined over the temperature range $5-44.2^{\circ}\text{C}$ (Figure 14) and is 13.73 Kcal. The ferrous sulfide used had been aged two months. A second series of experiments were conducted at pH 9 on a fresh ferrous sulfide suspension (aged 8 days). It was expected that the activation energy would reflect the higher surface area (smaller particles) in the younger solid. The activation energy is 15.5 Kcal over the temperature range $5-35^{\circ}\text{C}$. The activation energy of 15.5 Kcal at pH 9 for the fresh FeS compares well with the activation energy for the same fresh FeS at pH 7 in the high-temperature range.

Interpretation of the results is somewhat ambiguous. At pH 7 the rate-controlling mechanism appears to change at about 20°C . The activation energy for the oxidation reaction at pH 9 is very close to the activation energy at pH 7 in the higher temperature range ($20-35^{\circ}\text{C}$). There is insufficient information to tell whether the rate-controlling step is the same in both cases.

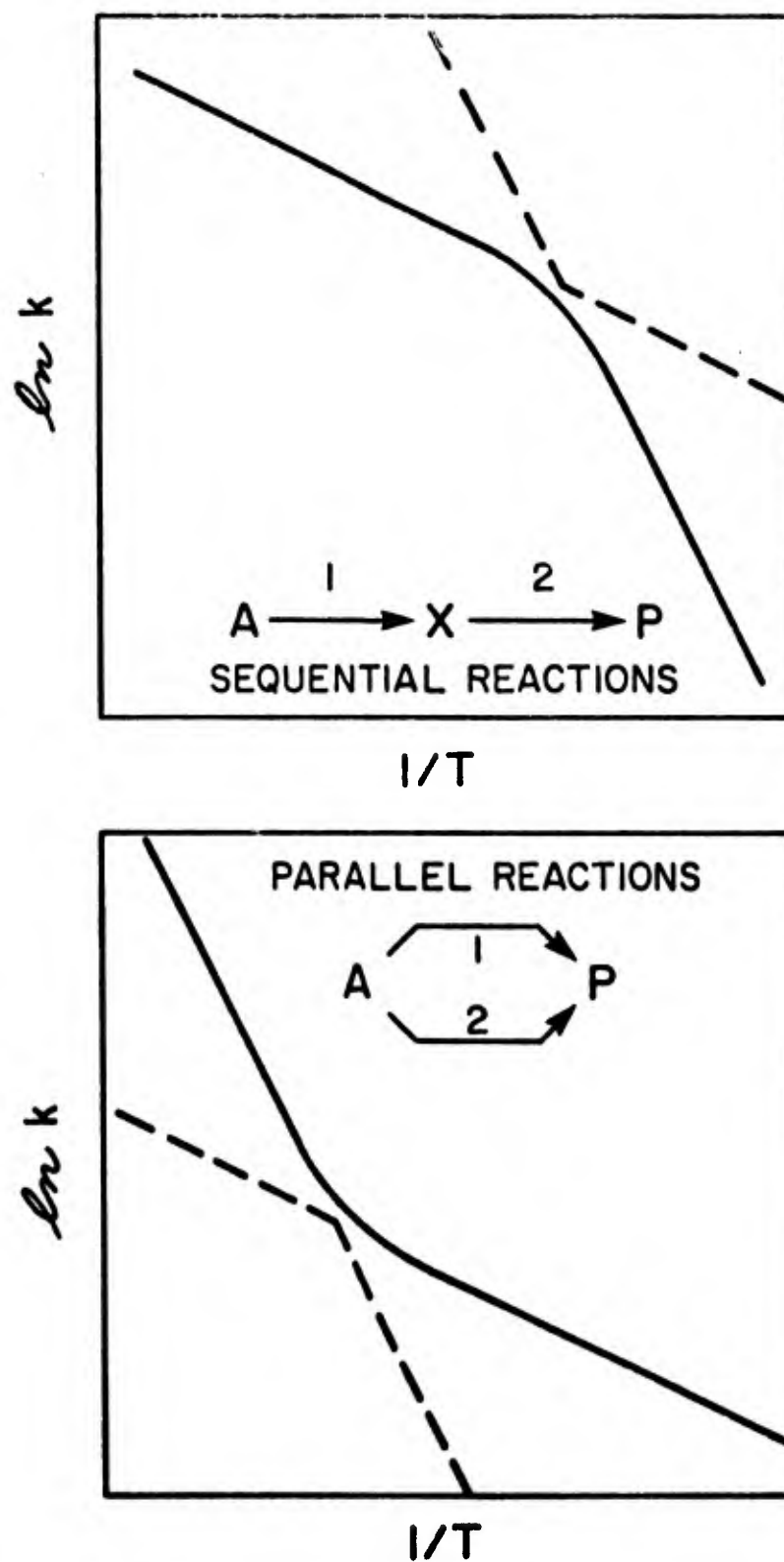


Figure 12. Arrhenius plots for sequential and parallel reactions.

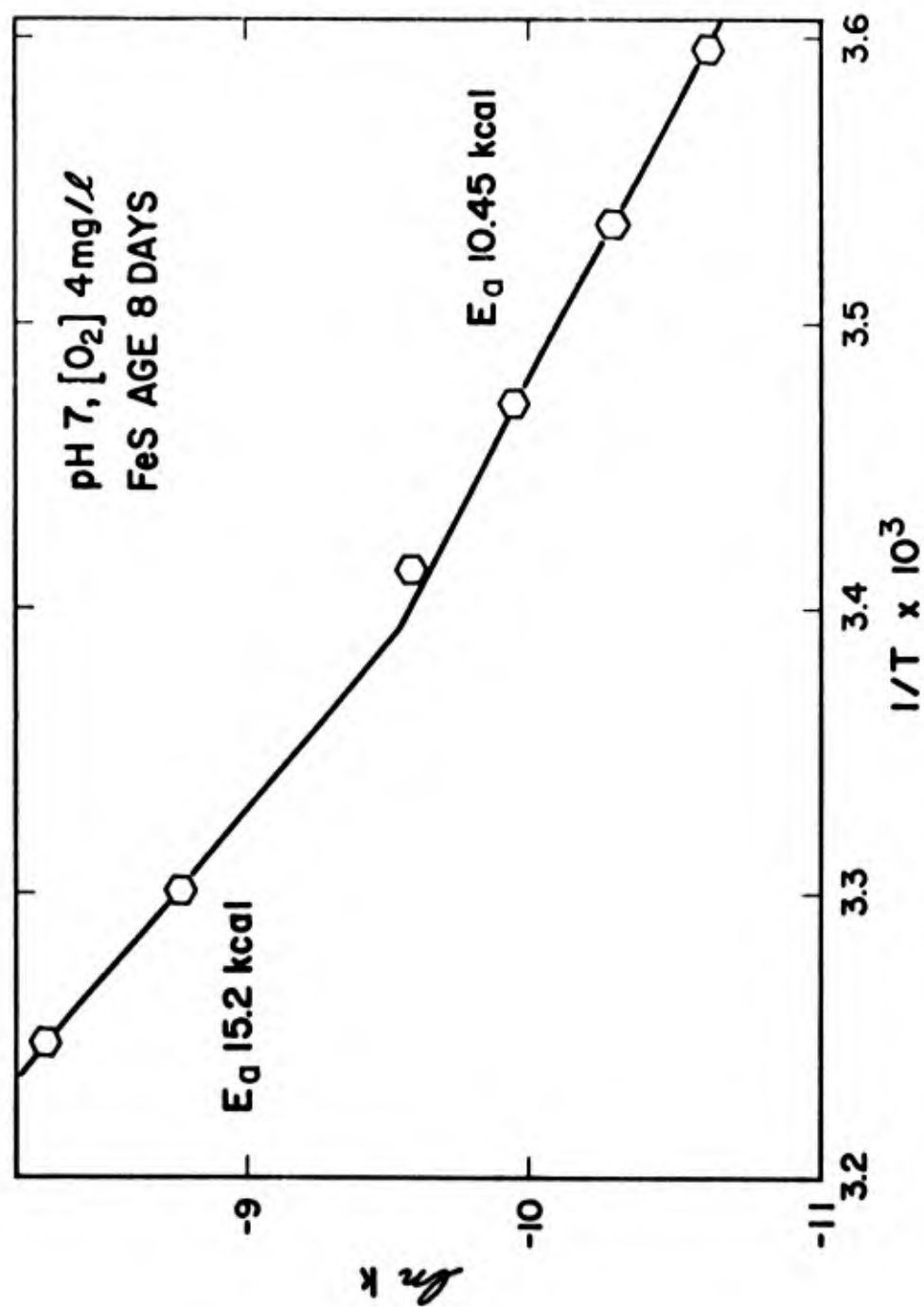


Figure 13. Arrhenius plot of overall oxidation rate at pH 7 and 4 mg/l O₂.

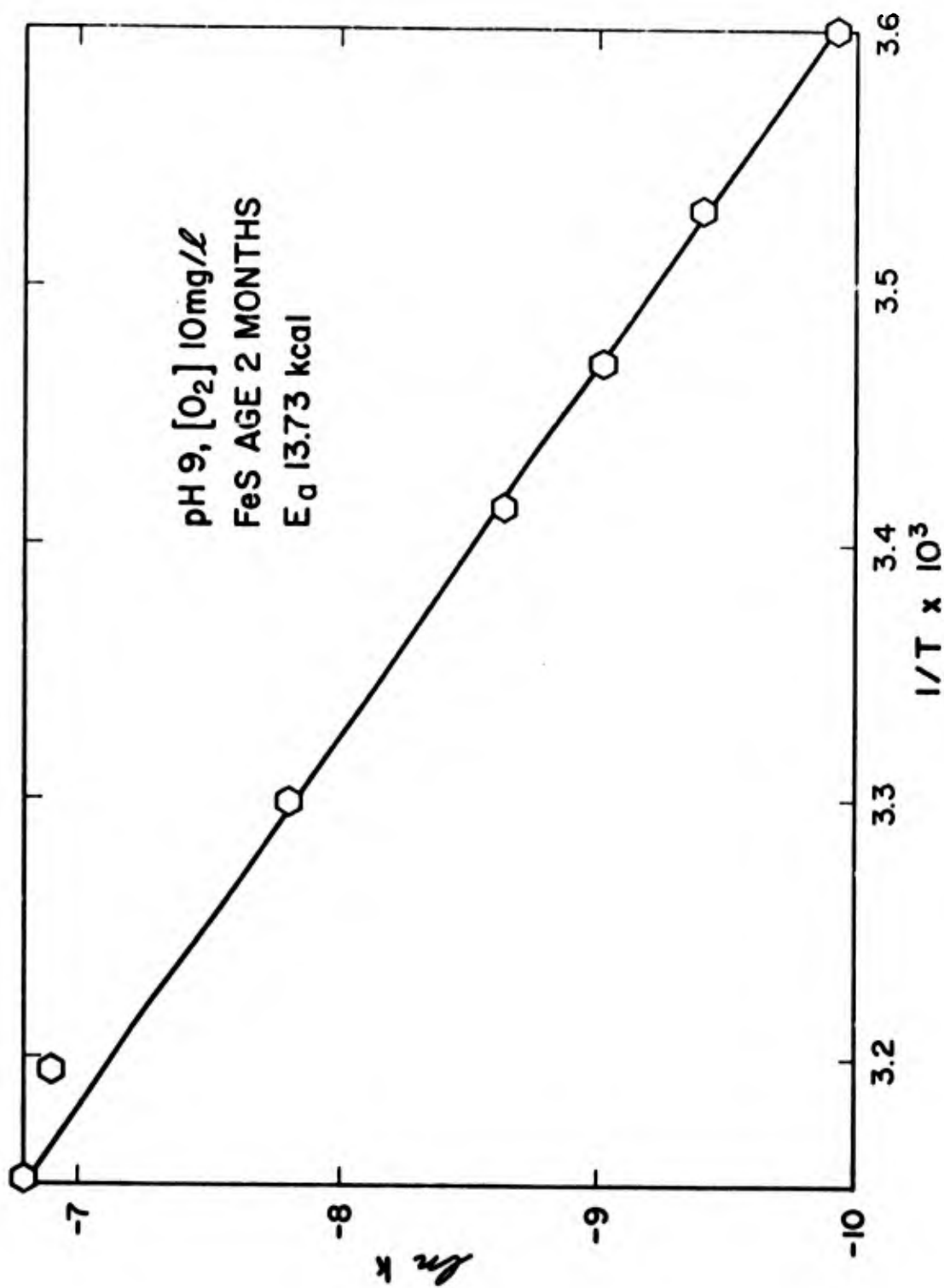


Figure 14. Arrhenius plot of overall oxidation rate at pH 9 and 10 mg/l O₂.

It can be concluded that at least two parallel reaction pathways are effective in the overall reaction at pH 7. The temperature range studied is not large enough for either mechanism to become totally dominant in the respective temperature range. An iterative computational technique could be used to refine the data if the need was evident.

Effect of Surface Area

The surface area is readily identified as an important parameter in describing the heterogeneous reaction between ferrous sulfide and dissolved oxygen. Two experimental approaches were taken to evaluate the relationship between surface area and rate of reaction. The first approach involves determining the rate of ferrous sulfide oxidation as a function of oxygen concentration over a range of ferrous sulfide concentrations and total surface areas. The experimental apparatus, design, and procedure are described earlier. The rate and extent of oxidation are determined by monitoring the concentration of dissolved oxygen remaining as a function of time. The stoichiometry of the oxygen-ferrous sulfide reaction is constant for a given set of experimental conditions; therefore, the rate of ferrous sulfide oxidation is directly proportional to the rate of oxygen consumption. The ferrous sulfide is added to the reaction vessel as a suspension, and the total surface area present to react is directly proportional to the concentration of ferrous sulfide added. The concentrations of ferrous sulfide used are sufficiently large that the change in surface area over the course of the reaction is negligible. The rate of oxidation of ferrous sulfide has been shown to fit the empirical relationship:

$$\frac{d[\text{FeS}]}{dt} = -k_c [\text{O}_2]$$

The surface area was held essentially constant throughout the experiment and is incorporated into the rate constant. The rate constant can be rewritten, separating the surface area out of the rate constant and assuming first-order dependence of the rate upon surface area:

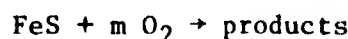
$$k_c = k'_c(S)$$

where S = surface area. Rewriting the rate expression yields:

$$\frac{d[\text{FeS}]}{dt} = -k'_c(S)[\text{O}_2]$$

This expression predicts that doubling the surface area will double the rate of oxidation.

The concentration of ferrous sulfide oxidized is related to the oxygen concentration which is reduced by the stoichiometry of the reaction



The value of m can vary from 0.75 when the oxidation product of sulfide is elemental sulfur to 2.25 when the sulfide is oxidized as far as sulfate. For any given set of experimental conditions where the pH, temperature, and other parameters are held constant, the value of m will remain constant. Therefore, the rate of change of the ferrous sulfide concentration is related to the rate of change of the oxygen concentration by

$$\frac{d[\text{FeS}]}{dt} = \frac{1}{m} \frac{d[\text{O}_2]}{dt}$$

This relationship can be substituted into the differential rate equation and integrated over the interval of the initial oxygen concentration to the concentration remaining at some time t . This yields a linear relationship between the logarithm of the oxygen concentration and time:

$$\log[\text{O}_2]_0 - \log[\text{O}_2] = \frac{mk'_c}{2.303}(S) t$$

The concentration of oxygen remaining was measured as a function of time at two different initial surface areas. The total surface area of ferrous sulfide in each experiment was varied such that the ratio of surface area present in each succeeding experiment increased in the ratio 1:2. Thus, the surface area of subsequent experiments can be expressed as a multiple of the first experiment; for example, $S_2 = 2S_1$. The relationship between the logarithm of the oxygen concentration remaining and time predicts that the value of $(mk'_c/2.303)S$ will be directly proportional to the total surface area present. The ratio of the values of $(mk'_c/2.303)S$ obtained experimentally are 1:2.02. These compare very well with the ratio of the total surface area present. This establishes that the rate of oxidation has first-order dependence with respect to the surface area present during the reaction.

The effect of surface area on the rate of reaction was also determined in experiments where the surface area was not held constant. The rate of

oxidation was determined as a function of the initial surface area present by monitoring the concentration of ferrous sulfide remaining as a function of time at both pH 7 and 9. In these experiments, the concentration of ferrous sulfide and the total surface area remaining change over the course of the experiment.

Well-aged (> one month) ferrous sulfide suspensions were prepared to ensure that the physical-chemical characteristics of the solid were uniform over the series of experiments. Aliquots of known amounts of FeS were oxidized under identical conditions of pH and dissolved oxygen. FeS remaining as a function of time at pH 7 and 9 is plotted in Figures 15 and 16. It is apparent that the time required for complete oxidation is essentially independent of the concentration of FeS. If there is negligible interaction between particles, then oxidation of individual particles will proceed independently and the overall rate will be dependent only upon available surface area and solution conditions. Although the initial concentration of FeS varied in these experiments, the particle-size distribution and, hence, specific surface area was the same. Thus, reaction dependence upon available surface area is confirmed by the linear acceleration of the overall reaction as a function of surface area and the fact the time to completion is independent of initial FeS concentration.

The relationship between the rate of oxidation and concentration of ferrous sulfide remaining at any point in the reaction provides some insight into how the reactive surface area changes as a function of the volume of the ferrous sulfide particle remaining. Further discussion of this is deferred until the discussion of kinetic models.

The surface area per unit mass of ferrous sulfide initially present in the ferrous sulfide suspensions was determined for two representative batches of ferrous sulfide using the BET method. Sample preparation consisted of centrifuging samples of ferrous sulfide suspension, decanting the solution containing the sodium sulfate medium, resuspending in deionized water and recentrifuging. This concentrates the ferrous sulfide and removes a majority of the soluble sodium sulfate salts. It also removes some of the ferrous sulfide fines. The excess liquid is decanted off under a nitrogen atmosphere, and the remaining material is freeze-dried. The freeze-dried material is transferred to a BET flask under a nitrogen atmosphere and degassed. The degassing is performed at 110°C to prevent the crystal structure of tetragonal ferrous sulfide from shifting to a more stable structure.

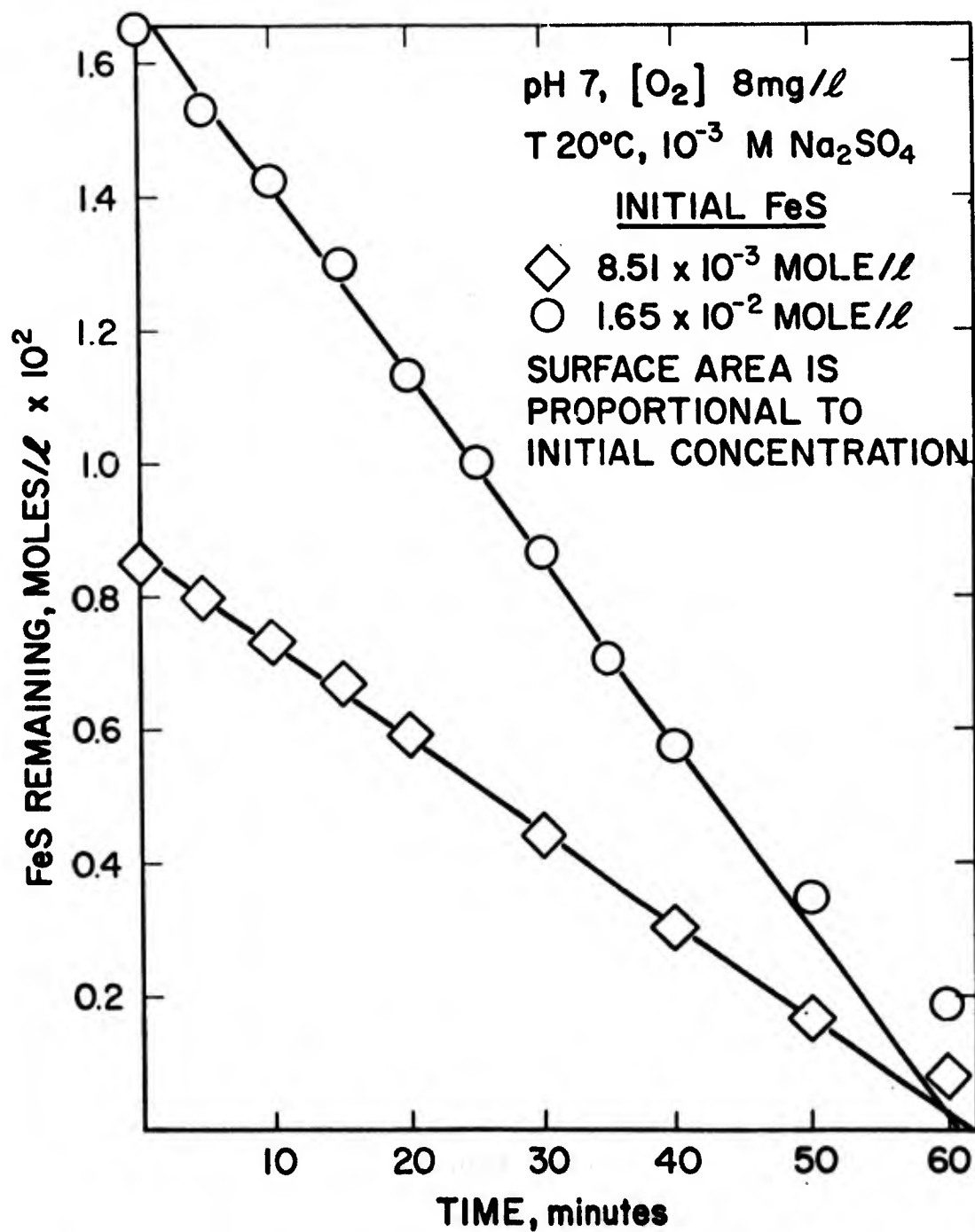


Figure 15. Concentration of FeS(s) remaining as a function of time during oxidative dissolution at pH 7.

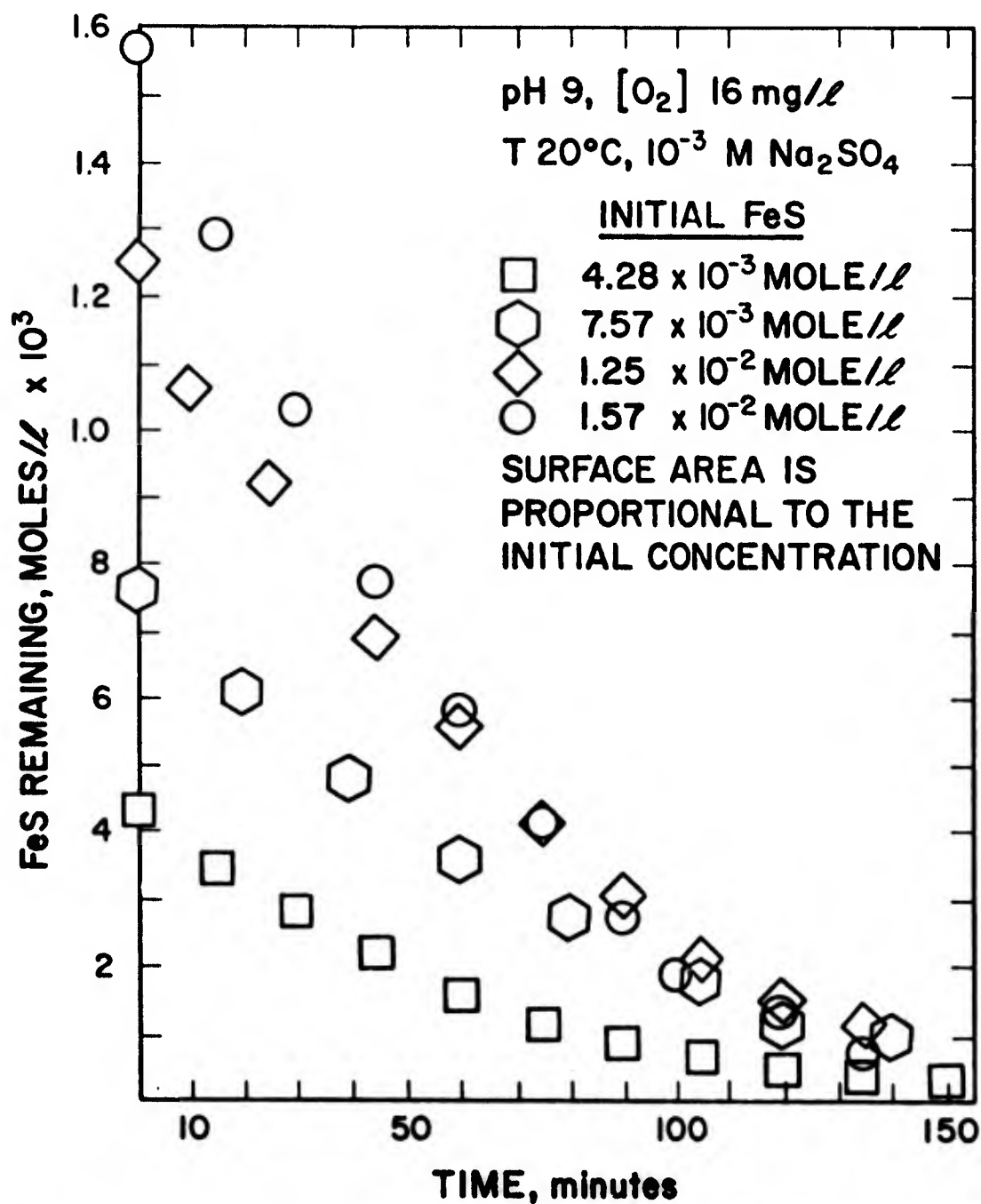


Figure 16. Concentration of FeS(s) remaining as a function of time during oxidative dissolution at pH 9.

Ferrous sulfide suspensions which had been prepared by precipitation from solution and aged 10 days had a surface area of $115 \text{ m}^2/\text{gm}$. A second batch, prepared by an identical procedure and aged 72 days, had a measured surface area of $59.6 \text{ m}^2/\text{gm}$. This gives a relative sense of the aging process and crystal growth occurring in the suspensions. Both values may be low due to the method of sample preparation and probable loss of the finest particles. The values provide an indication of the extremely small particle size present in the suspension.

Effect of Ionic Strength and Chloride

The electrolyte composition and concentration both affect the rate of oxidation of FeS and influence the nature of the reaction products. Increasing ionic strength reduces the equilibrium concentration of dissolved oxygen which can be achieved for a given partial pressure of oxygen (salting-out effect). Thus, the rate of oxidation of FeS at constant partial pressure of O_2 and increasing ionic strength should reflect the decrease in actual concentration of dissolved oxygen in the reaction system. The effect of increasing ionic strength in a reaction system with constant concentration of dissolved oxygen is minor. Figure 17 shows experimental data for reaction at pH 7 and 8 mg/l O_2 for ionic strengths of 3×10^{-3} , 0.1 and 0.5M. There is less than a 20 percent decrease in rate for greater than 100-fold increase in ionic strength.

The effect of chloride-ion concentration was investigated because chloride is ubiquitous in natural waters and is a major anion in estuarine and marine systems. Results of experiments conducted at pH 7, 8 mg O_2 , and 0.0, 0.1, and 0.5M sodium chloride are shown in Figure 18. The data show that there is a real inhibitory effect of chloride on the rate of oxidation of FeS.

The effect of ionic strength or chloride upon the rate of oxidation appears to be independent of the concentration of dissolved oxygen. That is, if the addition of sodium chloride or sodium sulfate decreases the rate of oxidation by 20% at 4 mg/l dissolved oxygen, it will also reduce the observed rate of oxidation by 20% at 16 mg/l dissolved oxygen. The inhibitory effect is greater than can be accounted for by ionic strength effects alone (Figure 17). Apparently, chloride interferes in the reaction mechanism at pH 7. Similar experiments at pH 9 indicate no influence of chloride on the

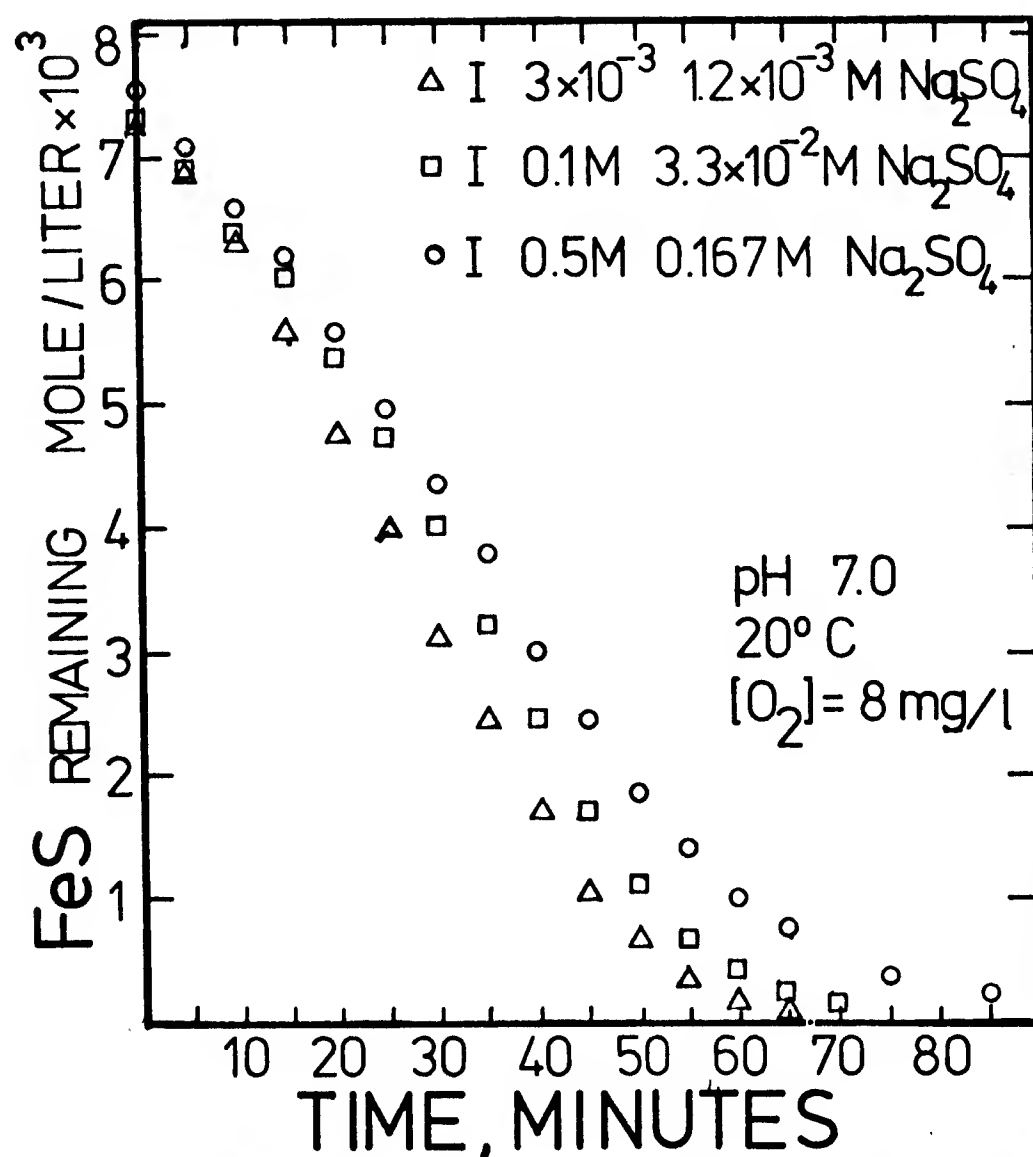


Figure 17. Influence of sulfate on oxidation rate at pH 7, 20°C, and 8 mg/l O_2 .

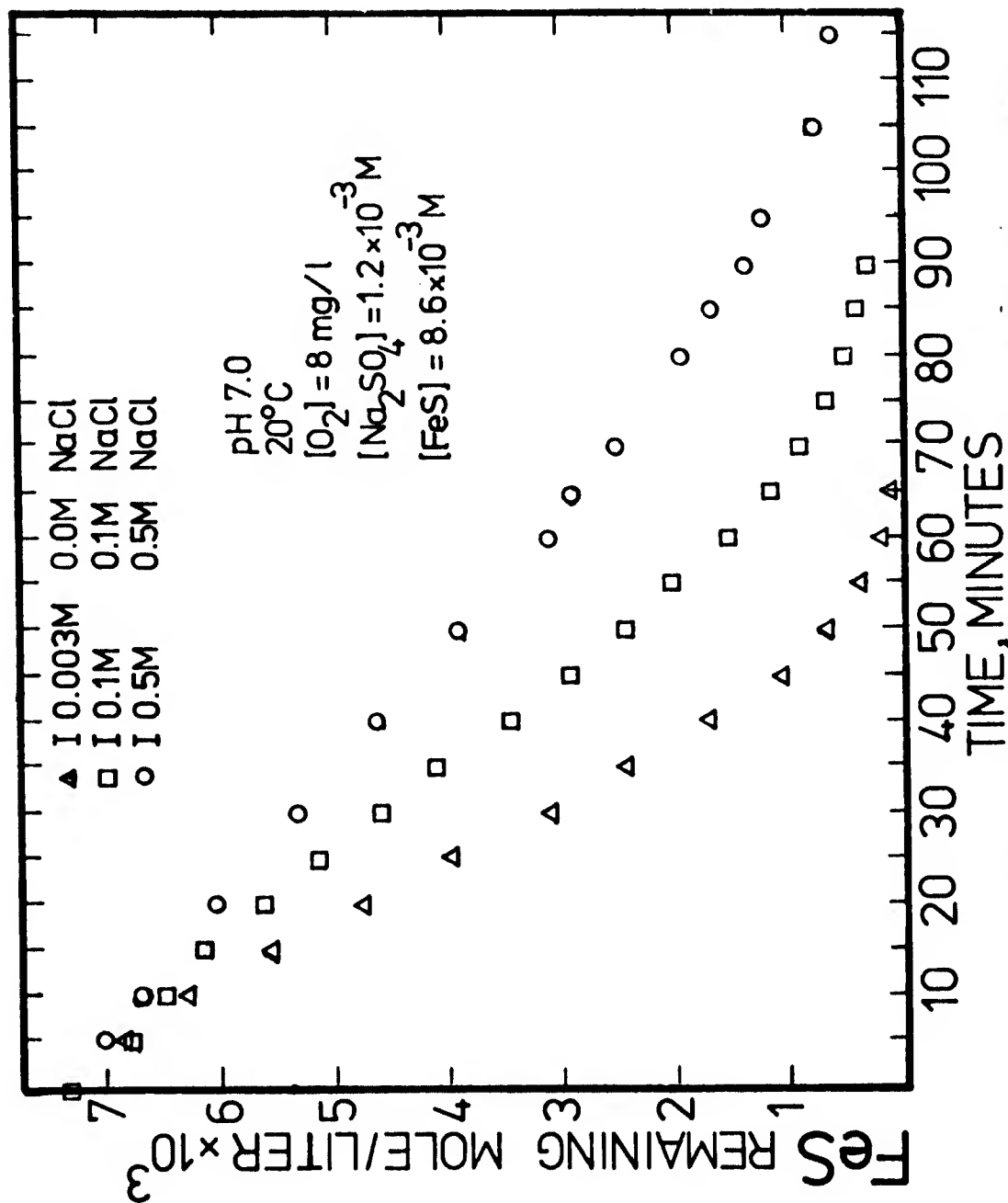


Figure 18. Influence of chloride on oxidation rate at pH 7, 20°C, and 8 mg/l O_2 .

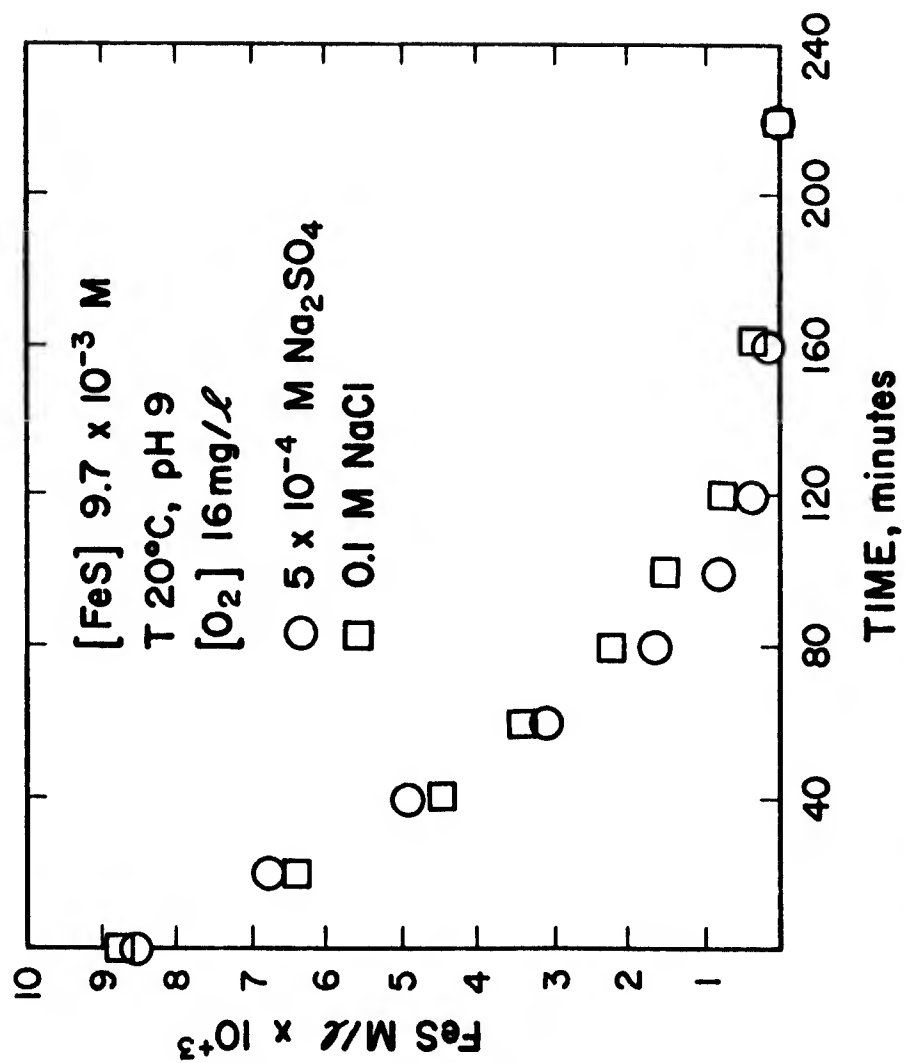


Figure 19. Oxidation of FeS(s) in presence and absence of chloride at pH 9.

rate of oxidation (Figure 19). The presence of 0.377M formaldehyde during the oxidation of ferrous sulfide at pH 9, 20°C, and 5×10^{-4} M Na_2SO_4 had no effect upon the rate of oxidation, either. Although neither chloride nor formaldehyde affect the rate of oxidation at pH 9, both substantially affect the nature of the sulfur reaction products. Implications of this observation in terms of sulfur reaction mechanisms are discussed later.

Effect of Catalytic Agents

The importance of catalytic agents in the oxidation of both ferrous iron and sulfide has been established by experimental work in homogeneous systems. In this investigation the studies on catalysis have been limited to the role that transition elements might play in accelerating the overall oxidation reaction. The experimental approach was to exchange the trace metal with the surface of aged FeS. A concentrated slurry of FeS was added to a dilute solution of trace metal to provide as uniform a distribution of trace metal as possible. Identical experiments in the absence of a catalyst were run for comparative purposes. Of the trace metals investigated for catalytic effects (Cu(II), Ni(II), Ag(I), Cd(II)), only Ni(II) showed any significant ability to accelerate the reaction.

Reactions were performed in the presence of 0, 1×10^{-5} , 3×10^{-5} , 1×10^{-4} , and 1×10^{-3} M Ni(II) where the FeS was 8.9×10^{-2} M. At the highest concentration of nickel the rate of oxidation is so rapid that the experimental design did not allow quantitative measurement. Results of experiments at the lower concentrations of nickel are given in Figure 20. A concentration of 1×10^{-5} M nickel has a small, reproducible catalytic effect on oxidation reaction, while 3×10^{-5} M Ni(II) has a substantial catalytic effect, increasing the rate by a factor of three. At 3×10^{-5} M Ni(II) the Ni(II)/Fe(II) ratio is 1:297, or nickel is 0.34 mole percent of the metal ions present. A slight increase in reaction rate occurs at 3×10^{-5} M Ni(II) when there is a slight excess of sulfide present. At 1×10^{-4} M Ni(II) the reaction rate is increased by about a factor of 10. Ni(II) is known to catalyze the oxidation of homogeneous sulfide solutions.

The catalytic effects of copper and silver were investigated in systems prepared similar to the nickel studies. Copper does not demonstrate any appreciable effect at a mole fraction of 0.34 percent (Figure 21). In this study an additional 10 ml of 1×10^{-2} M CuSO_4 solution was added, bringing the total copper concentration up to 1.41×10^{-4} M with a Cu(II)/Fe(II) ratio of 1:26.2. No effect was observed.

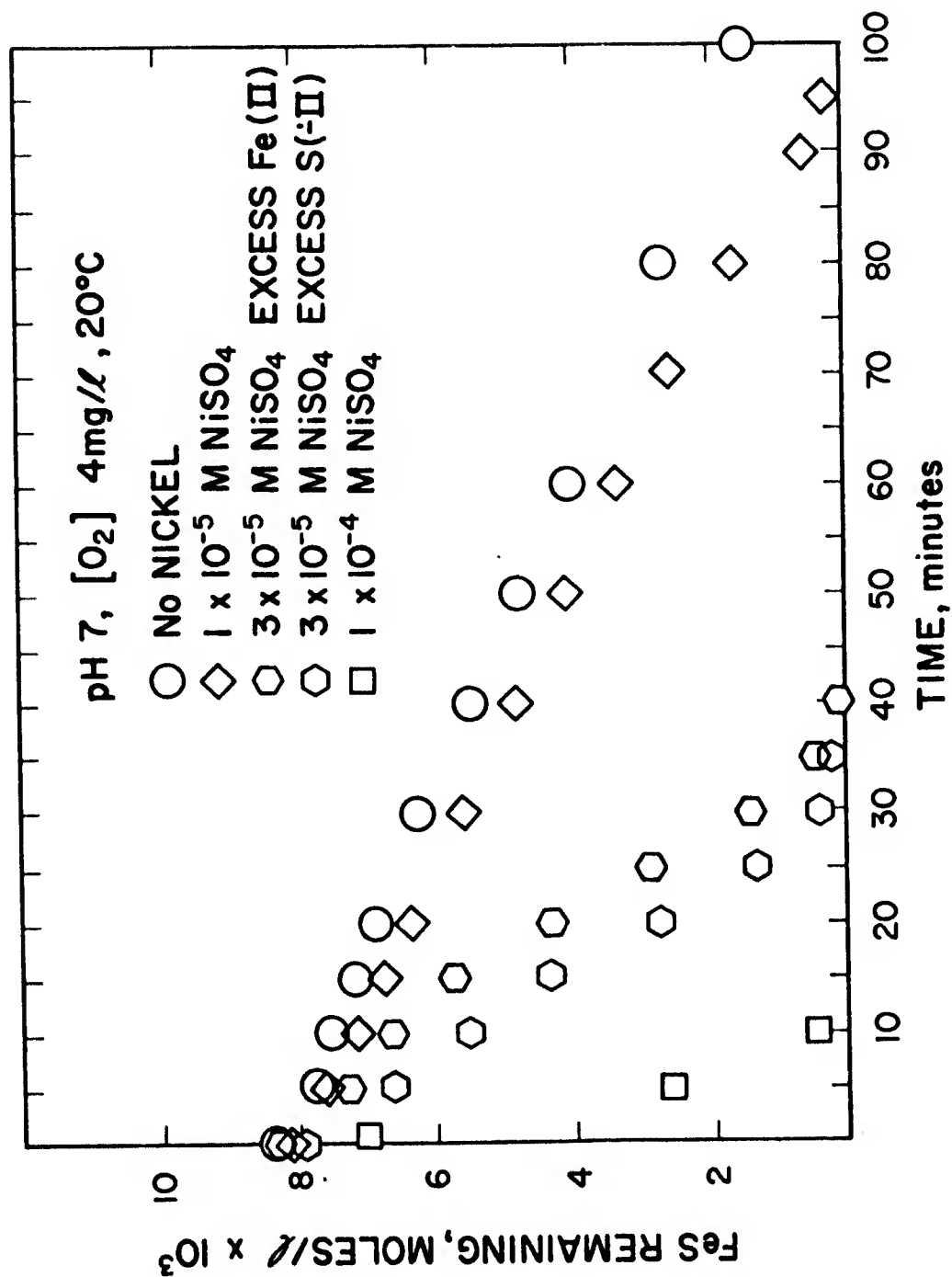


Figure 20. Catalytic effect of Ni on oxidation of FeS(s) at pH 7.

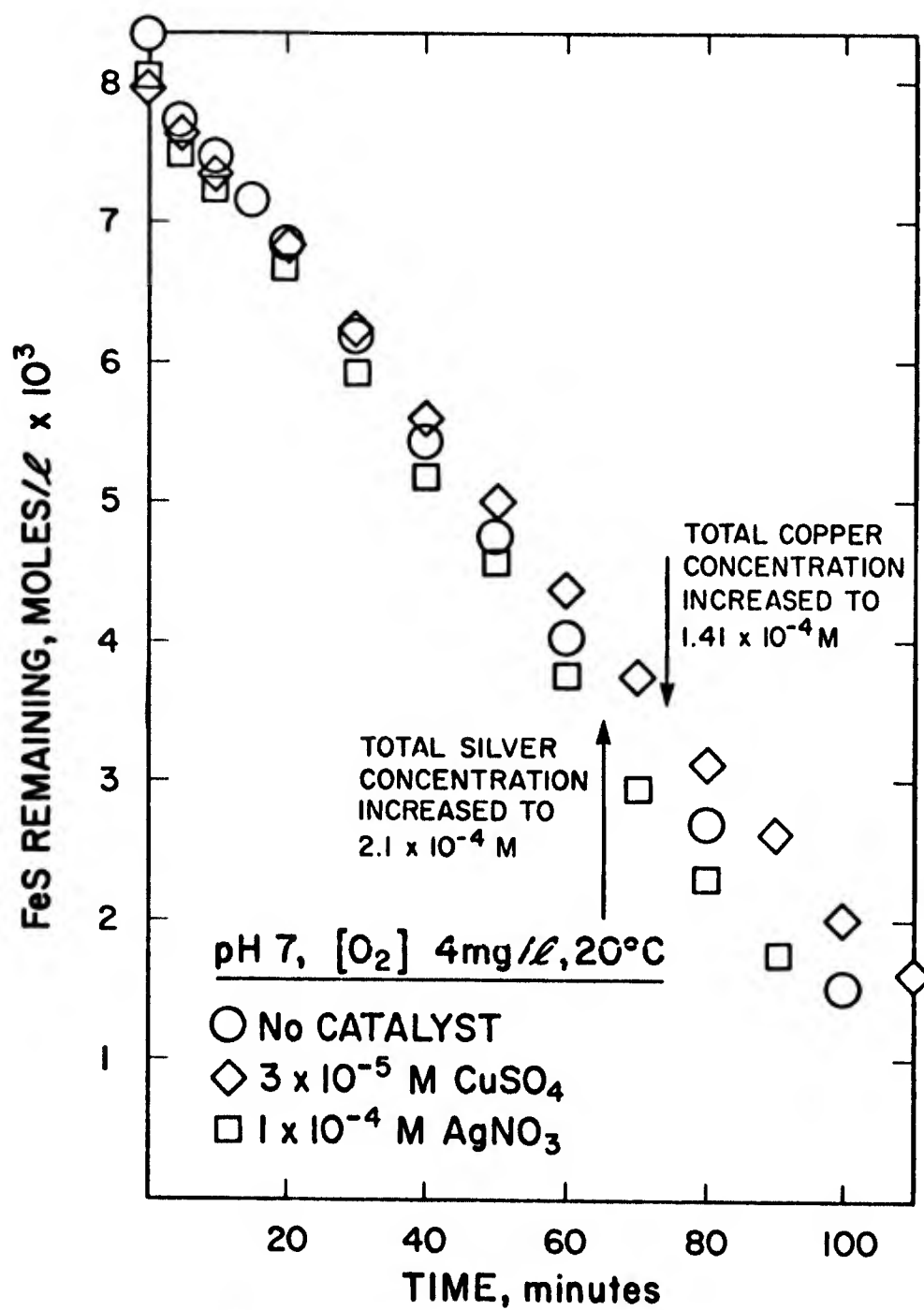


Figure 21. Oxidation of FeS(s) in the presence of Cu and Ag at pH 7.

Experiments with silver gave results very similar to those of copper. Ferrous sulfide containing 1.12 mole percent Ag(I) shows no catalytic activity during oxidation (Figure 21). An additional spike of silver (giving a Ag(I)/Fe(II) ratio of 1:17.5) at about 50 percent completion of reaction had no effect.

As expected, cadmium had no catalytic effect at Cd(II):Fe(II) ratios up to 1:17. Cadmium is not a transition metal and cannot participate in one-electron exchange oxidation-reduction reactions.

Of the trace metals studied, only nickel exhibited any appreciable catalytic capacity. The mechanism of the nickel catalysis is not understood. Galvanic effects, where the metal sulfide and ferrous sulfide form an electrolytic couple which increases the rate of oxidation of specie with the lower potential, while protecting the specie with the higher potential, are not consistent with the observed results. Any galvanic couple formed between ferrous sulfide and sulfides of the trace metals listed should enhance the rate of oxidation of FeS. Only Ni(II) shows this effect. On the other hand, there is not inhibition of the oxidation rate which might be observed if the adsorbed trace metals provided a protective coating to the FeS particles.

The presence of various organic molecules during the oxidation of homogeneous solutions of both ferrous iron and sulfide has been observed to inhibit oxidation (Chen, 1970). Phenol substantially reduces the rate of oxidation of sulfide, presumably by acting as a chain breaker in the propagation of free radical chains during the oxidation.

The effect of phenol on the heterogeneous oxidation of FeS has been studied (Figure 22). Phenol apparently has no appreciable effect on the oxidation rate at concentrations up to $1 \times 10^{-2}M$.

Effect of Mixing Rate

The rate of mass transfer to and from solid particles is controlled by the relative velocity of solid to liquid and the rate of renewal of the liquid layer which may depend on the intensity of turbulence around the solid particles. Experimental work (Nagata, 1975) confirms that the effect of mixing on the mass transport behavior of particles very much smaller than $1 \mu m$ is different than for particles greater than $1 \mu m$ size. Because sub- μm -size particles tend to move with the motion of eddies or are trapped in

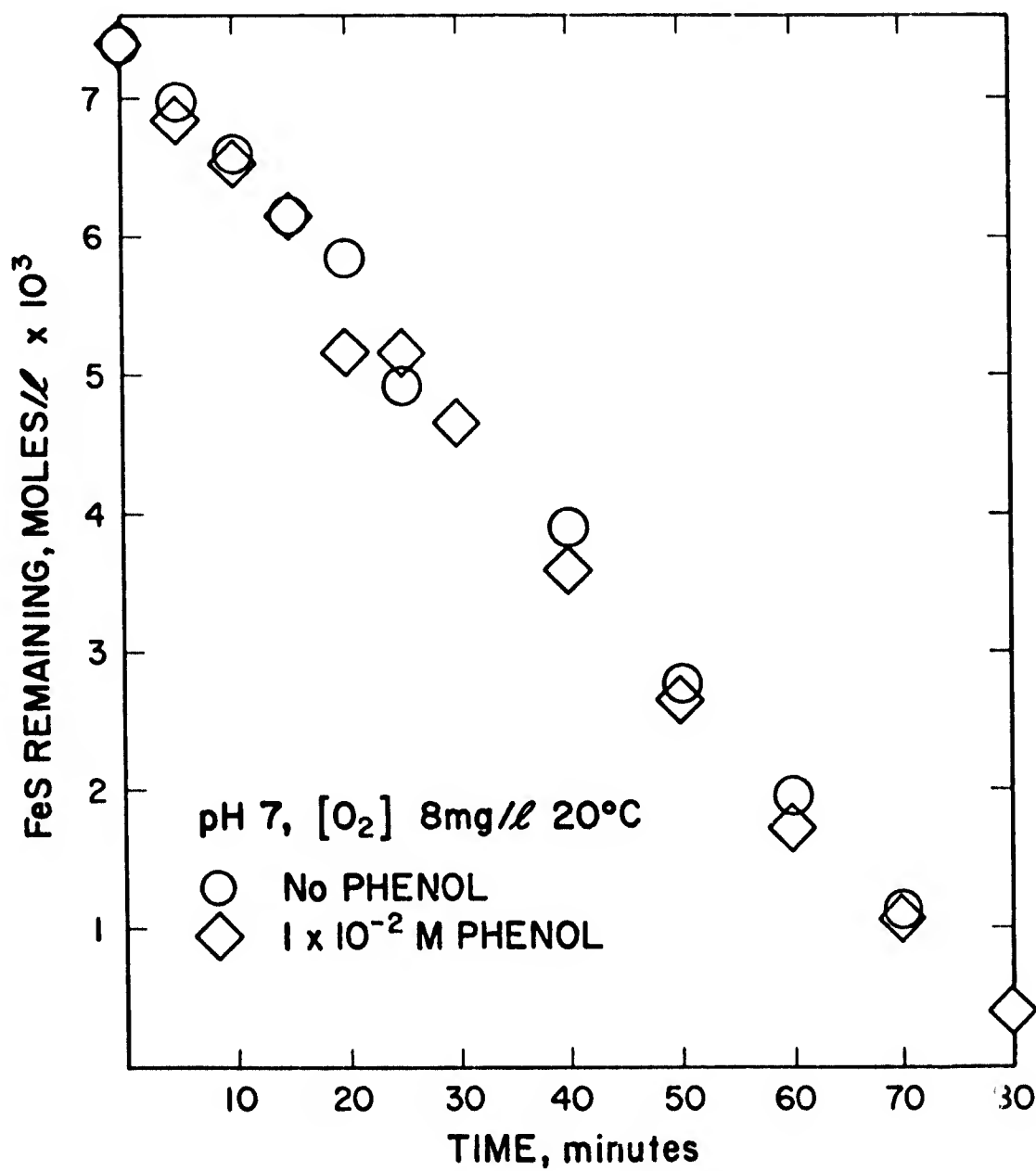


Figure 22. Oxidation of FeS(s) in the presence of phenol at pH 7.

the smallest eddies in which viscous effects prevail, the mass transfer coefficient appears to be independent of kinetic energy, that is, mixing intensity, since mass transfer is controlled by Brownian motion (Nagata, 1975).

Mixing intensity was varied in several otherwise similar experiments. The results indicated no effect of increased turbulence. Since the FeS-particle size ranges from 500 to 4000 Å, they should follow the flow streamlines and, thus, be independent of intensity of agitation. Because of the limitations imposed by the particle-size range of the FeS used in these experiments, it has been impossible to test possible mass transport limitations of the overall reaction rate directly.

Summary of Parametric Studies

The parametric study of the important parameters affecting the rate of oxidation of FeS indicates that the rate has a pseudo first-order dependence on the concentration of dissolved oxygen at lower oxygen concentrations and on the concentration of surface area (area/volume liquid). In addition, the results indicate that at least two possible mechanisms are involved in the oxidation reaction (temperature studies) and that one of these mechanisms is influenced by the presence of chloride ions. The overall reaction rate is catalyzed by Ni(II) and shows only a weak dependence upon the hydronium-ion concentration over the pH range 6.5 to 9 and no dependence at pH values above 9. Mixing intensities above that required to just suspend the FeS particles has no effect.

These results are discussed below in terms of a mechanistic model designed to account for the several effects observed experimentally. The products formed under various experimental conditions are presented next with some discussion as to the likely correlation between rate and products.

Iron Oxidation Products

Results. The rate of oxidation of tetragonal iron sulfide and the resultant products are a function of pH, dissolved oxygen concentration, surface area, and the composition of the reaction solution. There is no apparent correlation between the rate of oxidation and the iron-oxide phase formed.

The iron-oxyhydroxide phase produced is only dependent upon the pH of the solution. The iron-oxide phase present at the completion of the typical

oxidation experiments was determined by X-ray diffraction analysis. Diffraction patterns obtained from solids produced at pH 7 through 11 are shown in Figure 23. The sample prepared at pH 7 gives a very sharp clean pattern easily identified as lepidocrocite (γ -FeOOH). Elemental sulfur is the principle sulfur species produced when the oxidation is carried out at pH 7. The diffraction from elemental sulfur mixed with the iron oxide can be seen in the diffraction pattern at pH 7 at 2θ of 10.7. The intensity and definition of the peaks can be detected by this method of analysis. While presence of chloride partially inhibits the oxidation of sulfide past elemental sulfur, it does not appear to affect the iron-oxide phase produced. Lepidocrocite was identified as the iron-oxyhydroxide phase formed during reactions catalyzed by nickel.

Amorphous ferric hydroxide and freshly precipitated ferric-hydroxide gels dissolve readily at pH 8 and 80°C in a citrate-ascorbate solution (Nelson and Leckie, 1976). γ -FeOOH does not dissolve to any extent under these conditions. Dissolution of the solids prepared was attempted (on solids prepared at pH 7 and 11). The solid formed by oxidizing FeS at pH 11 dissolved completely in the reagents in 15 minutes. Very little of the solid prepared at pH 7 dissolved under the same conditions. This is indicative of the degree of crystallinity of the material and indicates that very little amorphous material is present in the products produced at pH 7.

Two crystal forms of γ -FeOOH have been reported in the literature. The most common shape observed are long, thin lathes. Lepidocrocite is also observed much less frequently to occur as serrated plates. Several iron-oxide samples obtained from different sources were investigated by transmission electron microscopy. A commercially prepared iron oxide was obtained from Pfizer Chemicals, New York. This was identified as lepidocrocite by X-ray diffraction. The method of preparation of the commercially prepared product is unknown. Electron micrographs (Figure 24) of the commercially prepared γ -FeOOH show the iron oxide as long thin rods or lathes on the order of 7000 Å by 650 Å.

Electron micrographs of the iron-oxide phases prepared by oxidation of ferrous sulfide look considerably different from the commercial iron oxide (Figure 24). Both are identified as γ -FeOOH by X-ray diffraction. The majority of the iron-oxide particles prepared by iron-sulfide oxidation are thin serrated plates. A portion of the plates are either lying on their

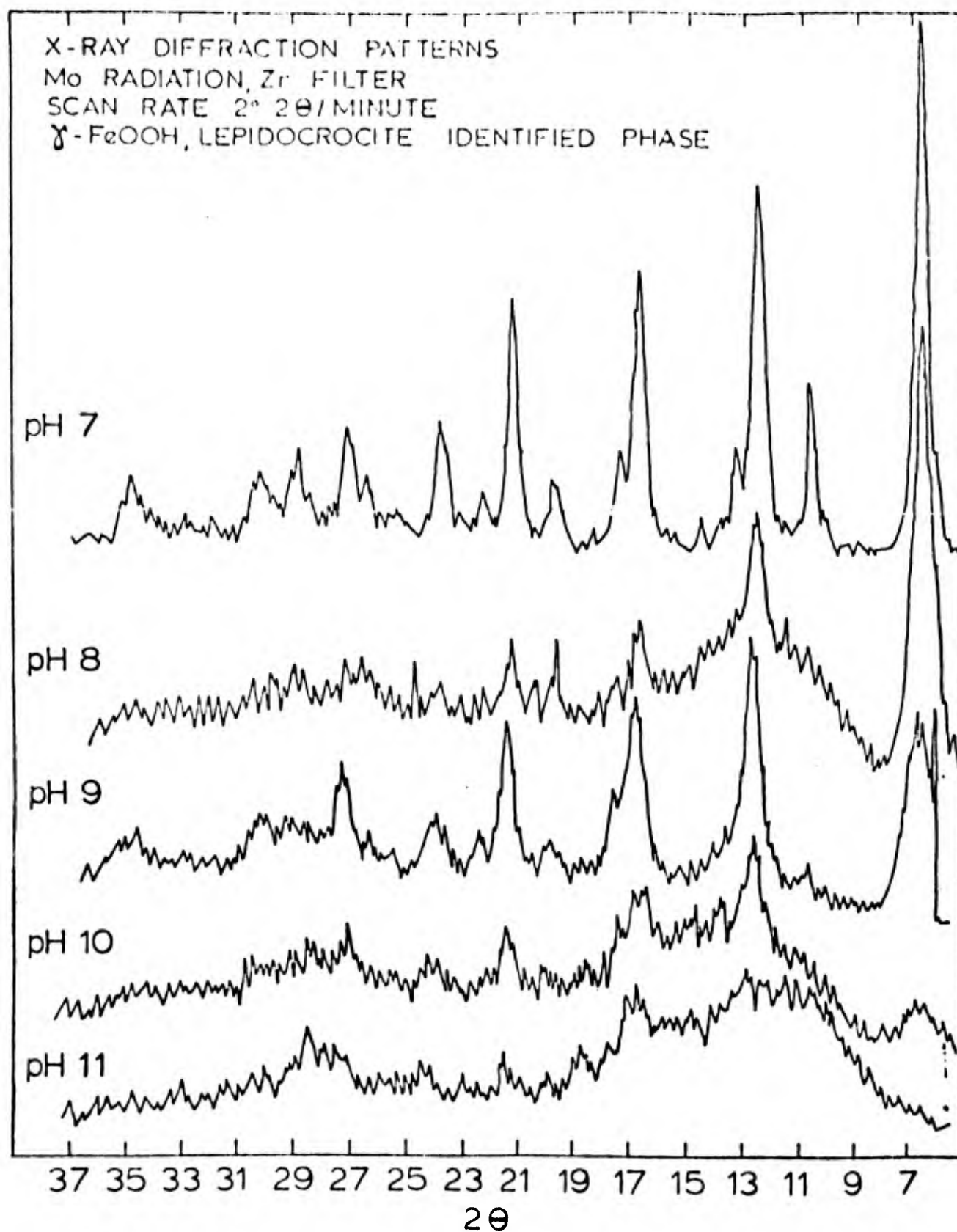


Figure 23. X-ray diffraction patterns of solid iron oxyhydroxide produced during oxidation of FeS(s).

A.



B.



C.



D.



E.



Figure 24. Electron Micrographs
of Iron Oxyhydroxide Products

I. γ -FeOOH purchased from Pfizer
Chemical Co. (HFC lot 37)

A. Magnification x 26,000

B. Magnification x 58,500

II. γ -FeOOH formed during oxidation
of FeS at pH 7, 20°C

C. Magnification x 26,000

D. Magnification x 58,500

E. Magnification x 58,500

side or are rolled up, which makes them appear rod-like. However, taking a series of images by changing the focal point of the microscope indicates that these are fairly thick. Therefore, it is not clear whether they are lathes, or plates turned sideways or rolled up. The majority of the material is present as serrated plates with dimensions on the order of 2500 \AA by 1000 \AA . The largest particle observed in any of the 8 samples prepared was 5800 \AA ($0.58 \text{ }\mu\text{m}$) long.

Elemental sulfur was known to be present in the samples and was observed as a transient phase with the electron microscope. It was impossible to get an electron micrograph of elemental sulfur because it vaporizes rapidly in the electron beam.

Discussion. The synthesis of $\gamma\text{-FeOOH}$ in the laboratory is described earlier. Ferrous iron either dissolved or as a solid is almost always required as the initial substrate. In general, the synthesis of $\gamma\text{-FeOOH}$ requires the slow oxidation of ferrous iron over a period of weeks or months in the pH range 2 to 6.5. When oxidation is conducted rapidly or in a higher pH range, goethite is typically reported as the crystalline phase formed rather than lepidocrocite.

Synthesis of lepidocrocite is reported in the neutral to slightly alkaline range under certain conditions. The identification of $\gamma\text{-FeOOH}$ during the rapid aerial oxidation of ferrous-sulfate solutions or ferrous-hydroxide suspensions is discussed earlier. A portion of the ferrous-iron present appears to have to be oxidized before the formation of lepidocrocite occurs. Soluble ferrous or ferrous-ferric complexes are reported as intermediates in the formation of $\gamma\text{-FeOOH}$. The role these complexes play is not clear. The oxidation of ferrous-sulfide suspensions reported here were conducted under conditions which are significantly different from the conditions under which lepidocrocite is normally observed to form in the laboratory. The oxidation experiments were conducted under neutral to alkaline conditions, and complete oxidation was obtained from 10 minutes to 6 hours. Based upon observations of the ferric-oxyhydroxide phases formed under these conditions, goethite or ferric-oxide gel would be expected to form. Lepidocrocite is not normally observed to form over the pH range 7 to 10, particularly when the rate of oxidation is rapid. Diffraction patterns in Figure 23 indicate that some $\gamma\text{-FeOOH}$ is present even in the material produced by oxidizing ferrous sulfide suspensions at pH 10. It is also significant that the remainder of the material is too poorly crystallized to yield a diffraction

pattern. The presence of dissolved carbon dioxide does not appear to inhibit the formation of γ -FeOOH or favor the formation of α -FeOOH, under these conditions, as Schwertmann (1959) reported during the oxidation of ferrous hydroxide.

The synthetic formation of γ -FeOOH generally depends upon oxidizing a solid or aqueous ferrous compound. The ferrous iron present in soil or sediment is typically transported in as a ferric oxide or oxyhydroxide. It is then reduced in the absence of oxygen during the biological decomposition of organic matter. Ferrous iron is only stable in the absence of oxygen, which necessitates its association with decomposing organic matter and limited diffusion of oxygen. Anaerobic sediments and poorly drained soils such as gleyed soils, peats, rich loams, and soils with high organics all have conditions which would lead to the reduction of ferric oxides and stability of the ferrous iron produced. The ferrous iron might be present in association with organic matter, adsorbed or exchanged on clays, as ferrous carbonate, or as ferrous sulfide if a source of sulfur is present. Ferrous hydroxide would not be present under normal environmental conditions. The anaerobic decomposition of organic matter generally results in the production of carbon dioxide and organic acids, thus creating a low pH environment.

Lepidocrocite is found above the reduced zone in poorly drained soils and is not found in well-drained soils (Brown, 1953). Why γ -FeOOH would form under these conditions is an interesting question. Lepidocrocite crystals found in soils are very similar to those produced synthetically, suggesting that they are formed by precipitation from solution rather than oxidation of coatings on particles (Schwertmann, 1973). The conditions in the anoxic zone in many soils and peat bogs are slightly acidic with slow oxidation occurring in the upper layer. Soluble ferrous iron in organic-rich anaerobic regions would be reasonably mobile and available to diffuse out of this zone. The rate of oxidation controlled by the diffusion rate of ferrous iron and dissolved oxygen is consistent with observations of γ -FeOOH formation from homogeneous ferrous iron solutions in laboratory experiments.

Sediments in estuarine environments are subject to periodic resuspension and turnover during tidal cycles and seasonal changes in runoff. Ferrous sulfide in this material would be exposed to conditions similar to those under which the synthetic ferrous sulfides were oxidized in this study. The identification of γ -FeOOH in sediments has not been reported (except

γ -FeOOH of terrigenous origin by Mallik, 1972). This may be due to its low concentration in the clay matrix making up the sediment, or its relatively short life span once it is redeposited in anaerobic sediments due to rapid reduction to ferrous iron under these conditions. Lepidocrocite should be the ferric-oxyhydroxide phase produced during the oxidation of sulfidic sediments, based upon observations of synthetic systems reported here.

Conditions under which various iron-oxide phases form in the laboratory indicate the formation of γ -FeOOH during the rapid oxidation of ferrous sulfide should not occur. Explanations are lacking for why γ -FeOOH rather than α -FeOOH or an X-ray amorphous phase is formed as the reaction product.

Insight into where the oxidation of ferrous iron and crystallization of γ -FeOOH occurs can be deduced from observations in natural systems, and the relationship between ferrous sulfide and lepidocrocite in laboratory experiments.

Schwertmann (1973a) observed that lepidocrocite crystals found in soils are not present as oxide coatings on clays but rather as separate crystals. The similarity between crystals formed in soils and synthetically leads Schwertmann to conclude that both are formed by precipitation from solution rather than direct oxidative conversion of reduced iron coatings to ferric-oxide coatings.

The dissimilarity of tetragonal iron sulfide and lepidocrocite observed on electron micrographs, coupled with the dissimilarity of their crystal structure, suggests that ferrous sulfide does not serve as a template for γ -FeOOH precipitation. Qualitative observation of partially oxidized ferrous sulfide solutions indicate that the iron oxide formed and the remaining ferrous sulfide are not associated. In quiescent suspensions, the iron rapidly flocculates and settles while the ferrous sulfide remains dispersed.

The initial step in the oxidation of metal sulfides proposed by Sato (1960) involved the oxidation of the sulfide to elemental sulfur and the release of the metal ion to solution. The formation of γ -FeOOH is consistent with the mechanism proposed by Sato (1960) and the hypothesis that the oxidation of ferrous iron does not occur at the ferrous sulfide surface.

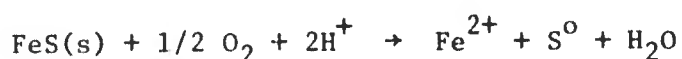
The formation of lepidocrocite in synthetic systems reportedly requires the formation of a soluble ferrous-ferric complex or a mixed solid phase ("green rust") as a precursor to the formation of lepidocrocite.

It is hypothesized that ferrous ions are released to solution during the initial reaction between oxygen and sulfide. This free ferrous iron is then

incorporated into freshly forming "green rust" or adsorbed onto the surface of forming lepidocrocite. The oxidation of the complexed ferrous iron then occurs while bound as a solid. This oxidation process is responsible for the conversion of "green rust" or ferrous-ferric surface complexes to γ -FeOOH. Catalysis of the oxidation of ferrous iron by ferric oxide surfaces is discussed in Section II.

There are alternate reaction sequences which compete for the ferrous iron as it is released from the ferrous sulfide surface. Ferrous iron is vulnerable to oxidation in solution by oxygen. The rate of oxidation of ferrous iron in homogeneous solution by oxygen is a function of pH, ferrous iron, and oxygen concentration.

The steady-state concentration of ferrous iron in solution during ferrous-sulfide oxidation is determined by the rate ferrous iron is released to solution during the initial reaction



and the rate of oxidation of the ferrous iron released. The rate of oxidation of ferrous iron in solution is given by

$$d[\text{Fe}^{2+}]/dt = -k[\text{Fe}^{2+}](\text{P}_{\text{O}_2})[\text{H}^+]^{-2}$$

This is discussed in detail in Section II. Under steady-state conditions, the rate of release of ferrous iron to solution due to the oxidation of ferrous sulfide is just equal to the rate of oxidation of ferrous iron. At pH 7, the steady-state concentration of ferrous iron would be on the order of 10^{-3}M using this approach. The concentrations of ferrous iron observed experimentally are far below this level. Therefore, the simple homogeneous oxidation of ferrous iron by oxygen cannot account for the removal of ferrous iron from solution.

As the pH of the reaction media increases, the rate of oxidation of ferrous iron increased with the square of the hydroxide concentration. From the expression for the rate of oxidation of ferrous iron, it is evident that the steady-state ferrous concentration will decrease rapidly with increasing pH. The concentration of ferrous iron in solution will also be a function of the distance from the surface of ferrous sulfide particles. The oxidation of ferrous iron in solution may compete successfully with the removal of

ferrous iron from solution by adsorption or as "green rust," with increasingly alkaline conditions.

This explanation is consistent with the general decrease in crystallinity and particle size observed for lepidocrocite formed under increasingly alkaline conditions.

In the example cited, the mechanism of oxidation of homogeneous ferrous iron presumes that the rate-limiting step in the oxidation of ferrous iron is the initial reaction between ferrous iron and oxygen. This reaction initiates a free radical chain which then reacts quickly. In the presence of ferrous sulfide, the oxidation of sulfide also probably results in the formation of free radicals. Therefore, the homogeneous oxidation of ferrous iron may be much more rapid, and steady-state concentrations much lower, than calculated in the simple case. The same arguments can be applied to the situation where the oxidation is due to free radicals as used for the reaction involving oxygen.

The presence of a greenish intermediate during the oxidation of ferrous sulfide was never observed. Ferrous sulfide has an intense black color which masks the color of everything else present, even when it represents a relatively minor fraction of the total solids present.

The oxidation of ferrous sulfide was conducted at pH 9 in the presence and absence of 0.38M formaldehyde. The formaldehyde had no detectable effect upon the rate of oxidation of ferrous sulfide. However, at the completion of the oxidation, the ferric oxyhydroxide phase was a flat olive green color rather than the normal yellow orange. Upon standing overnight, this changed to a bright yellow orange typical of lepidocrocite. Unfortunately, the crystal structure was not confirmed by X-ray diffraction analysis.

The observation of the greenish intermediate lends support to the hypothesis that a ferrous-ferric complex is a necessary intermediate in the conversion of ferrous iron to lepidocrocite. Although a portion of the discussion is speculation with respect to the formation of γ -FeOOH, the individual processes mentioned, such as mechanism of metal-sulfide oxidation, or necessity of presence of soluble iron during γ -FeOOH formation, are well established. The data are consistent with a mechanism involving the release of ferrous iron to solution, followed by homogeneous oxidation and precipitation from solution. This is consistent with the observations of ferrous-sulfide oxidation and the mechanisms proposed to explain this oxidation.

Sulfur Oxidation Products

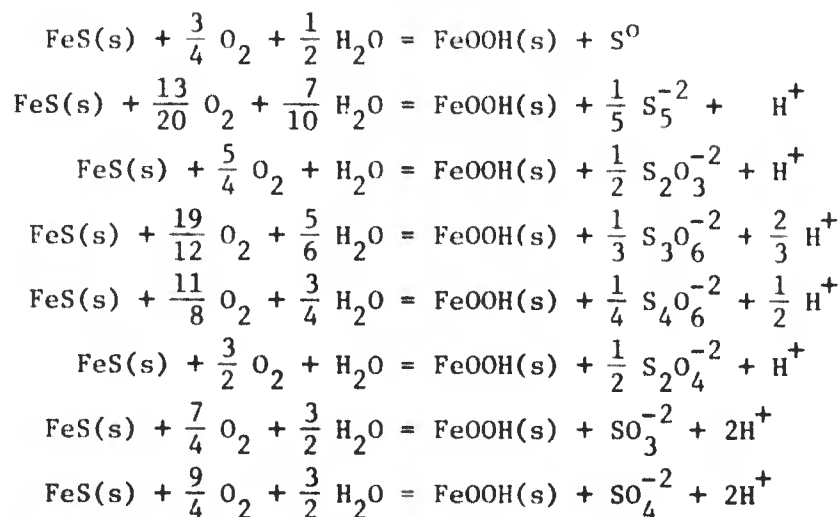
Identification of the oxidation products of sulfide and their dependence upon reaction conditions represents a formidable task. The chemistry of sulfur is discussed earlier along with many of the possible sulfide oxidation products. Virtually all of these reaction products may be formed to some extent under appropriate conditions.

The sulfur oxidation products were evaluated by two approaches. Analysis for specific sulfur species were performed, which has the advantage of providing highly detailed information on the products. This approach requires that analysis be performed for each species of interest. The potential complexity of the mixtures of oxidation products which may be formed is alluded to earlier. A second approach based upon changes in solution composition provides a method of monitoring similarities and differences in the distribution of species formed under varying experimental conditions. The use of indirect measurements, such as hydronium ion production and formation of iodine reactive species, provides a powerful tool for evaluating the response of sulfur oxidation products to experimental conditions. Much of the data concerning the effect of experimental parameters on sulfur oxidation products is presented using these relationships. Since this manner of data presentation may at first appear obscure or confusing, the discussion of the experimental results is preceded by a discussion of the interpretation and significance of comparisons of data obtained by indirect measurements.

Stoichiometric equations describing the oxidation of ferrous sulfide by molecular oxygen to ferric oxyhydroxide and various sulfur species are presented in Table 6. With relatively few exceptions, the number of protons liberated generally increases with the increasing average oxidation state of sulfur in the sulfur product formed. Oxidation leading to the formation of elemental sulfur does not result in a net excess of hydronium ions, while the formation of all remaining species, which are soluble, does result in a net excess of hydronium ions. Therefore, the formation of an excess of hydronium ions indicates that the oxidation is proceeding past elemental sulfur.

The interpretation of data on hydronium ion formation is limited by itself. However, several of the soluble sulfur species react with iodine and the iodine-consuming capacity of the species produced can be determined. The ratio of hydronium ions produced per equivalent of iodine-consuming capacity provides an empirical means of comparing the distribution of soluble sulfur

TABLE 6. SOME POSSIBLE OXIDATION PRODUCTS OF FeS



products formed under different experimental conditions. Similar ratios found for experiments conducted under different conditions indicate that the relative distribution of soluble sulfur species is similar in both cases. This does not mean the absolute concentrations are the same, only that the ratio of different soluble species remains the same. Even without knowing which soluble species are produced, changes in this ratio readily indicates changes in the composition of soluble sulfur species formed.

When the ratio of protons per equivalent of iodine-consuming species produced remains constant, but the absolute quantities change, the change indicates the extent of oxidation past elemental sulfur. This conclusion is based on the fact that the formation of elemental sulfur does not generate any protons or iodine-reactive species. Therefore, the ratio of soluble sulfur species to elemental sulfur produced may vary considerably, yet the ratio of proton to iodine-consuming species liberated will remain constant as long as the relative distribution of soluble species remains constant.

Because of the great number of soluble sulfur species, it is possible that both the concentration and distribution of species could vary in a manner that the ratios remained constant. The simultaneous determination of specific sulfur species confirms the interpretation drawn from the indirect data analysis.

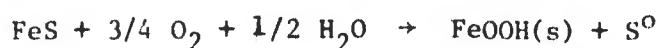
Experiments were conducted under varying conditions of pH, temperature, dissolved oxygen, and ionic media. The soluble iodine-reactive species

produced, hydrogen ions generated, and the concentrations of elemental sulfur and selected sulfur-oxyanions were determined. There is very little correlation between the dependence of the oxidation rate upon a specific parameter and the sulfur-oxidation products. However, the results do provide insight into the rate-controlling process of the oxidation reaction of iron sulfide.

Dependence on pH. The free hydrogen-ion concentration, or pH, is readily identified as an important parameter in determining the speciation of oxidation products of sulfide. The distribution of products initially formed is as much a function of kinetics as thermodynamics. As a result, the oxidation products identified are typically metastable intermediates, which are ultimately slowly oxidized to sulfate. However, experimental observations generally support the importance of hydrogen-ion concentration in determining the initial distribution of sulfur species.

During the oxidation of ferrous sulfide at pH 7, 20°C in $10^{-3}\text{M Na}_2\text{SO}_4$ solution the pH remains constant and does not require the addition of base to maintain a pH of 7 once the reaction has commenced. Soluble iodine-reactive species are absent in the solution, consistent with the absence of proton production.

The stoichiometric equation describing the oxidation of ferrous sulfide to elemental sulfur and ferric hydroxide is



There is no net production or consumption of hydrogen ions when elemental sulfur is the sole product of the oxidation of sulfide. Elemental sulfur is not oxidized by iodine at any appreciable rate, and therefore does not interfere with the analytical technique. Analysis of the suspension for elemental sulfur after complete oxidation of ferrous sulfide confirms that the oxidation of sulfide proceeds only as far as elemental sulfur.

The particle size of the elemental sulfur formed is quite small. A significant fraction of the sulfur formed passed through a 0.45 μm filter. In order to achieve quantitative recoveries of elemental sulfur, a 0.05- μm filter was required.

The oxidation of suspensions of ferrous sulfide at 20°C in $10^{-3}\text{M Na}_2\text{SO}_4$ was carried out at a number of successively higher pH values. The generation of hydrogen ions and soluble iodine-reactive species increases with increasing pH. This indicates that the oxidation of at least a portion of the sulfide is proceeding past elemental sulfur to higher oxidation states.

Results from the oxidation of ferrous sulfide at pH 7, 9, and 10 are shown in Figure 25. The concentration of soluble iodine-reactive species formed during oxidation is plotted as a function of the concentration of ferrous sulfide oxidized. The concentration of iodine-reactive species produced per mole of FeS oxidized increases with increasing pH. This is demonstrated in Figure 26, where the equivalents of soluble iodine-reactive species produced per mole of FeS oxidized is plotted as a function of the pH at which the oxidation is conducted. A very similar relationship holds for the concentration of hydrogen ions produced during the oxidation and the pH at which the oxidation is performed. The relationship between the soluble iodine-reactive species produced and the number of hydrogen ions produced appears to be fairly insensitive to pH during oxidation (Figure 27). The linear relationship between the two parameters suggests that the reactions involved do not change over the course of the oxidation. The relationship between the number of hydrogen ions produced per equivalent of soluble iodine-reactive species produced remains constant and independent of pH, even though the absolute concentration of both increases with increasing pH. This same phenomenon is observed when the oxidation is carried out at constant pH over a range of temperatures. The observation is particularly significant and is discussed at length below.

Identity of Soluble Sulfur Oxidation Products. Determination of the speciation of soluble sulfur products formed during the oxidation of ferrous sulfide proved to be a difficult task. The oxidation of ferrous sulfide under alkaline conditions leads to the formation of multiple sulfur oxidation products. The distribution of sulfur species present at the completion of oxidation is divided into two general classes. The fraction of sulfur which can be trapped by a 0.05- μ m filter and measured colorimetrically as elemental sulfur is termed filterable elemental sulfur. The fraction passing the 0.05- μ m filter is operationally defined as soluble for the purpose of classification. This fraction includes truly soluble sulfur species and colloidal elemental sulfur.

The oxidation of ferrous sulfide was conducted at pH 10, 20°C, and 8 mg/l oxygen to maximize the formation of the soluble species of interest. The initial concentration of ferrous sulfide present was determined by analyses for iron, sulfide, and total sulfur present. The background concentration of sulfate initially present which did not arise from the ferrous sulfide was

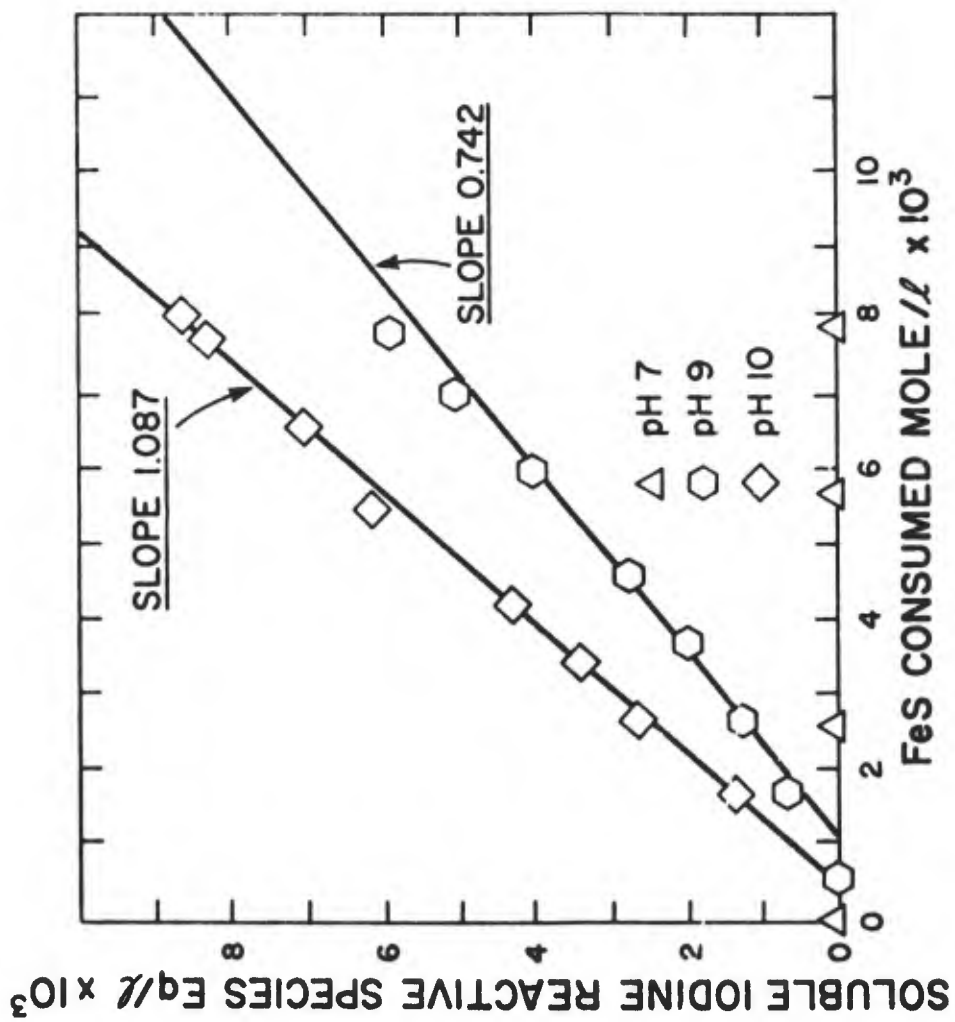


Figure 25. Equivalents of soluble iodine-consuming species formed as a function of moles/l FeS(s) oxidized at 20°C and 10 mg/l O₂.

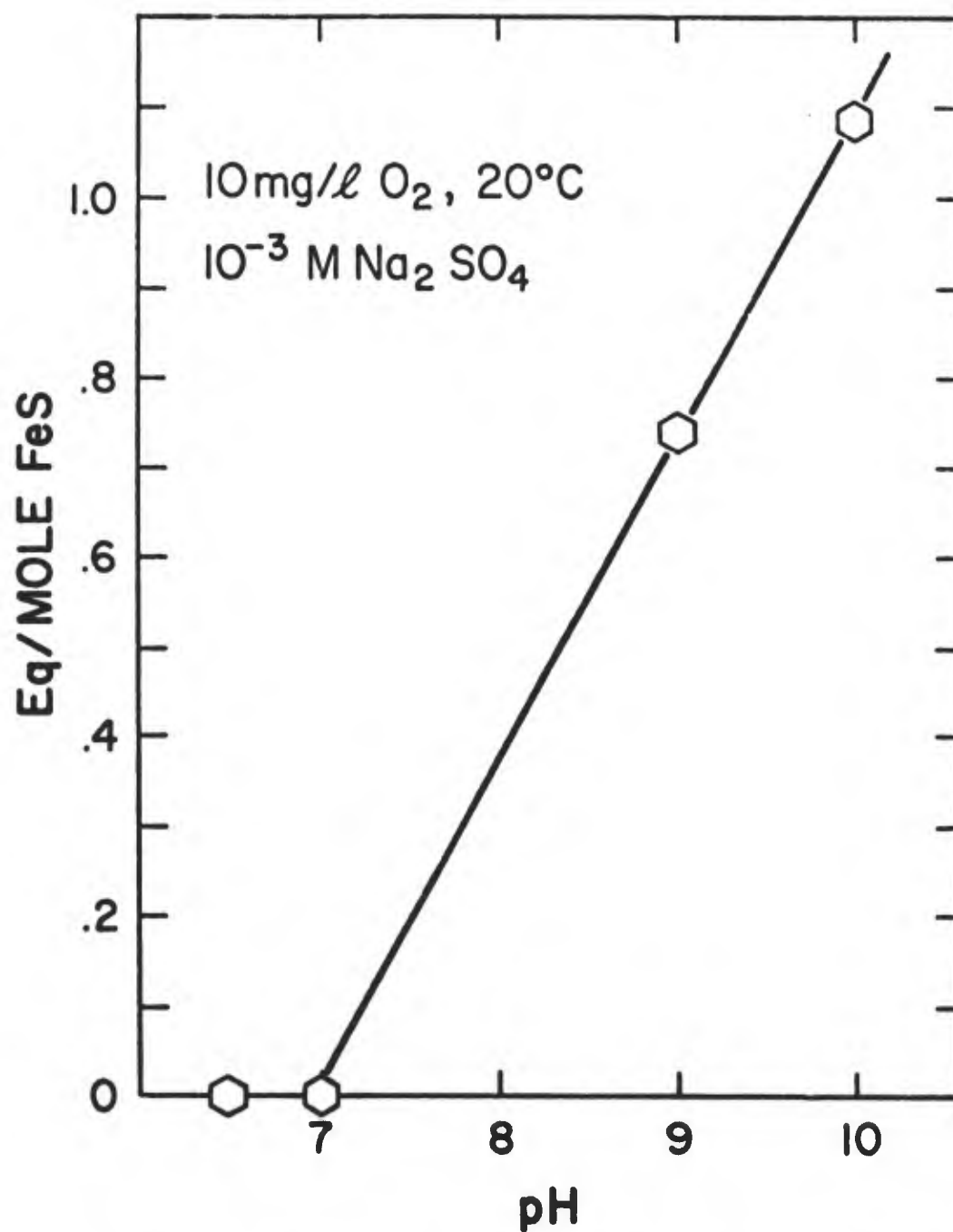


Figure 26. Ratio of equivalents of iodine-consuming species formed per mole of $FeS(s)$ oxidized as a function of pH during oxidation, indicating the extent of oxidation of sulfur.

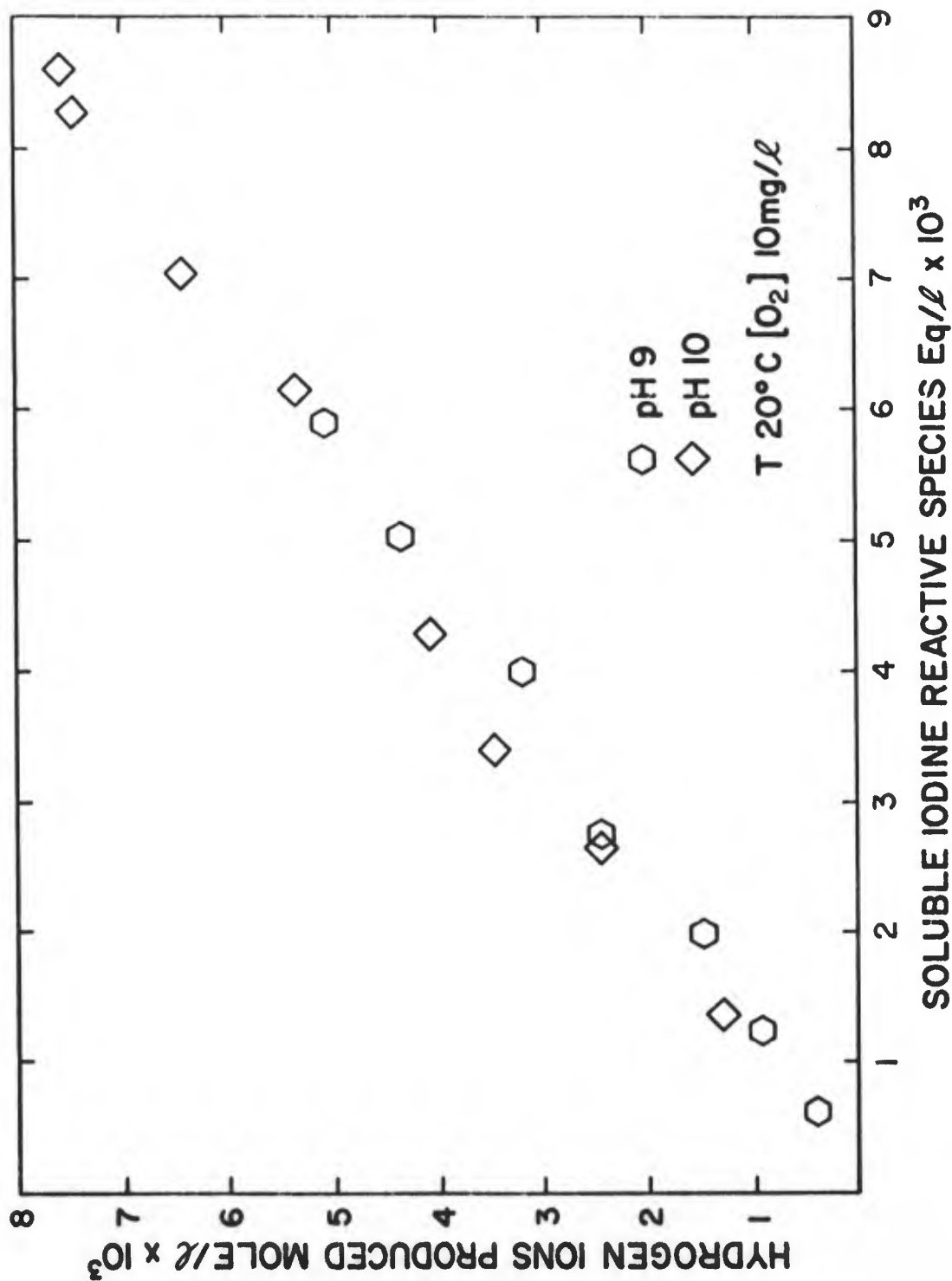


Figure 27. The relationship between hydrogen ions and soluble iodine-consuming species produced during FeS(s) oxidation. The extent of oxidation of soluble sulfur species is indicated. The similarity between results at pH 9 and 10 indicates the distribution of soluble sulfur species is similar at both pH values.

also determined. The results are shown in Table 7 (part 1). The oxidation was carried to completion under the conditions listed above. At the completion of the oxidation, the concentrations of filterable elemental sulfur, sulfate formed during the oxidation, and total sulfur in solution were determined. The total sulfur recovered after correction for the background concentration of sulfate initially present is shown in Table 7 (part 2). Agreement between the concentrations added and recovered is quite good. Approximately 98% of the sulfur added is found in the soluble phase at completion of the oxidation. Very little, about 3%, of the sulfide added is oxidized as far as sulfate. The major fraction, the remaining 95%, is oxidized to some intermediate oxidation state.

Identification of the remaining species was elusive, but has been established indirectly, using a number of techniques. Samples of the soluble phase were cyanolyzed under controlled conditions which allows a differentiation between thiosulfate, trithionate and higher polythionates. Colloidal elemental sulfur also reacts quantitatively with cyanide to form thiocyanate under the conditions leading to the cyanolysis of trithionate and can interfere to a lesser extent with the determination of higher polythionates.

Total sulfur in the soluble phase can be calculated, assuming alternately that the thiocyanate formed during the analysis for trithionate arises from either trithionate or colloidal elemental sulfur. The summation of the total sulfur present in all of the soluble sulfur species can then be compared with the total sulfur actually found in solution measured as sulfate after oxidation with hydrogen peroxide (Table 7, parts 3 and 4).

When the thiocyanate formed is assumed to arise from the cyanolysis of trithionate, the concentration of sulfur calculated far exceeds the concentration added. However, when the concentration of thiocyanate is assumed to arise from the cyanolysis of colloidal elemental sulfur, the concentration of sulfur calculated agrees very well with the concentration added.

The concentration of hydronium ions produced during the oxidation reaction was measured. The contribution from the formation of thiosulfate and sulfate can be calculated (Table 6). The difference which represents the contribution of all other species is small. The very low number of hydronium ions released per mole of sulfur oxidized ($0.31 \text{ H}^+/\text{S}$) indicates that the average oxidation state of the remaining sulfur is quite low. If the analyses for tetrathionate is assumed to measure tetrathionate with minimal interference from colloidal sulfur, tetrathionate formation more than accounts for the

TABLE 7. MASS BALANCE AND DISTRIBUTION OF SULFUR SPECIES BEFORE AND AFTER
AERIAL OXIDATION AT pH 10 (as moles/l as S or eq/l)

1. FeS added	
A. Fe(total) (measured colorimetrically with ferrozine technique)	$9.13 \times 10^{-3}M$
B. S(II) (measured by iodometric titration)	$9.26 \times 10^{-3}M$
C. Total sulfur in FeS as sulfate	
Total SO_4 (after H_2O_2 oxidation)	$1.115 \times 10^{-2}M$
Background SO_4 in FeS suspension	$2.16 \times 10^{-3}M$
Total sulfur from FeS	$8.99 \times 10^{-3}M$
2. Sulfur recovered at completion of aerial oxidation	
A. Elemental sulfur (filterable)	$1.53 \times 10^{-4}M$
B. Soluble sulfur formed during oxidation	
Total S found in filtrate	$1.133 \times 10^{-2}M$
SO_4 initially pres- ent (background)	$2.16 \times 10^{-3}M$
Total formed (difference)	$9.17 \times 10^{-3}M$
Total sulfur recovered	$9.32 \times 10^{-3}M$
3. Sulfur speciation	
A. Thiosulfate	
Mole/l SCN^- found upon cyanolysis	$3.16 \times 10^{-3}M$
S_2O_3	$6.32 \times 10^{-3}M$
B. 2-minute cyanolysis of filtrate $20^\circ C$	
Mole/l SCN^- found upon cyanolysis	$1.15 \times 10^{-3}(\pm 2.24 \times 10^{-4})M$
Mole/l as S assuming S_4O_2	$2.3 \times 10^{-3}M$
Mole/l as S assuming S^0	$1.15 \times 10^{-3}M$
C. 45-minute cyanolysis at $100^\circ C$	
Mole/l SCN^- found upon cyanolysis	$1.14 \times 10^{-3}(\pm 1.81 \times 10^{-3})M$
Mole/l as S assuming S_3O_6	$3.42 \times 10^{-3}M$
Mole/l as S assuming S^0	$1.14 \times 10^{-3}M$

TABLE 7. (CONTINUED)

D. Sulfate formed during oxidation

Final SO_4^{-2} in filtrate mole/l	$2.405 \times 10^{-3}\text{M}$
Initial SO_4 before oxidation	$2.16 \times 10^{-3}\text{M}$
Sulfate formed during oxidation	$2.45 \times 10^{-4}\text{M}$

4. Total sulfur recovered as calculated from summation of sulfur in specific species

A. Assuming SCN^- came from $\text{S}_2\text{O}_3^{-2}$, $\text{S}_4\text{O}_6^{-2}$ and $\text{S}_3\text{O}_6^{-2}$

Soluble sulfur

S_2O_3	$6.32 \times 10^{-3}\text{M}$
S_4O_6	$2.3 \times 10^{-3}\text{M}$
S_3O_6	$3.42 \times 10^{-3}\text{M}$
SO_4	$.245 \times 10^{-3}\text{M}$

Sum of sulfur 12.29×10^{-3} Elemental sulfur (filterable) $1.5 \times 10^{-4}\text{M}$ Total sulfur (soluble & filterable) $12.44 \times 10^{-3}\text{M}$ B. Assuming SCN^- came from $\text{S}_2\text{O}_3^{-2}$ and colloidal S^0

"Soluble" sulfur

$\text{S}_2\text{O}_3^{-2}$	$6.32 \times 10^{-3}\text{M}$
SCN^- 2-min cyanolysis	$1.15 \times 10^{-3}\text{M}$
SCN^- 45-min cyanolysis 100°C	$1.14 \times 10^{-3}\text{M}$
SO_4^{-2}	$.245 \times 10^{-3}\text{M}$

Sum of sulfur $8.86 \times 10^{-3}\text{M}$ Elemental sulfur (filterable) $1.5 \times 10^{-4}\text{M}$ Total sulfur (soluble & filterable) $9.01 \times 10^{-3}\text{M}$

5. Iodine reactive species

Soluble iodine reactive species found 8.89×10^{-3} eq/lEquivalents/l attributed
to $\text{S}_2\text{O}_3^{-2}$ 3.21×10^{-3} eq/lEquivalents/l unac-
counted for 5.68×10^{-3} eq/l

TABLE 7. (CONCLUDED)

6. Hydronium ions		
Hydronium ions released (measured by titration)		7.57×10^{-3} eq/l
Hydronium ions attributed to the formation of thiosulfate	6.32×10^{-3} eq/l	
Hydronium ions attributed to the formation of sulfate	0.49×10^{-3} eq/l	
Hydronium ions released and not accounted for	0.76×10^{-3} eq/l	
Hydronium ions attributed to S_4O_6	1.15×10^{-3} eq/l	
Total H^+ from S_2O_3 , S_4O_6 and SO_4	7.96×10^{-3} eq/l	
ΔH unaccounted for	-0.39×10^{-3} eq/l	

remaining hydronium ions released. The oxidation state of the remaining sulfur must be zero, or that of elemental sulfur. Colloidal elemental sulfur is reportedly stabilized by higher polythionates (Urban, 1960d) which may facilitate their passage through the filters. The tentative conclusion from these results is that the species present in solution are thiosulfate, higher polythionates, and colloidal elemental sulfur rather than trithionate. The capacity of the species in solution to consume iodine is inconsistent with the capacity calculated assuming thiosulfate is the only iodine reactive species.

This discrepancy is consistently observed. An evaluation of the sulfur products formed during the oxidation of ferrous sulfide at pH 9 is presented in Table 8. The unusually high percentage of the sulfur found as filterable elemental sulfur and relatively small values of the soluble species in question limit the interpretation of these results. The results do demonstrate the discrepancy between the iodine consumption observed and the consumption predicted from the thiosulfate concentration. Thiosulfate can only account for 43 and 36% of the total iodine consumed, yet represent 69 and 74% of the total sulfur in solution at pH 9 and 10, respectively. The iodine consumption which is unaccounted for can be linked directly to the species responsible for the thiocyanate formation attributed to trithionate or colloidal elemental sulfur. Both of these species are reportedly non-iodine reactive under the conditions of the analysis (Kolthoff and Belcher, 1957). An in-depth discussion of the iodine reactivity of this species is deferred until after the presentation of all of the experimental results, where it is discussed in detail.

TABLE 8. MASS BALANCE AND DISTRIBUTION OF SULFUR SPECIES BEFORE AND AFTER
AERIAL OXIDATION AT pH 9 (as moles/l as S or eq/l)

1. FeS added		
A. Fe(total) (measured colorimetrically with ferrozine technique)		$8.92 \times 10^{-3} \text{M}$
B. S(II) (measured by iodometric titration)		$8.88 \times 10^{-3} \text{M}$
2. Sulfur recovered at completion of aerial oxidation		
A. Elemental sulfur (filterable)		$5.27 \times 10^{-3} \text{M}$
B. Soluble sulfur formed during oxidation		
Total S found in filtrate	$5.32 \times 10^{-3} \text{M}$	
SO ₄ initially present (Background)	$2.16 \times 10^{-3} \text{M}$	
Total formed (difference)		$3.16 \times 10^{-3} \text{M}$
Total sulfur recovered		$8.43 \times 10^{-3} \text{M}$
3. Sulfur speciation		
A. Thiosulfate		
Mole/l SCN ⁻ found upon cyanolysis	$1.18 \times 10^{-3} \text{M}$	
S ₂ O ₃ mole/l as S		$2.36 \times 10^{-3} \text{M}$
B. 2-minute cyanolysis of filtrate 20°C		
Mole/l SCN ⁻ found upon cyanolysis	$.276 \pm .09 \times 10^{-3} \text{M}$	
Mole/l as S assuming S ₄ O ₆	$0.552 \times 10^{-3} \text{M}$	
Mole/l as S assuming S ⁰	$0.276 \times 10^{-3} \text{M}$	
C. 45-minute cyanolysis at 100°C		
Mole/l SCN ⁻ found upon cyanolysis	$1.30 \times 10^{-4} (\pm 1.09 \times 10^{-4}) \text{M}$	
Mole/l as S assuming S ₃ O ₆	$3.91 \times 10^{-4} \text{M}$	
Mole/l as S assuming S ⁰	$1.3 \times 10^{-4} \text{M}$	

TABLE 8. (CONCLUDED)

4. Total sulfur recovered as calculated from summation of sulfur in specific species

A. Assuming SCN^- came from $\text{S}_2\text{O}_3^{-2}$, $\text{S}_4\text{O}_6^{-2}$ and $\text{S}_3\text{O}_6^{-2}$

Soluble sulfur

S_2O_3	$2.36 \times 10^{-3}\text{M}$	
S_4O_6	$.55 \times 10^{-3}\text{M}$	
S_3O_6	$.39 \times 10^{-3}\text{M}$	
SO_4	-	
Sum of sulfur		$3.30 \times 10^{-3}\text{M}$
Elemental sulfur (filterable)		$5.27 \times 10^{-3}\text{M}$
Total sulfur ("soluble" & filterable)		$8.57 \times 10^{-3}\text{M}$

B. Assuming SCN^- came from $\text{S}_2\text{O}_3^{-2}$ and colloidal S^0

"Soluble" sulfur

$\text{S}_2\text{O}_3^{-2}$	$2.36 \times 10^{-3}\text{M}$	
SCN^- 2-min cyanolysis	$.276 \times 10^{-3}\text{M}$	
SCN^- 45-min cyanolysis	$.13 \times 10^{-3}\text{M}$	
SO_4^{-2}	-	
Sum of sulfur		$2.77 \times 10^{-3}\text{M}$
Elemental sulfur (filterable)		$5.27 \times 10^{-3}\text{M}$
Total sulfur (soluble & filterable)		$8.04 \times 10^{-3}\text{M}$

5. Iodine reactive species

Soluble iodine reactive species found		$2.75 \times 10^{-3} \text{ eq/l}$
Equivalents/l attributed to $\text{S}_2\text{O}_3^{-2}$	$1.18 \times 10^{-3} \text{ eq/l}$	
Equivalents/l unac- counted for	$1.57 \times 10^{-3} \text{ eq/l}$	

6. Hydronium ions

Hydronium ions released (measured by titration)		$2.41 \times 10^{-3} \text{ eq/l}$
Hydronium ions attributed to the formation of thiosulfate	$2.36 \times 10^{-3} \text{ eq/l}$	
Hydronium ions attributed to the formation of sulfate	-	
Hydronium ions released and not accounted for		$5 \times 10^{-5} \text{ eq/l}$

Dependence on Oxygen Concentration. The rate of oxidation of ferrous sulfide has a pseudo first-order dependence upon dissolved oxygen at the lower oxygen concentrations. In two experiments conducted at pH 9 (20°C), the oxidation was performed at concentrations of 10 and 43 mg/l of dissolved oxygen. The moles of hydrogen ions produced per mole of ferrous sulfide oxidized are shown in Figure 28 for both oxygen concentrations. The quantity of protons released generally reflects the average oxidation state of the sulfur which has reacted in the system. Since only the oxidation of sulfide to an oxidation state higher than elemental sulfur results in the release of protons, this indicates that a higher percentage of the initial sulfide present is oxidized past elemental sulfur at the lower oxygen concentration. This result is interesting because it was anticipated that higher oxygen concentration would tend to drive the oxidation of sulfur to a higher oxidation state. The soluble iodine-consuming species produced per mole of ferrous sulfide oxidized is also lower for the higher oxygen concentration (Figure 29). The ratio of hydrogen ions produced per equivalent of iodine-consuming sulfur species produced is constant and independent of the oxygen concentration (Figure 30). This suggests that the same distribution of soluble species is produced at both oxygen concentrations, but that the total concentration of soluble species produced is greater at the lower oxygen concentration. The concentration of thiosulfate formed during the oxidation and its concentration of thiocyanate liberated during the selective cyanolysis of the soluble species present at both dissolved oxygen concentrations were also determined at both oxygen levels. The ratio of these species produced per mole of iodine-consuming species produced is essentially constant and independent of the oxygen concentration during the reaction (Figure 31). This supports the earlier observation that the distribution of soluble sulfur species is independent of oxygen concentration but that the absolute concentrations are directly dependent. The ratio of thiocyanate formed from all cyanide reactive species to thiosulfate also appears to be constant and independent of oxygen concentration. Possible relationships between the two quantities are considered in the discussion. The relationship between sulfur speciation and the rate of oxidation or oxygen concentration is not evident. A review of the various observations suggests that the oxidation of sulfide may occur by several parallel mechanisms, and that the reactions leading to the formation of soluble sulfur oxyanions are at least one step removed from the initial oxidation of the ferrous sulfide.

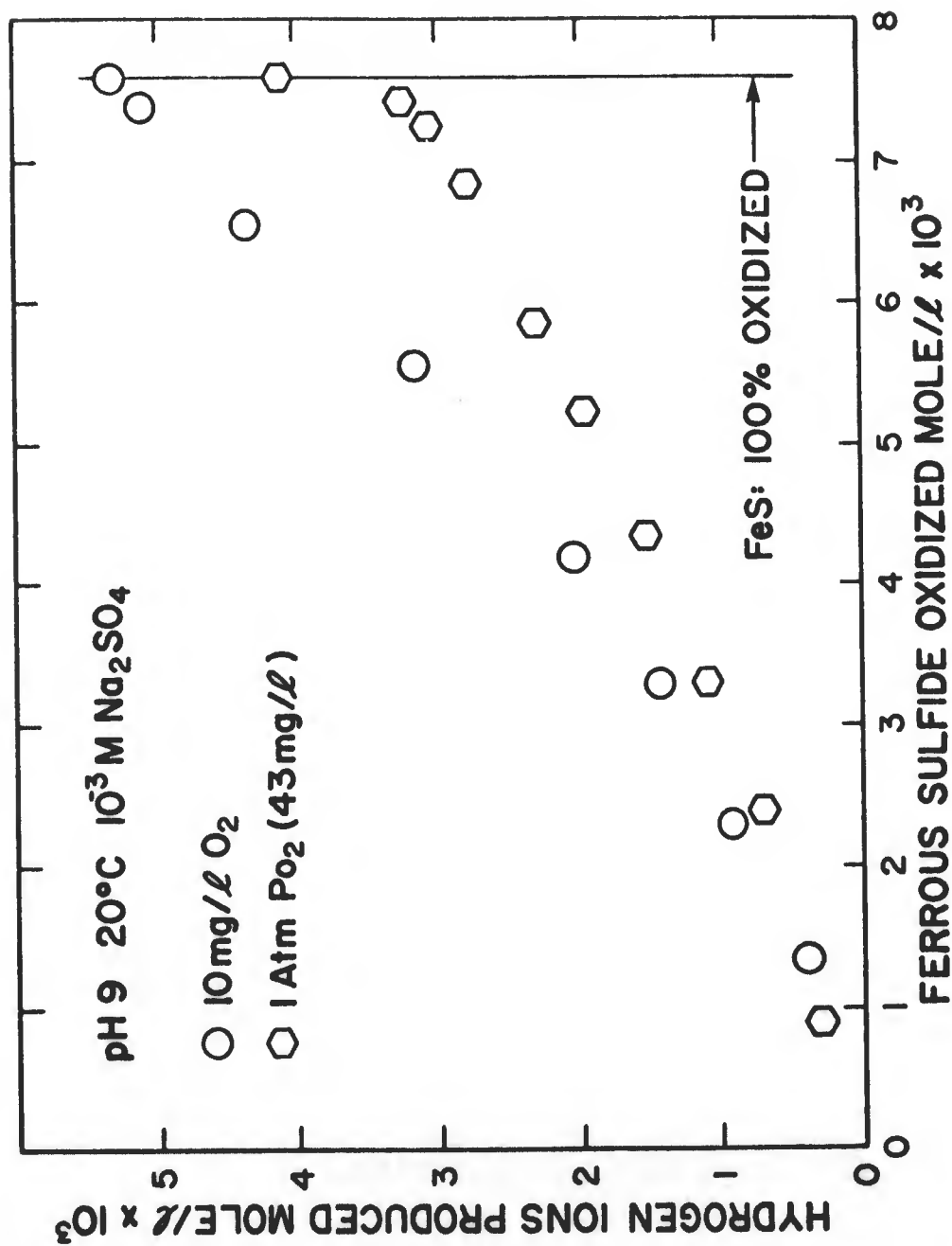


Figure 28. Effect of oxygen concentration during FeS oxidation on the extent of oxidation of sulfur species, as indicated by hydrogen ion formation.

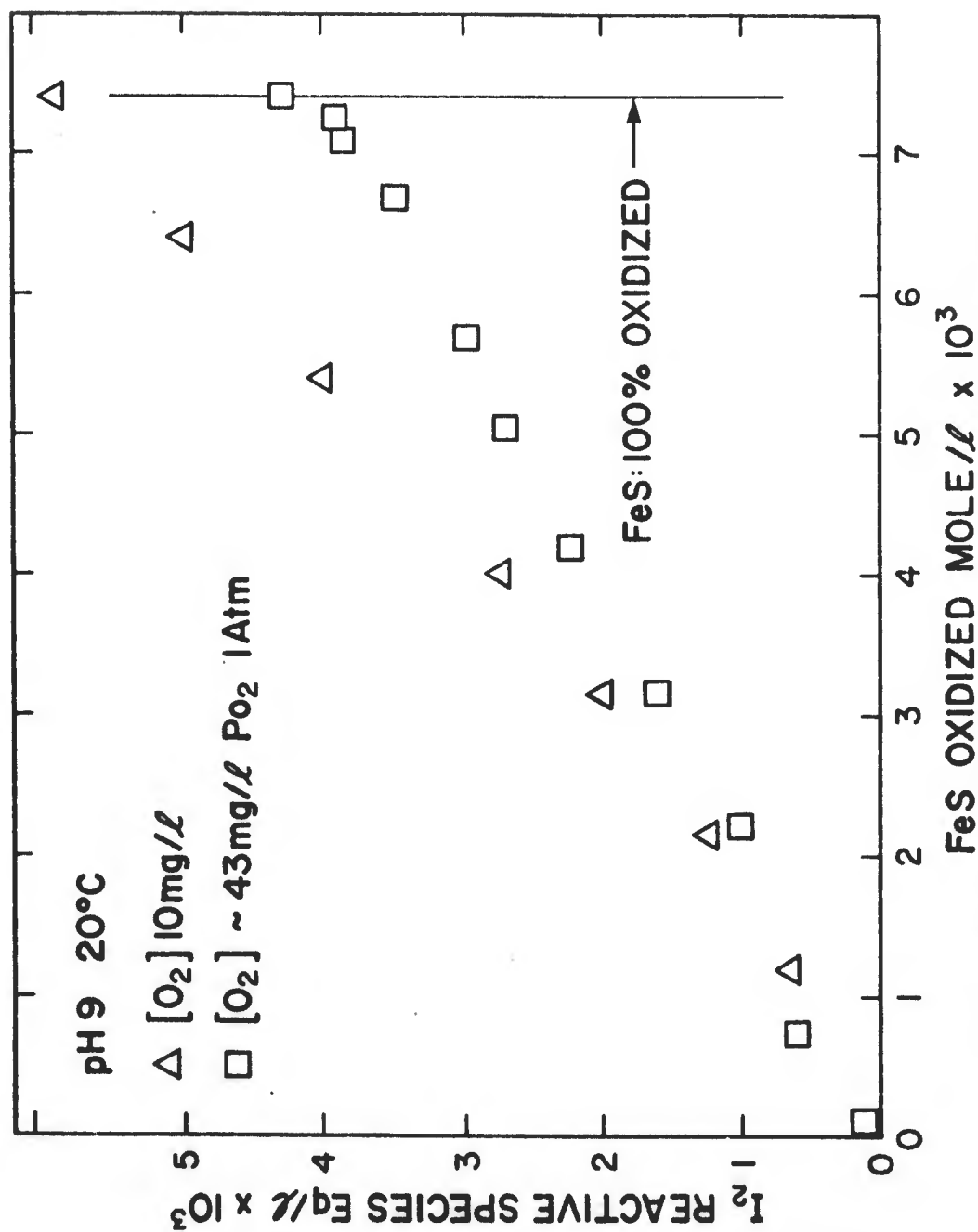


Figure 29. Effect of oxygen concentration during FeS oxidation on the extent of oxidation of sulfur species, as indicated by the soluble iodine-consuming species produced.

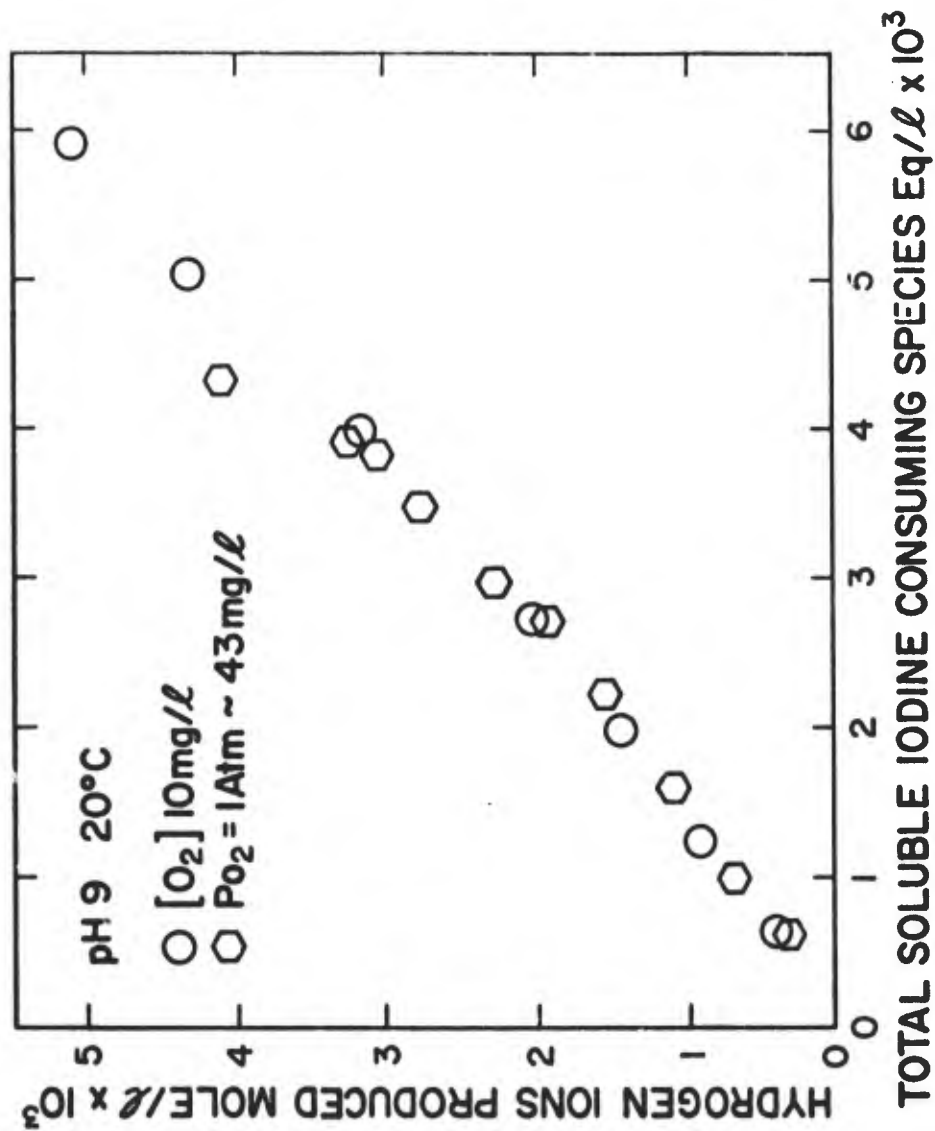


Figure 30. Relationship between hydrogen ions and soluble iodine-
 consuming species produced for the oxidation of FeS(s) at
 10 and 43 $\text{mg/l } O_2$.

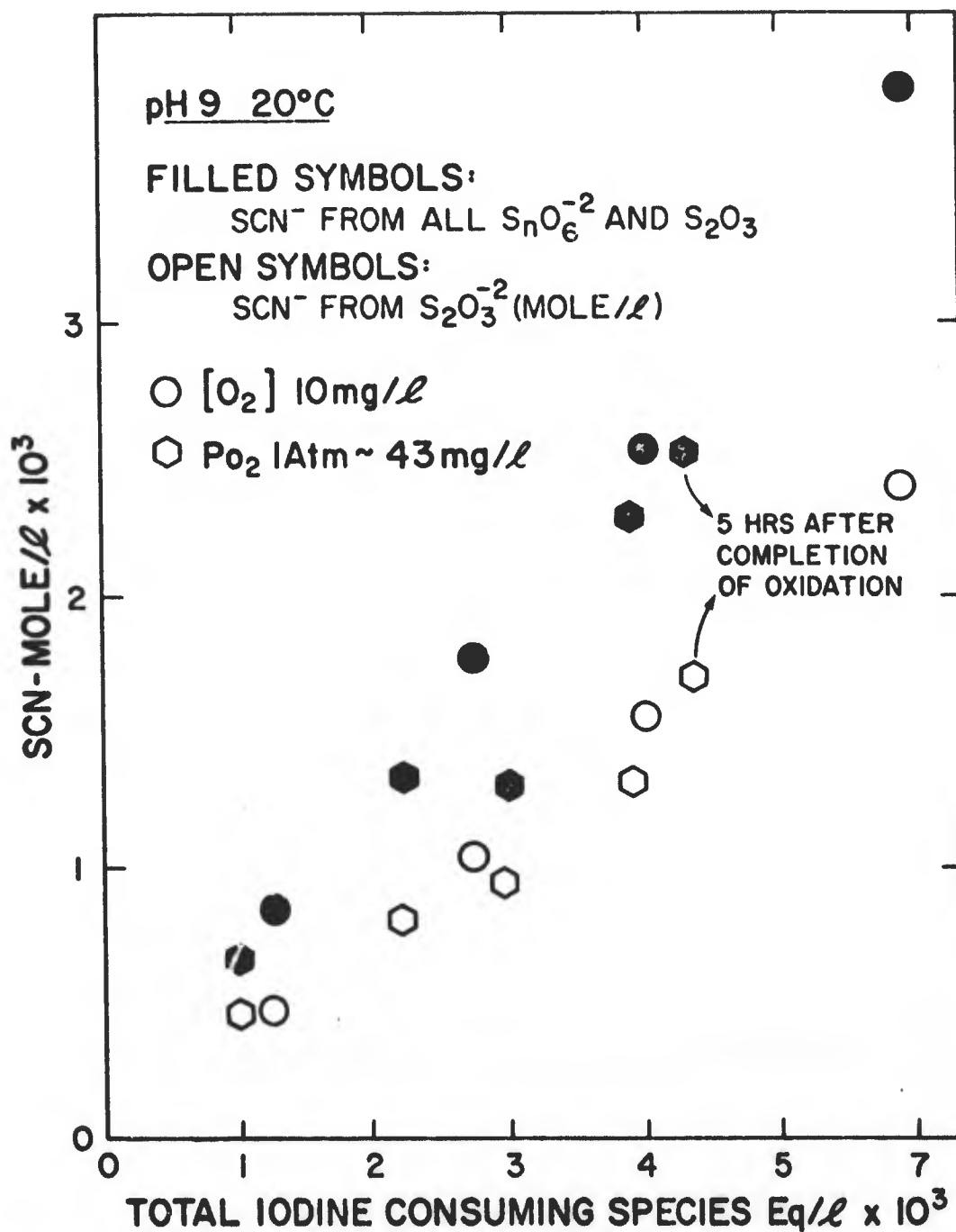


Figure 31. Relationship between soluble sulfur species and iodine-consuming species produced during the oxidation of FeS(s) at 10 and 43 mg/l O₂.

The percentage of the total sulfur oxidized past elemental sulfur is dependent upon the oxidation conditions, yet the ratio of the various soluble sulfur species formed appears to be constant and independent of the conditions. This implies that the differentiation between these species occurs at least one step beyond where the proportion of sulfur oxidized past elemental sulfur is determined. This is discussed in greater detail later.

Temperature Dependence of Sulfur Speciation. The dependence of the ferrous sulfide oxidation-rate constant upon temperature at pH 9 is discussed earlier. There is a linear relationship between the natural logarithm of the rate constant and the inverse of the absolute temperature, indicating that the same mechanism is controlling the rate of oxidation over the temperature range 5-44.5°C.

Temperature also influences the extent of oxidation of the sulfide. This is monitored by the hydrogen ions released during the oxidation at each temperature. The moles of hydrogen ions produced per mole of ferrous sulfide oxidized gives a general indication of the final oxidation state of sulfur. Figure 32 illustrates graphically the increase in average oxidation state of sulfur as a function of the temperature. There is a similar increase in the number of equivalents of iodine-consuming species generated per mole of ferrous sulfide oxidized with increasing temperature of oxidation. The relationship between hydrogen ions produced and iodine-consuming species produced over a range of temperatures is shown in Figure 33. As discussed earlier, the oxidation of ferrous sulfide by oxygen to ferric hydroxide and elemental sulfur produces no iodine-reactive species or hydrogen ions. Therefore, the information in Figure 32 suggests that the extent of oxidation of sulfide to oxidation states higher than elemental sulfur increases with increasing temperature. Figure 33 suggests that the distribution of soluble species produced is relatively constant and independent of the oxidation temperature. This information alone is inadequate to support that conclusion because there are a number of combinations of sulfur products which will yield the same ratio of equivalents of iodine-consuming species per equivalent of hydrogen ions produced in their formation. However, analysis for specific sulfur species lends support for this conclusion. The concentration of thiosulfate and thiocyanate from cyanide reactive species in the filtrate were determined during the oxidation of ferrous sulfide over the range of temperatures mentioned. The thiosulfate concentration and total thicyanate liberated from other

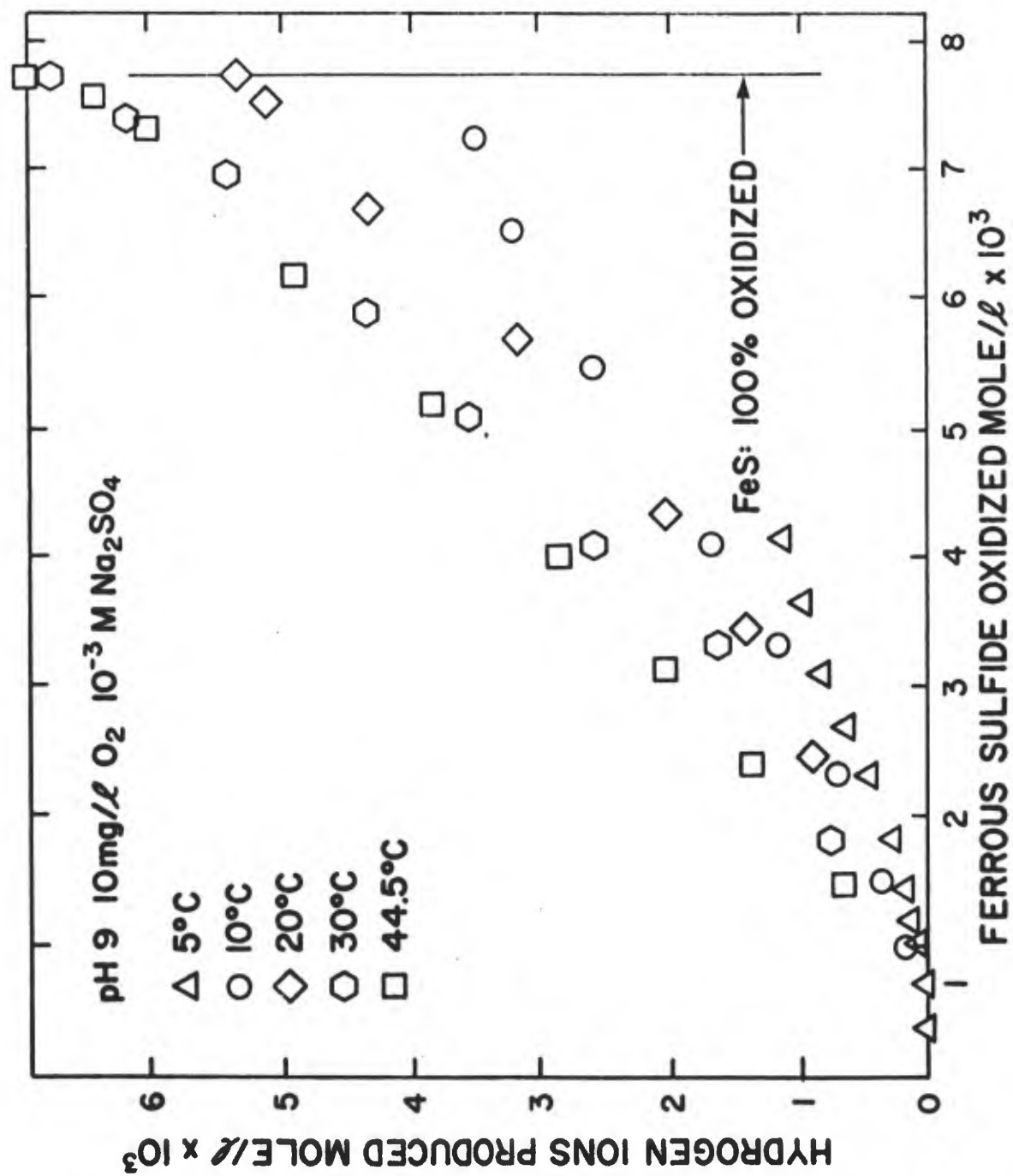


Figure 32. Hydrogen ions produced, indicating the extent of oxidation of sulfur species as a function of $FeS(s)$ oxidized over the temperature range 5 to 44.5°C.

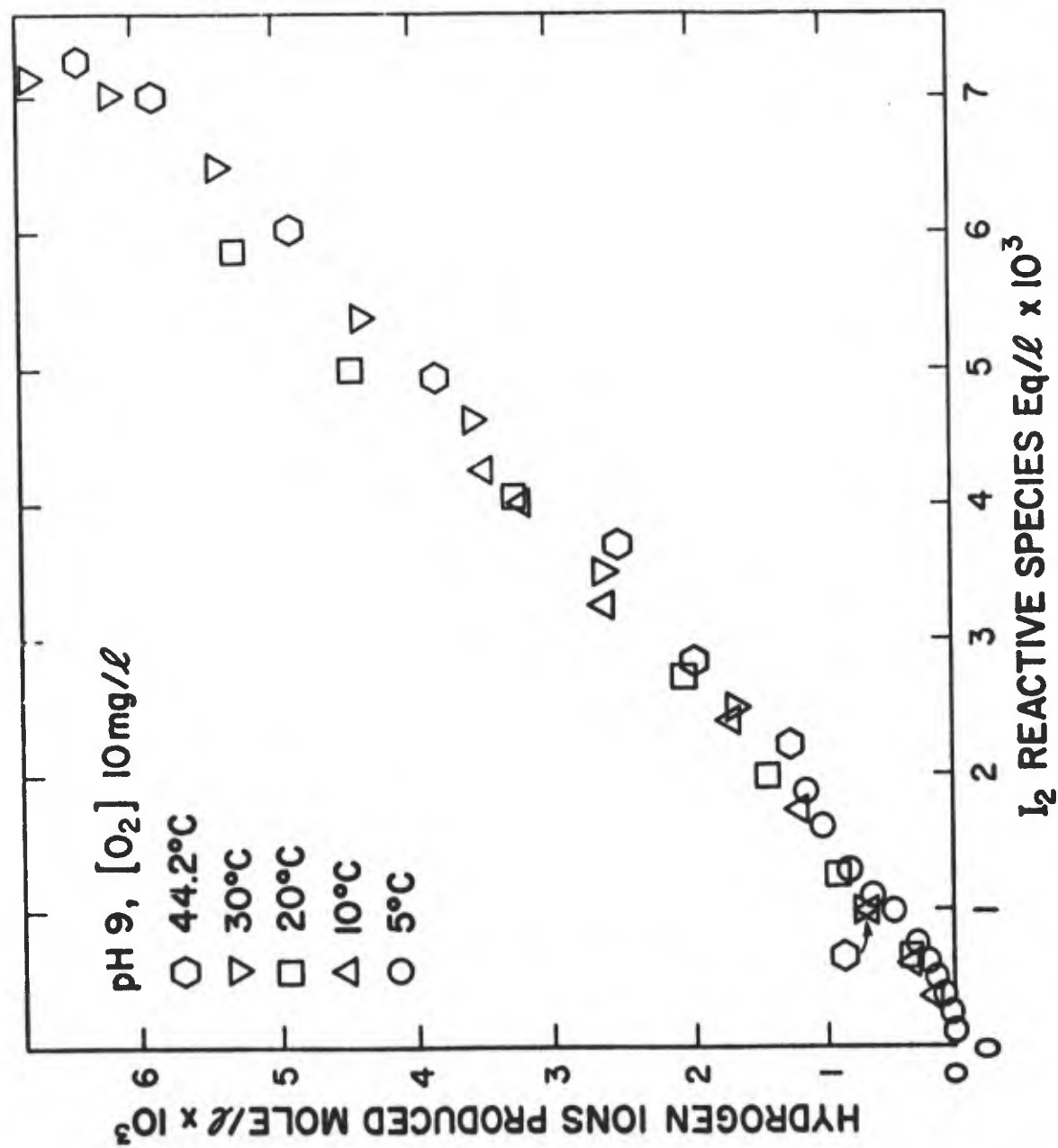


Figure 33. Hydrogen ions produced as a function of the equivalents of iodine-consuming species produced over the temperature range 5 to 44.5°C.

cyanide reactive species present are shown in Figure 34 as a function of the equivalents of soluble iodine-consuming species present. The data demonstrate two important points. First, there is a linear relationship between both the thiosulfate and total thiocyanate formed and the total equivalents of iodine-consuming species produced. This means that they are all being formed at the same rate or that the concentration of one is in equilibrium with the other. Second, the ratio of thiosulfate and total thiocyanate formed to total iodine-reactive species formed appears to be constant and independent of the oxidation temperature. The temperature range over which analyses for specific sulfur species were measured ranged from 10 to 44.5°C. At 40 and 44.5°C, the reaction rate is too rapid to monitor the intermediate thiosulfate and polythionate concentrations. Samples were taken and analysis for these species were performed near the end of the experiment. These data represent the final concentrations generated at these temperatures. These data points are also included in Figure 34 and can be seen to fall along the same line as predicted by experiments conducted at lower temperatures.

Effect of Catalysts on Sulfur Speciation. The oxidation of homogeneous solutions of both ferrous iron and sulfide is catalyzed by the presence of several transition metals. The catalytic activity appears to be related to the ability of the metal to participate in one-electron exchange reactions. The metals selected for this study include nickel, copper, silver, and cadmium. The catalytic activity of various metals towards the oxidation of sulfide is discussed earlier.

Nickel is the only metal investigated which demonstrated any catalytic activity. When nickel is present in alkaline solutions of sulfide, it results in a shift towards the formation of elemental sulfur as an end product rather than the formation of sulfur oxyanions of higher oxidation.

The ferrous sulfide to be oxidized was resuspended in a 5×10^{-5} M solution of NiSO_4 . Nickel forms a very insoluble sulfide. The nickel is believed to adsorb onto the surface of the existing ferrous sulfide particles. This approach is used to insure a uniform distribution of nickel over the surface. This method of preparation also allows ferrous sulfide with similar particle size, surface areas, and degree of crystallinity to be used, thereby allowing a comparison of results in the presence and absence of nickel.

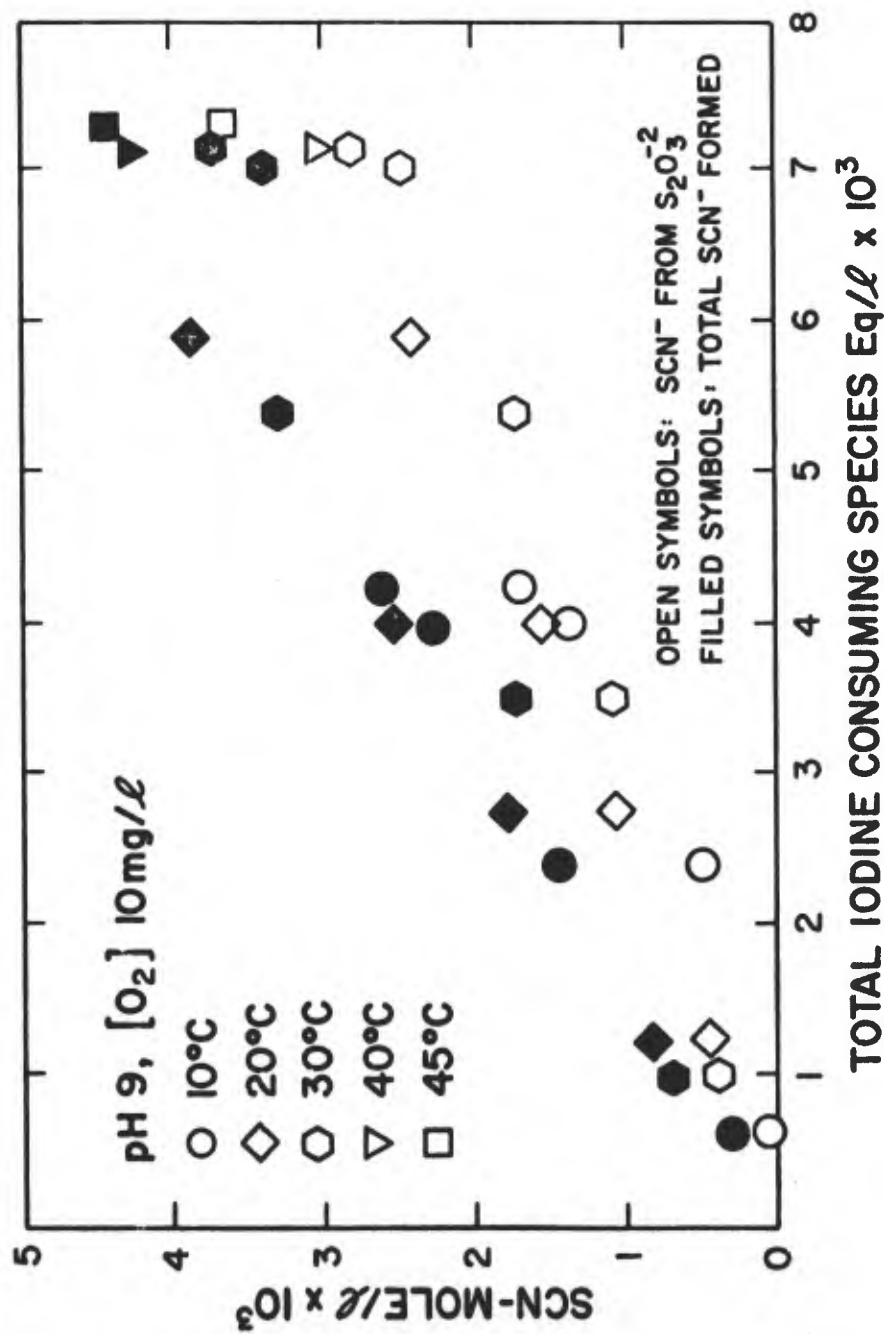


Figure 34. The relationship between soluble sulfur species and equivalents of iodine-consuming species produced for the oxidation of FeS(s) between 5 and 44.5°C.

As discussed earlier, the presence of as little as $5 \times 10^{-5}M$ nickel significantly increases the rate of oxidation at both pH 7 and 9.

At pH 7, elemental sulfur is the end product of the oxidation of sulfide in both the presence and absence of nickel.

The presence of nickel during the oxidation of ferrous sulfide at pH 9 results in a decrease in the average oxidation state of the oxidation products of sulfide. The equivalents of protons produced per mole of ferrous sulfide oxidized during the oxidation of ferrous sulfide by dissolved oxygen in the presence and absence of nickel is shown in Figure 35. There is a significant reduction in the ratio of protons produced per mole of ferrous sulfide oxidized in the presence of nickel. This is consistent with the formation of a higher percentage of elemental sulfur from the oxidation of sulfide. There is also a similar decrease in the ratio of equivalents of iodine-consuming species produced per mole of ferrous sulfide oxidized.

The presence of nickel does not appear to affect the speciation of the soluble sulfur oxyanions--only the percentage of sulfur which is oxidized past elemental sulfur. The species produced and their concentrations relative to each other appear to be independent of the presence of nickel. This is illustrated graphically in Figure 36 by the similarity in the relationship between the production of hydrogen ions per equivalent of iodine-reactive species produced in the presence and absence of nickel.

The presence of nickel directly catalyzes the oxidation of ferrous sulfide. It is not clear whether its influence upon the products of sulfide oxidation is direct. The oxidation proceeded much more rapidly in the presence of nickel, just as it does when the dissolved oxygen concentration is raised from 10 mg/l to 43 mg/l. The shift in sulfur oxidation products towards elemental sulfur may simply reflect the response of different oxidation mechanisms to an increase in the rate of formation of an intermediate specie.

The experimental results are consistent with an interpretation of this type. An increase in the oxygen concentration from 10 to 43 mg/l or the presence of $5 \times 10^{-5}M$ nickel and an oxygen concentration of 10 mg/l both result in an increase in the rate of oxidation by a factor of four. They also result in a decrease in hydrogen ions produced per mole of ferrous sulfide oxidized of 31 and 45 percent, respectively.

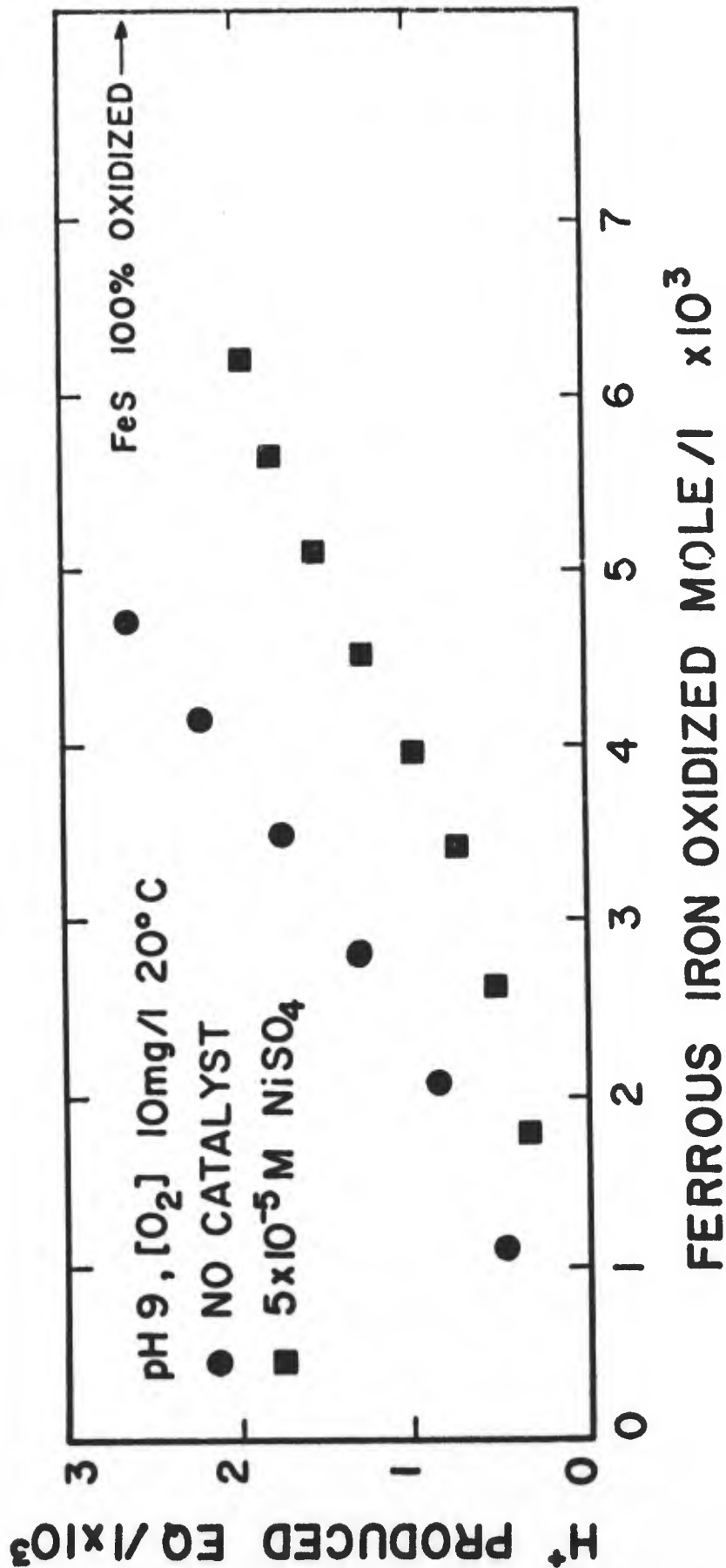


Figure 35. Formation of hydrogen ions as a function of the concentration of $FeS(s)$ oxidized in both the presence and absence of nickel.

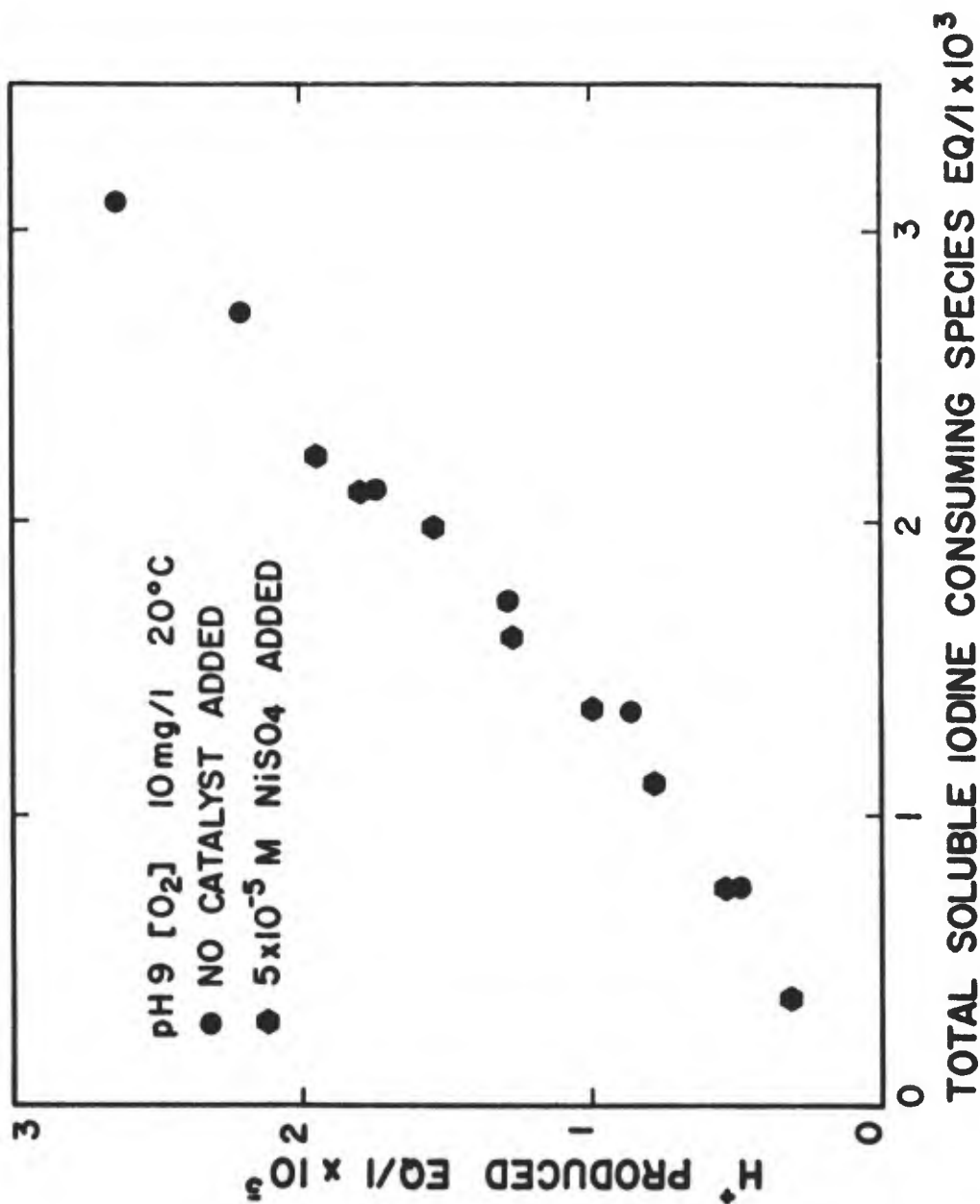


Figure 36. Equivalents of hydrogen ions liberated as a function of iodine-consuming species formed during the oxidation of FeS(s) at pH 9 in the presence and absence of nickel.

Ionic Medium and Chloride. The majority of the experiments were conducted in a dilute solution of sodium sulfate, usually on the order of 5×10^{-4} to 10^{-3} molar. The sulfate is present as a supporting electrolyte in the stock ferrous sulfide suspensions during preparation to enhance the settling of ferrous sulfide particles. Sulfate serves adequately as an inert electrolyte, as demonstrated by the minimal influence of sulfate concentration on the oxidation rate.

The influence of variations in the concentration of both sulfate and chloride upon the rate of oxidation of ferrous sulfide has been discussed.

At pH 7, the presence of chloride inhibits the oxidation of ferrous sulfide, particularly at the higher concentrations. The oxidation of ferrous sulfide at pH 7 leads to the formation of elemental sulfur under all experimental conditions investigated.

The effect of ionic strength and chloride concentration upon the oxidation of ferrous sulfide at pH 9 was investigated. Neither the composition of the aqueous media nor the presence of chloride appear to affect the rate of oxidation of ferrous sulfide. This is in contrast to the observations at pH 7. The presence of 0.1M sodium chloride has a significant effect upon the sulfur products formed at pH 9, however. Chloride inhibits the oxidation of sulfide to oxidation states higher than elemental sulfur. Elemental sulfur becomes the dominant sulfur species produced when 0.1M chloride is present during oxidation. The effect of chloride upon the soluble sulfur species produced and their relative proportions provides insight into the mechanisms involved in the formation of the various sulfur products. The same approach is used to monitor changes in soluble sulfur species produced and the proportions of each species as discussed earlier.

The hydrogen ions produced during the oxidation of ferrous sulfide in the presence and absence of chloride are shown in Figure 37. The oxidation of sulfide to oxidation states greater than elemental sulfur results in the formation of an excess of hydrogen ions. The number of hydrogen ions released increases with increasing final oxidation state. The number of hydrogen ions produced per mole of ferrous sulfide oxidized drops radically when chloride is present during the oxidation. This suggests that the average oxidation state of the sulfur which has been oxidized has dropped substantially and is very close to elemental sulfur. The oxidation of ferrous

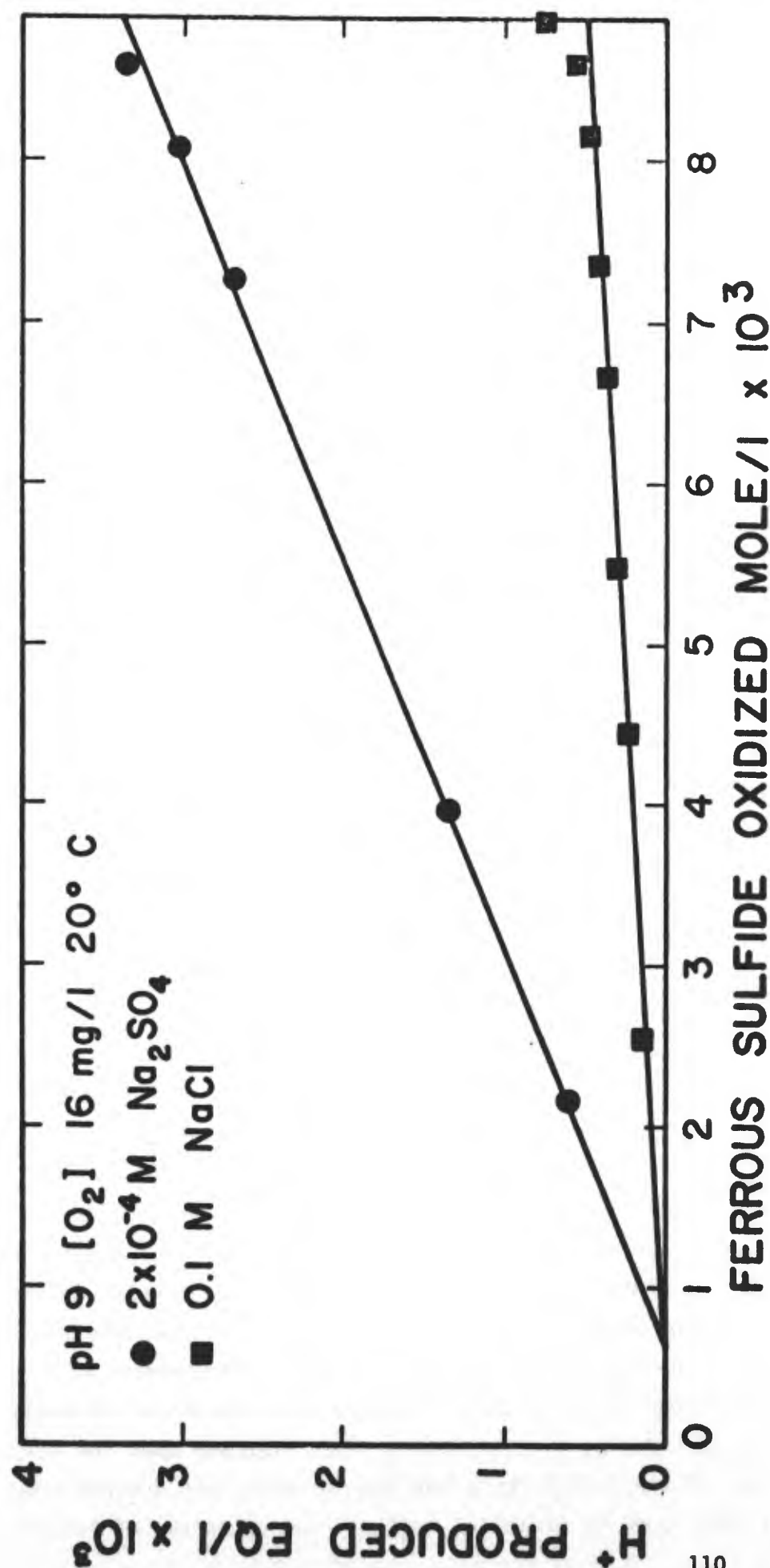


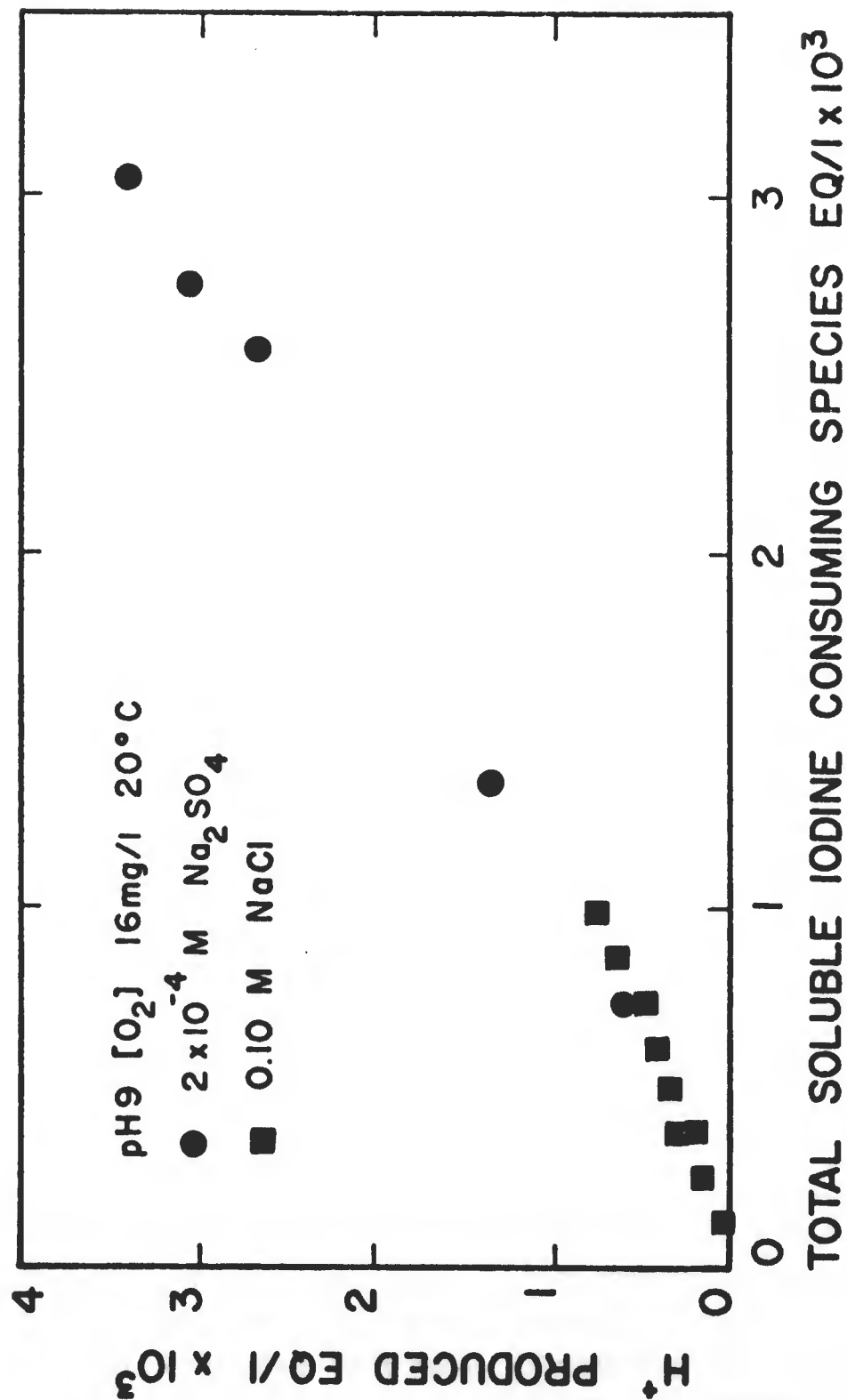
Figure 37. Equivalents of hydrogen ions liberated as a function of FeS(s) oxidized during oxidation at pH 9 in 2 x 10⁻⁴M Na₂SO₄ and 0.10M NaCl.

sulfide to elemental sulfur and ferric hydroxide does not liberate any hydrogen ions. A similar reduction in the number of equivalents of iodine-consuming species per mole of ferrous sulfide oxidized is also observed.

The equivalents of hydrogen ions produced per equivalent of iodine-consuming species produced during the oxidation of ferrous sulfide in the presence and absence of chloride are shown in Figure 38. Considerably more sulfide is oxidized past elemental sulfur in the absence of chloride, so the magnitude of the concentrations of both hydrogen ions and soluble iodine-consuming species produced is much greater than when chloride is present. The ratio of the two parameters provides a means of comparing the soluble products produced in both experiments. The results have some scatter due to the inherent error in determining such small differences in iodine-reactive species produced in the presence of chloride. More hydrogen ions per equivalent of iodine-consuming species appear to be produced in the absence of chloride. This indicates that the average oxidation state of the soluble sulfur species produced when chloride is present is slightly lower than when it is absent.

Speciation of the sulfur oxyanions formed during the oxidation process was determined. The concentration of thiosulfate and the total number of moles of thiocyanate formed during the cyanolysis of thisulfate and other cyanide reactive species are shown in Figure 39 as a function of the equivalents of soluble iodine-consuming species produced. There is reasonably good agreement between the various ratios, which suggests that the distribution of soluble sulfur species produced is similar in both the presence and absence of chloride. Chloride reduces the percentage of sulfide oxidized past elemental sulfur but does not appreciably affect the relative proportions of soluble species. Results of analysis of soluble sulfur species and elemental sulfur produced in the presence and absence of chloride are shown in Table 9.

The presence of colloidal sulfur interferes with the determination of trithionate because it also forms thiocyanate and is determined as trithionate. The data in Table 9 are reduced assuming that the thiocyanate formed came from trithionate and elemental sulfur, respectively. In addition, the concentration of hydrogen ions produced and iodine-consuming capacity of the species produced are calculated and compared with the experimentally determined concentrations (Table 9). In general, the calculated sulfur concentration exceeds



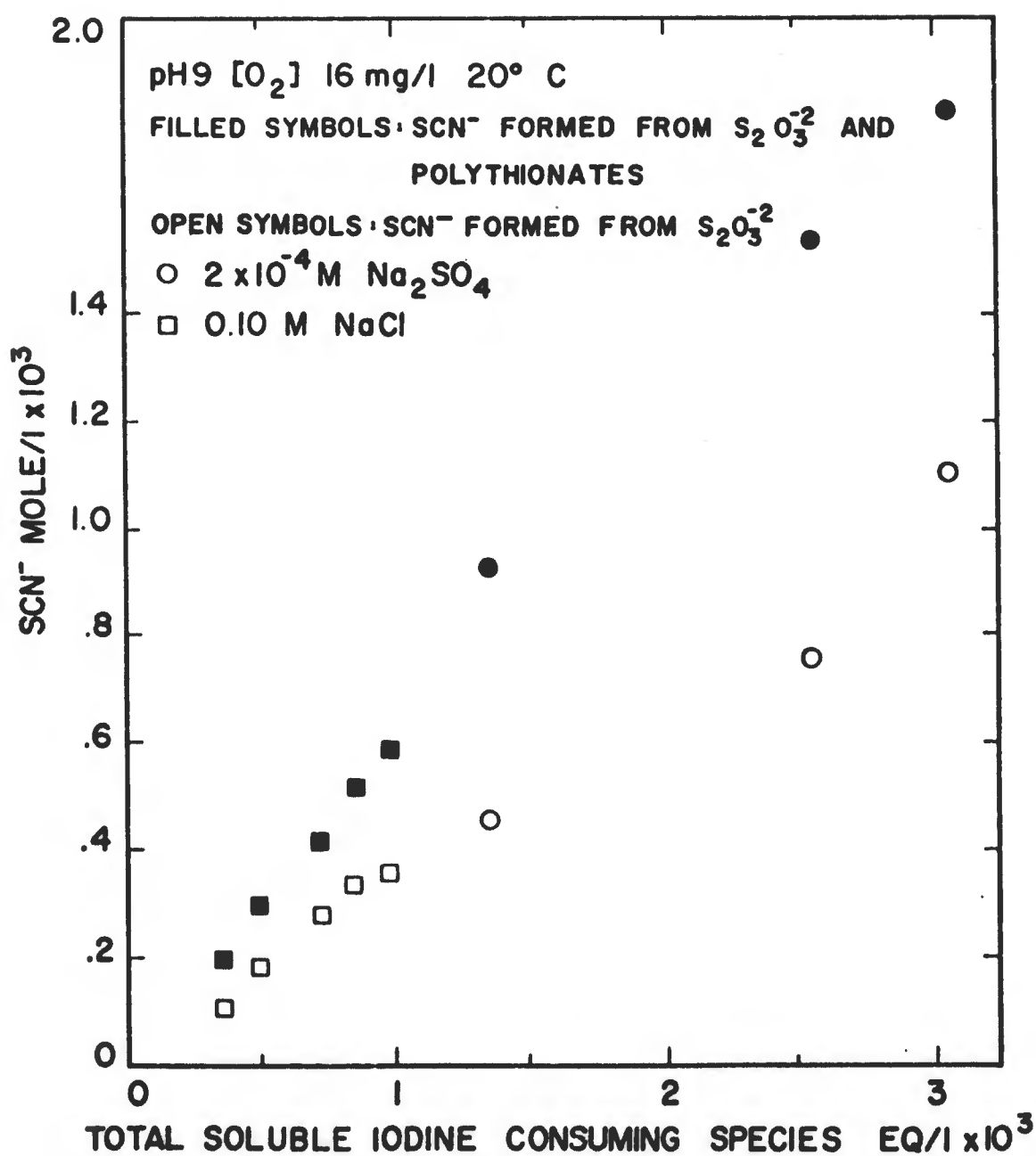


Figure 39. Thiocyanate formed as a function of total soluble iodine-consuming species including polythionates and S₂O₃⁻².

TABLE 9. SULFUR MASS BALANCE ASSUMING THIOCYANATE FROM SLOW CYANOLYSIS OF (1) $S_3O_6^{2-}$, (2) Colloidal S^0

pH	[O ₂] mg/l	Tempe- rature °C	NaCl mole/l	S ⁰ * Determined	Assumes $S_3O_6^{2-}$ Formation			Assumes S ⁰ Formation	
					$\frac{\sum S \text{ found}}{\sum S \text{ added}}$	$\frac{H^+ \text{ calc.}}{H^+ \text{ found}}$	$\frac{I_2 \text{ found}}{I_2}$	$\frac{\sum S \text{ found}}{\sum S \text{ added}}$	$\frac{H^+ \text{ calc.}}{H^+ \text{ found}}$
9	10	20	No	No	1.15	1.36	0.41	0.86	0.95
9	10	30	No	No	1.23	1.19	0.39	0.95	0.87
9	10	30	No	No	0.92	1.0	0.35	0.84	0.90
9	10	10	No	No	0.69	1.31	0.46	0.51	1.06
10	10	20	No	No	1.39	1.21	0.29	0.97	0.74
9	16	20	3×10^{-2}	3.76×10^{-3}	1.24	1.18	0.43	1.02	0.78
9	16	20	0.60	7.81×10^{-3}	0.95	1.27	0.22	0.94	1.0
9	16	20	0.1	No	0.12	1.47	0.38	0.10	1.16

*Note: Elemental sulfur analysis was not performed on many of the samples. The formation of S⁰ does not liberate protons.

the amount added, and the calculated hydrogen ion concentration released exceeds the actual amount released. The calculated iodine-consuming capacity of the species produced is consistently lower than the actual equivalents of iodine consumed experimentally.

Formaldehyde. Aldehydes react with sulfur ions and acids with direct S-H links. The chemistry of this reaction is discussed in Section II. Sulfur species, with which formaldehyde reacts, include: bisulfite (HSO_3^-), sulfoxylic acid (H_2SO_2), thiosulfurous acid ($\text{H}_2\text{S}_2\text{O}_2$), and dithionous acid ($\text{H}_2\text{S}_2\text{O}_4$).

The soluble oxidation products formed during the oxidation of ferrous sulfide at pH 9 were analyzed for their capacity to consume iodine in the presence and absence of formaldehyde. Formaldehyde showed no effect on the iodine-consuming capacity of the solution.

The oxidation of ferrous sulfide was conducted at pH 9, 20°C, and $5 \times 10^{-4}\text{M}$ Na_2SO_4 in the absence and presence of 0.377M (1.13% V/V) formaldehyde. The presence of formaldehyde during the oxidation of ferrous sulfide should compete for intermediate sulfur species, blocking or inhibiting the formation of some oxidation products and altering the distribution of end products normally observed.

The presence of formaldehyde had no effect upon the rate of oxidation of ferrous sulfide. The presence of formaldehyde did alter the composition of the soluble sulfur species produced significantly. The concentration of hydrogen ions produced in the presence of formaldehyde increased, indicating that the average extent of oxidation of soluble sulfur species had increased. The concentration of iodine reactive species produced dropped by roughly one-third suggesting that either their formation had been prevented or that their subsequent reaction with formaldehyde resulted in a product which is non-iodine reactive.

Analyses for specific sulfur species were also performed. The presence of formaldehyde reduced the formation of thiosulfate by over 50%. Higher polythionates or colloidal elemental sulfur could not be determined because formaldehyde reacts with cyanide under the alkaline conditions required for their cyanolysis.

The results demonstrate that the mechanism responsible for the differentiation of sulfur into the products observed is at least one step after the initial oxidation step.

Discussion of Sulfur Speciation

Sulfur Speciation. The sulfur oxidation products formed during oxidation of FeS are operationally divided in two classes. These are termed filterable elemental sulfur and soluble sulfur species. The latter class includes all soluble sulfoxyanions and any colloidal sulfur which passes through a 0.05- μ m filter. The final distribution of sulfur between these two classes is sensitive to the experimental conditions. The distribution of specific species in the soluble phase is determined by specific analysis for species and comparison of different properties including hydronium ion production and iodine-consuming capacity. The investigations demonstrate that the distribution of sulfur species in the soluble phase appears to be relatively consistent and insensitive to variations in experimental conditions. The presence of both chloride and formaldehyde have major and opposite effects upon the distribution of sulfur between elemental sulfur and soluble species, yet have no effect upon the rate of oxidation of ferrous sulfide. From this it can be inferred that either the two classes of end products occur by parallel pathways or that the point in the overall mechanism where the differentiation in end products occurs is at least one step past the rate-controlling step in the oxidation of ferrous sulfide.

The manner in which the experimental data are presented and correlations are drawn provides a useful means of comparing results from different experiments without having to know the exact composition or speciation of the respective tests.

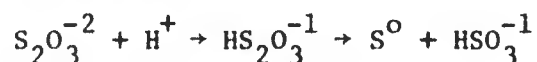
Throughout the results there is an apparent inconsistency which is manifested in the poor quantitative correlation between iodine-consuming capacity calculated based upon concentrations of specific sulfur species and the experimentally measured iodine consumption. The equivalents of iodine-consuming capacity calculated from the measured thiosulfate concentration is always lower than the experimentally observed iodine consumption. Typically the calculated value is on the order of 40% of the actual consumption.

Under the experimental conditions present, only sulfide, polysulfides, thiosulfate, and sulfite should be oxidized by iodine. (Dithionite $S_2O_4^{2-}$ is oxidized to SO_4^{2-} by iodine, or converted to SO_3^{2-} in acidic solution. Dithionite, however, is so susceptible to oxidation by oxygen it should not be present. Metabisulfite $S_2O_5^{2-}$ is also oxidized by iodine but should not be present due to its hydrolysis to SO_3^{2-} .) Sulfite reacts rapidly with oxygen

and is not stable enough to exist for the extended periods observed during and after the oxidation experiments. Sulfite also does not undergo cyanolysis, which would make it difficult to account for the correlation between iodine consumption observed and formation of thiocyanate.

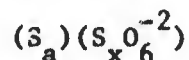
Sulfite is readily oxidized by iodine. However, treatment of sulfite solution under alkaline conditions with formaldehyde converts the sulfite to a non-reactive species. Experiments based upon this approach demonstrate that sulfite is not responsible for the unaccounted for iodine consumption. Formaldehyde also reacts with and alters the reactivity of other sulfur species with II-S bonds. Analysis of filtered samples for sulfide and polysulfide using methylene blue does not indicate the presence of either. Neither sulfide nor polysulfide is stable in a reacting system of this nature and should rapidly react with the ferric iron or dissolved oxygen. Polysulfides would liberate thiocyanate upon cyanolysis, however, and are precursors to thiosulfate and polythionate formation in alkaline solutions. This eliminates all of the sulfur species which are known to be iodine reactive as possible explanations for the discrepancy.

The analytical technique for the determination of thiosulfate was first believed responsible for the discrepancy. Thiosulfate is unstable under acidic conditions and decomposes according to



The procedure was evaluated in detail, and this possibility was positively eliminated. The presence of γ -FeOOH does not catalyze the decomposition. Ferric iron does oxidize thiosulfate to tetrathionate, but this reaction would tend to reduce the measured consumption of iodine. The presence of polythionates and colloidal elemental sulfur as reaction products in the filtrate has been established. The results of mass balances performed upon the sulfur species produced during the oxidation of ferrous sulfide at pH 9 and 10 are reported earlier. Thiosulfate and colloidal elemental sulfur are tentatively identified as the principal forms of sulfur in the "soluble" phase under these conditions.

The formation of stable sulfur sols is relatively common. Tetra- and higher polythionates are reported to stabilize sulfur sols (Urban, 1961d). The sol is described by the general formula



The average number of sulfur atoms in the formula $(a + x)$ has been reported to range from 15 to 140, while Urban (1961c) found an average of 17 in his suspensions. The average number of sulfur atoms $(a + x)$ per six oxygens decreases with aging. Urban (1961c) does not make it clear whether this is due to oxidation of elemental sulfur or precipitation from suspension of larger particles which lower the sulfur/oxygen ratio.

The very low number of hydrogen ions measured during the formation of the unidentified iodine-reactive sulfur species is consistent with the formation of elemental sulfur rather than sulfur species of higher oxidation state. The theoretically calculated capacity of the filtrate containing thiosulfate, polythionate and elemental sulfur to consume iodine must still be reconciled with the actual consumption observed. Both colloidal elemental sulfur and polythionate react with cyanide under alkaline conditions to form thiocyanate. A very good experimental correlation between the equivalents of iodine consumed and the concentrations of thiosulfate and thiocyanate (formed upon cyanolysis of the solution) was found. The correlation between the respective measurements suggests that they are related. During the oxidation of ferrous sulfide at pH 9, the concentrations of thiosulfate, thiocyanate formed upon cyanolysis, and equivalents of iodine consumed were measured as a function of time. The relative rates of formations for all three were the same (Figure 40). The oxidation was essentially complete after 560 minutes at pH 9. At this point the pH was allowed to drift overnight and shifted from 9 to 7.8. The equivalents of iodine-consuming capacity of the solution dropped substantially overnight at this lower pH. The concentration of thiocyanate formed upon cyanolysis also dropped to about 20% of its concentration after 560 minutes of oxidation. The thiosulfate concentration rose slightly and comes close to accounting for all of the remaining iodine-consuming species. Two explanations can be offered to account for this. The presence of polythionates or colloidal elemental sulfur alters the stoichiometry of the reaction of thiosulfate with iodine. This would result in the abnormally high iodine consumption. Samples were analyzed after adding known additions of thiosulfate to the samples. The results eliminate an alteration of the thiosulfate-iodine reaction stoichiometry as a possibility.

As a second explanation, the possibility that colloidal elemental sulfur is being oxidized must be considered. Support for the conclusion that colloidal elemental sulfur is responsible for the iodine consumption is

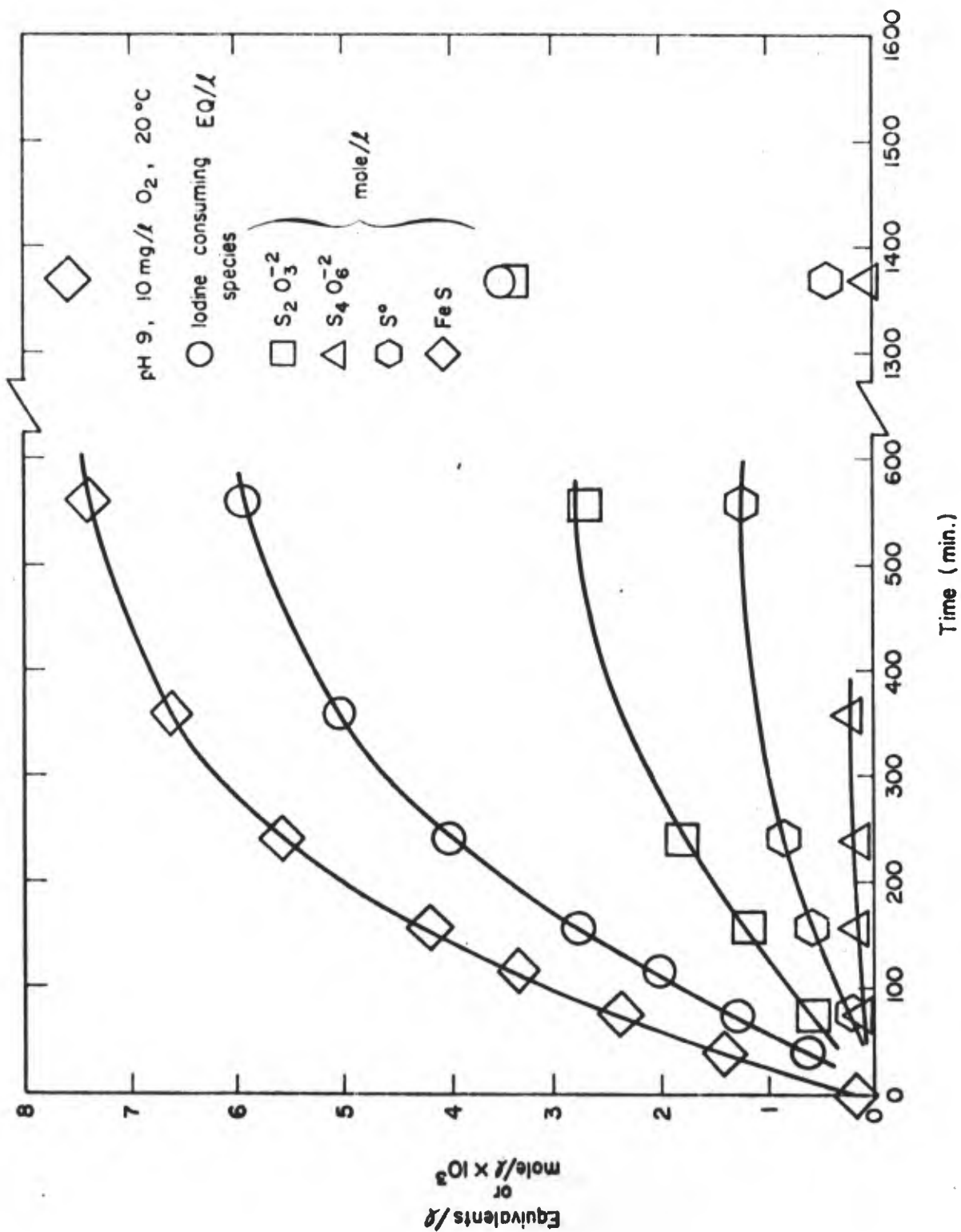


Figure 40. Relationship between the concentrations of polythionates, thiosulfate, and iodine-consuming species as a function of time of oxidation at pH 9.

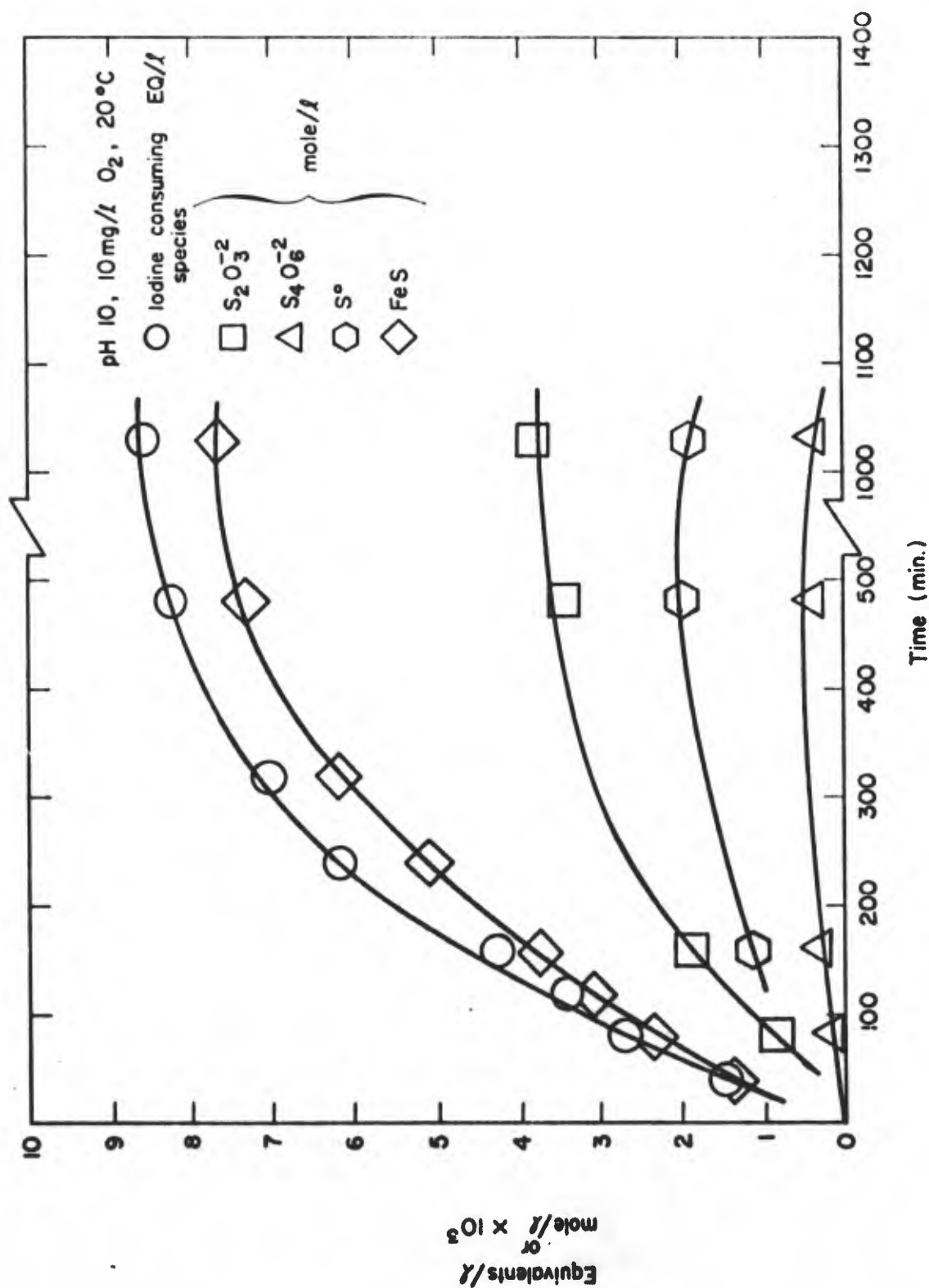


Figure 41. Relationship between the concentrations of polythionates, thiosulfate, and iodine-consuming species as a function of time of oxidation at pH 10.

contributed by the results of other oxidation experiments. The concentrations of thiosulfate, thiocyanate formed upon cyanolysis, and iodine consumption during the oxidation of ferrous sulfide at pH 10 are shown in Figure 41. The oxidation of the ferrous sulfide was essentially completely oxidized after 480 minutes. The suspension was maintained at pH 10 for an additional 600 minutes (10 hours) and sampled again. The concentrations of all three species remained constant within experimental error. Similar results are obtained at pH 9 when the pH is not allowed to drift.

Polythionates are not stable under alkaline conditions due to hydrolysis. The general trend is to trithionate, thiosulfate, and ultimately sulfate. Polythionates become increasingly stable with decreasing pH. Therefore if polythionates were responsible for the iodine consumption, there should be a more rapid decrease in polythionate concentration and iodine consumption with time under the more alkaline conditions. This is contrary to what is observed.

Elemental sulfur is also most stable under acidic conditions and becomes increasingly thermodynamically unstable with increasing pH. Under alkaline conditions, it is gradually oxidized to thiosulfate, among other intermediates, and ultimately to sulfate. This would suggest that the concentration of colloidal sulfur should also decrease more rapidly with time with increasing pH. There are other factors which may also affect the concentration of colloidal sulfur, however. Decreasing the pH of the solution may destabilize the colloid and allow it to be filtered. This would remove it from the filtrate, eliminating its contribution to the total iodine consumption observed. A number of mechanisms by which the colloidal sulfur sol is stabilized can be postulated. Stabilization by polythionates has been mentioned. The possibility of a surface charge resulting from slow hydrolysis or oxidation upon the surface leading to the formation of charged sulfoxy groups on the surface could both stabilize the colloid and contribute to its iodine reactivity. The experimental results suggest that there is a much more direct relationship between the concentration of iodine reactive colloidal sulfur and thiosulfate than that they are merely formed at the same rate. There seems to be a relatively constant stoichiometry between the iodine-consuming species, the thiosulfate concentration, and the colloidal sulfur concentration as measured by thiocyanate formation. The ratio of total elemental sulfur formed to the concentration of thiosulfate formed is observed to vary widely. Yet the ratio of colloidal sulfur which passes through a 0.05- μ m filter to thiosulfate

formed appears to be relatively constant. This suggests that the thiosulfate is responsible for the stability of the colloidal elemental sulfur. The observation that the ratio is essentially constant over such a wide range of experimental conditions indicates that there is a fixed stoichiometry between thiosulfate and colloidal elemental sulfur. That is, thiosulfate associates with the colloidal elemental sulfur in a specific stoichiometry and is responsible for its stability.

The explanation for the iodine consumption unaccounted for lies in this complex. In this form, the elemental sulfur may alter the stoichiometry of the thiosulfate-iodine reaction, or the elemental sulfur itself may become iodine-reactive when associated with thiosulfate in this manner. Which, if either, of these explanations is correct has not been established. From a phenomenological point of view, the non-thiosulfate consumption of iodine is observed to vary with the concentration of colloidal sulfur passing the filter. The concentration of colloidal sulfur passing the filter varies as a function of the concentration of thiosulfate.

The decrease in iodine-consuming species with time observed under neutral pH conditions can be explained in terms of a decrease in the stability of the thiosulfate-sulfur complex. The sulfur sol is destabilized thus forming larger aggregates or particles which are filterable. The destruction of the thiosulfate-sulfur complex also results in a decrease in the capacity of the solution to consume iodine.

Oxidation Mechanisms. The initial reaction involves the interaction of molecular oxygen with a sulfur atom on the surface of the ferrous sulfide crystal. This interaction is the rate-controlling step which determines the overall rate of oxidation of ferrous sulfide. The differentiation of sulfur into the observed oxidation products is removed by at least one step from the initial rate controlling step in the oxidation of ferrous sulfide. The rate at which individual species are formed is dependent upon the rate that sulfide is oxidized and made available for further reactions at the surface of the iron sulfide. This is demonstrated in Figures 40 and 41 where the increase in concentration of each species with time is parallel to the concentration of ferrous sulfide oxidized with time.

The presence of chloride and formaldehyde during oxidation substantially alters the sulfur species formed yet has no effect upon the rate of oxidation of ferrous sulfide. This suggests that the differentiation of sulfur into

the observed end products is a function of the solution conditions and is removed by at least one step from the initial rate-controlling step in the reaction. A system as complex as the oxidation of ferrous sulfide is not suitable for determining the mechanism involved in the oxidation of sulfide to the various observed end products. The mechanisms involved in the homogeneous oxidation of sulfide are far from being resolved, despite the work which has been done on homogeneous systems to date. A better understanding of homogeneous sulfide oxidation mechanisms is a necessary prerequisite to understanding the mechanisms involved during the heterogeneous oxidation of sulfide in ferrous sulfide.

Summary and Conclusions

The formation of soluble sulfur species appears to be separated from the initial oxidation of ferrous sulfide by at least one step. The pH of the system during the oxidation is the single, most important parameter in determining the speciation of the sulfur oxidation products. Elemental sulfur is the predominant end product under neutral to acidic conditions. The products shift to soluble sulfoxyanions including thiosulfate, trithionate, and higher polythionates with increasing pH. The concentration of colloidal elemental sulfur varies directly as a function of the thiosulfate concentration formed. This suggests that the stability of the sulfur sol is due to its association with thiosulfate and that there is a fairly consistent stoichiometric relationship between the colloidal sulfur and thiosulfate concentrations. The distribution of species present in the filtrate or soluble fraction appears to be constant and relatively insensitive to experimental conditions.

Increasing temperature causes a greater percentage of the total sulfur present to be oxidized past elemental sulfur. Increasing oxygen concentration and the presence of catalysts decrease the extent of oxidation past elemental sulfur. This is believed to be due principally to the increased rate of oxidation of ferrous sulfide rather than a direct effect upon the reaction leading to the formation of higher sulfoxyanions. Concentrations of chloride on the order of tenth molar or greater severely inhibit the oxidation of sulfur past elemental sulfur. This observation has implications in the oxidation of estuarine sulfidic sediments.

The identify of the specie or species responsible for the consumption of iodine has not been determined incontrovertibly. The important observations,

with which the proposed species must be consistent, are summarized as follows:

1. The concentration of iodine-consuming species varies directly with the thiocyanate liberated from non-thiosulfate species.
2. The average oxidation state of the sulfur in the sulfur species responsible for the iodine consumption is very low. This is based on the liberation of hydrogen ions.
3. Formaldehyde does not interfere with the iodine reactivity of the non-thiosulfate iodine reactive species. This positively eliminates sulfite and metabisulfite as possible species. This also provides a basis for rejecting dithionite and thiosulfite.
4. The experimentally measured iodine consumption is consistently greater than that calculated from the concentration of thiosulfate present. This is not an artifact of the experimental technique but represents the consumption of iodine due to the presence of additional iodine-consuming species.

Release of Cadmium During Oxidation of FeS

The fate of heavy metals such as cadmium entrapped in sulfidic sediments is of particular interest when the oxidation of the sulfide material is considered. Both the rate and extent of release during the oxidation reaction is of interest.

A series of studies were undertaken to investigate the behavior of 1 percent mole fraction of cadmium associated with FeS during oxidation. Ferrous sulfide suspensions were prepared with cadmium associated in two different ways: (1) Cadmium adsorbed on prepared, aged FeS, and (2) CdS precipitated simultaneously with FeS. It has been determined that Cd(II) and Fe(II) do not form solid solutions to any significant extent at ambient temperatures (Framson and Leckie, 1977), thus the cadmium precipitated simultaneously with ferrous iron is in the form of CdS. No significant difference in behavior was noted between adsorbed Cd and Cd precipitated simultaneously with FeS. Table 10 gives results of desorption studies on the reaction products after oxidation for up to 12 hours (720 minutes).

Desorption of Cd was accomplished by lowering the pH by adding appropriate aliquots of HCl. After centrifugation total cadmium in solution was determined. Distribution of cadmium among solid reaction products or unreacted reactants was not determined. Although the data must be considered

TABLE 10. RELEASE OF CADMIUM AFTER OXIDATION OF Cd-ENRICHED FERROUS SULFIDE
1 percent mole fraction (cations) cadmium in FeS

Solution Conditions during Oxidation	Time of Oxidation, minutes	pH of Desorption	Solution Cadmium Concentration, $\mu\text{g/l}$
pH 7 [O ₂] 8 mg/l 20°C 1 x 10 ⁻⁴ M Na ₂ SO ₄	100	7.0	1.47
	100	5.0	155.
	720	6.4	5.5
	720	5.0	450.
pH 7 [O ₂] 8 mg/l 20°C 0.1M NaCl	720	6.4	276
	720	5.0	650
pH 9 [O ₂] 16 mg/l 20°C 1 x 10 ⁻⁴ M Na ₂ SO ₄	720	9.0	-*
	720	5.0	89
	720	4.0	848
	720	3.0	1717
pH 9 [O ₂] 16 mg/l 20°C 0.1M NaCl	0	9	< 0.5
	0	5	< 0.5
	0	4	< 0.5
	0	3	1.5
	720	9	1.8
	720	5	1.8
	720	4	> 1600
	720	3	4500
* Analysis not valid.			

only as a first estimate of the redistribution of cadmium during oxidation of FeS, it is nevertheless very useful.

Time of Oxidation. Data for oxidation at pH 7 (Table 10) indicate that continued oxidation after all FeS has been oxidized (~ 2 hours) results in additional cadmium release when the iron oxyhydroxide is treated with acid to pH 5. Presumably this is a result of continued oxidation of cadmium sulfide remaining in the system.

Effect of Chloride. The effect of chloride upon the desorption of cadmium from reaction products is to increase the quantity of cadmium mobilized. Increased desorption of Cd in chloride solutions occurs at both pH 7 and 9. The presence of 0.1M NaCl increases the Cd desorbed at pH 5 almost 2.5 times when oxidation occurs at pH 9, as compared to an increase of about 1.5 for similar conditions when oxidative occurs at pH 7. The cadmium released to solution in the presence of chloride is most likely as chloride complexes. Since CdS solubility at pH 5 is negligible (verified by laboratory experiments), the cadmium released from the γ -FeOOH at pH 5 is probably adsorbed at the surface of the iron oxyhydroxide. Further interpretation requires additional detailed studies to investigate the mechanism of release and the form of the desorbed cadmium.

Oxidation Kinetics of Natural Sediments

Oxidation kinetics have been studied on anoxic sediment samples from India Basin, San Francisco Bay, California. The sediment samples were taken in the intertidal zone and pertinent physical-chemical characteristics are given in Table 11. These sediment samples are typical anoxic sediment materials in the intertidal zone of San Francisco Bay.

The oxygenation of real sulfidic estuarine sediments has been studied so that comparison can be made with the detailed experimental work on synthetic ferrous sulfides. Real sediments, of course, are considerably more complex than synthetic FeS, having organic matter and living biota.

The experimental procedures used with real sediment materials were essentially the same as those used with synthetic FeS. Data for the kinetics of oxidation for 89 gm wet sediment at pH 8.5 and 8 mg/l dissolved oxygen are given in Figure 42. During the oxidation samples were taken periodically and analyzed for both ferrous iron and iodine-consuming species. The total

TABLE 11. CHARACTERIZATION OF INDIA BASIN SEDIMENTS

Site Station	Total* Iron mg/kg	Acid* Soluble Iron mg/kg	Acid* Soluble Sulfide mg/kg	Percent Solids ($\frac{\text{dry wt}}{\text{wet wt}} \times 100$)	Percent Organic (wet wt)
1	2.28×10^4	5.83×10^3	248	51.8%	1.336
	2.20 "	5.87 "	496	52/5	1.321
2	2.11 "	7.27 "	1072	47.5	1.449
	2.25 "	7.59 "	1083	48.9	1.436
3	2.09 "	7.10 "	651	47.0	1.549
	2.04 "	7.10 "	1397	47.8	1.537
4	1.92 "	6.31 "	675	45.8	1.370
	1.98 "	7.04 "	396	45.8	1.354
	-	-	591	44.5	1.349
	-	-	588	-	-
Mean	2.11×10^4	6.76×10^3	719.7	47.95%	1.418
Standard Deviation	0.128 "	0.67 "	354.8	2.43	0.087
Mean**	2.12×10^4	7.27×10^3	1050.75	47.83%	1.493
Standard Deviation	0.090 "	0.23 "	306.	0.67	0.055

* Expressed in mg/kg wet sediment.

** Stations 2 and 3 only.

Total Iron: 8 gms wet sediment are refluxed in 200 ml 6N HCl 25 minutes.

Acid Soluble Iron: 8 gms wet sediment are suspended in 300 ml of 1:50 H₂SO₄, aerated and mixed 2 hours, filtered and analyzed for total soluble iron.

Acid Soluble Sulfide: 9 to 40 gms of wet sediment are suspended in 300 ml deaerated 1:50 H₂SO₄ under nitrogen. Nitrogen is bubbled through suspension while mixing, then passed through zinc acetate to trap sulfide released.

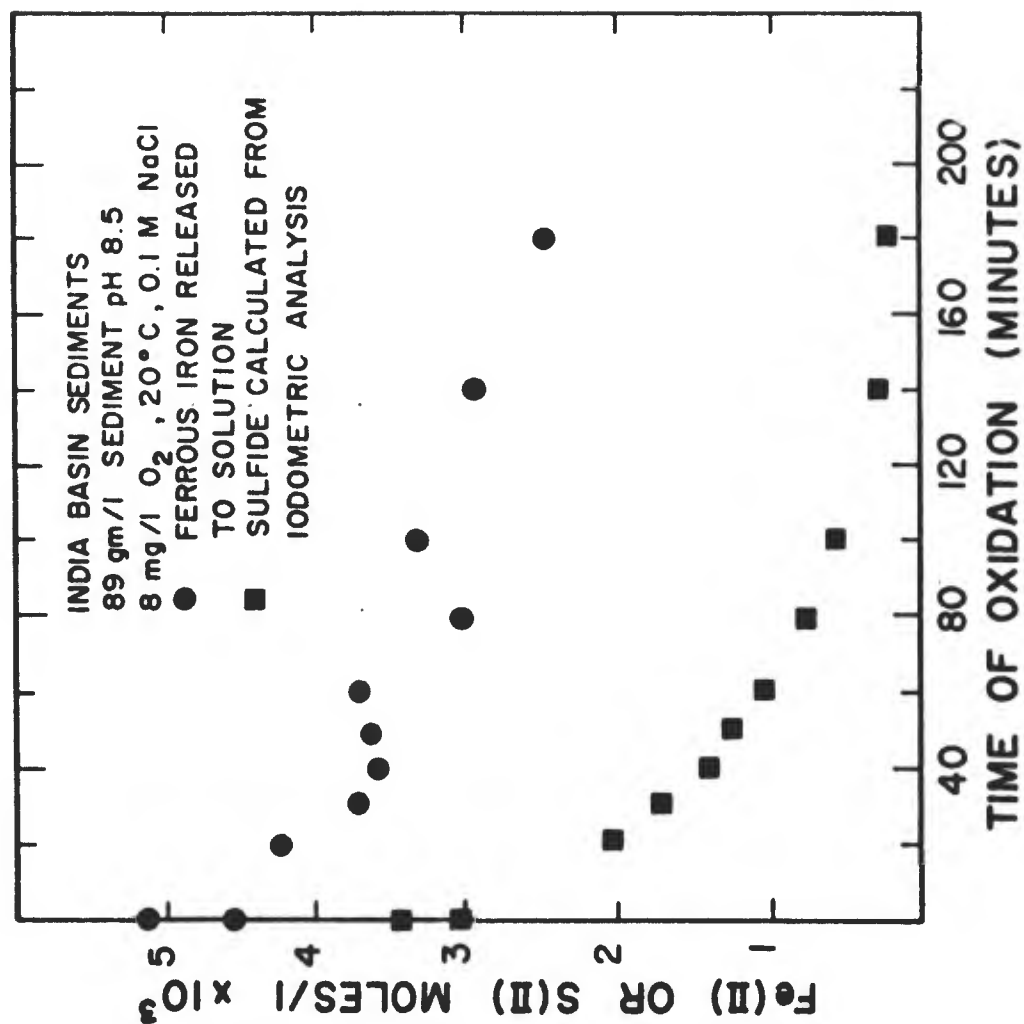


Figure 42. Oxidation of natural estuarine sulfidic sediments as a function of time. $Fe(II)$ and $S(-II)$ disappear with time.

concentration of ferrous iron is always significantly larger than the concentration of sulfide by approximately a constant amount. Since the total iron concentration in the sediment materials far exceeds the sulfide concentration, it indicates the presence of iron sources other than ferrous sulfide. Analysis indicates that a second source of ferrous iron was present, possibly ferrous carbonate. When the constant excess ferrous iron is subtracted from the total measure, the concentrations of ferrous iron and sulfide show the correlation expected (Figure 43).

The shape of curve describing the rate of oxidation of ferrous sulfide in natural sediments (Figure 43) at pH 8.5 is very similar to the equivalent type of data for synthetic FeS. In addition, the reaction is completed in approximately 160 minutes, comparing very well with 180-200 minutes for synthetic systems at pH 9. A more quantitative comparison requires information on surface area and presence of catalytic or inhibitory agents in the real system. No soluble iodine-consuming species or hydrogen ions were formed during the reaction, indicating that elemental sulfur is the major sulfur reaction product. This is in good agreement with observations on synthetic FeS systems in the presence of 0.1M NaCl at pH 9.

Discussion of Kinetic Results and Models

The objectives of the discussion are threefold. First, possible reaction mechanisms are discussed in terms of the observed experimental results. Mechanisms which are inconsistent with experimental observations have been rejected. Second, the discussion relates the theoretical model developed to experimentally observed results. Finally, the kinetic expression predicted from the theoretical mechanism is quantified using experimental results.

A number of general reaction mechanisms describing heterogeneous reactions between a species in solution and a solid phase have been developed in the literature. With the exception of a dissolution-controlled reaction, all of the mechanisms have the same general processes, or steps, in common. The relative speed of each of the steps in relation to the speed of the other steps determines which process controls the rate at which the overall reaction occurs. This, in turn, determines the form of the kinetic expression describing the reaction rate and how various parameters affect the

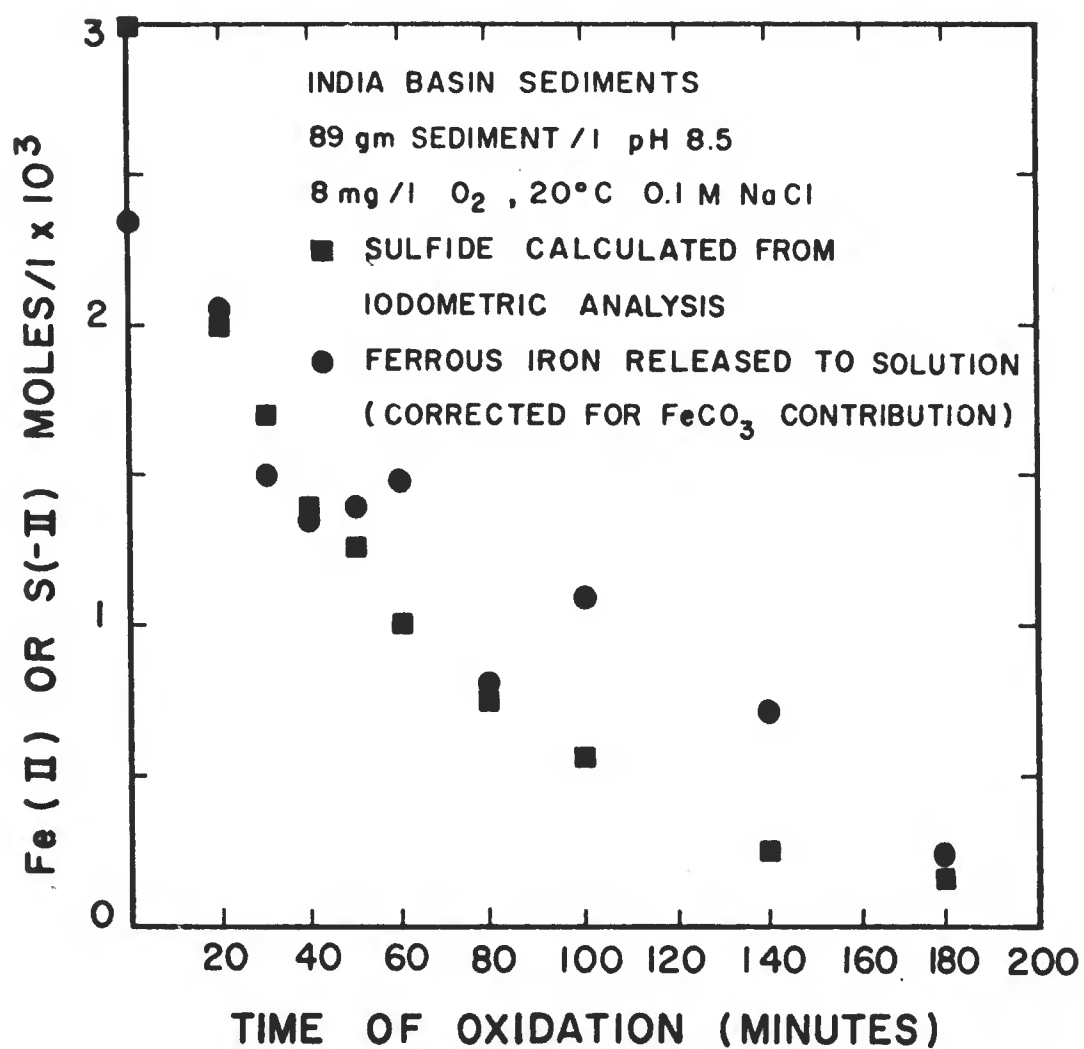


Figure 43. Oxidation data for natural estuarine sulfidic sediments corrected for $Fe(II)$ from $FeCO_3(s)$.

rate of oxidation. The experimental parameters chosen and the ranges over which they were investigated, were selected to provide an experimental basis for developing an appropriate mechanistic model, for differentiating between models, and to adequately cover significant ranges of natural conditions.

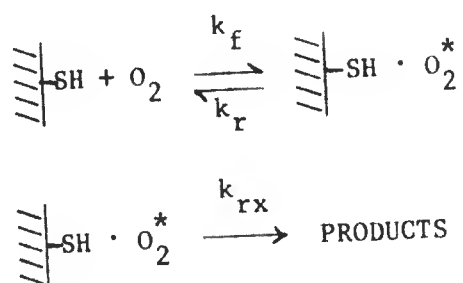
The rate of oxidation is predicted to be a function of both the dissolved oxygen concentration and surface area of ferrous sulfide by the kinetic expressions describing both diffusion-controlled and surface chemical reaction-controlled processes. Diffusion-controlled models have the appropriate form to explain the rate dependence on surface area and oxygen concentration. However, the activation energy of 15.5 Kcal is much too large for a diffusion-controlled mechanism, typically ≤ 6 Kcal (Glasstone et al., 1941). Increased turbulence had no measureable effect upon the rate of oxidation. The small particle size of FeS used ($\sim 2000 \text{ \AA}$) minimizes the significance of this observation as a test of diffusion-limited mass transport. The presence of Ni(II) on the surface of the ferrous sulfide significantly catalyzed the rate of oxidation. Since the presence of nickel on the surface should not affect the flux of oxygen to the surface, a solution-mass transport mechanism cannot be the rate-limiting process.

With the exception of a dissolution-controlled model, all other pertinent models are dependent upon a reaction step involving the interaction of oxygen with the solid FeS surface. A number of transport and reaction steps must occur in the overall oxidation reaction. Oxygen must first diffuse to the surface. Once at the surface, oxygen must attach to the surface in some manner. Either in the initial attachment step or in a subsequent step a rearrangement of the bonding in the oxygen molecule must occur, with a transfer of electrons from the sulfur to the oxygen. This step may also require participation of additional species such as free protons. Subsequent reaction steps may occur at the surface. Finally, the reaction products must diffuse to the bulk solution. The reaction between oxygen and sulfide on the surface of FeS can be modeled by a sequence of steps which include adsorption of oxygen onto a surface sulfide site, followed by a molecular rearrangement, and terminating in the oxidation reaction giving products.

This is a very general statement of the kinetic model. More than one detailed reaction sequence can be proposed for each step in the general reaction model. However, all yield similar kinetic expressions describing the rate

of reaction. Experimental data from the limited types of reactions conducted in this study, in general, do not allow detailed elucidation of the reaction mechanism. For example, how the oxygen-oxygen bond is broken or the nature of the species participating in the electron exchange between sulfur and oxygen cannot be determined from a study of this type. Only the general reaction steps and the rate at which each step occurs can be determined. Therefore, the proposed mechanistic model is presented at a low detail level.

In the absence of chloride, and at a given pH the sequence of events leading to oxidation can be described by the following sets of reactions.



The asterisk (*) denotes an activated state or complex.

The first reaction is a generalized form and represents one or more reversible steps which occur prior to the final rate-controlling step. The kinetic expression which evolves from this mechanism is

$$\frac{d[\text{PRODUCTS}]}{dt} = \frac{k_{rx} k_a [\text{O}_2]}{k_a [\text{O}_2] + 1} \frac{S \cdot N}{V_R}$$

where

$$k_a = k_f / (k_r + k_{rx}),$$

S = total surface area present, a function of [FeS],

N = number of surface sites/unit area, and

V_R = volume of reactor.

From the last expression it is clear that the reaction rate is dependent upon the dissolved oxygen concentration at low concentration levels ($K[\text{O}_2] \leq 1$). However, as $K[\text{O}_2] \gg 1$ the rate of reaction is predicted to become independent of the dissolved oxygen concentration, thus being limited to the rate at which the activated surface complex reacts (this does not necessarily imply a saturated surface). Quantitative values for k_{rx} can be determined

at constant temperature in the oxygen-independent range of the reaction. Obtaining a second set of data in the oxygen-dependent range of the reaction allows determination of K or the ratio $k_f/(k_r + k_{rx})$. An alternate method for determination of these constants can be used when data at the higher dissolved oxygen concentrations are not available. At a given temperature k_{rx} is constant and if the rate of reaction is known at two different oxygen concentrations in the oxygen-dependent range, the ratio of the two rates (at the same temperature) will be

$$\frac{r_1}{r_2} = \frac{\left(\frac{k_{rx} k_f [O_2]_1}{k_f [O_2]_1 + k_r + k_{rx}} \right)}{\left(\frac{k_{rx} k_f [O_2]_2}{k_f [O_2]_2 + k_r + k_{rx}} \right)}$$

Rearranging yields

$$\frac{k_f}{k_r + k_{rx}} = \frac{1 - \frac{r_1 [O_2]_2}{r_2 [O_2]_1}}{[O_2]_2 \left(\frac{r_1}{r_2} - 1 \right)}$$

Thus a value for the ratio of the rate constants can be computed for data at constant temperature. Comparison of values of the ratio at significantly different temperatures provides insight into differentiating whether the adsorption step is near equilibrium ($k_r \gg k_{rx}$) or the values of k_r and k_{rx} are of similar magnitude. Since adsorption processes are typically exothermic, K should decrease with increasing temperature for the equilibrium system. Failure of K to decrease indicates the adsorption step is not at equilibrium.

The design of the experimental apparatus used in this study limits the maximum operating gas pressure to one atmosphere. The rate of reaction at one atmosphere partial pressure of oxygen limits the temperature range over which the rate of reaction can be determined to 15°C or less. The oxidation rate of ferrous sulfide was determined at 10°C and 15°C over a range of oxygen concentrations using partial pressures of oxygen up to one atmosphere. The experimental results are shown in Figures 10 and 11.

The relationships between reaction rate and oxygen concentration clearly deviates from linearity with increasing oxygen concentration as

predicted by the model. Values for k_a and k_{rx} were determined at both 10 and 15°C using the rates at the lowest and highest oxygen concentration. At 10°C, the value for k_a and k_{rx} are 0.951 atm⁻¹ and 2.06×10^{-6} l-m⁻²-min⁻¹, respectively. Upon substitution of these values into the rate expression, the rate of oxidation predicted by the theoretical expression can be calculated at any oxygen concentration. The theoretically predicted relationship between the rate of oxidation and oxygen concentration is represented by the solid line in Figures 10 and 11.

With increasing temperature, the rate of reaction at the higher oxygen concentrations becomes too rapid to measure with the available analytical techniques. In the lower oxygen concentration range, there is very little curvature in the graphical presentation of the rate of oxidation as a function of oxygen concentration. The curvature is of the same order of magnitude as the error in determination of the experimental rate. In this region, the rate appears to have roughly a first-order dependence upon oxygen concentrations.

The temperature dependence of the constants was determined using two pairs of points determined at 10°C and 15°C using the Arrhenius relationship. Values of k_{rx} and k_a were calculated for the reaction at 20°C based upon the response of the constants to temperature between 10° and 15°C. Determination of an activation energy from only two points, particularly when separated by only 5°C is to be regarded with some reservation. The purpose of the procedure here is solely to evaluate the capacity of the model to be extrapolated outside of the range of conditions actually considered. The solid line in Figure 44 represents the theoretical relationship between reaction rate and oxygen concentration predicted using the values of k_{rx} and k_a calculated from the data generated at 10° and 15°C. The open symbols are reaction rates determined experimentally at 20°C. The agreement between the theoretical and experimental results is quite good, considering the number of variables involved. Below 20°C the activation energy for the reaction is 10 Kcal.

Values of k_{rx} and k_a were calculated for temperatures up to 40°C using the values and temperature dependence of the constants determined at 10° and 15°C. An activation energy of 10 Kcal was calculated for the reaction rates predicted using the calculated temperature compensated rate constants. The rate-controlling reaction appears to change around 20°C, and the activation

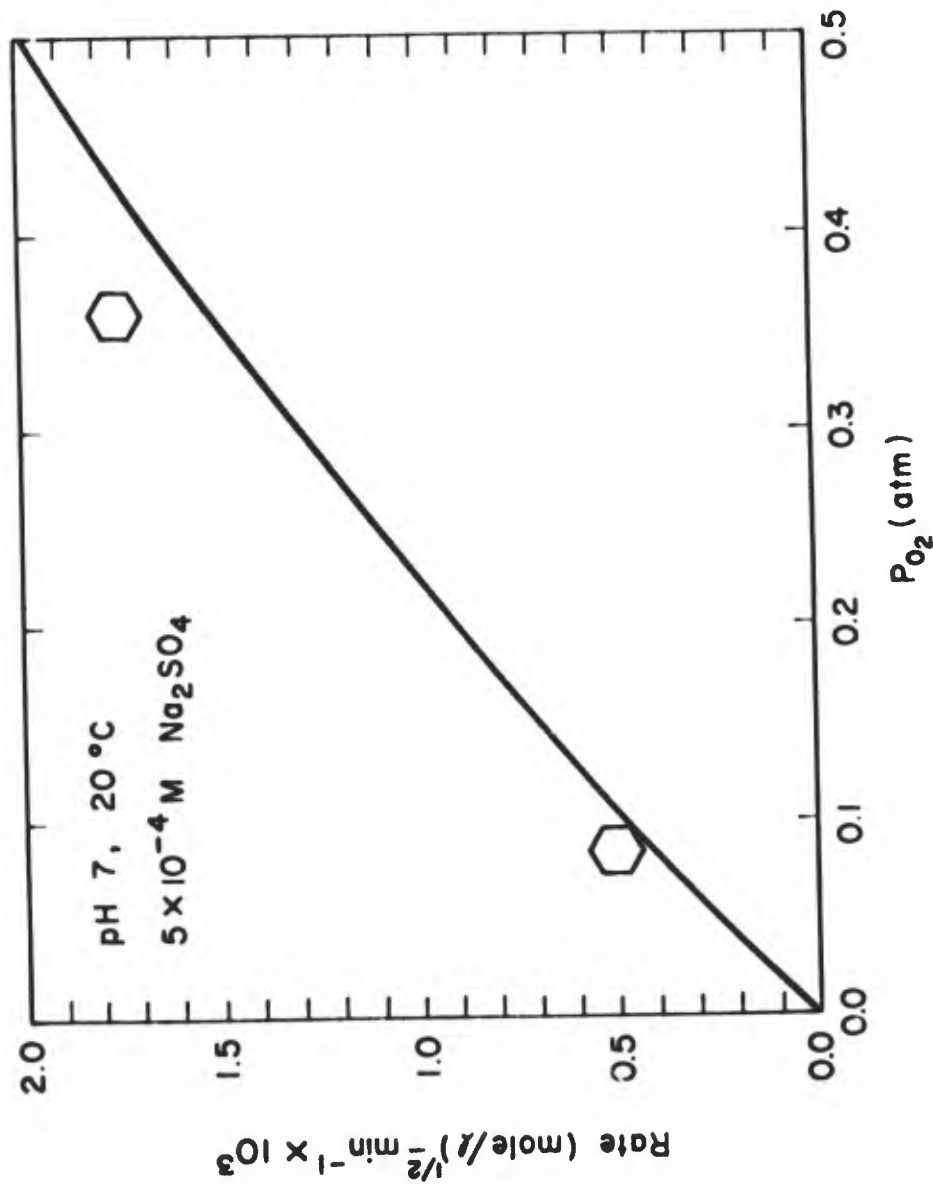


Figure 44. Oxidation rate vs partial pressure of oxygen at pH 7 and 20°C. Solid line represents theoretical relationship predicted by kinetic model using data at 10°C and 15°C.

energy for the reaction at temperatures greater than 20°C is roughly 15 Kcal.

The rate constants determined at 10° and 15°C should not be extrapolated above 20°C because of the shift in the rate-controlling reaction. The activation energy for the overall rate of reaction at pH 9 varied from 15.0 Kcal for FeS aged one week to 13.73 Kcal for FeS aged two months. The oxidation of ferrous sulfide at pH 9 appears to proceed by the same mechanism as at pH 7 as evidenced by the deviation from linearity in the relationship between date of oxidation and increasing oxygen concentration. Lack of reliable quantitative measurements of the higher oxygen concentrations prevent a more quantitative treatment of these data.

The observation that the activation energy shifts to a higher activation energy with increasing temperature at pH 7 indicates that two parallel reactions are contributing to the overall rate of reaction rather than a shift in mechanism to a different rate-controlling process.

The mechanistic models describe the interaction of oxygen with a surface site on the surface of the ferrous sulfide. The kinetic expression describing the rate of oxidation of ferrous sulfide is formulated in terms of surface sites per unit surface area and total surface area per unit volume present in the reactor. The mass of ferrous sulfide (or mass per particle times the number of particles) per unit volume is always directly proportional to the concentration of ferrous sulfide remaining at any point during the reaction. The initial surface area in the reaction vessel is proportional to the initial mass or volume per particle of ferrous sulfide in the reactor. However, as the reaction proceeds, the surface area per unit volume of ferrous sulfide changes. This is because the surface area per unit volume of solid increases as the size of the particle decreases.

Experimentally, the rate of oxidation of ferrous sulfide is determined as a function of the concentration of ferrous sulfide remaining as a function of time. This inevitably leads to the determination of pseudo rate constants in terms of the concentration of ferrous sulfide remaining rather than the surface area remaining and available to react.

In order to reconcile the experimentally observed rates based upon the concentration of ferrous sulfide remaining, and the theoretical kinetic expressions based upon surface area, a relationship between the concentration of ferrous sulfide and the surface area as a function of the extent of

oxidation must be found. The initial surface area of the ferrous sulfide can be measured with a BET adsorption technique, because ferrous sulfide is the only solid phase present. The surface area of ferrous sulfide remaining at some intermediate point in the oxidation cannot be measured because of the formation of ferric hydroxide which also has a high surface area.

The relationship between the surface area and ferrous sulfide remaining as a function of the extent of oxidation can be determined using an empirical approach. This approach also provides some insight into the particle morphology and the relationship between the reactive surface area and particle volume.

The relationship is based upon the assumption that the rate of oxidation is directly proportional to the reactive surface area remaining at any time during the reaction. Therefore, the reactive surface area remaining at any time in the reaction can be expressed as a function of the initial reactive surface area if the experimentally determined instantaneous rate of oxidation at each time is known.

Differentiation between total surface area and reactive surface area remaining must be made before developing this approach further.

A distinction may be made between reactive surface area and total surface area. For the purpose of discussion, consider a crystalline solid in the shape of a cube, each face representing a different crystallographic axis. All faces may be equally reactive, in which case each face would be attacked at the same rate. There is no reason to assume that different faces representing different crystallographic axes should be equally reactive. Quite the opposite is true. Considering the crystal structure of ferrous sulfide, it is clear that the degree of bonding an atom at the solid/liquid interface is able to participate in changes with different faces. Returning to the example of the cube, the rate of change of the volume of the cube will be a function of the rate of reaction per unit area of each face times the surface area of each face. The rate of reaction at any point during the reaction and the geometry of the remaining particle are also dependent upon the relative reactivities of each face and the surface area of each face remaining. This is the reason for differentiating between total surface area and reactive surface area remaining.

The experimentally measureable quantities obtained during the oxidation of ferrous sulfide are the concentration (or volume) of ferrous sulfide

remaining and time. The instantaneous rate of reaction is directly proportional to the reactive surface area remaining and could be determined from the slope of the graphical representation of the concentration of ferrous sulfide remaining as a function of time. The empirical relationship between the reactive surface area and extent of oxidation of a particle can be found by plotting the log of the rate versus the log of the remaining concentration. For a given particle size and shape, reacting under a given set of conditions, this manipulation shows how the reactive surface area remaining changes as a function of the volume of ferrous sulfide remaining. Neither the initial nor intermediate size, shape, and surface of ferrous sulfide particles need be known to apply this approach. This allows the reactive surface area remaining which cannot be measured directly to be expressed in terms of ferrous sulfide concentration remaining, which can be measured directly.

At pH 7, the concentration of ferrous sulfide remaining during the oxidation is close to a linear function of time. Therefore, the rate of change of FeS concentration is constant. Since the rate of change of the ferrous sulfide concentration is directly proportional to the reactive surface area present, this implies that the reactive surface area remaining is essentially constant over the course of the reaction. At the same time, the concentration of FeS, or volume remaining per particle, is decreasing. This situation can be conceptualized by considering a crystal which is only attacked along one crystallographic axis or plane. As the attack proceeds, the volume decreases and the shape of the crystal changes, but the surface area of the reactive face remains constant.

At pH 9, the concentration of ferrous sulfide remaining during the oxidation is not a linear function of time. The rate of oxidation decreases with increasing extent of oxidation and time of reaction. This implies that the reactive surface area remaining is changing as the volume of FeS remaining changes. This can be appreciated conceptually by considering a crystal which is attacked along two or more crystallographic axes or planes. As the reaction on one face proceeds, it decreases the surface area on the adjacent face available to react and vice versa. This provides a conceptual basis for understanding why the relationship between the concentration of ferrous sulfide remaining with time and the dependence of the rate of oxidation upon the ferrous sulfide concentration remaining change with experimental conditions.

When the initial shape of the crystal and the relative rate of reaction of each face are known, mathematical expressions describing the rate of change of the volume can readily be derived. The morphology and relative reactivity of the different crystallographic planes are not known for the ferrous sulfide used in the experiments reported here. The same concepts still apply to the approach used here, however. An empirical relationship between the reactive surface area and volume of ferrous sulfide remaining at any point in the reaction was determined for each set of experimental conditions. The relationship is based upon the assumption that the experimentally observed instantaneous rate of oxidation is directly proportional to the reactive surface area and the ability to experimentally determine the concentration of ferrous sulfide remaining at each point.

Determination of Rate of Reaction. The oxidation of ferrous sulfide is monitored experimentally by measuring the concentration of ferrous sulfide remaining as a function of time. The rate of oxidation at any point in the oxidation is proportional to the reactive surface area remaining at that point in the reaction. The reactive surface area remaining cannot be measured directly. However, it can be expressed empirically by the relationship $A = K[\text{FeS}]^n$, where A is the reactive surface area remaining and $[\text{FeS}]$ is the concentration of ferrous sulfide remaining expressed in moles per liter or $(\text{cm}^3/\text{particle}) \times (\text{number of particles}/\text{volume of reactor})$. The value of n varies from 0 to 1/2 depending upon the experimental reaction conditions. The rate of oxidation for a given set of conditions can be expressed as

$$\frac{d \text{ FeS}}{dt} = -k_c A$$

where

k_c = composite reaction rate constant including oxygen concentration,
 A = reactive surface area remaining.

The reactive surface area remaining is related to the concentration remaining and can be substituted into the rate expression yielding

$$\frac{d \text{ FeS}}{dt} = -k'_c [\text{FeS}]^n$$

where

$$k'_c = k_c \cdot K.$$

The value of n determines the form of the integrated equation. When $n = 0$, the integrated equation is

$$[\text{FeS}] = -k'_c t$$

The ferrous sulfide concentration which has been oxidized (or remaining) is a linear function of time with a slope of $-k'_c$. A value of k'_c can readily be determined from the experimentally measured ferrous sulfide concentration. When n is $1/2$, the integrated equation is

$$2[\text{FeS}]^{1/2} = -k'_c t$$

From this relationship a value of k'_c can be determined.

This approach provides an empirical method of expressing the reactive surface area remaining, which cannot be measured directly, as a function of the experimentally measureable concentration of ferrous sulfide remaining.

The relationships developed above were used as a basis for reducing experimental results.

Role of the Hydronium Ion in the Reaction Model. The pH, or hydronium ion concentration, was not observed to have a significant effect upon the rate of oxidation. This came as somewhat of a surprise, because the rate of oxidation of homogeneous solutions of both ferrous iron and sulfide are reported to be very pH dependent.

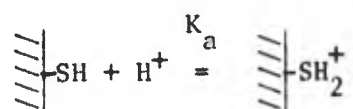
The concentration of hydronium ions plays a major role in determining the distribution of sulfur oxidation products and the degree of crystallinity of the ferric oxyhydroxide phase formed (lepidocrocite) during the oxidation of ferrous sulfide. Both sulfur products and iron oxide phase are sensitive to and vary regularly with, changes in pH. No direct correlation between the oxidation of ferrous sulfide and the products formed could be determined. This indicates that the processes leading to the formation of products are at least one step removed from the initial oxidation process.

The pH of the reaction media may affect the oxidation reaction directly or indirectly. The reaction involves the interaction of oxygen with the ferrous sulfide surface. The surface properties of the ferrous sulfide may affect the adsorption of oxygen, altering the equilibrium position which is reflected in the value of k_a or the reactivity of the surface complex

which is reflected in the value of k_{rx} . The surface of the ferrous sulfide solid interacts with water to form surface sulfhydryl groups, creating negative, neutral and positive sites, according to the degree of protonation. These sites may act as adsorption sites for oxygen. The adsorption of oxygen onto the ferrous sulfide surface and the reactivity of the resultant adsorbed complex are a function of the chemical characteristics of the surface.

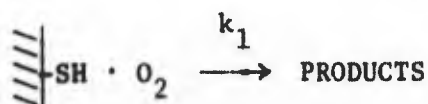
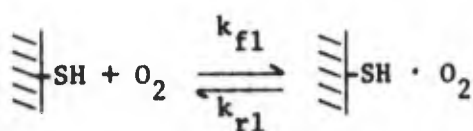
The hydronium ion concentration has no perceptible effect on oxidation rate at pH greater than 9 and only a minimal effect in the pH range 6.5 to 9. The degree of protonation of the FeS surface is a function of pH. The surface is composed predominantly of sulfide units, thus providing an electron-dense surface to solution. This surface is somewhat similar to an oxide surface, although there are significant differences in ionic radii, localization of charge, and degree of ionic versus covalent bonding in the solid. The physical-chemical surface properties of metal oxides and sulfides are determined by the type of solid and the solution composition. Although experimental data are lacking, it is reasonable to assume that the log of the surface acidity constant for the second proton on FeS should be on the order of 6-7. Thus, the surface would be positively charged below pH 6 and tend toward neutral above that pH. Observations of the rate of oxidation of a number of sulfide ores indicates that the rate of oxidation is relatively insensitive to pH over the pH range 3 to 11 (Majima and Peters, 1966).

The reaction model proposed here allows for interaction of solution protons with the surface and, through interaction between oxygen and surface sulfhydryl groups, some influence of solution pH on the overall rate of reaction. If we consider the surface to be a diprotic acid system, we can describe the acid-base reactions by the following stoichiometric relationship

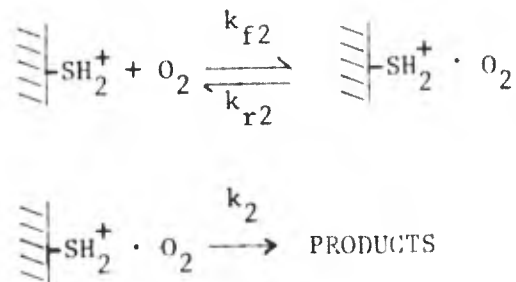


Now, consider adsorption of oxygen at the two types of sites followed by reaction.

For the monoprotonated site we have



and for the diprotic site



The number of surface sites of each type can be expressed as a fraction of the total number of surface sites, where

ϕ_1 is the fraction of monoprotic sites, ---SH

ϕ_2 is the fraction of diprotic sites, ---SH_2^+

θ_1 is the fraction of occupied monoprotic sites, $\text{---SH} \cdot \text{O}_2$

θ_2 is the fraction of occupied diprotic sites, $\text{---SH}_2^+ \cdot \text{O}_2$

The total number of sites is simply the sum of all sites

$$\text{TOTAL SITES No} = \sum_{i=1}^4 (\text{each type of site } n_i)$$

Expressing each site as a fraction we get

$$1 = \sum \left(\frac{n_i}{N_o} \right) = \phi_1 + \theta_1 + \phi_2 + \theta_2$$

Assuming equilibrium for the adsorption/desorption reactions, we can combine expressions to yield

$$k_f \phi [\text{O}_2] = k_r \theta$$

or

$$\frac{k_f}{k_r} = K = \frac{\theta}{\phi [O_2]}$$

and

$$\theta_1 = K_1 \phi_1 [O_2]$$

$$\theta_2 = K_2 \phi_2 [O_2]$$

Also

$$\phi_2 = K_a [H^+] \phi_1$$

Substituting these expressions into the mass balance expression for total sites gives

$$\phi_1 = \frac{1}{1 + K_1 [O_2] + K_a [H^+] + K_a [H^+] K_2 [O_2]}$$

The rate of formation of products can be expressed in terms of sites θ_1 and θ_2 ,

$$\frac{d[\text{PRODUCTS}]}{dt} = (k_1 \theta_1 + k_2 \theta_2) \frac{No A}{V}$$

where No is total number of sites per unit area, A is the total surface area, and V is the volume of reacting fluid.

Substituting for the more complete expression gives

$$\frac{d[\text{PRODUCTS}]}{dt} = \frac{No A}{V} (k_1 K_1 [O_2] \phi_1 + k_2 K_2 K_a [H^+] [O_2] \phi_1)$$

and now substituting for ϕ_1 we get

$$\frac{d[\text{PRODUCTS}]}{dt} = \left(\frac{No A}{V} \right) \frac{[O_2] (k_1 K_1 + k_2 K_2 [H^+] K_a)}{1 + K_1 [O_2] + K_a [H^+] + K_a K_2 [H^+] [O_2]}$$

Thus, we can express the overall rate of reaction as a function of the concentration of hydronium ions, oxygen, and surface area.

The value of K_a is not available in the literature. Electrokinetic measurements could not be made because the particle size is too small to be observed in a light microscope. The small particle size is subject to excessive brownian motion. The surface charge could not be determined by titrimetric methods because the solubility of ferrous sulfide increases with decreasing pH. The sulfide released consumes titrant, which masks the reaction occurring at the surface of the solid.

Measurements of electrokinetic behavior of zinc and nickel sulfide were reported by Healy et al. They indicated in personal communication that the presence of a partial monolayer of elemental sulfur determined the iso-electric point (pH_{iep}) of most sulfide minerals. The conditions of preparation and storage are also reportedly important in determining the pH_{iep} . ZnS pre-equilibrated at pH 6.5 for 17 hours had a pH_{iep} of 6.7 in both 10^{-2} and 10^{-3} M KNO_3 .

The settling characteristics of the ferrous sulfide suspension at pH 7 and 9 were also observed. The suspension appears to settle more rapidly at pH 9 than pH 7, consistent with a more highly charged surface at pH 7. A value for K_a can be determined from the experimental results using a method of successive approximations.

The general expression for the rate of oxidation is given by

$$r = \left(\frac{N_o A}{V} \right) P_{O_2} \left(\frac{k_1 K_1 + k_2 K_2 K_a [H^+]}{1 + K_1 P_{O_2} + K_a [H^+] (1 + K_2 P_{O_2})} \right)$$

If the rate of oxidation is known at two or more different pH values under otherwise identical conditions, the ratio of the two expressions yields

$$\frac{r_{H_1}^+}{r_{H_2}^+} = \frac{\left(\frac{N_o A}{V} \right) (P_{O_2}) \left(\frac{k_1 K_1 + k_2 K_2 K_a [H_1^+]}{1 + K_1 P_{O_2} + K_a [H_1^+] (1 + K_2 P_{O_2})} \right)}{\left(\frac{N_o A}{V} \right) (P_{O_2}) \left(\frac{k_1 K_1 + k_2 K_2 K_a [H_2^+]}{1 + K_1 P_{O_2} + K_a [H_2^+] (1 + K_2 P_{O_2})} \right)}$$

Simplifying yields

$$\frac{r_{H_1}^+}{r_{H_2}^+} = \frac{(k_1 K_1 + k_2 K_2 K_a [H_1^+])}{(k_1 K_1 + k_2 K_2 K_a [H_2^+])} \frac{1 + K_1 P_{O_2} + K_a [H_2^+] (1 + K_2 P_{O_2})}{1 + K_1 P_{O_2} + K_a [H_1^+] (1 + K_2 P_{O_2})}$$

A number of assumptions can be made to simplify this expression further. If the reactions are conducted at relatively low oxygen concentrations, $K_1P_{O_2}$ and $K_2P_{O_2}$ are far less than unity. In addition, the rate of oxidation above pH 9 is independent of pH. Therefore,

$$k_1K_1 \gg k_2K_2K_a(10^{-9})$$

The value of $K_a(10^{-9})$ can also be shown to be much less than unity by comparing the ratio of the rates at pH 9, 10, and 11. Using these deductions, the value of K_a can be found from the ratio of the rates of oxidation observed in a pH-independent and pH-dependent range. Simplifying the expression for the ratio of the rates, assuming the denominator is the rate at pH 9 or greater, yields

$$\frac{r_H}{r_9} = \left(\frac{k_1K_1 + k_2K_2K_a[H^+]}{k_1K_1} \right) \left(\frac{1}{1 + K_a[H^+]} \right)$$

Rearranging this expression,

$$\frac{r_H}{r_9} (1 + K_a[H^+]) = 1 + \frac{k_2K_2}{k_1K_1} [K_aH^+]$$

or

$$\frac{\frac{r_H}{r_9} (1 + K_a[H^+]) - 1}{K_a[H^+]} = \frac{k_2K_2}{k_1K_1}$$

The value of k_2K_2/k_1K_1 is a constant. Therefore if the value of r_H is known at a number of different pH values, the equation for k_2K_2/k_1K_1 can be solved iteratively for a number of different pH values and assumed K_a values. The values of K_a which yields the same value for k_2K_2/k_1K_1 at all pH values is the appropriate constant. Kinetic data reduced in this manner are given in Table 12.

Results indicate that the value of K_a is approximately $10^{6.9}$. Table 12 also indicates that the ratio of k_2K_2/k_1K_1 is approximately 6:1. These numbers are only approximate because of the limitations in determining the reaction rates and the simplifying assumptions.

TABLE 12. VALUES OF (k_2K_2/k_1K_1) COMPUTED BY ITERATIVE METHOD ASSUMING VALUESOF K_a

pH	r	r/r _g	$K_a \cdot 10^6$	$K_a \cdot 10^7$	$K_a \cdot 10^{6.8}$	$K_a \cdot 10^{6.9}$
6.5	4	4.44	15.3	5.53	6.16	5.81
7.0	2.9	3.22	25.4	5.44	6.74	6.01
7.5	1.8	2.0	33.6	5.16	7.01	5.98
8.0	1.5	1.67	68.7	8.37	12.3	10.1
9	0.9	1.0	-	-	-	-

Mathematically, the kinetic equation developed from the kinetic model describes the experimentally observed reaction rates very well. The description of the manner in which the hydronium ions are associated with the sites on the surface is general. The hydronium ions may be associated with the specific sites participating in the reaction as described in the conceptual model. The protonation of the surface may affect the reactivity of the surface by altering the properties of the surface. The dependence of the rate of oxidation upon the hydronium ion concentration in the mathematical expression remains the same.

A discussion of the role of protons in the reaction occurring at the surface necessarily involves a discussion of the properties of the surface and factors which influence them.

The model just developed is somewhat simplistic since it only considers possible interactions between the surface and hydronium ions.

The reactivity of the ferrous sulfide-oxygen complex may also be affected by surface properties of the ferrous sulfide which are only indirectly dependent upon the free hydronium ion concentration in solution. Surface properties of metal sulfides have not been given the attention that many other solids such as oxides or silicates have received. The electro-kinetic properties of the zinc and nickel sulfide-water interfaces were studied in detail, and a summary of properties these and other metal sulfides have was reported by Healy and co-workers in personal communication. They reported that, with the exception of pyrite, all other metal sulfides have an iso-electric point (pH_{iep}) of 2.5 ± 1.0 . The similarity of the iso-electric

point of elemental sulfur and the experimentally observed pH_{iep} of metal sulfides suggested the possibility that a partial surface coating of elemental sulfur is responsible for the observed behavior. This layer is estimated at less than half of a monolayer coverage, yet is apparently enough to layer the properties of the metal sulfide surface. Under conditions of increasing pH, elemental sulfur becomes increasingly less stable and tends to form sulfoxy anions, presumably reducing the surface coverage by elemental sulfur. Hydrolyzed metal hydroxo species or surface complexes of basic metal salts are believed to be present on the surface at higher pH and affect the electrokinetic mobility of the particles.

The formation of a layer of either elemental sulfur or metal hydroxo complexes on the surface is a function of pH. Their presence, in turn, may alter the reactivity of the surface. Their presence on the surface also interferes with a determination of the value of the dissociation constants for the protonated surface sites.

The surface chemistry of metal sulfides is very poorly understood and, hence, places a severe limitation upon the discussion of how the protonation of the surface or presence of other species on the surface will affect the overall rate of reaction.

The exact mechanism of the dependence of the overall rate of oxidation on the hydronium ion concentration has not been resolved. The rate is relatively insensitive to changes in pH over the range investigated. The model proposed is useful in that it predicts the dependence of the rate of oxidation on the hydronium concentration over the range studied.

Role of Ionic Strength in Reaction Model. The ionic strength of the media determines the activity:concentration ratio of reacting species and thus, in turn, influences the reaction rate to some extent. The reacting system in which the oxidation of ferrous sulfide was investigated involves gaseous, aqueous, and solid phases, plus the interactions at each interface.

Oxygen is one of the two principal reactants involved in the initial reaction. In the discussion up to this point no distinction between activity and concentration has been made. At constant temperature, pressure, and ionic strength, the activity and concentration are directly proportional. Therefore a distinction between the two was unnecessary. As the composition of the reacting media changes, the activity:concentration ratio changes. In order to compare the results obtained under different reaction conditions, both activity and concentration must be known.

The ionic strength of the reaction media alters the activity of all of the reacting species. In order to evaluate the effect of ionic strength on the oxidation reaction, the ionic strength effect on the solubility of oxygen must first be evaluated.

The concentration of oxygen in solution is most frequently expressed in terms of the partial pressure of gas with which the solution is in equilibrium. The solubility of oxygen decreases with increasing ionic strength (salting-out effect). However, when both the gas and aqueous phase are in equilibrium, the activity of oxygen in solution remains the same with increasing ionic strength. Therefore, the actual number of molecules of oxygen in solution and available to react at the ferrous sulfide surface is decreasing with increasing ionic strength, even though the activity of oxygen in solution and in equilibrium with the gas phase remains constant.

This brings up the question as to which measurement, activity, or concentration is more appropriate to use when considering the effect of ionic strength or other parameters in different ionic-strength media, as they relate to the oxidation rate. The decision was made very early in the course of experimental work that the concentration of oxygen in solution and available to react with the surface of the iron sulfide is a more appropriate measure when comparing the effect of ionic strength upon oxidation rate. Results are discussed in terms of both the concentration and activity of oxygen in solution.

The operation of the dissolved oxygen probe used to monitor the activity of oxygen in solution provides some insight into how the adsorption of oxygen onto the ferrous sulfide surface should vary with ionic strength if oxygen is the only species affected by the ionic media. The dissolved oxygen probe consists of an anode and cathode immersed in a concentrated electrolyte solution and separated from the bulk solution by a teflon membrane. Oxygen is reduced at the cathode and the meter reads the current which is generated. The rate at which oxygen arrives at the electrode is limited by the rate at which it diffuses across the teflon membrane. The rate at which it diffuses across the teflon membrane is directly proportional to the concentration gradient across the membrane. Since the concentration on the inside of the membrane is essentially zero, the rate of oxygen transfer is proportional to the concentration in the bulk solution. More accurately, it is proportional to the activity of the oxygen in solution. An increase in the ionic strength of a solution decreases the solubility of oxygen in solution at equilibrium

but not its activity. The rate at which oxygen diffuses across the teflon membrane is proportional to the activity of the oxygen rather than the actual concentration. This is why the meter reads in partial pressure rather than concentration. This means that the "salting-out" effect of increasing ionic strength not only reduces the tendency of oxygen to go into solution but tends to force it out through the teflon membrane as well. An analogy between the driving force for diffusion across the teflon membrane and the driving force for adsorption of oxygen onto the surface of ferrous sulfide can be drawn.

The concentration and activity of oxygen in solution are known for each set of experimental conditions. The effect of ionic strength on the oxygen in solution is known, and its effect on the rate of oxidation can be predicted. Some information on how the surface complexes must change with ionic strength can be inferred from the effect of ionic strength on the overall rate of reaction and the manner in which the activity of oxygen is known to vary.

The oxidation of ferrous sulfide was conducted at pH 9 in $5 \times 10^{-4} \text{ M Na}_2\text{SO}_4$ ($I = 1.5 \times 10^{-3}$) and 0.1M NaCl at 16 mg/l dissolved oxygen. The rate of oxidation in both cases was identical. If the only effect of ionic strength was on the activity of oxygen in solution, the rate of oxidation should have increased at the higher ionic strength because the activity of oxygen was greater.

The observation that the rate does not increase indicates that the ionic strength interferes with the reaction in some other manner, such as altering the partition coefficient for adsorption or reducing the reactivity of the complex.

The oxidation of ferrous sulfide was conducted in a number of different ionic strengths and ionic media at pH 7, constant temperature, and constant oxygen concentration. At a given oxygen concentration, the rate of oxidation decreases with increasing ionic strength. This indicates that the activity of the reactants at the surface are decreasing faster than the activity of oxygen in solution is increasing.

The interaction between an aqueous ionic media and solid surface is not understood well enough to quantify the alterations in the activity of species present at the interface.

The effect of ionic strength and composition of the reaction media on the reaction rate can be explained in terms of the adsorption model in two

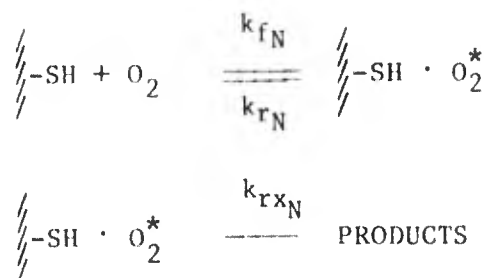
ways. The ionic strength of the solution may alter the reactivity of the activated surface complex. That is, the composition of the ionic media immediately adjacent to the surface may alter the rate at which the activated complex decomposes into products. The rate of decomposition of the activated complex is conceived to be a function of the internal vibrational frequency of the complex. In order to alter this, the ionic media would have to influence the electron population and distribution in the complex. Intuitively, this is readily conceivable; however, the pursuit of this in a more rigorous way is beyond the scope of this investigation.

The composition of the ionic media may also alter the adsorption of oxygen onto the surface. This may be due to an alteration of the surface properties of ferrous sulfide or an alteration of the propensity of the oxygen to adsorb or desorb. Either of these effects would be manifested in a change in the adsorption partitioning coefficient k_a ($k_f/(k_r + k_{rx})$). The salting-out effect of increasing ionic strength tends to increase the extent of adsorption. The ionic strength of the media must affect the surface properties of the solid which increases the tendency of oxygen to desorb.

Inhibition of the rate of oxidation with increasing ionic strength is readily observed experimentally. The manner in which this inhibition occurs is not known.

Changes in the reactivity of species in solution as a function of ionic strength are normally corrected for with an activity coefficient. The activity coefficient relates the actual concentration of a species to its apparent concentration or activity in solution. The procedures for calculating activity coefficients and the validity of the results are well developed and readily available. Similar techniques for determining coefficients to correct for changes in the activity of species on the surface of solids or at the solid-aqueous interface are not available. This is in part due to the fact that intensive efforts to understand the interface on a fundamental basis are relatively recent and partly due to the difficulty in studying the interface.

The difference in the effect of ionic strength on the rate of oxidation observed at pH 7 and 9 has been discussed but not explained. Consider the simple two-step reaction sequence used to develop the steady-state model earlier. This can be used to demonstrate the effect of ionic strength on the activity of the surface complexes. The reaction sequence proposed is:



The rate at which each reaction occurs is a function of the activity of each species. The activity is related to the actual concentration by the activity coefficient (not known). The number of surface sites present can be expressed as a fraction of the total sites present, where:

$$\phi_N = \text{fraction of unoccupied sites } \text{\\-SH}$$

$$\theta_N = \text{fraction of sites complexed with oxygen } \text{\\-SH} \cdot \text{O}_2^*$$

At steady-state conditions the rate of formation and destruction of activated complexes is equal and is a function of the activity of each type of site present,

$$\frac{d(\text{cmplx}^*)}{dt} = 0 = k_{fN} \gamma_{\phi_N} \phi_N P_{\text{O}_2} - k_{rN} \gamma_{\theta_N} \theta_N - k_{rxN} \gamma_{\theta_N} \theta_N$$

where γ_{ϕ_N} and γ_{θ_N} are activity coefficients for the respective surface species. Following a similar procedure to that used earlier the overall rate of reaction is:

$$\frac{d[\text{PRODUCTS}]}{dt} = \frac{k_{rxN} \left(\gamma_{\theta_N}^2 / \gamma_{\phi} \right) \left(\frac{k_{fN}}{k_{rN} + k_{rxN}} \right) P_{\text{O}_2}}{1 + \left(\gamma_{\theta_N} / \gamma_N \right) \left(\frac{k_{fN}}{k_{rN} + k_{rxN}} \right) P_{\text{O}_2}}$$

When $k_{rN} \gg k_{rxN}$, then $K_N = k_{fN}/k_{rN}$ and

$$\frac{d[\text{PRODUCTS}]}{dt} = \frac{k_{rxN} \left(\gamma_{\theta}^2 / \gamma_{\phi_N} \right) K_N P_{\text{O}_2}}{1 + (\gamma_{\theta} / \gamma_{\phi}) K_N P_{\text{O}_2}}$$

This demonstrates how the rate of oxidation is predicted to change with changes in the ionic strength of the reaction media.

The lack of a theoretical basis for making activity corrections for surface reactivity presents some limitations to the discussion. The observations in various ionic strength media provides an empirical means of determining composite activity coefficients, however.

The rate of oxidation at pH 9 shows very little dependence upon ionic strength. The rate of oxidation in low ionic strength media ($5 \times 10^{-4} \text{M Na}_2\text{SO}_4$) is essentially the same as the rate in 0.1M NaCl (Figure 19).

If the partial pressure and rate of oxidation are known and the values of the constants are independent of ionic strength, the manner in which the activity coefficients vary with ionic strength can be determined from the relationship

$$\frac{r_H}{r_L} = \frac{\left[\frac{k_{rx} (\gamma_{\theta_H}^2 / \gamma_{\phi_H}) K(P_{O_2})_H}{(1 + \gamma_{\theta_H} / \gamma_{\phi_H}) K(P_{O_2})_H} \right]}{\left[\frac{k_{rx} (\gamma_{\theta_L}^2 / \gamma_{\phi_L}) K(P_{O_2})_L}{1 + (\gamma_{\theta_L} / \gamma_{\phi_L}) K(P_{O_2})_L} \right]}$$

where the subscripts H and L signify high and low ionic strengths, respectively. If the experiments are run at oxygen concentrations where $1 \gg (\gamma_{\theta} / \gamma_{\phi}) K(P_{O_2})$, the equation simplifies to

$$\frac{r_H}{r_L} = \frac{(\gamma_{\theta_H}^2 / \gamma_{\phi_H}) (P_{O_2})_H}{(\gamma_{\theta_L}^2 / \gamma_{\phi_L}) (P_{O_2})_L}$$

If the further assumption is made that the activity coefficients in low ionic strength media are essentially unity, the expression can be rearranged to yield

$$\frac{\gamma_{\theta_H}^2}{\gamma_{\phi_H}} = \frac{r_H (P_{O_2})_L}{r_L (P_{O_2})_H}$$

Experimentally, the value of this is determined as a composite activity coefficient where

$$\gamma_{\text{exp}} = \gamma_{\text{H}}^2 / \gamma_{\phi_{\text{H}}}$$

At pH 9, the rate of oxidation at high and low ionic strength is essentially the same within experimental error. If γ_{L} is assumed to be unity, γ_{H} is 1.04. This is essentially one within experimental error. This suggests that the surface sites and surface complex at pH 9 are uncharged. This would explain why the rate of oxidation at pH 9 is insensitive to ionic strength.

At pH 7, the rate of oxidation is observed to be a function of ionic strength. Using the same assumptions and method of data reduction, the apparent activity coefficients of the surface complex in 0.1 and 0.5M NaCl are $\gamma_{0.1} \approx 0.6$ and $\gamma_{0.5} \approx 0.4$, respectively. This suggests that the surface sites and surface complexes have a net charge on them at pH 7.

For the purposes of comparison and discussion, representative activity coefficients for mono- and divalent ions in ionic strength media of 0.1 and 0.5 are shown in Table 13.

TABLE 13. CALCULATED ACTIVITY COEFFICIENTS FOR SOLUTION AND SURFACE*

Species	Ionic Strength		
	.001	0.1	0.5
Monovalent ions	0.97	0.78	0.69
Divalent ions	0.87	0.36	0.23
FeS surface pH 7	1 (by definition)	0.60	0.40
*Activity coefficients are calculated using the Davies equation. The values can be considerably refined by using more exact equations for specific ions, but for purposes of comparison here the added sophistication is not needed. Extension of the Davies equation beyond 0.1 molar to 0.5 molar ionic strength is approximate; beyond 0.5, only order of magnitude values obtain.			

The activity coefficients of aqueous species and surface complexes cannot be compared directly because of the difference in chemical environments surrounding each. The activity coefficient for the surface reaction may also represent a composite or quotient of more than one activity coefficient.

The principal point of this discussion is to provide a basis for explaining why the overall rate of oxidation would be more sensitive to ionic strength in one pH range than in another. The observation also lends support to the surface protonation model. The degree of protonation and therefore surface charge increase with decreasing pH. The ionic strength would affect the activity of charged surface complexes much more than neutral complexes.

Role of Catalysts in the Reaction Model. The most notable observation of the effect of species known to catalyze or inhibit the homogeneous oxidation of ferrous iron or sulfide is the insensitivity of the rate of oxidation of ferrous sulfide to such a wide range of conditions. The oxidation of homogeneous solutions of both ferrous iron and of sulfide by oxygen is believed to proceed via free radical mechanisms (discussed in Section II). Heavy metals, particularly those which participate in one-electron exchange reactions, are reported to catalyze the oxidation of both ferrous iron and sulfide. The catalytic or inhibitory action of a species is explained in terms of their propensity to initiate, propagate, or terminate free radical chains. In homogeneous solution, these species are uniformly distributed which allows them to interact with oxygen or other species. The heterogeneous oxidation of ferrous sulfide in the presence of potential catalysts differs from homogeneous reactions in at least two important ways. Ferrous sulfide is present as a solid phase, and the reaction between ferrous sulfide and oxygen or the reactive free radical occurs at the surface of the solid. Second, all of the heavy metals used form extremely insoluble sulfides. After their addition to the ferrous sulfide suspension, they can be assumed to be either adsorbed onto the surface of the ferrous sulfide particle or to be present as a separate metal sulfide phase. The concentration of free or complexed metal in solution is very small. Therefore, it is very unlikely that the interaction of heavy metals in solution resulting in the formation of free radicals contributes to the overall rate of reaction.

The mechanism proposed to explain the oxidation of ferrous sulfide involves the formation and reaction of a ferrous sulfide-oxygen surface complex. In order for heavy metals to influence the rate of oxidation, they must

either alter the reactivity of this complex or provide an alternate mechanism by which the reaction can proceed.

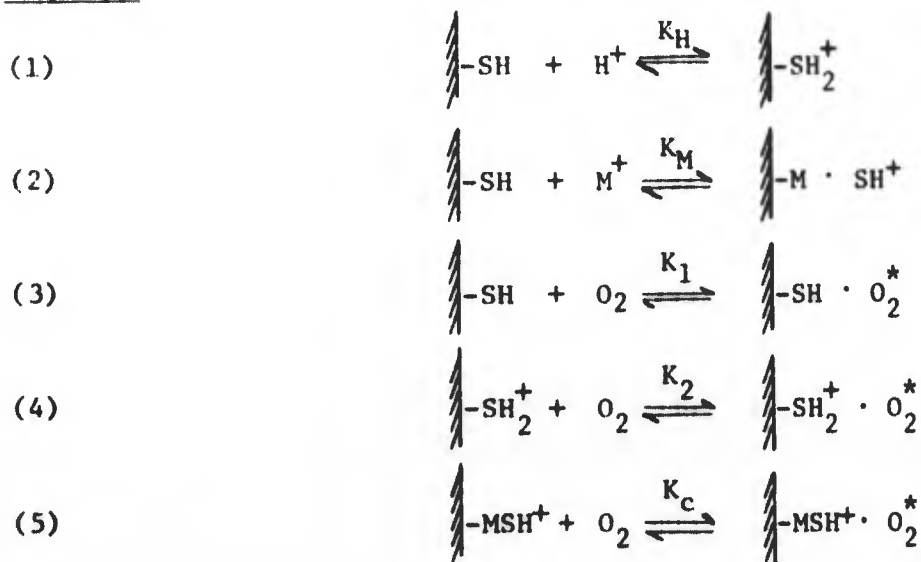
The overall rate of reaction is influenced by the fraction of the total surface which is associated with oxygen and the rate at which the surface complexes react to form products. The presence of heavy metals on the surface of ferrous sulfide is analogous to two discrete metal sulfide crystals in contact with each other. Gottschalk and Buehler (1912) observed that when two dissimilar metal sulfides in the same solution are placed in contact, an emf is generated between the two. The rate of oxidation of the less noble metal sulfide is accelerated, while the more noble metal sulfide is protected cathodically from oxidation (see Section II).

The manner in which the metal catalyst is present upon the surface or how it exerts its catalytic behavior is not known. Experimental results provide some insight into the process and the information necessary to model the effect.

The presence of a heavy metal may affect the overall rate of reaction by increasing the average reactivity of the surface or by increasing the reactivity of the sites which it occupies or is immediately adjacent to. The reactivity of the sites affected by the presence of the metal catalyst then becomes a function of the concentration of catalysts.

A simplified sequence of reactions describing various catalyzed and uncatalyzed reactions is proposed as follows:

Reaction Sequence:





Performing a mass balance on the total sites available yields

$$1 = \phi_1 + \theta_1 + \phi_2 + \theta_2 + \phi_M + \theta_M$$

where

ϕ_1 = fraction of total sites which are monoprotonated and unoccupied,

θ_1 = fraction of total sites which are monoprotonated and complexed with oxygen,

ϕ_2 = fraction of total sites which are diprotonated and unoccupied,

θ_2 = fraction of total sites which are diprotonated and complexed with oxygen,

ϕ_M = fraction of total sites which have metal adsorbed, and

θ_M = fraction of total sites which have metal and oxygen adsorbed.

The fraction of the total sites occupied by a heavy metal catalyst could be expressed as a concentration of the heavy metal concentration in solution. It is more practical to express this in terms of the total amount of catalyst present.

The assumption can be made that essentially all of the heavy metal present will be either adsorbed onto the FeS surface or as a separate metal sulfide phase, when the heavy metal forms a less soluble sulfide than ferrous iron, and the ferrous sulfide surface is not saturated with the heavy metal.

The fraction of the total sites occupied by a heavy metal atom is therefore directly proportional to the amount of heavy metal added and inversely proportional to the total number of sites present. The fraction of the total sites occupied by heavy metal is

$$\phi_M + \theta_M = \frac{[M \text{ mole/l}](N_A \text{ atom/mole})(\text{sites/atom})(\text{area/site})}{(\text{total sites/l})(\text{area/site})}$$

Defining,

$$q = \frac{(N_A)(\text{site/atom})}{(\text{total sites/l})}$$

M = analytical concentration added, not the concentration in solution

the fraction of sites with a heavy metal atom adsorbed $(M)(q)$ may be further divided into sites with or without oxygen adsorbed, where

$$(M)(q) = \phi_M + \theta_M$$

The fraction of sites available which are not associated with a heavy metal are given by:

$$[1 - (M)(q)] = \phi_1 + \theta_1 + \phi_2 + \theta_2$$

Using these relationships and the procedures developed earlier, the equations can be combined to yield an expression for the overall rate of oxidation which considers the fractional surface coverage by an adsorbed heavy metal.

$$\frac{d[\text{PRODUCTS}]}{dt} = \left[\frac{(k_1 K_1 + k_2 K_2 [H^+] K_H) (P_{O_2}) (1 - [M]q)}{1 + K_1 (P_{O_2}) + K_H [H^+] + K_H [H^+] K_2 (P_{O_2})} \right] + \left[\frac{k_c K_c P_{O_2} [M](q)}{1 + K_c P_{O_2}} \right]$$

The form of this expression is somewhat different than developed earlier. The value of $[M](q)$ is directly proportional to the amount of catalyst added. As the amount of catalyst added increases, the importance of the reaction occurring at the sites adjacent to the sites with adsorbed heavy metal becomes increasingly important.

This model also predicts the effect of the adsorption of an inert species onto the surface; that is, a species which does not affect the reactivity of the adjacent sites but merely prevents a reaction of the occupied site. The presence of a concentration M of an inert species should decrease the value of the first term by $(1 - [M]q)$ and therefore of the overall rate of reaction.

The catalytic effect of a number of heavy metals upon the rate of oxidation of ferrous sulfide is reported earlier. Both copper and silver are capable of participating in one-electron exchange reactions, and both form extremely insoluble sulfides. Neither demonstrates any catalytic behavior.

An attempt was made to determine the surface area of ferrous sulfide by measuring the adsorption of silver 110. Silver was added to a suspension of ferrous sulfide, and the concentration of silver in solution was measured as a function of the silver added. It was hoped that a surface coating of silver sulfide would form upon the ferrous sulfide. Then at the completion of the coating, further removal of silver from solution would be much slower, because it must diffuse through this layer into the interior of the particle. This would be observed by an increase in silver in solution at this point. The concentration of silver remained below the detection limit until all of the ferrous iron had been displaced and all of the sulfide was bound to silver. This indicates that either the diffusion of silver is very rapid through the solid or that silver is forming a separate silver sulfide phase.

The crystal structure of both silver and copper sulfide is substantially different from ferrous sulfide and both are far less soluble. The method of preparation of the ferrous sulfide-heavy metal suspension was designed to promote the formation of a uniform adsorbed layer of heavy metal upon the existing ferrous sulfide surface, but it is very possible that both silver and copper precipitated out as a separate phase. As a separate phase, they would not affect the rate of oxidation of ferrous sulfide.

Silver sulfide is much less susceptible to oxidation than ferrous sulfide. If silver is displacing iron and forming a silver sulfide coating upon the ferrous sulfide rather than a separate phase, the presence of silver should affect the observed rate of oxidation. One possible effect is the galvanic acceleration discussed earlier. The formation of a protective coating reduces the surface area available to react. Therefore the formation of a silver sulfide coating should inhibit the rate of oxidation. Neither of these effects is observed experimentally. This strongly suggests that the silver added is forming a separate silver sulfide phase.

A similar argument can be made for copper. If copper is present on the ferrous sulfide surface, it should exhibit a galvanic effect upon the adjacent ferrous sulfide surface and tend to increase the observed rate of oxidation. Countering this effect is the protective effect covering a fraction of the reactive surface area. This should reduce the observed rate of oxidation. In either case, the presence of copper upon the surface should alter the observed reaction rate. No effect is observed, which strongly suggests that the bulk of the copper is present as a separate phase.

Cadmium does not participate in one-electron exchange reactions and therefore is not expected to interact directly in reaction mechanisms involving the formation of free radicals. However, if the rate of oxidation of ferrous sulfide is enhanced by galvanic effects of the presence of more noble heavy metals upon the surface, then cadmium is eligible as a potential catalyst. The presence of cadmium during the oxidation reaction neither increased the rate of oxidation as predicted by galvanic affects nor reduced the rate of oxidation due to partial coverage of the surface with a protective inert layer of cadmium sulfide.

The solubility of cadmium in ferrous sulfide is very low. The difference in crystal structure and bonding in cadmium sulfide and ferrous sulfide is significant. The failure of cadmium to exert any effect upon the rate of oxidation of ferrous sulfide suggests that the cadmium is present as a separate phase rather than on the surface of the ferrous sulfide. Of all of the metals tested, only nickel demonstrated any catalytic activity. This activity was dramatic, however. The rate of oxidation is also observed to increase with increasing amount of nickel added. Nickel forms an extremely insoluble sulfide, much less soluble than ferrous sulfide. The concentration of nickel in solution should be extremely low. The concentration of nickel in solution should also be relatively independent of the amount added and only dependent upon the solubility of nickel sulfide and the fraction of the total surface covered by nickel sulfide. Therefore, its catalytic activity is undoubtedly due to its activity on the surface rather than in solution.

It is significant that nickel sulfide precipitates with the same crystal structure as tetragonal ferrous sulfide. The cell dimensions are very similar and ferrous iron and nickel substitute freely for each other, forming solid solutions of continuous composition from one end member to the other. Naturally occurring mackinawite (tetragonal FeS) is rarely found without significant amounts of nickel. Nickel is typically present in concentrations on the order of a percent or more. On this basis, it is reasonable to assume that the nickel added is associated with the ferrous sulfide rather than forming a separate phase.

The mechanism by which this catalysis occurs is not clear. One possibility is a galvanic effect where the reactivity of the ferrous sulfide is increased, analogous to the effects observed by Gottschalk and Buehler (1912).

The nickel sulfide might also participate directly by being oxidized itself. The nickel released upon oxidation of the nickel sulfide then displaces a ferrous iron atom upon the surface and the process is repeated, the concentration of nickel sulfide on the surface increasing as the remaining concentration of ferrous sulfide decreases. This would cause the rate of oxidation per unit surface area to increase as the reaction progresses. Some evidence for this is observed in the shape of the curves of ferrous sulfide remaining as a function of time in the presence of nickel. This same effect can be explained by the presence of nickel on the surface exhibiting a galvanic effect however, so this cannot be used to differentiate between the two mechanisms.

FeS remaining versus time of oxidation in the presence of varying amounts of nickel is shown in Figure 20. The minimum concentration required to exert a noticeable catalytic effect on the rate is on the order of $1 \times 10^{-5} \text{M Ni}$. Below this level, the rate of oxidation reflects the uncatalyzed reaction. As the concentration increases above this level, the overall rate of reaction also increases rapidly. In these terms, the results are not particularly useful without an additional frame of reference.

The crystal structure of ferrous sulfide is discussed in Section II. From the packing of the sulfur atoms on the surface, the area per surface site can be calculated. Each site takes up roughly 13.5 \AA^2 . This is not to be confused with the cross-sectional area of a nickel ion. Ignoring the propensity of nickel and iron to become involved in metallic bonding, which would result in a much smaller area per site, each metal ion will occupy one site.

If the surface area of the ferrous sulfide solid is $100 \text{ m}^2/\text{g}$ (a typical value), the concentration of ferrous sulfide in suspension is 6.786 g/l , and the concentration of nickel added is $1 \times 10^{-5} \text{ mole/l}$, the percentage of the surface covered is approximately one percent. At $1 \times 10^{-4} \text{ mole/l}$, the coverage is approximately 10 percent.

The model predicts that the rate of oxidation will increase with increasing concentration of nickel on the surface. The experimental rates of oxidation in the presence of increasing nickel concentrations are estimated from data presented in Figure 45. The overall rates of oxidation determined are plotted as a function of nickel added. The rate does increase with increasing nickel concentration, as seen in Figures 20 and 45. The kinetic expression derived from the assumed mechanism does not quite fit the experimental results at the

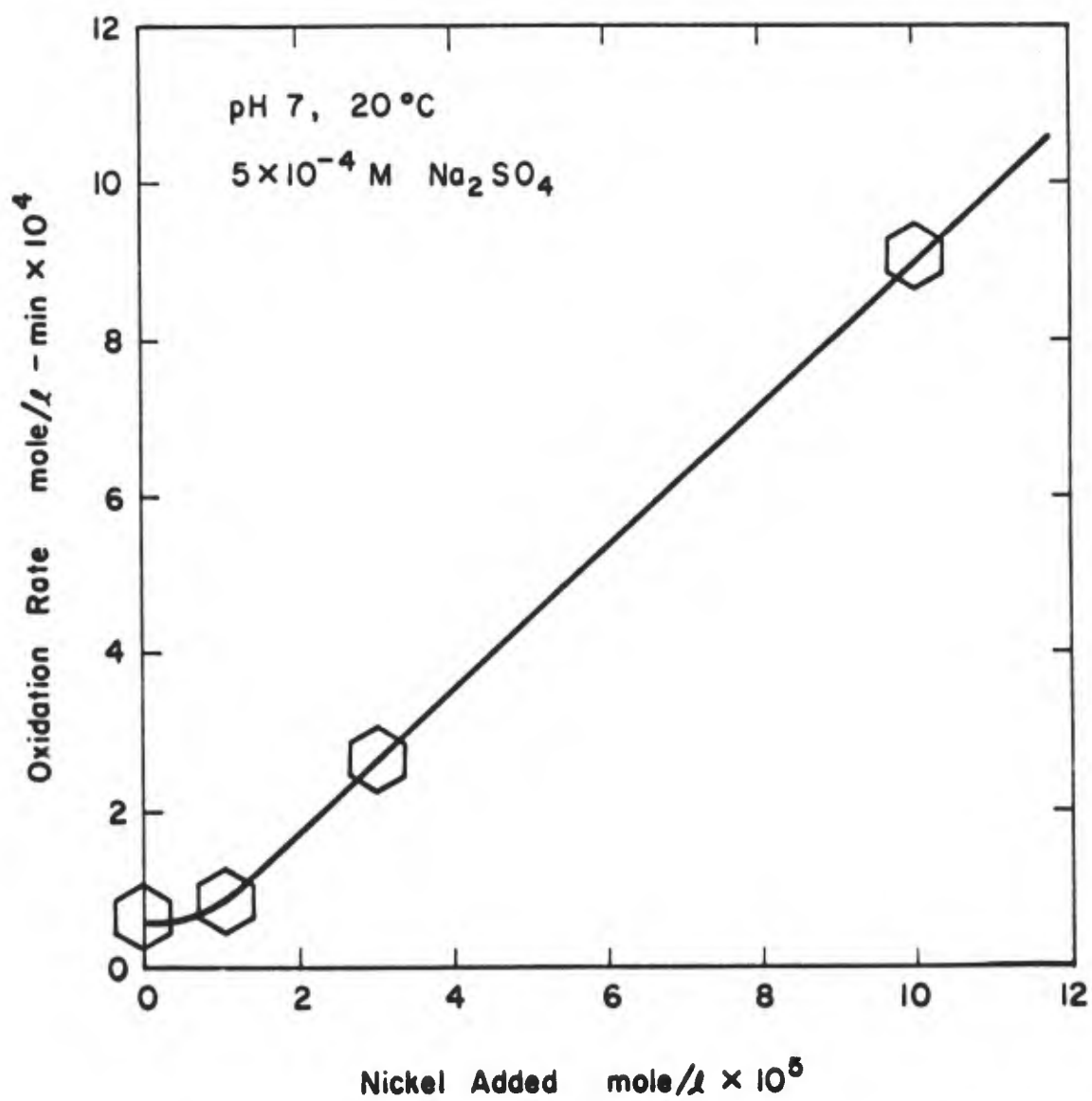


Figure 45. Oxidation rate vs concentration of nickel in system at pH 7 and 20°C.

lower nickel concentrations. The effect of nickel added on the oxidation rate becomes insignificant sooner than predicted. This may be because the model is an oversimplification. The presence of nickel on the surface may have more extended effects than the sites immediately adjacent to them. A minimum threshold amount may be necessary to exert any influence such as a galvanic effect.

Experiments investigating the catalytic activity of various heavy metals on the rate of oxidation were conducted principally to provide insight into the reaction mechanisms involved. It was never the intent to model this effect quantitatively, so unfortunately insufficient data is available to evaluate the model in terms of nickel catalysis.

Comparison of the effect of different heavy metals upon the observed rate of oxidation and the relationships between catalytic activity and similarity in crystal structure provide insight into the processes occurring at the ferrous sulfide-water interface.

Complete Model: Relationship between Experimental Constants and Mechanistic Constants. In the preceding sections, kinetic expressions were developed to explain the effect of each parameter studied upon the overall rate of oxidation. Each of the reaction sequences proposed contributes to the overall rate of oxidation observed to a greater or lesser extent depending on the conditions.

All of the parameters observed to affect the oxidation rate can be combined into one overall expression for the rate of oxidation, as follows:

$$\frac{d[\text{PRODUCTS}]}{dt} = \left[\frac{N_o}{V} A \right] \left\{ \frac{P_{O_2} \left(\frac{\gamma_{\theta 1}^2}{\gamma_{\phi 1}} k_1 K_1 + \frac{\gamma_{\theta 2}^2}{\gamma_{\phi 2}} k_2 K_2 K_2 [H^+] \right) (1-Q)}{\left[1 + \frac{\gamma_{\theta 1}}{\gamma_{\phi 1}} K_1 P_{O_2} + K_a [H^+] + \frac{\gamma_{\theta 2}}{\gamma_{\phi 2}} K_2 K_H [H^+] P_{O_2} \right]} + \frac{k_c K_c P_{O_2} Q}{1 + K_c P_{O_2}} \right\}$$

where

Q = fraction of total sites with a heavy metal adsorbed = $[M](q)$,

γ = activity coefficients of various type sites.

The overall rate of reaction is observed to be quite temperature dependent. The temperature dependency of the rate constants has been deleted for simplicity. The rate constants can be corrected for temperature if the rate

constants at one temperature and the activation energy of the reaction are known. The relationship between the rate constants and temperature are

$$k_{T_2} = k_{T_1} e^{-E_{act}/R(T_1-T_2/T_1T_2)}$$

The activation energy for the overall rate of oxidation has been determined at pH 7 and 9 in the absence of catalyst and in low ionic strength media as reported above. The activation energy for the catalyzed reaction and the reaction in high ionic strength reaction media was not determined.

Many of the experimentally determined constants represent composites of two or more of the constants in the theoretical model. For example, the experimental activity coefficient determined at various ionic strengths is a composite of a number of activity coefficients of proposed intermediates, (e.g., $\gamma_{exp} = (\gamma_\theta^2/\gamma_\phi)$).

Each of the generalized reaction steps proposed, which the rate expression evolves from, may consist of a series of more detailed reaction steps. This will not change the form of the overall expression. The constants for the generalized reaction sequence represents a composite of the individual rate constants comprising the overall expression.

Some of the experimentally determined constants represent a composite of the individual constants which are developed in the mechanistic model. The expression used to reduce the experimental results is given by

$$\frac{d[FeS]}{dt} = - \left(\frac{N_o A}{V} \right) P_{O_2} \left(\frac{k_{rx} k_a}{k_a P_{O_2} + 1} \right)$$

The expression resulting from the mechanistic model is

$$\frac{d[FeS]}{dt} = - \left(\frac{N_o A}{V} \right) P_{O_2} \left(\frac{k_1 K_1 + k_2 K_2 K_a [H^+]}{1 + K_1 P_{O_2} + K_a [H^+] (1 + K_2 P_{O_2})} \right)$$

The expression for the value of k_a is developed earlier, where

$$k_a = \frac{\left(\frac{r_1 (P_{O_2})_2}{r_2 (P_{O_2})_2} - 1 \right)}{(P_{O_2})_2 (1 - r_1/r_2)}$$

Using a similar manipulation of the mechanistic rate expression yields

$$\frac{K_1 + K_2 K_a [H^+]}{1 + K_a [H^+]} = \frac{\left(\frac{r_1 (P_{O_2})_2}{r_2 (P_{O_2})_1} - 1 \right)}{(P_{O_2})_2 (1 - r_1/r_2)}$$

The experimental value of k_a is related to the constants in the mechanistic model by

$$k_a = \frac{K_1 + K_2 K_a [H^+]}{1 + K_a [H^+]}$$

The expression for k_{rx} is determined by substituting the value of k_a into the original expression, where

$$k_{rx} = \frac{(r)(V)}{(N_o A)} \frac{(k_a P_{O_2} + 1)}{(k_a P_{O_2})}$$

Using a similar method of algebraic manipulation, the mechanistic model yields

$$(k_1 K_1 + k_2 K_2 K_a [H^+]) = \frac{rV [(1 + K_a [H^+]) + (K_1 + K_2 K_a [H^+]) P_{O_2}]}{(N_o A) P_{O_2}}$$

The experimental reaction rate constant k_{rx} is related to the constants in the mechanistic model by

$$k_{rx} = \frac{k_1 K_1 + k_2 K_2 K_a [H^+]}{K_1 + K_2 K_a [H^+]}$$

or

$$k_1 K_1 + k_2 K_2 K_a [H^+] = k_{rx} k_a (1 + K_a [H^+])$$

At $pH \geq 9$, the rate of oxidation becomes independent of the pH. Experiments were not conducted at high enough concentrations of oxygen to allow a determination of k_a . Therefore, the experimental rate constant k'_{rx} is a composite of $(k_{rx}) \times (k_a)$. Under the experimental conditions at pH 9, and low P_{O_2} , where $K_1 P_{O_2} \ll 1$ and $K_2 P_{O_2} \ll 1$, the mechanistic model reduces to

$$\frac{d[\text{FeS}]}{dt} = - \frac{N_o}{V} A_{pO_2} \frac{k_1 K_1 + k_2 K_2 K_a [H^+]}{1 + K_a [H^+]}$$

Therefore,

$$k'_{rx} = \frac{k_1 K_1 + k_2 K_2 K_a [H^+]}{1 + K_a [H^+]}$$

Using the relationships determined earlier at 20°C, where $K_a = 10^{+6.9}$ and $k_2 K_2 \approx 6 k_1 K_1$, the relationship at pH 9 reduces to

$$k'_{rx} = 1.039 k_1 K_1$$

Therefore, the experimental value reflects the value of the constants in the model quite well in the pH range 9 to 11. In this range, the contribution by the reaction of protonated sites to the overall rate of reaction is quite small.

With decreasing pH, the number of protonated sites and their contribution to the overall rate of reaction increases rapidly. At pH 7, the value of the term $k_2 K_2 K_a [H^+]$ dominates the composite rate constant ($k_1 K_1 + k_2 K_2 K_a [H^+]$) at 20°C. The values of k_{rx} and k_a determined at pH 7 and 10°C and 15°C were reported earlier. If the relationship $k_2 K_2 = 6 k_1 K_1$ found earlier at 20°C is assumed to hold down to 10°C, values for $k_1 K_1$ and $k_2 K_2$ can be determined, since

$$k_a = \frac{K_1 + K_2 K_a [H^+]}{1 + K_a [H^+]}$$

and

$$k_1 K_1 + k_2 K_2 K_a [H^+] = k_{rx} (k_a) (1 + K_a [H^+])$$

At pH 7, $K_a = 10^{+6.9}$, values for $k_1 K_1$ and $k_2 K_2$ can be calculated using these relationships. The results are tabulated in Table 14. Therefore, at pH 7 the reaction of the protonated sites does dominate the overall rate of reaction. The experimentally determined constants largely reflect the rate constants of the protonated sites but are slightly reduced due to the contribution of the unprotonated sites.

TABLE 14. CALCULATED VALUES OF k_1K_1 AND k_2K_2 AT 10° AND 15°C

T	k_a	$K_1 + K_2K_a [H^+]$	k_{rx}	$k_1K_1 + k_2K_2K_a [H^+]$	k_1K_1	k_2K_2
10°C	0.951 atm^{-1}	0.755 atm^{-1}	$2.06 \times 10^{-6} \text{ l/m}^2\text{-min}$	$1.56 \times 10^{-6} \text{ l/m}^2\text{-min}$	$0.271 \times 10^{-6} \text{ l/m}^2\text{-min}$	$1.62 \times 10^{-6} \text{ l/m}^2\text{-min}$
15°C	0.704 atm^{-1}	0.600 atm^{-1}	$3.38 \times 10^{-6} \text{ l/m}^2\text{-min}$	$2.03 \times 10^{-6} \text{ l/m}^2\text{-min}$	$0.352 \times 10^{-6} \text{ l/m}^2\text{-min}$	$2.11 \times 10^{-6} \text{ l/m}^2\text{-min}$
<p>where $(k_1K_1 + k_2K_2K_a [H^+]) = 0.961 k_2K_2$</p> <p>$(k_1K_1 + k_2K_2K_a [H^+]) = 5.77 k_1K_1$</p> <p>assuming $K_a = 10^{6.9}$, $k_2K_2 = 6 k_1K_1$, pH 7.</p>						

Summary and Conclusions. The oxidation of suspensions of ferrous sulfide in aqueous solution has been demonstrated to proceed via a surface reaction involving ferrous sulfide and molecular oxygen. The general reaction sequence consists of the adsorption of molecular oxygen onto the ferrous sulfide surface. This is followed by a redistribution of electrons resulting in the breaking of the oxygen double bond. The electronic rearrangement is the rate-limiting step in the overall reaction.

This initial reaction may result in the formation of free radicals which then proceed to react rapidly, completing the reaction sequence.

The experimental design was not favorable for studying the reaction sequence following the initial rate-limiting step. The presence of phenol, which acts to terminate free radical chains, had no measurable effect on the rate of oxidation, however.

The rate of oxidation appears to have first-order dependence on the surface area present and the concentration of oxygen complexes present on the surface. At low oxygen concentrations (≤ 10 mg/l), which are relevant in natural systems, the rate of oxidation exhibits a pseudo first-order dependence upon the partial pressure of oxygen in solution.

A number of other parameters, including pH, temperature, catalysts, and ionic strength also influence the overall rate of oxidation observed. The effect of each parameter is incorporated into an expression describing the overall rate of oxidation. The kinetic expression describes the rate of oxidation quite well as a function of all of the parameters investigated.

The reactions leading to the formation of various sulfur oxidation products appears to occur at least one step removed from the initial rate-limiting reaction step. This is indicated by the lack of correlation between the rate of oxidation and sulfur products formed at pH 9 under various conditions.

The information and interpretations presented provide a basis for understanding the oxidation of ferrous sulfide in natural systems. The observed effects of various heavy metals upon the oxidation rate of ferrous sulfide provides insight into the distribution of heavy metals in sulfidic sediments and their association with ferrous sulfide. This provides a sound starting point for determining the probable redistribution of heavy metals in sulfidic sediments upon exposure to oxygenated environments.

SECTION V

AQUEOUS CHEMISTRY OF SILVER

Electronic Structure and Oxidation States

Elemental silver has the electronic configuration $1s^2 2s^2 2p^6 3s^2 3p^6 3d^{10} 4s^2 4p^6 4d^{10} 5s^1$ and is a member of subgroup Ib in the Periodic Table, which also contains copper and gold. The members of this group differ from the alkalis in that they are not readily oxidized. Like copper and gold, silver has a single s electron outside a completed d shell, but in spite of the similarity in electronic structures and ionization potentials there are few resemblances among the three elements.

The intervening filled 4d-shell of silver shields very imperfectly the 5s electron from the increased attractive force of the nucleus. This results in a much greater amount of energy required to remove the 5s electron as compared to rubidium (electronic structure: $1s^2 2s^2 2p^6 3s^2 3p^6 3d^{10} 4s^2 4p^6 5s^1$). The increased nuclear attraction for the extranuclear electrons also results in a smaller ionic radius of silver(I) as compared to rubidium(I), 1.26 Å to 1.48 Å, respectively. Removal of subsequent electrons from the 4d subshell of silver(I) is more difficult than from the 3d subshell of copper(I) because of the intervention of an empty 4f subshell in the silver ion. Consideration of the electronic structure thus explains the loss of reactivity towards the formation of monovalent ions when compared to rubidium and the increased stability of the I state when compared to copper (Thompson, 1973).

Twenty-seven isotopes of silver are known; two of these, ^{107}Ag and ^{109}Ag , are not radioactive and are found in nature with an abundance of 51.82% and 48.18%, respectively. Four oxidation states are known: 0, I, II, and III. The two higher oxidation states are either unstable in water or can only exist in insoluble compounds under special conditions. The chemistry of these higher oxidation states is not included in this discussion.

Elemental silver has the highest electrical and thermal conductivities, a very high reflectivity, and probably the lowest emissivity (black body coefficients) of all the elements. The metal appears to have only one crystal form, a face-centered cubic arrangement with a lattice constant $a = 4.086 \text{ Å}$. The distance between silver atoms is 2.884 Å. Silver is appreciably diamagnetic, and its magnetic susceptibility is almost independent

of temperature. Although silver is the middle element of the Ib series, its physical properties exhibit extreme values rather than values that fall between copper and gold, e.g., melting point (minimum), boiling point (minimum), and thermal conductivity (maximum). The metal exhibits a steel-gray color similar to that of the majority of the metals rather than a color similar to copper and gold (Thompson, 1973).

Bonding and Structure of Silver(I) Complexes

Hard and Soft Acids and Bases Principle. Pearson (1969) has summarized a unifying concept by which chemical reactivities, selectivities, and stabilities of compounds may be readily rationalized. Chemical entities including atoms, molecules, ions, and free radicals are characterized as "hard" and "soft" Lewis acids or bases. The hard species in general have small atomic radius, high effective nuclear charge, and low polarizability, whereas soft species possess the opposite characteristics. It is known from classical theory that a strong acid and a strong base form a stable complex, and a weaker acid and base will form a less stable one. The strength of Lewis acids and bases is heightened by increased charge and decreased radius of cations and anions. However, the complex stability cannot be adequately estimated by considering the intrinsic strengths alone; softness parameters have to be introduced. Acids show greater affinity for bases of the same class and vice versa. Thus, hard acids (acceptors) tend to form strong bonds with hard bases (donors) and bind reluctantly or weakly to soft bases. The latter class of compounds interacts preferably with soft acids.

Ligands coordinated to hard acceptors are generally held by bonds of an essentially electrostatic character, while the less numerous group of soft acceptors forms bonds which are markedly covalent. With a certain group of ligands of the same charge, e.g., the halide ions, the complexes formed by hard acceptors are invariably stronger with decreasing ligand size. The complexes also become stronger with increasing charge or decreasing size of the acceptor involved. For soft acceptors on the other hand, the strongest complex is not formed by the smallest ligand of a series, but by a succeeding one (e.g., I^- instead of F^-). Strong complexes are often formed with uncharged ligands of low polarity, or even no polarity at all,

e.g., the olefins. Soft acceptors form strongly covalent bonds, especially when the ligands are also very soft. Such ligands as a rule exert only weak electrostatic attraction and are therefore not coordinated by hard acceptors.

Only aqueous systems are considered here and the complex formation is therefore, in fact, a substitution of ligands for water molecules within the inner coordination sphere of the acceptor. The reaction thus involves not only the formation of acceptor/ligand bonds, but also the breaking of acceptor/water bonds (where oxygen is a hard base or donor), and hence a liberation of water molecules. The solvation energy is thus not only a function of charge but the softness of the acceptor.

Silver(I) is the normal stable oxidation state for silver in aqueous media. As an acceptor silver(I) behaves in a markedly different manner than first-row transition elements in that it is generally classified as soft in character. This difference in behavior is apparent in the preference of silver(I) for coordination to the heavier donor atoms of groups VB and VIB and with the olefinic bond which are classified as soft donors (see Table 15). Since silver(I) has a low cationic charge with filled d-orbitals and a moderate ionic radius, it presents orbitals of suitable size and symmetry for back π -bonding and is strongly polarizing towards the large polarizable donors. This latter property appears to be the more important factor in the coordination chemistry of silver(I). When coordinated to many ligands, especially the harder donors such as nitrogen, silver(I) appears to prefer a linear (sp) stereochemistry with a coordination number of two. However, with softer donors a coordination number of four (sp^3) or some intermediate value (1 or 3) is often preferred.

Silver(I) Bonds with Oxygen and Nitrogen. Oxygen and nitrogen cannot form donor π -bonds with silver(I) since neither oxygen nor nitrogen have vacant d- or p-orbitals. Ligands containing oxygen or nitrogen as donors are usually classified as hard donors. Silver(I) shows a pronounced tendency to exhibit linear two-fold coordination with such donors. This may be due to a relatively small energy difference between the filled d-orbitals and the unfilled s-orbital which permits extensive hybridization of the d_{z^2} - and s-orbitals (Cotton and Wilkinson, 1972). However, most chemists characterize the linear structure about the silver atom as produced by sp

TABLE 15. CLASSIFICATION OF LEWIS ACIDS AND BASES*

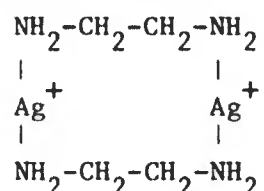
<u>Lewis Acids:</u>	Hard --	H^+, Li^+, Na^+, K^+
		$Be^{2+}, Mg^{2+}, Ca^{2+}, Sr^{2+}$
		$Al^{3+}, Cr^{3+}, Fe^{3+}, As^{3+}, Co$
		$Si^{4+}, Zr^{4+}, Th^{4+}, Hf^{4+}$
	Borderline --	$Fe^{2+}, Co^{2+}, Ni^{2+}, Cu^{2+}, Zn^{2+}, Pb^{2+}$
		$SO_2, C_6H_5^+$
	Soft --	$Cu^+, Ag^+, Au^+, Hg_2^{2+}$
		$Pd^{2+}, Cd^{2+}, Hg^{2+}, CH_3Hg^+$
<u>Lewis Bases:</u>	Hard --	H_2O, OH^-, F^-
		$CH_2COO^-, PO_4^{3-}, SO_4^{2-}$
		CO_3^{2-}, ClO_4^-
		ROH, RO^-
		NH_3, RNH_2
	Borderline --	$C_6H_5NH_2, C_5H_5N, Cl^-, Br^-, NO_2^-$
	Soft --	R_2S, RSH, RS
		$SCN^-, S_2O_3^{2-}, CN^-, I^-$
		R_3P, R_3As
		C_2H_4, C_6H_6
* After Pearson (1969).		

hybridization (Thompson, 1973). Regardless of the type of hybridization, these donors are characterized by a coordination number of two with a linear structure. For monodentate ligands, the species AgL , AgL_2 , AgL_3 , and AgL_4 can exist, but the stability constants K_1 and K_2 are usually high whereas K_3

and K_4 are relatively small. Hence the main species are of the linear AgL_2 type, e.g., complexes with OH^- , NH_3 , and CN^- in Table 16.

Silver(I) is evidently solvated in aqueous solution, but an aquo ion does not occur in salts, practically all of which are anhydrous. Silver nitrate and silver perchlorate are water soluble, but silver sulfate and silver acetate are only sparingly so. Silver(I) is weakly hydrolyzed, leading to only two species, $AgOH^0$ and $Ag(OH)_2^-$. Silver(I) complexes are also weak with other oxo anions such as sulfate, acetate, phosphate, carbonate, and nitrate.

Since the most stable silver(I) complexes with oxygen and nitrogen have a linear structure, bidentate and other chelating ligands cannot form simple ions and hence tend to give polynuclear complexes. For example, 1,2-diaminoethane (en) forms the following polynuclear complex allowing silver to retain a linear stereochemistry:



This behavior contrasts silver with first-row transition elements (harder acceptors) which form simple stepwise complexes of the type $M(en)_x^{z+}$.

A comparison of ligands with first-row heteroatoms (hard donors), where only a donor interaction to silver exists, shows the coordination affinity sequence $N > O > F$ for a similar series of ligands, e.g., $NH_3 > H_2O > HF$. This can be explained by the fact that the lone electron pairs of the heteroatoms in the p-orbitals become more numerous in this sequence, and so there will be an increasing repulsion between these non-bonding pairs and the electrons in the 4d-orbital of silver. Thus, nitrogen donor complexes are more significant in the complex chemistry of silver(I), e.g., NH_3 and CN^- in Table 16. Silver is primarily bonded to the amino group in amino acids as evidenced by similar stability constants for amino acids with different locations of the amino group (Sillén and Martell, 1964, 1971):

	$\log K_1$	$\log \beta_2$
2-aminopropanoic acid	3.6	7.1
3-aminopropanoic acid	3.4	7.3
4-aminobutanoic acid	3.5	7.2

TABLE 16. SOLUBILITY AND COMPLEX FORMATION EQUILIBRIA FOR SILVER

No.	I. Solubility Equilibria	pK^* (25°C)
1.	$Ag(s) = Ag^+ + e^-$	13.51
2.	$\frac{1}{2}Ag_2O + \frac{1}{2}H_2O = Ag^+ + OH^-$	7.71
3.	$Ag_2CO_3(s) = 2Ag^+ + CO_3^{2-}$	11.07
4.	$Ag_2SO_4(s) = 2Ag^+ + SO_4^{2-}$	4.92
5.	$Ag_3PO_4(s) = 3Ag^+ + PO_4^{3-}$	15.98
6.	$AgCl(s) = Ag^+ + Cl^-$	9.75
7.	$AgCN(s) = Ag^+ + CN^-$	16.23
8.	$AgSCN(s) = Ag^+ + SCN^-$	11.99
9.	$Ag_2S(\alpha, s) = 2Ag^+ + S^{2-}$	49.18
10.	$Ag_2S(\beta, s) = 2Ag^+ + S^{2-}$	48.97
	II. Complex Formation Equilibria	$\log k^*$ (25°C)
	<u>Oxygen Donors</u>	
11.	$Ag^+ + OH^- = AgOH^0$	2.1
12.	$Ag^+ + 2OH^- = Ag(OH)_2^-$	4.0
13.	$Ag^+ + NO_3^- = AgNO_3^0$	-0.3
14.	$Ag^+ + SO_4^{2-} = AgSO_4^-$	1.3
15.	$Ag^+ + Ac^- = AgAc^0$	0.7 ^a
16.	$Ag^+ + Ph^- = AgPh^0$	0.3 ^{a,e}
	<u>Nitrogen Donors</u>	
17.	$Ag^+ + NH_3 = Ag(NH_3)^+$	3.3
18.	$Ag^+ + 2NH_3 = Ag(NH_3)_2^+$	7.2
19.	$Ag^+ + 2NH_3 + Cl^- = Ag(NH_3)_2Cl^0$	6.9
20.	$Ag^+ + EtA = AgEtA^+$	3.4 ^{a,f}
21.	$Ag^+ + 2EtA = Ag(EtA)_2^+$	7.3 ^a

TABLE 16. (CONTINUED)

		<u>log k* (25°C)</u>
22.	$\text{Ag}^+ + \text{en} = \text{Ag(en)}^+$	4.7 ^{a,g}
23.	$\text{Ag}^+ + 2\text{en} = \text{Ag(en)}_2^+$	7.7 ^{a,g}
24.	$2\text{Ag}^+ + 2\text{en} = \text{Ag}_2(\text{en})_2^{2+}$	13.2 ^{a,g}
25.	$\text{Ag}^+ + \text{H(en)}^+ = \text{AgH(en)}^{2+}$	2.35 ^{a,g}
26.	$\text{Ag}^+ + \text{Pip} = \text{Ag(Pip)}^+$	3.1 ^{a,f}
27.	$\text{Ag}^+ + 2\text{Pip} = \text{Ag(Pip)}_2^+$	6.6 ^{a,f}
28.	$\text{Ag}^+ + \text{Gly}^- = \text{Ag(Gly)}^0$	3.5 ^a
29.	$\text{Ag}^+ + 2\text{Gly}^- = \text{Ag(Gly)}_2^-$	6.9 ^a
30.	$\text{Ag}^+ + \text{Pyr} = \text{Ag(Pyr)}^+$	2.0 ^a
31.	$\text{Ag}^+ + 2\text{Pyr} = \text{Ag(Pyr)}_2^+$	4.1 ^a
32.	$\text{Ag}^+ + \text{Imid} = \text{Ag(Imid)}^+$	3.2 ^{a,g}
33.	$\text{Ag}^+ + 2\text{Imid} = \text{Ag(Imid)}_2^+$	7.0 ^{a,g}
34.	$\text{Ag}^+ + \text{Hista} = \text{Ag(Hista)}^+$	4.9 ^a
35.	$\text{Ag}^+ + \text{Histid}^- = \text{Ag(Histid)}^0$	6.5 ^a
36.	$\text{Ag}^+ + 2\text{Histid}^- = \text{Ag(Histid)}^-$	14.3 ^a
37.	$\text{Ag}^+ + 2\text{CN}^- = \text{Ag(CN)}_2^-$	20.4
38.	$\text{Ag}^+ + 3\text{CN}^- = \text{Ag(CN)}_3^{2-}$	21.4 ^a
39.	$\text{Ag}^+ + \text{CN}^- + \text{OH}^- = \text{Ag(CN)(OH)}^-$	13.5
40.	$\text{Ag}^+ + \text{SCN}^- = \text{Ag(SCN)}^0$	4.75
41.	$\text{Ag}^+ + 2\text{SCN}^- = \text{Ag(SCN)}_2^-$	8.3
42.	$\text{Ag}^+ + 3\text{SCN}^- = \text{Ag(SCN)}_3^{2-}$	9.5
43.	$\text{Ag}^+ + 4\text{SCN}^- = \text{Ag(SCN)}_4^{3-}$	9.8
<u>Halide Donors</u>		
44.	$\text{Ag}^+ + \text{Cl}^- = \text{AgCl}^0$	3.3
45.	$\text{Ag}^+ + 2\text{Cl}^- = \text{Ag(Cl)}_2^-$	5.3

TABLE 16. (CONTINUED)

		<u>log k* (25°C)</u>
46.	$\text{Ag}^+ + 4\text{Cl}^- = \text{Ag}(\text{Cl})_4^{3-}$	6.1 ^a
47.	$\text{Ag}^+ + \text{I}^- = \text{AgI}^0$	6.6 ^a
48.	$\text{Ag}^+ + 3\text{I}^- = \text{AgI}_3^-$	13.8 ^a
49.	$\text{Ag}^+ + 4\text{I}^- = \text{AgI}_4^-$	14.4 ^a
<u>Sulfur Donors</u>		
50.	$\text{Ag}^+ + \text{HS}^- = \text{Ag}(\text{HS})^0$	16.2 ^b
51.	$\text{Ag}^+ + 2\text{HS}^- = \text{Ag}(\text{HS})_2^-$	18.0 ^b
52.	$\text{Ag}^+ + \text{S}_2\text{O}_3^{2-} = \text{AgS}_2\text{O}_3^-$	8.9 ^a
53.	$\text{Ag}^+ + 2\text{S}_2\text{O}_3^{2-} = \text{Ag}(\text{S}_2\text{O}_3)_2^{3-}$	13.2 ^d
54.	$\text{Ag}^+ + \text{S}_2\text{O}_3^{2-} + \text{Cl}^- = \text{Ag}(\text{S}_2\text{O}_3)\text{Cl}^{2-}$	10.8 ^{a,e}
55.	$\text{Ag}^+ + 2\text{S}_4^{2-} = [\text{Ag}(\text{S}_4)_2]^{3-}$	20.8 ^c
56.	$\text{Ag}^+ + \text{S}_4^{2-} + \text{S}_5^{2-} = [\text{Ag}(\text{S}_4)(\text{S}_5)]^{3-}$	20.2 ^c
57.	$\text{Ag}^+ + \text{HS}^- + \text{S}_4^{2-} = [\text{Ag}(\text{HS})(\text{S}_4)]^{2-}$	20.4 ^c
58.	$\text{Ag}^+ + 3\text{tu} = \text{Ag}(\text{tu})_3^+$	13.1 ^a
59.	$\text{Ag}^+ + 2\text{Thioacet}^- = \text{Ag}(\text{Thioacet})_2^-$	13.7 ^{a,f}
60.	$\text{Ag}^+ + \text{EtSPhSulf}^- = \text{Ag}(\text{EtSPhSulf})^0$	2.6 ^{h,g}
<u>Key to Ligand Abbreviations</u>		
Ac = acetate	Pyr = pyridine	
Ph = phenol	Imid = imidazole	
EtA = ethylamine	Hista = histamine	
en = ethylenediamine	Histid = histidine	
Pip = piperidine	tu = thiourea	
Gly = glycine	Thioacet = thioacetamide	
EtSPhSulf = p-ethylthiobenzenesulphonate		
<p>* Equilibrium constants presented here were calculated from free energy data for solution conditions of 25°C and zero ionic strength, unless indicated otherwise. From National Bureau of Standard Technical Notes 270-3 and 270-4, "Selected Values of Chemical Thermodynamic Properties, U.S. Dept. of Commerce, Washington, D.C. (1969).</p>		

TABLE 16. (CONCLUDED)

^aConstant selected from L. G. Sillén and A. E. Martell, "Stability Constants of Metal-Ion Complexes," The Chemical Society (London), Special Publications No. 17 (1964) and No. 25 (1971).

^bConstants from Y. I. Ol'shanskii, V. V. Ivanenko, and A. V. Khromov (1959). See references.

^cConstants modified from Cloke (1963b). See references.

^dCalculated from free-energy data from W. M. Latimer, "Oxidation Potentials," 2nd ed., Prentice-Hall (1952).

^eSolution conditions: 1 molar electrolyte, 25°C.

^fSolution conditions: 0.5 molar electrolyte, 25°C.

^gSolution conditions: 0.1 molar electrolyte, 25°C.

^hConstants from Ahrlund, Chatt et al., 1958a. See references.

Lanza (1968) shows that silver(I) forms complexes with glycine even when the carboxyl hydrogen is still present, e.g., $^+Ag-NH_2-CH_2-COOH$. The complex is stable enough that it comprises about 10% of the total silver at pH 5.0 in $H_2O-Ag(I)$ -glycine systems containing excess ligand. Aromatic amines and other conjugated cyclic ligands containing nitrogen as a heteroatom form weaker complexes with silver(I) than aliphatic amines because the lone electron pair is strongly conjugated with the aromatic system. For example, compare the stability constants of ammonia and 1,2-diaminoethane with pyridine and aniline:

	$\log K_1$	$\log \beta_2$
ammonia	3.3	7.2
1,2-diaminoethane	4.7	-
pyridine	2.0	4.1
aniline	1.4	-

The large stability constants for silver(I) with cyanide are due to p_π -bonding but still show twofold coordination.

Silver(I) Bonds with Sulfur, Selenium, Phosphorus, and Arsenic.

The difference in behavior of silver(I) compared to the first-row transition metal ions is apparent in the preference of silver for coordination to the

heavier donor atoms of groups VB and VIB, i.e., sulfur, selenium, phosphorus, and arsenic. This difference in behavior is a result of back π -bonding of silver(I) with these ligands. A metal-ligand complex is stabilized in cases where a donor π -bond is formed between the metal and ligand in addition to the ordinary coordinative σ -bond. This π -bond is formed by the transition of d-electrons from the metal ion to the vacant d- or p-orbitals of the ligand. The presence of the π -bond also results in a strengthening of the coordinative σ -bond, which is formed by the electron pair transferred by the ligand donor atom to the silver ion. In fact, a transfer of d-electrons from the silver ion to the ligand results in an increase of electron affinity of the silver ion which, in turn, produces an intensified retention of the electron pair of the σ -bond. The same ligand atom which participates in the complex formation may act both as an electron donor in the σ -bond and as an electron acceptor in the donor π -bond. The formation of a π -bond with the silver ion assumes that the ligand has vacant d- or p-orbitals in its outer electron shell capable of receiving d-electrons from silver. This requirement is satisfied almost exclusively by the heavier elements of groups VB and VIB, ligands and chelons containing phosphorus, sulfur, arsenic, selenium, or tellurium as donor atoms (Cotton and Wilkinson, 1972).

d_{π} -bonding by the donor atom of a ligand has a marked effect on the coordination number and stereochemistry of silver(I) complexes. d_{π} -bonding by the ligand atom on the x-coordinate would involve d_{xy} - and d_{xz} -orbitals of the metal, probably hybridized with the p_y - and p_z -orbitals, respectively. These orbitals and electrons in them would also have to be used for d_{π} -bonding to a second ligand molecule if it were attached in the diametrically opposite position to the first. Since they are already used in bonding to the first, they are not so readily available for the second ligand and its attachment is delayed. Indeed, if d_{π} -bonding by the ligand atom contributes significantly to the bond strength, the second ligand will not attach in the diametrically opposite position but rather in a trigonal or tetrahedral position. Thus, it can be seen that strong d_{π} -bonding, such as occurs in complexes of silver(I) with ligands containing the heavier elements of groups VB and VIB, lowers the stability of the linear complex, AgL_2 , and increases that of the first complex, AgL (Ahrland et al., 1958b).

A demonstration of this effect is evident in the complex formation of silver(I) with sulfur-containing ligands. Silver sulfide is probably the least soluble solid in water of all silver compounds. It dissolves to an insignificant extent in dilute non-oxidizing acids; the most significant solution species are the bisulfide complexes in the neutral pH range. Note the enhanced stability of the $\text{Ag}(\text{HS})^0$ complex compared to the stability of $\text{Ag}(\text{HS})_2^-$ in Table 16. It is also known that the bonding in silver sulfide and the bisulfide complexes is not linear (Thompson, 1973). Both of these characteristics are indicative of strong d_{π} -bonding.

Although sulfide and bisulfide complexes of silver(I) are not strong enough to significantly increase the solubility of silver sulfide, Cloke (1963b) shows that the polysulfide complexes of silver(I) can increase the solubility to 10^{-5} total dissolved silver. The important complexes are $\text{Ag}(\text{S}_4)_2^{3-}$, $\text{Ag}(\text{HS})(\text{S}_4)^{2-}$, and $\text{Ag}(\text{S}_4)(\text{S}_5)^{3-}$ but probably other polysulfide complexes also exist. The experiments were conducted at 25°C in solutions of varying sodium polysulfide concentrations, and Cloke (1963b) makes estimates of the stability constants of the three aforementioned complexes. The stability constants determined by Cloke have been modified to be consistent with the NBS value for the free energy of formation value of the sulfide ion since Cloke (1963a) uses a different value to compute the stability constants. The modified constants are shown in Table 16. The importance of these complexes is dependent on the kinetic stability of the polysulfide species.

The strength of complexes of silver(I) with ligands containing sulfur depends on the electron environment in which the sulfur donor atom exists in the ligand molecule. The usual qualitative observation that aliphatic derivatives of the donor atom form more stable complexes than aromatic derivatives holds true for sulfur. Sulfur-containing chelons with a thioether group, $\text{R}_1\text{-S-R}_2$, give a more stable π -bond than those with a sulfhydryl group, R-SH (Cotton and Wilkinson, 1972). The strength of complexes of silver(I) with the various oxoanions of sulfur depend on the availability of the sulfur atoms for bonding. Thus, silver thiosulfate forms strong complexes whereas silver sulfate does not. The thiosulfate complexes are decreased in strength as compared to the bisulfide complexes, and all show the enhanced stability of the AgL complex (see Table 16).

Little data is available for silver-phosphorus bonding. It is known that silver(I) forms its strongest d_{π} -bonds when phosphine is the donor atom. Ahrland et al. (1958b) show that aromatic phosphines form complexes with silver(I) significantly stronger than those formed with analogous aromatic sulfides. This is probably due to the strengthening of the coordinative σ -bond for group VB elements as compared to the VIB elements, as previously mentioned in the case of nitrogen and oxygen. Silver phosphate is less soluble than silver sulfate, and silver phosphate complexes are probably stronger than silver sulfate complexes. No data is available for aliphatic phosphorus-containing ligands, which theoretically would form even stronger bonds with silver(I).

Ahrland et al. (1958a) confirm the observations of earlier workers that silver(I) complex stabilities increase in the order sulfur < selenium < tellurium for analogous ligands containing the donor atoms. In general, the polarizability and soft character of the donor atom increase as the element in the group becomes heavier. Phosphorus and arsenic do not fit in this pattern in the case of silver(I) complexes, but arsenic appears to be a special case since there is no known example of a complex in which arsenic as the donor atom is more stable than its phosphorus analog (Ahrland et al., 1958b).

Silver(I) Bonds with Halogens and Other Donors. The strength of silver(I)-halide bonds follows from a consideration of the hard-soft character of the halides. The solubility decreases and the stability constants for complexes increase in the order: $F < Cl < Br < I$. This trend illustrates the soft character of silver(I) as an acceptor in its preference for the larger and more polarizable ligands. The bonds become more covalent with the heavier halide atoms, indicating some d-electron contribution of silver to the unfilled d-orbitals of the halide. The contribution of the d_{π} -bonding is diminished with respect to the analogous heavier elements of groups VB and VIB by the electron repulsion of the unused lone pairs of the halide ligands. The resulting strength of the bonds is thus intermediate between that observed for nitrogen and oxygen bonding and that of the heavier elements of groups VB and VIB (see Table 6, Cl^- and I^- complexes). The coordination number and stereochemistry effects of the ligands are also intermediate in nature.

Silver(I) shows its soft character in the strength of its complexes with the olefinic bond as compared to other transition metals. Complexes between silver(I) and olefins have probably been more extensively studied than those of any other metal ion, mainly because of its importance as a catalyst in carbonium ion reaction chemistry. Bonding between an alkene and silver(I) can be described in the following way: a σ -type bond, as a result of donation of π -electrons from the occupied 2p-bonding orbital of the olefinic system into the vacant 5s-orbital of the silver ion, and a π -type bond, as a result of back-donation of d-electrons from occupied 4d-orbitals of the silver into the unoccupied π^* -2p antibonding orbitals of the olefinic system, thus decreasing the stability of the olefinic bond itself. The stability of this complex is weak when compared to complexes of silver(I) with other donors, roughly equivalent to the stabilities of acetate and fluoride ions with silver(I). Complex stability and bonding will be affected by the availability of electrons in the filled orbitals of the olefinic system, which is dependent on the inductive and steric effects of substituents. An increased electron density at the carbon-carbon double bond should enhance σ -type bond formation and weaken the π -type bond. Although both σ - and π -type bonds are important for complex stability, their relative importance is not known and this makes the influence of electronic effects difficult to predict, particularly because the study of substituent effects causes a blend of steric and electronic influences (Beverwijk et al., 1970).

In silver(I) coordination complexes with aromatic compounds an interaction exists between the silver ion and the π -electronic system, including σ - and π -type molecular bonds similar to the interaction just described for the olefinic bond. However, in arene-silver coordination σ -type bonding seems to be more significant. Substituent effects are again a blend of factors. An increasing capacity of the substituent to donate electrons to the ring causes an increase of the stability constant, suggesting that primarily σ -type bonding contributes to the coordination. Thus, the stability of the complexes increases when the donor molecules are changed from benzene to toluene and to the xylenes. However, upon further substitution the stability constants decrease due to a steric interference between the ring alkyl groups and the water molecules in the hydration sphere of the silver ion (Beverwijk et al., 1970).

Andrews and Keefer (1949) and Smith and Rundle (1958) have proposed structures for solution complexes and solid complex compounds containing silver(I)-arene coordinative bonds. For both types of complexes silver ions are positioned above and below the plane of the benzene ring and equidistant from the six carbon atoms comprising the ring. The π -electrons of the benzene molecule are considered to be polarized toward the silver atoms.

Comparison of Bond Strengths Among Donor Groups. The type of bonding, coordination number, and the relative strength of bonding of various donor groups can be deduced from plots of the formation curves of unidentate ligands containing the donor group. Formation curves show the average ligand number per silver atom, \bar{n} , versus total concentration of ligand added, assuming excess ligand present (see Figure 46). The formation curves are of three main types: 1) those (NH_3 , Cl^-) which have a stop or inflection at $\bar{n} = 2$, 2) an intermediate type (S, Se) where the formation of complexes proceeds uniformly to $\bar{n} = 4$, and 3) those (P, As, I^- , HS^-) with a stop or inflection at $\bar{n} = 1$ and $\bar{n} = 3$.

Curves of type (1) are indicative of small or no contribution of d_π -bonding to the complexes. It is easily seen from Figure 46 that the linear AgL_2 complex whose special stability would cause a stop or inflection at $\bar{n} = 2$ is not favored by many of the donor groups, especially phosphorous, arsenic, sulfur, selenium, and iodide, whose contribution to d_π -bonding is expected to be significant. It is clear that silver(I) has no characteristic coordination number but that the number of unidentate ligand molecules which can be accommodated is very sensitive to the nature of the coordinating atoms (Ahrlund et al., 1958b).

The strength of bonds for analogous ligands containing the appropriate donor group or atom increases approximately in the following order: olefins = fluorides < oxides < amines < chlorides < bromides < sulfides < selenides < arsines < iodides < phosphines. Qualitative evidence suggests that the series agrees with the tendency toward d_π -bond formation. Aliphatic derivatives of the coordinating atom usually allow the strongest binding of silver(I) since donor electrons may be strongly conjugated in aromatic systems. Compare the formation curves of HS^- and S in Figure 46.

p_π -bonding capacity on the part of the coordinating atom does not alter the shape of the formation curve in the same manner. In such a case

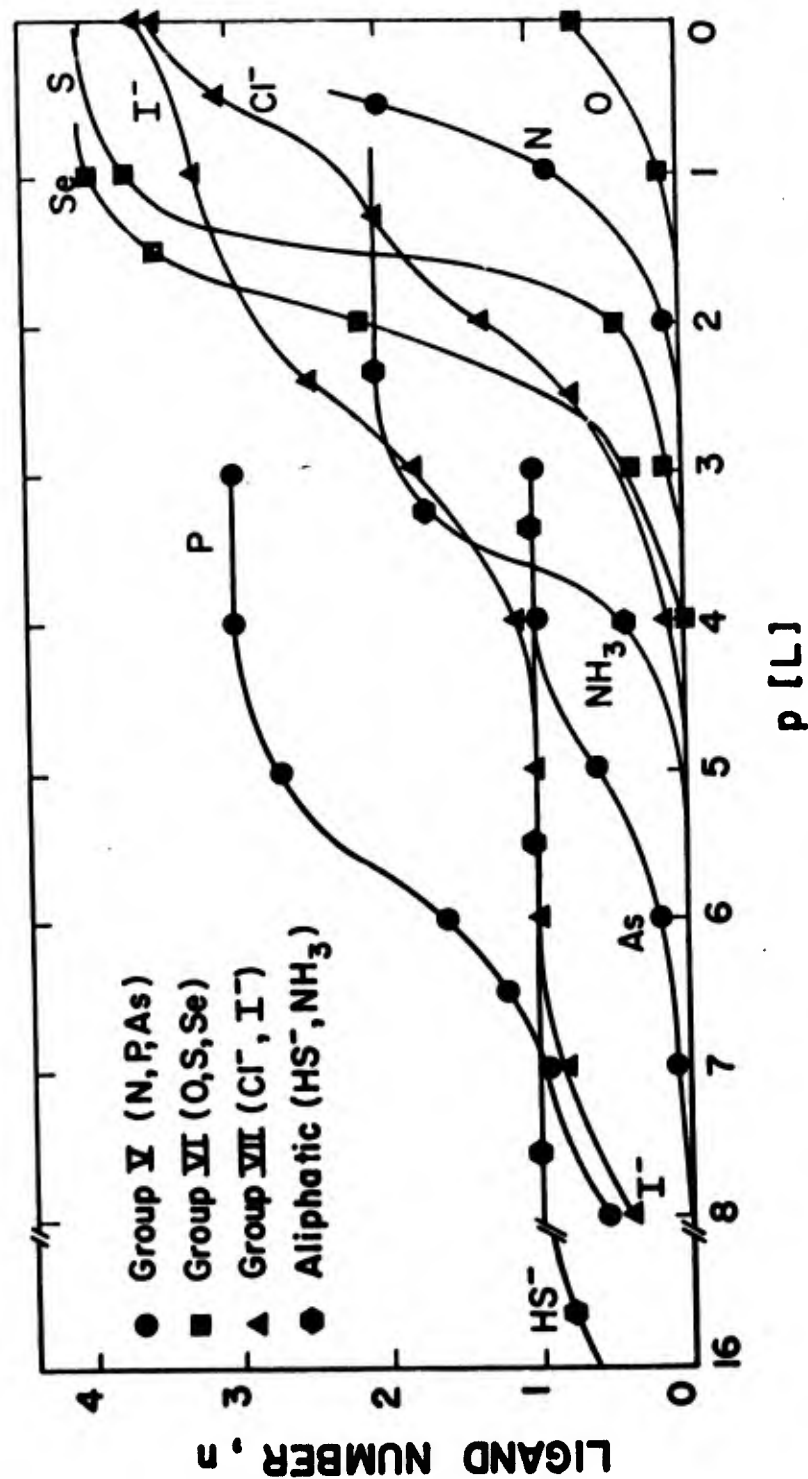
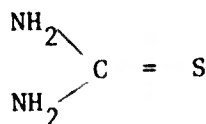


Figure 46. Complex-formation curves for silver(I) with unidentate ligands containing various coordinating atoms. Group V and VI curves are for p-phenyl (atom) benzenesulphonic acid with the appropriate atom in the ligand. Additional curves are shown for Cl⁻, I⁻, HS⁻, and NH₃.

attachment of the first ligand molecule will involve only the electrons of one d-orbital of silver, e.g., d_{xy} . The electrons from the d_{xz} -orbital will then remain available to attach the second ligand in the diametrically opposite position. Thus, the special stability of the linear AgL_2 type of complex is not destroyed by p_π -bonding on the part of the ligand, e.g., CN^- and SCN^- in Table 16 (Ahrland et al., 1958b).

There are many ligands which contain more than one type of donor group or atom, in which case the characterization of the bonding becomes even more complex. Israeli and Pettit (1975) show that silver(I), in contrast to most other transition metal ions, has significant metal-olefin interaction as well as coordination to the amino nitrogen in complexes with unsaturated α -amino acids. In this case, silver(I) deviates from the marked preference for linear coordination typical for nitrogen donor complexes. Bonding in complexes with thiourea changes with the number of ligands



coordinated to the silver atom. For the complex formed with one thiourea molecule, $Ag(tu)$, silver bonds to the extended sulfur atom. For the complex, $Ag(tu)_2$, silver is coordinated in a linear arrangement to one nitrogen atom from each thiourea molecule. For $Ag(tu)_3$, silver is bonded to two nitrogen atoms and one sulfur atom (Enea and Berthon, 1973). As the number of donor atoms available to silver increases in chelates and multidentate ligands, the bonding and structure becomes increasingly more complex.

Photochemistry of Silver(I)

The hydrated silver ion in aqueous solution practically lacks photosensitivity (Clark and Vondjidis, 1968). Mahlman and Willmarth (1964) show that small amounts of elemental silver can be precipitated from 2M aqueous solution of silver nitrate after prolonged exposure to an intense mercury source and other ionizing radiations. The particles are essentially spherical, and the volume of the spheres is directly proportional to the exposure time. For a 20-hr exposure, the spheres have a maximum diameter of 8.75 microns.

Goetz and Inn (1948) find that silver ions adsorb on ZnO or TiO_2 very rapidly and that aqueous suspensions of the particles are extremely photosensitive. Radiation with wavelengths less than 5800 \AA is capable of rapidly reducing the adsorbed silver ions to silver atoms. The silver atoms migrate over the surface of the particle and coalesce into one or several minute silver crystals, occupying a negligible amount of surface area when compared to the adsorbed silver ions. The chemical equilibrium of the surface is destroyed by this reaction, and more silver ions migrate to the surface from the solution to reestablish equilibrium with the surface. By this process of replenishment and subsequent reduction to elemental silver, an almost unlimited amount of silver can be collected on the exposed surface of the particle.

Clark and Vondjidis (1968) report on similar experiments with titanium dioxide and discuss the nature and mechanisms of the interaction with the semiconductor oxide surface. These authors confirm that the adsorbed silver ions were reduced to the metal rather than oxidized, as has been postulated by other workers. The catalytic influence that the oxide surface exhibits on the silver ion must be considerable. The effect is most marked for exposure to wavelengths within the fundamental absorption region of the oxide. The nature of the better-known photolysis of silver halides is certainly different than that of silver which has been sorbed on the oxide surface from an aqueous solution. The absorption of light quanta of sufficient energy results in the production of pairs of electrons and holes; less energetic quanta can be thought to produce excitons which may interact with the crystal to produce electrons and holes. Although the light energy is absorbed within the titania crystallites, the consequent photochemical changes are produced by secondary processes on their surfaces. An electron localized at a surface trap may well be able to become associated with an adsorbed silver ion, producing a silver atom (with high electrical conductivity) which, in turn, is likely to promote the formation of additional atoms (Clark and Vondjidis, 1968).

The results of Fleischauer, Kan, and Shepherd (1972) are in agreement with Goetz and Inn (1948) and Clark and Vondjidis (1968). These workers have found that titanium dioxide is inert with respect to thermal electron transfer to adsorbed silver ions, but under near-UV irradiation, surface

electrons are generated that reduce Ag(I) with quantum efficiencies up to 10% in a matter of seconds for solutions of varying concentration (10^{-4}M to 2M).

The amount of silver reduced in these experiments is negligible compared to the total amount of silver in the experiment. However, this is simply a result of the fact that the amount adsorbed is negligible in comparison to the total silver present since high silver concentrations were used. Titanium dioxide particles covered with a monolayer of reduced silver atoms are obtained in some experiments (Fleischauer, 1975).

In subsequent work Fleischauer and Shepherd (1974) find that after an initial exposure to radiation capable of reducing adsorbed silver ions, additional silver is reduced thermally by treatment with an appropriate reducing agent. The reaction with Fe(II) in particular is investigated. Only adsorbed silver ions are reduced. The process is believed to be electrochemical; a silver nucleus behaves simultaneously as the cathode and anode. Thus, silver nuclei produced by the initial photolytic reaction are required to serve as catalytic sites for the subsequent thermal reduction.

Struempfer (1973) reports that 100% adsorption of silver occurs in six days from 10^{-8}M silver solutions acidified to pH 2 and exposed to normal lighting conditions in glass and polyethylene containers. Identical solutions maintained in the dark do not absorb a significant quantity of silver ($< 2\%$). The rate of adsorption is constant at about 20% per day for the first four days.

Zhitnikov and Paugart (1966) report that silver ions can be reduced on silica surfaces. Fleischauer (1975) expresses doubt about the possibility of the photolysis reaction at the silica-water interface, based on the fact that the absorption region for silica is well into the UV region. Fleischauer (1975) stated that iron and manganese oxides are probably both capable of the photolytic reduction of adsorbed silver, although both are probably less photosensitive than titanium dioxide.

Not enough information is available in the literature to determine whether photolysis of silver in short-term (< 24 hr) adsorption experiments with dilute silver solutions ($< 10^{-5}\text{M}$) is significant. Anderson et al. (1973) have not taken special precautions for shielding experimental solutions from normal laboratory lighting. Experimental work on this question is summarized in a later section.

Silver(I) in Natural Aquatic Systems

The content of silver in natural fresh waters is low and averages 0.2 ppb (Boyle, 1968) with considerable spatial variations. Relatively high concentrations of silver are found in suspended and streambed sediments and in soils over silver-enriched rocks (Turekian and Scott, 1967; Boyle, 1968) ranging from < 1 ppm to over 100 ppm. Turekian, Harriss, and Johnson (1967) find that high concentrations of silver may arise from pollution, but adsorption of silver(I) on suspended stream sediment keeps the solution concentration at a low level. Photoprocessing effluents are the primary source of human technological input of silver to the environment. Photoprocessing effluents usually contain silver as thiosulfate complexes, or precipitates of silver bromide or silver sulfide, depending on the process involved (Bard, Murphy et al., 1976). The removal of silver from natural waters is caused by chemical or physio-chemical interactions occurring between silver and solid components of the sediments and soils. The mechanisms involved may include ion exchange, adsorption, and/or coprecipitation. The mechanisms responsible for controlling the concentration of most trace metals in soils and sediments are dependent upon the speciation and distribution of the metal in the water column. Of the solid components of sediments and soils, hydrous manganese and iron oxides are credited with being strong scavengers for trace metals in the weathering cycle (Jenné, 1968). The great affinity of hydrous oxides of manganese and iron for silver is indicated by the high content of silver in these oxides that occur in nature (Boyle, 1968; Chao and Anderson, 1974). It is not yet clear whether the common abundance and high surface areas of these oxides are solely responsible for the observed adsorptive properties (Leckie and James, 1974).

The composition of natural aquatic systems ranges from highly saline marine water to pristine oligotrophic fresh water to stagnant organic-rich bog and marsh water to anoxic high-sulfide interstitial water of sediments. In typical oxygenated waters the predominant ligands of importance are the oxoanions (NO_3^- , SO_4^{2-} , PO_4^{3-} , CO_3^{2-} , OH^-), chloride, and organic ligands, polymers, and macromolecules whose coordinating functional groups are dominated by those containing the donor atoms nitrogen and/or oxygen (fatty

acids, amino acids, sugars, carbohydrates, alcohols, proteins, amines, fulvic and humic acids). Of course, local pollution inputs to natural waters can change the ligand environment dramatically. Because nitrogen, oxygen, and chloride are the predominant donor atoms available in complexing ligands in oxygenated waters, silver(I) gets little chance to engage in d_{π} -bonding and is usually less complexed than most transition metals in surface waters. Speciation of trace metals is important in the prediction of adsorptive behavior of the metal (MacNaughton and James, 1974).

The ligand and electrochemical environment in anoxic interstitial sedimentary waters is radically different. Such waters are often in contact with ferrous sulfide and other sulfidic mineral phases and may contain high concentrations of dissolved sulfide. The suite of inorganic and organic ligands available for complexation of trace metals likely contains higher concentrations of some ligands, notably those containing sulfur as a donor atom. The distribution of silver in this environment is far more complex, but the predominant solid phases are silver sulfide and elemental silver. Figure 47 shows a stability field diagram for solid silver phases in aqueous solution for total sulfur of $10^{-3}M$ and total chloride of $10^{-4}M$. Higher chloride concentrations increase the predominance area for silver chloride. Note the large areas of predominance for elemental silver and silver sulfide and the small area of silver oxide even for the low chloride concentration chosen. Leckie and Nelson (1975) have computed the concentration of silver species in equilibrium with the dominant solid phase as a function of pE for a solution composition typical of estuarine sediment interstitial waters (see Fig. 48). The dominant solid phase changes from elemental silver to silver sulfide at approximately $pE = -3.7$. The bisulfide complex apparently approaches an upper concentration of $10^{-7}M$ as the pE is decreased below this point. An increase in pH or total sulfide would increase the upper limiting concentration reached by the bisulfide complex.

The small area of predominance for silver oxide in Fig. 47 occurs in a very high pH range, and thus it is unlikely that silver oxide would be found in natural environments. This is a result of the extremely weak binding strength of oxygen for silver(I). This is also apparent in Fig. 49 which graphically displays the hydrolysis behavior of silver(I). The hydroxo complexes of silver(I) are not numerically significant for $pH < 11$,

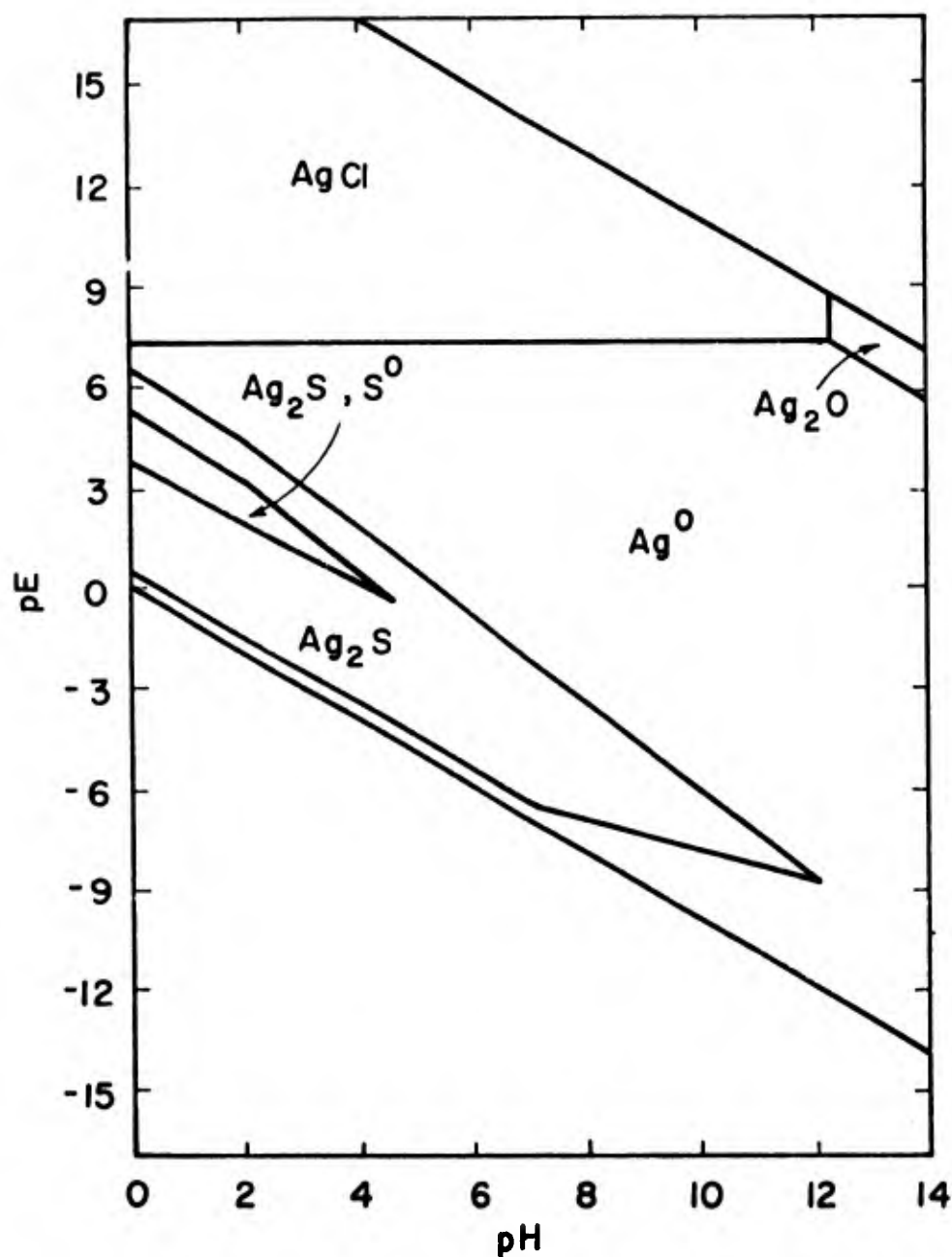


Figure 47. Stability field diagram showing dominance regions for solid silver phases in equilibrium with aqueous solution at 25°C and 1 atm total pressure. pE-pH diagram is computed for conditions of total sulfur of 10^{-3} M, total chloride of 10^{-4} M and total carbonate of 10^{-1} M.

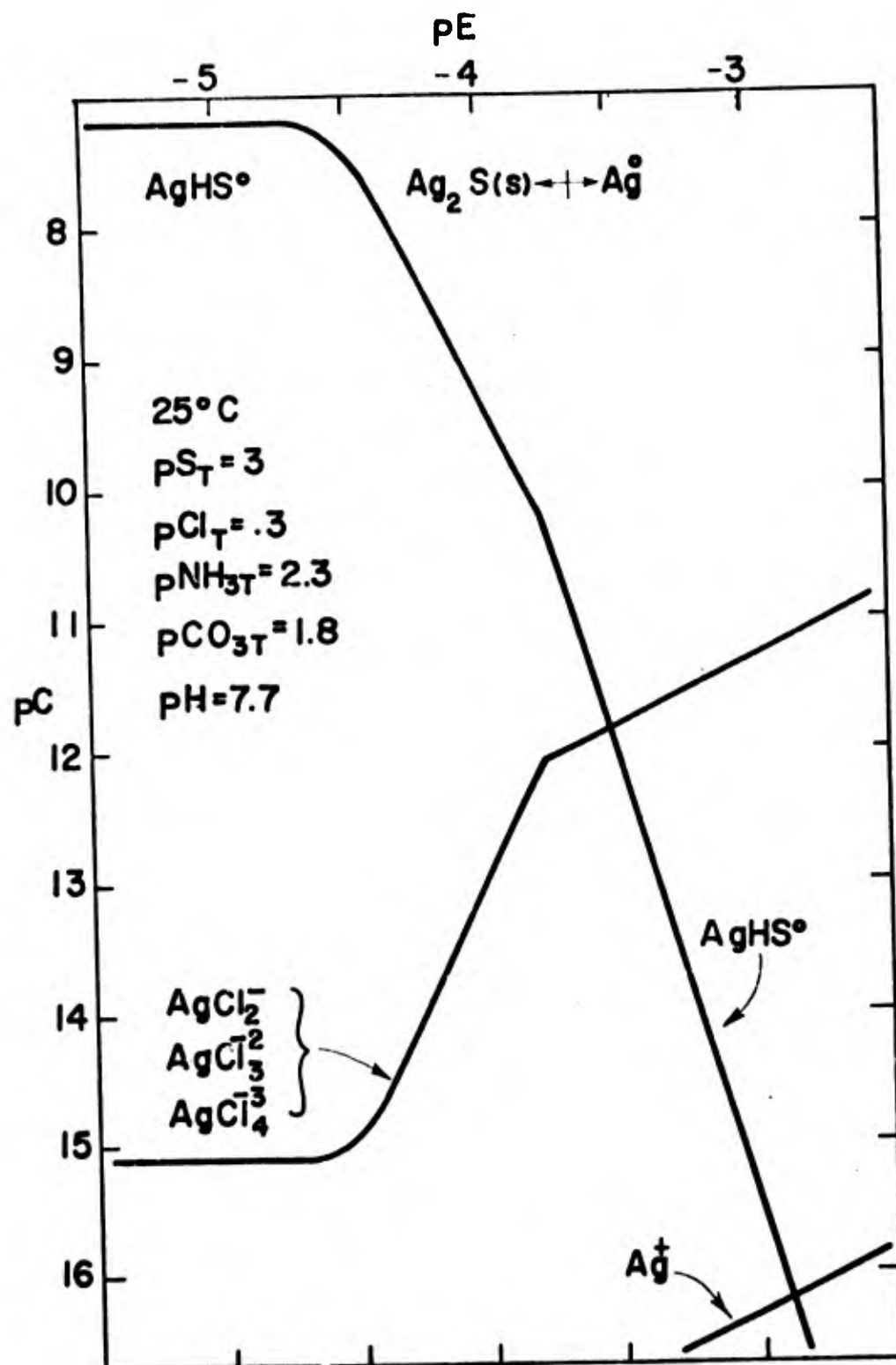


Figure 48. Equilibrium aqueous concentrations of silver species as a function of pE . Note that a phase transition occurs at about pE of -3.7 between $Ag_2S(s)$ and $Ag^\circ(s)$. Solution composition is typical of estuarine sediment interstitial waters.

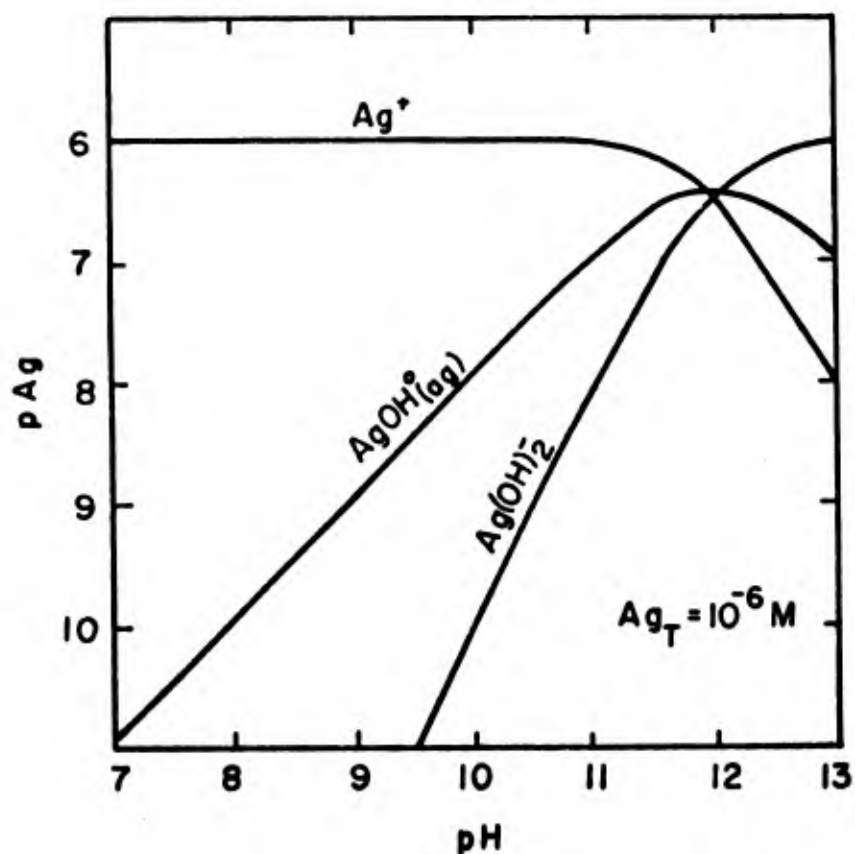
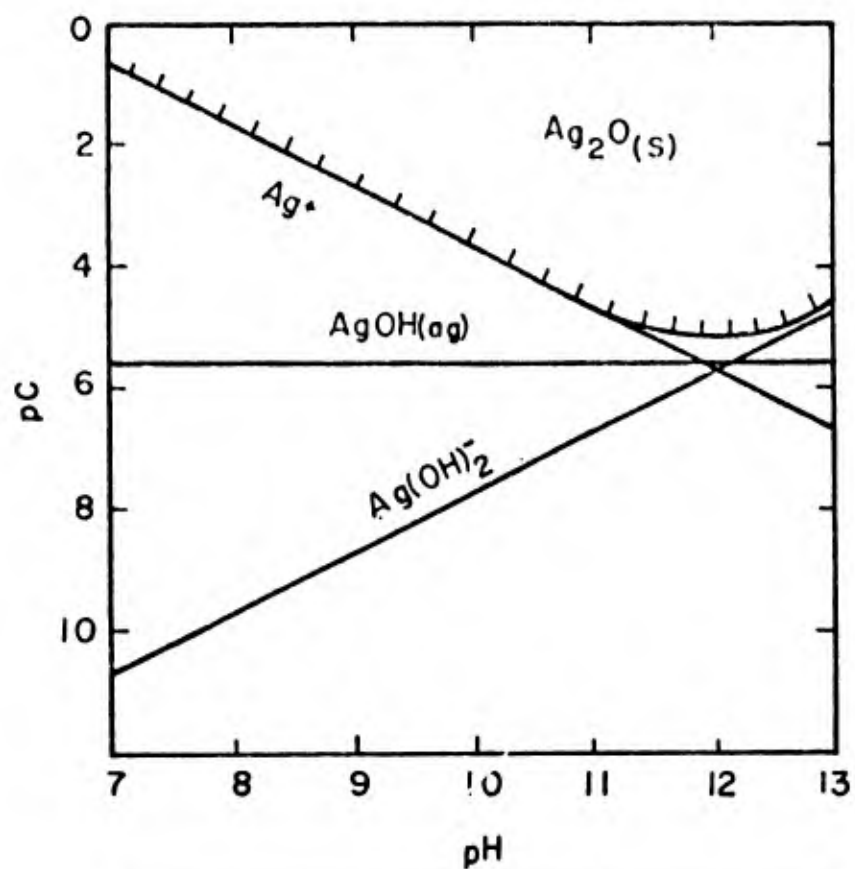


Figure 49. Log concentration diagrams for silver at 25°C and 1 atm total pressure. The upper diagram shows the stability field of silver oxide and the major hydrolytic species. The hash-marked curve represents the sum of all dissolved silver species. The lower diagram shows the speciation of silver computed for total silver of $10^{-6} M$.

a dramatic difference from the hydrolysis behavior of other transition metals.

Thermodynamic data are not available for complexes of silver(I) with catechol, salicylic acid, or phthalic acid. These silver complexes are presumed much weaker than those of other transition metals because of the weak interaction of silver(I) and oxygen and the non-linear stereochemistry forced upon the silver ion by these chelating groups. The importance of fulvic and humic acids in the environmental chemistry of silver is uncertain. However, the similarities in functionality of humic material to the aforementioned weak aromatic acids lead to a similar conclusion that its importance is less than that observed for other transition metal ions.

Ammonia nitrogen complexation of silver(I) is considerably greater than that of any oxoanion but probably not large enough to be significant in most environmental situations. Figure 50 shows the distribution of silver species as a function of pH for total chloride of 10^{-3}M and total ammonia of 10^{-2}M . In reducing environments ammonia concentrations may well reach this level, but sulfur-containing ligands are then likely to dominate the distribution of silver.

Thiosulfate is an important ligand to consider in the aquatic chemistry of silver since it will usually occur in excess of silver(I) in waters where it is added by photoprocessing effluents. Figure 51 shows the speciation of silver at pH 7.0 for a fixed total concentration of silver(I) of 10^{-6}M as a function of total thiosulfate concentration. This diagram and Figure 52 illustrate the larger strength of the thiosulfate complex compared to those previously discussed. Figure 52 shows the distribution of silver among species at pH 7.0 as a function of total chloride concentration. The minimum solubility of silver chloride occurs at $\text{pCl} \sim 2.7$. An additional concentration relationship shows the dominating effect of a total concentration of 10^{-6}M thiosulfate which sequesters an equimolar amount of silver(I) for chloride concentrations less than $5 \times 10^{-2}\text{M}$.

No information has been found on the importance of redox behavior for silver(I) in the natural environment. Equilibrium calculations based on the thermodynamic data available show that elemental silver is an important solid phase in reducing environments (see Figures 47 and 48).

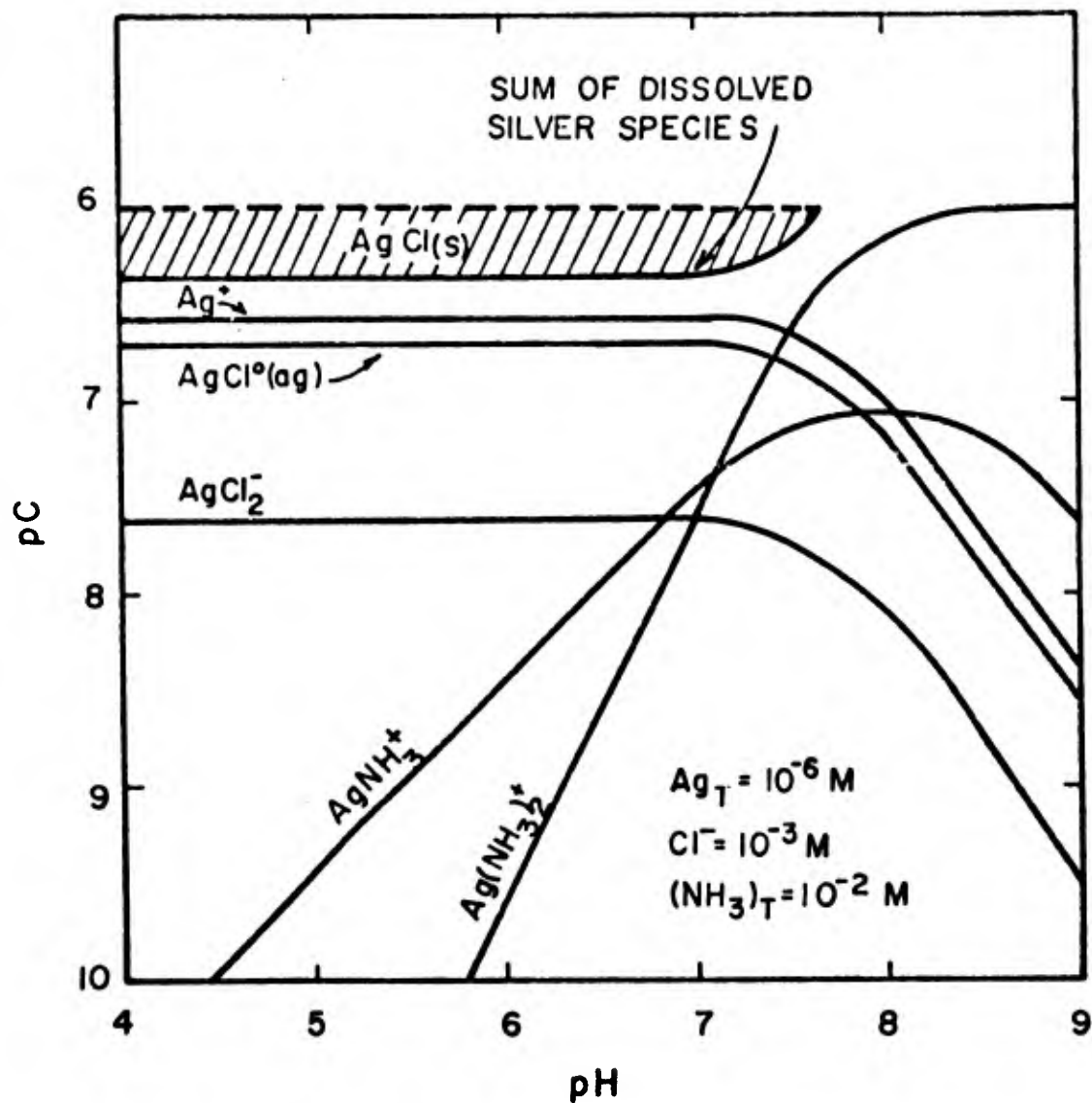


Figure 50. Log concentration-pH diagram for silver at 25°C and 1 atm total pressure. Computed for total silver of $10^{-6}M$, total chloride of $10^{-3}M$, and total ammonia of $10^{-2}M$. The dashed region represents the formation of $AgCl(s)$ at equilibrium conditions. The lower boundary of the dashed region shows the sum of all dissolved silver species.

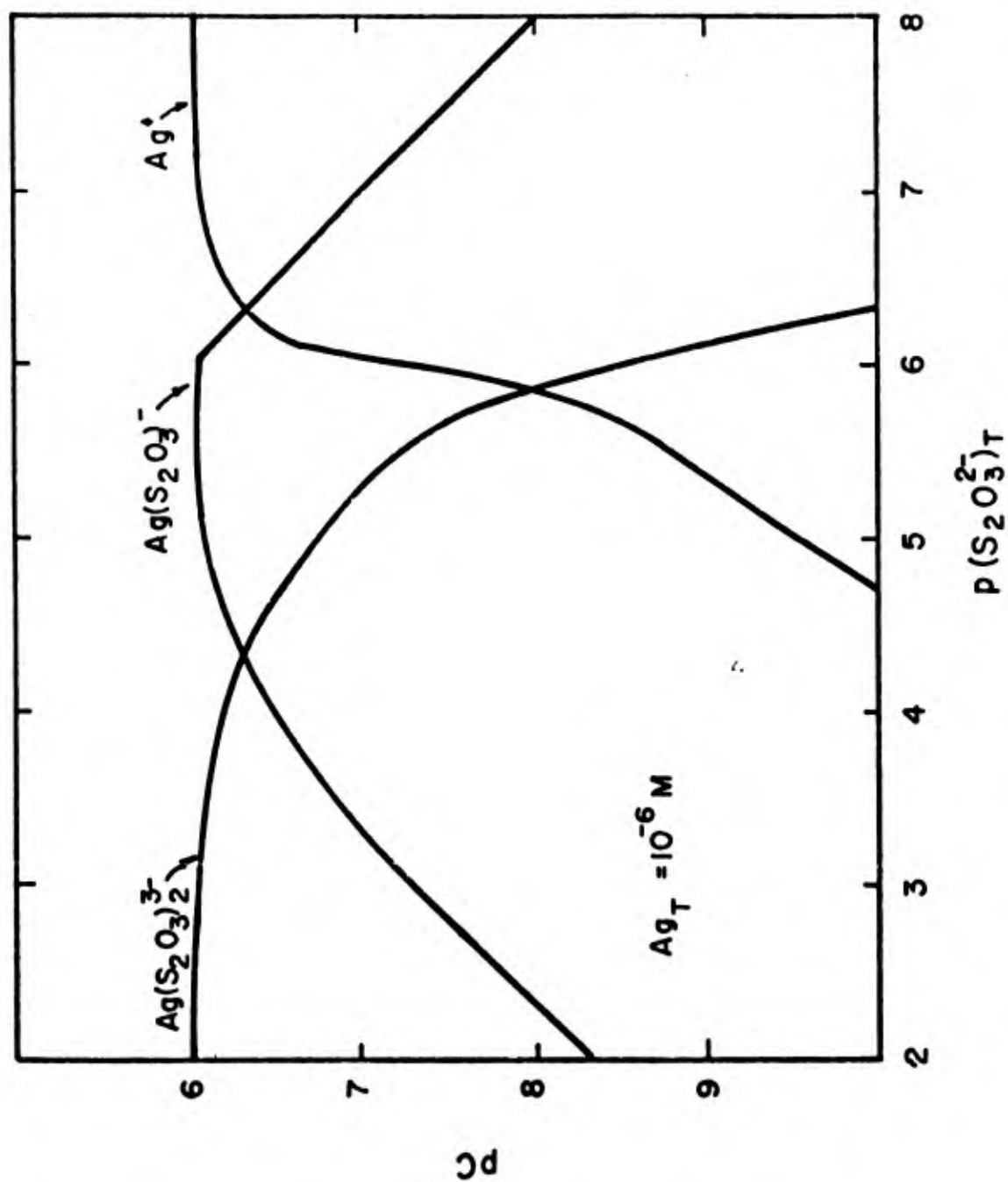


Figure 51. Log concentration diagram showing the major thiosulfate species at 25°C and 1 atm total pressure as a function of the total thiosulfate concentration. Computed for total silver of $10^{-6}M$ at pH 7.

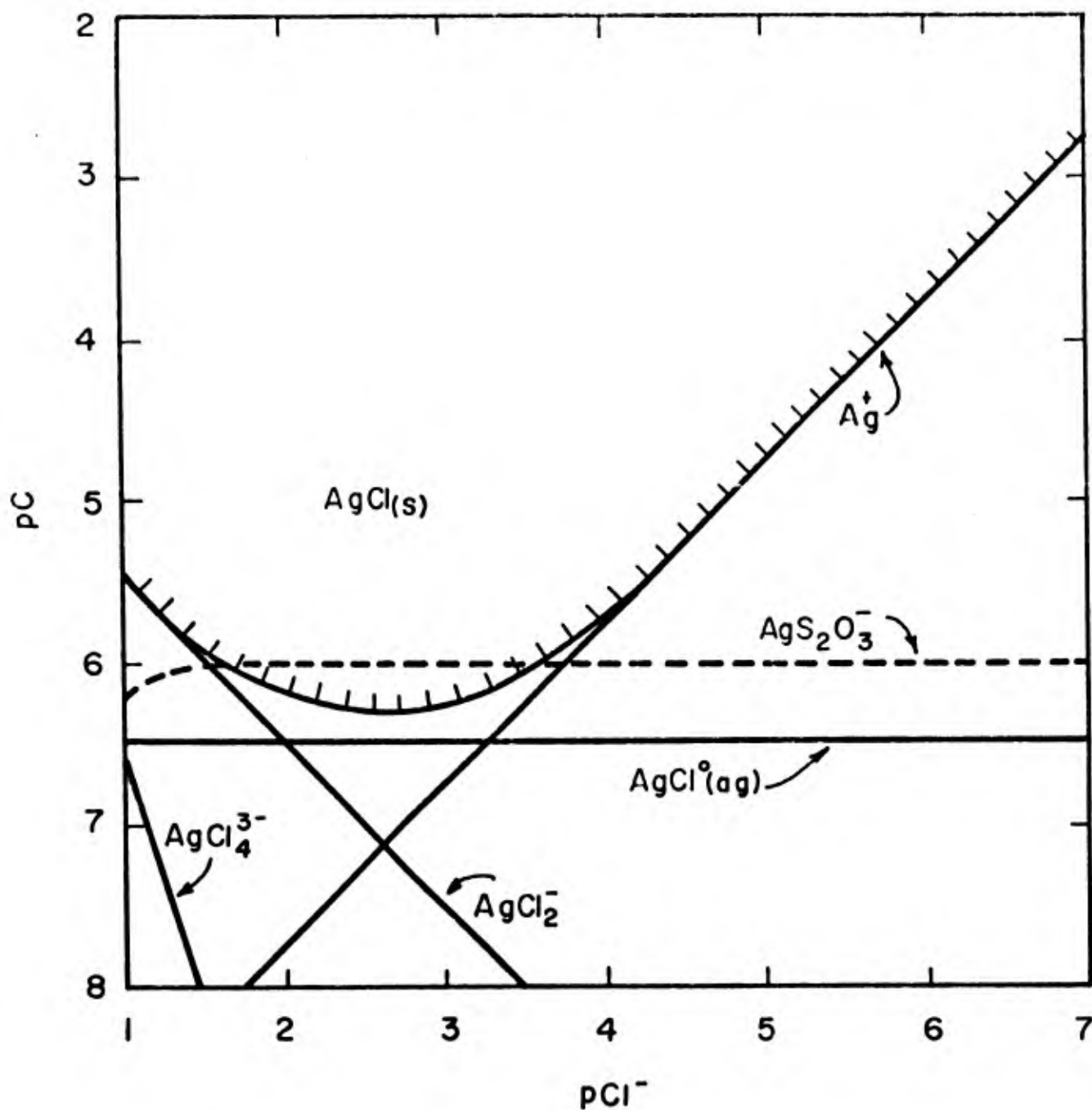


Figure 52. Log concentration diagram for $AgCl(s)$ showing stability fields for solid silver chloride and major argentous chloride complexes at $25^\circ C$ and 1 atm total pressure. The hash-marked curve represents the sum of all dissolved silver species. An additional concentration relationship is shown for a total thiosulfate concentration of $10^{-6} M$.

Indeed, the likelihood of silver reduction is higher than for most transition metals. The importance of photoreduction at solid surfaces in the natural environment is also unknown. Surfaces in the natural environment are likely to be coated with organic compounds, and it is known that reducing agents at the surface aid in the photoreduction of silver(I). The lack of understanding of these aspects of silver chemistry complicate the prediction of silver distribution in natural aquatic environments.

SECTION VI

AQUEOUS CHEMISTRY OF CADMIUM

Electronic Structure and Oxidation States

Cadmium is atomic number 48 and has atomic mass 112.40. It occurs naturally as a mixture of eight stable isotopes with the following abundances: Cd-106 (1.2%), Cd-108 (.9%), Cd-110 (12.4%), Cd-111 (12.8%), Cd-112 (24%), Cd-113 (12.3%), Cd-114 (28.9%), and Cd-116 (7.6%). The position of Cd in the periodic table is in group IIB, below Zn and above Hg. Cadmium has electronic structure $4s^2 4p^6 4d^{10} 5s^2$, outside 3 filled lower orbitals and retains a full 4d subshell in all its compounds. For this reason, its chemistry is in some respects more analogous to the IIA elements Mg and Ca than to the transition elements (Cotton and Wilkinson, 1972).

Cadmium exhibits only two stable oxidation states in aqueous solution, 0 and +2. Although the Cd_2^{2+} species can be stable in some organic solids and solutions, it rapidly dissociates to Cd^0 and Cd^{2+} in water.

Cadmium Compounds

Solids. Cadmium forms insoluble crystalline oxides, hydroxides, carbonates, and sulfides. Solubility products for some of these minerals are listed in Table 17. The crystal structures possible are tetrahedral and octahedral. For the hydroxide and sulfide, both forms are known.

TABLE 17. STABILITY CONSTANTS FOR CADMIUM INORGANIC LIGAND COMPLEXES

<u>Reaction</u>	<u>log K*</u>
REDOX	
$Cd^{2+} + 2e^- = Cd^0(c)$	-13.51 ($E^0 = -402.5$ mV)
SOLUBILITY PRODUCTS	
$Cd(OH)_2(s) = Cd^{2+} + 2OH^-$	-13.6 (active $Cd(OH)_2$)
$CdCO_3(s) = Cd^{2+} + CO_3^{2-}$	-12 (-11.2)
$Cd[B(OH)_4]_2(s) = Cd^{2+} + 2B(OH)_4^-$	-8.64
$CdS(s) = Cd^{2+} + S^{2-}$	-27.8

TABLE 17. (CONTINUED)

Reaction	log K*
SOLUBLE COMPLEXES	
$\text{Cd}^{2+} + \text{OH}^- = \text{Cd}(\text{OH})^+$	3.92 ^a
$\text{Cd}^{2+} + 2\text{OH}^- = \text{Cd}(\text{OH})_2^0 \text{ (aq)}$	7.65 ^a
$\text{Cd}^{2+} + 3\text{OH}^- = \text{Cd}(\text{OH})_3^-$	< 8.7 ^a
$\text{Cd}^{2+} + 4\text{OH}^- = \text{Cd}(\text{OH})_4^{2-}$	8.6 ^a
$2\text{Cd}^{2+} + \text{OH}^- = \text{Cd}_2\text{OH}^{3+}$	4.61 ^a
$4\text{Cd}^{2+} + 4\text{OH}^- = \text{Cd}_4(\text{OH})_4^{4+}$	23.15 ^a
$\text{Cd}^{2+} + \text{CN}^- = \text{CdCN}^+$	5.5
$\text{Cd}^{2+} + 2\text{CN}^- = \text{Cd}(\text{CN})_2^0 \text{ (aq)}$	5.1
$\text{Cd}^{2+} + 3\text{CN}^- = \text{Cd}(\text{CN})_3^-$	4.6
$\text{Cd}^{2+} + 4\text{CN}^- = \text{Cd}(\text{CN})_4^{2-}$	3.6
$\text{Cd}^{2+} + \text{SCN}^- = \text{CdSCN}^+$	1.5
$\text{Cd}^{2+} + 2\text{SCN}^- = \text{Cd}(\text{SCN})_2^0 \text{ (aq)}$	2.2
$\text{Cd}^{2+} + \text{CO}_3^{2-} = \text{CdCO}_3^0 \text{ (aq)}$	4.0 ^b , (5.4 ^c)
$\text{Cd}^{2+} + \text{HCO}_3^- = \text{CdHCO}_3^+$	2.2 ^c (1.6 ^d)
$\text{Cd}^{2+} + \text{NH}_3 \text{ (aq)} = \text{CdNH}_3^{2+}$	2.5
$\text{Cd}^{2+} + 2\text{NH}_3 \text{ (aq)} = \text{Cd}(\text{NH}_3)_2^{2+}$	4.5
$\text{Cd}^{2+} + 3\text{NH}_3 \text{ (aq)} = \text{Cd}(\text{NH}_3)_3^{2+}$	5.8
$\text{Cd}^{2+} + 4\text{NH}_3 \text{ (aq)} = \text{Cd}(\text{NH}_3)_4^{2+}$	6.4
$\text{Cd}^{2+} + \text{NO}_2^- = \text{CdNO}_2^+$	1.3
$\text{Cd}^{2+} + \text{NO}_3^- = \text{CdNO}_3^+$	0.1
$\text{Cd}_3(\text{PO}_4)_2 \text{ (s)} = 3\text{Cd}^{2+} + 2\text{PO}_4^{3-}$	-32.6
$\text{Cd}_3(\text{AsO}_4)_2 \text{ (s)} = 3\text{Cd}^{2+} + 2\text{AsO}_4^{3-}$	-32.66

TABLE 17. (CONCLUDED)

Reaction	log K*
$\text{Cd}^{2+} + \text{HS}^- = \text{CdHS}^+$	7.55
$\text{CdHS}^+ + \text{HS}^- = \text{Cd}(\text{HS})_2^0 (\text{aq})$	7.06
$\text{Cd}(\text{HS})_2^0 (\text{aq}) + \text{HS}^- = \text{Cd}(\text{HS})_3^-$	1.88
$\text{Cd}(\text{HS})_3^- + \text{HS}^- = \text{Cd}(\text{HS})_4^{2-}$	2.36
$\text{Cd}^{2+} + \text{S}_2\text{O}_3^{2-} = \text{CdS}_2\text{O}_3^0 (\text{aq})$	3.9
$\text{Cd}^{2+} + 2\text{S}_2\text{O}_3^{2-} = \text{Cd}(\text{S}_2\text{O}_3)_2^{2-}$	6.2
$\text{Cd}^{2+} + \text{SO}_4^{2-} = \text{CdSO}_4^0 (\text{aq})$	2.3
$\text{Cd}^{2+} + 2\text{SO}_4^{2-} = \text{Cd}(\text{SO}_4)_2^{2-}$	3.5 ^c
$\text{Cd}^{2+} + \text{F}^- = \text{CdF}^+$	0.46
$\text{Cd}^{2+} + \text{Cl}^- = \text{CdCl}^+$	2.0
$\text{Cd}^{2+} + 2\text{Cl}^- = \text{CdCl}_2^0 (\text{aq})$	2.7
$\text{Cd}^{2+} + 3\text{Cl}^- = \text{CdCl}_3^-$	2.7
$\text{Cd}^{2+} + 4\text{Cl}^- = \text{CdCl}_4^{2-}$	2.4
$\text{Cd}^{2+} + \text{Br}^- = \text{CdBr}^+$	2.2
$\text{Cd}^{2+} + 2\text{Br}^- = \text{CdBr}_2^0 (\text{aq})$	3.0
$\text{Cd}^{2+} + 3\text{Br}^- = \text{CdBr}_3^-$	3.3
$\text{Cd}^{2+} + \text{I}^- = \text{CdI}^+$	2.3
$\text{Cd}^{2+} + 2\text{I}^- = \text{CdI}_2^0 (\text{aq})$	3.6
$\text{Cd}^{2+} + 3\text{I}^- = \text{CdI}_3^-$	4.9

* Constants selected from L. G. Sillén and A. E. Martell, "Stability Constants of Metal-Ion Complexes," The Chemical Society (London), Special Publications No. 17 (1964) and No. 25 (1971) unless otherwise noted.

^a Constants from Mesmer and Baes (in press). See References.

^b Constants from Gardiner (1974a). See References.

^c Constants from Zirino and Yamamoto (1972). See References.

^d Constants estimated from data of Gardiner (1974a) using method of Zirino and Yamamoto (1972). See References.

Cadmium oxide, CdO , is formed when monatomic Cd^0 gas is released during smelting of ores and mixes with atmospheric oxygen. The gas is oxidized to fine particulates. The CdO(s) is kinetically stable if it remains dry, although it can slowly absorb CO_2 from the atmosphere and be converted to $\text{CdCO}_3(\text{s})$. If the particles get wet, they may be converted to either $\text{Cd(OH)}_2(\text{s})$ or $\text{CdCO}_3(\text{s})$, depending on the pH and CO_2 content of the water. Figure 53 shows the relationship between these two solids and indicates that in any water system saturated with atmospheric CO_2 , $\text{CdCO}_3(\text{s})$ is the thermodynamically stable phase.

In strongly reducing environments containing sulfide CdS will precipitate. Figure 54 shows conditions of pE and pH under which CdS is the stable solid phase, assuming 10^{-1}M total dissolved sulfur species. More detailed physical and chemical information concerning these minerals is available in references by Cotton and Wilkinson (1972) and Aylett (1973).

Solid cadmium salts of the halides, sulfate, nitrate, and a number of other common inorganic ligands have been prepared and characterized. These solids are very soluble in water and are never found in natural systems. They are not discussed here. For thermodynamic data and information concerning crystal structures and preparation techniques, see Chizhikov (1962).

Organo-cadmium compounds are usually liquids or low-melting solids of co-ordination number two. These compounds are much less stable than the analogous organomercurials, since the 14-4f electrons in Hg make it a considerably "softer" metal than Cd. Organocadmium compounds are not important in aqueous systems (Fleischer et al., 1974).

Soluble Complexes. A summary of dissolved inorganic equilibria involving cadmium is presented in Table 17. Cadmium can form soluble complexes with N, S, O, P, or the halides as donor atoms. Consistent with its intermediate position in the Periodic Table, Cd forms complexes which are stronger than the alkaline earth elements but weaker than most transition metals.

Most monodentate ligands have four stepwise stability constants of decreasing strength, i.e., $K_1 > K_2 > K_3 > K_4$. In concentrated Cd solutions, polynuclear species are formed, but these are not expected in any natural waters.

Of the inorganic complex equilibria listed the most important are the chloro-, hydroxo-, carbonato-, sulfato-, cyano-, and ammine complexes. Due

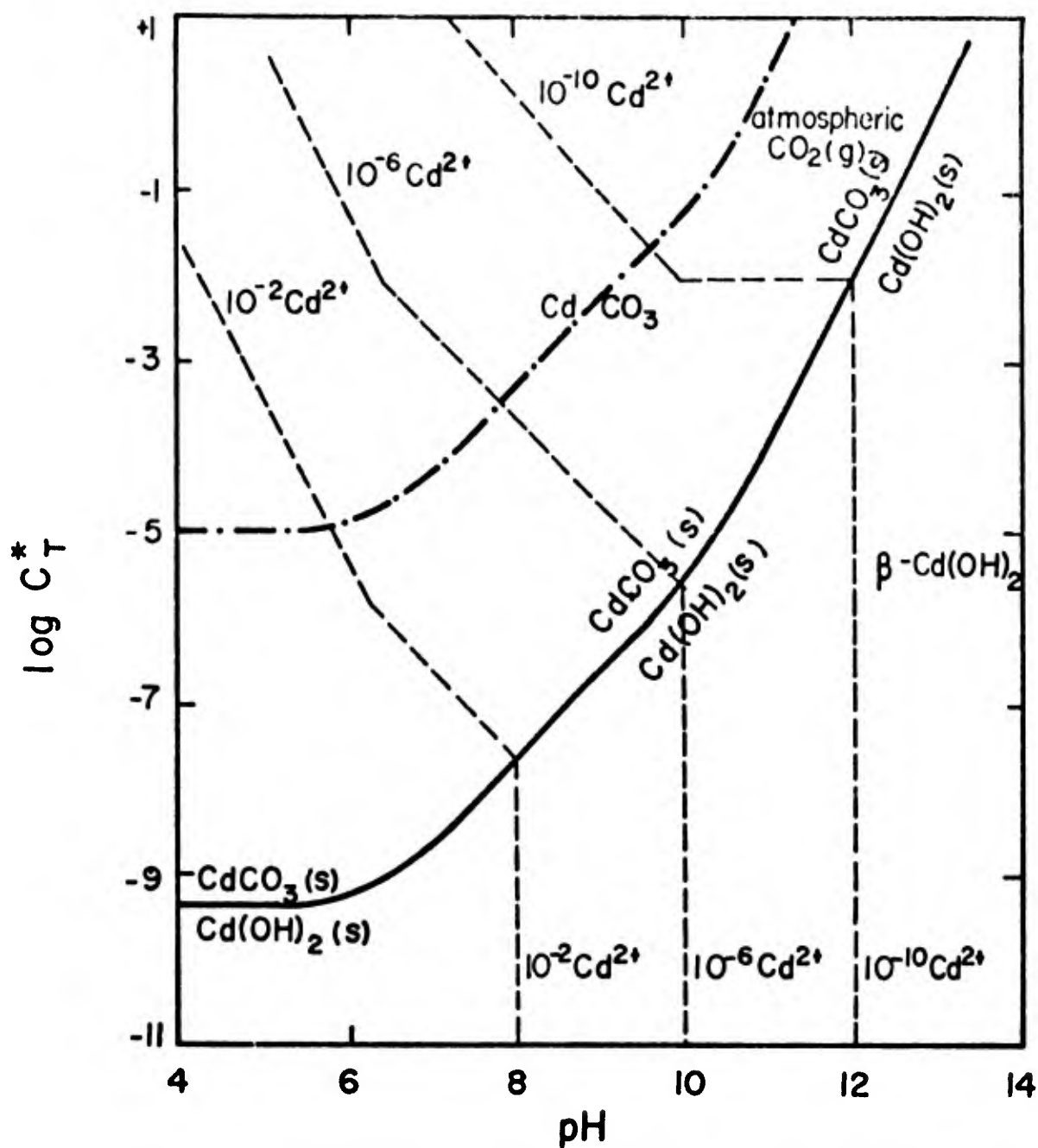


Figure 53. Cd-CO₂-H₂O system. Above and to the left of the solid line CdCO₃(s) is the solubility-limiting phase at equilibrium. Below and to the right Cd(OH)₂(s) predominates. Dashes (---) indicate Cd²⁺ solubility. Dotted line (-.-) indicates the case of water in equilibrium with atmospheric CO₂. Note that CdCO₃(s) is the equilibrium solid in all systems equilibrated with air. $C_T^* = \text{CO}_2(\text{aq}) + \text{HCO}_3^- + \text{CO}_3^{2-}$.

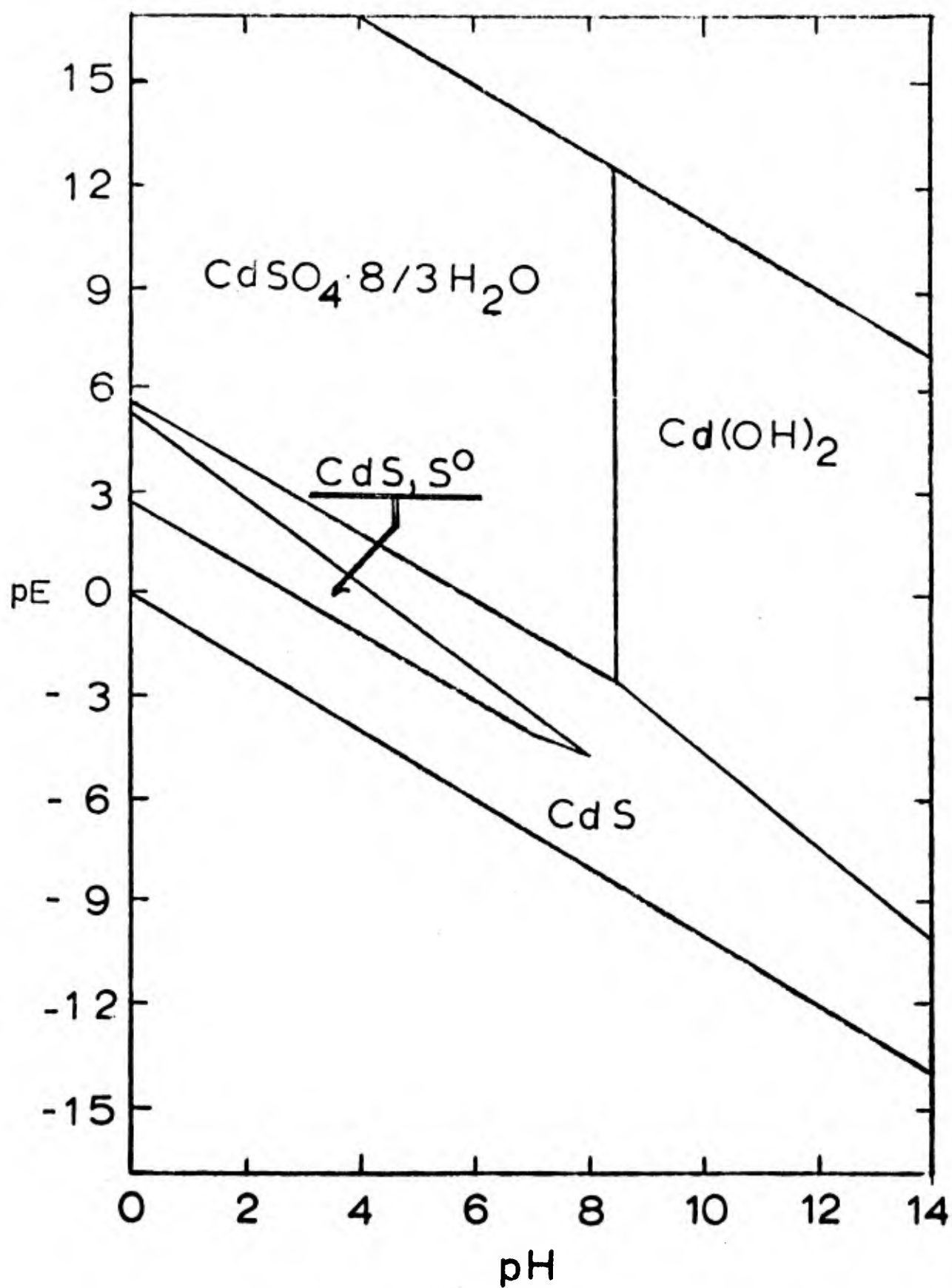


Figure 54. Stability field diagram showing dominance regions for solid cadmium phases in equilibrium with aqueous solution at 25°C and 1 atm total pressure. Total dissolved sulfur is 0.1M.

to the insolubility of the corresponding solids, values for the stability constants of the hydroxo- and carbonato-complexes are not well known. Based on the critical analysis by Mesmer and Baes (1975), the hydroxo-species are unimportant at pH below 9. While the stability constants for complexation by CN^- , SO_4^{2-} , and NH_3 are relatively large, these ligands are typically present at low concentrations in natural waters and would be expected to complex significant quantities of Cd only in unusual natural waters and domestic and industrial waste waters. The chloro-complexes are the major species in sea water.

In reducing environments, polysulfide complexes can solubilize significant quantities of heavy metals (L. Gardiner, 1974). Since the $\text{Cd}^{2+}\text{-S}_x^{2-}$ bond is strong, it is likely that $\text{Cd}(\text{HS})_x^{2-x}$ and $\text{CdS}_x^{2(1-x)}$ species will be important in reducing waters.

A summary of stability constants for Cd with various organic ligands is presented in Table 18. In general, cadmium complexes are less stable than those formed by transition metals except when the donor atom is sulfur. This is consistent with the hard-soft acid-base theory, according to which Cd is classified as a soft metal by virtue of its filled 4d-orbital. Softness of donor ligands increases in the order $\text{S} > \text{N} > \text{O}$. Theory states that soft metals bond more strongly as the softness of the donor ligand increases. The relative strengths of bonding of cadmium and several other metals with bidentate ligands are shown in Figure 55.

Sources and Uses of Cadmium

Cadmium is a rare element, comprising only about 0.15 to 0.20 ppm of the earth's crust. By comparison, its sister element Zn is about 500 times as abundant (Aylett, 1965). Except for a few minor deposits of CdS and CdCO_3 , no pure Cd mineral deposits are known. However, Cd is highly chalcophilic and is a minor constituent in sulfidic ores of other heavy metals. It is present at levels of 0.2-5% of the Zn and Pb concentrations in sphalerite and galena, respectively. In addition to these ores, Cd is concentrated in organic-rich shales, sediments, Mn nodules, and marine phosphorites (Fleischer et al., 1974). In igneous rocks, Cd is associated with Zn and the Zn:Cd ratio averages ~750 (range 25-7000) while in sedimentary rocks Cd is found to correlate with organic content better than with Zn concentration. The total, natural flux of Cd to the oceans is estimated to be 500 tons/yr (Fleischer et al., 1974).

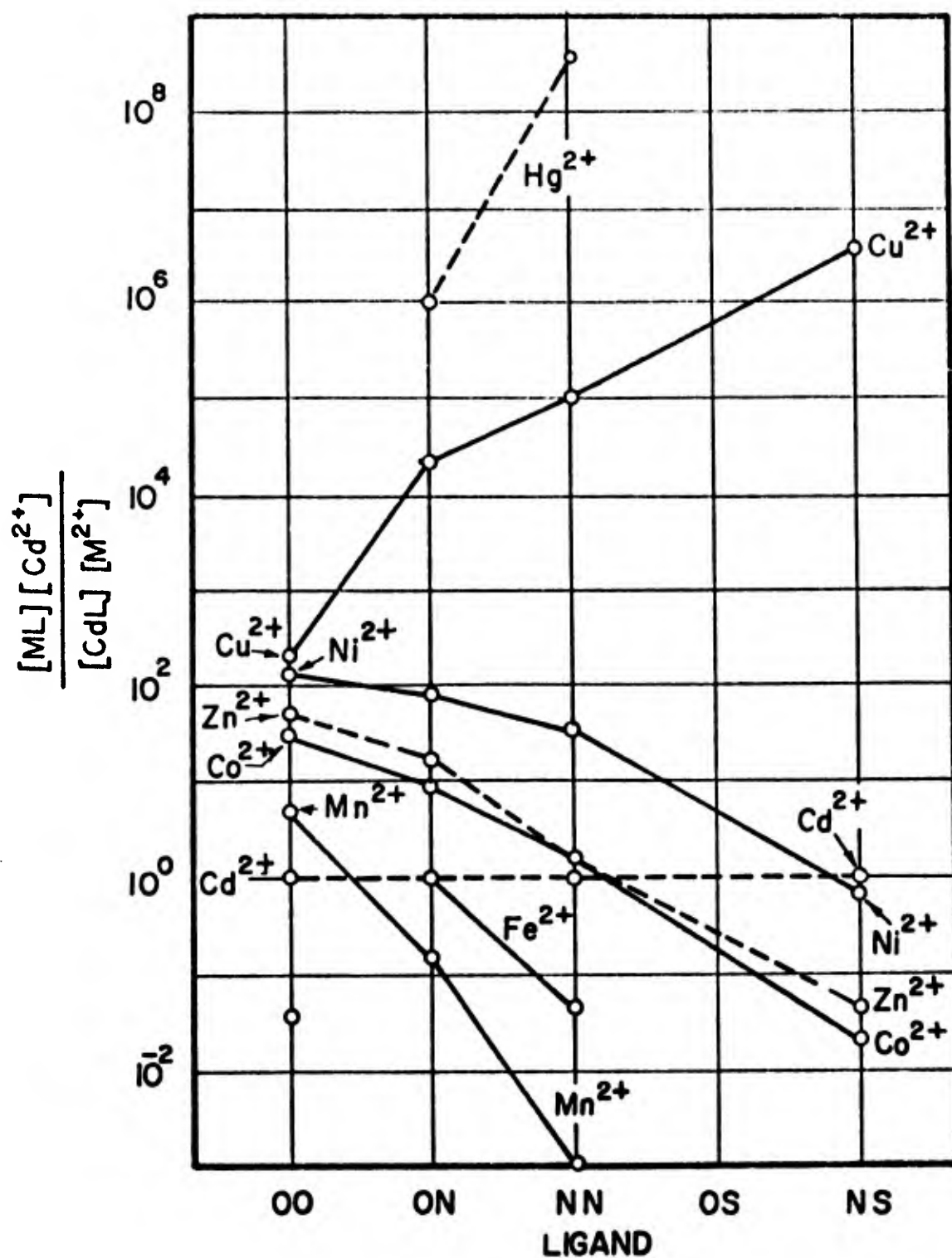


Figure 55. Relative strengths of cadmium bonds with bidentate ligands. The tendency of cadmium ion to displace other metal ions from bidentate ligands involving oxygen (O), nitrogen (N), and sulfur(s) donating ligands is shown.

TABLE 18. STABILITY CONSTANTS FOR CADMIUM ORGANIC LIGAND COMPLEXES

Reaction	log K*	Possible Donor Groups			
		N	COO ⁻	s	(TOT)
$\text{Cd}^{2+} + (\text{G1})^- = \text{Cd} - (\text{G1})^+$	1.3	0	1	0	(1)
$\text{Cd}(\text{G1})^+ + (\text{G1})^- = \text{Cd} - (\text{G1})_2^0$	0.8				
$\text{Cd}^{2+} + (\text{T1})^0 = \text{Cd} - (\text{T1})^{2+}$	1.38	2	0	1	(3)
$\text{Cd}(\text{T1})^{2+} + (\text{T1})^0 = \text{Cd} - (\text{T1})_2^{2+}$	0.3				
$\text{Cd}^{2+} + (\text{S1})^{2-} = \text{Cd} - (\text{S1})^0$	2.2	0	2	0	(2)
$\text{Cd}^{2+} + (\text{P1})^{2-} = \text{Cd} - (\text{P1})^0$	2.5	0	2	0	(2)
$\text{Cd}^{2+} + (\text{X1})^{2-} = \text{Cd} - (\text{X1})^0$	3.7	0	2	0	(2)
$\text{Cd}(\text{X1})^0 + (\text{X1})^{2-} = \text{Cd}(\text{X1})_2^{2-}$	0.3				
$\text{Cd}^{2+} + (\text{D1})^0 = \text{Cd}(\text{D1})^{2+}$	2.6	1	0	0	(1)
$\text{Cd}(\text{D1})^{2+} + (\text{d1})^0 = \text{Cd}(\text{D1})_2^{2+}$	2.1				
$\text{Cd}^{2+} + (\text{I1})^0 = \text{Cd}(\text{I1})^{2+}$	2.8	2	0	0	(2)
$\text{Cd}(\text{I1})^{2+} + (\text{I1})^0 = \text{Cd}(\text{I1})_2^{2+}$	2.1				
$\text{Cd}(\text{I1})_2^{2+} + (\text{I1})^0 = \text{Cd}(\text{I1})_3^{2+}$	1.5				
$\text{Cd}(\text{I1})_3^{2+} + (\text{I1})^0 = \text{Cd}(\text{I1})_4^{2+}$	1.1				
$\text{Cd}^{2+} + (\text{D2})^{2-} = \text{Cd}(\text{D2})^0$	3.3	0	2	0	(2)
$\text{Cd}^{2+} + \text{H}(\text{C1})^{2-} = \text{CdH}(\text{C1})^0$	2.3	0	3	0	(3)
$\text{Cd}^{2+} + (\text{M1})^- = \text{Cd}(\text{M1})^+$	3.7	1	1	1	(3)
$\text{Cd}(\text{M1})^+ + (\text{M1})^- = \text{Cd}(\text{M1})_2^0$	3.4				
$\text{Cd}^{2+} + (\text{A1})^{2-} = \text{Cd}(\text{A1})^0$	4.4	1	2	0	(3)
$\text{Cd}(\text{A1})^0 + (\text{A1})^{2-} = \text{Cd}(\text{A1})_2^{2-}$	4.5				
$\text{Cd}^{2+} + (\text{G2})^{2-} = \text{Cd}(\text{G2})^0$	5.3	1	2	0	(3)
$\text{Cd}(\text{G2})^0 + (\text{G2})^{2-} = \text{Cd}(\text{G2})_2^{2-}$	2.9				

TABLE 18. (CONTINUED)

Reaction	log K*	Possible Donor Groups			
		N	COO ⁻	s	(TOT)
$\text{Cd}^{2+} + (\text{G3})^- = \text{Cd}(\text{G3})^+$	4.6	1	1	0	(2)
$\text{Cd}(\text{G3})^+ + (\text{G3})^- = \text{Cd}(\text{G3})_2^0$	3.9				
$\text{Cd}^{2+} + (\text{A2})^- = \text{Cd}(\text{A2})^+$	4.0	1	1	0	(2)
$\text{Cd}(\text{A2})^+ + (\text{A2})^- = \text{Cd}(\text{A2})_2^0$	3.6				
$\text{Cd}^{2+} + (\text{H1})^0 = \text{Cd}(\text{H1})^{2+}$	4.8	1	0	0	(1)
$\text{Cd}(\text{H1})^{2+} + (\text{H1})^0 = \text{Cd}(\text{H1})_2^{2+}$	3.4				
$\text{Cd}^{2+} + (\text{P2})^0 = \text{Cd}(\text{P2})^{2+}$	5.4	2	0	0	(2)
$\text{Cd}(\text{P2})^{2+} + (\text{P2})^0 = \text{Cd}(\text{P2})_2^{2+}$	4.5				
$\text{Cd}(\text{P2})_2^{2+} + (\text{P2})^0 = \text{Cd}(\text{P2})_3^{2+}$	2.2				
$\text{Cd}^{2+} + (\text{D3})^0 = \text{Cd}(\text{D3})^{2+}$	5.5	2	0	1	(3)
$\text{Cd}(\text{D3})^{2+} + (\text{D3})^0 = \text{Cd}(\text{D3})_2^{2+}$	3.5				
$\text{Cd}^{2+} + (\text{S2})^{2-} = \text{Cd}(\text{S2})^0$	5.6	2	1	0	(3)
$\text{Cd}^{2+} + (\text{H2})^- = \text{Cd}(\text{H2})^+$	5.6				
$\text{Cd}(\text{H2})^+ + (\text{H2})^- = \text{Cd}(\text{H2})_2^0$	5.5				
$\text{Cd}^{2+} + (\text{E1})^0 = \text{Cd}(\text{E1})^{2+}$	5.5	2	0	0	(2)
$\text{Cd}(\text{E1}) + (\text{E1})^0 = \text{Cd}(\text{E1})_2^{2+}$	4.6				
$\text{Cd}(\text{E1})_2^{2+} + (\text{E1})^0 = \text{Cd}(\text{E1})_3^{2+}$	2.1				
$\text{Cd}^{2+} + (\text{I2})^{2-} = \text{Cd}(\text{I2})^0$	5.7	1	2	0	(3)
$\text{Cd}(\text{I2})^0 + (\text{I2})^{2-} = \text{Cd}(\text{I2})_2^{2-}$	4.4				
$\text{Cd}^{2+} + (\text{C2})^{2-} = \text{Cd}(\text{C2})^0$	6.5 ^a	1	1	1	(3)
$\text{Cd}(\text{C2})^0 + (\text{C2})^{2-} = \text{Cd}(\text{C2})_2^{2-}$	3.5				
$\text{Cd}^{2+} + (\text{H3})^- = \text{Cd}(\text{H3})^+$	7.2	1	phenol		
$\text{Cd}(\text{H3})^+ + (\text{H3})^- = \text{Cd}(\text{H3})_2^0$	6.2				
$\text{Cd}^{2+} + \text{H4}^- = \text{Cd}(\text{H4})^+$	6.7	1	COO ⁻		
$\text{Cd}(\text{H4})^+ + \text{H4}^- = \text{Cd}(\text{H4})_2^0$	5.7				
$\text{Cd}^{2+} + (\text{D4})^0 = \text{Cd}(\text{D4})^{2+}$	8.0	3	0	0	(3)
$\text{Cd}(\text{D4})^{2+} + (\text{D4})^0 = \text{Cd}(\text{D4})_2^{2+}$	5.8				

TABLE 18. (CONCLUDED)

Reaction	log K*	Possible Donor Groups			
		N	COO ⁻	s	(TOT)
$\text{Cd}^{2+} + (\text{N1})^{3-} = \text{Cd}(\text{N1})^{-}$	9.9	1	3	0	(4)
$\text{Cd}(\text{N1})^{-} + (\text{N1})^{3-} = \text{Cd}(\text{N1})_2^{4-}$	5.7				
$\text{Cd}^{2+} + (\text{M2})^{-} = \text{Cd}(\text{M2})^{+}$	11.0	1	0	1	(2)
$\text{Cd}(\text{M2})^{+} + (\text{M2})^{-} = \text{Cd}(\text{M2})_2^0$	8.8				
$\text{Cd}^{2+} + (\text{E2})^{2-} = \text{Cd}(\text{E2})^0$	10.6	2	2	0	(4)
$\text{Cd}(\text{E2})^0 + (\text{E2})^{2-} = \text{Cd}(\text{E2})_2^{2-}$	6.0				
$\text{Cd}^{2+} + (\text{C3})^{2-} = \text{Cd}(\text{C3})^0$	10.8	2	phenoxy		(2)
$\text{Cd}(\text{C3})^0 + (\text{C3})^{2-} = \text{Cd}(\text{C3})_2^{2-}$	8.2				
$\text{Cd}^{2+} + (\text{T2})^0 = \text{Cd}(\text{T2})^{2+}$	10.8	4	0	0	(4)
$\text{Cd}^{2+} + (\text{T3})^0 = \text{Cd}(\text{T3})^{2+}$	16.2	6	0	0	(6)
$\text{Cd}^{2+} + (\text{E3})^{4-} = \text{Cd}(\text{E3})^{2-}$	16.5	2	4	0	(6)

A1 = Aspartate	H2 = Histidine
A2 = Alanine	H3 = 8-hydroxyquinoline
C1 = Citrate	H4 = 1-hydroxy-2-naphtoic acid
C2 = Cysteine	I1 = Imidazole
C3 = Catechol	I2 = Iminodiacetate
D1 = Diethylamine	M1 = Methionine
D2 = Diglycollate	M2 = Mercaptoethylamine
D3 = Diaminodiethylsulfide	N1 = Nitrilotriacetate
D4 = Diethylenetriamine	P1 = Phthallate
E1 = Ethylenediamine	P2 = Propylenediamine
E2 = Ethylenediaminediacetate	S1 = Succinate
E3 = Ethylenetriaminetetraacetate	S2 = Salicylate
G1 = Glycollate	T1 = Thiourea
G2 = Glutamate	T2 = Triethylenetetramine
G3 = Glycine	T3 = Tetra-2-(aminoethyl)ethylenediamine
H1 = Histamine	X1 = Oxalate

* Constants selected from L. G. Sillén and A. E. Martell, "Stability Constants of Metal-Ion Complexes," The Chemical Society (London), Special Publications No. 17 (1964) and No. 25 (1971) unless otherwise noted.

^a Constant from Ramamoorthy and Manning (1975). See References.

Anthropogenic mobilization of Cd is far more important than natural mobilization and is estimated at 12,000 tons annually. Of this, approximately one-third is released in the United States.

Uses of Cd include electroplating, pigments, plastic stabilizers, and batteries. These uses are highly dispersive, leading Fulkerson and Goeller (1973) to dub Cd "the dissipated element."

Transport of Cadmium through the Environment

The most important mechanism for release of Cd to the environment is through the flue gas emissions of smelters. Cadmium is more volatile than most heavy metals, with a boiling point of 790°C and vapor pressures of 0.01 and 0.1 atm at 470°C and 610°C, respectively. Because of this, significant quantities of Cd are released to the air during processing of Zn and Pb ores, predominantly as the monatomic gas (85-100%) or as $\text{CdSO}_4(\text{g})$ or $\text{CdCl}_2(\text{g})$ (0-15%). The $\text{Cd}^0(\text{g})$ is rapidly oxidized to $\text{CdO}(\text{s})$ in the form of fine particulates which then settle to earth nearby. Typical Cd levels in uncontaminated soils are 0.05 to 0.5 ppm, and concentrations in soils near mining and smelting operations can be several tens of ppm (Zasoski, 1974; Page and Bingham, 1973). Other ways in which a major Cd burden is applied to land include the use of super-phosphate fertilizer or land disposal of sewage sludge either as fertilizer or landfill.

Major controls on Cd mobility in the terrestrial environment are not well understood. The CdO particles released near smelters must be somewhat mobile, since abnormally high Cd concentrations have been found 30 cm below the surface in such areas (Fleisher et al., 1974). It is not clear whether the particles migrate or the Cd dissolves and re-associates with soil particles. The strength of the Cd-soil bond has been studied by several investigators, but results are inconsistent. Zasoski (1974) estimated that only 10-20% of the Cd in soil is "labile." Huckabee and Blaylock (1973) simulated rainfall containing Cd-115m on a model ecosystem, followed by Cd-free rainfall at intervals for 3 months. At the end of the period, 70% of the Cd remained in the soil, 25% was in other compartments of the terrestrial system, and only 3% had been leached into the water phase. The Cd associated with the soil was not released by shaking with ammonium acetate. John (1971) found that the fraction of Cd which could be leached from a soil by shaking with Na-acetate was proportional to the soil organic content. However, in a

second study by John (1972), the Cd content of soils correlated with the amount of exchangeable Zn and Al in the soil, but not with soil organic content. Riffaldi and Levi-Minzi (1975) found that 50% of the Cd adsorbed onto a soil-derived humic acid was released upon leaching with Na-acetate, but 100% was released when a Cu-acetate solution was used. Lehman and Wilson (1971) flooded a field with sewage effluent several times for periods of 2-5 weeks over the course of 3 years. At the end of that period the soil was apparently saturated with Fe, Mn, Cu, Pb, and Ni, but not with Cd or Zn, suggesting that the soil-Cd bond is weak and labile. Clearly, considerable work remains to be done before the processes controlling Cd transport through soil are understood.

Cadmium in Natural Water Systems

The major pathways of Cd to the aquatic ecosystem, include leaching of soils and rocks into surface and groundwaters and disposal of domestic and industrial wastewaters. In addition, Cd can be leached from galvanized water pipes under some conditions (Posselt, 1971).

Once transported into an aquatic ecosystem, Cd can participate in several processes including complexation by organic or inorganic ligands, precipitation as a separate phase, co-precipitation, sorption/desorption reactions, and incorporation into biota. The dissolved Cd concentration in surface and groundwaters ranges from $< 1 \mu\text{g}/\ell$ to several tens of $\mu\text{g}/\ell$, and the median is slightly less than $1 \mu\text{g}/\ell$ (Hem, 1972). In open ocean water, dissolved Cd is present at concentrations of $0.1\text{--}0.2 \mu\text{g}/\ell$ (Fleischer et al., 1974).

Both suspended and bottom sediments concentrate Cd by a factor of $10^3\text{--}10^4$ relative to dissolved levels. Uncontaminated coastal sediments contain $0.2\text{--}0.6 \text{ ppm}$ Cd (Taylor, 1974) while those in industrial areas contain $1\text{--}20 \text{ ppm}$, and occasionally much more. Kubota et al. (1974) found that suspended solids in rural areas contain about one-half the Cd of those from urban areas. Despite the large concentration factors for sediments relative to dissolved species, more Cd is transported in solution than by particulate matter in both the Tennessee River (Perhac, 1972) and British Isles coastal water (Preston et al., 1972).

The most important solid species from an environmental standpoint are $\text{CdCO}_3(\text{s})$ and $\text{Cd}(\text{OH})_2(\text{s})$. Both of these minerals are extremely insoluble and

could conceivably control the solubility of Cd in oxidized natural waters. As can be seen in Figure 53, $\text{CdCO}_3(\text{s})$ is the dominant solid in waters equilibrated with atmospheric CO_2 . However, Posselt (1971) found that attainment of equilibrium with CdCO_3 from a supersaturated solution is extremely slow. It is therefore possible that some natural waters could be supersaturated with respect to solid $\text{CdCO}_3(\text{s})$. Hem (1972) found only 10 of 80 surface and ground waters had Cd concentrations approaching the solubility of either $\text{Cd}(\text{OH})_2$ or CdCO_3 . He felt that in some cases a mixed hydroxide-carbonate phase might be controlling. The Cd concentration in seawater is well below saturation also, and Krauskopf (1956) hypothesized that sorption equilibria operated to maintain the low levels. Another possibility is that a mixed $(\text{Ca},\text{Cd})\text{CO}_3$ is the controlling phase. The chemistry and ionic radii of Cd and Ca are similar enough that formation of such a solid seems likely (Fulkerson, 1975). Leckie and Nelson (1975) have pointed out that the concentration of dissolved Cd in equilibrium with a solid solution of which Cd is a minor component would be much less than that in equilibrium with a pure Cd solid phase. Other than $\text{Cd}(\text{OH})_2(\text{s})$ and $\text{CdCO}_3(\text{s})$, the only Cd solid occurring naturally is $\text{CdS}(\text{s})$, which is extremely insoluble and should precipitate in reducing environments. A pE-pH diagram showing the region in which CdS is the equilibrium solid phase is presented in Figure 54. Leckie and Nelson (1975) indicate that in anoxic sediments, FeS is likely to precipitate and could reduce soluble Cd concentrations below those in equilibrium with CdS by sorption of Cd or formation of a $(\text{Fe},\text{Cd})\text{S}$ solid solution. Chizhikov (1962) reports the formation of at least one such solid solution in the laboratory with a mole ratio of $\text{Fe}:\text{Cd}$ equal to 6:1 in the solid. Conditions conducive to production of sulfide in natural systems are dependent on a complex interaction of biological and physico-chemical parameters which may change on a regular (seasonal) cycle, or when an exterior stress is applied, such as dredging.

McLerran and Holmes (1974) cultured bacteria from the top sediments of Corpus Christi Bay. Within 6 days after addition of Cd-109 to the culture solution, 85% of the Cd had been removed to the sediments, possibly as a $\text{FeS}-\text{CdS}$ co-precipitate. Knauer and Martin (1973) found dissolved Cd levels in the Pacific varied inversely with plankton productivity. Holmes et al. (1974) report that during the summer Cd is precipitated as CdS in Corpus Christi Bay, but that in winter it is oxidized and transported to the ocean,

where it sorbs onto particulate matter and settles. If FeS and CdS oxidize simultaneously, the possibility also exists that Cd could adsorb onto or co-precipitate with solid ferric hydroxide.

In some natural water systems, adsorption may be the major control limiting Cd solubility. Adsorption will occur on clays and metal oxides, predominantly in alkaline waters, and will vary with particle size and surface area, concentration of major and minor elements and the quantity and nature of organics in the system. Humic acids, in particular, are likely to have a large effect on the extent of adsorption. A dramatic increase in sorption of Cd has been reported on a clay, African vermiculite, as pH is increased from 6 to 8 (ORNL, 1973). The selectivity coefficient $[(Cd/Ca)_{surf.}]/[(Cd/Ca)_{sol'n}]$ of Cd relative to Ca increased from the range 0.5-10 at pH 5 to the range 100-1000 at pH 8 for a number of clays, and the coefficient was even greater when a humic acid was used as the substrate. Similarly, J. Gardiner (1974b) found the concentration factor $(Cd_{surf.}/Cd_{sol'n})$ for Cd on humic acid was 20 times greater than on silica and 50 times greater than on kaolin. He felt the humic substances were largely responsible for adsorption of Cd on river muds. An interesting combination of mineral equilibria and sorption controls on dissolved Cd concentration in the Tennessee River was found by Perhac (1974). He reports that as the suspended sediments are transported downstream from a dolomitic Cd source, the coarse carbonate sediments settle to the bottom and as Cd is released by dissolution it sorbs onto clay-size particles and is transported further.

Counteracting the limits on Cd solubility imposed by precipitation and sorption reactions are the ligands which form soluble complexes with Cd, thereby keeping it in solution. Referring again to Table 17, it is clear that in most natural systems the only inorganic ligand capable of complexing significant quantities of Cd under oxidizing conditions is Cl^- . This prediction is verified in Table 19, which shows that in groundwater and river water no inorganic Cd complex is important, while in seawater more than 90% of the total soluble Cd is present as a chloro-complex. Ammonia-, cyano-, and sulfato-complexes may be important factors in the solubilization of Cd in industrial and domestic waste streams, but not in natural systems.

A number of strong soluble organic complexes of cadmium are known (Table 18) with the strength of the bond depending on the identity of the donor atom, and increasing in the order $O < N < S$. However, regardless of

TABLE 19. SPECIATION OF CADMIUM IN NATURAL WATERS

(Data given as % total dissolved Cd as the given species)							
Water Type	Ref.	Speciation		Water Type	Ref. Speciation		
Seawater	a	Cd^{2+}	2.5	River Water ^f	c	Cd^{2+}	44-55
		CdCl^+	39			CdCl^+	2-10
		CdCl_2^0	51			CdCO_3^0	3-21
		CdCl_3^-	6			CdOH^+	2-7
		$\text{Cd}(\text{CO}_3)^0$	1.5			CdSO_4^0	2-7
Sulfidic Marine Water	b	Cd^{2+}	<< 1	Filtered Settled Sewage	c	Cd^{2+}	41
		CdOH^+	<< 1			CdCl^+	1
		CdCl^+	<< 1			CdCO_3^0	9
		CdSO_4^0	<< 1			CdOH^+	2
		$\text{Cd}(\text{NH}_3)^{2+}$	<< 1			CdSO_4^0	3
		$\text{Cd}(\text{HS})^+$	100			Cd-H.A.	39
		Cd-org^d	<< 1				
Fresh Ground- water	c	Cd^{2+}	92				
		CdCl^+	1.8				
		CdCO_3^0	3.9				
		CdOH^+	1.4				
		CdSO_4	.6				
		Cd-H.A.^e	0				

^aZirino and Yamamoto (1972). Considered only inorganic complexes.

^bL. Gardiner (1974). Did not consider complexation by humic substances.

^cJ. Gardiner (1974a).

^dSum of 25 organic species typically found in such waters.

^eA humic substance of average M.W. = 700.

^fRange given is for several small rivers in England, pH = 7.7-8.1.

of the donor atom, it is doubtful that the bond is sufficiently strong to complex significant amounts of Cd at naturally-occurring concentrations of organics for mono-, bi-, and tridentate ligands, except in areas of intense biological activity. The strength of tetra- and hexadentate Cd complexes is suggested by the last equilibria in Table 18. Combining these data with the information in Figure 55, it appears that multidentate N- and S-donating ligands are the most likely candidates for complexing Cd in natural systems. Biological metabolites such as proteins and by-products from their degradation as well as anthropogenic organic chelating agents could provide such ligands. During diagenesis, these molecules can combine with other organics to form polymeric humic and fulvic acids which may play an important role in solubilizing, precipitating, or sorbing Cd. These substances contain varying numbers and types of functional groups. Gardiner (1974a) studied the interaction of a humic substance of molecular weight 700 (apparently a fulvic acid) with Cd and found the following relationship:

$$\frac{(\text{Cd} - \text{cpx})}{(\text{cd}^{2+})} \propto \frac{(\text{Humic})^{.64}}{(\text{H}^+)^{.2}}$$

Schnitzer and Skinner (1965) found carboxyl and phenolic hydroxyl groups to be the most important complexing agents for exchangeable Fe(III), Al(III), and Cu(II) from an imperfectly drained soil. These groups may also be important in Cd retention. However, a major fraction of the metal associated with humic acid may be non-exchangeable, and bound by different groups. Goodman and Cheshire (1973) found that non-exchangeable Cu(II) was complexed in humic acid by the nitrogen in porphyrin groups. This evidence, the affinity of Cd for S- and N-donors and the fact that humic acids at the sediment-water interface would be less oxidized than those in a soil, all argue in favor of sulfide, sulfhydryl, disulfide, amine, amide, and imide groups dominating Cd complexation in natural water systems. Banat et al. (1974) point out that in natural systems, biodegradability as well as strength of the metal-ligand bond affects the stability of a complex. They solubilized Cd, Cu, Ni, Pb, and Zn from sediments by shaking them with solutions of 0-100 mg/l NTA. Only the Ni, Cd, and Cu chelates were stable, though, since the Pb and Zn complexes were readily degraded, releasing the metals which then resorbed.

Regions where intense biological activity produce significant concentrations of organic chelators are likely to be strongly reducing, with high concentrations of sulfide species. Under these conditions soluble polysulfides, bisulfide, and polythionate complexes may represent the dominant dissolved species (Gardiner, 1974). Leckie and Nelson (1975) have made some model calculations of the speciation of Cd in reducing waters. Assuming pS_T of 3, and the presence of six typical chelons at $10^{-6}M$ each, the bisulfide complex $Cd(HS)_2^0$ would be the major dissolved species at a pE less than -4. For a pE greater than -4, the free aquo Cd^{2+} species dominates in fresh waters and the chlorocomplexes dominate in estuarine and seawater systems (Figure 56). Under no conditions is an organo-Cd complex predicted to dominate. However, the model considered only well-defined species and therefore does not include complexes with polymeric metabolites or humic or fulvic acids. Leckie and Nelson (1975) also point out that equilibrium models can put bounds on dissolved heavy-metal concentrations but that in any real systems kinetic controls might be more important.

Results from either analyses or model calculations of Cd speciation in several different types of aqueous systems are presented in Table 19.

Although speciation of dissolved Cd will vary from location to location, some general conclusions can be drawn. Typically, the dominant species are chloro-complexes in seawater, humic complexes and free aquo Cd^{2+} in fresh waters, and bisulfide complexes in sulfidic marine waters. In any system these complexes, which tend to increase total dissolved Cd concentrations, will oppose the limits placed on them by solubility and sorption reactions and uptake by biota. Kinetic constraints must be considered in addition to thermodynamic ones, and from the complex interaction of all these factors with the physical parameters of the system (temperature, mixing rates, etc.) concentration and flux of Cd through a given system will be established.

Ecological Aspects of Cadmium

Cadmium is an extremely toxic metal in all forms. It has no known biological function and is thought to act as a poison primarily by competing with the essential metal zinc in metalloprotein and enzyme systems (Luckey et al., 1973).

In man, Cd poisoning has been linked to hypertension, renal disorder, emphysema, anemia, and in particularly severe cases to a disease known as

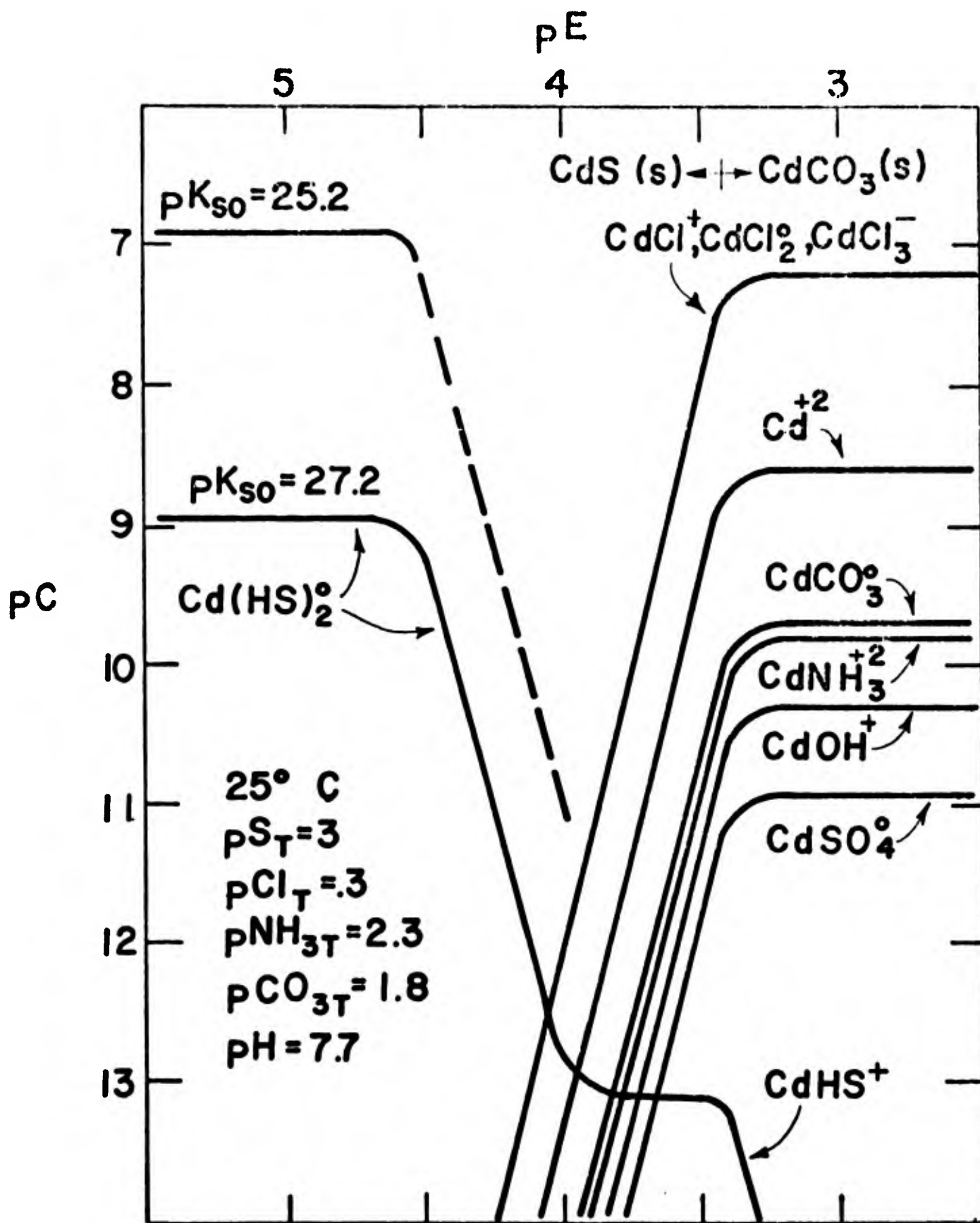


Figure 56. Equilibrium aqueous concentrations of cadmium species as a function of pE. Note that a phase transition occurs at about a pE of -3.5 between CdS(s) and $\text{CdCO}_3\text{(s)}$. Solution composition is typical of estuarine sediment interstitial waters.

Itai-itai. The nature of Cd distribution in the world is such as to make an incident of acute, single-dose Cd poisoning unlikely. However, Cd is an insidious poison in that it accumulates slowly over the course of a lifetime, there being no known mechanism for ridding the body of Cd once it has been absorbed. The principle source of Cd for non-smokers is ingestion. It has been estimated that the average diet contains ~50 µg Cd/day, of which 5% is absorbed through the intestinal wall. Cigarettes contain about 1 µg Cd/cigarette, and the efficiency of Cd absorption in the lungs is probably greater than in the intestine (Fleischer et al., 1974). Once in the blood stream, Cd can be complexed by α-globulins or can accumulate in red blood cells by complexing to the sulfhydryl functional groups in the cell membrane. Eventually, most of the absorbed Cd reaches the kidneys and liver, which contain about 2/3 of the total body burden of Cd in the average adult. There, Cd stimulates production of a protein known as metallothionein, which chelates Cd with 3 sulfhydryl groups complexing each Cd ion (Copenhagen et al., 1973). One of every three amino acid residues in metallothionein is cysteine. The metallothionein-Cd complex is subsequently assimilated into the kidneys and liver, where it remains.

The most severe outbreak of Cd poisoning in humans occurred in the Jintsu Valley in Japan, where over 100 people were afflicted with Itai-itai disease. The disease is characterized by brittle, weakening bones and extreme pain. The source of the Cd was ingestion for several years of apparently normal rice which contained up to 3 ppm Cd. There is no known cure. However, some of the symptoms can be counter-acted by administration of Zn, Se, Vitamin C, or sulfhydryl-containing chelating agents (Fleischer et al., 1974).

Most marine organisms accumulate Cd to concentrations $10-10^4$ times the concentration in surrounding water, but there is no evidence of biomagnification between trophic levels (Mathis and Cummings, 1973). The 24-hr TL_m for fish is in the range 0.6-80 mg/l but decreases rapidly as the time of the experiment increases. The seven-day TL_m can be as low as 8 µg/l (Fleischer et al., 1974).

Due to its long-term accumulation and the uncertainties concerning the interaction of Cd with organic ligands and other metals, considerable work remains to be done before the full biological impact of Cd poisoning can be assessed.

Summary

Cadmium is a rare element present in the earth's crust primarily in association with Zn and Pb ores. It is released and dispersed during the processing of these ores and by leaching of products containing Cd.

The transport mechanisms for Cd in the environment are not well understood. As a soluble species, Cd can be complexed with organic or inorganic ligands or transported as the free aquo ion. Either a simple or complexed form may adsorb to particulate matter and be transported in this form. Limits on Cd solubility are imposed by $\text{CdCO}_3(\text{s})$, $\text{Cd}(\text{OH})_2(\text{s})$, and $\text{CdS}(\text{s})$ in various types of waters.

Cadmium is a toxic, bio-accumulating metal which may interfere with protein activity. Over long periods of time, it is toxic to man and animals at low concentrations.

Further work on transport and reactions in natural systems is required to assess the full environmental impact of Cd.

SECTION VII

MODELS FOR ADSORPTION AT THE SOLID/SOLUTION INTERFACE

Although almost all natural waters contain some amount of organic matter, most laboratory experimental work on the adsorptive behavior of trace-metal ions has been done in the absence of organic ligands or organic colloids. Even though organics must be included in experimental work at some point, it is useful and necessary to know and understand the inorganic experimental systems well enough to be able to identify and model the role of ligands in the adsorption process. A short discussion of inorganic systems is presented here for background purposes since most theoretical and experimental information is available for the development of phenomenological models of inorganic adsorptive systems.

The adsorption behavior of hydrolyzable metal ions at the solid/water interface is strongly pH dependent and is characterized by general agreement between the hydrolysis of the aqueous metal ions and their enhanced adsorption, charge reversal, and coagulant properties. Models which can be used to describe the phenomena (Leckie and James, 1974; MacNaughton, 1973), including ion exchange and the specific adsorption of certain species, have been compared to a recently proposed model (James and Healy, 1972a,b,c) in which all the species of a hydrolyzable metal ion are considered as potential adsorbates; however, only the lower charged, less strongly hydrated hydrolysis complexes have favorable free energies for the adsorption process.

With the current awareness of heavy metals as pollutants in aquatic systems, there is much interest in factors which appear to be involved in the distribution of metal ions between solids and the aqueous phase. The processes described here are of direct application to treatment removal systems. Of course, the chemistry of sediments and natural waters is complicated by the presence of a variety of organic solutes, colloids, and solid phases. However, the interaction of hydrolyzable metal ions at oxide/water interfaces is a convenient reference system for comparison with other data and studies alluding to adsorption mechanisms (Leckie and James, 1974).

Hydrolytic Behavior of Metal Ions

From a wide range of investigations in different disciplines, it has been shown that adsorption or uptake of aqueous metals by mineral/water interfaces

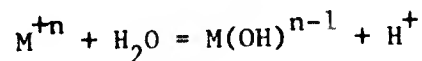
increases abruptly in the pH range where hydrolysis products become a significant fraction of the concentration of the aqueous metal ion (James and Healy, 1972; MacNaughton, 1973; Leckie and James, 1974).

The general interfacial behavior of hydrolyzable metal ions can be summarized as follows:

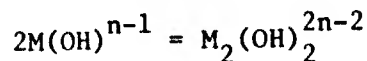
(1) For each metal there is a critical pH range, often less than 1 unit wide over which the fractional amount of metal adsorbed increases from almost zero to unity, i.e., almost complete adsorption or removal from solution. There appear to be some subtle differences for different substrates, but this usually has only a small effect on the critical pH range.

For example, the adsorption density of Fe(III) and Pb(II) on quartz increases abruptly when the following types of hydrolysis reactions occur for both iron(III) and lead(II) (Fuerstenau et al., 1970).

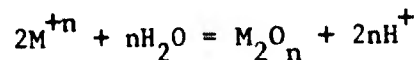
Mononuclear species



Polynuclear and high polymeric species



Insoluble precipitate formation



The usual sequence in the hydrolysis reactions is monomeric species forming transient polymeric species which yield crystalline oxide precipitates after long aging times (Parks, 1972; Smith, 1971; Bilinski and Tyree, 1971).

The adsorption of aqueous Co(III), Mg(II), and Ca(II) on quartz also increases abruptly when pH approaches hydrolysis conditions (Fuerstenau, 1970; James and Healy, 1972b).

(2) If the substrate has a negative surface charge and, hence, a negative surface potential, the experimentally observed double layer potential, ξ , usually reverses sign when the metal ion hydrolyses and metal hydroxides

are precipitated. The free aquo specie appears to have relatively little effect on the ξ potential of the solid.

Observation of the electrical properties of the mineral/water interface during an adsorption experiment reveals reversal of the sign of the surface charge from - to + when the pH is suitable for high adsorption densities and hydrolysis. This result is confirmed by the data of Mackenzie (1966, 1969) and Fuerstenau et al. (1970) on the electrokinetic behavior of quartz in Fe(III) (Mackenzie, 1966), Co(II) (Mackenzie, 1969), and Pb(II) (Fuerstenau et al., 1970) solutions. This type of evidence has been interpreted by Healy et al. (1968) to show that the original substrate oxide becomes coated with hydroxides and hydrous oxides of the adsorbing metal ion. The + to - charge reversal at high pH often corresponds to the pH_{pzc} of the pure oxide of the adsorbing metal ion.

(3) Concurrent with changes in the ξ potential, changes are observed in the stability of colloid dispersions. Generally, rapid coagulation and settling of colloids occur when the ξ potential decreases to a low magnitude. In some instances the formation of hydrolysis products is claimed to have been detected by coagulation techniques (Matijevic et al., 1960).

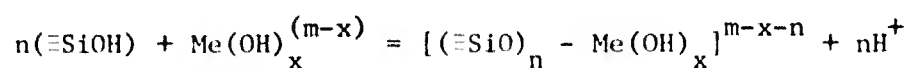
The importance of metal ion hydrolysis and precipitation in adsorption, electrokinetic, and coagulation behavior (and in water-treatment processes) is evident from the many experimental studies on trace metal adsorptive behavior. Adsorption, electrokinetic, and coagulation experiments have all contributed to our knowledge of adsorption processes.

Phenomenological Models for Adsorption of Hydrolyzable Metal Ions

It has been recognized for several years that the adsorption of hydrolyzable metal ions on most substrates, and particularly on hydrous metal oxides, is inextricably related to the hydrolysis behavior of the dissolved metal. A number of phenomenological models have been proposed to explain the experimental observations, which most often show an abrupt increase in adsorption from nil to near 100% in a narrow pH range at or slightly below the pK of the first hydrolysis product. Adsorption is sometimes accompanied by a reversal of the surface charge as measured by electrophoresis and by rapid coagulation. While the various models differ conceptually, it is difficult to distinguish among them experimentally due to our inability to take measurements and detect speciation at the solid/solution interface. Here we

describe three phenomenological models, ion exchange, surface complexation, and adsorption of hydrolytic complexes, and compare their basic assumptions and limitations.

The distinctive features of the ion exchange model are that it requires at least one proton to be released for each metal ion adsorbing and that only charged species sorb. This model was first proposed by Dugger et al. (1964) who studied sorption of 20 metal ions on silica. The reaction taking place at the surface can be written as:



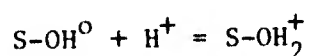
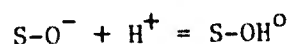
for $(m = x + n)$

$$K_{\text{ads}} = \frac{(\overline{\text{Me}(\text{OH})_x})(\text{H}^+)^n}{(\text{Me}(\text{OH})_x)(\text{H}^+)^n}$$

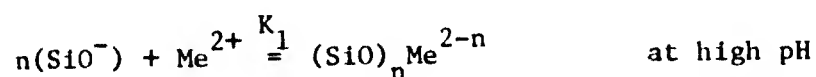
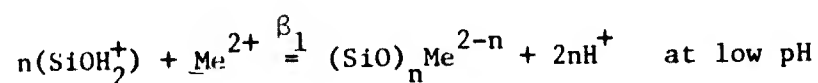
Dugger et al. (1964) found that $\log K_{\text{ads}}$ varied linearly with $^*\text{p}K_1$ leading to the observed correlation of increased adsorption with hydrolysis. There has been some confusion in the literature about the restrictions on m , n , and x . In the original description of the model (Dugger et al., 1964), all the solutions investigated were in the pH range where $x = 0$. It was further assumed for mathematical simplicity and in the absence of contradictory information that $m = n$, but this assumption is not a requirement of the model. The restriction that $x = 0$ is not explicitly stated in the model and we see no need to exclude hydrolyzed species as long as they are positively charged and can take part in traditional types of ion-exchange reactions. The second assumption is equivalent to assuming a constant-charge surface. Since this is an important variable in adsorption work, we have chosen to retain the restriction. In applying the model and comparing results from various investigators, it is important to know which of the model's assumptions they accept.

The constancy of the surface charge is a major objection to the ion-exchange model, since it fails to explain the observed variation of zeta potential with adsorption. The other main objection to the ion-exchange model is that it is inapplicable on surfaces where H^+ and OH^- are not the potential determining ions. Yet the adsorptive behavior of hydrolyzable metal ions is very similar on these surfaces to their behavior on oxides.

An obvious improvement in the ion-exchange theory would be to remove the constant surface charge restriction. Thus changed, and with some mathematical refinement of the forces acting on ions near the interface, the model can be called the "surface coordination" adsorption model. As described by Stumm et al. (1970) this model treats the surface as a poly-acid undergoing the reversible reactions:



in response to solution pH changes. A metal ion can then bond to one or more surface sites, with the accompanying release of 0, 1, or 2 protons per binding site, e.g.



Since the strengths of the surface- H^+ and surface- Me^{2+} bonds are dependent on the total surface charge, which changes with pH, β_1 and K_1 are not true thermodynamic constants. They are a combination of two energy terms, one of which describes the strength of the bond in the absence of surface charge, and a second which describes the coulombic energy associated with bringing the two charged species together. The first term represents an "intrinsic" equilibrium constant, K_{int} (or β_{int}), which is dependent only on the solid and metal species involved. K_{int} bears the same relation to K_1 that thermodynamic equilibrium constants bear to conditional solubility constants in heterogeneous systems.

Methods for measuring the intrinsic and conditional constants associated with metal/silica and metal/ γ -alumina systems are described in Stumm et al. (1970), Holm and Stumm (1975), Schindler et al. (1975). These workers found that, regardless of whether the metal was Fe^{3+} , Cu^{2+} , Cd^{2+} , Pb^{2+} , or Ca^{2+} , the unhydrolyzed free metal ion was the reactive species. As with the simpler ion-exchange model, a linear relationship was found between the exchange coefficient and the first hydrolysis constants for various metals. A critical conclusion concerning this model is that metal ions are "chemisorbed." That

is, they lose part of their inner hydration sheath and the metal ion binds directly with surface oxygens. This leads to stronger sorption of the more highly-charged species (i.e. unhydrolyzed) and is in contrast with the James-Healy "sorption of hydrolytic species" model, which is discussed next.

The critical aspect of the James-Healy model, or the related "adsorption and surface hydrolysis" model, is that the ions are "physically" adsorbed, i.e., they retain their inner hydration spheres and a layer of water one molecule thick separates the adsorbate from the surface. This model treats all solution species as potential adsorbates, and the extent to which each adsorbs is governed by a combination of coulombic, solvation, and chemical terms. The coulombic term can either favor or oppose adsorption, depending on the sign of the surface charge. The solvation term expresses the energy required to remove part of the outer hydration sphere of the metal ion and replace it with "structured water" of low dielectric constant near the surface. It opposes adsorption and is proportional to the square of the charge of the sorbing species. The third term represents a chemical interaction between sorbate and sorbent. It favors enhanced adsorption and is used as a fitting parameter in the model. The model predicts that in most cases when a hydrous oxide is the adsorbent the solvation term dominates the coulombic term. This leads to enhanced adsorption of hydrolyzed, lower charged species over that of the free aquo ion. A variation of this model proposes that the unhydrolyzed species adsorbs and hydrolyzes on the surface. While the two models differ conceptually, they predict identical configurations at equilibrium. James and Healy (1972a,b,c) report comparisons of predicted and experimental adsorption values in several systems.

Since the surface coordination model can be considered as an extension of the ion-exchange model, the main distinction among the models discussed is that the first two are chemical models describing coordinative bonds between metal ions and surface atoms, while the James/Healy model is a physical model, which attempts to define the physical parameters which control adsorption. It concludes that the adsorbing ions retain their inner hydration sphere. One advantage of this is that at the present time the James-Healy model is predictive while the others are not. Ignoring the question of whether a water molecule separates the adsorbed metal from the surface, it may be possible to combine the models, with the James-Healy model describing the relevant

physical parameters controlling the chemical processes taking place as described by the surface complexation model. Since the James-Healy model assumes, somewhat unrealistically, a spread-out uniform surface charge, altering the model to account for discrete surface sites would be an obvious refinement. The surface complexation model may provide insight into the mathematical expression of that refinement.

SECTION VIII

EXPERIMENTAL METHODS AND MATERIALS FOR ADSORPTION STUDIES

Reagents

All chemicals used in this research are Analytical Reagent Grade or better. Experimental adsorption systems are prepared with doubly-distilled deionized water, with the second distillation from potassium permanganate solution. Ionic strength is adjusted to $10^{-1}M$ in adsorption experiments by the addition of sodium nitrate. In some cases sodium perchlorate is used because of the interference of nitrate in subsequent analyses.

Silver stock solutions are prepared from silver nitrate and stored at pH 1.0 in dark glass containers. Copper stock solutions are prepared from the dissolution and oxidation of analytical reagent grade copper wire by nitric acid and stored in glass containers with ground glass stoppers. Stock solutions of ligands used in adsorption experiments are prepared from the sodium salts or the neutral molecule and stored in dark glass containers under refrigeration. Some stock solutions are pH adjusted to aid in dissolution of the ligand or to prevent biological or chemical degradation of the compound during storage.

Preparation of Amorphous Iron Oxide

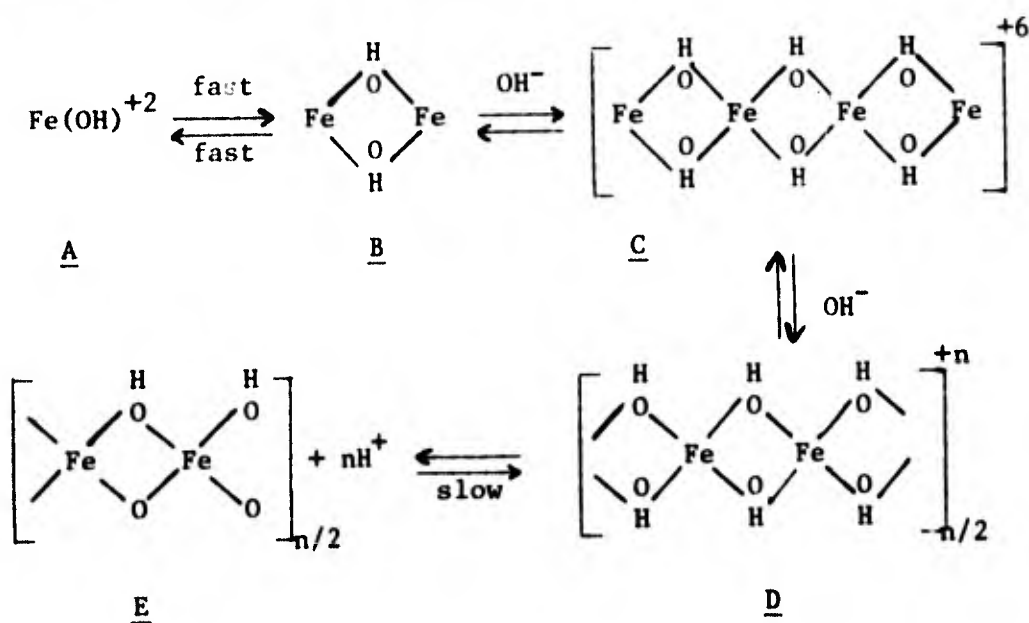
The hydrous iron oxide used in adsorption experiments is prepared in the following manner. Double-distilled water is maintained under a nitrogen atmosphere in a glass-jacketed pyrex reaction flask for several hours. A constant temperature of $25^{\circ}C \pm 1$ is maintained at all times. Nitrogen gas passes through dilute potassium permanganate and sodium hydroxide solutions before entering the reaction flask through a fritted glass gas sparger. Sodium nitrate is added in an amount sufficient to obtain an ionic strength of $10^{-1}M$ after the addition of all reagents. Acidified stock ferric nitrate solution is added, and the iron oxide is precipitated by dropwise addition of carbonate-free sodium hydroxide until a solution pH of 7.5 to 8.5 is attained.

A rapid change in solution pH is observed during the first few hours of ageing after precipitation. To simplify the problems of pH control in adsorption experiments, the iron oxide suspension is stirred in a closed container with a nitrogen atmosphere for a four-hour ageing period before adsorption experiments begin. During this ageing period the solution pH

decreases as hydrolysis reactions continue. During the first hour of ageing pH usually decreases from 8.0 to about 6.5. After this first hour the change in pH with time decreases significantly. During the final hour of ageing pH adjustments are made to bring the solution pH to the desired experimental value. After the ageing period solution conditions are more easily controlled.

Preliminary adsorption experiments showed that the amount of iron ageing had little effect on the kinetics or equilibria of silver adsorption. The adsorptive behavior of iron oxide aged for three days is similar to that aged for four hours. Since solution conditions can be adequately controlled after four hours, this ageing period was chosen for the preparation of freshly precipitated amorphous iron oxide for adsorption experiments.

Recent studies of hydrolysis and precipitation in ferric nitrate solution provide information that can be used to characterize the amorphous iron oxide produced. Dousma and de Bruyn (1976) show evidence that the formation of monomers and dimers are fast and reversible reactions. However, above a critical pH (dependent on solution conditions) higher polymers are formed which result in increased optical density in solution. The formation of these higher polymers is slower but increases with increasing ionic strength and temperature. Drop-wise base addition of sodium hydroxide leads to a faster rate of formation of the higher polymers than a method of homogeneous injection. Oxolation of the higher polymers occurs at a slow rate and results in a relaxation of pH with time. This relaxation is only observed above the critical pH necessary to form the higher polymers. The proposed hydrolysis scheme of Dousma and de Bruyn (1976) is shown below:



The oxobridges formed in structure E react very slowly with acid so a back titration does not decrease the optical density of the solution and primarily changes the solution pH.

Murphy, Posner, and Quirk (1976) characterize the ferric hydroxy polycations formed in a range of ferric nitrate solutions by electron microscope and density gradient ultracentrifugation techniques. The variables of interest are iron concentration, OH/Fe ratio, and ageing time. In all solutions studied the ferric polycations were spherical and in the same size range (15-30 Å in diameter) after 3-4 hours of ageing. An increase in the OH/Fe ratio generally increases the modal distribution of particle sizes at any given time of ageing; however, at 3-4 hours of ageing there is little difference in particle sizes with OH/Fe ratio. Ageing leads to the formation of short rods of 2-5 polycation particles which then form raftlike structures composed of the rods. With further ageing the spheres comprising the rods become indistinct and appear to be coalescing. The individual rods and spheres give no electron diffraction pattern, but goethite is identified in rafts where coalescence has occurred. At high ionic strengths rafts are formed more rapidly by shorter rods since side-by-side collisions are more effective.

Avotins (1975a) examines the effect of solution conditions and ageing periods on iron oxide precipitation. Ferric iron precipitated from solution by a dropwise addition of base to pH values between 6 and 9 forms an amorphous iron oxide. No signs of crystalline structure are evident after two days of ageing at intermediate pH. Some signs of crystallinity (goethite) become evident after fifteen days of ageing. Precipitation of iron oxide at pH values greater than 10 results in an increased rate of crystal formation with ageing. Goethite is primarily present after 15 days of ageing. Goethite precipitates are also observed in aged precipitates at low pH (Dousma and de Bruyn, 1976; Murphy, Posner, and Quirk, 1976). Hematite is formed at elevated temperatures and low pH.

Structure E in Dousma and de Bruyn's hydrolysis-precipitation scheme would account for the formation of goethite as the higher polymers coalesced into the rods and rafts observed by Murphy, Posner, and Quirk. The increased rate of crystal formation in alkaline solutions observed by Avotins (1975a) may be due to an increased rate of the oxolation reactions since the concentration of the hydrogen ion (a product) is suppressed.

Dousma and de Bruyn's data indicate that the rapid dropwise addition of sodium hydroxide used in our preparation procedure would result in the rapid formation of the higher polymers followed by a slow oxolation process during the four-hour ageing period. Thus, the decrease in pH observed during the four-hour ageing period is the pH relaxation ion phenomena due to the slow oxolation reaction. These higher polymers correspond to the 15-30 Å diameter polycation particles observed by Murphy, Posner, and Quirk (1976), who also show that decreasing iron concentration lowers the average particle size in the range (15-30 Å diameter). Since the iron concentrations used in these studies are generally an order of magnitude lower than the lowest concentration studied by Murphy, Posner, and Quirk (.0165M Fe), we can conclude that the diameter of the iron oxide polycations is approximately 20 Å diameter at the end of four hours of ageing. Also, since our precipitations were always performed at high ionic strength, it is likely that the formation of rods is suppressed somewhat. The OH/Fe ratio is higher in our systems (~ 3.0), but a range of OH/Fe ratio values (0.95-2.37) in the solutions of Murphy, Posner, and Quirk had little discernible effect in the first four hours on the formation of rods and coalescence reactions which introduce short-range order into the rods and eventually in the precipitate.

To summarize, it is believed that the amorphous iron oxide used for these adsorption studies is composed of flocculated aggregates of 20 Å (or so) spherical polycations and rafts of these particles similar to those observed by other workers (structure D of Dousma and de Bruyn). The formation of structure D and suppression of rod formation is favored by high ionic strengths and the short ageing period. Spiro et al. (1966) report the formation of high polymeric components in ferric nitrate solutions with the empirical composition $\text{Fe}(\text{OH})_x (\text{NO}_3)_{3-x}$ where x is between 2.3 and 2.5. This is in agreement with the model of Dousma and de Bruyn; it is likely that the high concentrations of the negatively-charged nitrate ion are in close association with the particle to balance the charge of the polycations of structure D. The coalescence of particles into an ordered structure is probably negligible in the four-hour ageing period.

X-ray diffraction analysis of freeze-dried material prepared by our method confirms that it is amorphous. The freeze-dried material has a surface area of 182 m²/gm as measured by BET nitrogen adsorption with 48 hours of outgassing at room temperature. Yates (1975) and Avotins (1975a) have

measured the BET surface area of amorphous iron oxides prepared from ferric nitrate solution in a similar manner and obtained values of 257 and 159 m²/gm, respectively. Yates estimated the chemical composition thermogravimetrically as Fe₂O₃ · H₂O. The water content was approximately 10% as determined by weight loss on heating at 980°C in air after outgassing to constant weight at room temperature (Yates, 1975).

The BET nitrogen surface area measurement must be used with some caution. Yates (1975) has studied weight loss of the amorphous iron oxide as a function of time and temperature of outgassing. As the temperature increases, amorphous iron oxide loses chemisorbed water and the surface structure is undoubtedly altered. Yates presents evidence that outgassing of amorphous iron oxide even at room temperature causes some surface decomposition. The result is probably an underestimate of the surface area.

Avotins (1975a) measured a surface area of 700 m²/gm for amorphous iron oxide by negative adsorption of Mg²⁺ at pH 5. Sodium negative adsorption experiments in this laboratory at pH 4 are in the range 270-335 m²/gm. However, a gel layer porous to water but not to Na⁺ or Mg²⁺ could result in an erroneously low value for surface area by this method.

Both negative adsorption and BET measurement techniques may provide low estimates of surface area for amorphous iron oxide because of porosity and surface decomposition, respectively. Assuming spherical particles and the density (3.57 g/cm³) given by Murphy, Posner, and Quirk (1976), a surface area of 750 m²/gm is an upper value of the surface area of amorphous iron oxide. A more likely value of the surface area is probably somewhere between 750 m²/gm and the value determined by negative adsorption (~300 m²/gm). All figures in this report are based on the BET measurement of 182 m²/gm.

All adsorption experiments are conducted in the pH range 4-13 on amorphous iron oxide. The solubility of amorphous iron oxide never exceeded 1% of the total iron present in any of the systems studied. Soluble iron was measured by the ferrozine method.

Preparation of α-Quartz

The quartz used in adsorption experiments is obtained from Pennsylvania Glass Sand Corporation under the trade name "Min-u-sil" 5. The median particle size is approximately five microns as reported by the manufacturer. X-ray diffraction analyses by MacNaughton and James (1974) and Vuceta (1975) confirm the structure as that of α-quartz. BET nitrogen gas

adsorption analyses indicate a surface area of $3.3 \text{ m}^2/\text{gm}$. MacNaughton and James (1974) and Vuceta (1975) report a specific surface area of $4\text{--}5 \text{ m}^2/\text{gm}$ for this material. BET analyses in this laboratory, performed in triplicate, give a surface area of $3.3 \text{ m}^2/\text{gm}$ for the α -quartz. This was confirmed at an independent laboratory (Department of Mineral Science and Engineering, University of California, Berkeley). Spectrographic analysis shows the presence of many trace impurities in Min-u-sil 5. Organic impurities are removed by oxidation at 550°C for 48 hours. Inorganic impurities are removed by refluxing in 4N nitric acid for several hours. The suspension is then washed with deionized water until a pH of about 6 is maintained. This process is repeated to adequately remove all traces of iron contamination. This is followed by an addition of sodium hydroxide to bring the suspension to approximately pH 10 for a weak base washing. The suspension is then washed with double-distilled water until pH 7.0 is reached. The material is dried and stored in covered glass containers. Subsequent spectrographic analysis of the cleaned particles indicates a dramatic decrease in the level of inorganic impurities (MacNaughton and James, 1974; Vuceta, 1975).

Experience with the washing procedure reveals that equilibration of the silica surface with solution is not rapid with respect to hydrogen ions. Liberation of protons from the surface during the washing procedure is slow. This phenomenon was not studied carefully, but qualitative observations indicate that equilibration is not reached in three days. Van der Lier, de Bruyn et al. (1960) attribute this phenomenon to the existence of a film of amorphous silica on the exterior of quartz particles due to grinding. The final washing procedure in weak base may also contribute to the development of an outer coating of amorphous silica on the quartz particles. The base cleaning procedure used by Vuceta (1975), shaking in 4N NH_4OH , would have even more drastic effects on the surface layers. The slow equilibration of protons with the surface may be a result of diffusion of protons in and out of the amorphous surface layer.

pH Measurement and Adjustment

Most pH determinations in these experiments are made with a glass electrode and a double-junction reference electrode with an outer salt bridge containing 10% potassium nitrate to prevent chloride contamination of the solution. In some cases a combination electrode is used for experimental

convenience. Correction for sodium error is made for very alkaline solution measurements. The pH meter used is a Beckman Expandomatic Model #SS-2. pH adjustments are made with redistilled GFS (G. Frederick Smith Chemical Co.) nitric acid or with carbonate-free sodium hydroxide. The stock acid and base solutions are prepared with double-distilled water.

The determination of pH in iron oxide suspensions is difficult. In the systems studied in this research the response time of the electrodes is very slow, usually requiring ten to thirty minutes to reach a stable value. The rate of drift is rapid immediately after immersing the electrodes but decreases asymptotically with time. The drift is very slow after five minutes, and it is necessary to monitor the change in measured potential with time in order to establish the attainment of a stable value. Because the rate of change slows asymptotically, it is necessary to make an arbitrary definition for the "equilibrium potential." For the purposes of these experiments a drift less than .01 pH unit in three minutes is defined as acceptable for the determination of pH. The slow response of the electrode was also observed by Avotins (1975). He used an arbitrary time of immersion of five minutes for the measurement of pH. The experimental apparatus used by Yates (1975) would eliminate many of the errors in our method. The agreement of the potentiometric titration data of Yates with our data for amorphous iron oxide is encouraging.

Since the slow attainment of a stable potential is observed only in freshly precipitated iron oxide suspensions, this phenomenon may be caused by the effect of highly charged particles and polymers moving by the electrode or hydrolytic reactions occurring at the surface of the electrodes. In an attempt to discover the cause of this phenomena, various methods of pH measurement were employed. The following statements summarize the results of these investigations: 1) The response time of the electrodes is related to the buffer capacity of the suspension. Rapid electrode equilibration is obtained in iron oxide suspensions that are moderately to highly buffered; 2) pH measurements made in the stirred suspension are slightly higher by .05 to .2 pH units than those made in the same suspension without stirring but can be dramatically different than measurements of the centrifugate of the suspension. Figure 57 shows the pH dependence of $\Delta\text{pH} = \text{pH}(\text{stirred suspension}) - \text{pH}(\text{centrifugate})$. Significant differences are observed in systems containing 10^{-3}M sodium bicarbonate; 3) pH measurements made with the

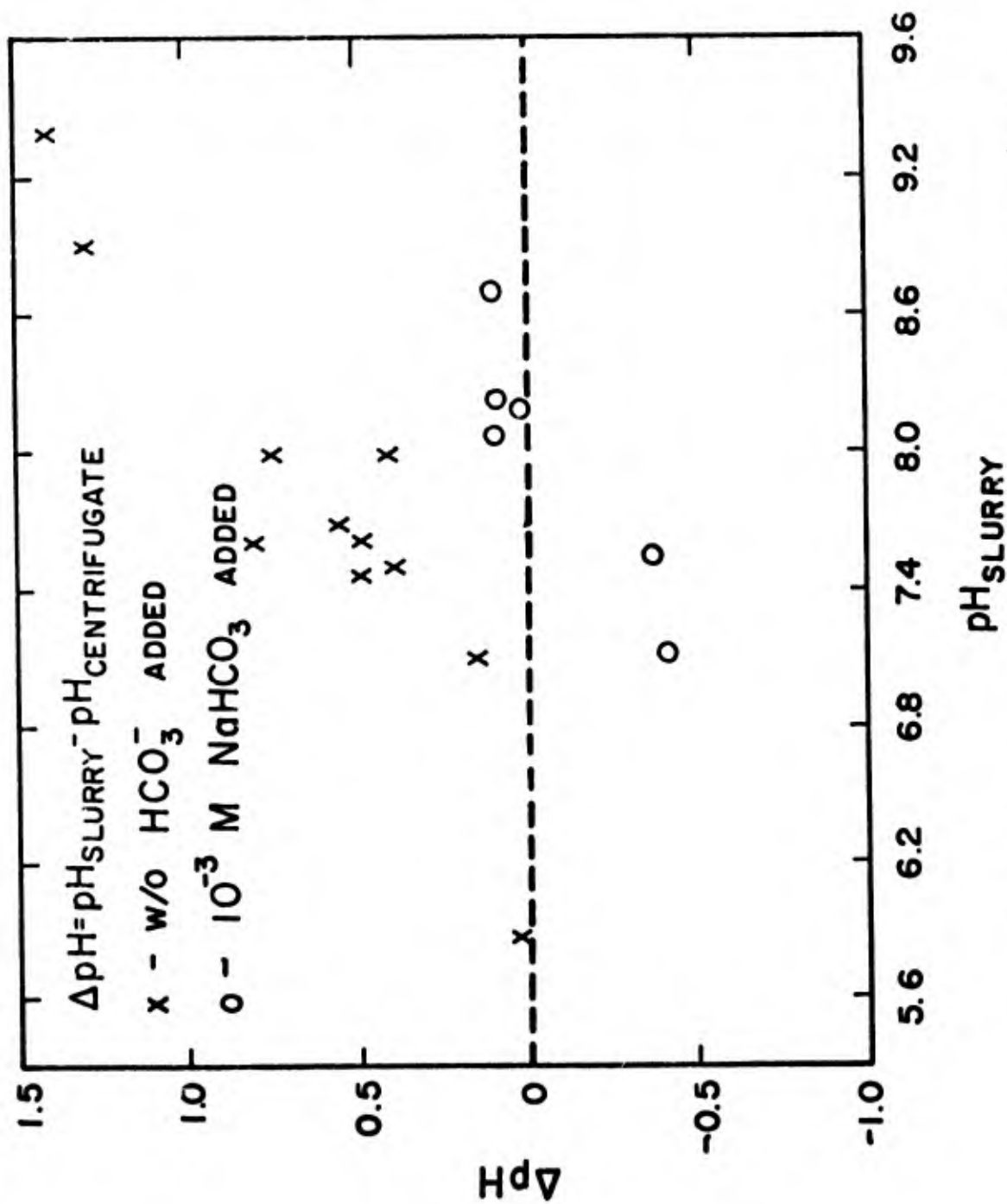


Figure 57. pH dependence of the difference between experimental pH measurement techniques in amorphous iron oxide systems at 25°C and $10^{-1}M$ ionic strength.

electrodes inside dialysis membranes immersed in a stirred iron oxide suspension are in close agreement with measurements made by immersion of the electrodes in the same suspension without stirring. This is also true for systems containing $10^{-3}M$ added sodium bicarbonate; 4) Adsorption experiments of silver(I) performed with and without a maintained nitrogen atmosphere indicate that centrifugate pH measurements are affected by the removal or addition of carbon dioxide to iron oxide suspensions of low buffer capacity; 5) Adsorption experiments of silver(I) in systems buffered with CO_2 /bicarbonate or with a maintained nitrogen atmosphere indicate that the best method of pH measurement in iron oxide slurries is the immersion of the electrodes in the suspension without stirring and before centrifugation. This is the method used by Avotins (1975a) and is used for all pH determinations in these experiments. pH determinations in the quartz suspensions are made by the same method.

Adsorption Experiments in Silver(I)/Amorphous Iron Oxide Systems

Preparation of freshly precipitated amorphous iron oxide for adsorption studies is discussed in a previous section. After the four-hour ageing period adsorption experiments are conducted in batch by one of the following methods: 1) pH adjustment is made in the iron oxide suspension if necessary. Silver(I) is added to the suspension from stock silver nitrate solution containing Ag-110m as a tracer. The silver addition is accomplished by Eppendorf micropipet with an acid-rinsed pipet tip. The tracer comprises less than 0.1% of the silver added. A nitrogen atmosphere and a temperature of $25^\circ C$ are maintained throughout the entire experiment. No pH adjustments are made during the adsorption experiment. A final pH determination is made upon the attainment of adsorption equilibria; 2) The iron oxide is transferred to a repipet flask with a 25-ml delivery spout. 25-ml aliquots of the suspension are delivered to pyrex centrifuge tubes. Small additions of acid or base are made to the iron oxide suspensions to obtain the experimentally desired range of pH. These suspensions are rotated at 15 rpm for one hour in a tube roller. Silver(I) is added with Ag-110m tracer to each of the iron oxide suspensions. The tubes are sealed with polycarbonate screw caps.

Silver(I) adsorption experiments conducted by the first method (under nitrogen atmosphere) show no detectable differences from similar experiments in the presence of an ambient atmosphere of air. Thus, the loss of the

nitrogen atmosphere in the latter method is not important with respect to silver(I) adsorption. Comparative adsorption equilibria experiments show that both methods produce identical results within experimental error.

Figure 58 displays the results of a short-term kinetic investigation of silver(I) adsorption on amorphous iron oxide. The time of measurement refers to the time at which an aliquot is withdrawn from the reaction vessel and does not include the time of centrifugation (fifteen minutes) and its possible effects. The curve indicates a rapid uptake of silver from solution in the first few minutes of reaction. This is in agreement with the results of Dyck (1968), who states that equilibration is reached within five minutes. However, Figure 58 shows a slight increase in adsorption from 3.5 to 15 hours. A second experiment was devised to determine the extent of long-term uptake. The results for two separate batch experiments are shown in Table 20. The results confirm that adsorption is not complete at the end of the initial rapid uptake. Avotins (1975a) finds similar kinetic behavior for the adsorption of mercury on amorphous iron oxide. Mercury adsorption continues at a slow rate for two months after a rapid initial uptake. Although the rate of this additional long-term uptake is slow, it is quantitatively significant when compared to the initial adsorption of mercury. Avotins (1975a) attributes the long-term uptake to diffusion of mercury into the interior of iron oxide particles. Yates (1975) presents some evidence that amorphous iron oxide may be porous to ions. An additional

TABLE 20. KINETIC ADSORPTION EXPERIMENTS

$\text{Ag}_T 5 \times 10^{-6}\text{M}$ $\text{Fe}_2\text{O}_3 \cdot \text{H}_2\text{O}$, amorphous, $4 \times 10^{-3}\text{M}$ Fe, $64.7 \text{ m}^2/\text{l}$ Ionic strength 10^{-1}M		
<u>Experiment</u>	<u>Time of Reaction</u>	<u>% Adsorption</u>
1. pH ~ 7.0	21 hr.	47.7
	44 hr.	50.9
	90 hr.	53.5
2. pH ~ 7.4	21 hr.	58.2
	44 hr.	60.6
	90 hr.	64.5

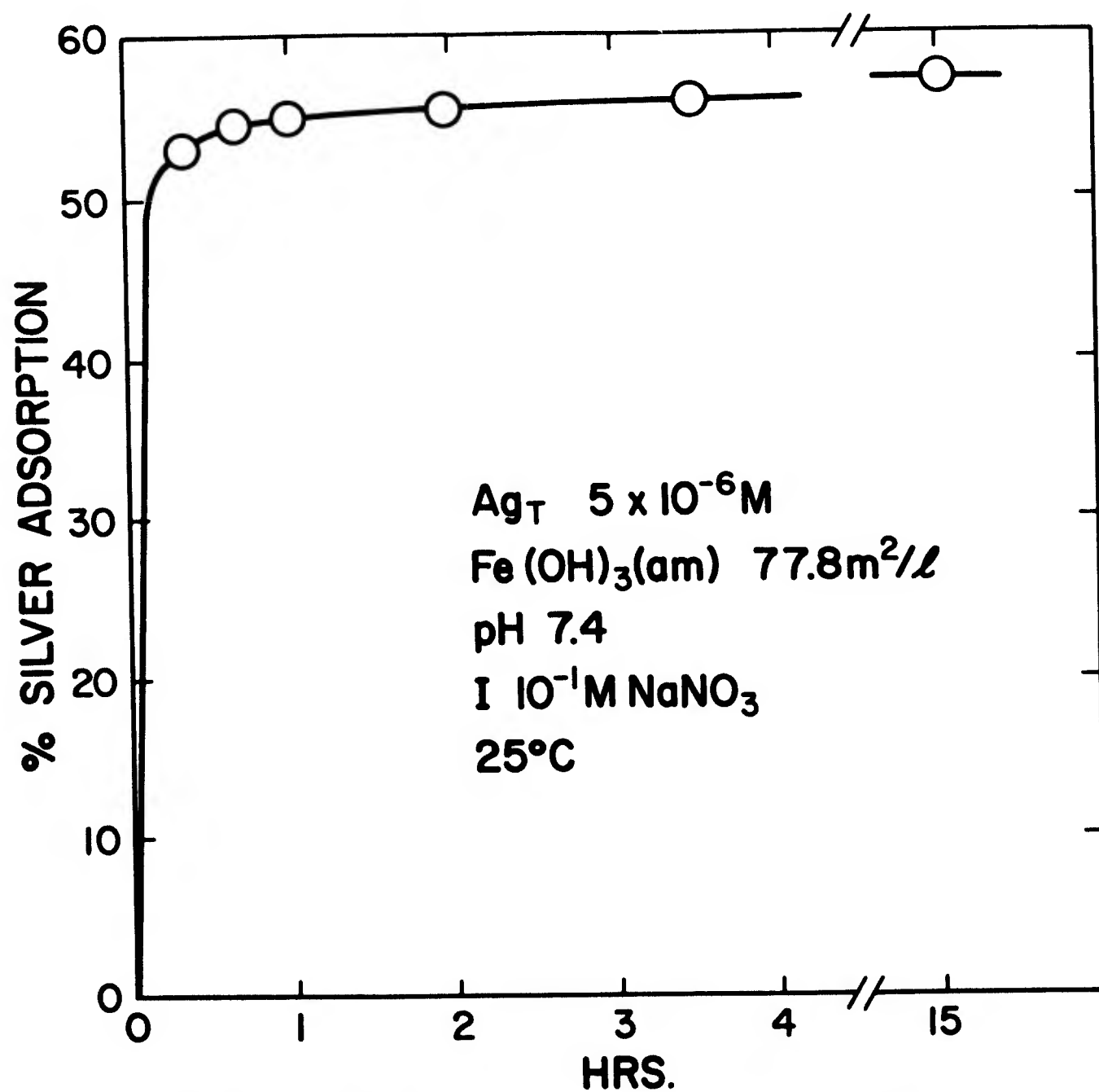


Figure 58. Kinetics of silver adsorption on amorphous iron oxide. Solution conditions of 25°C, 10^{-1}M ionic strength and $5 \times 10^{-6} \text{M}$ initial silver.

long-term kinetic experiment was conducted over a six-week period with batch suspensions of iron oxide in centrifuge tubes. The centrifuge tubes were wrapped with an opaque tape and rotated in a dark room to avoid photoreduction of silver ions. Overhead fluorescent lighting was used only at brief intervals to make necessary experimental measurements. The iron oxide suspension in each tube was originally obtained from one large batch and each tube had the same initial solution pH.

The results of the experiment are shown in Table 21. Each adsorption measurement is the average value of three batch suspensions analyzed at the same time. These results confirm that complete equilibrium is not attained in a short period of time. The slow uptake of silver continues over a period of weeks. It is possible that this additional slow uptake is due to a mechanism proposed by Avotins (1975a), diffusion of silver into the interior of iron oxide particles. However, interpretation of the data is difficult because of the changes occurring in the iron oxide phase and pH changes occurring as a result of the oxolation and coalescence reactions discussed earlier. The settling characteristics and color of the iron oxide phase changed during the course of the experiment. The pH changes observed over time in the suspensions are similar to changes in tubes containing iron oxide without silver addition. Thus, the observed decrease in pH is due to hydrolytic reactions or phase changes of the iron oxide. After two weeks the pH of some of the suspensions had decreased dramatically, in some cases to values as low as 3-4. In one case the iron oxide dissolved.

TABLE 21. LONG-TERM KINETIC ADSORPTION EXPERIMENT

$\text{Ag}_T 4 \times 10^{-6}\text{M}$ $\text{Fe}_2\text{O}_3 \cdot \text{H}_2\text{O}$, amorphous, $3.2 \times 10^{-3}\text{M Fe}$, $51.8 \text{ m}^2/\text{l}$ Aged 24 hours before silver addition Ionic strength 10^{-1}M		
<u>Time</u>	<u>pH</u>	<u>% Adsorbed</u>
5 hours	6.39	22.4
2.75 days	6.37	28.4
7 days	6.35	30.3
21 days	6.12	29.7
38 days	6.07	39.9

Avotins (1975a) and Dousma and de Bruyn (1976) indicate that the phase was probably changing to goethite during the course of the

objective of the preliminary experiments was to establish a reaction for adsorption equilibria experiments. Because the continued slow uptake of silver is studied. A four-hour reaction period is selected for the study of short-term "equilibria" (see Fig. 58). This reaction is used in all silver(I)/amorphous iron oxide equilibrium adsorption experiments. Figure 59 shows that laboratory lighting does not affect the extent of silver adsorption in the four-hour equilibration period.

A few experiments investigated the adsorption of silver(I) on iron sulfide. These results are presented in Appendix B.

Adsorption Experiments in Silver(I)/ α -Quartz Systems

The preparation of the quartz is discussed in a previous section. The desired amount of quartz is weighed in a beaker and then placed in a sonication chamber for several minutes in double-distilled water. The sonication ruptures the dried, flocculated material into the five micron particles. This slurry is added to double-distilled water and sufficient sodium nitrate to obtain an ionic strength of 0.1M after the addition of all reagents. The pH is adjusted to 7.0, and the system is allowed to equilibrate for two hours. Twenty-five ml aliquots of the suspension are added to centrifuge tubes containing small amounts of acid or base that will result in the desired experimental pH. The tubes are rotated overnight at 15 rpm to allow equilibration of the surface with the solution. This initial surface equilibration with the experimental solution is necessary to obtain reproducible results for silver adsorption. Because of the slow equilibration of the proton with the surface of quartz, the solution pH is not an accurate indication of the "surface pH" until sufficient time has been allowed for equilibration.

After twenty-four hours of rotating the suspension at the desired experimental pH, silver(I) is added from stock silver nitrate solution containing Ag-110m as a tracer. The silver addition is accomplished by Eppendorf micropipet with acid-rinsed pipet tips. The tubes are rotated in a dark room to prevent photoreduction of silver ions.

The work of Avotins (1975a) and Dousma and de Bruyn (1976) indicate that the iron oxide phase was probably changing to goethite during the course of the experiment.

The objective of the preliminary experiments was to establish a reaction time for adsorption equilibria experiments. Because the continued slow uptake poses experimental problems for the study of equilibria, only the initial rapid uptake of silver is studied. A four-hour reaction period is selected for the study of short-term "equilibria" (see Fig. 58). This reaction period is used in all silver(I)/amorphous iron oxide equilibrium adsorption experiments. Figure 59 shows that laboratory lighting does not affect the extent of silver adsorption in the four-hour equilibration period.

A few experiments investigated the adsorption of silver(I) on iron sulfide. These results are presented in Appendix B.

Adsorption Experiments in Silver(I)/ α -Quartz Systems

The preparation of the quartz is discussed in a previous section. The desired amount of quartz is weighed in a beaker and then placed in a sonication chamber for several minutes in double-distilled water. The sonication ruptures the dried, flocculated material into the five micron particles. This slurry is added to double-distilled water and sufficient sodium nitrate to obtain an ionic strength of 0.1M after the addition of all reagents. The pH is adjusted to 7.0, and the system is allowed to equilibrate for two hours. Twenty-five ml aliquots of the suspension are added to centrifuge tubes containing small amounts of acid or base that will result in the desired experimental pH. The tubes are rotated overnight at 15 rpm to allow equilibration of the surface with the solution. This initial surface equilibration with the experimental solution is necessary to obtain reproducible results for silver adsorption. Because of the slow equilibration of the proton with the surface of quartz, the solution pH is not an accurate indication of the "surface pH" until sufficient time has been allowed for equilibration.

After twenty-four hours of rotating the suspension at the desired experimental pH, silver(I) is added from stock silver nitrate solution containing Ag-110m as a tracer. The silver addition is accomplished by Eppendorf micropipet with acid-rinsed pipet tips. The tubes are rotated in a dark room to prevent photoreduction of silver ions.

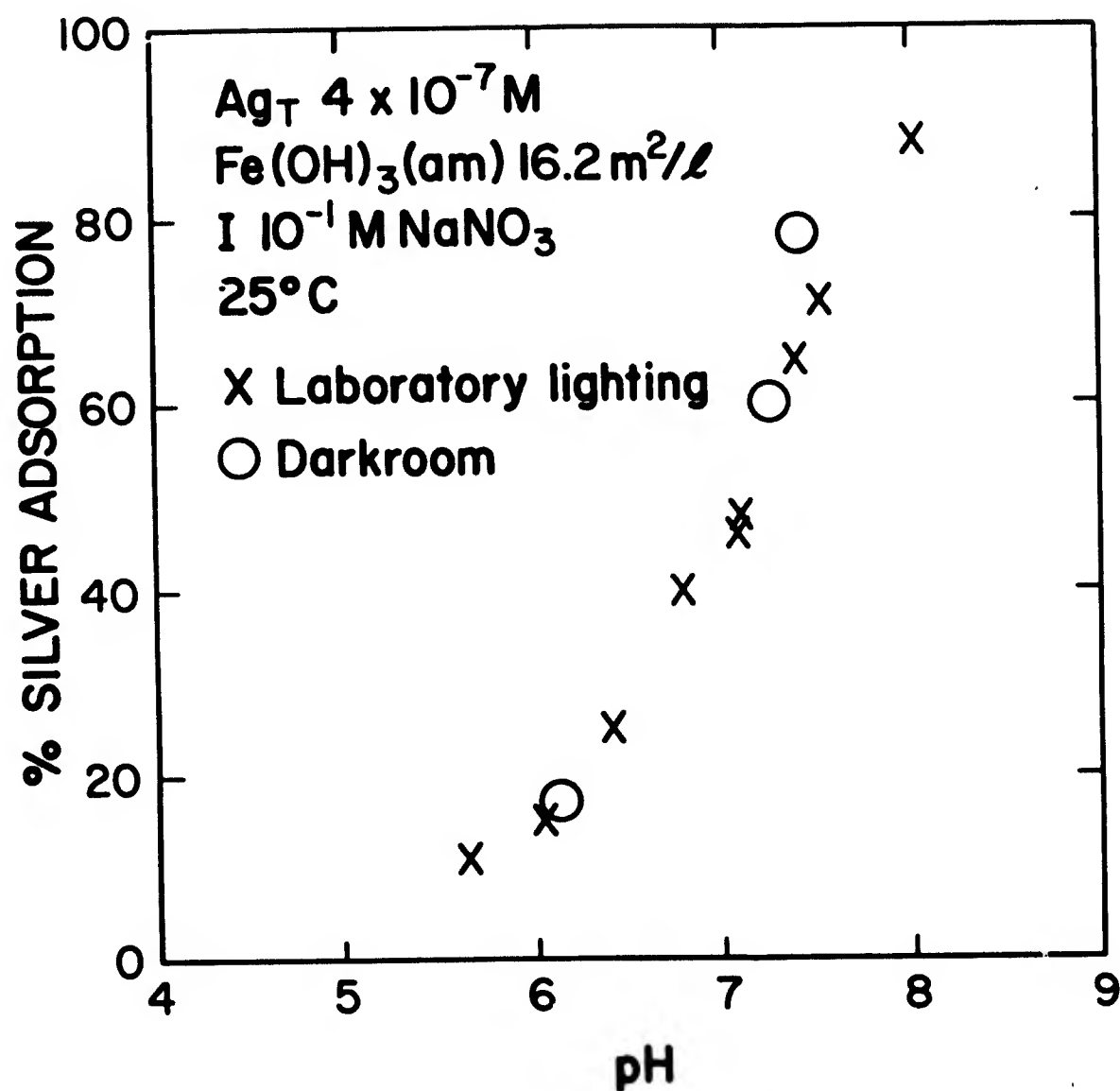


Figure 59. The adsorption of silver(I) on amorphous iron oxide as a function of pH under darkroom and laboratory lighting conditions. Data shown are for short-term 4-hr equilibria, ionic strength of 10^{-1} M , and 25°C .

The uptake of silver(I) on α -quartz is substantially slower than that observed for silver(I) on iron oxide. In addition to this kinetic difference, the rate and amount of silver uptake on α -quartz are dramatically influenced by laboratory lighting. Figure 60 shows the rate of adsorption of silver(I) in identical batch systems in the darkroom and under normal laboratory lighting conditions. Adsorption to the container is also dramatically enhanced by experiments conducted in laboratory lighting. Adsorption to the container in the darkroom and in iron oxide adsorption experiments is generally less than 2% of the total silver present. It is believed that this additional removal of silver from solution is due to photoreduction of adsorbed silver ions by the mechanism reported in the section on the aqueous chemistry of silver.

Figure 60 shows that silver adsorption has not yet reached equilibrium in twenty-four hours under darkroom conditions. Additional kinetic experiments have revealed that silver uptake increases only slightly after one to two days. A four-day reaction period is used for all silver/quartz systems to ensure that equilibrium is attained. The slow uptake of silver(I) on the quartz surface may be due to diffusion of silver ions into an amorphous silica surface layer. A similar postulate has been made for proton equilibration.

Adsorption Experiments in Copper(II)/Amorphous Iron Oxide and Copper(II)/ α -Quartz Systems

Amorphous Iron Oxide Systems. Preparation of amorphous iron oxide is discussed in a previous section. After the four-hour ageing period copper is added from stock cupric nitrate solution to the glass-jacketed pyrex reaction vessel. A nitrogen atmosphere is maintained during the preparation and ageing of the iron oxide and during the adsorption experiments. The temperature of the suspension is constant at 25°C. Sufficient sodium nitrate is added to obtain an ionic strength of 10^{-1}M after the addition of all reagents.

Figure 61 displays the rate of uptake of copper(II) on amorphous iron oxide. Contrary to the kinetic behavior reported for silver and mercury (Avotins, 1975a), copper adsorption appears to be complete at the end of the initial rapid uptake. Equilibration in copper(II)/amorphous iron oxide systems is allowed for ninety minutes before sampling. Experience with this system has revealed that adsorption and desorption of copper(II) is

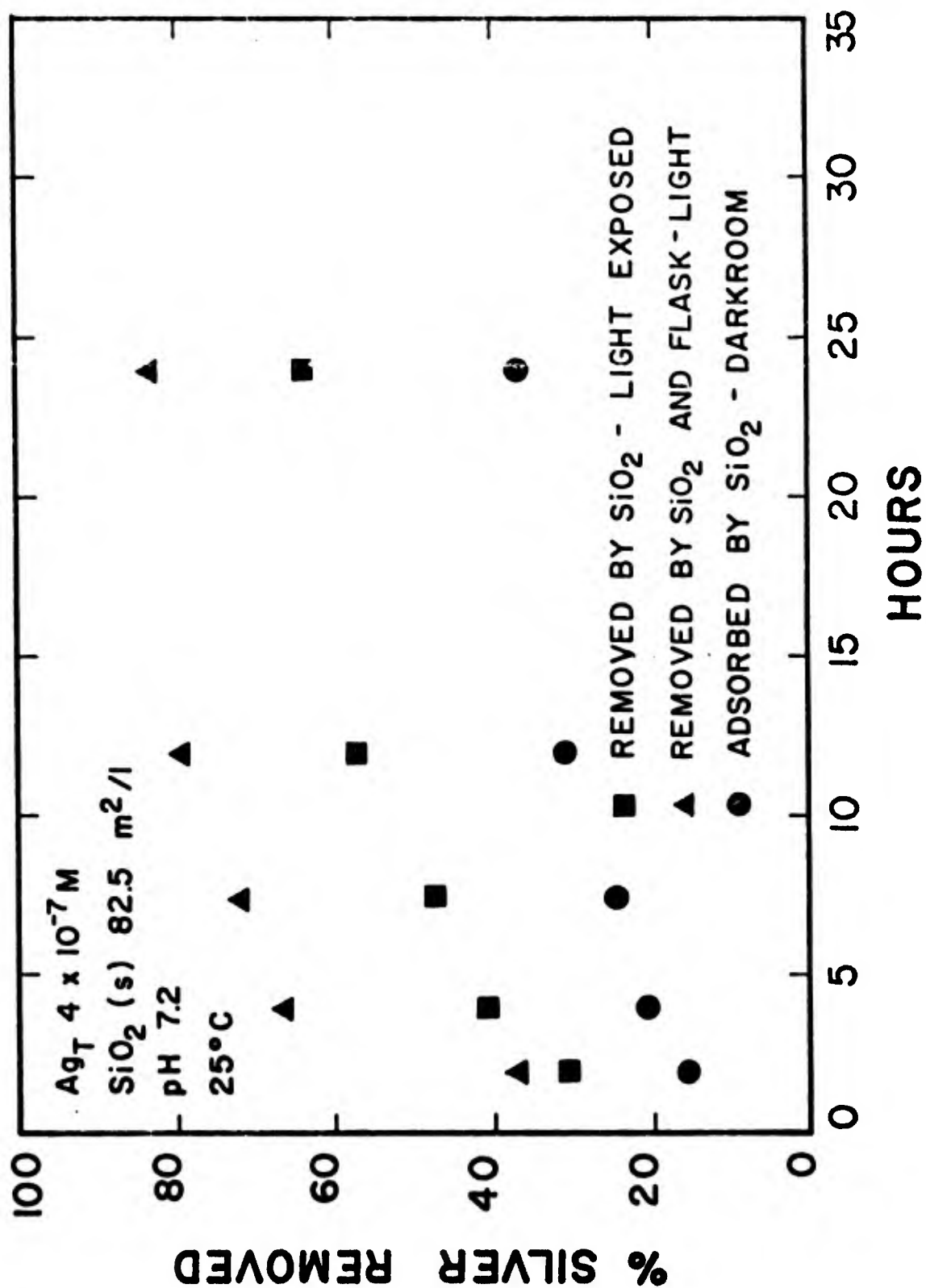


Figure 60. Rate of silver(I) removal from solution by α -quartz under darkroom and laboratory lighting conditions. Container adsorption is significant in laboratory lighting but absent in the dark. Ionic strength = 10^{-1} M NaNO_3 , 25°C .

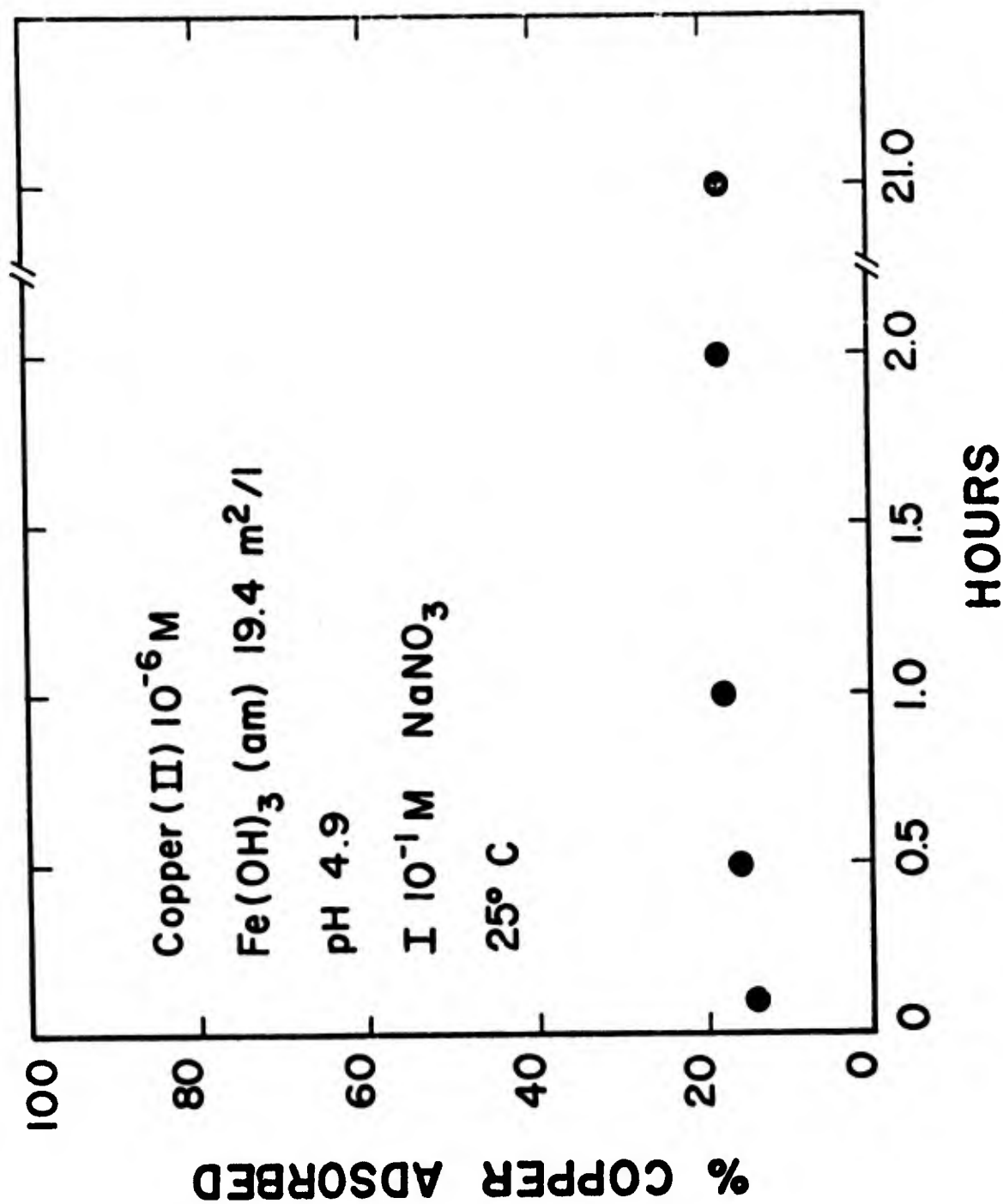


Figure 61. Rate of copper(II) adsorption on amorphous iron oxide at pH 4.9, 25°C , and ionic strength = 10^{-1}M .

sufficiently rapid to allow a change in pH and the measurement of additional equilibrium states with the same batch. A maximum of three points is obtained with each copper/amorphous iron oxide batch system. The characteristics of the iron oxide do not change significantly in this period of time (270 minutes). Comparative adsorption experiments have shown that this method produces equilibrium measurements identical to single measurements in batch systems.

α -Quartz Systems. Experimental methods in copper(II)/ α -quartz systems are similar to those in silver(I)/ α -quartz experiments. The quartz is weighed, sonicated and then equilibrated with the solution for twenty-four hours in 10^{-1} M sodium nitrate in double-distilled water. A nitrogen atmosphere and a constant temperature of 25°C are maintained. pH adjustments are made before the twenty-four hour equilibration to obtain the desired experimental value.

Figure 62 shows the rate of uptake of copper(II) on quartz. The rate is slower than that observed for amorphous iron oxide and equilibrium is attained in approximately 5-6 hours. A six-hour reaction period is used for adsorption equilibrium experiments in copper(II)/ α -quartz systems. The rate is slower than that observed by Vuceta (1975) for the same system. However, it is possible that the strong base-washing procedure used by Vuceta (1975) may have produced a different type of surface with respect to the material used in these experiments.

Adsorption Experiments in Systems Containing Complexing Ligands

In systems containing complexing ligands the ligand is added to the suspension before a trace metal unless otherwise stated. The investigations of the adsorption of ligands are conducted in a manner similar to the methods used in the trace-metal system to which it is to be compared. For example, if the effect of salicylic acid on copper adsorption on iron oxide is to be studied, the adsorption of salicylic acid on iron oxide is determined under the same conditions and methods used for copper adsorption. All silver/complexing ligand systems are investigated under darkroom conditions to avoid photoreduction. Adsorbing ligands appear to attain equilibrium conditions within the same period used for trace metal adsorption systems. After the addition of the ligand, a period of one to two hours is allowed for reequilibration of the system before the trace metal is added. Then, the usual period of equilibration is allowed for trace-metal adsorption.

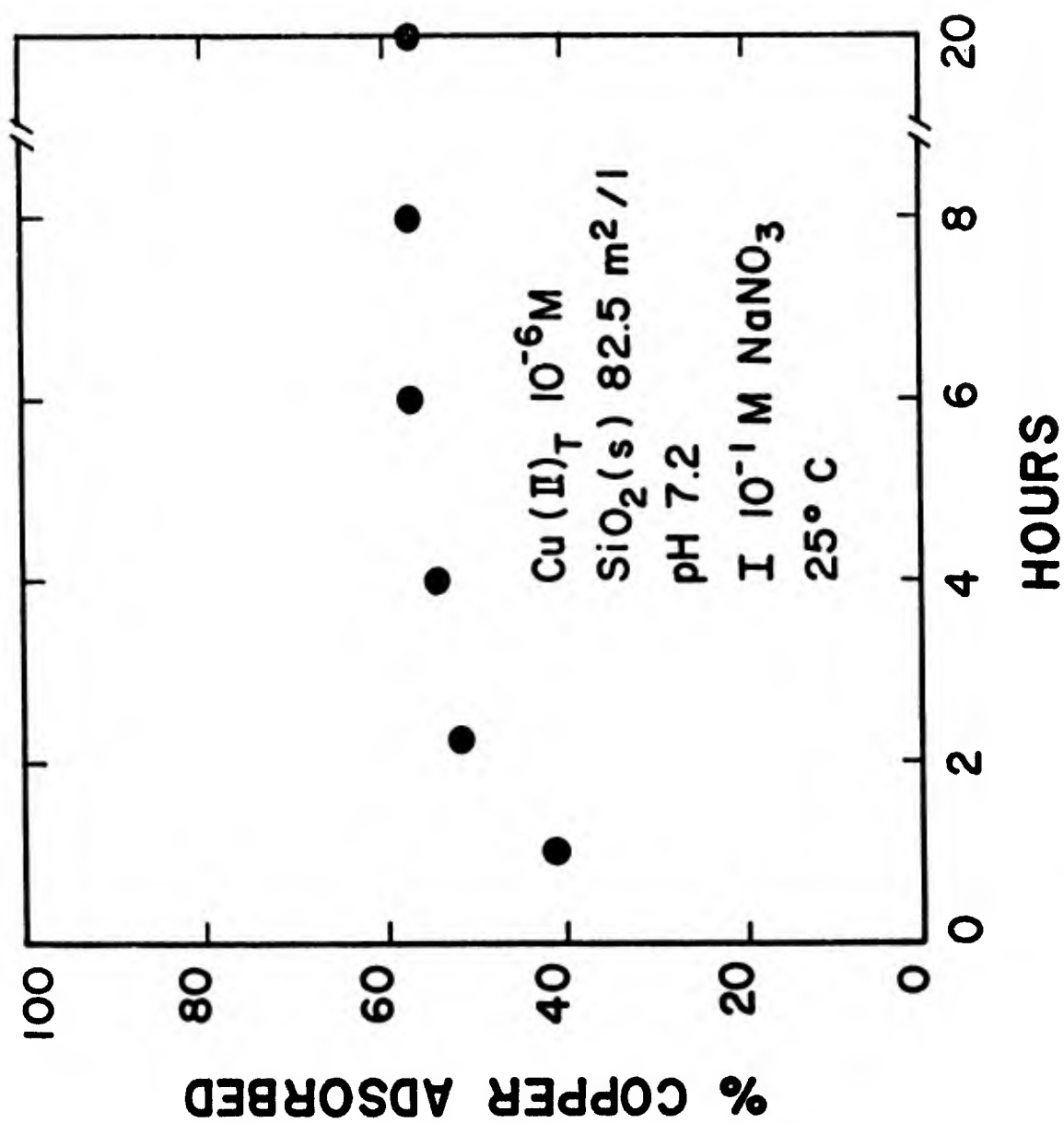


Figure 62. Rate of copper(II) adsorption on α -quartz at pH 7.2, 25°C , and ionic strength of 10^{-1}M .

Sampling and Analysis

Sampling is accomplished by the removal of twenty-five ml aliquots of suspension and transfer to a centrifuge tube for solid/liquid phase separation. Preliminary studies showed that a fifteen-minute centrifugation period in a clinical centrifuge achieves iron and quartz removal efficiencies equivalent to longer centrifugation periods at 10,000 rpm in a larger centrifuge. Precautions are taken to prevent significant temperature changes during centrifugation. Tests of the centrifugate for iron content have consistently shown that the iron concentration is below the detection limit of the ferrozine test (0.1 mg/l). Therefore, any colloidal iron left in the centrifugate would generally represent less than 0.1% by weight of the total iron used in adsorption experiments.

In silver(I) adsorption experiments Ag-110m is used as a tracer. A two-ml aliquot is taken from the centrifugate for scintillation counting to determine the amount of silver remaining in solution. A two-ml aliquot is also taken from the suspension at this time to determine the amount of silver removed by the container.

In copper adsorption experiments a three-ml aliquot is withdrawn from the centrifugate and stored in acid-washed vials for analysis by flameless atomic absorption spectrometry. Twenty microliters of concentrated redistilled GFS (G. Frederick Smith Co.) nitric acid are added to the vial to acidify the sample to pH 1. A Perkin-Elmer Model 403 Spectrometer with HGA carbon furnace attachment is used for the analysis. Copper standards are prepared with double-distilled water and acidified to pH 1 with GFS nitric acid. The standards contain 0.1M sodium nitrate to eliminate matrix effects in the analysis.

In systems containing complexing ligands, additional aliquots are sometimes taken from the centrifugate for analysis of the ligand concentration. Analysis of ligands is accomplished by several methods. These analytical techniques are discussed in the following sections.

Crystal Scintillation Counting. Crystal scintillation counting is the preferred method of analysis for Ag-110m. This method is typically used for gamma-emitting radioisotopes. Ag-110m emits gamma rays at the following energy levels: 0.116, 0.438, 0.446, 0.471, 0.499, 0.542, 0.575, 0.619, 0.657, 0.677, 0.705, 0.723, 0.764, 0.817, 0.884, 0.937, 1.384, and 1.504 MeV. Spectral analysis shows that the events overlap to produce a large plateau

rather than several distinct peaks. Because of the great number and wide range of the events, the use of wide-window discriminator settings is preferable to allow the detection of many events rather than using a narrow window centered around one particular peak. This method has the disadvantage of coping with a relatively large background count, but reduces the amount of isotope necessary to detect a sufficient number of counts to achieve the desired level of accuracy (10,000 cpm). The reduction of the amount of isotope used is important because of the high energies of the gamma rays of Ag-110m. A Baird-Atomic Model 810c well counter with sodium iodide crystal is used for gamma counting. The well counter signal is received by integrated Ridd amplifier, discriminator, scales, and timer (Model numbers 40-9B, 33-13A, 49-26, and 54-7, respectively).

Liquid Scintillation Counting. A technique has been developed that allows the simultaneous determination of Ag-110m and beta-emitting isotopes in aqueous solution using liquid scintillation counting. Gamma-emitting isotopes are usually analyzed by crystal scintillation counting. Liquid scintillation counting is typically used for radioisotopes with much lower energy, usually beta-emitting isotopes. The advantage of liquid scintillation counting for these experiments is that isotopes can be used for both silver and complexing ligands with simultaneous analysis. Ligands analyzed by this technique include sulfate and thiosulfate (S^{35}), salicylic acid and thiourea (C^{14}), and glycine, glutamic acid, and histidine (H^3). Appendix A presents background information on the use of liquid scintillation counting. The instrument used is a Packard Model 3320 Tri-Carb Liquid Scintillation Counter.

The mechanism of detection of Ag-110m by the liquid scintillator involves the detection of high-energy electrons that are produced by Compton interactions of the gamma rays, identical to the mechanism used for external standardization. Since Ag-110m has gamma rays of energies ranging from 0.116 to 1.5 MeV, the energies of the electrons produced by the Compton interactions also cover a wide range. As the gain level increases on the instrument, the percentage of total counts for Ag-110m increases at the high end of the detection scale. Beta-emitting isotopes (S^{35} , C^{14} , H^3) emit particles of lower energy. The beta particles of tritium are detected at the low end of the detection scale at high gain values. The counting efficiency of tritium decreases substantially as the gain decreases from 50%.

Intermediate energy emitters such as C^{14} and S^{35} have energies that can appear anywhere on the detection scale by varying the instrument gain level.

The counting of aqueous samples containing only a beta-emitter is simple. However, samples containing Ag-110m and a beta-emitter cannot be analyzed in the same manner. It is desirable to maximize the separation of the energies of the isotopes on the detection scale. Unfortunately, Ag-110m produces Compton electrons at all energy levels on the detection scale at all gain levels. Under these circumstances it is best to increase the gain level as high as possible to minimize the percentage of Ag-110m counts at the lower end of the detection scale. However, the gain level cannot be set so high as to move the energies of the beta events into the upper region of the detection scale. The following gain settings are found to be optimal for the counting of samples containing Ag-110m and the designated beta emitter:

1) S^{35} -20% gain, 2) C^{14} -20% gain, and 3) H^3 -60% gain.

Both channels ratio and external standardization techniques are used to determine the degree of quenching in samples. The degree of quenching must be known as accurately as possible to estimate the counting efficiency of each isotope. In addition, the degree of quenching affects the distribution of energies of the light pulses. An increase in the degree of quenching skews the distribution of counts toward the lower end of the detection scale. Thus, an increase in quenching increases the number of Ag-110m counts in the energy window selected for counting the beta-emitter.

External standardization or channels ratio in two high-energy windows can be used to determine the counting efficiency of Ag-110m. The gain settings are selected so that only Ag-110m counts are in the high-energy windows and direct calculation of the Ag-110m counts can be made after the determination of the counting efficiency for Ag-110m. This counting efficiency is correlated by previous calibration experiments to a channels ratio of Ag-110m counts in the high-energy window selected for silver counting and the low-energy window selected for the beta-emitter. Thus, the Ag-110m counts in the low-energy window can be subtracted from the total counts in that window for a sample containing both isotopes. The remaining counts in the low-energy window are due to the beta-emitter and must be corrected for counting efficiency by external standardization.

Satisfactory quenching curves are derived that allow the simultaneous counting of aqueous samples containing Ag-110m and S^{35} , C^{14} , and H^3 .

Quantitative analysis shows that the counting rates of Ag-110m and any of the beta-emitters are determined with a precision of 3% by this method.

Other Methods of Ligand Analysis. Many complexing ligands are unavailable as tracers, and an alternate method of analysis must be found. Fortunately in these experiments, most other complexing ligands can be satisfactorily analyzed by ultraviolet spectrometry because of their aromaticity. Ligands analyzed by ultraviolet absorbance include syringic acid, protocatechuic acid, picolinic acid, and 2,3-pyrazinedicarboxylic acid. The total concentrations of ligands added to adsorption experimental systems were chosen so that sample concentrations would be in the optimal range of analysis without dilution or concentration. All standards and samples are measured at the same pH by adjustment with a non-absorbing buffer.

Ammonia and ethylenediamine are determined by the use of a Technicon Auto-Analyzer.

Container Adsorption and Cleaning Techniques

Numerous investigators have examined the adsorption of silver on sample containers of many materials (Chao, Jenne, and Heppting, 1968; Robertson, 1968; Durst and Duhart, 1970; Dyck, 1968). Struempfer (1973) provides an adequate review of this literature. Adsorption of silver by containers varied with concentration, pH, contact time with the container, competition of dissolved salts, types of containers, and the presence of complexing agents. Negligible silver is adsorbed on glass and polyethylene containers from 0.5 ppb silver solutions acidified to pH 2 during a thirty-six day reaction period. At pH 4.5, both glass and polyethylene containers adsorb silver ions, somewhat rapidly at first, then linearly with time, and after twenty-four days one-half of the silver is adsorbed. Desorption from the container occurs upon acidification at about the same rate as adsorption. Chao, Jenne, and Heppting (1968) and Dyck (1975) express uncertainty as to whether complete desorption can always be achieved. The increased adsorption of silver from solutions exposed to light has been previously mentioned, apparently resulting from the photoreduction of adsorbed silver ions. Both light-exposed solutions and those maintained in the dark are subject to erratic adsorption behavior with time.

Experiments in this laboratory show that the amount of silver container adsorption is a function of the previous history and nature of the surface

of the container as well as solution conditions. Containers not previously exposed to silver adsorb significantly more silver than those with previous contact. Polycarbonate centrifuge tubes adsorbed 20% of the total silver present in a 10^{-6} M silver nitrate solution in two hours at pH 6.2 during the first exposure of the tubes of silver(I). A new beaker containing a solution of 10^{-5} M silver nitrate solution with Ag-110m tracer at pH 3 lost 52% of the silver from solution in twenty-four hours. About one-half of this silver was recovered by a six-hour immersion of the beaker in 10% nitric acid. Some silver was adsorbed on electrodes that had been immersed in the solution of silver nitrate during the twenty-four hour period. It was not possible to recover all of the silver from the electrodes by overnight immersion in 10% nitric acid. The reaction vessels used for adsorption experiments adsorb significant quantities (up to 18% has been observed from 10^{-6} M silver nitrate solution) of silver during first use but negligible quantities in subsequent adsorption experiments. This initial adsorption is considerably higher than expected when compared to reports in the literature.

Adsorption on containers is not a problem in these adsorption experiments. Container adsorption is minimized by previous exposure of the apparatus to silver solutions of similar concentrations and the fact that the surface area of the container is small compared to the surface area of the solid substrate used in the adsorption experiments. Total losses of silver during adsorption experiments are usually less than 2% of the total silver present. To prevent cross-contamination of the glassware used in the experiments, all glassware is designated for a specific use in the experimental scheme and is used only for that procedure. Glassware exposed to silver solutions is used only for a narrow range of silver concentrations. All used glassware and other experimental apparatus are immersed in chromic acid for twenty-four hours, then in 10% nitric acid for twenty-four hours, rinsed four times with deionized water, and finally air-dried in a filtered air chamber before reuse.

Adsorption Experiments in Cadmium(II)/ α -Quartz and Cadmium(II)/ γ -FeOOH Systems

Description of System. Batch adsorption experiments are performed either in 600-ml water-jacketed beakers or in 30-ml centrifuge tubes. When carbon dioxide is excluded from the system, the solid is dispersed ultrasonically in

deionized water adjusted to the appropriate ionic strength with reagent-grade chemicals. The pH is adjusted to ≤ 4.5 with 0.1M HNO_3 , and the suspension is purged with nitrogen for at least 30 minutes. The pH is adjusted to pH ~ 7.5 (~ 8 for silica) and the solid equilibrated for an additional period of 1 to 4 hours. The cadmium is then added to the suspension as a solution of normal cadmium and cadmium-109 in 0.1M HNO_3 . The stock solution is sufficiently concentrated so that in most cases ≥ 1 ml of solution is added per 500 ml of suspension. If competing ligands are included in the system, they are added before the initial pH adjustment. The pH is then adjusted with CO_3 -free 1.0M NaOH to the desired level. After a predetermined time period has elapsed, an aliquot of suspension is transferred to a centrifuge tube using a glass syringe fitted with a teflon tip and the suspension is centrifuged in a clinical centrifuge for 10 to 15 minutes. Samples of the supernatant and suspension are transferred to counting vials, and the activity of each is measured in a well-type crystal scintillation counter. Cadmium-109 decays via γ -radiation of energy 88 MeV. At least 10,000 counts above background are recorded for each sample. The pH of the suspension is then adjusted with 1M NaOH , and the equilibration and analysis are repeated. The entire system is stirred and purged with nitrogen continuously, and the temperature is maintained at $20 \pm 1^\circ\text{C}$.

Most of the lepidocrocite experiments are performed in systems including CO_2 . For these, the procedure is the same as for the CO_3 -free systems through the addition of the cadmium. At this point, the nitrogen purge is shut off and the pH is adjusted by addition of 1M CO_3 -free NaOH and 0.1M NaHCO_3 . Sufficient NaHCO_3 is added so the system is in equilibrium with air. An aliquot of suspension is then transferred to a centrifuge tube, which is placed on a roller. The pH of the suspension is adjusted with additional NaOH and NaHCO_3 , and the sampling procedure is repeated. The roller rotates at 5 to 10 rpm for a predetermined interval after which the pH of the sample is measured. It is then centrifuged and a portion of the supernatant is removed for cadmium-109 counting. For these samples, the activity of the slurry in all the tubes is assumed to be the same as the activity of the slurry in the main suspension. An occasional check of this assumption shows it to be acceptable. The temperature of these experiments is not controlled. Ambient temperatures are in the range $22 \pm 5^\circ\text{C}$.

Measurement. The pH of the slurry for experiments performed in large beakers is measured with a Radiometer pH meter, Model 22r. The electrodes are glass electrode type 202C, from Radiometer, and a Beckman double-junction reference electrode. When measuring pH in a centrifuge tube, the Metrohm Model E300B pH meter is used in conjunction with the Model EA147 combination electrode. All pH values are measured while the slurry is stirred magnetically, and extensive tests show the slurry effect to be negligible.

Desorption Experiments. Desorption experiments were run in the silica systems using the same techniques as for adsorption studies. After a system has reached an equilibrium condition, the pH is adjusted by addition of 1M HNO_3 and samples of the slurry and supernatant are analyzed for Cd-109. When desorption is studied as a result of addition of competing ligands, the ligand is added as the dry salt to an equilibrated system.

Acid-Base Filtration of the Solid. The solids are titrated with 0.100M CO_3 -free NaOH from pH ~ 3.5 to pH ~ 10.5 . The suspensions are somewhat more concentrated than those used for adsorption experiments in order to magnify any effects. Suspensions of the solids in the presence and absence of cadmium, as well as appropriate blanks, are stirred continuously and maintained at $20 \pm 1^\circ\text{C}$ during the titrations. They are first degassed at pH ~ 3 for ≥ 30 minutes, and those from which CO_2 is to be excluded are purged with CO_2 -free nitrogen continuously. Three minutes elapses between an addition of NaOH and the measurement of pH. The pH appears to stabilize within 30 seconds after the addition of base in most cases. In some experiments, after the degassing step the flow of nitrogen gas is stopped and an amount of NaHCO_3 is added to bring the total concentration of carbonate species in solution (CO_3, T) to $3.4 \times 10^{-4}\text{M}$, after which the titration proceeds normally.

If the amount of adsorption is to be measured, an aliquot of the suspension is vacuum-filtered through 0.45- μm Millipore filter mounted in an all-plastic filter holder. The process takes 1 to 2 minutes. The liquid is collected in glass bottles and acidified until it is transferred to counting vials for cadmium-109 analysis. Filtration of a solid-free solution of 10^{-4}M cadmium at pH 7.6 shows that 5% or more of the total cadmium is retained by the filter and holder.

Batch Adsorption Experiments

Adsorption Kinetics. Kinetics of adsorption of cadmium onto lepidocrocite and silica were studied. The results are shown in Figures 63 and 64. Equilibrium sorption levels are attained in less than 15 minutes on silica, but on lepidocrocite adsorption increases slowly for at least 14 days after an initial rapid uptake.

Due to the fact that reproducible results are not attained in CO_3 -free systems containing lepidocrocite (Figure 63), all results for such systems are for solution in equilibrium with the atmosphere. From the limited data available, it appears that this has the effect of increasing sorption slightly at any pH over that attained under a nitrogen atmosphere.

The rapid uptake step followed by a much slower, continual increase in adsorption is typical of amorphous iron oxides (Avotins, 1975; Davis, this report). Equilibrium adsorption of cadmium onto freshly precipitated hydrous manganese oxides has been reported to be rapid (Posselt, 1971; Zasosky, 1970) but may be much slower on well-ordered crystalline phases (Cabans et al., 1965). Equilibration times of 2 to 24 hours are used in a study of cadmium adsorption onto goethite and titania (James et al., 1975), but no long-term tests were undertaken to verify that thermodynamic equilibrium had been attained as reported by James in personal communication.

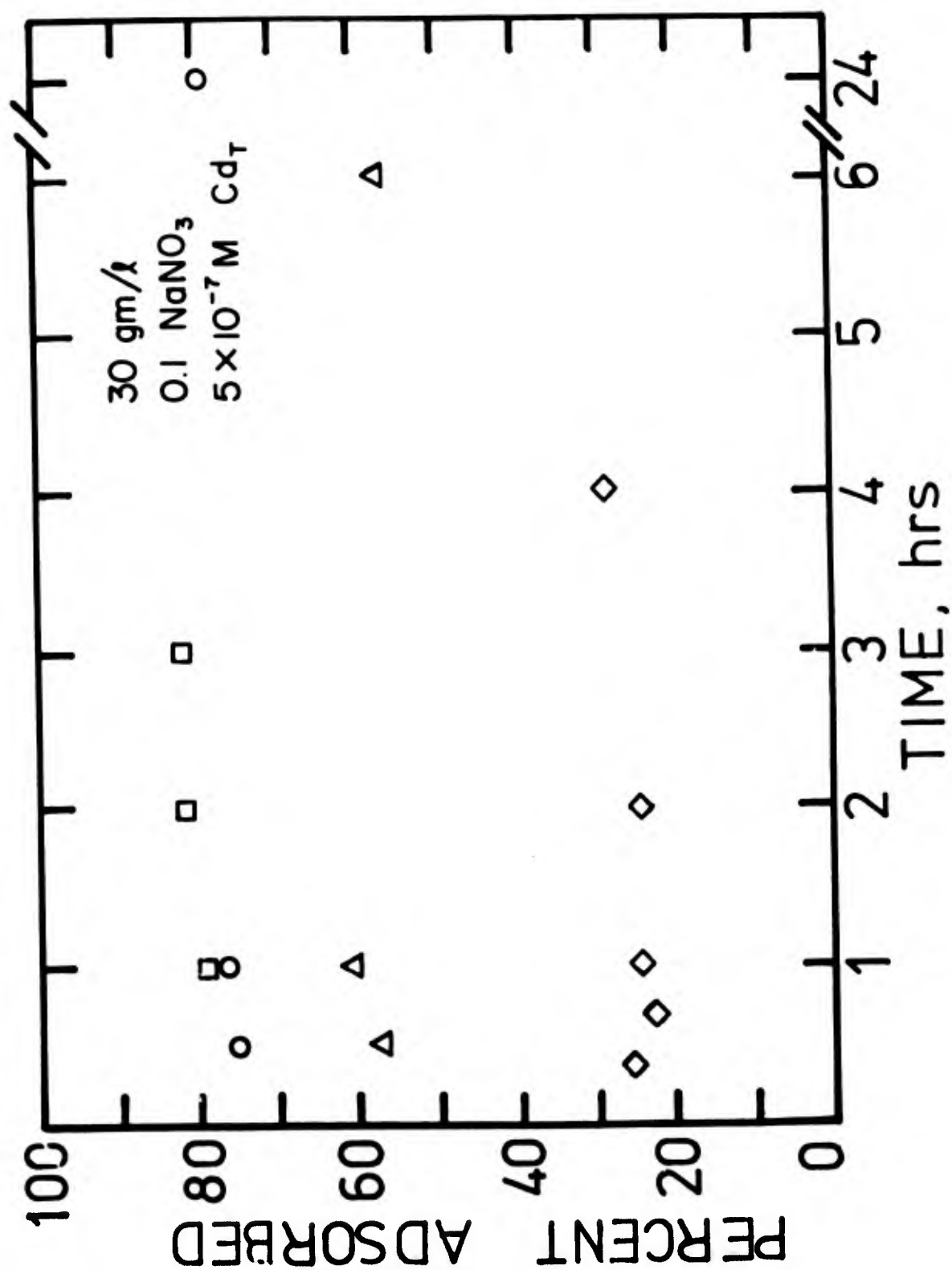


Figure 63. Kinetics of adsorption of Cd onto SiO₂.

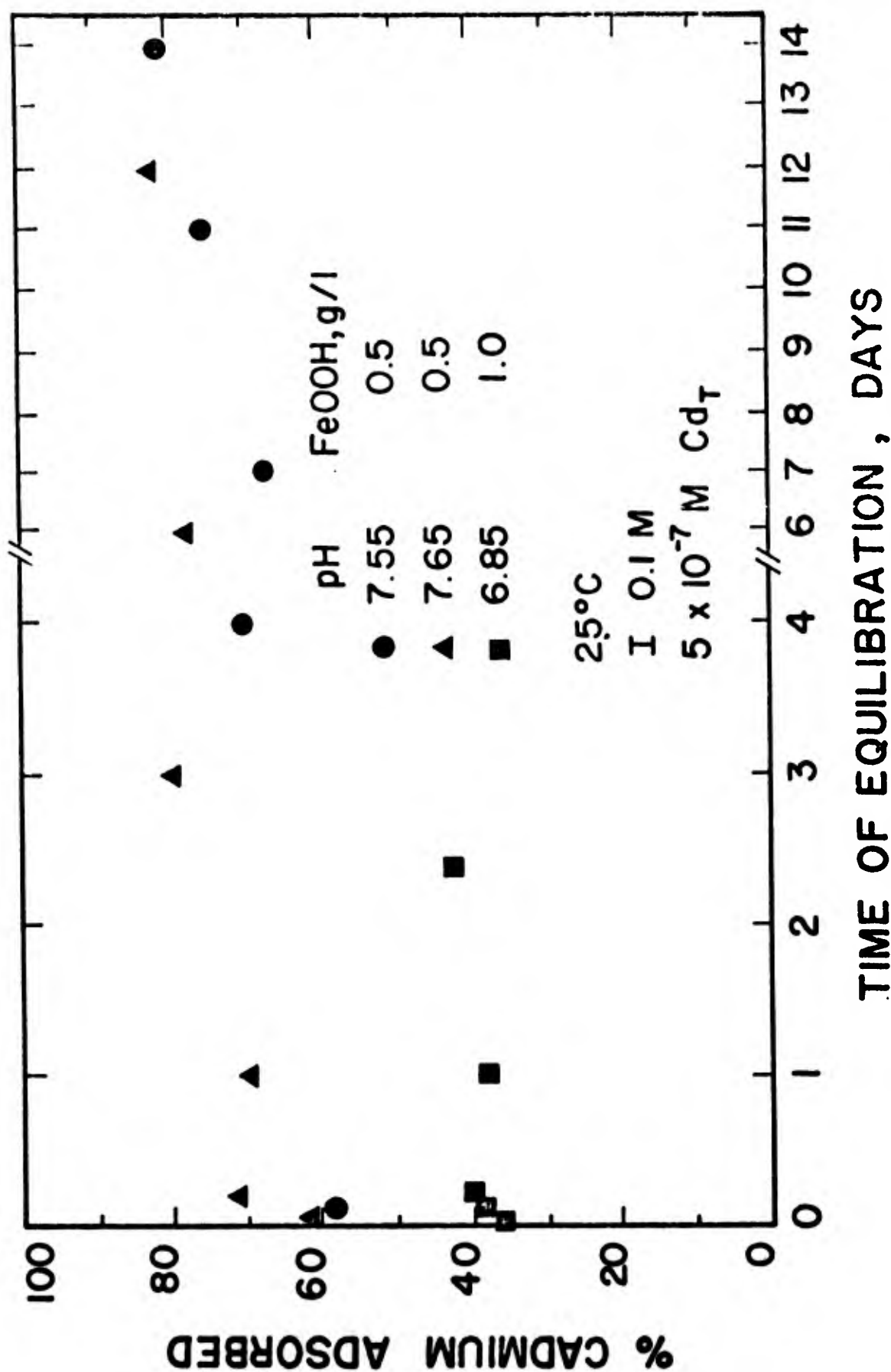


Figure 64. Kinetics of adsorption of Cd onto γ -FeOOH in the presence of dissolved CO₂.

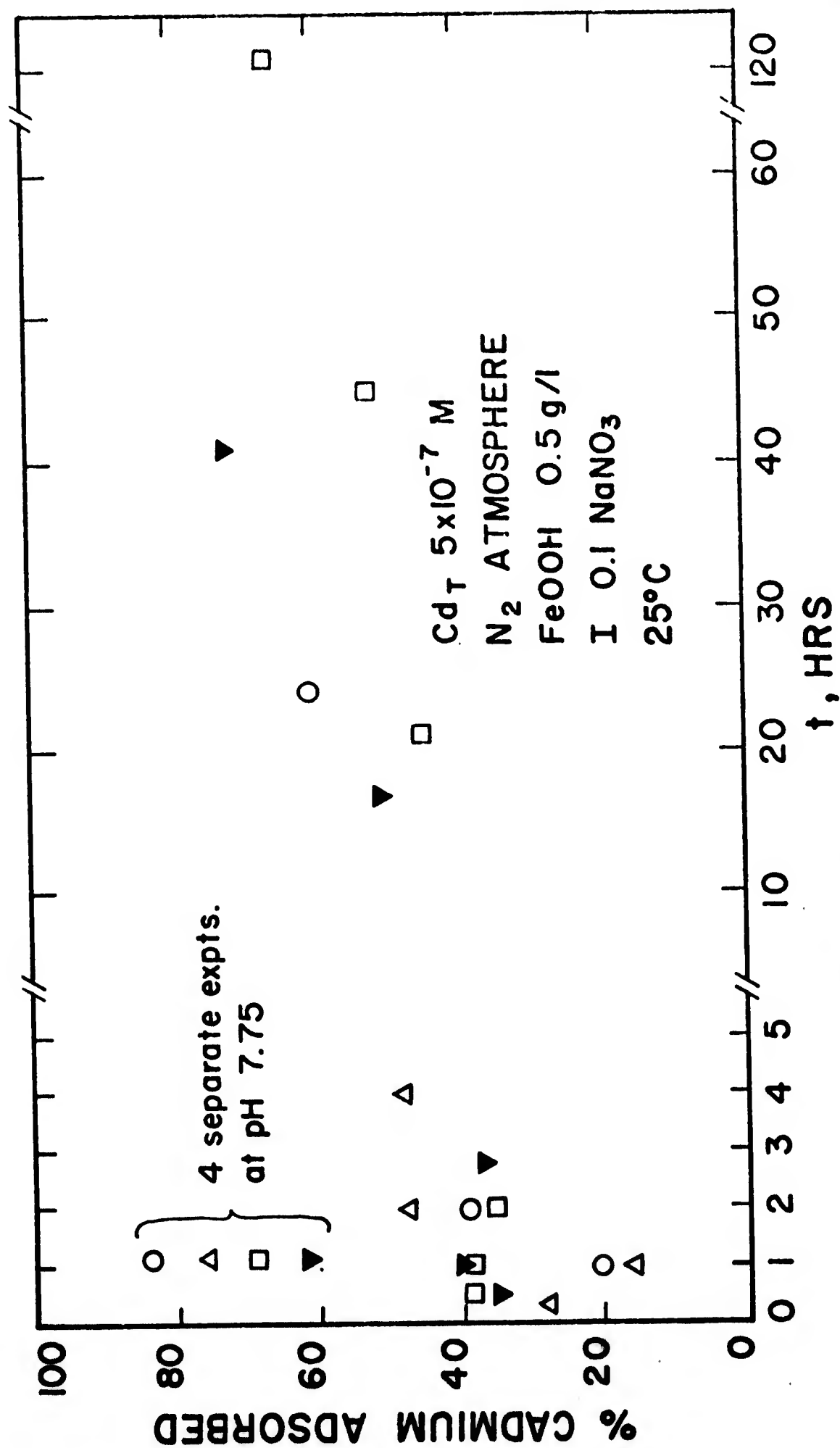


Figure 65. Kinetics of adsorption of Cd onto γ -FeOOH in the absence of dissolved CO_2 .

SECTION IX

ADSORPTION OF TRACE METALS ON HYDROUS OXIDES

Surface Characteristics of Hydrous Oxides

Amorphous Iron Oxide. Potentiometric titration is presently the most useful experimental technique for the determination of surface charge on oxides. Unfortunately, experimental difficulties were encountered in acid-base titrations of amorphous iron oxide. Hysteresis problems are serious. In the pH region 6-9 an acid titration curve is sometimes separated by as much as 0.4 pH units from a base titration curve. Similar problems are reported by Yates (1975). As a result, there are difficulties in the determination of the PZC by potentiometric titration. Batch acid titrations at different ionic strengths narrow the location of the PZC to the pH region 7.5-8.5. The PZC of most iron oxides are in this region (Parks, 1965; Yates, 1975). Yates (1975) states that the PZC for amorphous iron oxide is 8.0 but does not show the titration data at different ionic strengths.

A salt titration method provides better results for amorphous iron oxide. The salt titration is accomplished simply by observing the change in pH upon addition of electrolyte to batches of iron oxide suspensions. The iron oxide batches are aged in a nitrogen atmosphere for four hours according to the normal preparation procedure. pH adjustments are made during the aging period. Sodium nitrate is then added to increase the ionic strength. The addition of salt shifts the pH towards the PZC by increasing the surface charge. At the PZC there is theoretically no change in pH. Figure 66 displays ΔpH , the change in pH upon addition of salt versus the pH at low ionic strength. A PZC of 7.9 is indicated which is in good agreement with the PZC (8.0) determined by Yates (1975) and others (Parks, 1965).

Figure 67 shows the surface charge on amorphous iron oxide as a function of pH at various ionic strengths. The surface charge is determined by potentiometric titration of amorphous iron oxide and comparison with titrations of the ionic medium. A surface area of $182 \text{ m}^2/\text{gm}$ (BET) and a PZC of 7.9 are used for the surface charge calculation. Figure 68 displays the results of Yates (1975) for three different iron oxides. Yates believes that the higher surface charge and differential capacities observed for amorphous iron oxide are indications that a porous double layer or gel layer

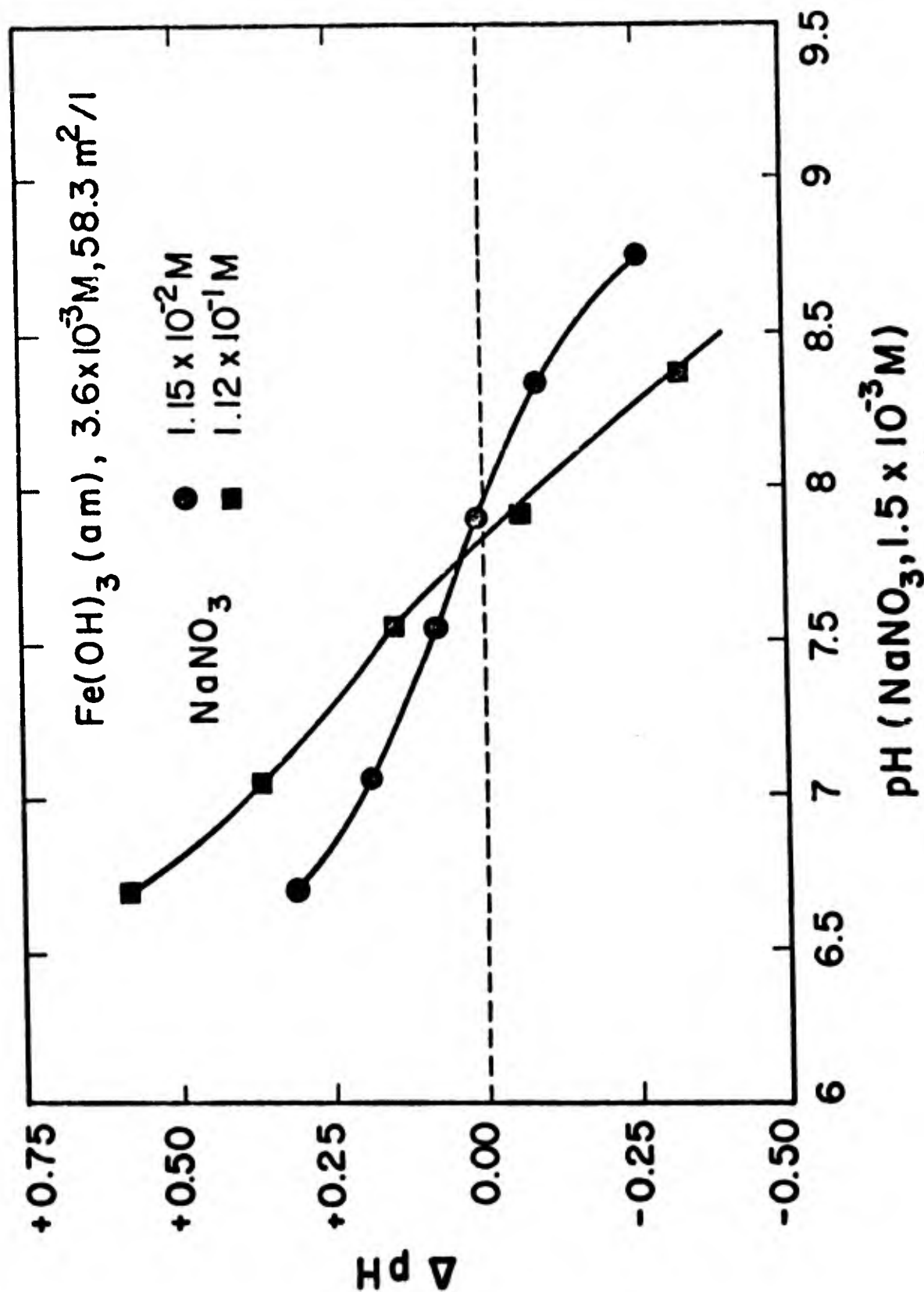


Figure 66. Change in pH (ΔpH) upon addition of sodium nitrate to amorphous iron oxide suspensions as a function of pH at low ionic strength. PZC = 7.9.

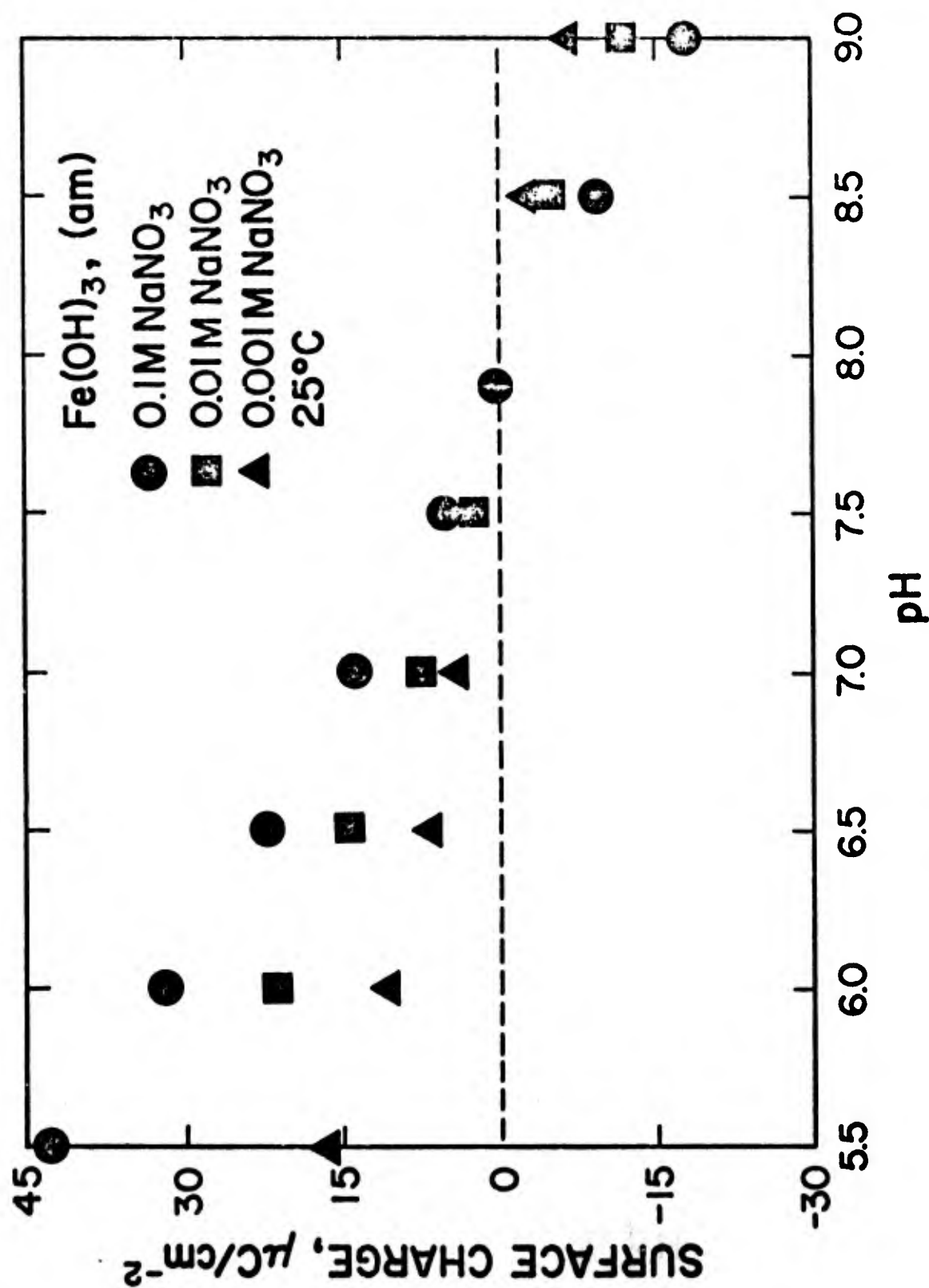


Figure 67. Surface charge of amorphous iron oxide as a function of pH at various ionic strengths. BET surface area of 182 m²/gm and PZC of 7.9 assumed.

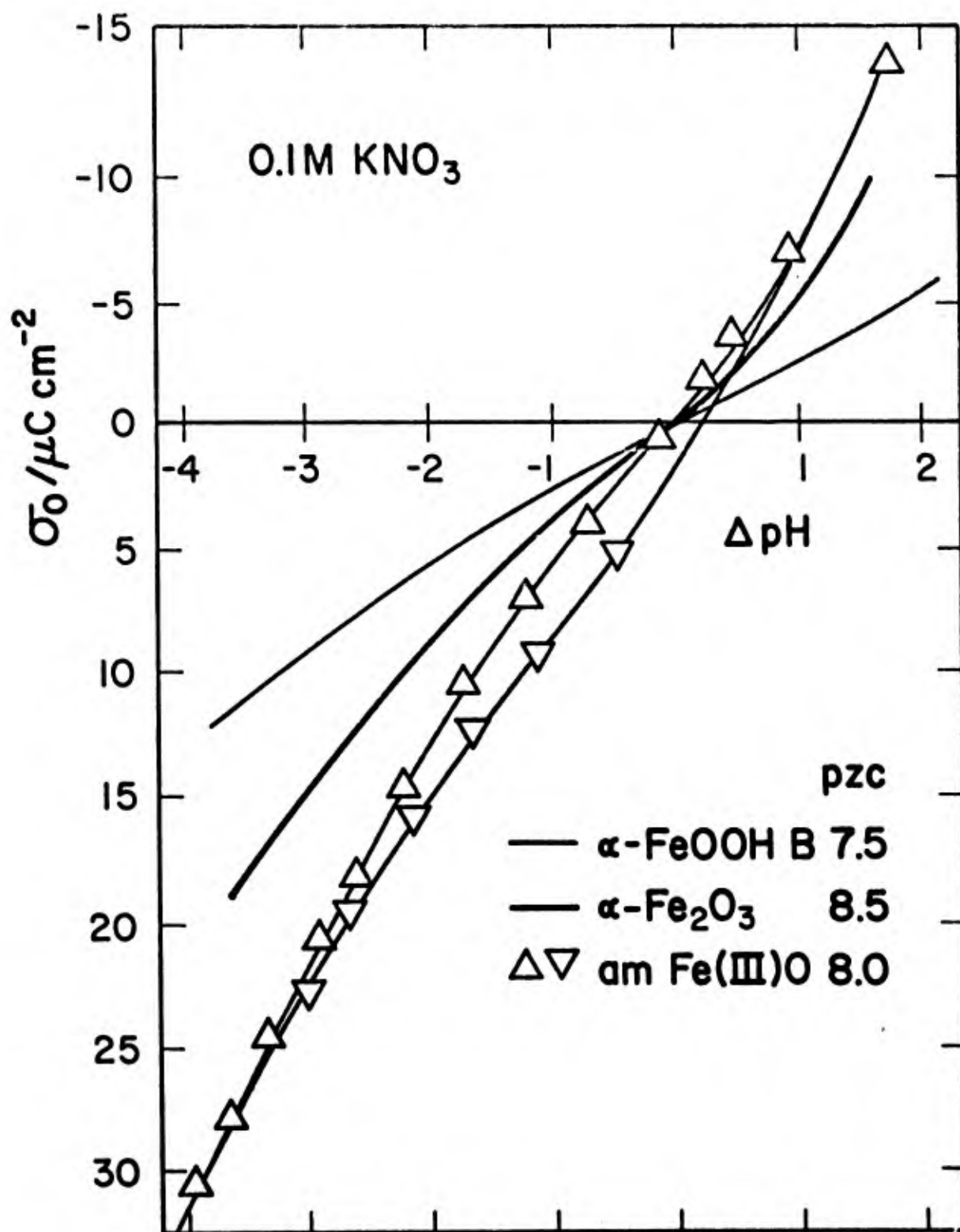


Figure 68. Surface charge curves for goethite, hematite, and amorphous iron oxide in 0.1M KNO₃. After Yates (1975).

exists at the surface. A comparison of the results of our potentiometric titrations (Figure 67) with Yates' amorphous iron oxide data shows that significant higher surface charge and differential capacity are indicated for the iron oxide used in this study. However, the surface charge observed in our experiments are much higher than has been reported for most oxides. The surface charge curve for 0.1M NaNO_3 increases to $\sim 65\text{--}70 \mu\text{C}/\text{cm}^2$ at pH 4. It is highly likely that the surface areas measured by BET nitrogen gas adsorption are low because of surface decomposition during outgassing (see discussion in Section VIII). Thus, the surface charge calculated for amorphous iron oxide by Yates (1975) and in Figure 67 is too large. The surface charge curves of Yates (1975) and in these experiments are very similar when surface charge is computed per mole of iron rather than on the basis of surface area. Thus, the major difference between the data of Yates (1975) and our potentiometric titration data is the BET surface area. The surface charge curve for goethite in Figure 68 is similar to that of most crystalline oxides. A higher surface area would lower the surface charge and differential capacity calculated for amorphous iron oxide.

Using the experimental data of Yates (1975) for the determination of sites on amorphous iron oxide, the intrinsic acidity constants are $\text{pK}_{\text{a1}}^{(\text{int})}$ 5.8 and $\text{pK}_{\text{a2}}^{(\text{int})}$ 10.0 in 0.1M NaNO_3 . The method of calculation is published in several papers (Hohl and Stumm, 1976; Schindler and Gamsjager, 1972) and the results are illustrated in Figures 69 and 70. α_+ and α_- are the fractions of positive and negative sites. The charged sites represent less than 10% of the total number of sites for pH values less than 3 pH units from the PZC. Thus, most of the sites remain uncharged over the mid-pH region. This also corroborates the hypothesis that the surface charge calculations in Figure 67 are based on an erroneously small surface area value.

α -Quartz. Potentiometric titrations have not been undertaken on Min-u-sil 5, the quartz used in these experiments. The surface charge on Min-u-sil 5 is expected to be similar to other non-porous silicas. Potentiometric titration data for various types of silicas are found in the literature (Schindler and Kamber, 1968; Schindler, Furst, et al., 1976; Yates, 1975; Bolt, 1957; Tadros and Lyklema, 1968). Li and de Bruyn (1966) determined the zeta potential on quartz particles as a function of pH. The

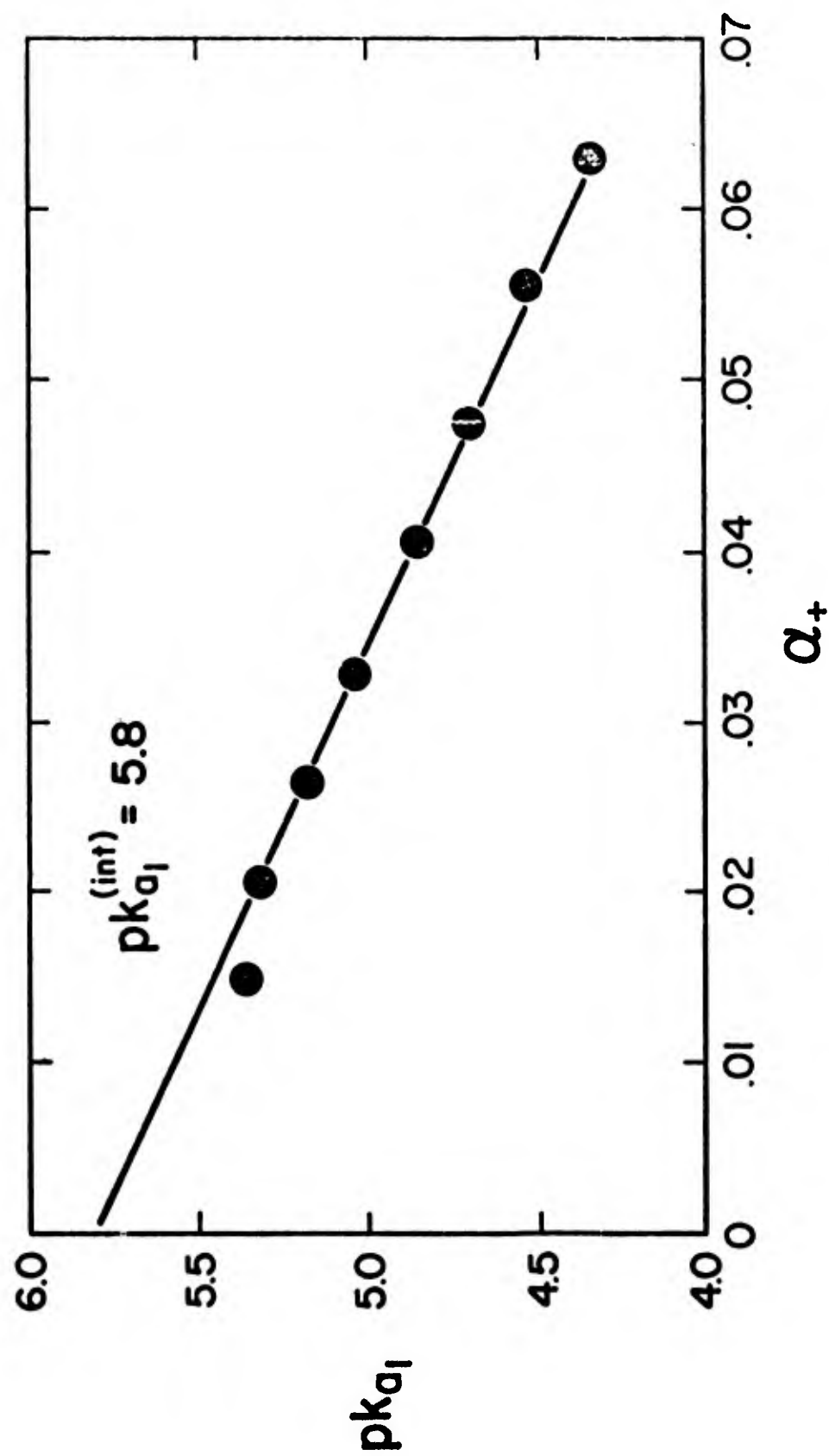


Figure 69. Determination of $pK_{a1}^{(int)}$ for amorphous iron oxide.

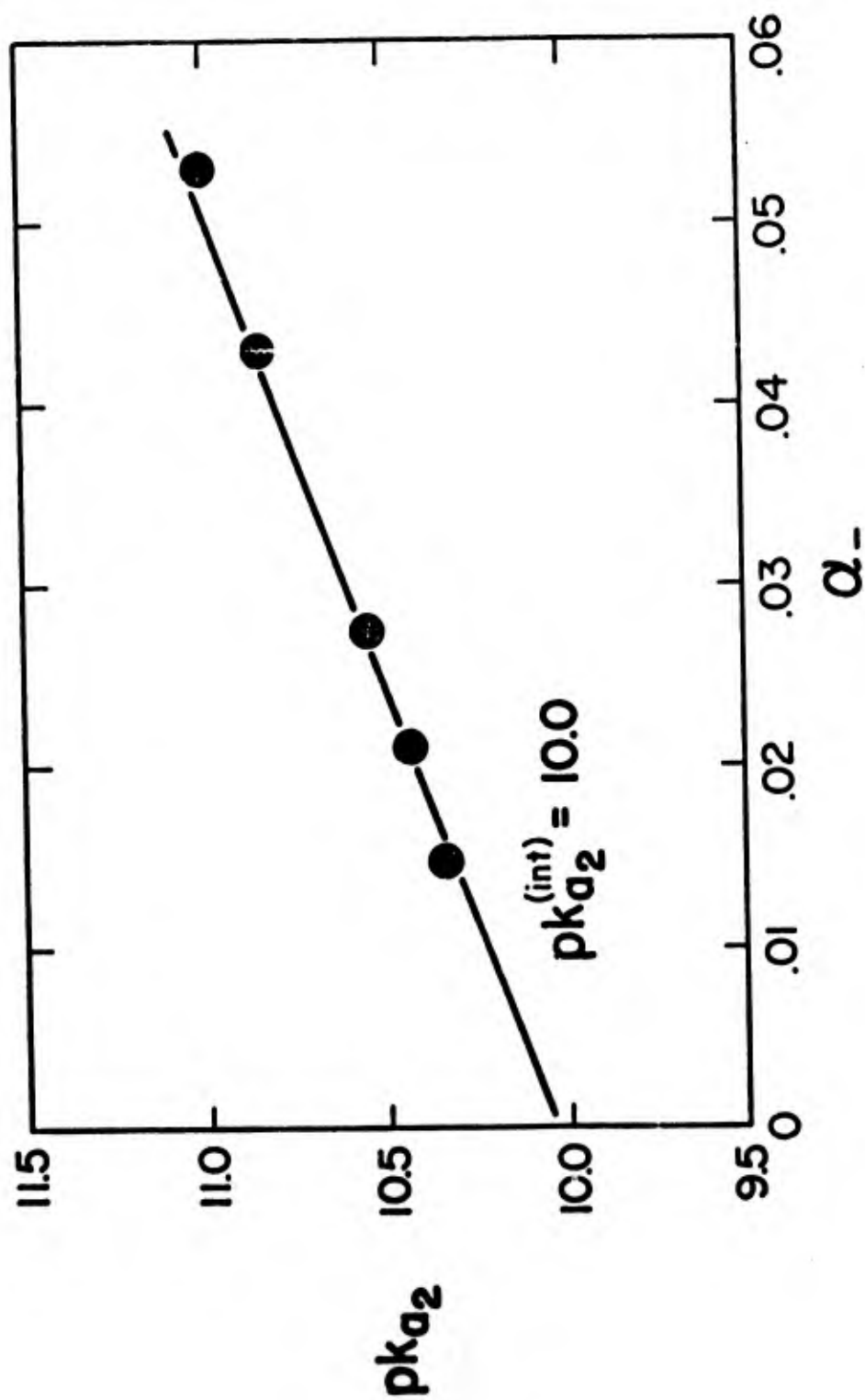
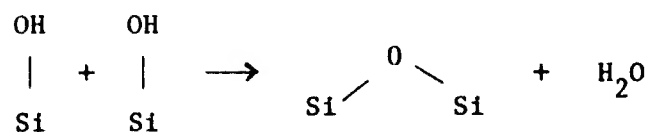


Figure 70. Determination of $pK_{a2}^{(int)}$ for amorphous iron oxide.

results of these experiments show that the surface charge and capacitance of silica are lower near the PZC than most oxides and the classical surfaces of mercury and silver iodide. Yates (1975) believes this is a result of the weak acidity properties of the silanol group. Schindler and Kamber (1968) report a $pK_{a2}^{(int)}$ of 6.8 for silica gel. Calculation of the acidity constant from the titration data of Bolt (1957) and Yates (1975) also yields a value of 6.8. The exact value of the PZC is not known but probably is between 2.0 and 3.0. Fortunately this uncertainty is not critical in calculating surface charge because the charge isotherms are nearly horizontal at the PZC.

Nearly all experimentally determined values for the total number of sites on non-porous silica lie between 3 and 6 sites/nm². Hockey (1967) concludes that 4.6 sites/nm² is the most reliable value for fully rehydrated, well-annealed silica. Heating silica above 450°C can cause irreversible dehydration of surface hydroxyls and the formation of strained siloxane groups according to the following reaction:



The presence of stable siloxane groups even after extensive rehydration is possible for the material used in these experiments since it was heated at 550°C for 48 hours. The number of active adsorption sites could be reduced by the dehydration reaction. However, the acid refluxing may restore the hydrated surface.

γ-FeOOH, Lepidocrocite. Two samples of lepidocrocite, one purchased from Pfizer and another produced in the laboratory, were determined to be pure γ-FeOOH within the limits of sensitivity of X-ray diffraction analysis (+5%). In particular, no peaks suggested the presence of goethite (α-FeOOH). The specific surface areas of silica, lepidocrocite purchased from Pfizer Chemical Co., and lepidocrocite produced in-house by oxidation of ferrous sulfide were determined by the BET method as follows:

Silica	3.3	m ² /g
Pfizer γ-FeOOH	20	m ² /g
In-house γ-FeOOH	36	m ² /g

The specific surface area of the Pfizer γ -FeOOH was determined by negative adsorption of sodium ions to be $24 \text{ m}^2/\text{g}$.

The BET surface area determined for silica is about one-third less than that determined by MacNaughton (1973) for Min-u-sil 5. The lower value is felt to be accurate since the BET isotherm is highly linear. In any case, when modeling metal adsorption from solution, an error in specific surface area of the adsorbate will change the magnitude of the fitting parameters but will not alter predictions made by the models or any conclusions about the models' applicability.

The BET isotherms for the Pfizer and in-house lepidocrocite samples are also linear. Since the production process for the Pfizer lepidocrocite is not known, the cause of the difference in specific surface area between it and the in-house sample is not clear. The precision of the negative adsorption experiment is not as good as that of the BET measurement, so the value of $20 \text{ m}^2/\text{g}$ for the Pfizer sample is used in the modeling studies.

A plot of ΔpH vs pH_{final} (Figure 71), where ΔpH is the change in pH accompanying an addition of inert salt to the suspension, shows that the PZC of the lepidocrocite is in the range 7.0 to 7.3. The final pH of several systems is 7.16, and this pH is approached from solutions of both higher and lower initial pH. An independent determination of the PZC using titration data indicates a similar range (7.10 to 7.35), as does a literature value of 7.4 ± 0.2 quoted by Parks (1965). Therefore, the value of $\text{PZC} = 7.16$ is used in subsequent modeling calculations.

The iso-electric point (IEP) of the lepidocrocite is determined by electrophoresis to be 3.15. Since this value is considerably lower than the PZC, specific adsorption of an anionic species is indicated. Repeated rinsing of the solid in deionized water has no effect on the IEP. Information on the production process for the Pfizer lepidocrocite is not available. However, the lepidocrocite produced in-house has a similar IEP, suggesting that sulfate is the specifically adsorbed anion. It is also possible that sulfate is present as a minor constituent throughout the iron oxide lattice. The inclusion of sulfate into hydrous oxide sols generally lowers the IEP, but the magnitude of the effect is variable and not well understood (Matijevik et al., 1975). Specific adsorption of sulfate onto a sulfate-free hydrous iron oxide can drastically lower the IEP (James, 1976). Structural impurities of less than 2 mole percent of SO_4 in Fe_2O_3 can decrease the IEP by at least 1.6 pH units (Parks, 1965).

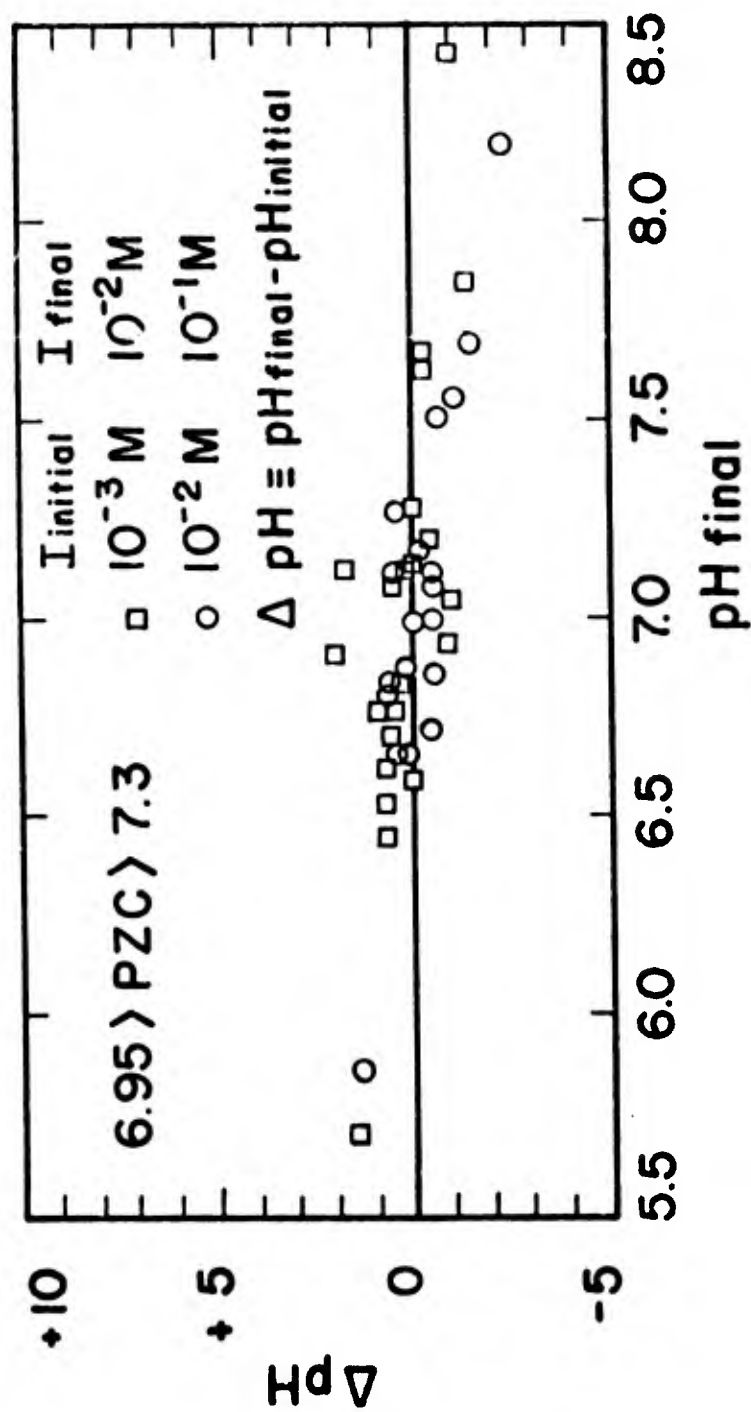


Figure 71. Change in pH upon addition of solid NaNO_3 to a suspension of $\gamma\text{-FeOOH}$ as a function of final pH.

Adsorption of Silver on Hydrous Oxides

Literature Review. Dugger et al. (1964) examined the surface exchange of metal ions with the silanol group (SiOH) of hydrated silica gel. The experiments were conducted in a pH region for each metal where hydrolysis of the ion is insignificant. The free energy of the surface exchange at infinite surface dilution for silver, copper, and sodium are -1.5, -4.3, and 0.0 kcal/mole at 25°C, respectively. However, the free energies are calculated based on the assumption that the value for sodium is zero. All free energy values are normalized against sodium.

The adsorption of silver on titanium dioxide and zinc oxide has been examined by several research groups. The objectives of these experiments are related primarily to photochemical surface reactions, and the data are frequently not presented in the quantitative form desired for adsorption modeling. Misra (1968) studied the adsorption of silver on titanium dioxide in darkness to avoid photoreduction of silver ions. Langmuir isotherms are reported for silver nitrate in the concentration range 0.01-2M for two different commercial preparations of TiO_2 . Clark and Vonjdis (1968) and Goetz and Inn (1948) also refer to the adsorption behavior of silver on titanium dioxide as Langmuir type adsorption.

Dyck (1968, 1971) reports on the adsorption of silver on hydrous oxides of iron and manganese. Most of the work concerns adsorption on iron oxides; a few experiments with manganese oxides are discussed for comparative purposes. The iron adsorption experiments are undertaken in the pH region 4-8 with silver equilibrium concentrations reported in a range of 10^{-9}M to 10^{-3}M . Kinetic experiments indicate equilibrium is established in less than five minutes for both iron and manganese oxides. The results fit Freundlich isotherms with the slope (not reported) less than one and roughly the same for all pH values in the region 4-8. Adsorption maxima are not determined and the isotherms are linear up to the highest concentration used. Adsorption is strongly dependent on pH and the manner in which the precipitate is prepared, but is independent of temperature (0-50°C range), ionic strength (dilute to $< 10^{-1}\text{M NaNO}_3$), and trace concentrations of chloride ($> 10^{-4}\text{M}$). Adsorption and coprecipitation experiments in identical solutions approach the same equilibrium value; however, the time to reach equilibrium is longer for the coprecipitation experiments.

Anderson, Jenné, and Chao (1973) studied the adsorption of silver by poorly crystallized manganese oxides in the pH region 3-7. Several structural modifications of manganese dioxide are known and extensive substitutions exist. The adsorbents used by Anderson et al. (1973) are from the birnessite and γ - MnO_2 groups. All four oxides studied adsorb significant quantities of silver. The manganous manganites show the greatest sorption (up to 0.5 mole silver/mole MnO_x at pH 7) and the γ - MnO_2 group the least (0.3 mole silver/mole MnO_x at pH 7). The adsorption behavior is described by the Langmuir equation over a considerable concentration range (10^{-5} - 10^{-3}M). The relationship fails at low pH values and high equilibrium silver concentrations. These results are in good agreement with the silver uptake experiments of Posselt, Anderson, and Weber (1968).

Anderson, Jenné, and Chao (1973) find that more silver is adsorbed by manganese oxide preparations (0.3-0.5 mole silver/mole MnO_x) than that reported by Dyck (1968) for amorphous iron oxide (.01 mole silver/mole $\text{Fe}(\text{OH})_3$). However, the sorption maxima on the manganese oxides are greater than can be explained by "surface adsorption." The processes involved include exchange of silver with structural potassium, sodium, and manganese as well as surface exchange. Thus, the sorption maxima are not directly related to surface area but appear to vary with the amount of occluded sodium and potassium present in each manganese oxide preparation. Dyck (1971) also reports increased adsorption on hydrous manganese oxides in comparative experiments. The amount of iron present in mixed suspensions of manganese oxide and iron oxide has little effect on the amount of silver adsorbed.

Chao and Anderson (1974) analyzed digested stream sediment samples for silver, manganese, and iron content. The sediment samples were collected from two Colorado drainage areas which contain anomalous amounts of silver. Linear and multiple regression analyses show a highly significant correlation between silver and manganese content and little dependence on iron content. The authors suggest that manganese oxides are the major control on the scavenging of silver by stream sediments. Dyck (1971) investigated the adsorption of silver on natural hydrous oxides collected from several drainage areas in Canada. The results of the experiment show a high degree of silver removal from solution. Dyck (1971) attributes the removal to surface precipitation of insoluble silver compounds, such as the chloride.

Adsorption of Silver on Amorphous Iron Oxide. The adsorption of silver on amorphous iron oxide has been studied as a function of silver concentration, surface area available, and pH. All measurements are made after an equilibration period of four hours at 25°C in 0.1M NaNO₃. For most experiments, the total silver concentration is 4×10^{-7} M. Thus, equilibrium conditions are characterized by low surface coverage of adsorbed silver and trace solution concentrations of silver. These conditions are expected in natural waters.

Figure 72 shows the adsorption of silver as a function of pH and surface area in batch experiments. The total silver concentration is 4×10^{-7} M in each batch experiment. The amount of silver adsorbed is highly dependent on pH and surface area. Monovalent silver ion is the primary solution species involved in the surface reaction since the concentrations of hydrolyzed species are extremely low in the mid-pH region (see Figure 49). Changes in the surface characteristics as a function of pH are responsible for the observed adsorption behavior since silver speciation does not change significantly.

The PZC of amorphous iron oxide is 7.9. Like other transition metals the adsorption of silver can be classified as "specific adsorption" since adsorption occurs at the PZC. The adsorption behavior of many transition metals is characterized by an increase from zero to nearly 100% adsorption in one pH unit. However, the increase from zero to > 90% adsorption of silver is apparently less dependent on pH and more dependent on the amount of surface area available. This observation is in qualitative agreement with an ion exchange model for trace metal adsorption where hydrogen ions are released when the metal adsorbs (Dugger et al., 1964). Usually the number of hydrogen ions released equals the charge on the trace metal. The number of protons released for silver is expected to be less than for a divalent metal ion. Thus, divalent metals should have steeper adsorption edges than silver.

An alternative hypothesis for decreased dependence on pH is based on the importance of the coulombic term in silver adsorption as compared to other transition metals. The change in free energy for the reaction of silver with the silanol group is less than that of other transition metals (Dugger et al., 1964). This is in agreement with the weak hydrolysis behavior of silver.

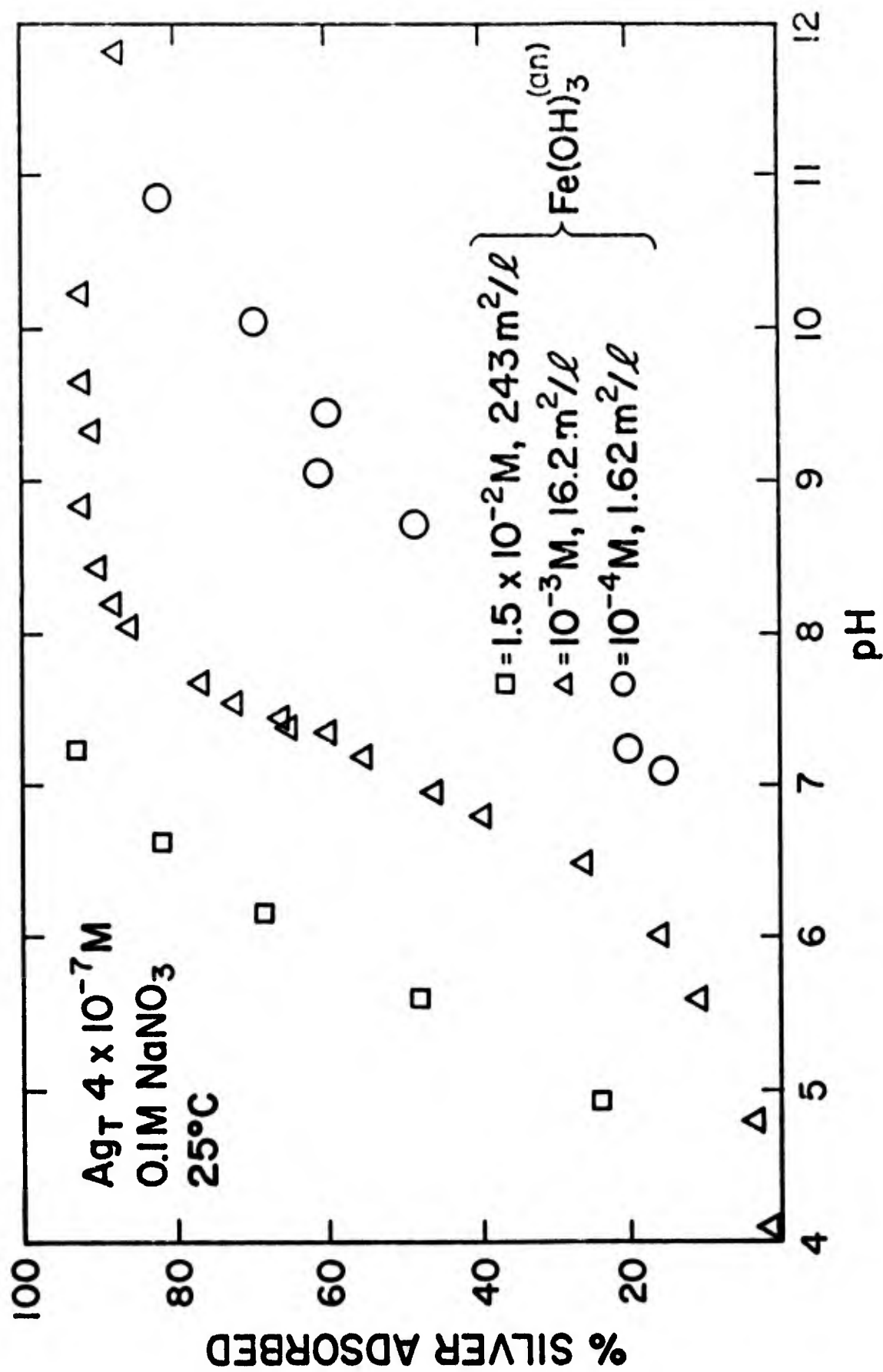


Figure 72. Adsorption of silver on amorphous iron oxide as a function of pH and surface area.

If the overall free energy of adsorption is a combination of coulombic and chemical terms, the coulombic term may be more significant for silver than for other transition metals despite its lower charge. Thus, the slope of the adsorption edge for silver will be more dependent on the charge characteristics of the solid as a function of pH. This may explain the shape of the adsorption edges in Figure 72. A combination of the two hypotheses is possible.

Figures 73 and 74 show adsorption isotherms for silver on amorphous iron oxide at pH 6.5 and 10. A surface area of $182 \text{ m}^2/\text{gm}$ is used to calculate adsorption density. Both isotherms are linear over a large concentration range of silver and have approximately the same slope (~ 0.6). The adsorption behavior is best fit with a Freundlich type isotherm. These are in good agreement with the adsorption isotherms of Dyck (1968) for pH 4-8. Dyck's isotherms are linear (slope ~ 0.6) up to the maximum concentration investigated, 10^{-3}M . No isotherms are reported for pH greater than 8. The isotherm at pH 10 (Figure 74) shows a similar slope, but the highest silver concentration is limited by the solubility of silver oxide at pH 10. The highest adsorption density shown in Figure 74 is near the point of silver oxide precipitation. Both total silver concentration and total surface area were varied in these experiments to obtain the isotherms. All points represent adsorption isotherms between 20-80% removal of the total silver present to minimize errors in calculating adsorption density and silver concentration.

Anderson, Jenné, and Chao (1973) compare the adsorption maxima for manganese oxides with the highest adsorption densities reported by Dyck (1968) and conclude that manganese oxides are probably more significant as silver adsorbents in natural waters. However, the adsorption densities in these experiments and those of Dyck (1968) are not maxima. Kinetic experiments also reveal that adsorption may increase by as much as a factor of two over a period of six weeks on iron oxide. Figure 73 indicates that silver adsorption can vary from zero to nearly quantitative removal in the pH region of typical natural waters. Surface area and surface charge characteristics may be the most important factors in assessing the importance of substrates as silver scavengers in natural systems. Manganese oxides generally have lower PZC's than iron oxides (Parks, 1965).

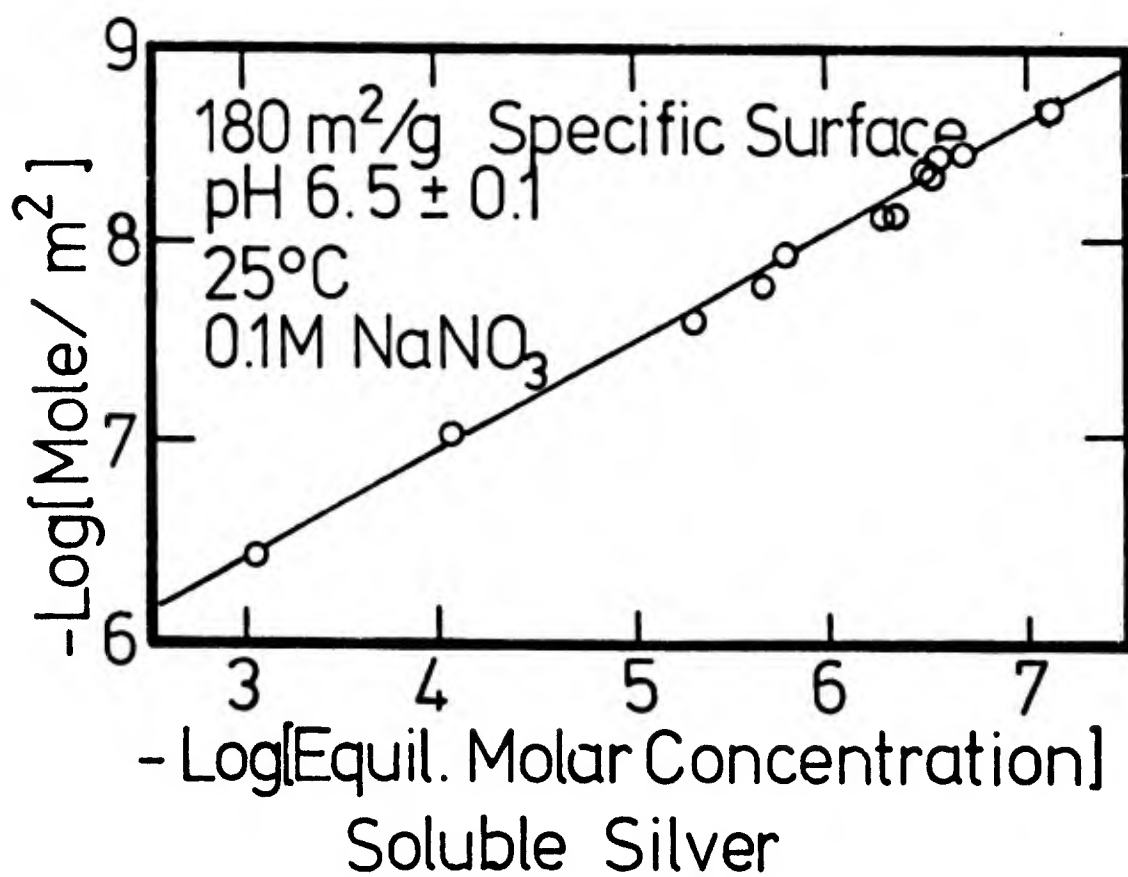


Figure 73. Freundlich adsorption isotherm plot for silver on amorphous iron oxide at pH 6.5.

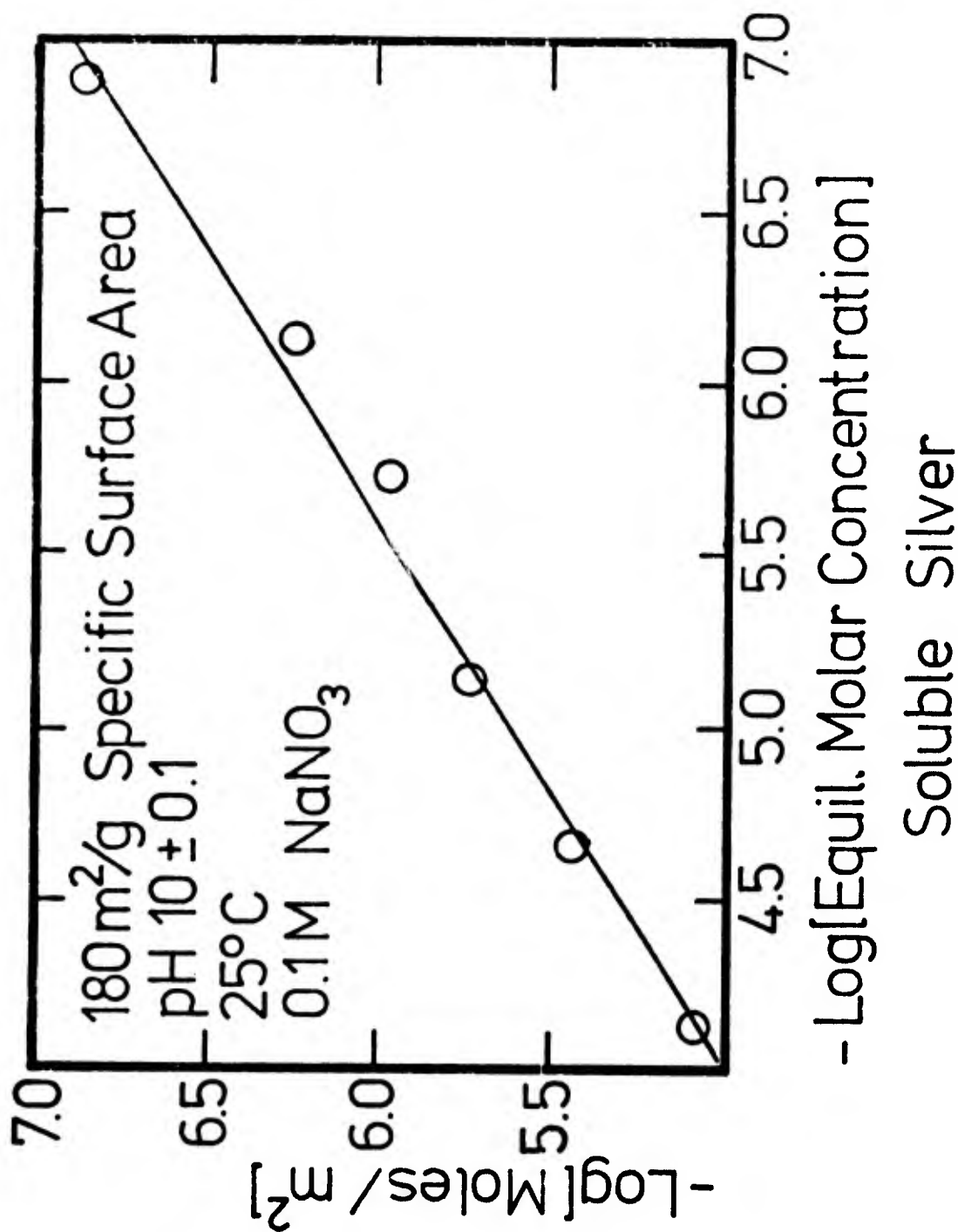
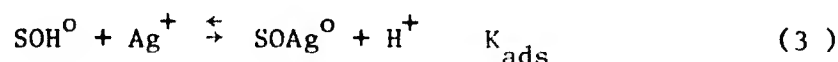


Figure 74. Freundlich adsorption isotherm plot for silver on amorphous iron oxide at pH 10.0.

The surface coordination model used by Stumm, Huang, and Jenkins (1970) and Schlinder, Fürst et al. (1976) proposes that the surfaces of hydrous oxides act as poly-acids undergoing the following reversible proton-exchange reactions:



A metal ion can then bond to one or more surface sites with the accompanying release of 0, 1, or 2 protons per binding site. Assume for the moment that silver reacts with the neutral surface sites according to the following reaction:



Since the strengths of the surface $-\text{H}^+$ and surface $-\text{Ag}^+$ bonds are dependent on surface charge, which changes with pH, the constants of Eqs.(1),(2), and (3) are not true thermodynamic constants. They are a combination of two energy terms, one of which describes the strength of the bond in the absence of surface charge and a second describing the coulombic energy.

Ignoring the coulombic term for the moment, the equilibria of (3) can be written:

$$[\text{SOAg}^0] a_{\text{H}^+} = K_{\text{ads}} [\text{SOH}^0] [\text{Ag}^+] \quad (4)$$

$$\Gamma = \frac{[\text{SOAg}^0]}{S_T}$$

where Γ is the adsorption density of silver and S_T is the total number of adsorption sites, defined as follows:

$$S_T = [\text{SOH}_2^+] + [\text{SOH}^0] + [\text{SO}^-] + [\text{SOAg}^0]$$

Dividing (4) by S_T ,

$$\Gamma(a_{\text{H}^+}) = K_{\text{ads}} \frac{[\text{SOH}^0]}{S_T} [\text{Ag}^+]$$

It has already been shown that $[\text{SOH}] \approx S_T$ for 2 pH units on either side of the PZC (7.9) of amorphous iron oxide (within 5-6%). If the equilibrium concentration of silver is constant, then

$$\Gamma = [\text{constant}] a_{\text{H}^+}^{-1}$$

or

$$\text{p}\Gamma = -\text{pH} - \log[\text{constant}]$$

where

$$[\text{constant}] = K_{\text{ads}} \frac{[\text{SOH}]}{S_T} [\text{Ag}_{\text{equil}}^+]$$

Thus, a plot of $\text{p}\Gamma$ vs pH should be a straight line in the pH region near the PZC. Figure 75 shows the relationship for a constant equilibrium concentration of $2 \times 10^{-7}\text{M}$ silver. There is a linear region in the pH region 7-8.5 and deviations from linearity become more severe as $|\text{pH}-\text{PZC}|$ increases. This deviation from linearity shows that the coulombic term omitted from this analysis is an important term to be taken into account in evaluating the adsorption constant for silver.

Figure 76 shows the results of two batch experiments to determine the kinetics and extent of silver desorption from amorphous iron oxide. The desorption is attempted in one case by an addition of acid and in the other by addition of chloride to the iron oxide suspension after four-hour silver equilibration. In the case of the acid addition, most of the adsorbed silver is desorbed rapidly and the system is slowly approaching the equilibria observed at four hours. In the case of the chloride addition, most of the silver is again desorbed rapidly but the approach toward equilibrium is complicated by a significant decrease in pH during the desorption period.

Adsorption of Silver on α -Quartz. The adsorption of silver on quartz is studied as a function of surface area and pH. All experiments are conducted at 25°C with a total concentration of $4 \times 10^{-7}\text{M}$ silver in 0.1M NaNO_3 , corrected for acid or base addition. A four-day equilibration period is used under darkroom conditions to avoid photoreduction.

Figure 77 shows the dependence of silver adsorption on surface area and pH. Since the increase in charge with respect to pH is small, the free

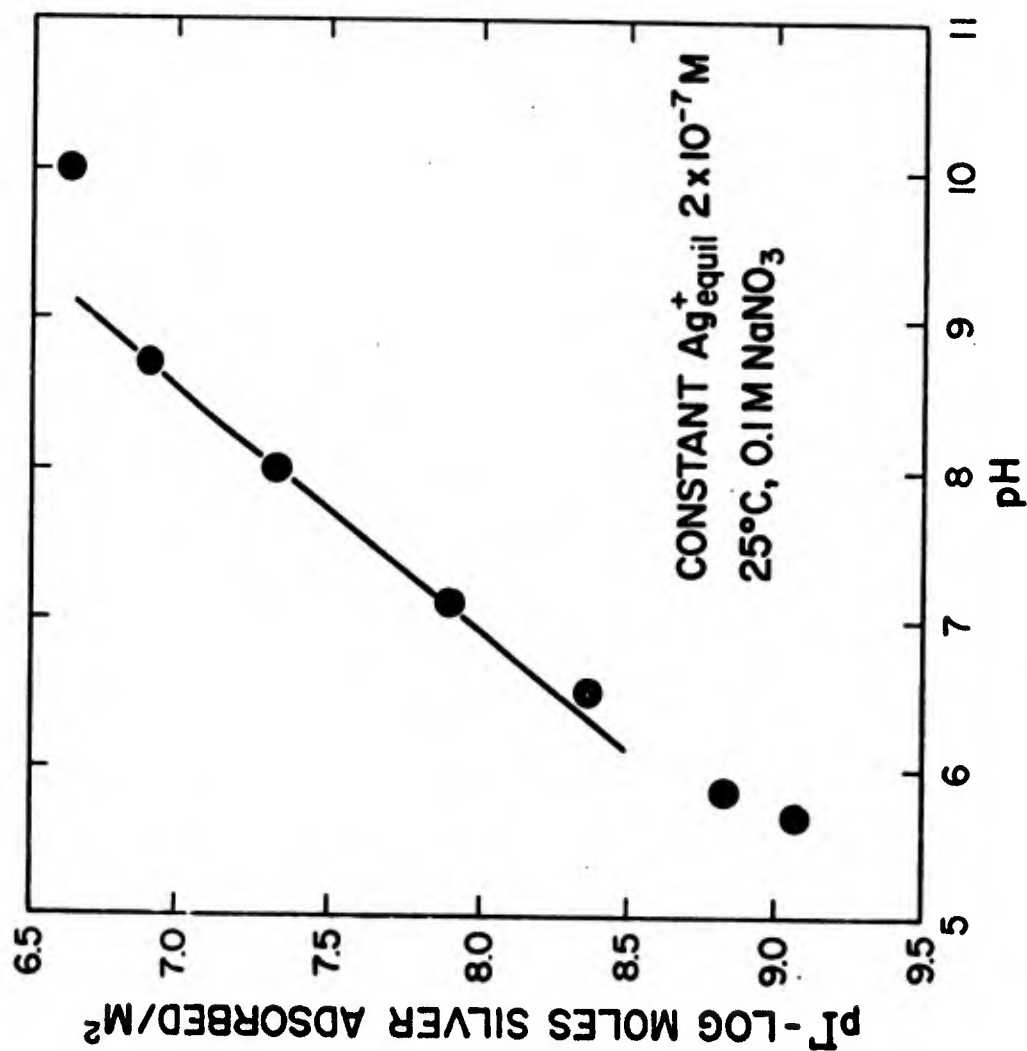


Figure 75. Adsorption density of silver on amorphous iron oxide as a function of pH at constant $\text{Ag}^+_{\text{equil}}$ of $2 \times 10^{-7} \text{ M}$.

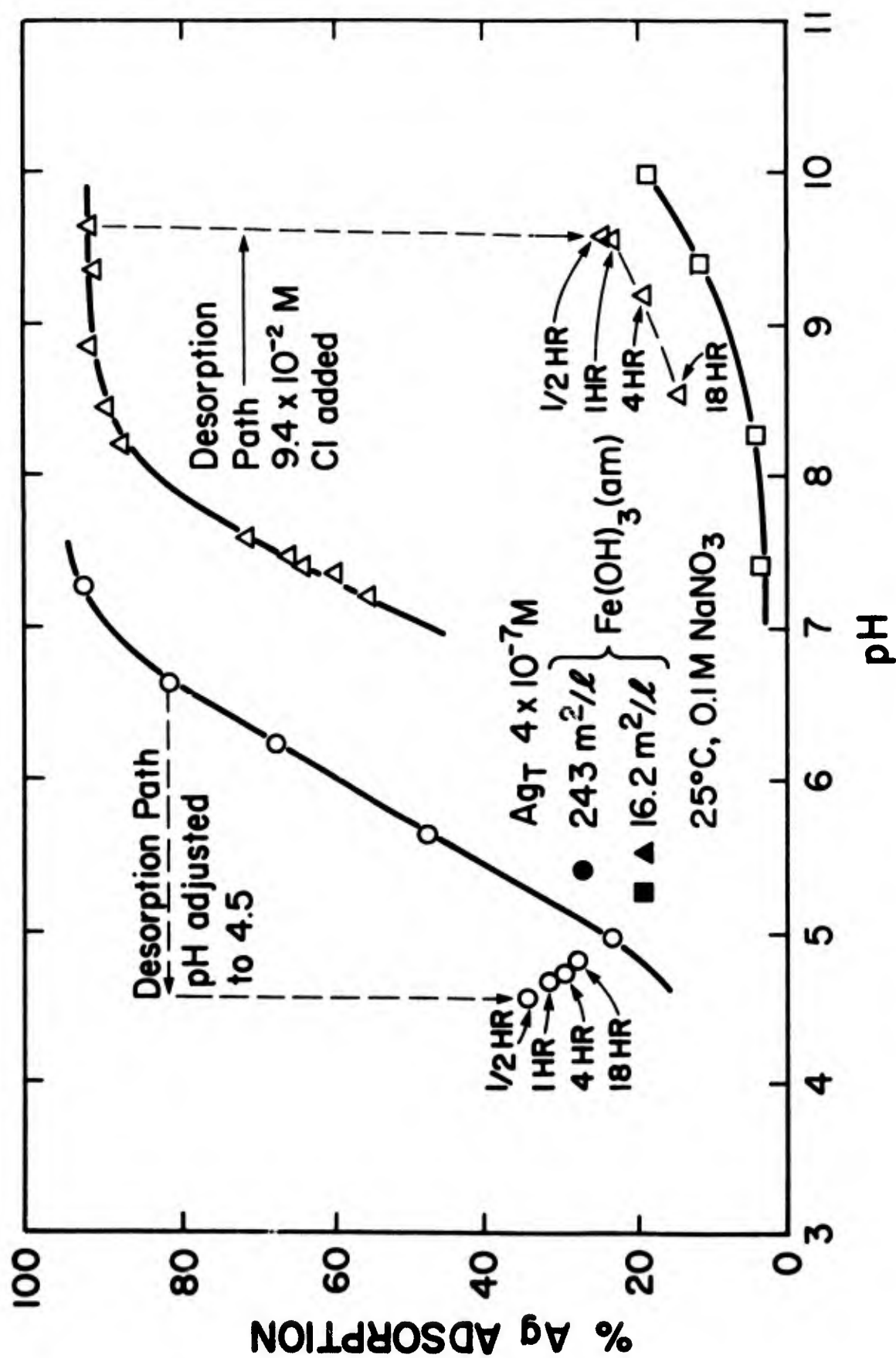


Figure 76. Adsorption-desorption data for silver on amorphous iron oxide. Experimental data denoted by squares is for adsorption equilibria in the presence of 9.4×10^{-2} M chloride.

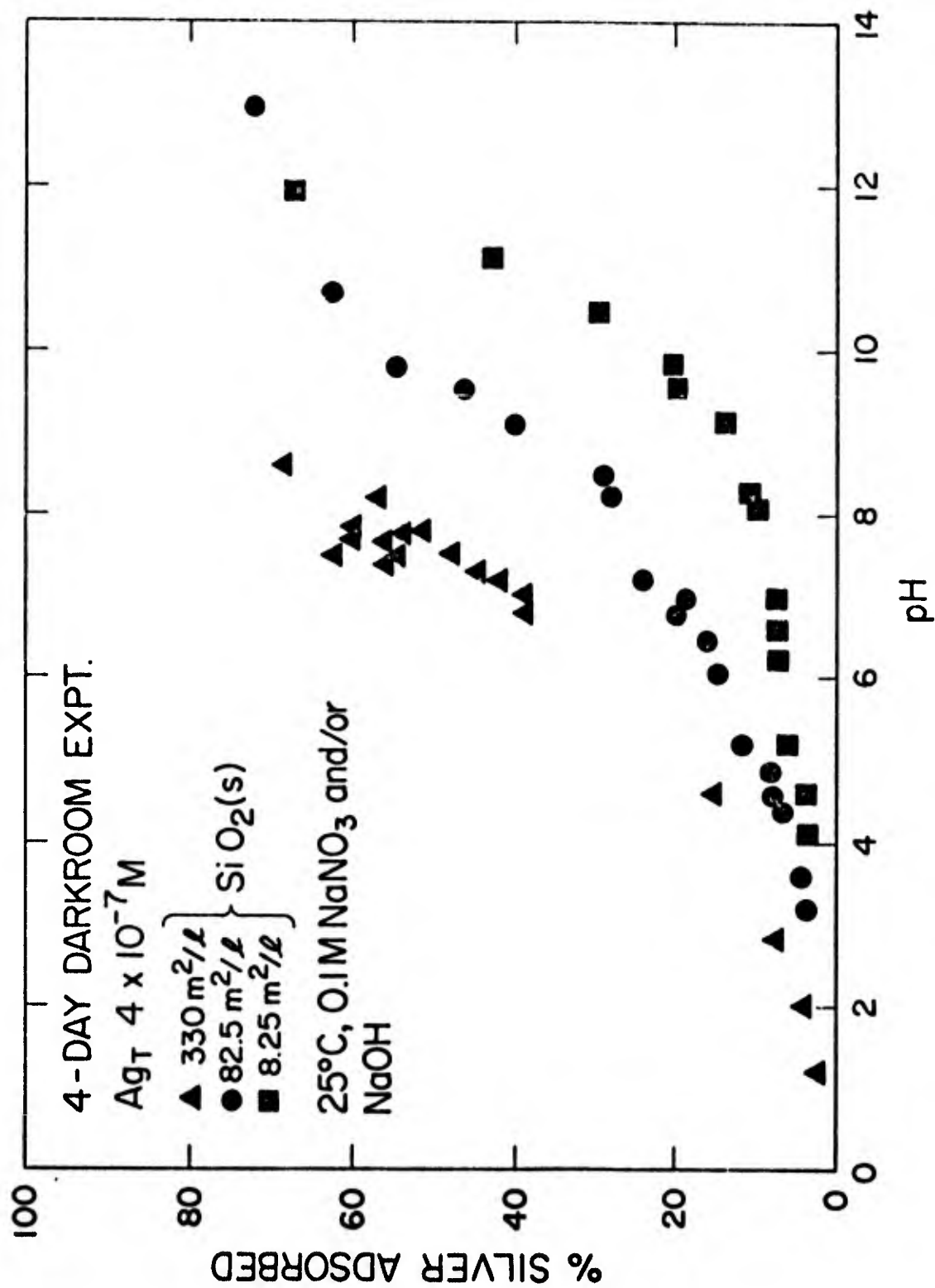


Figure 77. Adsorption of silver(I) on α -quartz under darkroom conditions as a function of pH and surface area available.

energy of adsorption will have a smaller coulombic dependence than that observed for adsorption on amorphous iron oxide. It is difficult to compare the chemical terms of the two oxides at this point because of the uncertainty in the surface area determination for amorphous iron oxide.

Adsorption does not increase significantly until the pH approaches pK_{a2} (6.8) of silica. Then the rate of increase of adsorption appears to be slightly dependent on surface area. The shape of the curves at high pH indicates there is a strong possibility that $AgOH^0$ is an adsorbing species as well as Ag^+ . The highest surface area curve represents a suspension of 100 g/l of α -quartz. Since this is an extremely concentrated suspension, it is probable that α -quartz is not as important as amorphous iron oxide in determining the distribution of silver in natural waters. However, amorphous silicas with much higher specific surface areas and porosity could presumably assume a greater role.

Adsorption of Copper on Hydrous Oxides

Literature Review. A number of investigators examine the adsorption of copper on silica. Kozawa (1961) and Huang, Elliott, and Ashmead (1975) studied adsorption for copper concentrations greater than $10^{-3}M$. Kozawa (1961) states that four hydrogen ions are released for each copper ion adsorbed on silica gel. However, the analysis is complicated by the use of 1M ammonium acetate as background electrolyte. Kozawa proposes that two hydrogen ions are released from the silica surface and two from complexation of the adsorbed copper by ammonia. However, the solution chemistry of copper is ignored in making the calculations.

Huang, Elliott, and Ashmead (1975) find that adsorption of copper is negligible when the pH is less than 5, but adsorption increases abruptly between pH 5 and 6 in 0.1M sodium chloride. The same adsorption behavior is observed for silica (type not mentioned), $\gamma-Al_2O_3$, and two Delawarean soils.

Schindler, Fürst et al. (1976) and Vuceta (1975) studied the adsorption of copper on silica in more dilute solutions. Schindler's results show a rapid increase in adsorption between pH 5 and 6 for silica gel. A total copper concentration slightly greater than $10^{-4}M$ is used in an ionic medium of 3M sodium perchlorate. Vuceta (1975) finds an adsorption edge between

pH 5 and 6 in 0.1M NaCl for trace concentrations of copper in α -quartz suspensions. A decrease in ionic strength to 10^{-3} M NaCl moves the adsorption edge nearly 1.5 pH units to about pH 4. However, the surface of the quartz particles used by Vuceta (1975) may be coated with amorphous silica as a result of the base-washing procedure.

Adsorption of Copper on Amorphous Iron Oxide and α -Quartz. Figures 78 and 79 show the adsorption of copper as a function of pH on amorphous iron oxide and α -quartz, respectively. All experiments are conducted at 25°C in a nitrogen atmosphere with a total copper concentration of 10^{-6} M in 0.1M sodium nitrate. The adsorption edge on amorphous iron oxide occurs in the pH region 5-6, as has been observed by other investigators. It seems likely that the primary adsorbing species is CuOH^+ since the adsorption edge is near the pH where hydrolysis begins on many solids with varying surface characteristics. In Figure 78 it can be seen that there is some adsorption at pH 4 and a slight increase to pH 5. This adsorption is probably due to Cu^{+2} .

A similarly shaped curve is observed in Figure 79 for α -quartz. The interaction of copper with this α -quartz must be extremely weak because the adsorption edge is less steep and occurs in the pH region 6-7.5. The adsorption curve appears to change shape at pH 7 with an abrupt increase in adsorption. This may be the result of a change in predominant adsorbing species from Cu^{+2} to CuOH^+ , as postulated for the iron oxide. It is possible that some dehydration of the surface during preparation causes the observed weak interaction of copper with the α -quartz in these experiments. The dehydration reaction reduces the number of adsorption sites by the production of stable siloxane groups.

Adsorption of Cadmium(II) on Hydroxides Oxides

Equilibrium curves for adsorption of cadmium onto α -quartz and γ -FeCOH are shown in Figures 80 through 83. For the lepidocrocite experiments, the equilibration time is chosen to be two hours at which time the initial rapid uptake step is complete.

Effect of Cadmium and Substrate Concentrations. Adsorption isotherms are plotted in Figures 84 and 85 for sorption of cadmium onto silica and lepidocrocite, respectively. The data represent experiments in which the

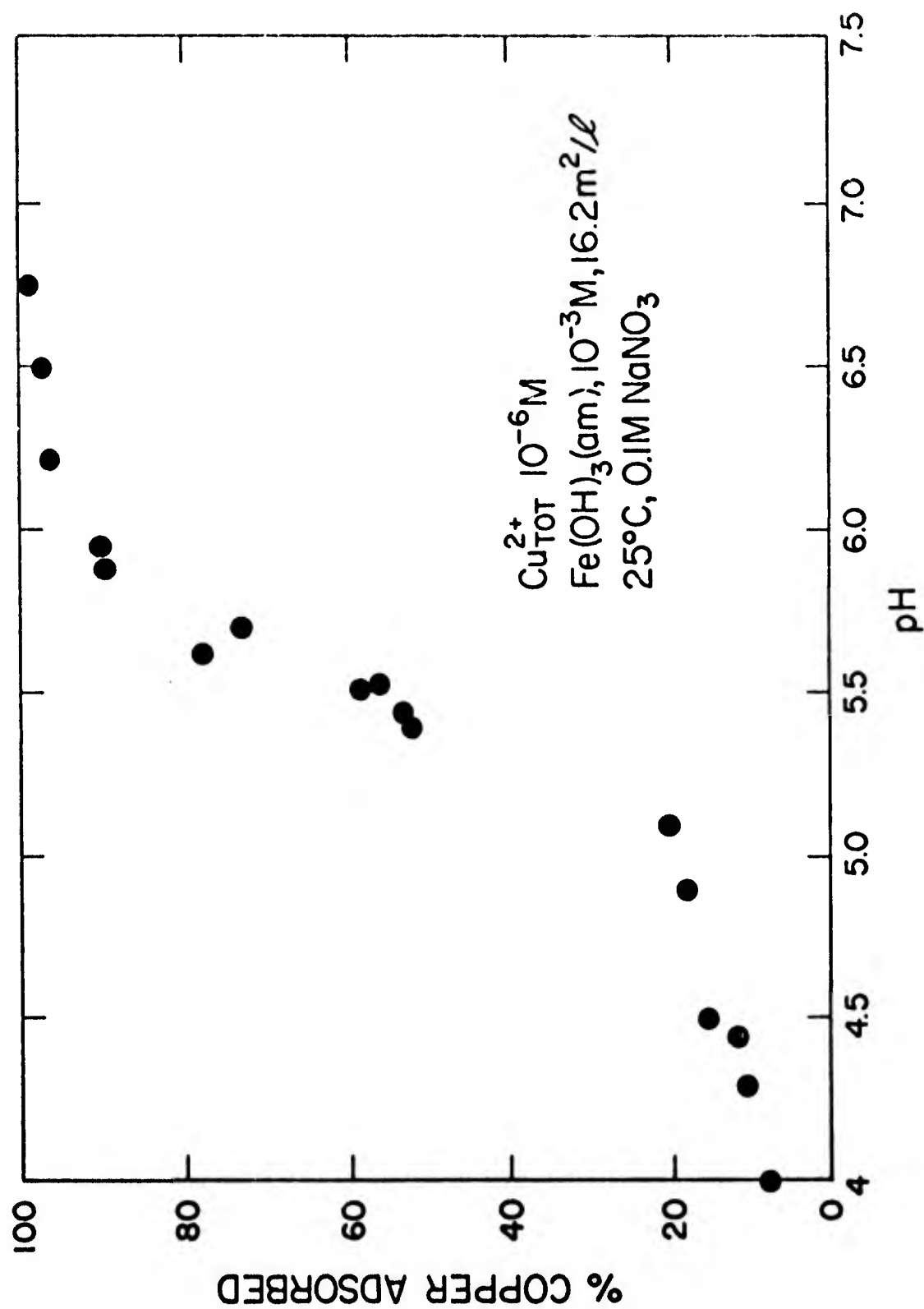


Figure 78. Adsorption of copper(II) on amorphous iron oxide as a function of pH.

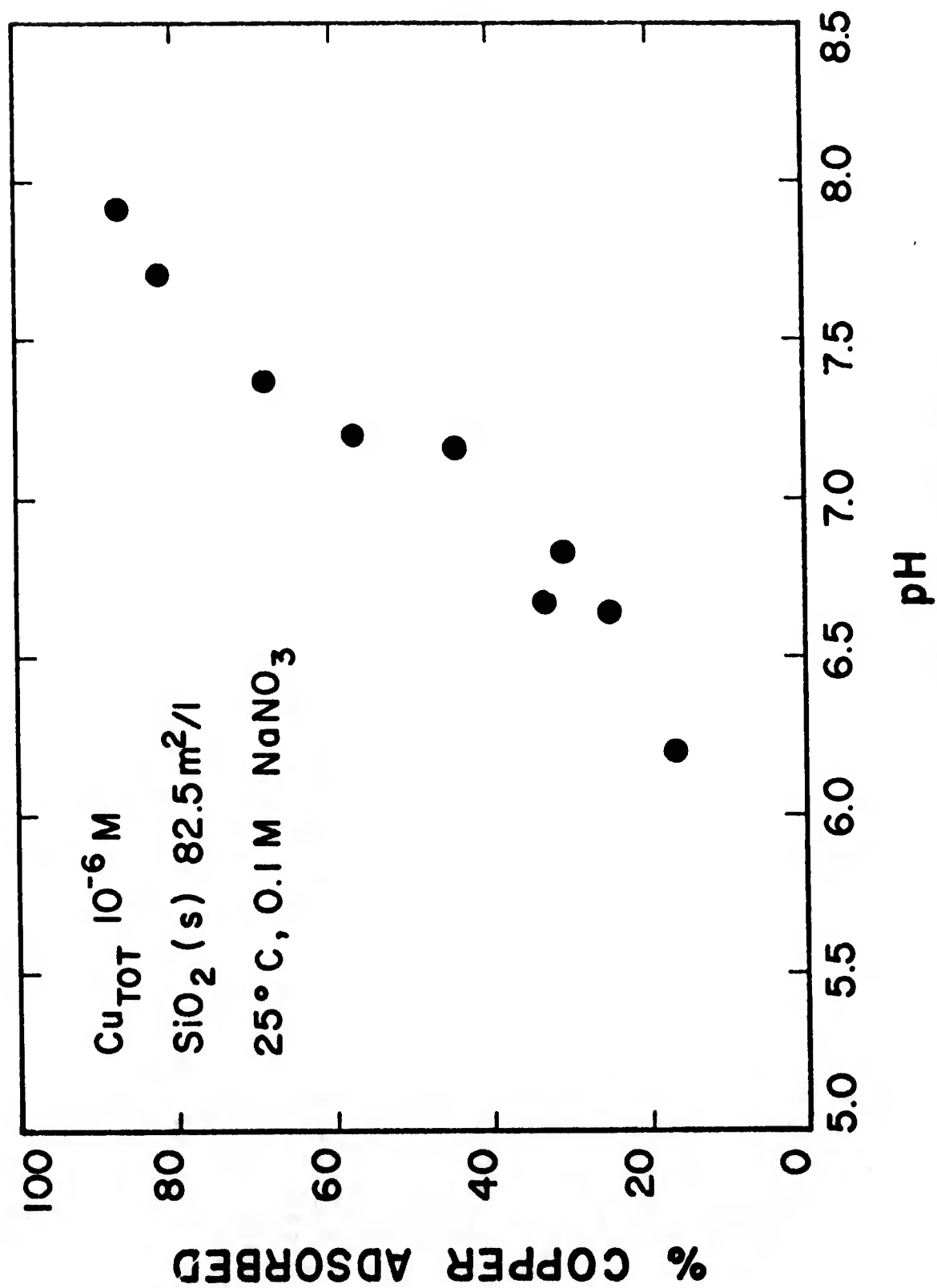


Figure 79. Adsorption of copper(II) on α -quartz as a function of pH.

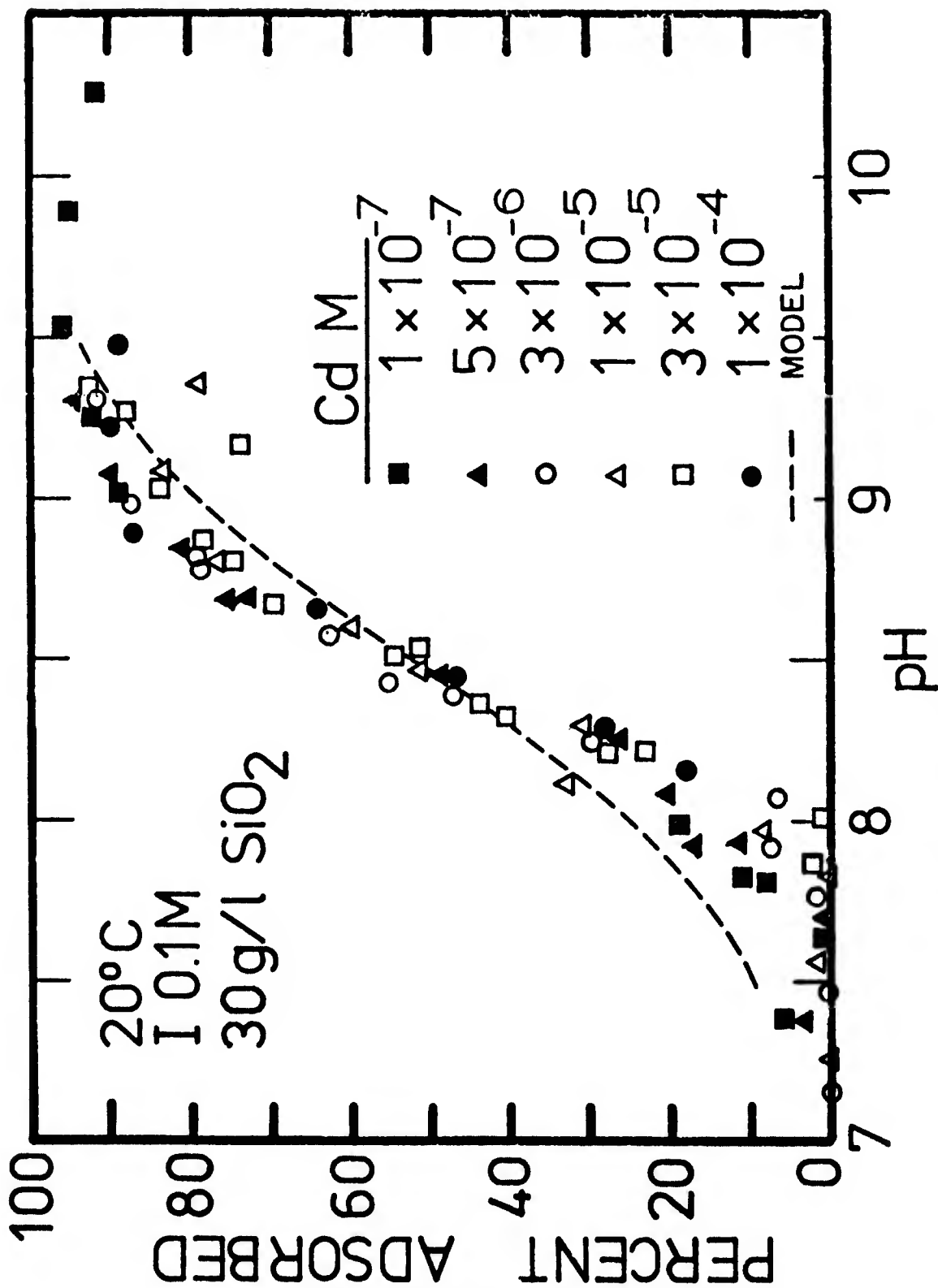


Figure 80. Fractional adsorption of Cd onto SiO₂ as a function of pH and Cd concentration.

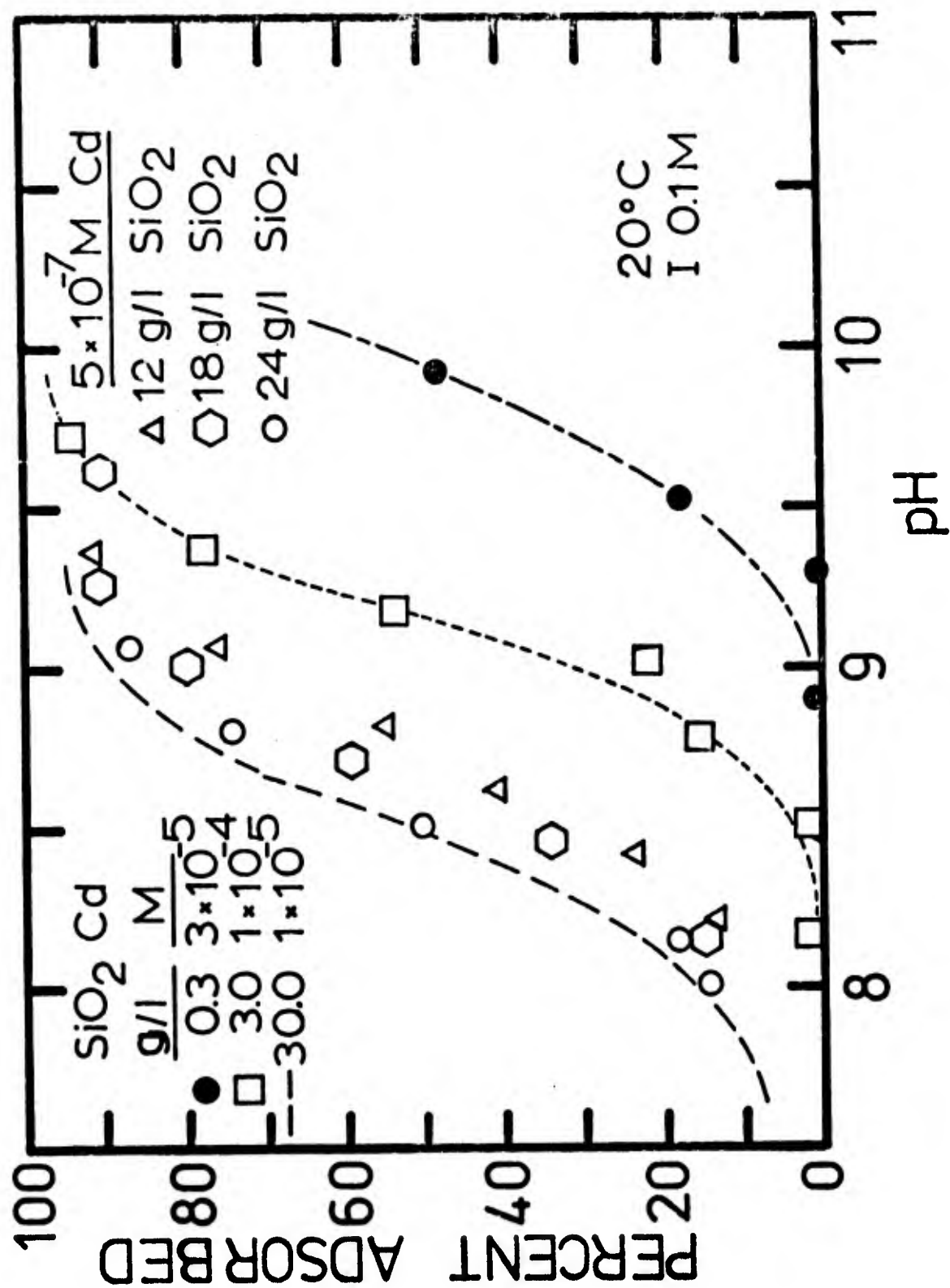


Figure 81. Fractional adsorption of Cd onto SiO₂ as a function of pH, Cd concentration, and SiO₂ concentration.

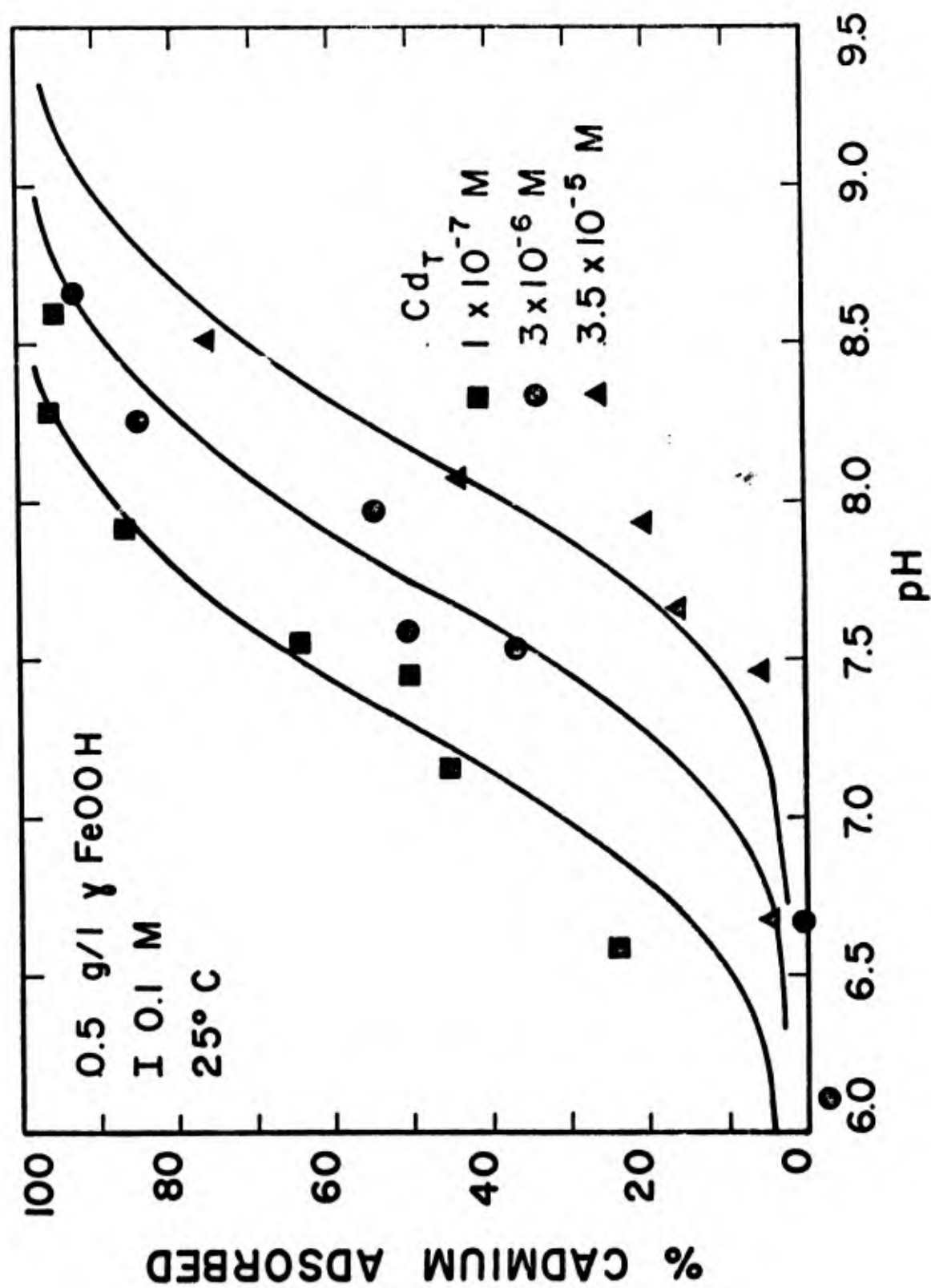


Figure 82. Fractional adsorption of Cd onto γ -FeOOH as a function of pH and Cd concentration.

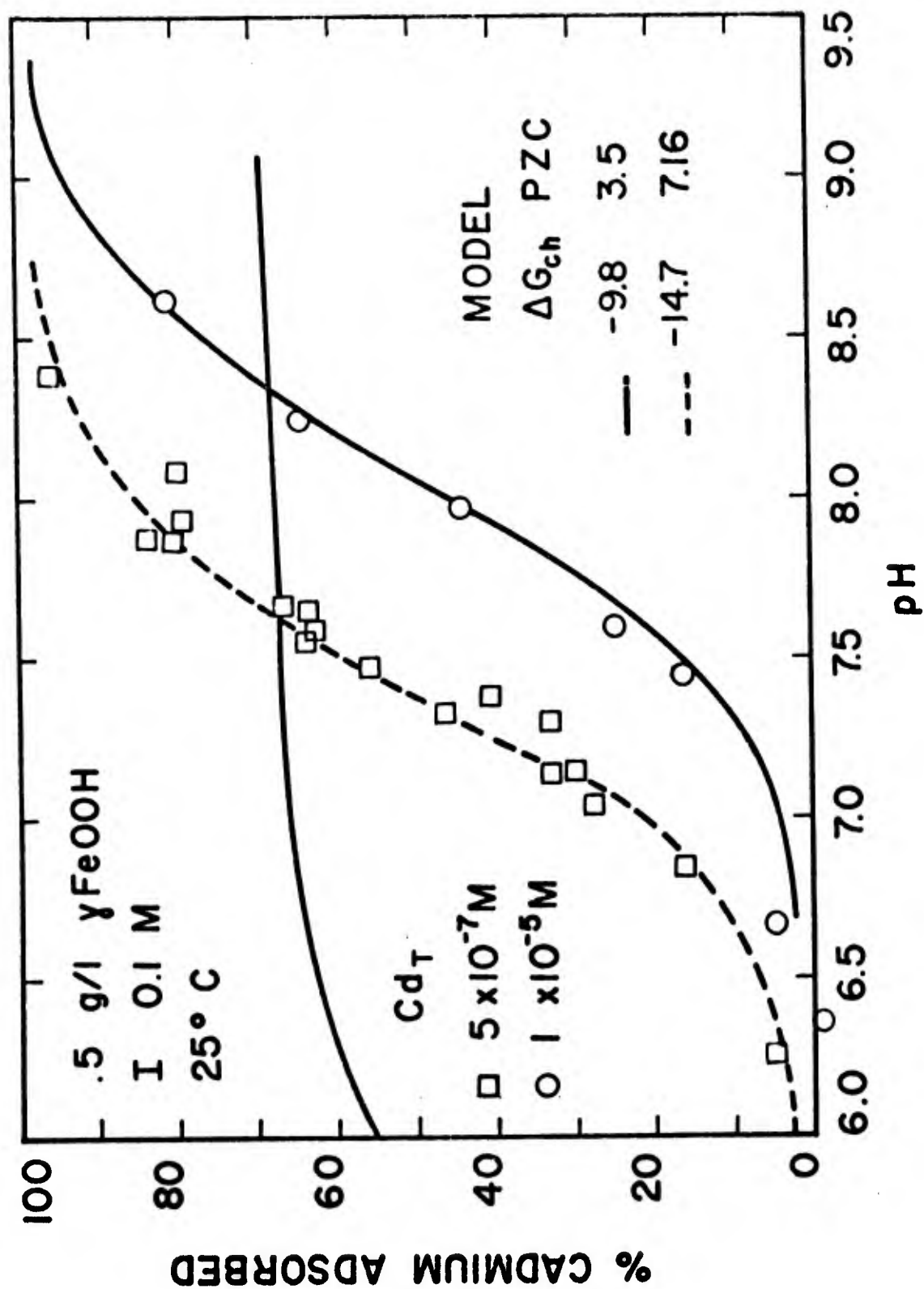


Figure 83. Fractional adsorption of Cd onto $\gamma\text{-FeOOH}$ as a function of pH and Cd concentration.

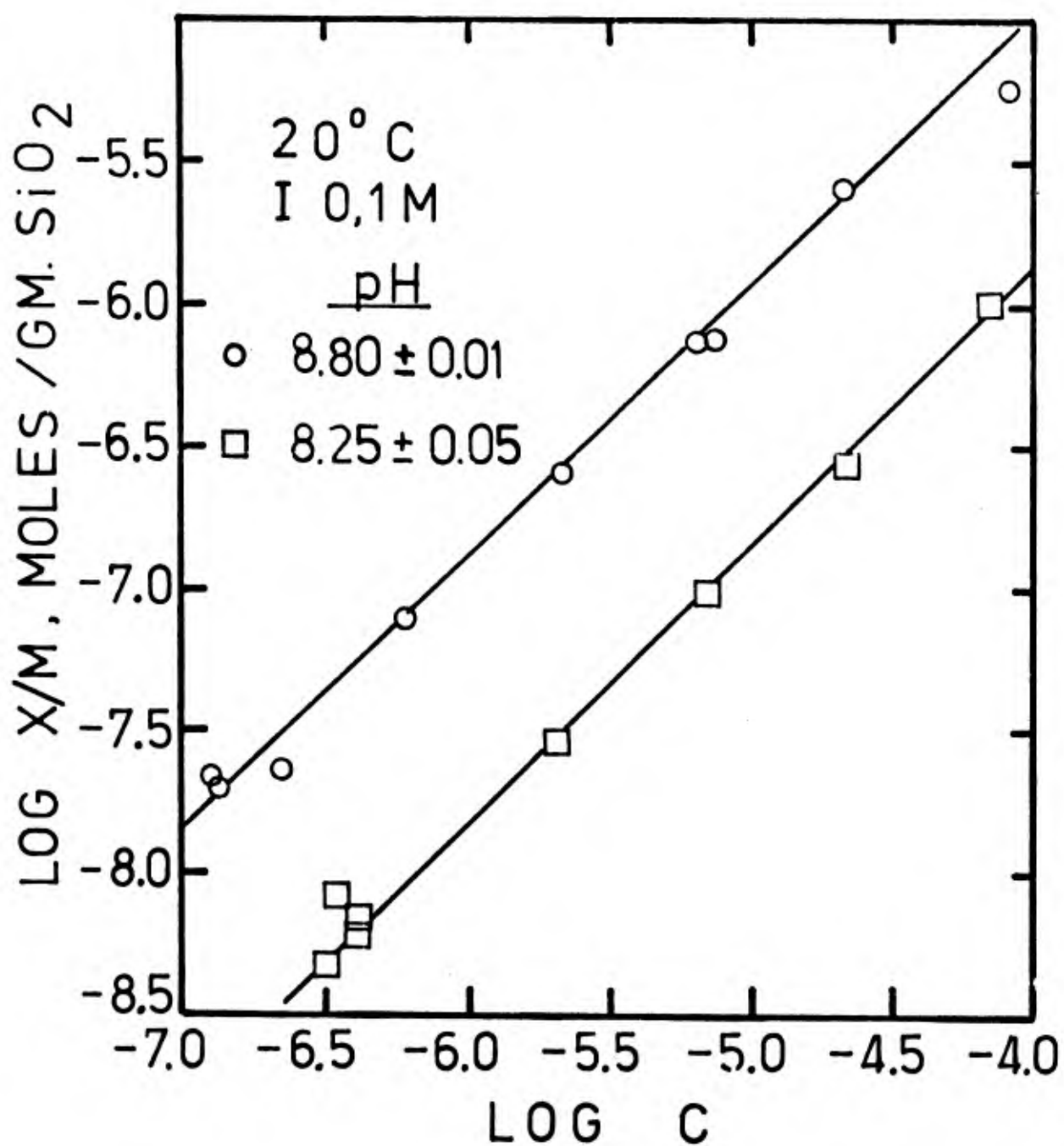


Figure 84. Adsorption isotherms for the system Cd/SiO₂ at two pH values.

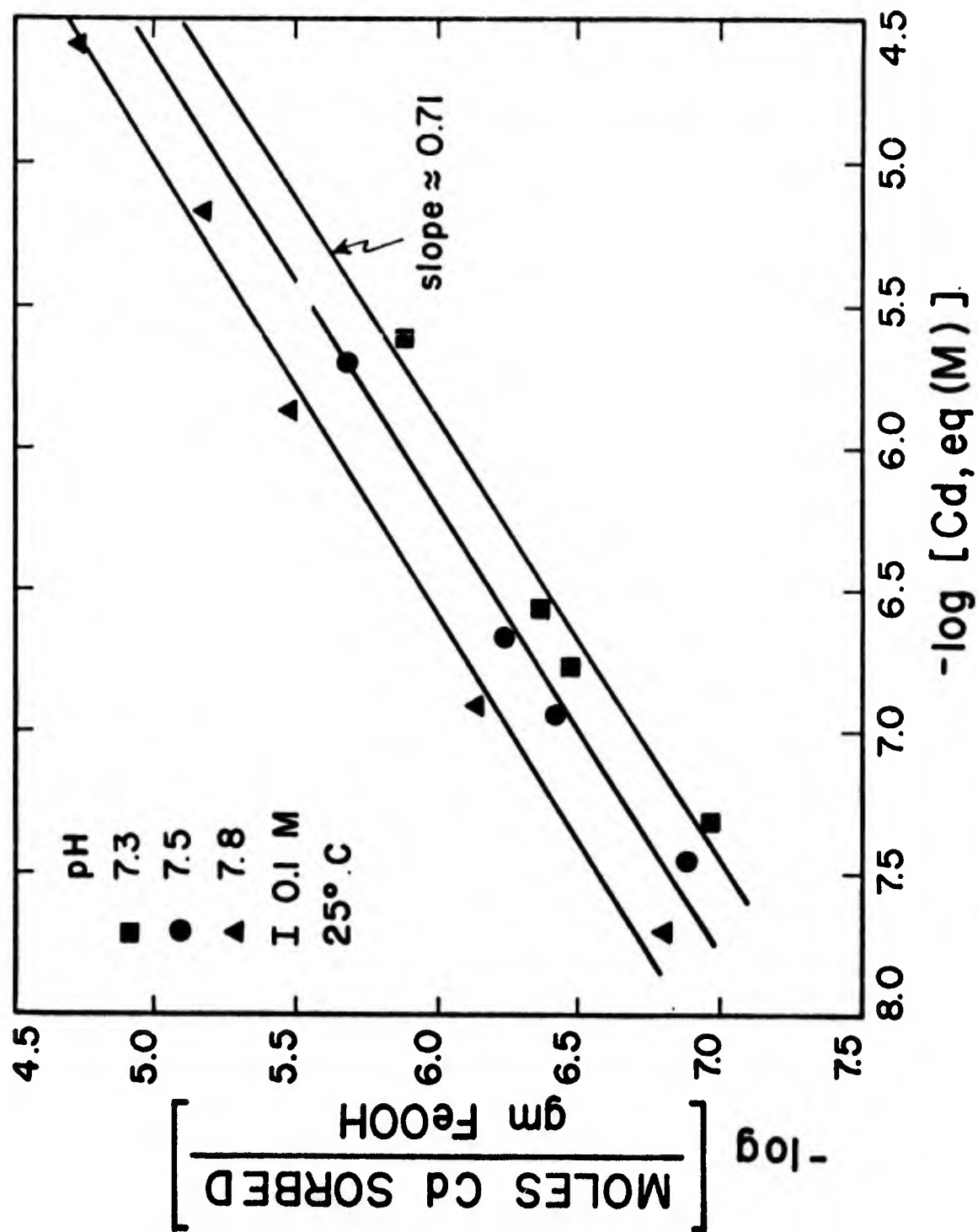
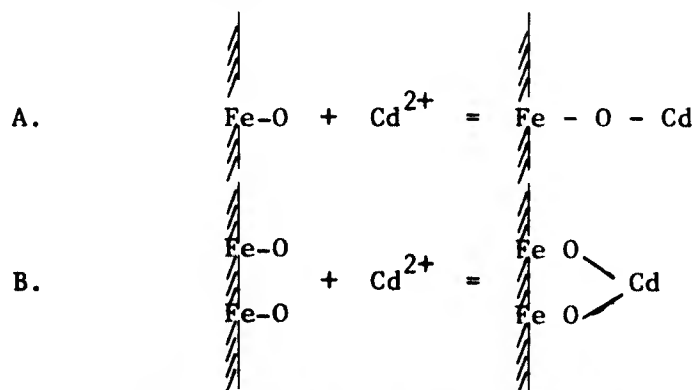


Figure 85. Adsorption isotherms for the system Cd/ γ -FeOOH at three pH values.

total cadmium in the system, Cd_{tot} , varies over at least 2-1/2 orders of magnitude in each case. Substrate concentrations are varied over 2 orders of magnitude in the case of silica but are not varied in the lepidocrocite experiments. The slopes of the isotherms are 0.71 and 1.00 for lepidocrocite and silica, respectively.

A slope of 1.0 is predicted by a Langmuir-type isotherm at low surface coverage. As availability of surface sites becomes the limiting factor, the slope should gradually decrease to zero, but no such trend is evident in the range of cadmium and silica concentrations studied. A slope of 1.0 also indicates an adsorption reaction in which each cadmium ion bonds to one and only one surface site. Such a reaction is found for the adsorption of 20 metals onto silica-gel at low pH (Dugger et al., 1964).

A slope of 0.71 for an adsorption isotherm is indicative of a reaction in which, on the average, each cadmium ion bonds to 1/0.71 or 1.4 surface sites. One possible conceptual scheme which satisfies this condition is if the cadmium can bond in two ways



and if the equilibrium between the two reactions is such that for every 10 cadmium ions adsorbed, six are in configuration A and four are in configuration B. A slightly different model is one in which each cadmium binds to a single oxide site, but in doing so, decreases the likelihood that a second cadmium ion will adsorb at a neighboring site. Other models are also possible. Adsorption isotherm slopes of less than 1.0 have been found by Davis (this report) and Dyck (1968, 1971) for adsorption of silver onto hydrous iron oxides.

Equilibrium adsorption curves for several different ionic strengths for each solid substrate are presented in Figures 86 and 87. As expected, increasing ionic strength decreases cadmium adsorption due to the compression of

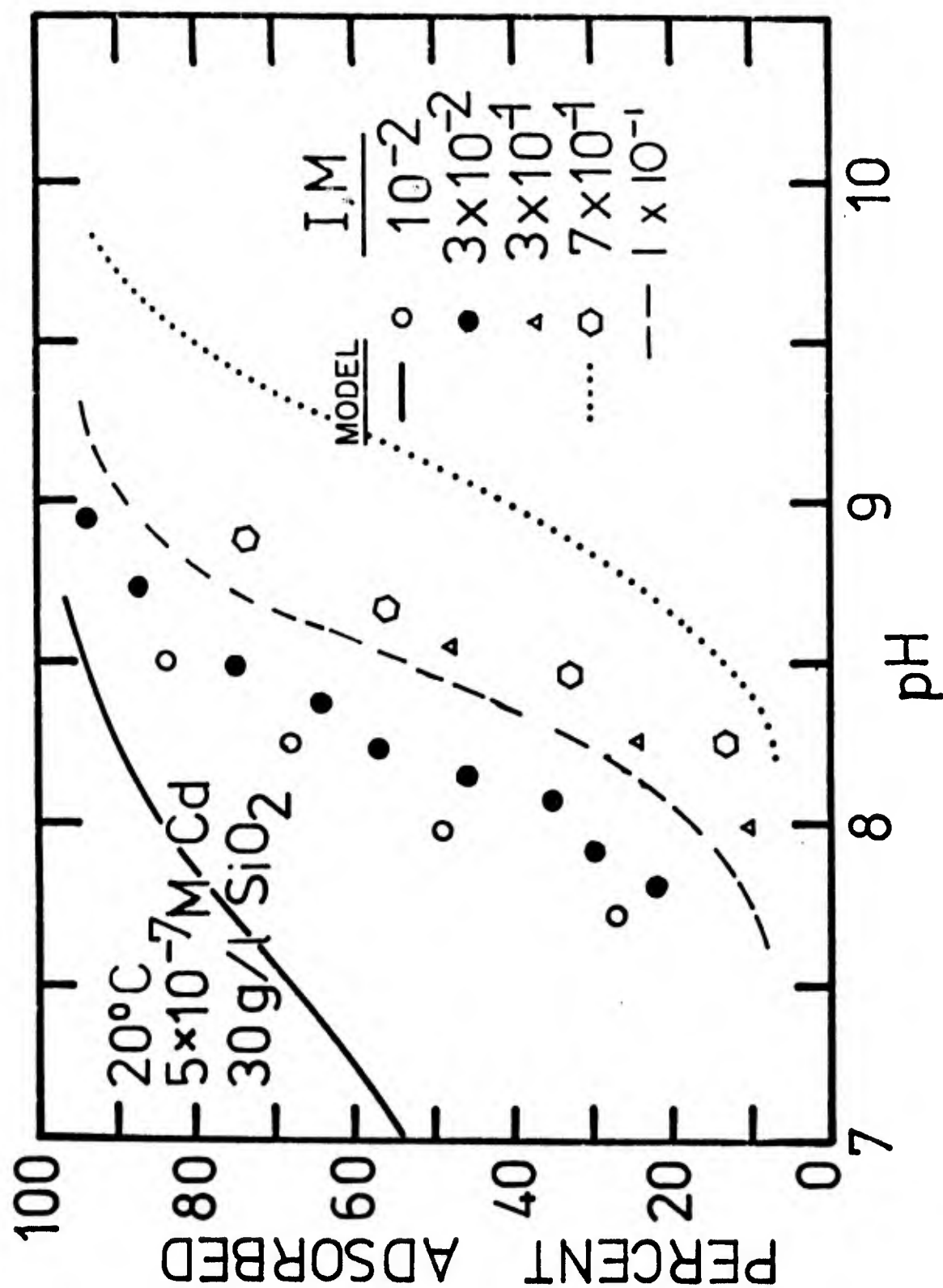


Figure 86. Adsorption of Cd onto SiO₂ as a function of pH and ionic strength.

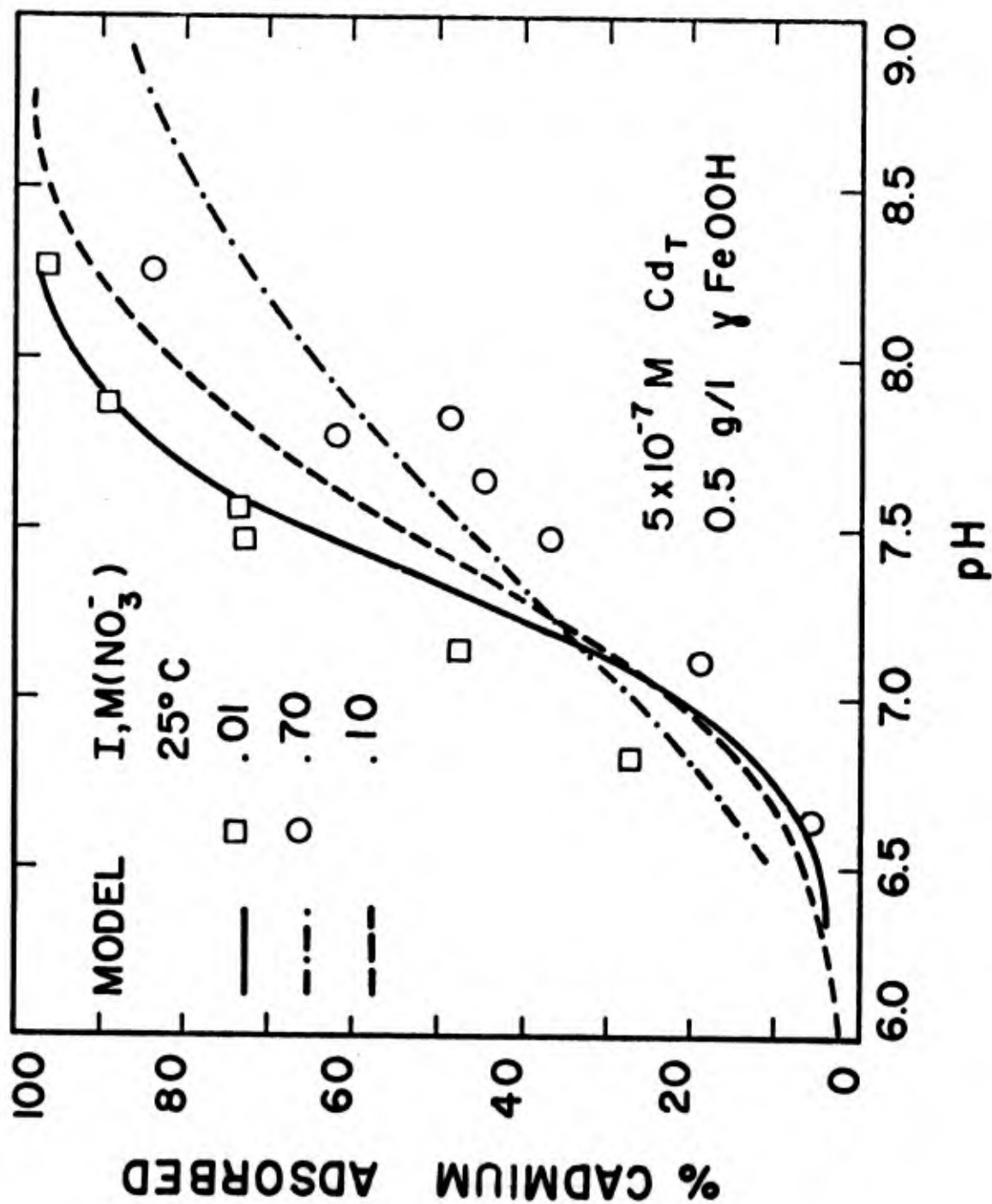


Figure 87. Adsorption of Cd onto γ -FeOOH as a function of pH and ionic strength.

the electrical double layer. In the case of lepidocrocite, this effect is partially masked by the fact that as ionic strength increases, the activity of the cadmium decreases, leading to an increase in the percentage of Cd_{tot} adsorbed. The shift in the adsorption edge is ~ 0.3 to 0.5 pH units for a change of one order of magnitude in total ionic strength.

Both cadmium hydroxide and cadmium carbonate are insoluble species which could potentially precipitate at high pH. If these solids precipitate, the measured values for % Cd_{tot} adsorbed will have a positive error.

Figure 88 shows that the presence of dissolved carbonate has no effect on the adsorption of cadmium onto silica. If the solution is in equilibrium with $\text{CdCO}_3(\text{s})$, more than 90% of the total cadmium in solution should have been removed at any pH above 8. Apparently precipitation is not a problem. Similarly, in the absence of carbonate, cadmium hydroxide could precipitate at high pH. However, in the case where cadmium hydroxide is most likely to form (Figure 81), the system becomes super-saturated without any evidence to suggest precipitation is occurring.

Acid-Base Titrations of the Surfaces. Extensive titration data were obtained for systems containing lepidocrocite, in the presence and absence of cadmium and dissolved carbonate, and at two different solids concentrations (Figures 89-91). In addition, two titration curves were obtained for the silica system, one with and one without cadmium (Fig. 92).

Lepidocrocite. Carbonate-free systems. The lepidocrocite titrations are normalized to coincide at pH 4.5, mls added = 0.0. The curves are extremely reproducible. In the absence of cadmium, the buffering effect of the lepidocrocite is evident throughout the pH range 4.5 to 10.5. The total number of protons released to solution per gram of solid during the titration is computed from knowledge of the excess volume of base required in the presence of solid compared to the blank. It is assumed that all surface sites are double-protonated at pH 4, and deprotonated at pH 10. Using a specific surface area of $20 \text{ m}^2/\text{g}$, the number of oxide sites available for reversible protonation is computed from two independent experiments using solids concentrations of 1.5 and 5.0 gm/l. The values obtained are 1.00 and 1.05 oxide surface sites per 100\AA^2 , respectively. When 10^{-4}M Cd^{2+} is added to the system, the titration curve is shifted to the right at pH above 6.5 (Figure 90). In the absence of solid, addition of cadmium has no

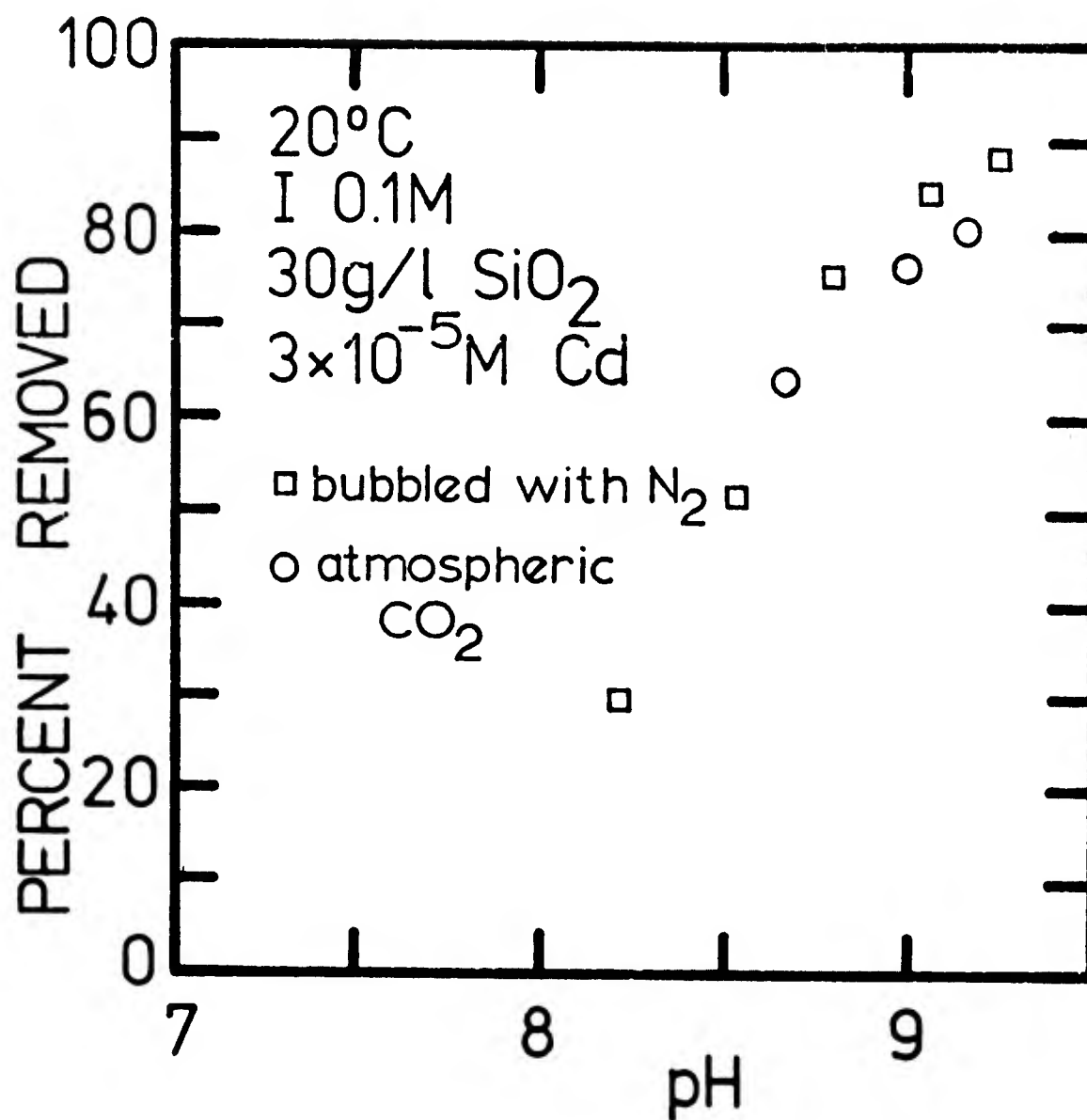


Figure 88. Adsorption of Cd onto SiO₂ as a function of pH. Effect of dissolved CO₂(g).

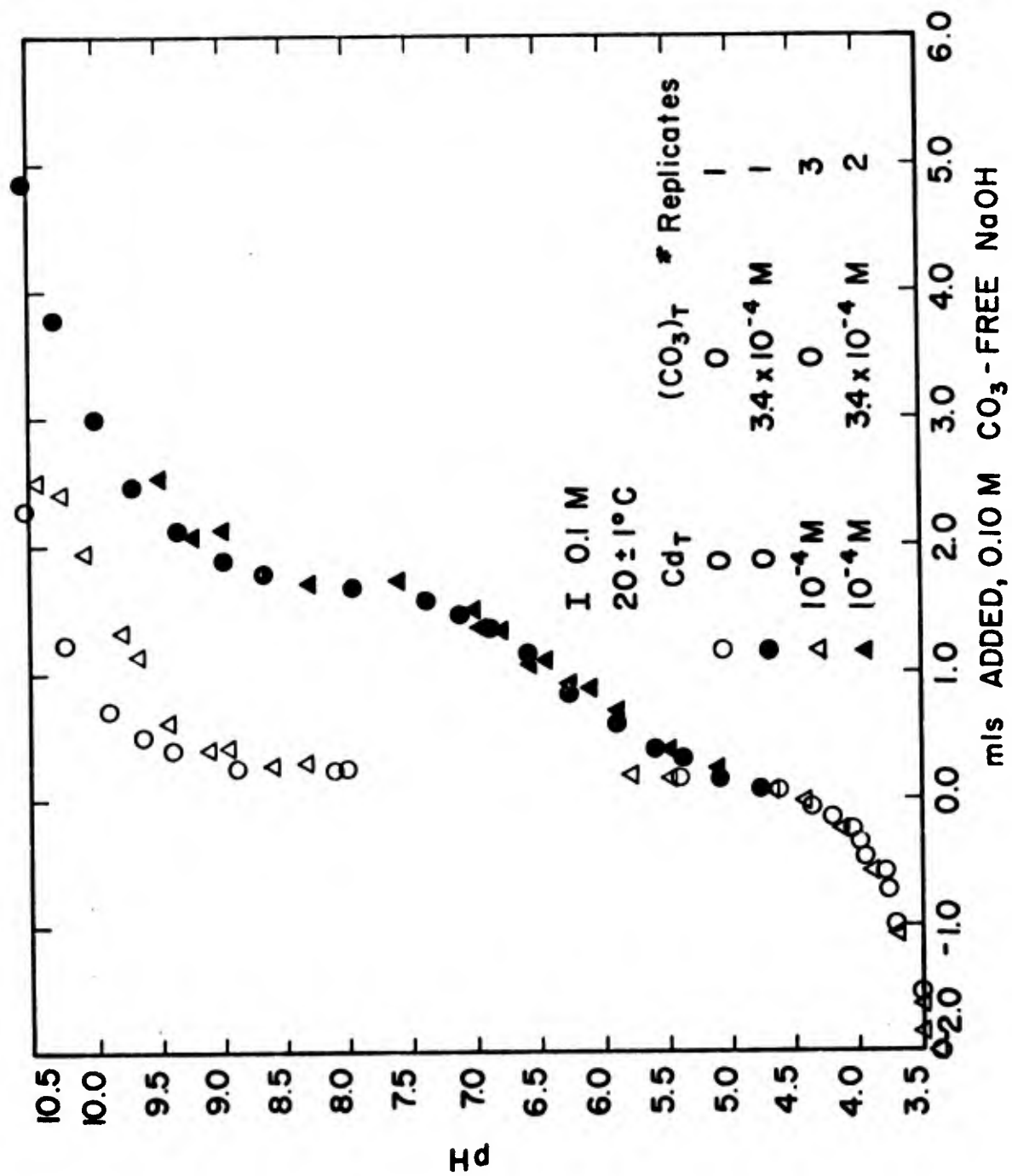


Figure 89. Acid-base titration of the system Cd/CO₂/H₂O.

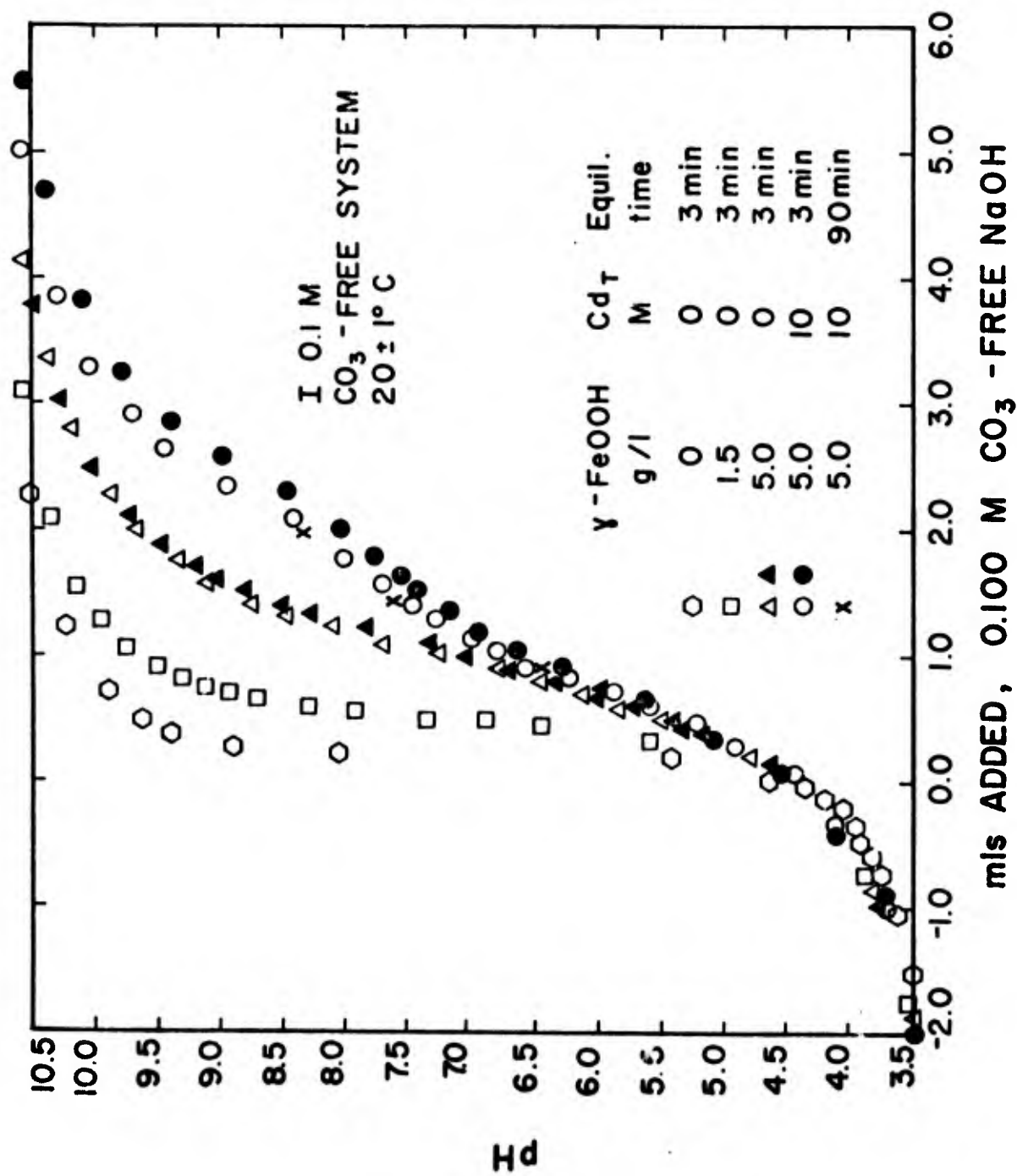


Figure 90. Acid-base titration of the system Cd/γ-FeOOH/H₂O.

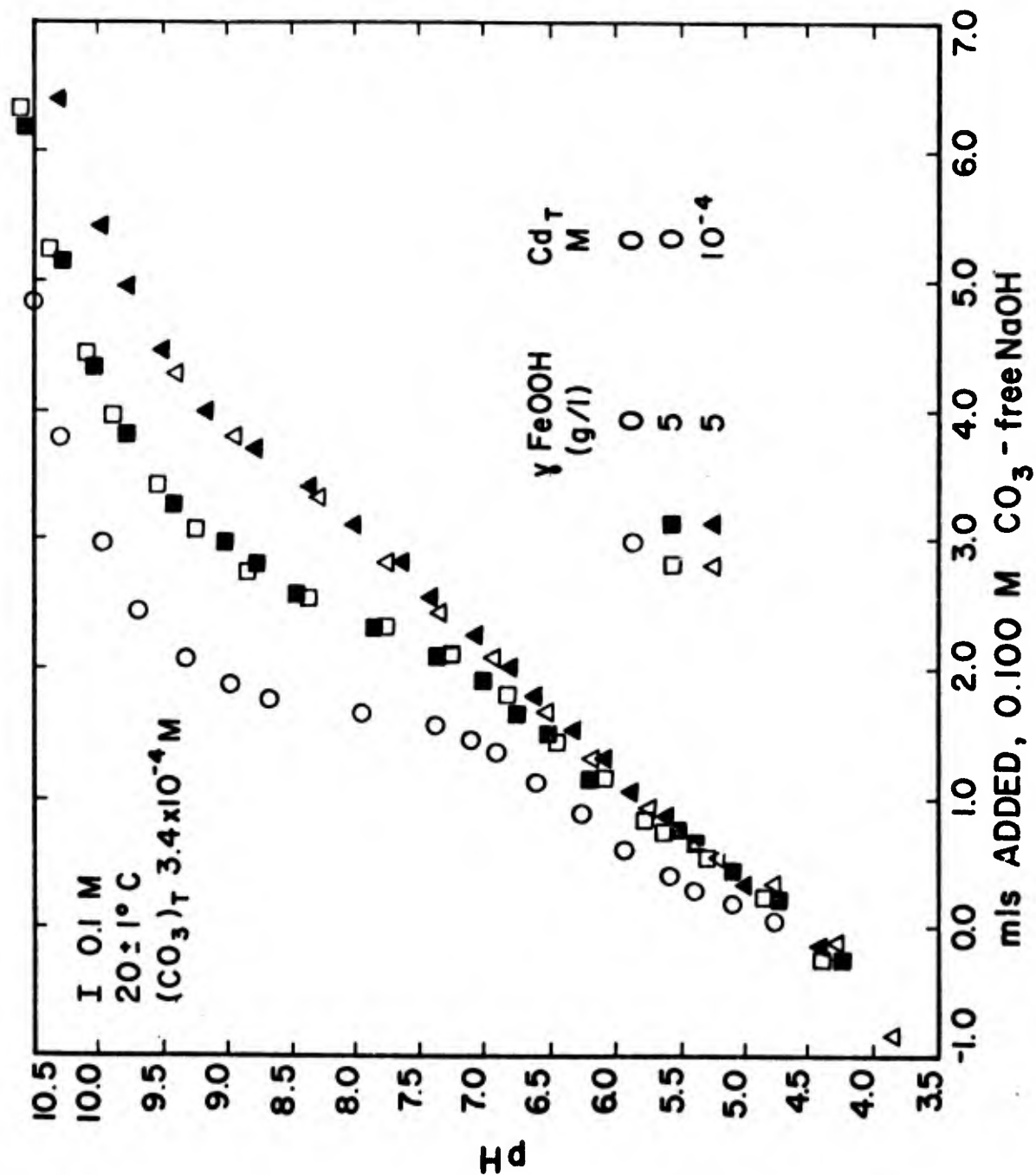


Figure 91. Acid-base titration of the system Cd/ γ -FeOOH/CO₂/H₂O.

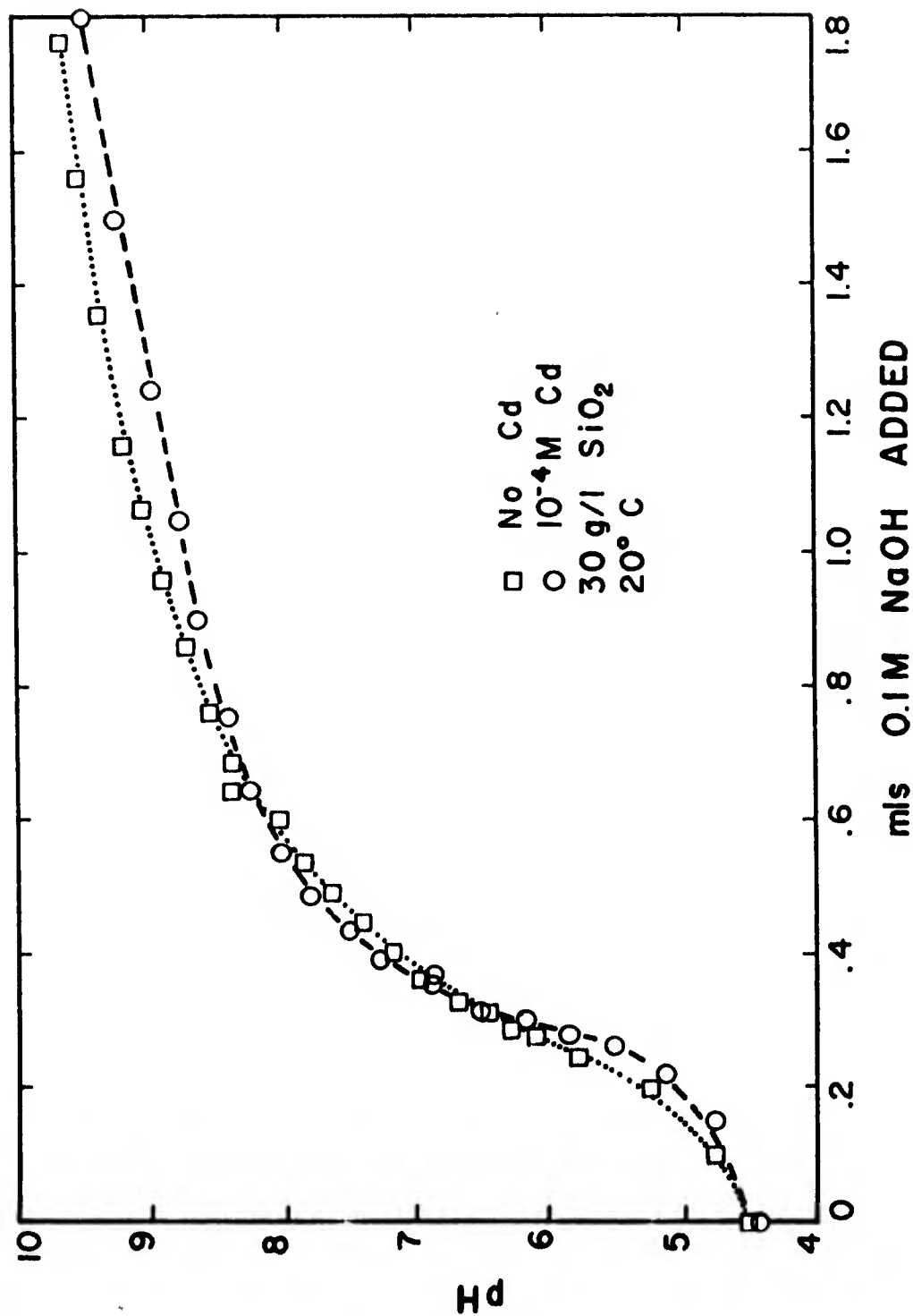


Figure 92. Acid-base titration of the system Cd/SiO₂/H₂O.

effect on the titration curve at pH 9 or less (Figure 89). Therefore, the additional protons titrated between pH 6.5 and 9.0 must be released by a reaction involving lepidocrocite. Short-term adsorption experiments (Figure 93) show that pH ~ 6.5 is also the pH at which significant adsorption of cadmium begins. Combining the adsorption and titration data shows that 2 protons are released per cadmium ion adsorbed over the range $6.0 \leq \text{pH} \leq 8.5$ (Figure 94). There is some indication that the ratio decreases at pH > 8.5, but the data are insufficient to draw a firm conclusion. A few longer-term adsorption experiments were run, allowing 90 minutes or more for equilibration instead of the usual 3 minutes. No significant additional adsorption was detected.

Assuming that each cadmium ion bonds to one or two oxide sites, that no oxide site can bond more than one cadmium, and that the only sites at which cadmium can be adsorbed are those which are reversibly protonatable, then when 100% of the cadmium is adsorbed, more than 60% of the surface oxide groups are bound to cadmium ions.

Yates (1975) has estimated surface site densities of 10 to 25 oxides per 100\AA^2 on various iron oxides. He has also shown that the assumption that two protons are released when iron oxide is titrated from pH 4 to pH 10 is probably incorrect. In addition, using the value of 1 oxide site per 100\AA^2 , at the highest concentration of cadmium investigated, there would be 5 cadmium ions adsorbed per surface site. While this situation is possible if surface precipitation occurs, it seems more likely that the estimated density of surface sites is low by at least one order of magnitude. If this is true, then at no time during the titration experiments are more than 6% of the surface sites bound to cadmium.

Systems containing carbonate. When carbonate is added to the system, it is added as NaHCO_3 to systems at low pH (~ 3.5). This means the system is super-saturated with H_2CO_3 with respect to equilibrium with the atmosphere until the titration raises the pH to above 6.3. The time period involved is 10 to 15 minutes. Analysis of the titration curves in the absence of solid (Figure 91) indicates that no $\text{CO}_2(\text{g})$ is lost to the atmosphere during this period and that cadmium and carbonate do not interact in a way that removes or releases protons at any pH less than 9. In the system containing carbonate and lepidocrocite but no cadmium, the titration curve is shifted to the right. At low pH (< 6), the shift is equal to that for the

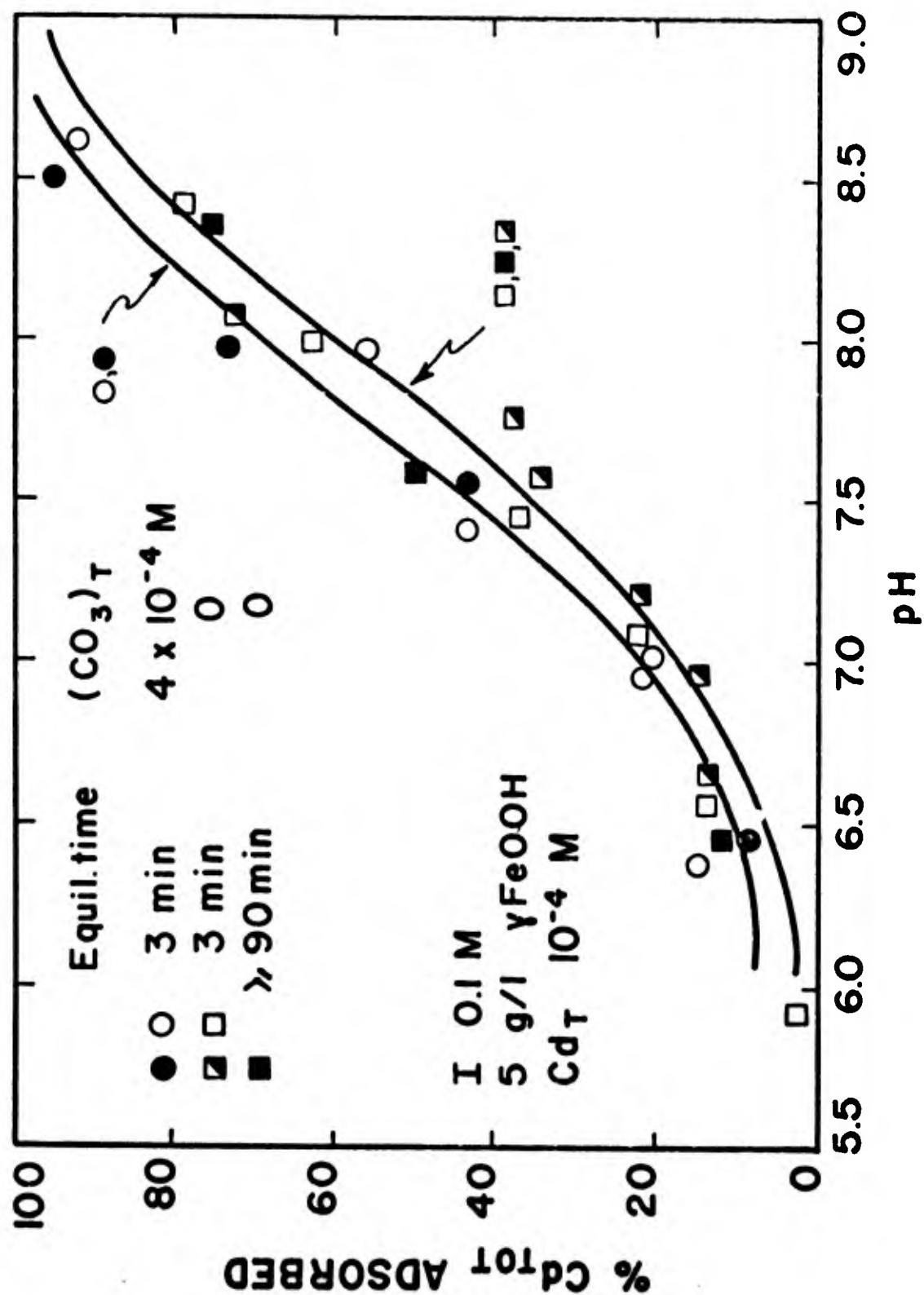


Figure 93. Short-term adsorption of Cd onto γ -FeOOH as a function of pH and CO_2 concentration.

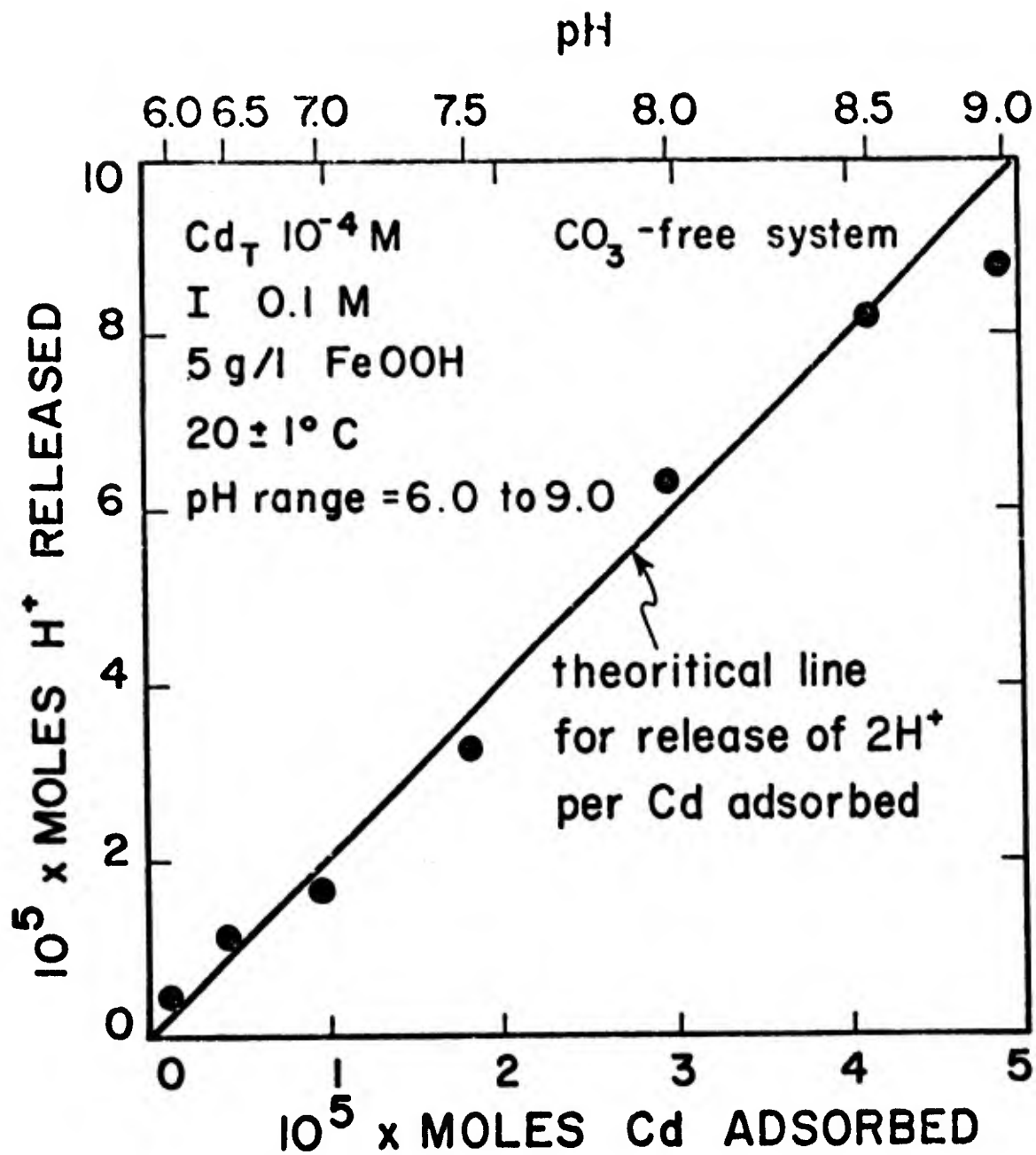
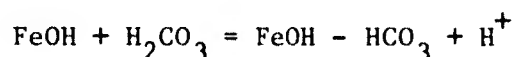
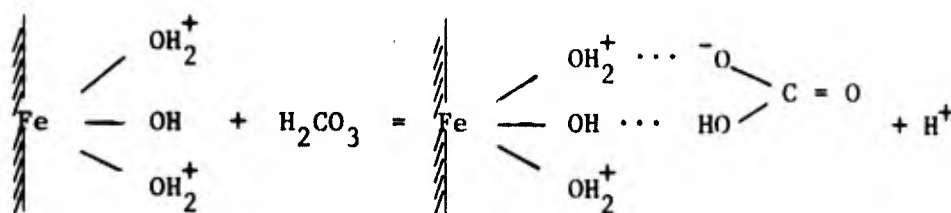


Figure 94. Release of protons as a function of Cd adsorption in the system $\text{Cd}/\gamma\text{-FeOOH}/\text{H}_2\text{O}$.

carbonate-free systems, but in the range $6.0 < \text{pH} < 7.5$, the shift due to the presence of solid is less in the carbonate system. At pH 7.5 or above, the shifts in the curves are again equal (Figure 95). In other words, when the solid is present, less carbon dioxide is titrated to bicarbonate than when there is no solid present. There are at least two possible explanations for this. One is that $\text{H}_2\text{CO}_3(\text{g})$ is nucleating on the lepidocrocite particles and is being removed from solution. This is unlikely since such a process would probably be dependent on stirring rate and duration of the super-saturated period. Since these factors are not controlled and since equilibration with atmospheric CO_2 is never attained at low pH, the amount of CO_2 remaining in the suspension would be expected to be quite variable. In fact, it is highly reproducible. An hypothesis consistent with this fact is that at low pH, an equilibrium is attained for the adsorption of H_2CO_3 onto lepidocrocite according to the following reaction:



In other words, part of the H_2CO_3 is deprotonated to HCO_3^- at low pH by a surface reaction before the manual titration begins. Since less H_2CO_3 remains to be titrated, the carbonate concentration determined experimentally is less than the total carbonate in solution. The bonding of the HCO_3^- to the surface might be some combination of covalent and hydrogen bonding. Since at low pH most of the oxide sites are doubly protonated, a possible adsorption reaction process is



Such a reaction predicts that adsorption of bicarbonate is probably increased at higher pH. It is not possible to verify or disprove such a prediction with only the titration curves available. If this hypothesis is correct, and if there are 10 surface sites per 100\AA^2 , then between 4 and 20% as many bicarbonate ions would be adsorbed as there are total surface sites.

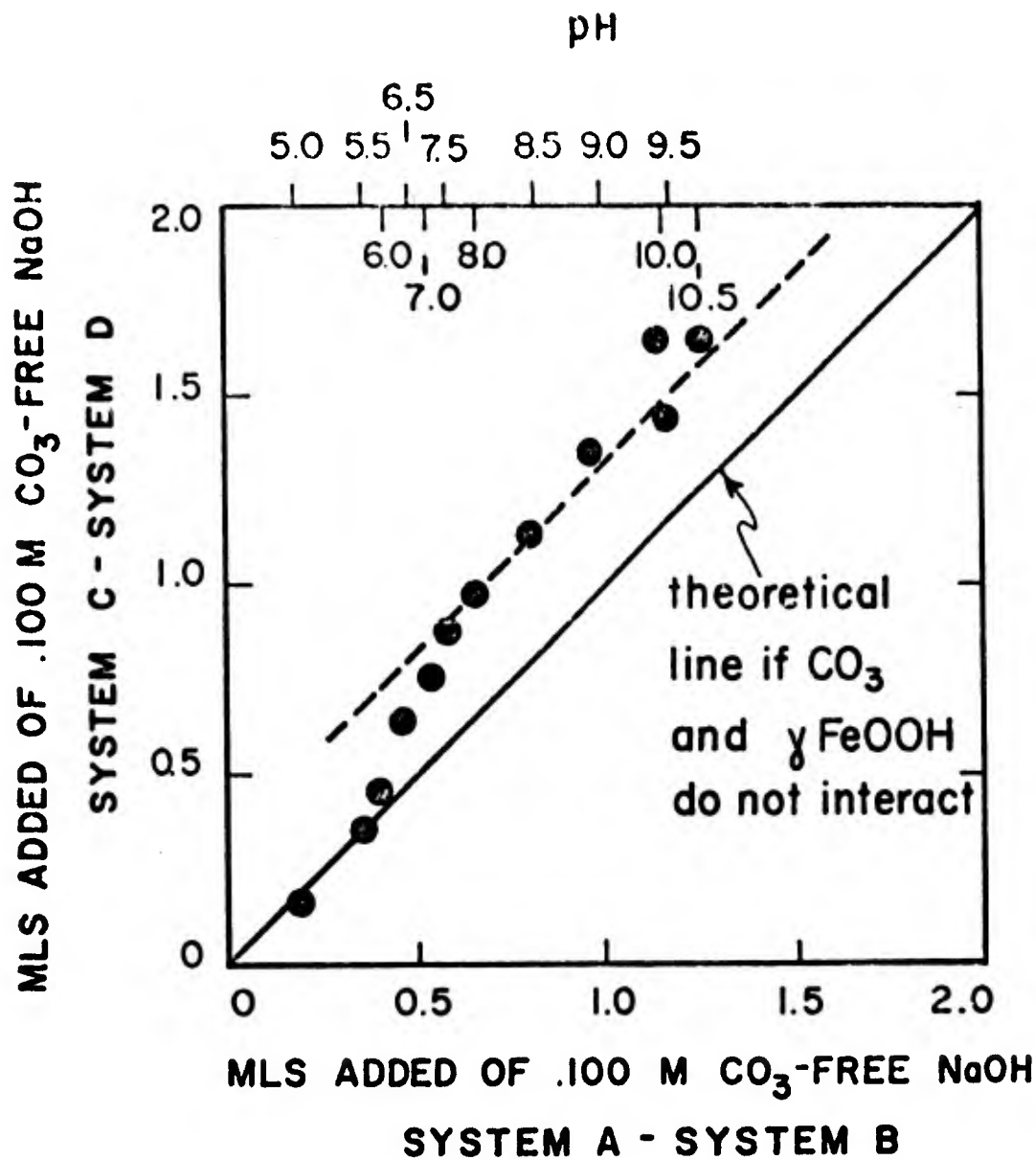


Figure 95. Interaction of γ -FeOOH and CO_3 . For no interaction, the effect of addition of CO_3 to the system $\text{Cd}/\text{H}_2\text{O}$ and $\text{Cd}/\gamma\text{-FeOOH}/\text{H}_2\text{O}$ would be identical. System A: $\text{Cd}/\text{CO}_3/\text{H}_2\text{O}$. System B: $\text{Cd}/\text{H}_2\text{O}$. System C: $\text{Fe}/\text{Cd}/\text{CO}_3/\text{H}_2\text{O}$. System D: $\text{Fe}/\text{Cd}/\text{H}_2\text{O}$.

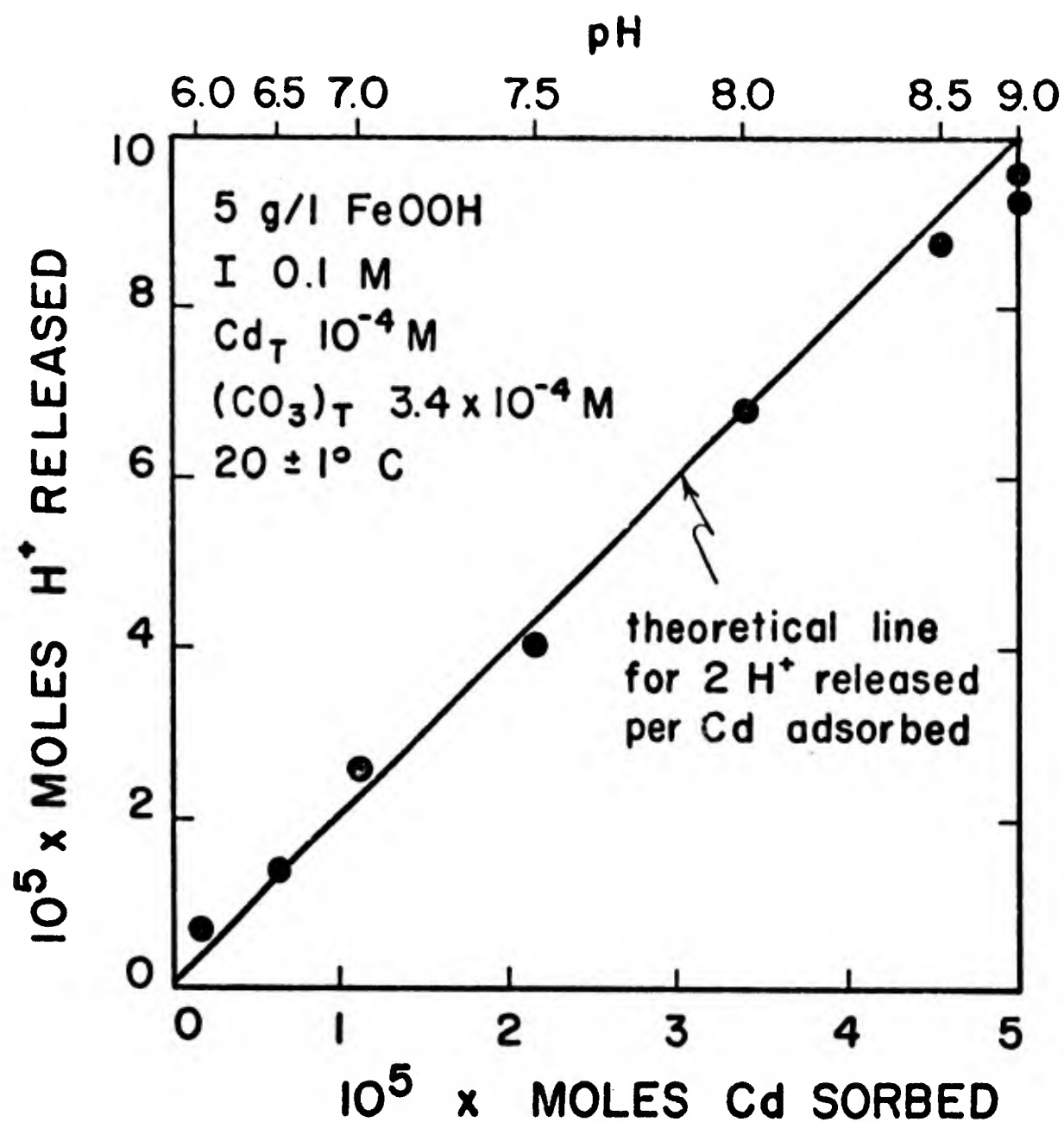


Figure 96. Release of protons as a function of Cd adsorption in the system Cd/ γ -FeOOH/CO₂/H₂O.

As in the carbonate-free system, combination of the adsorption curve (Figure 93) and the titration data (Figure 91) indicate that 2 protons are released per cadmium ion adsorbed (Figure 96).

Silica. Analysis of the titration curves in the silica system (Figure 92) shows that the curves separate in a slightly higher pH range than where adsorption of cadmium becomes significant. A plot of protons released versus cadmium adsorbed (Figure 97) shows that no protons are released until $\text{pH} > 8.2$, after which approximately one is released for each cadmium which adsorbs. Because of the flatness of the titration curves in the range of interest, the derived values for number of protons released are considerably more uncertain than in the lepidocrocite systems.

Modeling of the Adsorption Reactions. The adsorption data are used to test two conceptual and mathematical models, adsorption of hydrolytic complexes, the James-Healy model, and the surface coordination model.

Adsorption of Hydrolytic Complexes. In this physical model of adsorption, the main fitting parameter is the chemical-free energy of adsorption, ΔG_{ch} . The best fit of the model to experimental results is obtained using the following parameters:

	<u>Silica</u>	<u>Lepidocrocite</u>
ΔG_{ch}	7.55 Kcal/mole	8.73 Kcal/mole
IEP	2.0	7.16
ϵ_s^*	4.3	12.0
Surface area	3.3 m^2/g	20 m^2/g

* Dielectric constant of surface.

The adsorption curves predicted using these parameters are shown as the dotted lines in Figures 80 and 83. The PZC of lepidocrocite is used rather than the IEP because no value of ΔG_{ch} gives a satisfactory fit when the IEP is used (Figure 83).

Since the James-Healy model assumes a Langmuir-type isotherm, it predicts that at low surface coverage the fractional adsorption of a metal will be independent of the total metal concentration in solution. Since this is not true in the lepidocrocite experiments, the value of ΔG_{ch} is chosen to

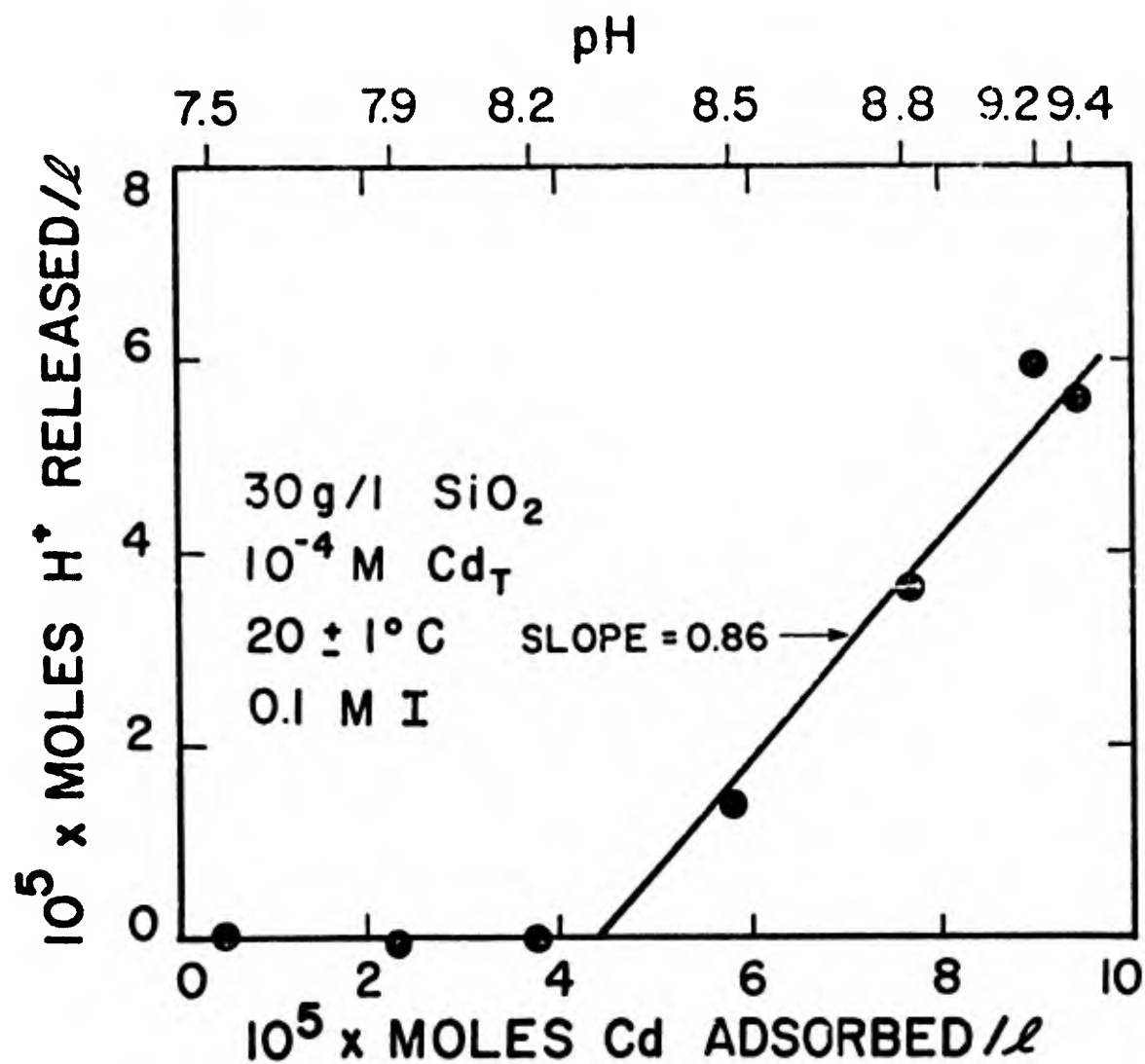


Figure 97. Release of protons as a function of Cd adsorption in the system $\text{Cd/SiO}_2/\text{H}_2\text{O}$.

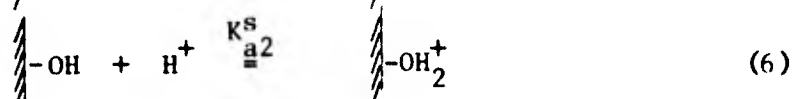
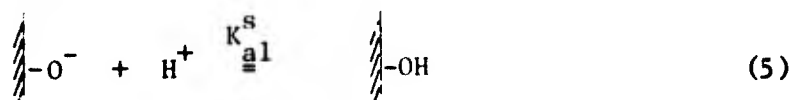
fit the data for $Cd_T = 5 \times 10^{-7} M$. The shape of the model curve fits the lepidocrocite data well, but the silica experiments show a slightly steeper adsorption edge than predicted.

In almost all cases, when a change in the composition of the solution causes a shift in the adsorption edge, the shift predicted by the model is considerably greater than the shift observed. This is true for changes in ionic strength (Figures 86 and 87) as well as for addition of sulfate or chloride as complexing ligands.

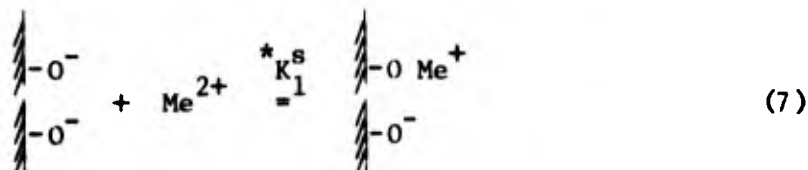
The model assumes that the only effect of changing ionic strength is to change the thickness of the double layer. A corollary is that adsorption will be independent of ionic strength at the IEP, at which pH there is no double layer, and that the curves for various ionic strengths cross each other at $pH = IEP$. This is the only prediction of the model which is clearly incorrect as a result of using the PZC instead of the IEP.

Only in the case of thiosulfate as a complexing ligand does the model predict the shift with good accuracy (see next section).

Surface Coordination Model. In this chemical model, oxide surfaces are assumed to undergo two reversible hydrolysis reactions:



The equilibrium constants K_{a1}^s and K_{a2}^s are functions of the intrinsic affinity of the protons for the surface and the surface potential. The intrinsic acidity constants $^*K_{a1}^s$ and $^*K_{a2}^s$ are defined as the apparent acidity constants when the surface potential, ψ_0 , is zero. Knowledge of the titration curve allows the intrinsic constants to be calculated. The model treats adsorbing metals in much the same way as protons, except that the possible reactions are:



and



The model has not been applied to solids for which the IEP does not equal the PZC. Normally, the apparent acidity constants are plotted against surface charge, and the intrinsic constants are obtained from the intercept, where surface charge and potential are both zero. It is felt that the data, obtained in the pH range 6.0 to 9.5, are not accurate enough to allow extrapolation to the IEP (3.5), and that there is no conceptual basis for claiming the apparent acidity constants at $\text{pH} = \text{PZC}$ are the intrinsic constants. Instead, values of $(\log ([\text{FeOH}_2^+]/[\text{FeOH}]))$ and $(\log ([\text{FeOH}]/[\text{FeO}^-]))$ are derived and plotted against pH (Figure 98). For an ordinary diprotic acid, these plots should be straight lines of slope -1.0 and x-intercept at $\text{pH} = \text{pK}$. For the solid, reasonably straight lines of slopes -0.7 to -0.9 are obtained, with intercepts $\text{pK}_{\text{a1}}^{\text{S}} = 5.8$ and $\text{pK}_{\text{a2}}^{\text{S}} = 8.8$. The deviation from linearity and unit slope may be related to the effects of a non-constant surface potential or simply experimental error. The slopes become very nearly equal to -1.0 if the PZC is taken to be 7.30 (Figures 99 and 100), which is within experimental error of the previously determined value of 7.16. A slope of between 0 and -1.0 is predicted if the increasingly negative potential at the surface, as pH increases, has a significant effect on the surface deprotonation equilibrium.

In other words, a non-zero surface potential has the effect of shifting the apparent acidity constants farther than the intrinsic constants from the PZC. Unfortunately, the acidity constants are sensitive functions of the total number of surface sites, a number which has been shown to be in doubt by at least one order of magnitude. For example, the values of the apparent acidity constants at pH 5.8 and pH 8.8 for 1 and 10 sites per 100\AA^2 are:

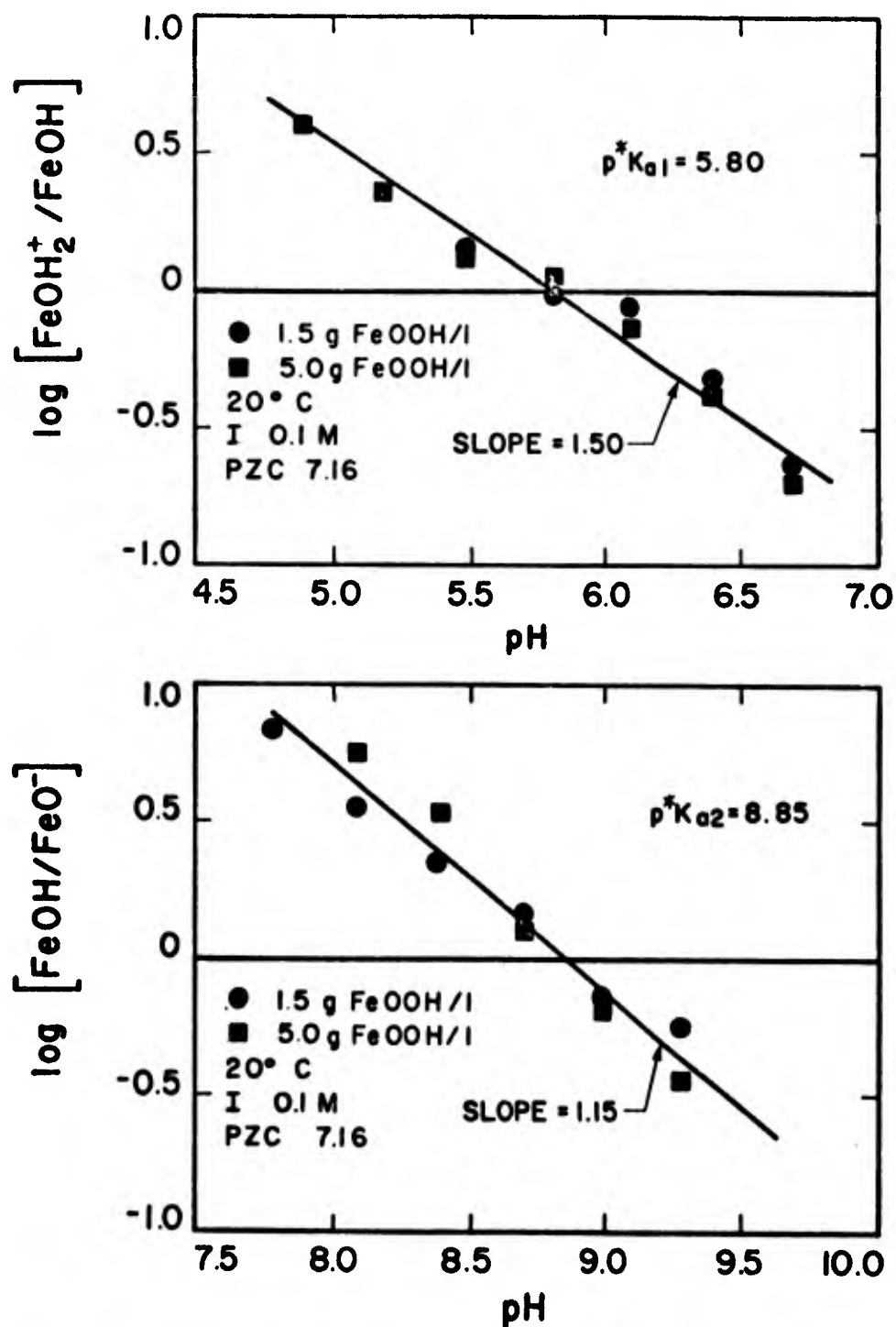


Figure 98. Degree of protonation of surface sites on γ -FeOOH as a function of pH, assuming a PZC of 7.16.

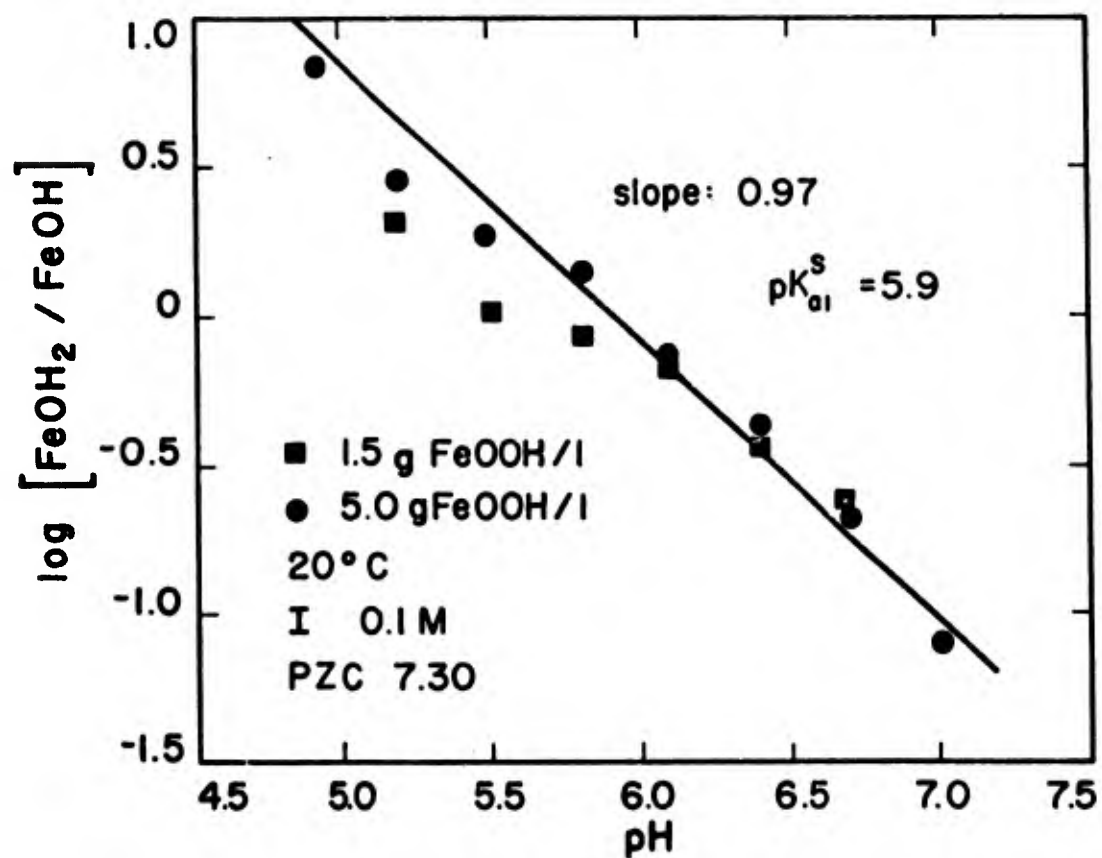


Figure 99. Ratio of doubly- to singly-protonated surface sites on γ -FeOOH as a function of pH, assuming a PZC of 7.30.

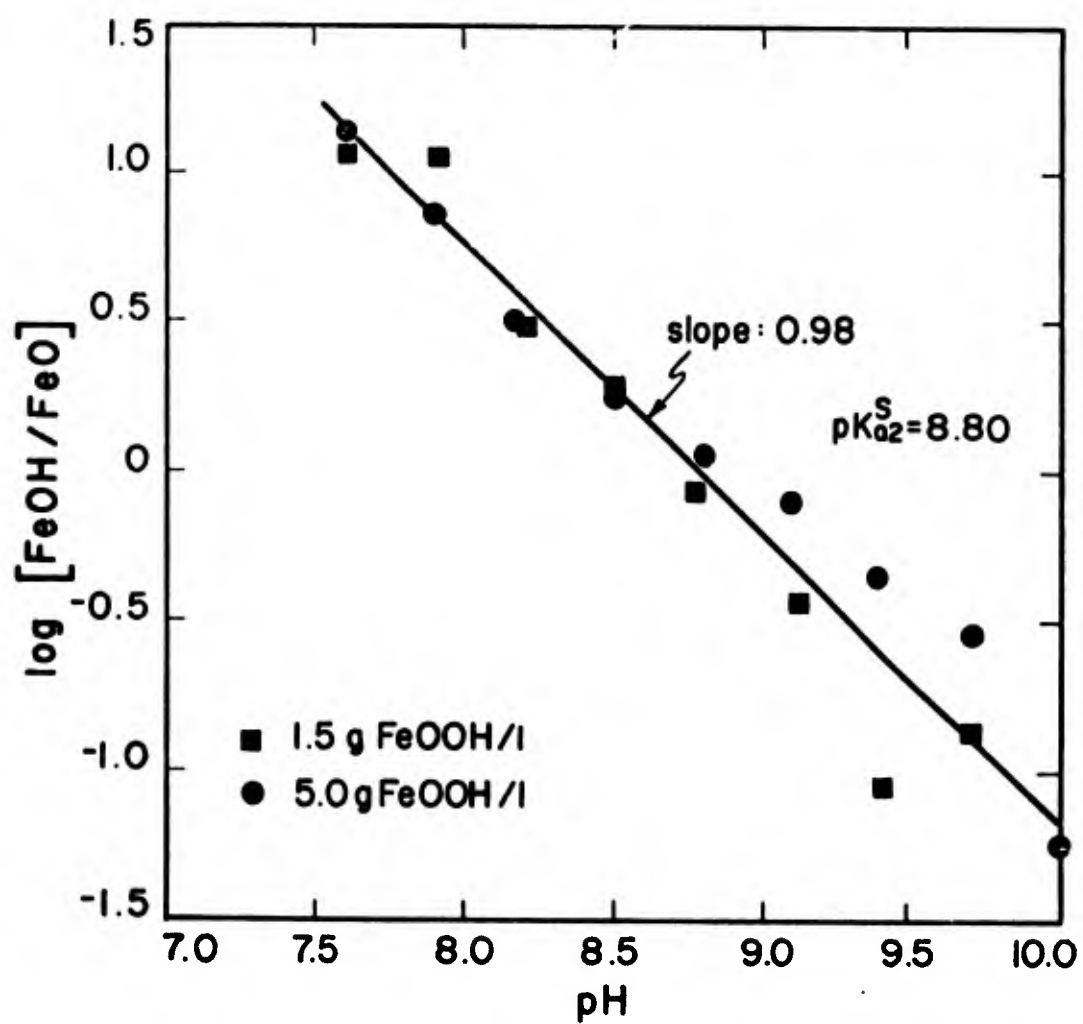
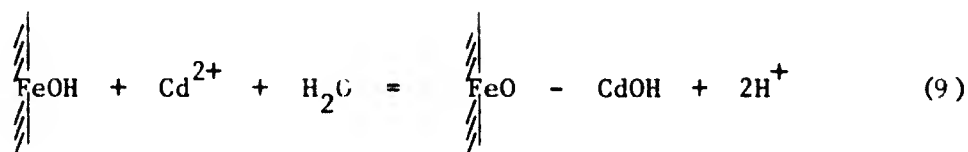


Figure 100. Ratio of singly-protonated to deprotonated surface sites on γ -FeOOH as a function of pH.

Surface site density	$pK_{a1}^S \big _{pH=5.8}$	$pK_{a2}^S \big _{pH=8.8}$	PZC
$1/100\text{\AA}^2$	5.8	8.8	7.3
$10/100\text{\AA}^2$	4.8	9.8	7.3

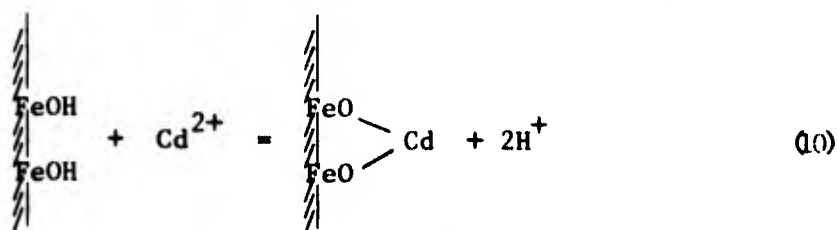
Using the values for the intrinsic acidity constants, assuming 1 site/ 100\AA^2 , it is not possible to calculate surface complexation constants for the adsorption of cadmium because more protons are released during the adsorption reaction than are calculated to be present on the entire surface.

A Combined Model. One possible explanation for the anomaly in number of protons released is that hydrolyzed cadmium species are adsorbing according to the reaction:



This would allow 2 protons to be released during adsorption of one cadmium ion, only one proton of which would originate at the surface. Such a reaction is actually a combination of the James-Healy and surface-complexation models and, while neither model has suggested such a reaction, it does not violate the basic assumptions of either.

If a surface site density of $10/100\text{\AA}^2$ is assumed, all the protons released during adsorption of cadmium can be accounted for by the reaction



Since 2 protons are released per cadmium ion adsorbed over the pH range 6.5 to 8.5, and since the fraction of doubly protonated surface sites is negligible throughout this pH range, the number of cadmium ions adsorbing to a single surface site (Eq. 7) must be negligible compared to those adsorbing according to Eq.(10). But it was shown earlier that an adsorption isotherm slope of 0.7 suggests that 6 of every 10 adsorbed cadmium ions attaches according

to reaction (7). Thus the only reaction mechanisms which can account for all the data include four unhydrolyzed Cd^{2+} ions each bonding to 2 surface oxide groups for every six hydrolyzed $\text{Cd}(\text{OH})^+$ ions attached to a single surface oxide site. Such a system requires that every adsorbed cadmium ion be bonded to two oxygen atoms, which is intuitively reasonable for an ion in a state intermediate between free solution and precipitation as the hydroxide, $\text{Cd}(\text{OH})_2$.

To summarize the analyses of the various models:

1. The James-Healy model allows for release of protons during adsorption which do not originate at the solid surface. It predicts a Langmuir-type isotherm.
2. The surface-coordination model can predict an adsorption isotherm of slope ± 1 , but cannot account for release of protons other than from the surface.
3. A combined model can account for all the observed data for adsorption of cadmium onto lepidocrocite, which neither of the models can do individually. The models can be combined in such a way that the conceptual integrity of each is maintained. Only assumptions which are peripheral to the basic concepts need be discarded.

SECTION X

EFFECT OF LIGANDS ON TRACE-METAL ADSORPTION

Ligand Adsorption on Hydrous Oxides

Literature Review. A considerable body of literature exists describing the adsorption of anions on hydrous oxides and clays. Only a few will be mentioned here to illustrate the approaches used by various research groups.

Huang (1975) uses the model of James and Healy (1972c) to describe the adsorption of phosphate from dilute solution on $\gamma\text{-Al}_2\text{O}_3$ in 0.1M NaCl. The extent of adsorption is affected by pH, surface area, and phosphate concentration. The adsorption data fit a Langmuir isotherm and the maximum monolayer capacity is of the same order of magnitude as that observed for gibbsite (Mujaldi, Posner, and Quirk, 1965) and amorphous $\text{Al}(\text{OH})_3$ (Hsu and Rennie, 1962). H_2PO_4^- and HPO_4^{2-} are assumed to be the major solution species involved in the surface reactions. The best fit of the model to the experimental data is obtained with a specific free energy term (ΔG chemical) of -3.8 kcal/mole. No attempt is made to describe the mechanism of the adsorption reaction.

Hingston et al. (1967) show that the adsorption of anions correlates with the pK_a values of the anion acids. A linear relationship is found for the pK_a values of weak acids and the pH of observed inflections in the slope of adsorption curves for orthophosphate, pyrophosphate, tripolyphosphate, selenite, silicate, and fluoride. The isoelectric point (IEP) is shifted to more acid values because of the adsorption of anions. The adsorption reaction is viewed as a ligand exchange reaction; a coordinated hydroxyl or water molecule is displaced from the surface. The relationship between anion adsorption and release of hydroxyl is not simple. If the anion is polyprotic, it appears that more than one of the acid-base forms can adsorb. In many cases released hydroxyl ions are not detected in solution, and the authors attribute this to an accompanying proton release from the anion. The bonding of the adsorbed molecule thus directly involves a metal atom of the metal oxide.

Many infrared studies have been undertaken to determine the bonding of adsorbed molecules. Groenewegen and Sachtler (1974) show that the strength of adsorption bonds for a series of amino acids depends on the position of the amino group with respect to the carboxylic group. From the location of the $\text{C}=\text{O}$ stretching frequencies the authors conclude that two types of

adsorption complex exist, a surface ester and a hydrogen-bonded complex:



The surface ester is formed by the elimination of a water molecule from the hydrogen-bonded complex. Little (1966) and Eyring and Wadsworth (1956) present IR evidence that water is eliminated during adsorption reactions.

Han, Healy, and Fuerstenau (1973) question the applicability of these findings to the bonding mechanisms of interfacial reactions that occur in aqueous solution. These authors feel that the preparation of the sample (dehydration, etc.) influences the bonding of the adsorbed species. Therefore, it is difficult to ascertain whether the bonding mechanisms determined by IR spectrometry are identical to those in aqueous solution.

Han, Healy, and Fuerstenau (1973) use microelectrophoresis to determine the effect of adsorbed saturated and unsaturated fatty acids on the zeta potential of iron and aluminum oxides. The results show that there are three types of adsorption: a) non-specific physical adsorption, b) chemical specific adsorption, and c) hydrophobic specific adsorption. Simple physical adsorption occurs when the only adsorption energy is the coulombic attraction of ions from solution to an oppositely charged surface. Chemical specific adsorption causes a shift in the isoelectric point (IEP) of the oxide. Hydrophobic specific adsorption occurs only when surface coverage reaches a certain density (the hemi-micelle concentration) such that a lowering of the free energy of the system occurs by the aggregation or condensation of the alkyl chains at the interface. After this phenomenon occurs a charge reversal may result; however, at lower concentrations there is no effect on the IEP. The authors believe that the dehydration of samples for infrared analysis may provide ambiguous results because of this hydrophobic effect.

The type of bonding that occurs when ligands adsorb at oxide interfaces has not been adequately described by current experimental methods.

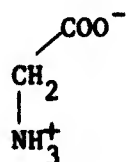
Study of cation adsorption has reached the same point of development. Significant advances in the field of interfacial chemistry will be made when techniques are developed that allow an examination of surfaces of particles without removal from solution.

Adsorption of Ligands on Amorphous Iron Oxide. The adsorption of several ligands on amorphous iron oxide has been studied experimentally as a function of pH and total ligand concentration. All experiments are conducted at 25°C in either 0.1M NaNO₃ or 0.1M NaClO₄.

Figure 101 shows the adsorption of sulfate on amorphous iron oxide for total sulfate concentrations of 10⁻³M and 10⁻⁵M. The adsorption curves show little evidence of specific adsorption since adsorption approaches zero at pH 8 even for a sulfate concentration of 10⁻⁵M. The low percent adsorption of sulfate at 10⁻³M indicates that adsorption may be approaching high surface coverage. Adsorption approaches quantitative removal of sulfate at pH 4 with total sulfate of 10⁻⁵M. Thus, the coulombic interaction must be large between the positively charged surface and the negative charge on sulfate.

Figure 102 displays a similar adsorption behavior for thiosulfate. Little specific interaction is observed. The extent of adsorption is apparently independent of total thiosulfate concentration in very dilute solution. This is to be expected if the interaction at the surface is primarily related to coulombic interaction. The strength of the interaction is diminished when compared to that of sulfate since higher removals of sulfate are observed even at higher sulfate concentrations. This may be a result of chemical or geometrical differences between the adsorbed species that allow greater net coulombic attraction for sulfate than for thiosulfate.

An investigation of the adsorptive behavior of glycine shows that it does not adsorb on amorphous iron oxide. In the mid-pH region, glycine exists primarily as the zwitterion with localized charge on the carboxyl and amino groups:



glycine in mid-pH region

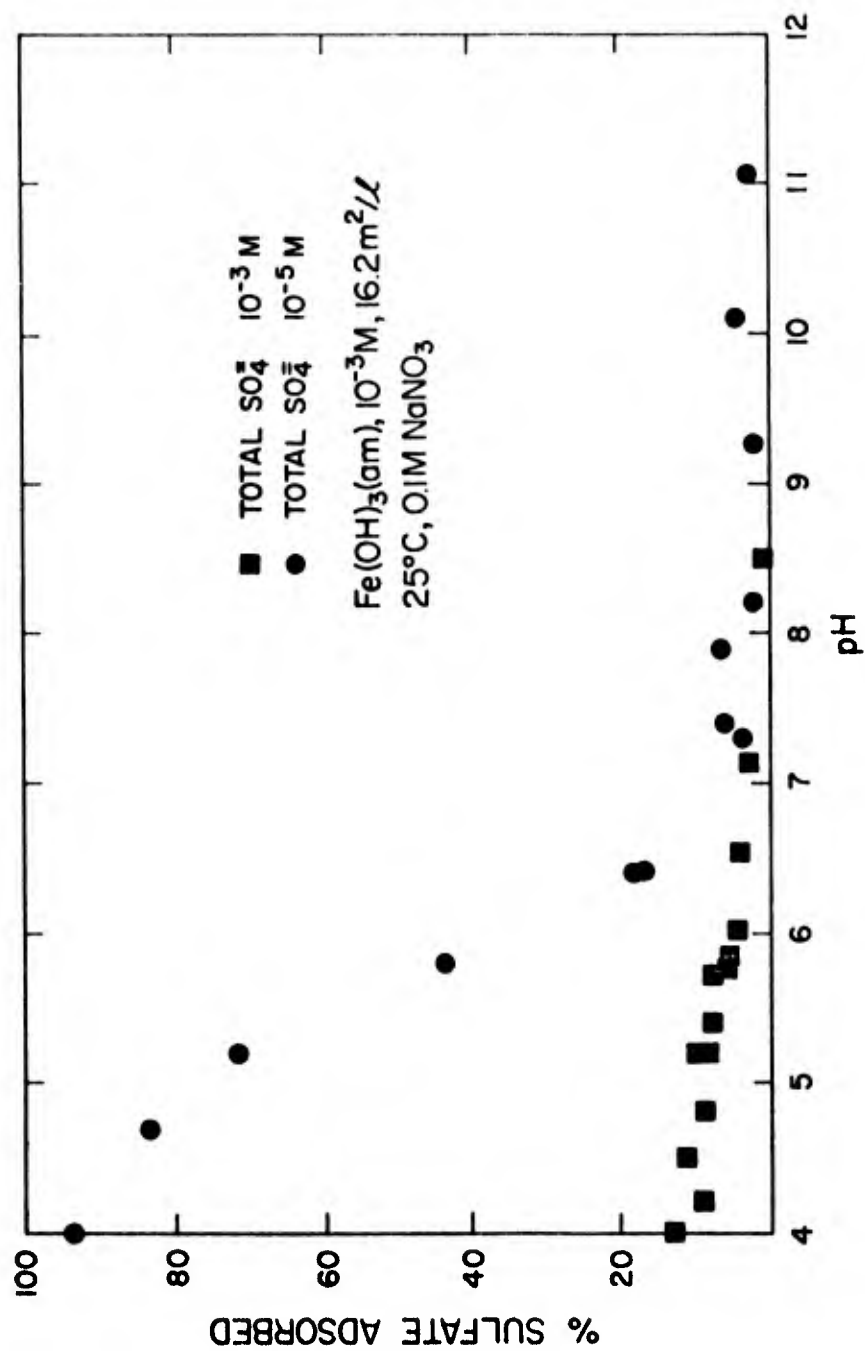


Figure 101. Adsorption of sulfate on amorphous iron oxide as a function of pH and total sulfate concentration.

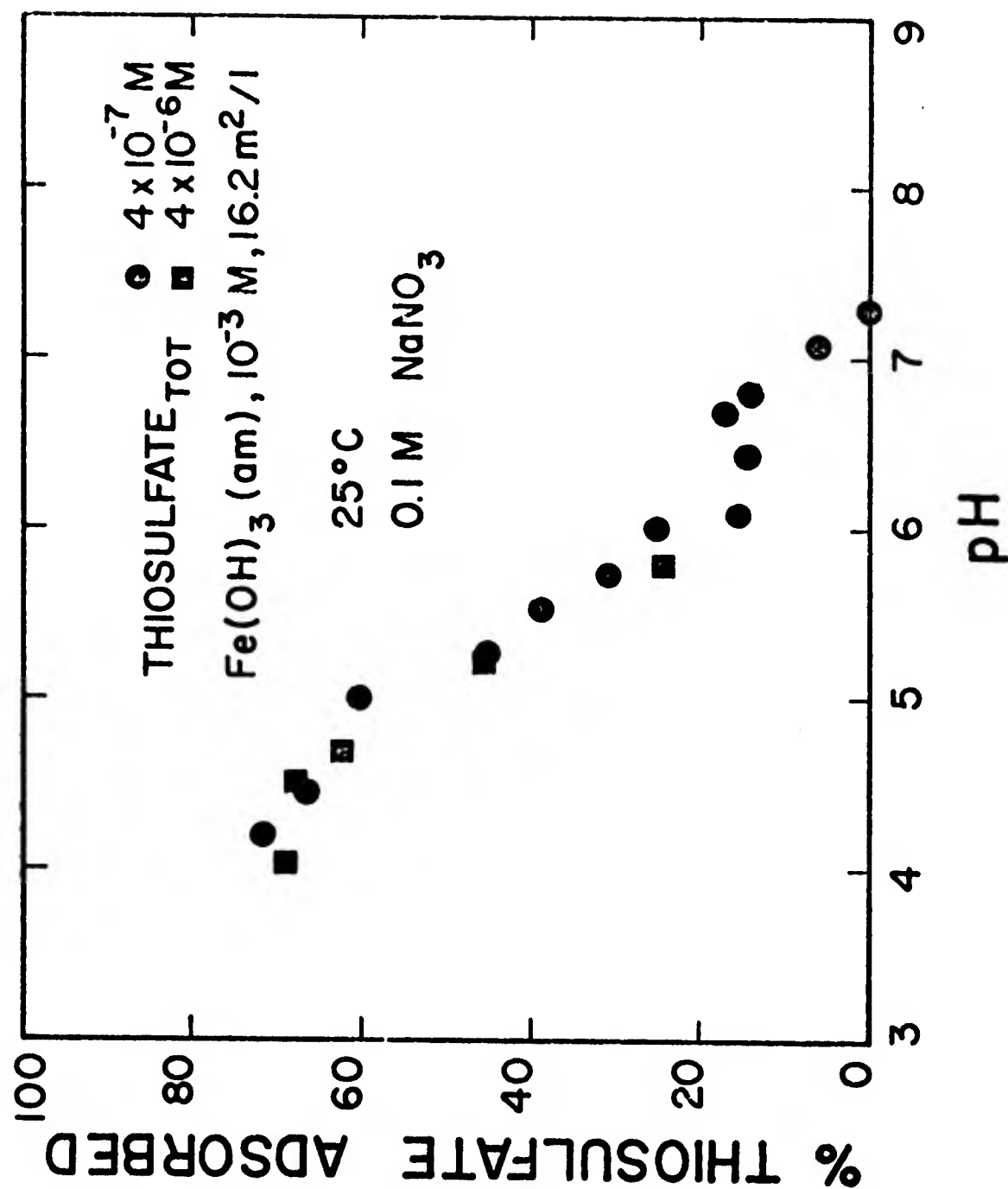


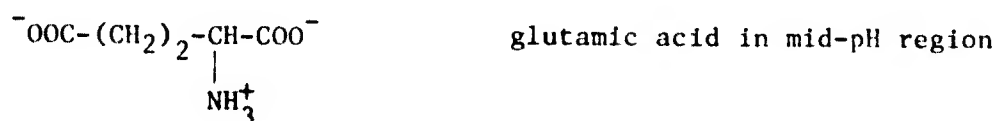
Figure 102. Adsorption of thiosulfate on amorphous iron oxide as a function of pH and total thiosulfate concentration.

Apparently the iron oxide has little affinity for the zwitterion, either coulombically or chemically. Less than 3% adsorption of glycine is observed in the pH region 4-10 for concentrations as low as 10^{-6} M glycine. This is in qualitative agreement with the results of Sridharan and Lee (1972) who find the following trends in co-precipitation of trace glycine with ferric chloride:

<u>total glycine concentration</u>	<u>pH</u>	<u>% glycine co-prec.</u>
5.5×10^{-8} M	9	32
1.1×10^{-7} M	9	29
2.2×10^{-7} M	9	9
1.1×10^{-7} M	6	20
1.1×10^{-7} M	8	23
1.1×10^{-7} M	10	27

Note that the co-precipitation decreases significantly to less than 10% for a total glycine concentration of 2.2×10^{-7} M at pH 9, the pH of maximum glycine removal.

The adsorption of glutamic acid on amorphous iron oxide is shown in Figure 103. Glutamic acid adsorption is strikingly similar to sulfate adsorption behavior. Very little specific interaction is observed and the coulombic attraction is roughly the same for each ion. The adsorption reaction occurs such that the terminal carboxyl group is involved in the surface bond formation.



This can be inferred from the results of the glycine experiments which show that there is little attraction of the iron oxide for the zwitterion.

The adsorption of syringic acid on amorphous iron oxide is illustrated in Figure 104. The extent of adsorption is considerably weaker than that observed for other ligands. Specific adsorption does not occur. There is a break in the adsorption curve near the pK_a (4.3) of syringic acid, in agreement with the correlation observed by Hingston et al. (1967). The acidity constants for syringic acid and the terminal carboxyl group on glutamic acid are very close in value. However, the negative charge for syringic acid

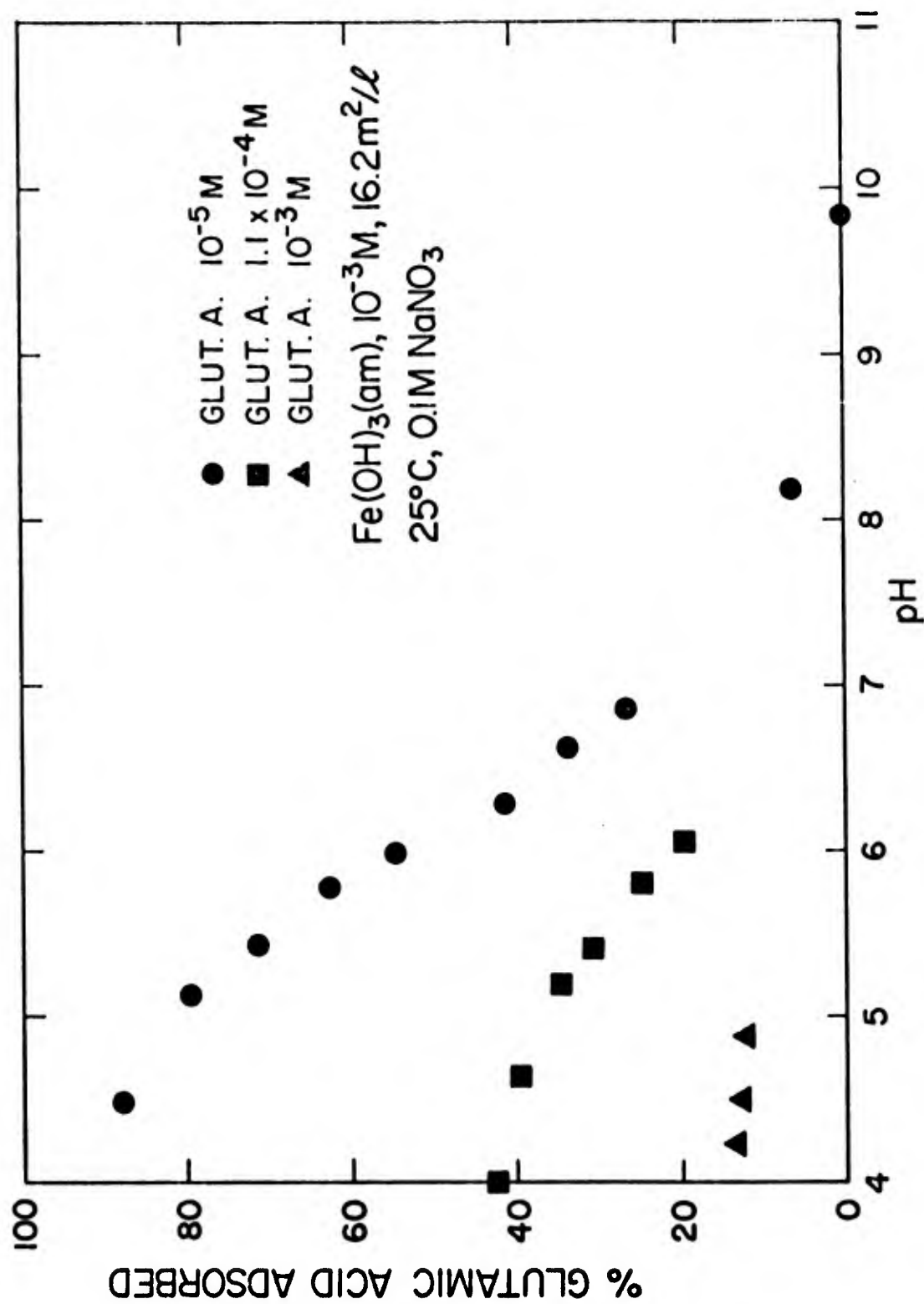


Figure 103. Adsorption of glutamic acid on amorphous iron oxide as a function of pH and total glutamic acid concentration.

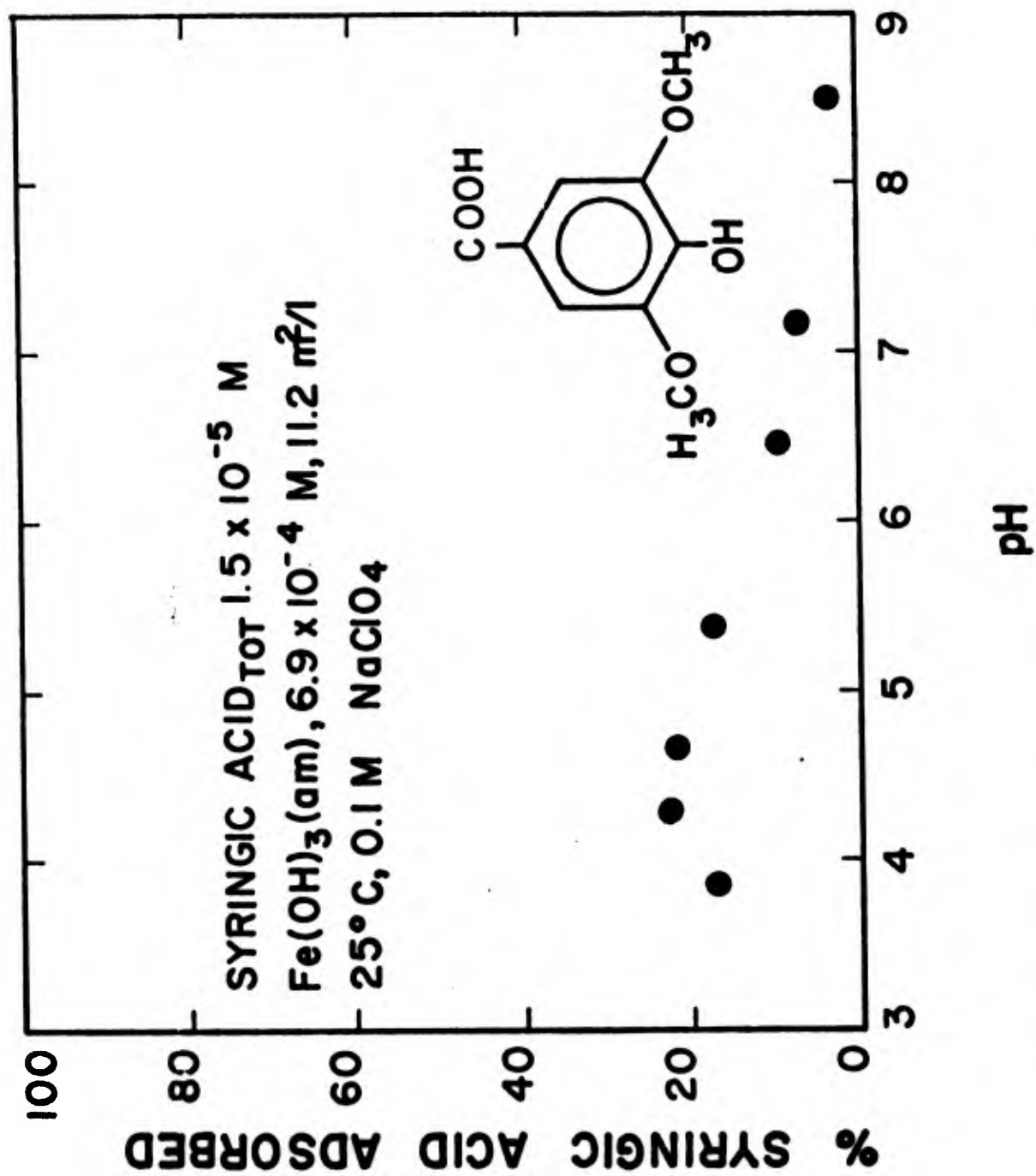
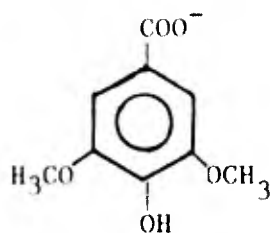


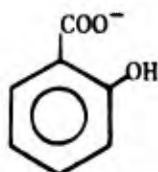
Figure 104. Adsorption of syringic acid on amorphous iron oxide as a function of pH.



syringic acid in mid-pH region

is distributed throughout the entire aromatic system. Thus, the net coulombic interaction should be less for syringic acid than for glutamic acid. Syringic acid is probably prevented from aligning parallel to the surface because of the substituent groups. This may explain the decreased intensity of interaction observed for syringic acid.

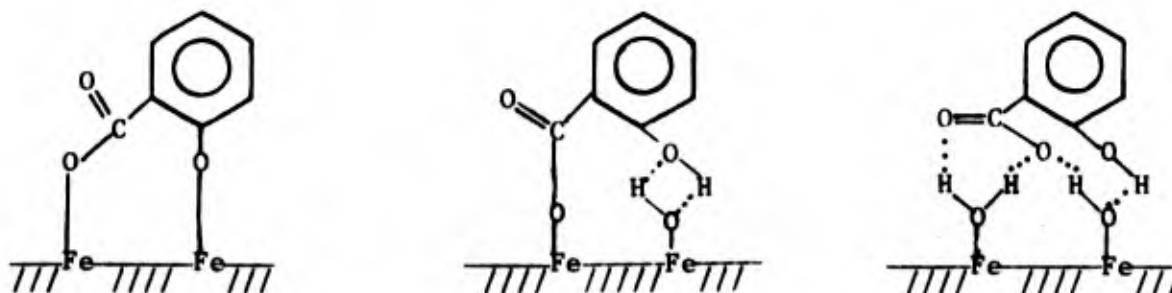
Figure 105 shows the adsorption of salicylic acid on amorphous iron oxide as a function of pH and total salicylic acid concentration. Salicylic acid shows a slight amount of chemical interaction, but the coulombic



salicylic acid in mid-pH region

attraction appears to dominate the adsorption behavior. The beta hydroxyl increases the acidity of the carboxylic group (pK_a 3.0), but the acidity of the phenolic group is significantly less (pK_a 13.0). Thus, the electrical charge is distributed throughout the aromatic system with some charge on both the carboxyl and phenolic oxygens. This enhances the ability of salicylic acid to form hydrogen-bonded arrangements and/or surface esters:

Possible bonding arrangements for adsorbed salicylic acid



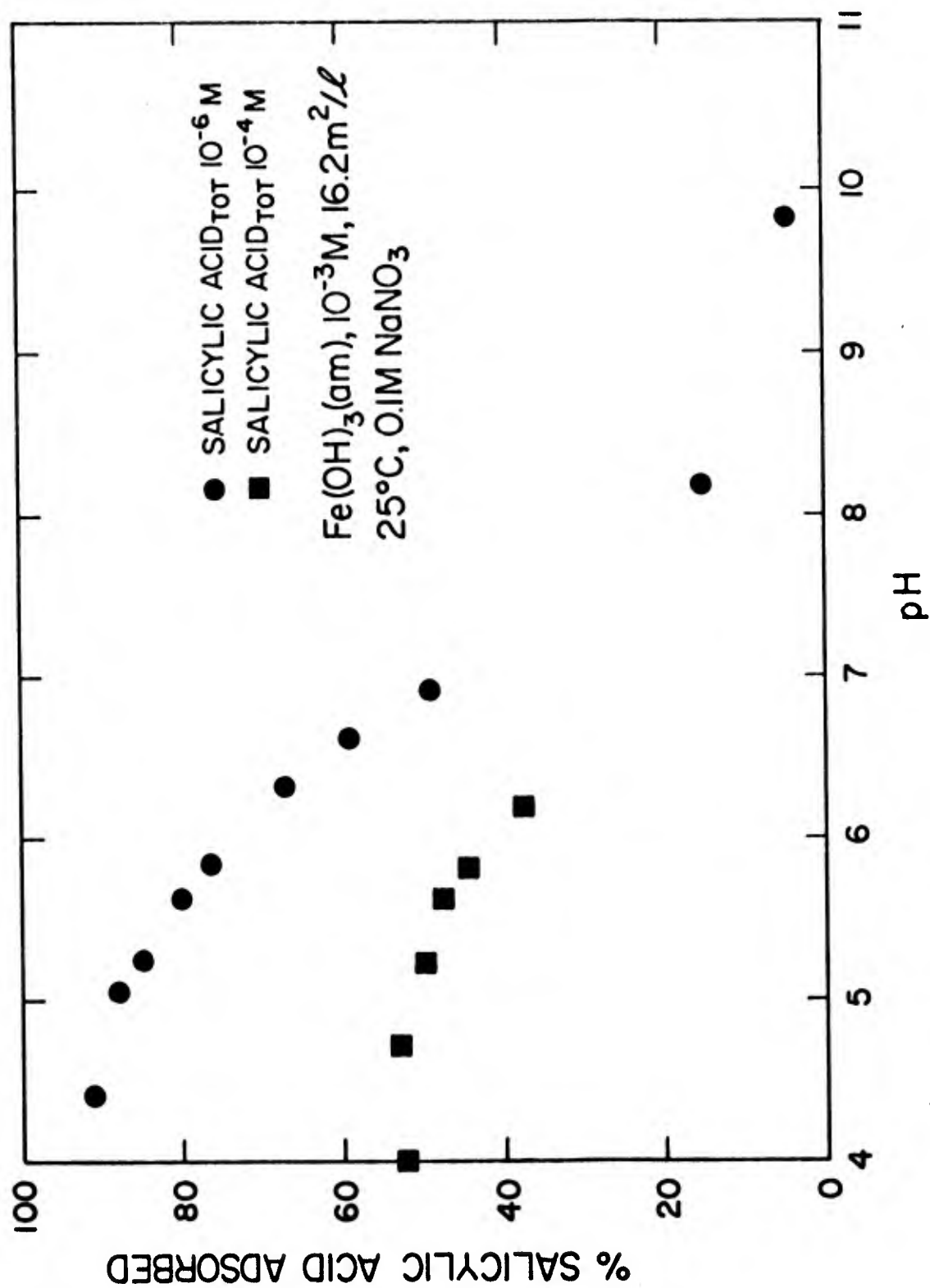
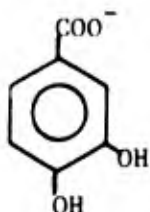


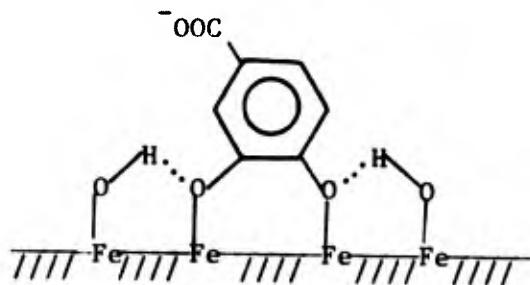
Figure 105. Adsorption of salicylic acid on amorphous iron oxide as a function of pH and total salicylic acid concentration.

The adsorption of protocatechuic acid on amorphous iron oxide is displayed in Figure 106. Protocatechuic acid shows specific adsorption over a large pH range, and the bonding of the surface interactions must be radically different from that discussed for previous ligands. Transition metal ions



protocatechuic acid in mid-pH region

form stronger complexes with catechol than with salicylic or phthalic acids so the binding power of the two adjacent phenolic oxygens must be considerable. The surface interaction must be either a strong specific chemical interaction or a strong physical interaction such as that observed in the hydrophobic interactions of adsorbed fatty acids. The following is a possible bonding scheme that would produce a strong chemical surface interaction:



Two water molecules would be liberated by the removal of two hydroxyls from the surface iron atoms and removal of two phenolic hydrogens. Slight changes in slope are observed near the carboxylic pK_a (4.4) and the most acidic phenolic pK_a (8.7). The adsorption intensity decreases at higher pH as the surface and the molecule become more negatively charged.

Figure 107 illustrates the adsorption of picolinic acid on amorphous iron oxide. The intensity of adsorption is similar to that observed for glutamic acid and sulfate. There is little evidence of specific interaction. There appears to be an inflection point near the pK_a (5.2) of the carboxylic group as predicted by the correlation observed by Hingston et

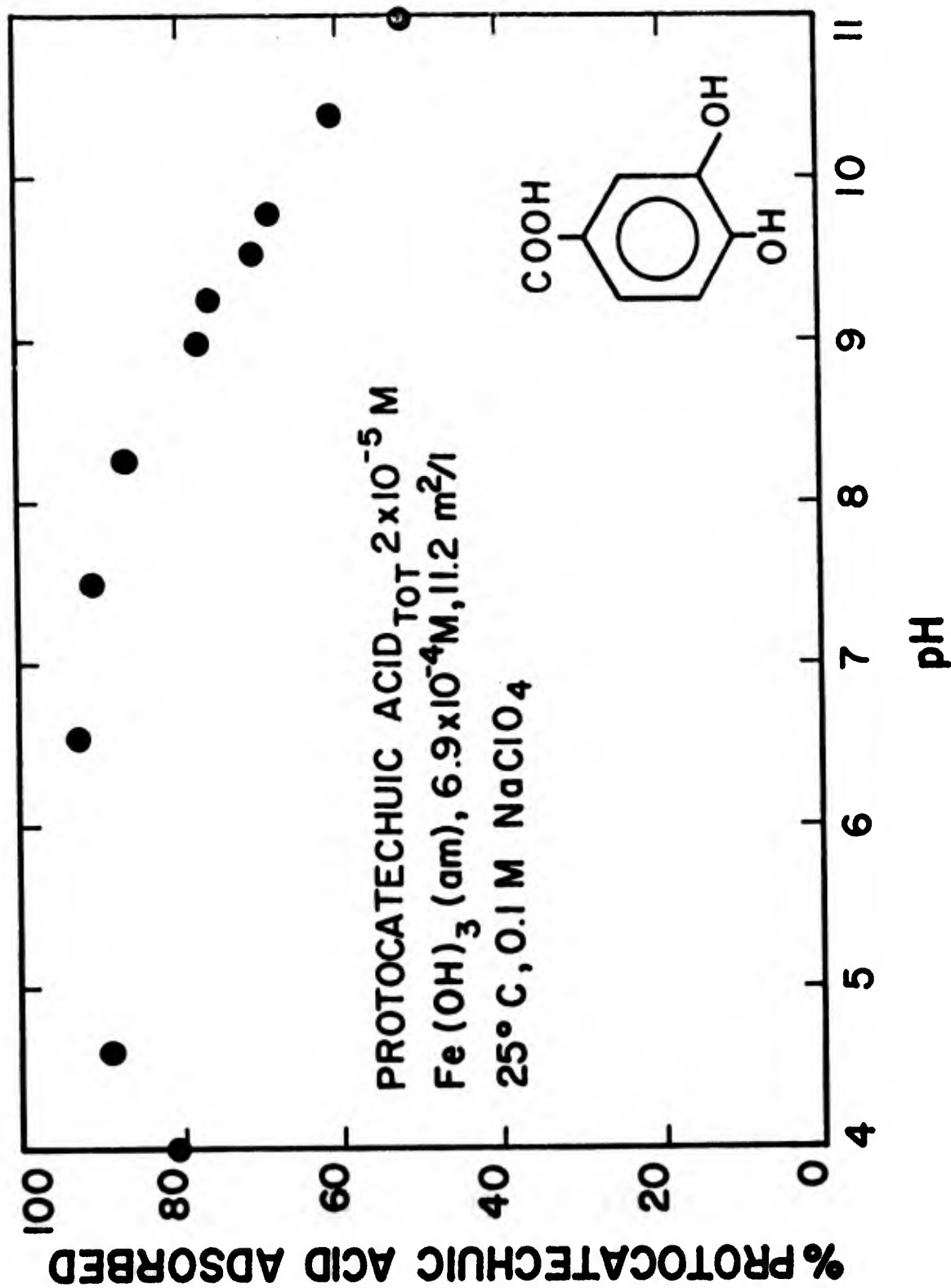


Figure 106. Adsorption of protocatechuic acid on amorphous iron oxide as a function of pH.

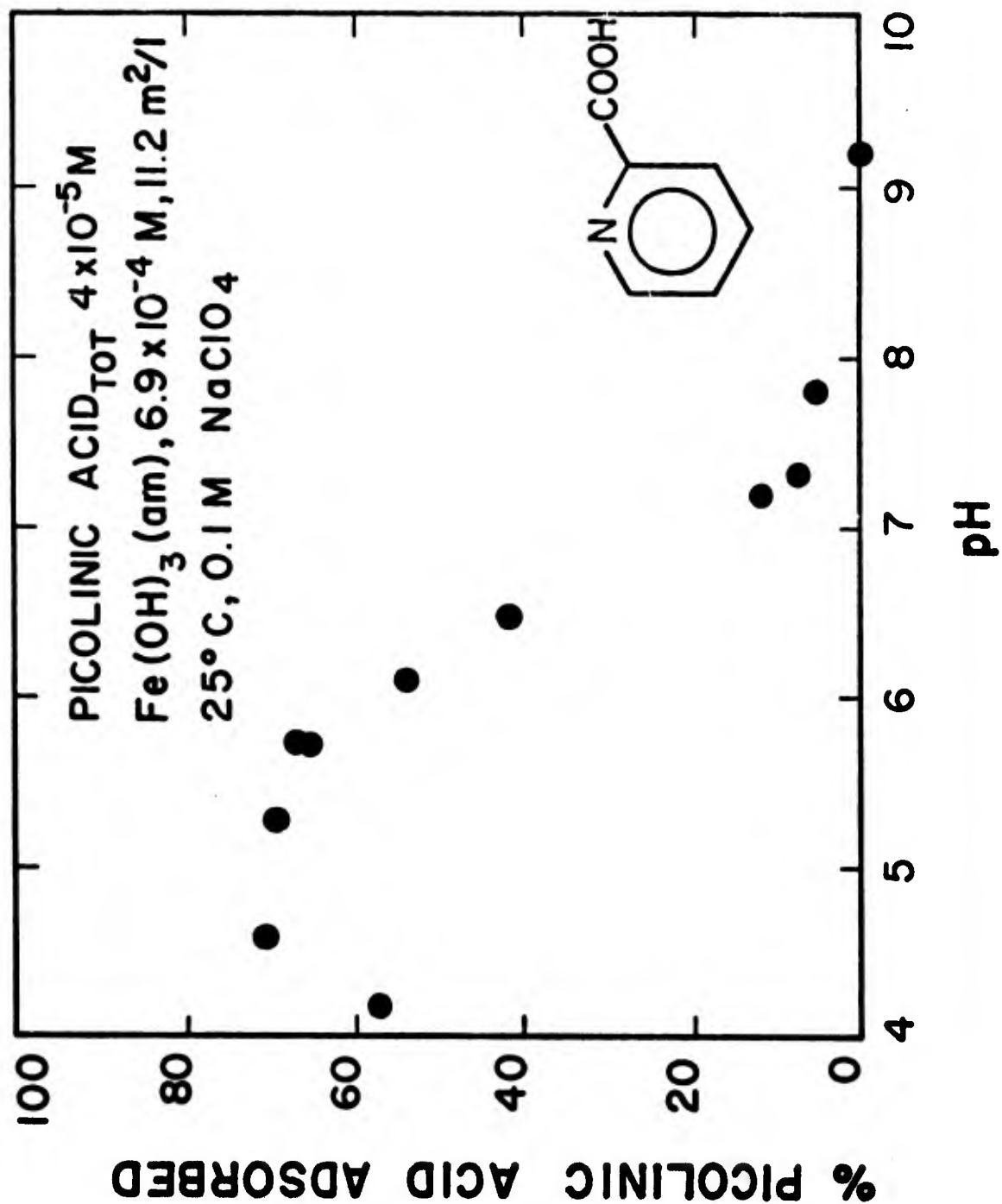
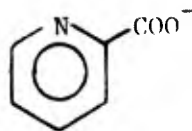
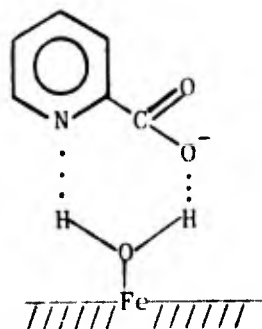


Figure 107. Adsorption of picolinic acid on amorphous iron oxide as a function of pH.



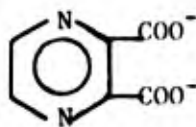
picolinic acid in mid-pH region

al. (1967). The free energy of adsorption must be primarily coulombic in nature; some slight hydrogen-bonding contribution is possible:



One important point is that the surface-bonding scheme undoubtedly involves the electrons from the carboxyl and the nitrogen heteroatom in some fashion. As a result an adsorbed picolinic acid molecule will have weak trace metal complexation capability since both ligand sites are occupied.

Adsorption of 2,3-pyrazinedicarboxylic acid (2,3-PDCA) on amorphous iron oxide is shown in Figure 108. The adsorption behavior is similar to other



2,3-PDCA in mid-pH region

ligands in that no specific interaction is observed. However, the decrease in adsorption from its maximum to zero adsorption is comparatively steep. This may be an indication that the two negatively charged carboxyl groups are facing the surface.

Adsorption of Ligands on α -Quartz. The adsorption of histidine and ammonium ions in 0.1M NaNO_3 on quartz has been investigated but no adsorption is observed for either ligand in the pH region 3-9. Total concentrations of ligands in the experiments were 10^{-5}M and 10^{-4}M for histidine and

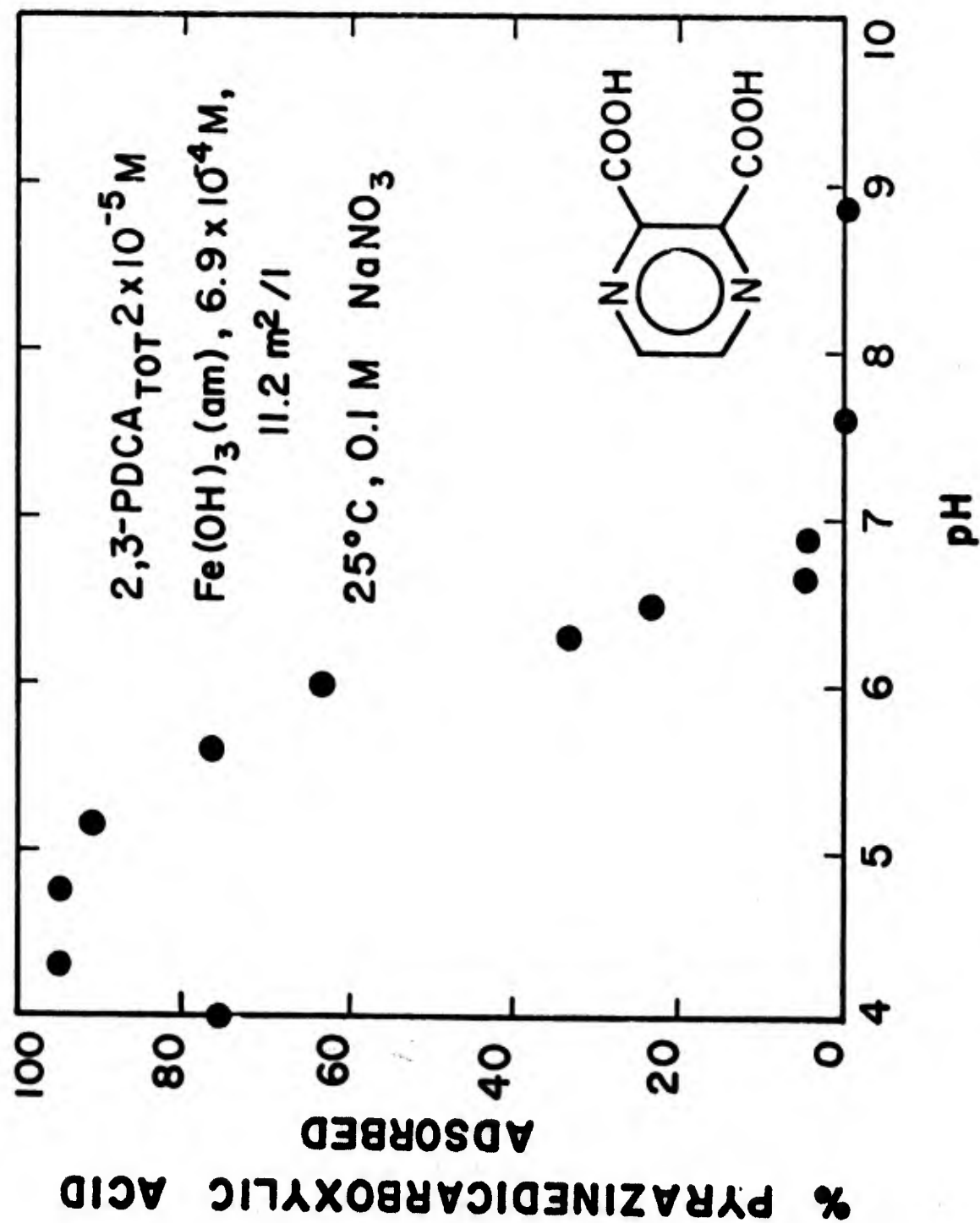


Figure 108. Adsorption of 2,3-pyrazinedicarboxylic acid on amorphous iron oxide as a function of pH.

ammonia, respectively. A surface area of $82.5 \text{ m}^2/\text{g}$ of quartz was used in the experiments.

Adsorption of Silver on Amorphous Iron Oxide and α -Quartz in Systems Containing Ligands

All silver adsorption experiments in systems containing ligands were conducted in the dark to avoid photoreduction of silver. A total silver concentration of $4 \times 10^{-7} \text{ M}$ and ionic medium of 0.1 M NaNO_3 is present in all experiments.

Figure 109 shows the adsorption of silver on amorphous iron oxide as a function of pH and various chloride concentrations. Silver chloride precipitation should not occur at these solution conditions (see Figure 50). Moderate concentrations of chloride have little effect on the adsorption behavior of silver. At a chloride concentration of $9.4 \times 10^{-2} \text{ M}$, the predominant silver solution species is AgCl_2^- . Silver does not adsorb significantly for $\text{pH} < 9$ with this chloride concentration. The hydrolysis products of silver become significant only at $\text{pH} > 11$. Since the increase in adsorption continues until pH 12 in $9.4 \times 10^{-2} \text{ M}$ chloride, a hydrolysis product of silver (AgOH) may be involved in the surface reaction in alkaline solutions. It is unlikely that AgCl^0 is an adsorbing species. Several transition metals are desorbed by high chloride concentrations (MacNaughton and James, 1974).

Adsorption in the presence of glutamic acid, salicylic acid, and cyanide is displayed in Figure 110. A trace concentration of cyanide effectively prevents silver adsorption when $\text{pH} > 7$. The stability of the silver cyanide complex, $\text{Ag}(\text{CN})_2^-$, is large, and this should be the predominant silver solution species, even at trace concentrations of silver and cyanide. No experiments are conducted for $\text{pH} < 7$ since equilibrium calculations indicate the formation of $\text{HCN}(\text{aq})$ and $\text{HCN}(\text{g})$.

Salicylic acid (10^{-6} M) has little effect on silver adsorption. Salicylic acid is probably a weak complexer of silver. No stability constants are found in the literature. Greater than 50% of the salicylic acid is adsorbed when $\text{pH} < 7$ (Figure 105), but silver adsorption remains the same. A slight decrease in silver adsorption due to complexation is possible for $\text{pH} > 8$ where little salicylic acid is adsorbed.

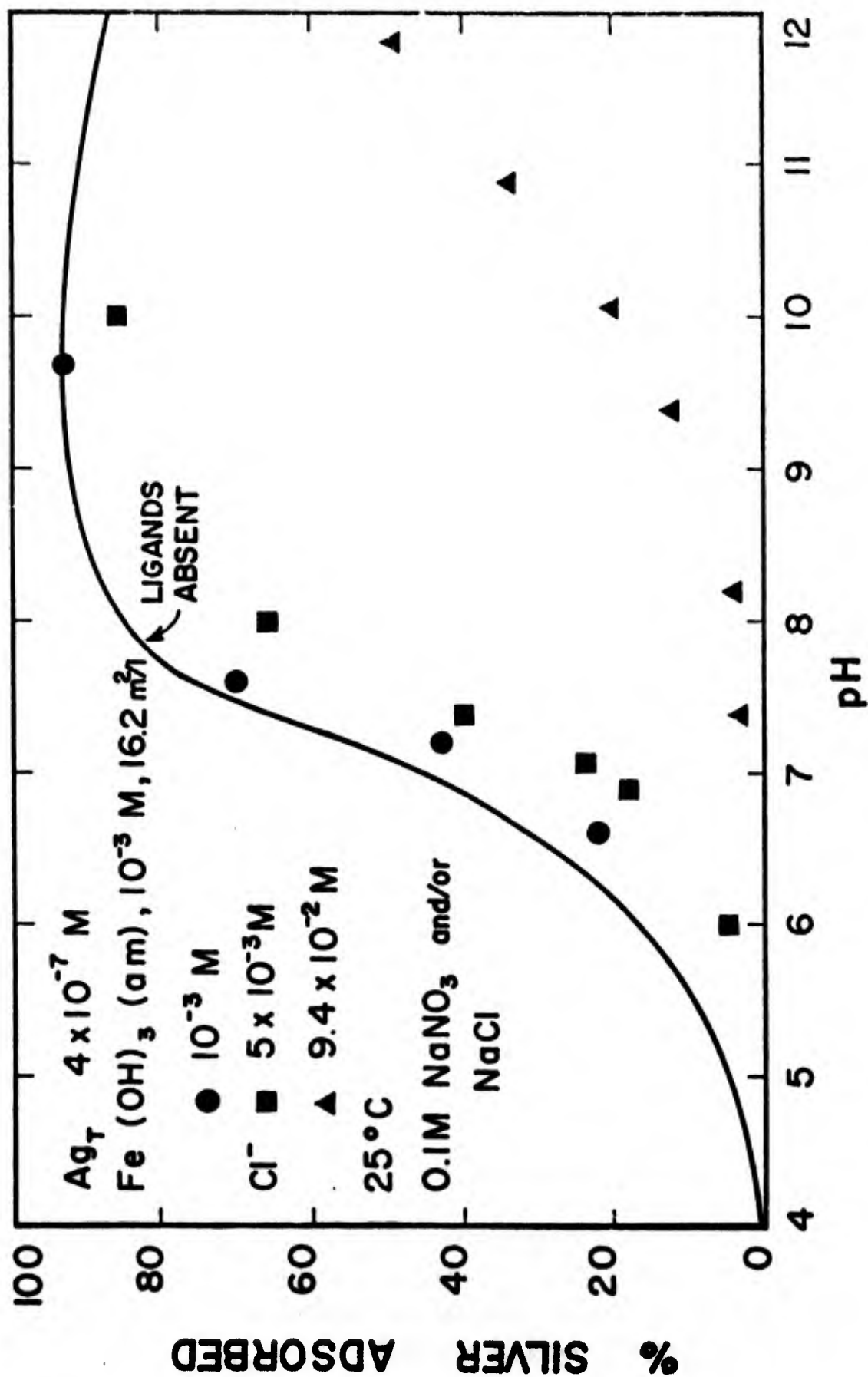


Figure 109. Adsorption of silver on amorphous iron oxide as a function of silver and chloride concentration.

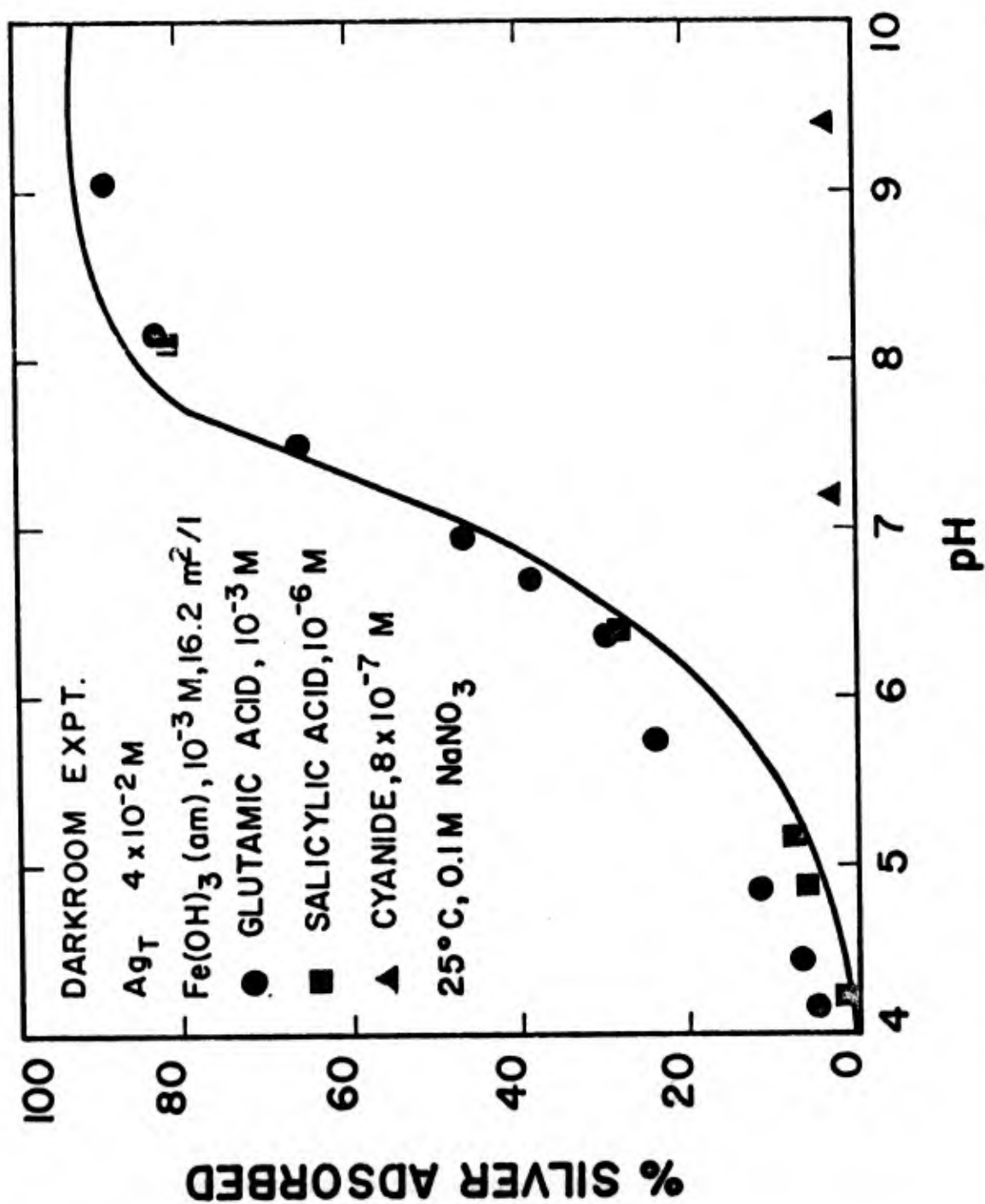
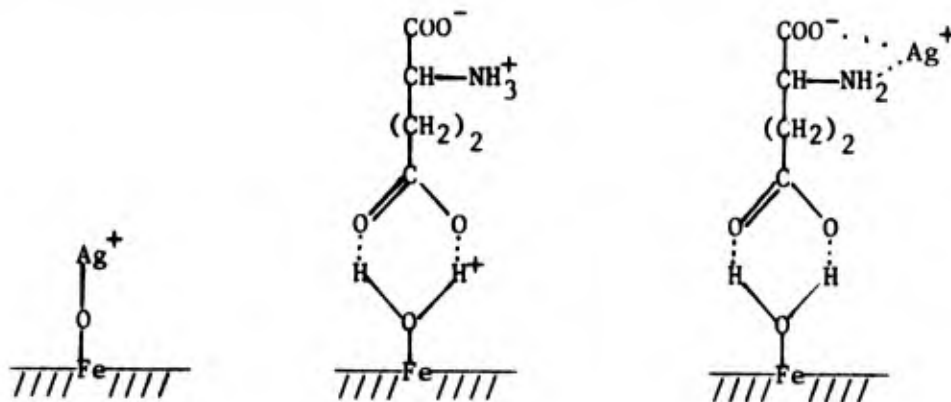


Figure 110. Adsorption of silver on amorphous iron oxide as a function of pH in the presence of glutamic acid, salicylic acid, and cyanide.

The presence of 10^{-3}M glutamic acid affects silver adsorption slightly. Silver adsorption is increased in the pH region 4-6.5. Approximately 10^{-4} moles glutamic acid are adsorbed in this pH region (Figure 103). The adsorbed glutamic acid may increase silver adsorption by lowering the surface charge on amorphous iron oxide. The coulombic term for silver is repulsive in this pH region. However, it is possible that the surface charge is not affected by the adsorbed glutamic acid since a ligand exchange reaction with adsorbed nitrate cannot be ruled out. An alternate hypothesis for increased silver adsorption concerns the complexation of silver by adsorbed glutamic acid. Silver forms complexes of moderate strength with the zwitterion functional groups. These functional groups should still be available for complexation since the terminal carboxyl group of glutamic acid is involved in its surface reaction. Thus, silver may adsorb as an ion or by complexing with an adsorbed glutamic acid molecule:

Adsorbing species in silver (I)/glut. acid/iron oxide system



An alternate reaction scheme is that the silver-glutamate complex forms in solution first and then adsorbs. The two hypotheses are thermodynamically indistinguishable.

Figure 111 illustrates the effect of sulfate and tellurate on silver adsorption. Sulfate (10^{-3}M) has a smaller effect on silver adsorption than glutamic acid (Figure 110). The adsorption behavior of sulfate is similar to glutamic acid. If silver adsorption is increased by coulombic effects of these adsorbed ligands, then sulfate should have a greater effect on silver adsorption than glutamic acid. The small effect of sulfate on silver

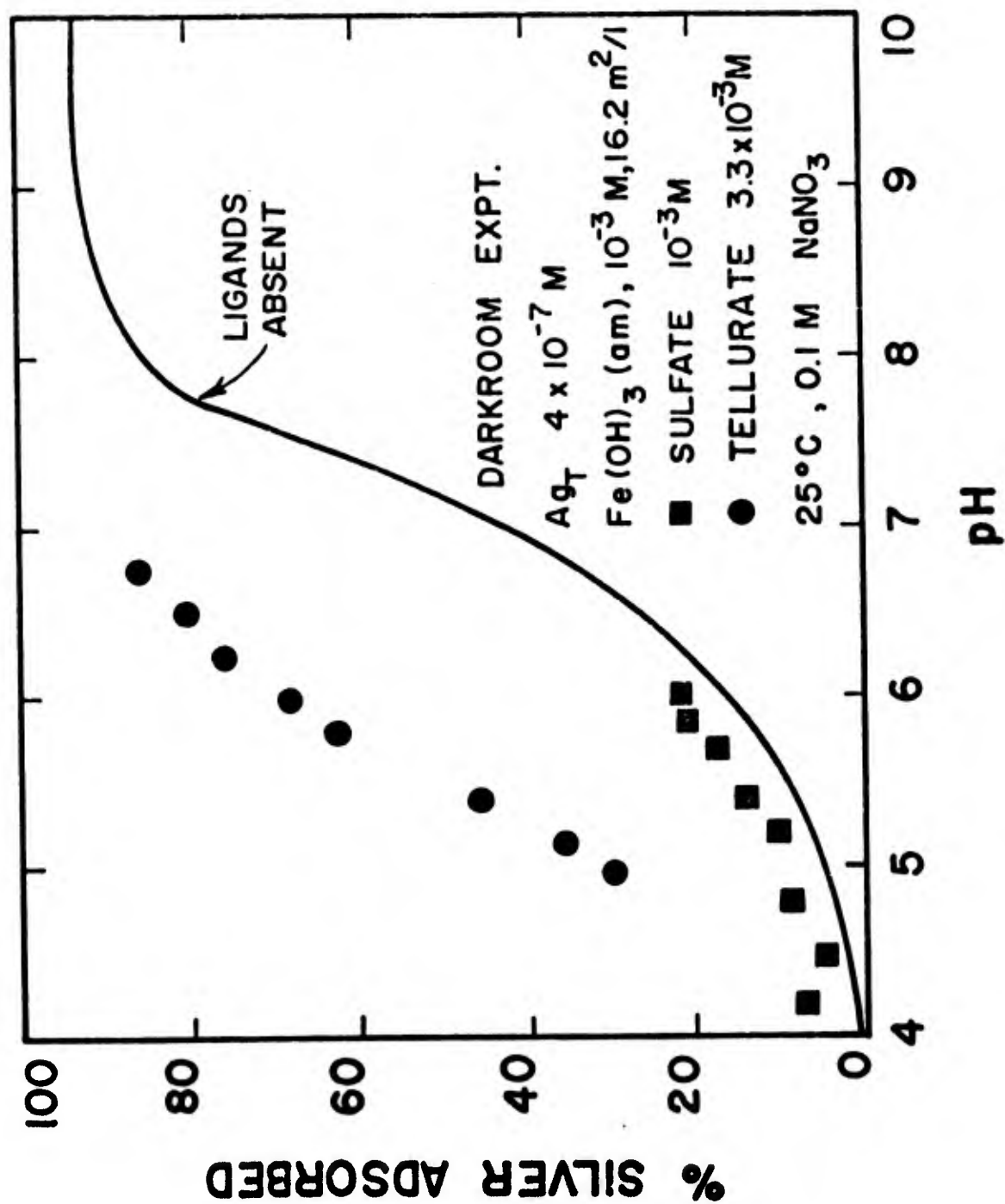


Figure 111. Adsorption of silver on amorphous iron oxide as a function of pH in the presence of sulfate and tellurate.

adsorption favors the surface complexation argument since silver forms weak sulfate complexes.

The effect of tellurate is not well understood at present because the adsorption of tellurate has not been determined. It is known that the adsorption of tellurate is accompanied by a significant release of protons but the release has not been determined quantitatively. Telluric acid is a weak acid (pK_{a1} , 6.2; pK_{a2} , 7.8), and probably is adsorbed strongly on amorphous iron oxide. No information has been found in the literature on the stability of silver-tellurate complexes or the solubility of silver tellurate. The observed increase in silver removal is probably due to the formation of silver tellurate bonds on the surface of iron oxide. This would presumably occur by the strong chemisorption of a stable silver-tellurate complex or surface precipitation of silver tellurate.

Silver forms strong complexes with thiosulfate. In solutions containing $4 \times 10^{-7}M$ total silver concentration and an equal total thiosulfate concentration, approximately 90% of each is complexed as $AgS_2O_3^-$. The adsorption of silver as a function of pH and thiosulfate concentration is shown in Figure 111. Adsorption of silver is dramatically increased in the pH region 4-6.5 and decreased for $pH > 7$ in the presence of thiosulfate. Moreover, an increase in thiosulfate concentration magnifies the observed effects. Nearly quantitative removal of silver occurs at pH 4 for a total thiosulfate concentration of $4 \times 10^{-6}M$. The adsorption of silver for $4 < pH < 6.5$ closely parallels the adsorption of thiosulfate in Figure 101. Clearly the increased adsorption of silver is related to the adsorption of thiosulfate.

Figure 112 displays the adsorption of silver and thiosulfate on amorphous iron oxide in the system containing $4 \times 10^{-7}M$ total silver and an equal concentration of total thiosulfate. In the pH region 4.5-6.5 the amount of silver adsorbed is equal to the amount of thiosulfate adsorbed. Thiosulfate adsorption is slightly greater than in the absence of silver. Since the predominant solution species for silver and thiosulfate is $AgS_2O_3^-$, the best explanation for the observed behavior is the adsorption of the silver-thiosulfate complex. The strength of the interaction is roughly equal to the coulombic term for thiosulfate. Adsorption of the silver-thiosulfate complex occurs by the attraction of the negatively charged complex to the positively charged surface. As pH increases and the positive charge

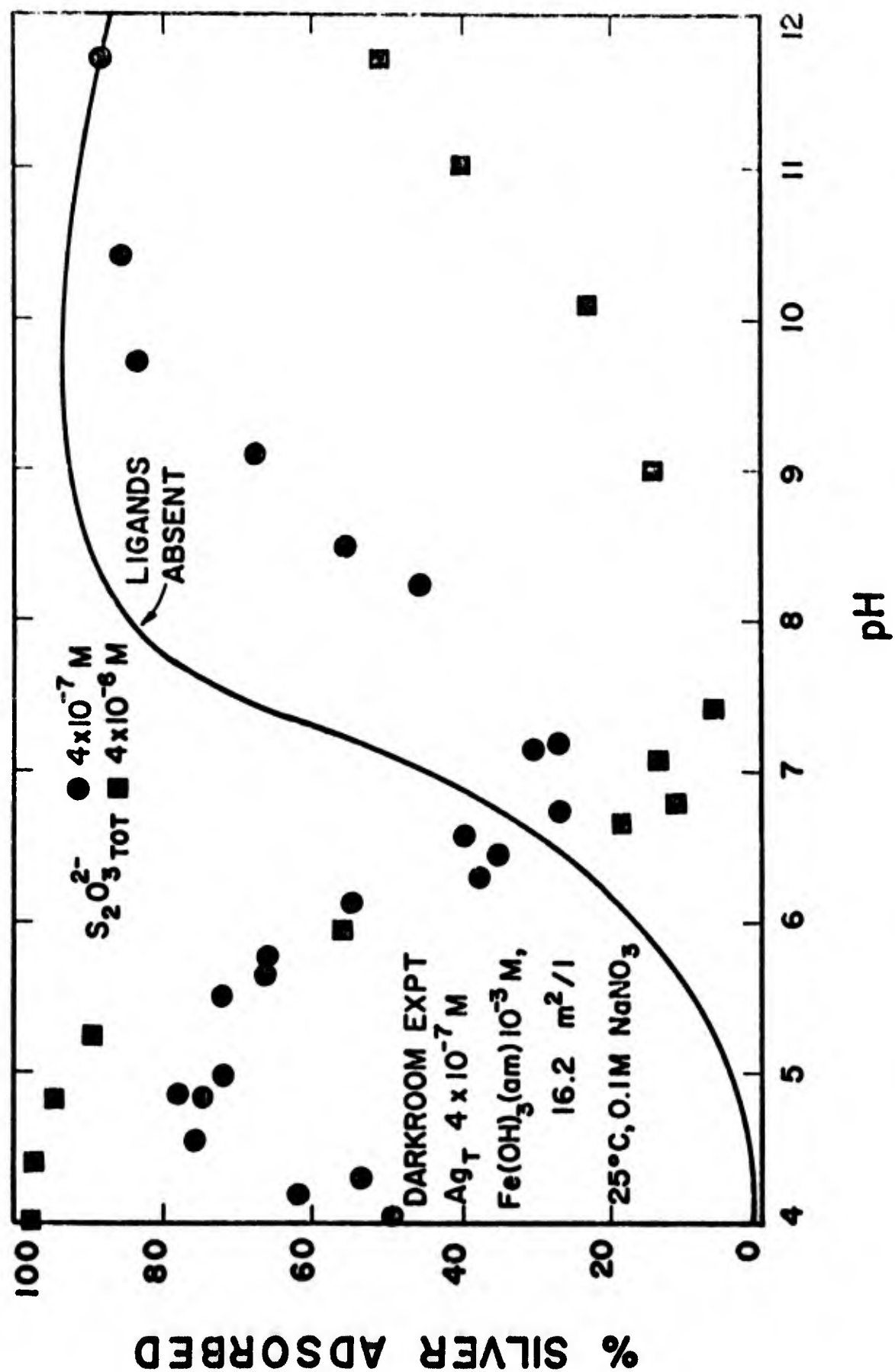


Figure 112. Adsorption of silver on amorphous iron oxide as a function of pH and total thiosulfate concentration.

decreases on the surface, adsorption of silver thiosulfate decreases to zero near pH 7.5.

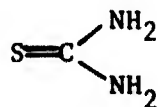
At pH 6.5 silver adsorption begins to increase again in Figure 113. However, thiosulfate adsorption continues to decrease. The increase in silver adsorption at pH 6.5 is thus due to the surface reaction that occurs in the absence of thiosulfate. At pH 7.5 thiosulfate adsorption is near zero. So, when the pH > 7.5, thiosulfate functions as a simple complexing agent in solution. Thiosulfate and the iron oxide surface compete for the complexation of silver.

The proposed reaction scheme is consistent with the results at higher thiosulfate concentration. Since the surface concentration of thiosulfate is now increased, more silver-thiosulfate complex can be adsorbed. Thus, silver adsorption is greater at low pH. At higher pH where thiosulfate is not adsorbed the decrease in silver adsorption is much greater.

The case of thiosulfate confirms the hypothesis that transition metal complexes can adsorb or that transition metals can be complexed by adsorbed ligands.

The fate of silver in natural systems will be partly determined by its redox behavior at the sediment/water interface. The stability of its complexes with some organic compounds is not great. Decomposition of the complexes may or may not be accompanied by redox reactions. Photoreduction is also enhanced by the presence of reducing agents at oxide interfaces.

The effect of the presence of thiourea on silver removal is illustrated in Figure 115. Thiourea (10^{-6} M) is not adsorbed in the pH region 4-10 in separate adsorption experiments. Thiourea concentration is monitored by C^{14}



Thiourea

activity. In the batch experiments shown in Figure 114, C^{14} activity in the solution phase did not decrease. Although silver forms very strong complexes with thiourea, decomposition of the complexes can occur rapidly. The complex decomposes by the removal of the sulfur atom from thiourea and the subsequent precipitation of silver sulfide (Stephen and Townshend, 1966).

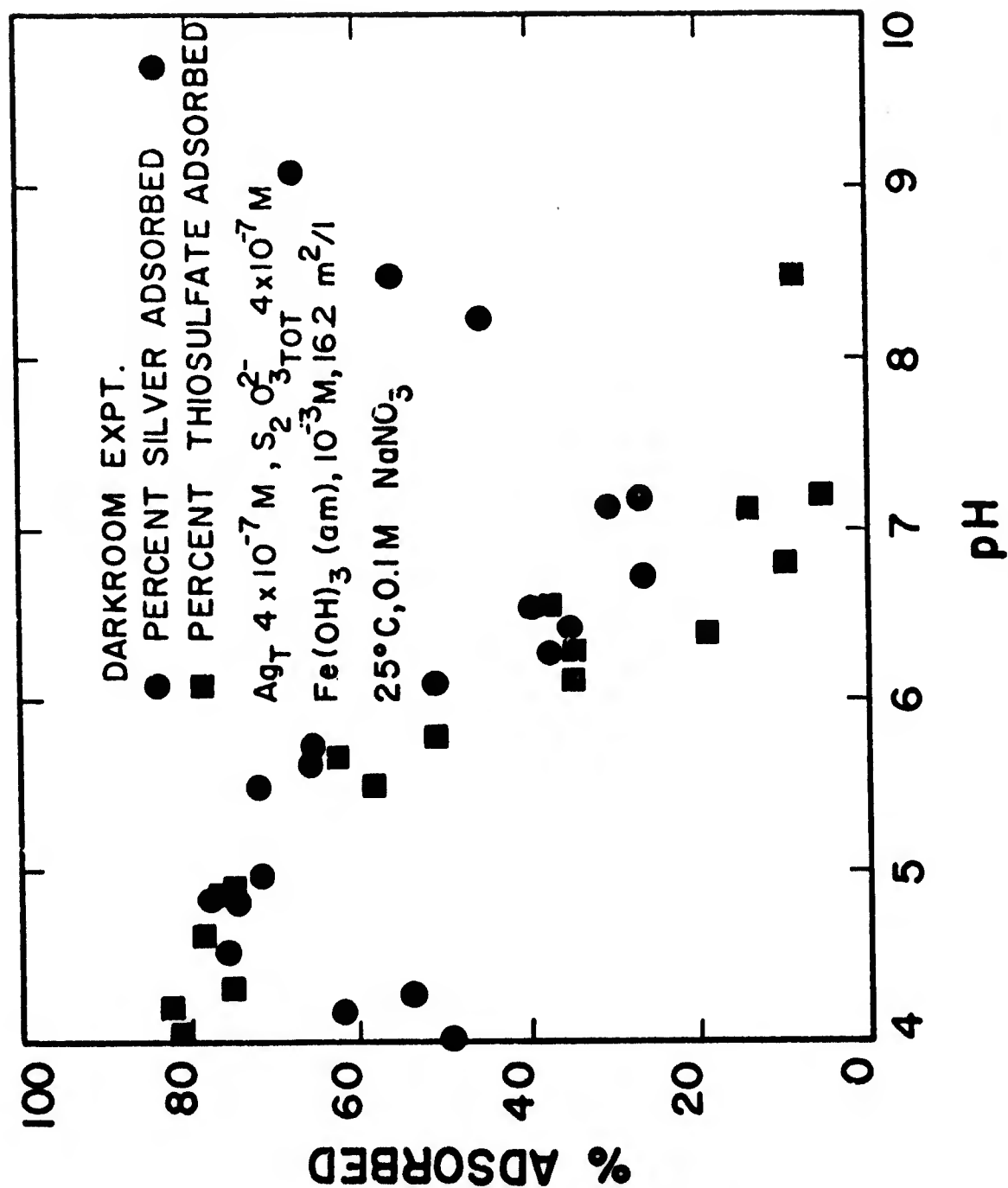


Figure 113. Adsorption of silver and thiosulfate from an equimolar solution ($4 \times 10^{-7} \text{ M}$) on amorphous iron oxide as a function of pH.

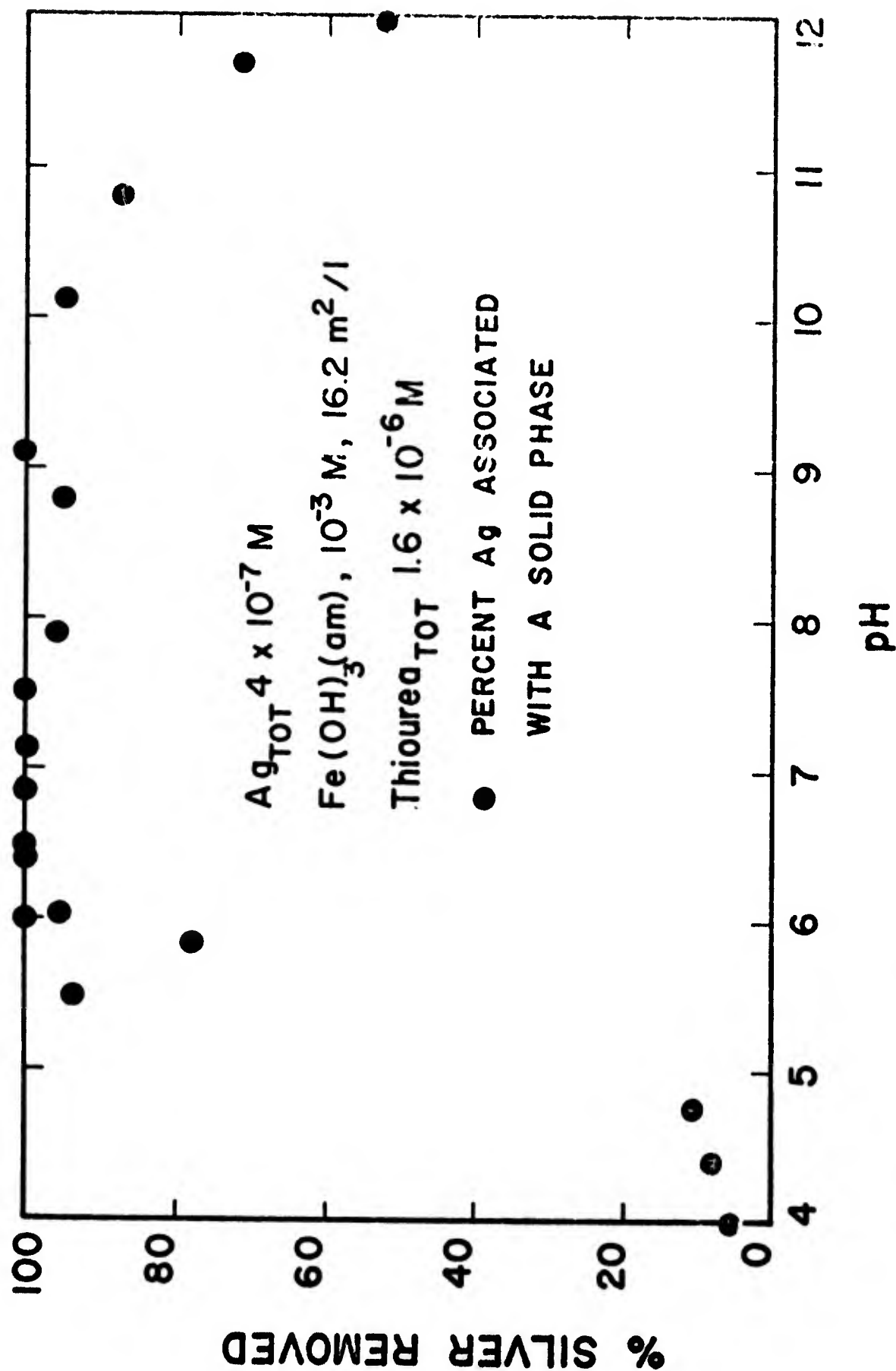
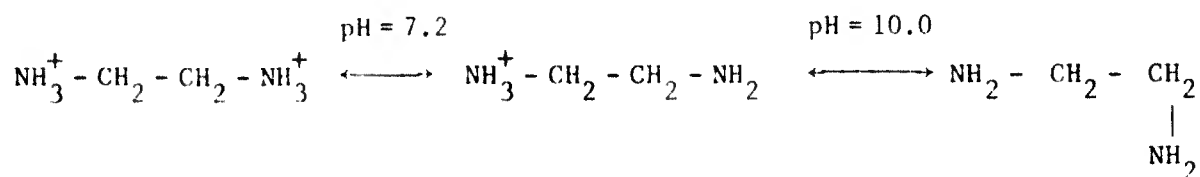


Figure 114. Removal of silver from solution as a function of pH in the presence of thiourea and amorphous iron oxide.

Decomposition of the silver-thiourea complex is the most plausible explanation for the results of these experiments. Stephen and Townshend (1966) report that the decomposition reaction is markedly reduced in slightly acidic solution. This is in agreement with the decrease in silver removal near pH 4-5 (Figure 114). The high removals of silver cannot be explained by adsorption of the complex since C^{14} activity in solution did not decrease. A redox reaction causing the reduction of silver to the metal cannot be ruled out, but the experiments were conducted in the dark to avoid photoreduction. An experiment with S^{35} -labelled thiourea could confirm that silver removal is a result of silver sulfide precipitation.

Figure 115 shows the adsorption of silver on α -quartz in the presence of ethylenediamine. Ethylenediamine adsorption on quartz has not yet been studied so the hypotheses for this system are tentative. Silver adsorption on α -quartz is apparently increased in the pH region 8-10 by the presence of ethylenediamine. Ethylenediamine is positively charged over most of the pH range of interest according to the following reactions:



Silver forms complexes of moderate strength with an uncharged amino group.

α -quartz is negatively charged only slightly between pH 4 and 6, but the increase in surface charge with pH is rapid above pH 7. Thus, the positively charged ethylenediamine species should be weakly adsorbed by the coulombic attraction above pH 7. Above pH 7.2 the predominant ethylenediamine species has one positively charged amino group. The uncharged amino group is available for silver complexation. Thus, silver adsorption is probably increased in the pH region 8-10 by adsorption of the ethylenediamine complex. As the pH increases the ethylenediamine speciation changes again to the uncharged ligand. Complexation of silver in solution then becomes more important and silver adsorption decreases.

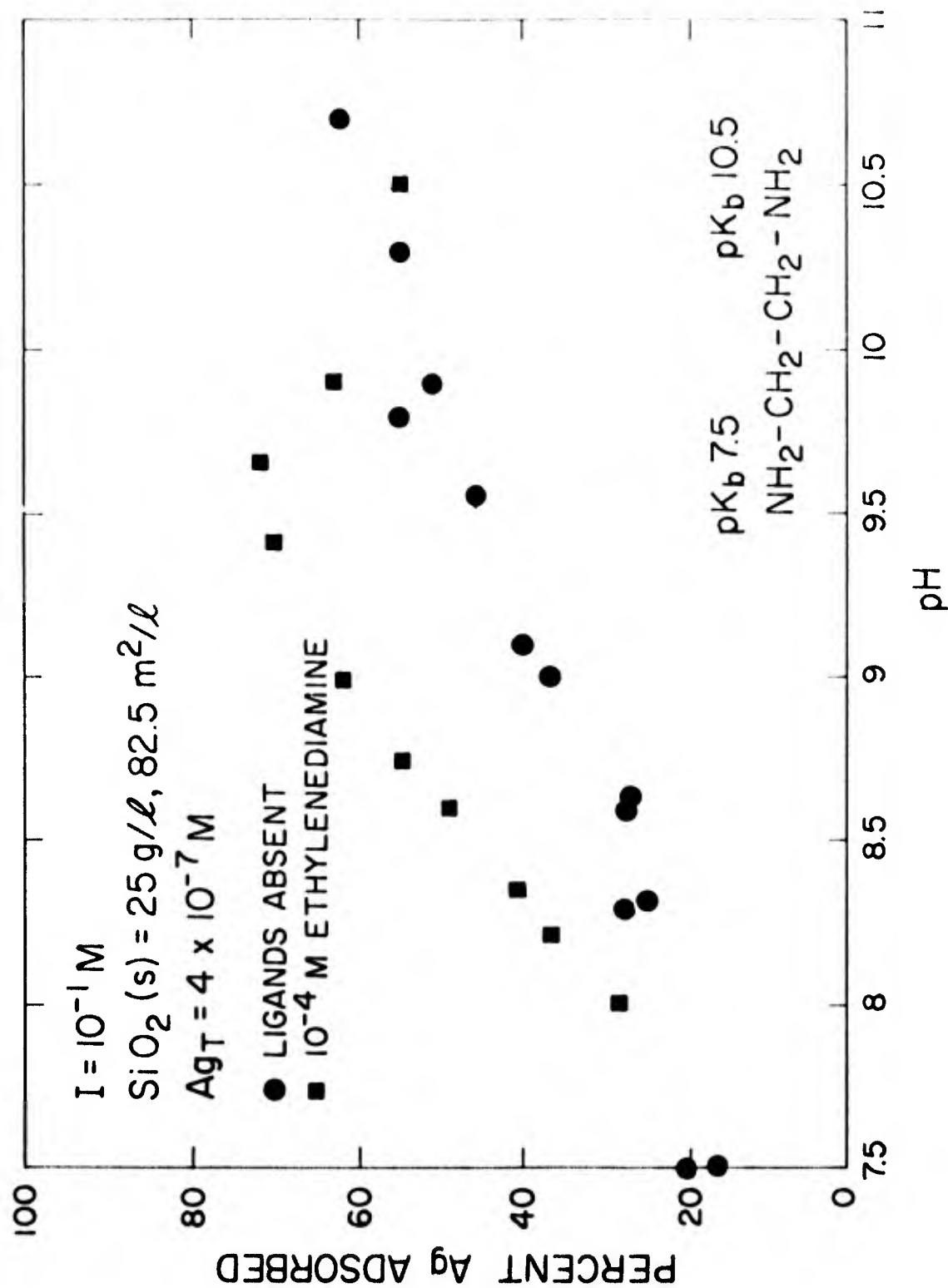


Figure 115. Adsorption of silver on α -quartz as a function of pH in the presence of ethylenediamine.

Adsorption of Copper on Amorphous Iron Oxide and α -Quartz in Systems Containing Ligands

The effect of salicylic acid, protocatechuic acid (PCCA), and sulfate on copper adsorption on amorphous iron oxide is illustrated in Figure 116. None of the ligands has a significant effect despite the fact that two form moderate to strong complexes with copper. However, only a portion of the complexing ligands remains in solution since the copper adsorption edge overlaps the pH region where the ligands are coulombically adsorbed. Protocatechuic acid (PCCA) is strongly adsorbed over the entire pH range (Figure 106).

Apparently the sorptive behavior of these complexing ligands has little effect on copper adsorption. In the case of salicylic acid and protocatechuic acid, this is to be expected since the coordinating functional groups used in complexation of metals are the same groups likely to be involved in adsorption reactions. This also suggests that the complexes do not form and adsorb with copper adjacent to the surface. To test this hypothesis, experiments were conducted with PCCA where 1) copper was added to the iron oxide suspension and equilibrated before PCCA addition, and 2) copper and PCCA were added to the iron oxide suspension simultaneously. These results were compared with the normal procedure of PCCA addition and equilibrium before copper addition. There are no detectable differences in copper or PCCA adsorption among the three methods.

Figure 117 displays the results for copper/iron oxide suspensions containing glutamic acid or 2,3-pyrazinedicarboxylic acid (2,3-PDCA). Both ligands increase the concentration of copper. The case of glutamic acid is analogous to that already explained for silver. Copper adsorption is increased either by adsorption of the copper-glutamate complex or complexation by an adsorbed glutamate ion. The terminal carboxylic group is involved in the surface reaction, and the zwitterion functional groups are available for complexation. Thus, an important distinction between glutamic acid and salicylic acid is that an adsorbed glutamate ion can still complex a trace metal whereas salicylic acid cannot.

Apparently, 2,3-PDCA also has coordinating atoms (two nitrogens) available for increasing adsorption. The actual mechanism is unknown since the stereochemistry of an adsorbed 2,3-PDCA molecule is not known. It is probable that both carboxyl groups of 2,3-PDCA face the surface, as suggested

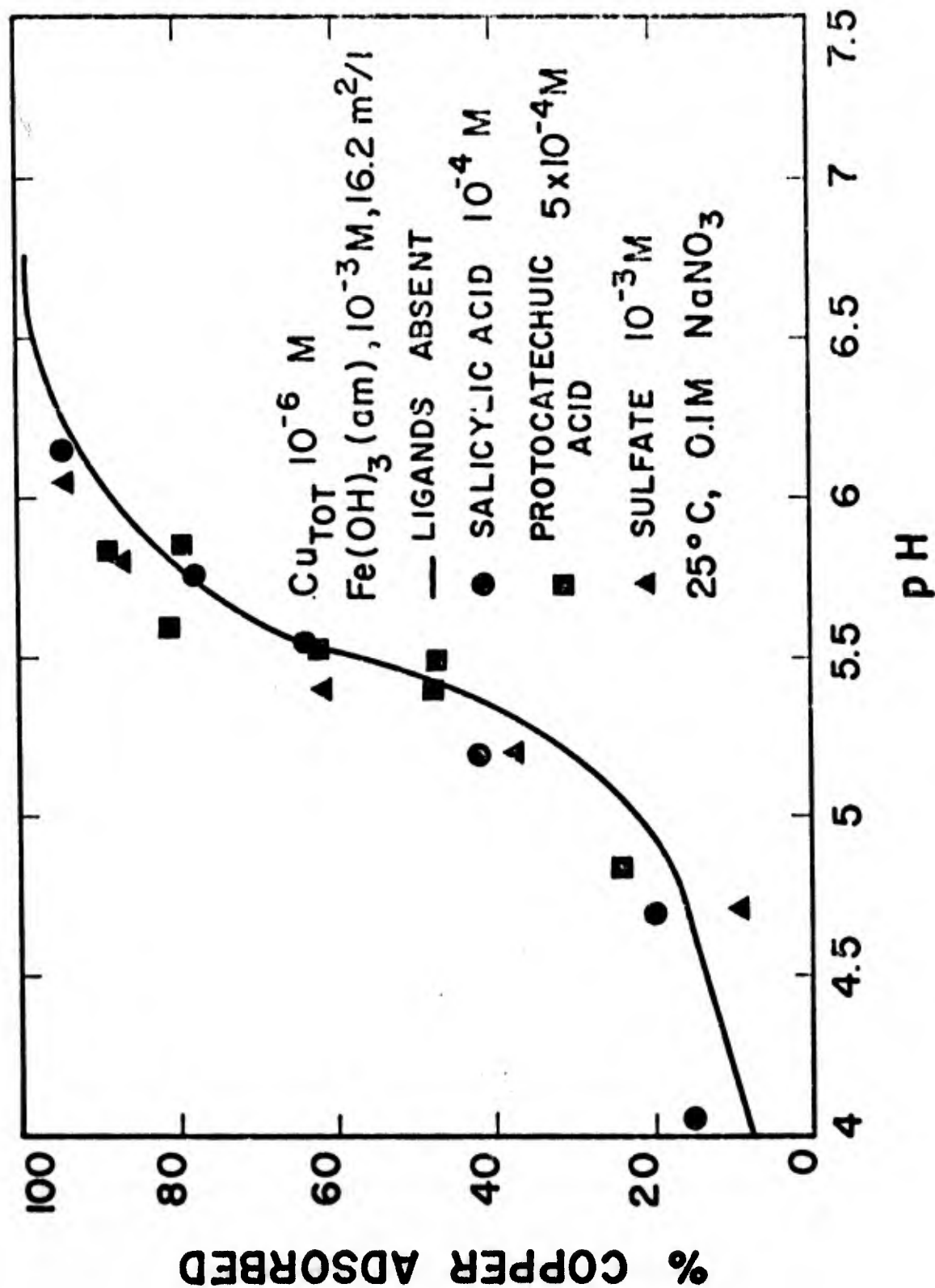


Figure 116. Adsorption of copper on amorphous iron oxide as a function of pH in the presence of salicylic acid, protocatechuic acid, and sulfate.

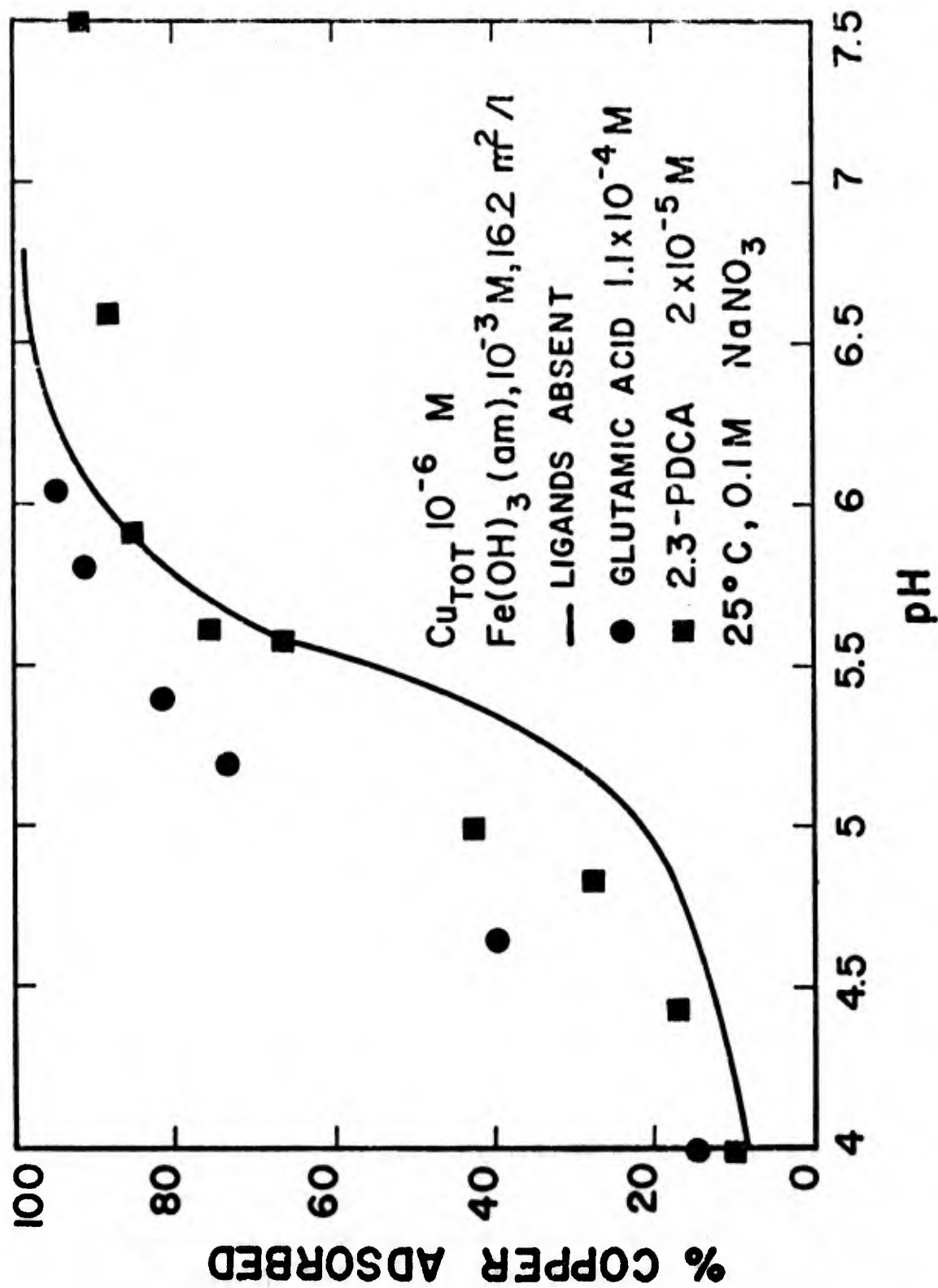


Figure 117. Adsorption of copper on amorphous iron oxide as a function of pH in the presence of glutamic acid and 2,3-pyrazinedicarboxylic acid.

by the comparatively steep slope in Figure 108. Perhaps surface sites adjacent to an adsorbed 2,3-PDCA molecule are stabilized (with respect to copper adsorption) by the presence of a nitrogen heteroatom. At pH 6.5 adsorption of 2,3-PDCA approaches zero. Copper adsorption is enhanced in the pH region 4.5-5.5 where 2,3-PDCA adsorption is high and then approaches normal levels at pH 6. At higher pH values there is some evidence of decreased adsorption of copper, presumably due to complexation of copper in solution by 2,3-PDCA.

Figure 118 includes the same data for 2,3-PDCA effect on copper adsorption and a comparison with the effect of picolinic acid. Picolinic acid effectively prevents copper adsorption by complexation in solution. The adsorptive and complexation (in solution) behavior of picolinic acid and 2,3-PDCA are similar. The orientation of an adsorbed picolinic acid ion is probably different from that of an adsorbed 2,3-PDCA ion. However, it is more likely that the nitrogen atoms in picolinic acid are involved in the surface reaction than those of 2,3-PDCA. As a result, 2,3-PDCA can increase copper adsorption by some association of adsorbed copper and 2,3-PDCA ions.

Figure 119 shows the adsorption of copper on α -quartz in the presence of histidine and ethylenediamine. Both ligands form strong complexes with copper. Histidine, a non-adsorbing ligand, prevents copper adsorption by complexation in solution. Ethylenediamine also controls the sorptive behavior of copper by complexation. As the pH increases, the surface of α -quartz becomes more negative and ethylenediamine adsorption should be increasing. Copper adsorption increases slightly, possibly in response to the increased adsorption of ethylenediamine and the ethylenediamine-copper complex.

Adsorption of Cadmium on γ -FeOOH and α -Quartz in Systems Containing Ligands

In many cases a ligand which forms a soluble complex with a metal will decrease the degree of adsorption of the metal onto a surface. Therefore, for each surface studied, the effect of adding various cadmium-complexing ligands to solution was investigated. The ligands chosen were Cl^- , SO_4^{2-} , and $\text{S}_2\text{O}_3^{2-}$, since they form relatively strong complexes with cadmium at concentrations likely to be found in natural waters or specialized waste streams (e.g. photographic wastes). For each solid, when a given fraction of the cadmium in solution was complexed by the ligand, the effect on the adsorption of cadmium increased in the order $\text{SO}_4^{2-} < \text{Cl}^- < \text{S}_2\text{O}_3^{2-}$ (Figures 120 through

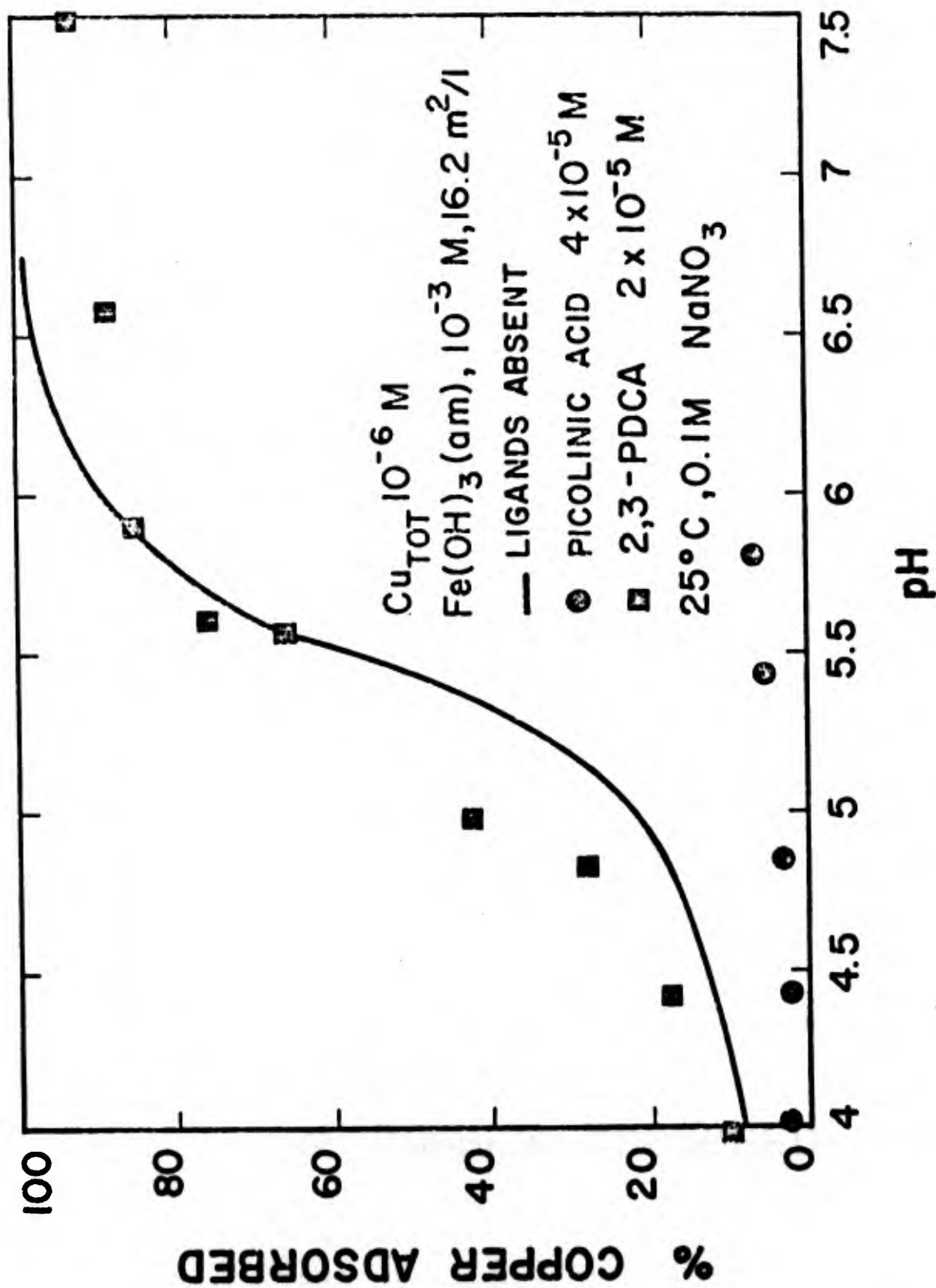


Figure 118. Adsorption of copper on amorphous iron oxide as a function of pH in the presence of picolinic acid and 2,3-pyrazinedicarboxylic acid.

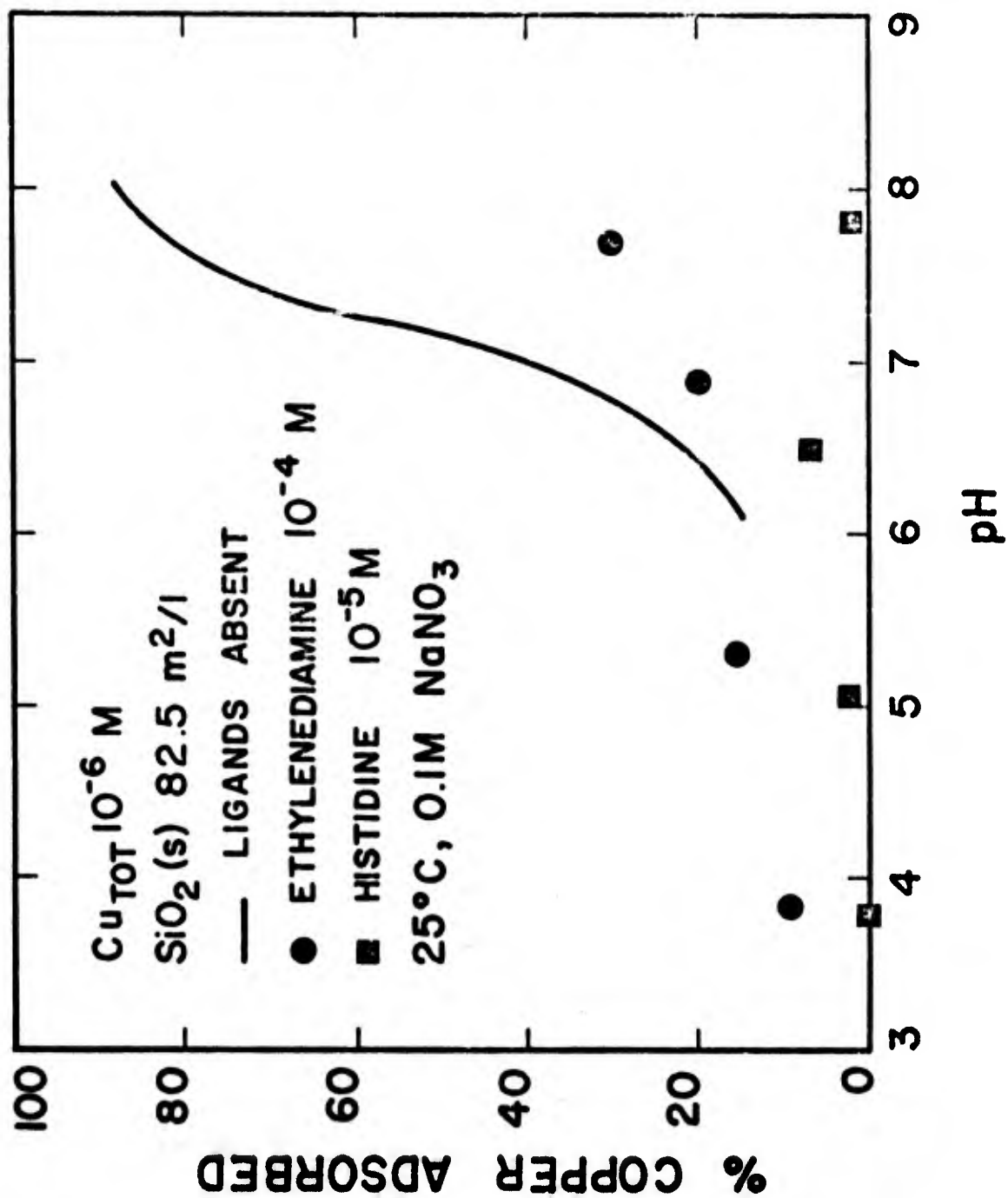


Figure 119. Copper adsorption on α -quartz as a function of pH in the presence of histidine and ethylenediamine.

125) . When lepidocrocite was the adsorbent and sulfate the ligand, the equilibrium adsorption curve was not affected even when the ratio of complexed to uncomplexed cadmium in solution was 25:1. Under similar conditions, when thiosulfate was the complexing ligand, the adsorption edge was shifted approximately 0.8 pH units to the right.

If complexed cadmium is unavailable for adsorption, then at a given ratio of (complexed Cd:free Cd²⁺), the adsorption should be independent of the ligand. This is clearly not the case. Apparently some ligands interact with the surface in such a way that metal adsorption is affected. Several types of interactions can be envisioned. The ligand may adsorb and alter the electrostatic interaction of the surface with the metal. Alternatively, the metal-ligand complex may adsorb as a single species. These possibilities and any other conceptual models to explain the effects of the various ligands cannot be distinguished at this time.

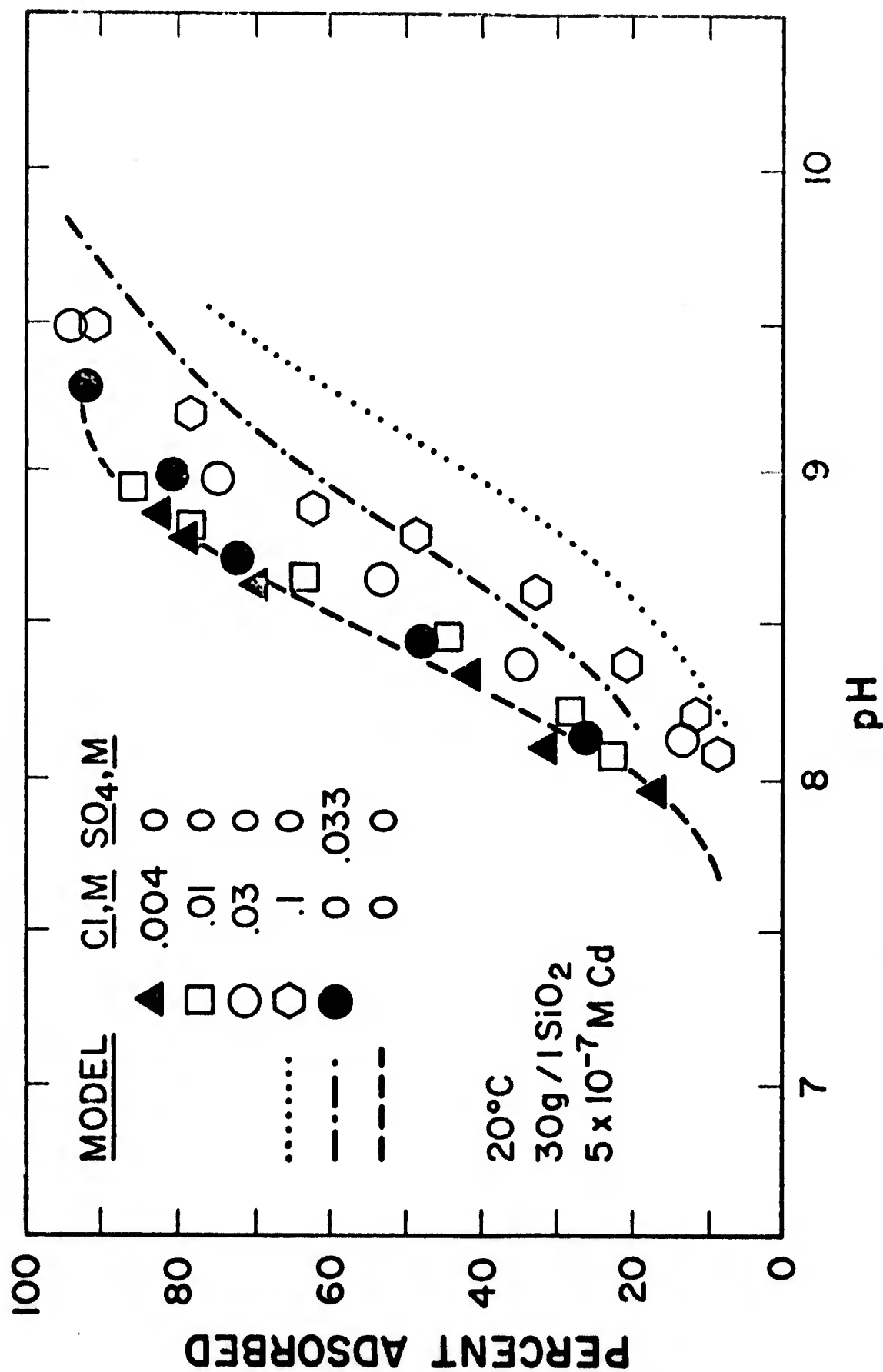


Figure 120. Adsorption of Cd onto SiO₂ as a function of pH and concentration of complexing ligands (Cl or SO₄) at 0.1M ionic strength.

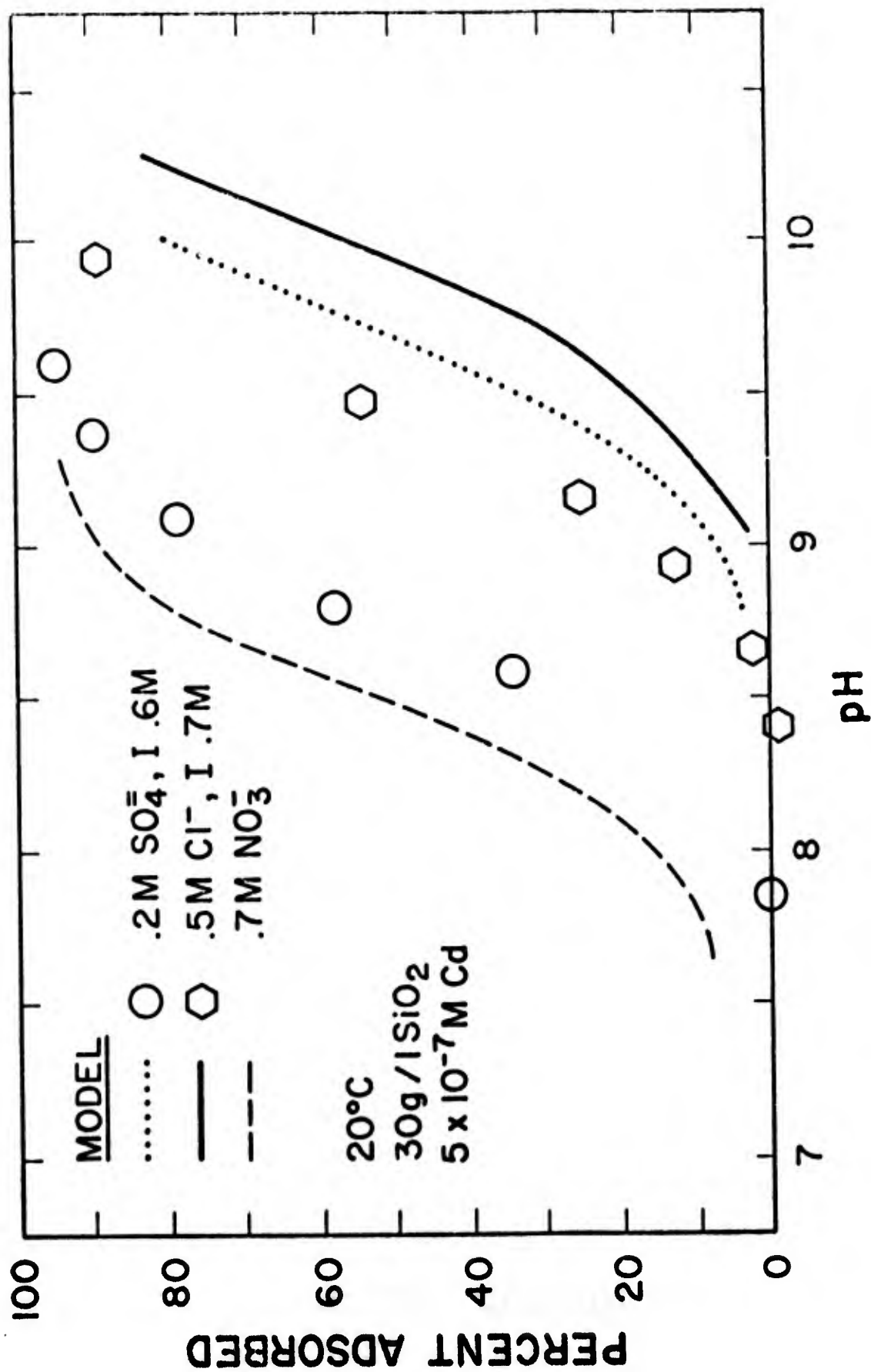


Figure 121. Adsorption of Cd onto SiO₂ as a function of pH and concentration of complexing ligands (Cl or SO₄) at 0.7M ionic strength.

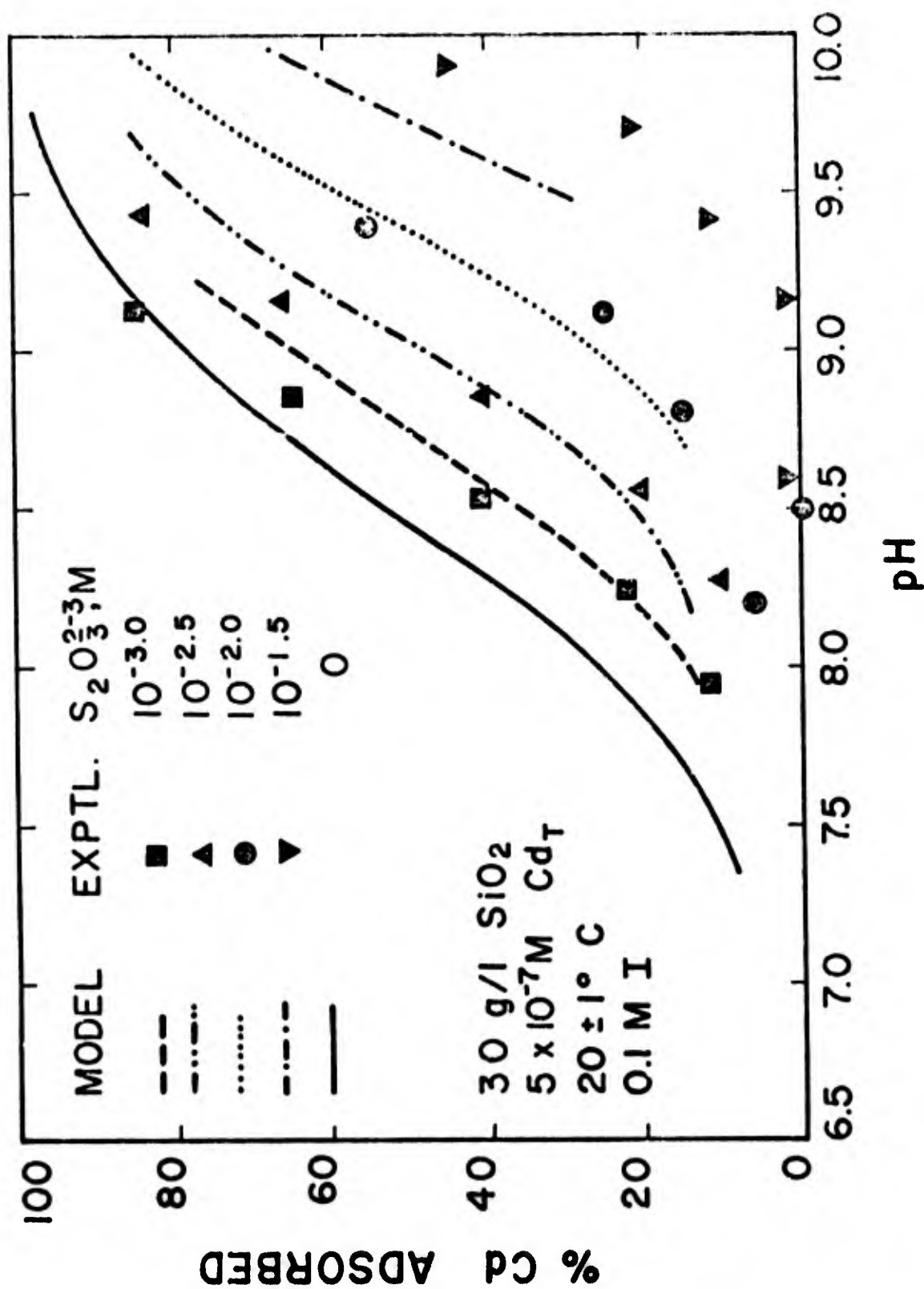


FIGURE 22 Adsorption of Cd onto SiO₂ as a function of pH and concentration of dissolved thiosulfate.

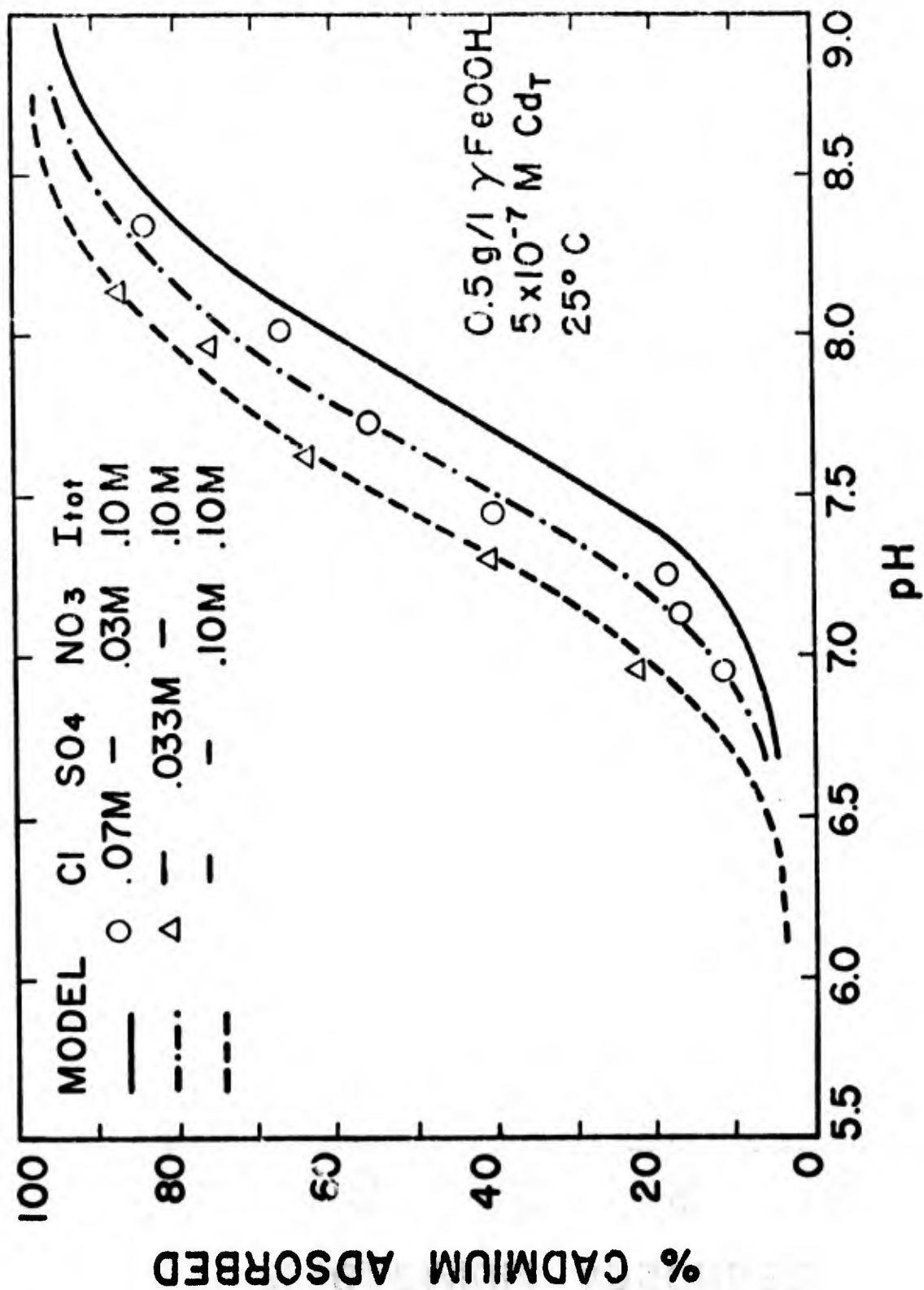


Figure .23 Adsorption of Cd onto γ -FeOOH as a function of pH and concentration of complexing ligands (Cl or SO_4) at 0.1M ionic strength.

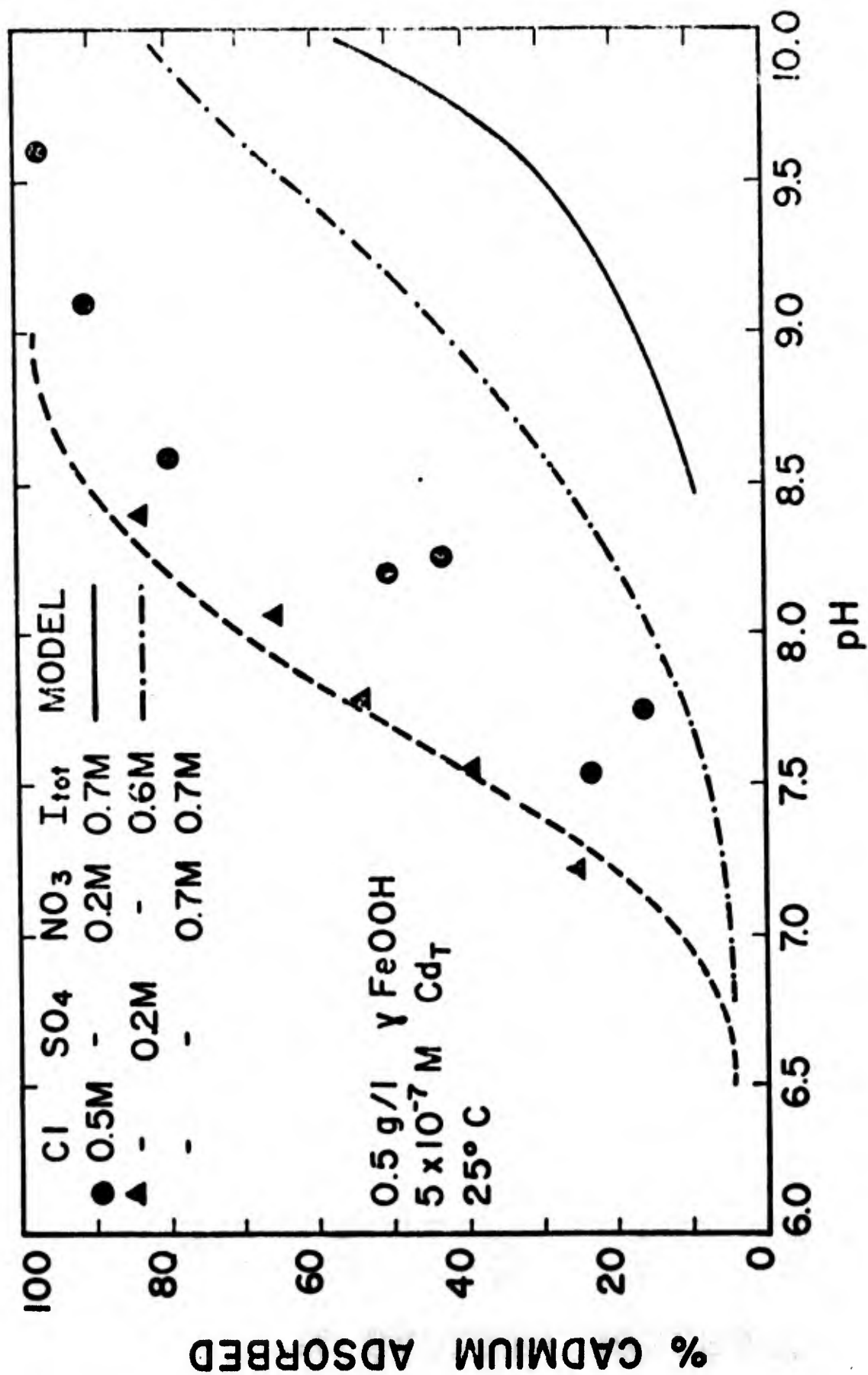


Figure 124. Adsorption of Cd onto γ -FeOOH as a function of pH and concentration of complexing ligands (Cl or SO₄) at high ionic strength.

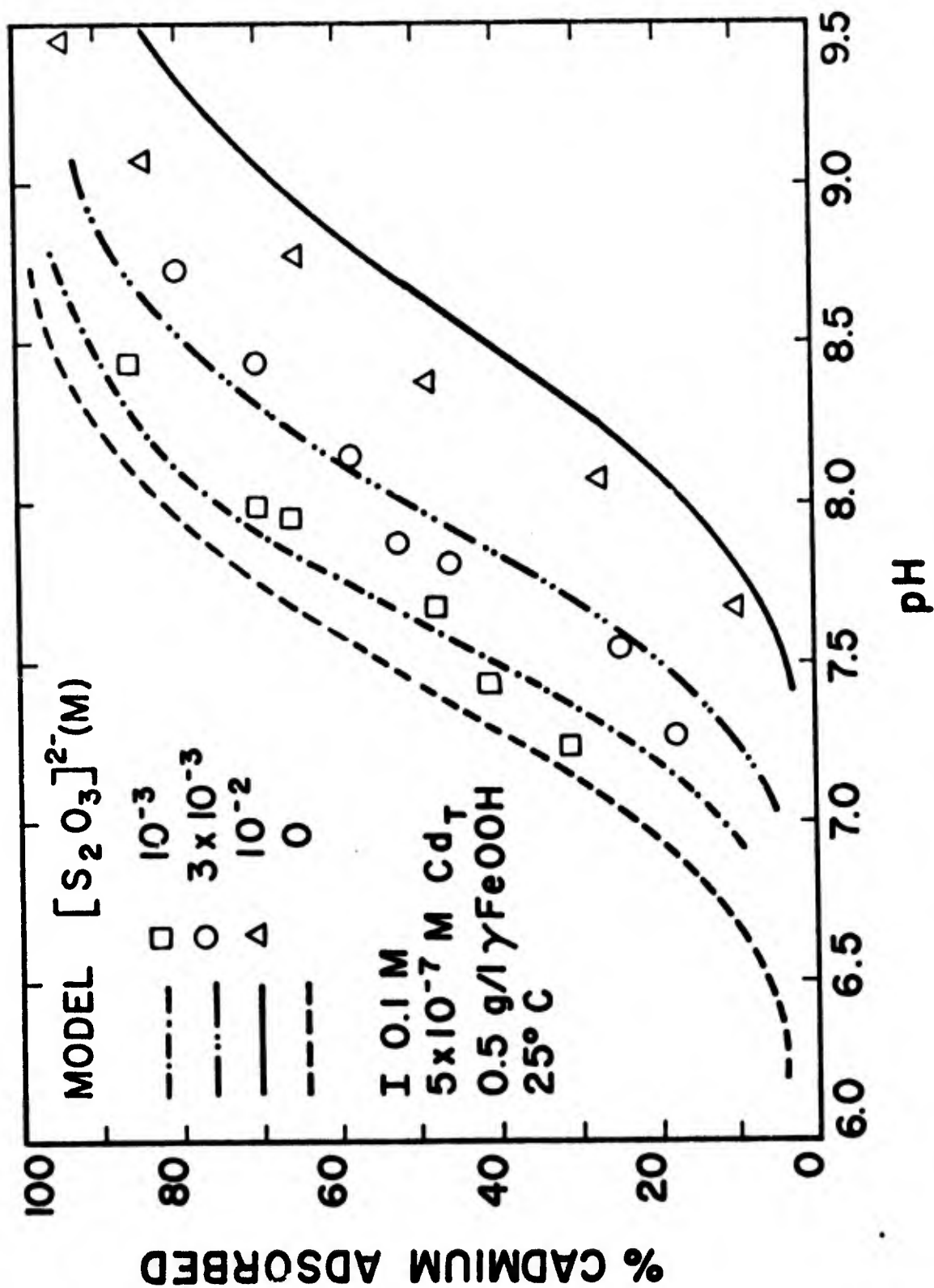


Figure 125. Adsorption of Cd onto γ -FeOOH as a function of pH and concentration of dissolved thiosulfate.

1. The rate of oxidative dissolution of the ferrous monosulfide, mackinawite, has first-order dependence on dissolved oxygen concentration and total surface area of FeS. The rate of oxidation shows a fractional (1/4) dependence on the hydronium ion concentration. The empirical rate equation is

$$-\frac{d[\text{FeS}]}{dt} = k(\text{Area}) P_{\text{O}_2} [\text{H}^+]^{1/4}$$

2. Chloride ion concentration has the effect of retarding the rate of oxidation at pH 7 but shows no effect on the rate of oxidation at pH > 9.
3. The iron reaction product is γ -FeOOH (lepidocrocite) over the pH range 6.5 to 10. Above pH 10 the crystal structure cannot be definitely identified.
4. The sulfur reaction products vary with pH and chloride concentration. At pH 7 the sulfur reaction product is always elemental sulfur. At pH > 7 the sulfur reaction products begin shifting to thiosulfate and the polythionates. The ratio of the dissolved sulfur oxyanion products remains constant even though the fraction of sulfur oxidized past elemental sulfur changes. Increasing concentrations of chloride shift the sulfur reaction product increasingly to elemental sulfur. Thus, in estuarine and marine systems elemental sulfur will invariably be the reaction product while in freshwater systems dissolved sulfur oxyanions may be important in slightly alkaline waters.
5. Trace concentrations of nickel catalyzes the oxidation reaction. Nickel, adsorbed on the FeS surface, accelerates the surface reaction. Nickel is known to enter into one-electron transfer reactions. Trace amounts of copper, cadmium, and silver do not affect the reaction kinetics or products. Implications of possible catalytic behavior of trace metals concerns oxidation of FeS in undisturbed sediments where diffusion-controlled mass transport of oxygen and reaction products is important.

6. Adsorption of Ag, Cu, and Cd on SiO_2 , am $\text{Fe}(\text{OH})_3$, and $\gamma\text{-FeOOH}$ in simple aqueous systems occurs in the pH range 6 to 9. The pH adsorption edge is much steeper for Cu and Cd than for Ag. All three metals are expected to have adsorptive interaction with silicate minerals, clays, and iron and manganese hydrous oxides in freshwater systems. The degree of interaction is dependent on concentration of metal, available surface area, and only slightly on the nature of the solid substrate.
7. The hydrated surfaces of oxides can, in general, be characterized as behaving as ligand sites for adsorbed trace metals. Thus, interaction between solution ligands such as Cl^- , SO_4^{2-} , $\text{S}_2\text{O}_3^{2-}$, CN^- and others and adsorbable trace metals is characterized as competition between ligands and can be quantified by examining the relative strengths of the stability constants for non-adsorbing ligands.
8. Both organic and inorganic ligands may adsorb at the oxide/solution interface. The adsorption can be both electrostatic and specific, depending on the degree of chemical interaction and orientation of the ligand on the surface. The ability of an adsorbing ligand to enhance the adsorption of a trace metal depends on the availability of coordination sites on the adsorbed ligand or, conversely, the ability of the metal-ligand complex to adsorb. Experimental work confirms that organic and inorganic ligands and chelons can either decrease, increase, or have no effect on the adsorption behavior of trace metals. Specific examples pertinent to this study are Cl^- and SO_4^{2-} which decrease adsorption of Ag and Cd such that at seawater concentration and pH no significant adsorption is expected. On the other hand, $\text{S}_2\text{O}_3^{2-}$ significantly increases adsorption of Ag but decreases the adsorption of Cd. Similar behavior is found for various organic chelons.
9. Cd is mobilized into solution during the oxidation of Cd-containing FeS(s) in the presence of high concentrations of chloride. Thus, under appropriate conditions trace metals may be mobilized during the oxidation of trace-metal-contaminated sulfidic sediments.
10. Oxidation of sulfidic estuarine sediments at pH 8.5 shows rate behavior predicted from the laboratory rate studies, and elemental sulfur is the reaction product, consistent with the presence of high concentrations of chloride.

SECTION XII

RECOMMENDATIONS

The following recommendations for further study are suggested as the most important and potentially fruitful investigations needed to gain greater insight into the behavior of trace metals associated with ferrous monosulfides and the details of oxidation of heterogeneous sulfide systems.

1. Extensive studies of the kinetics of oxidation of natural sulfidic sediments using techniques and procedures developed in this study would be very useful.
2. Continued study of the oxidation mechanisms of FeS(s) and the solution sulfur reaction sequence would be very useful.
3. Investigations of the oxidation kinetics of solid solutions of Ni, Zn, and Co with FeS(s) should be undertaken. Included should be studies on the fate of the trace metals during the oxidation reaction.
4. Studies of the slow homogeneous co-precipitation of FeS(s) and trace metals (Ni, Zn, Cu, Co) under near-ambient conditions would give added insight into the fate of trace metals deposited in sulfidic surficial sediments.
5. Investigation of competitive adsorption between several trace metals and single substrates should yield insight into the possible mode of redistribution of trace metals in depositing sediments and the adsorptive behavior of trace metals released to natural aquatic systems.
6. Investigations of competitive adsorption between several solids and a single trace metal should give added insight into the redistribution of trace metals deposited in recent surficial sediments.
7. Additional work on the role of natural organics on modifying the behavior of trace metals in natural aquatic systems should be undertaken.

REFERENCES

- Ahrland, S., Chatt, J., et al. (1958a) The relative affinities of co-ordinating atoms for silver ion. Part I. Oxygen, sulphur, and selenium. *J. Chem. Soc.*, 1958, 264.
- Ahrland, S., Chatt, J., et al. (1958b) The relative affinities of co-ordinating atoms for silver ion. Part II. Nitrogen, phosphorus, and arsenic. *J. Chem. Soc.*, 1958, 276.
- Amer. Public Health Assoc. (1971) Standard Methods for the Examination of Water and Wastewater, 13th ed., Amer. Publ. Health Assoc., Washington, D.C.
- Anderson, B. J., Jenne, E. A., and Chao, T. T. (1973) The sorption of silver by poorly crystallized manganese oxides. *Geochim. Cosmochim. Acta* 37, 611.
- Andrews, L. J., and Keefer, R. M. (1949) Cation complexes of compounds containing carbon-carbon double bonds. IV. The argentation of aromatic hydrocarbons. *J. Am. Chem. Soc.* 71, 3644.
- Arnold, R. G. (1962) Equilibrium relations between pyrrhotite and pyrite from 325°C to 745°C. *Econ. Geol.* 57, 72-90.
- Atkinson, R. J., Posner, A. M., and Quirk, J. P. (1968) Crystal nucleation in Fe(III) solutions and hydroxide gels. *J. Inorg. Nucl. Chem.* 30, 2371-2381.
- Avotins, P. V. (1975) Adsorption and coprecipitation studies of mercury on hydrous iron oxides. University Microfilms, Ann Arbor, Michigan.
- Aylett, B. (1973) Group II B in: Comprehensive Inorganic Chemistry, V. 3, ed. by J. Bailar et al., Pergamon Press, 1973, 187-328.
- Banat, K., Förstner, U., and Müller, G. (1974) Experimental mobilization of metals from aquatic sediments by NTA. *Chem. Geol.* 14, 199-207.
- Bard, C. C., Murphy, J. J., Stone, D. L., and Terhaar, C. J. (1976) Silver in photoprocessing effluents. *J. Water Poll. Cont. Fed.* 48, 389-394.
- Bartlett, J. K., and Skoog, D. A. (1954) Colorimetric determination of elemental sulfur in hydrocarbons. *Anal. Chem.* 26(6), 1008-1011.
- Baudisch, O., and Albrecht, W. H. (1932) Gamma-ferric oxide hydrate. *J. Amer. Chem. Soc.* 51(1), 943-947.
- Berner, R. A. (1964) Iron sulfides from aqueous solution at low temperature and atmospheric pressure. *J. Geology* 72, 293-306.
- Bertolacini, R. J., and Barney, J. E., II (1957) Colorimetric determination of sulfate with barium chloranilate. *Anal. Chem.* 29(2), 281-283.
- Beverwijk, C. D. M., van der Kerk, G. J. M., et al. (1970) Organosilver chemistry. *Organometal. Chem. Rev. A* 5, 215.

- Bolt, G. H. (1957) Determination of the charge density of silica sols. J. Phys. Chem. 61, 1166.
- Boyle, R. W. (1968) The geochemistry of silver and its deposits. Geol. Surv. of Canada, Dept. of Energy, Mines, and Resources, Bull. 160.
- Brown, G. (1953) The occurrence of lepidocrocite in some British soils. J. Soil Sci. 4, 220-228.
- Brown, G. (1954) Soil morphology and minealogy. A qualitative study of some gleyed soils from North-West England. J. Soil Sci. 5(1), 145-153.
- Chao, T. T., Jenne, E. A., and Heppting, L. M. (1968) Adsorption of traces of silver on sample container. USGS Prof. Paper 600-D, D13.
- Chao, T. T., and Anderson, B. J. (1974) The scavenging of silver by manganese and iron oxides in stream sediments collected from two drainage areas of Colorado. Chem. Geol. 14, 159.
- Chen, K. Y. (1970) Oxidation of aqueous sulfide by O_2 . Ph.D. thesis submitted to Division of Eng. and Appl. Physics, Harvard Univ., Cambridge, Mass., April 1970.
- Chen, K. Y., and Morris, J. C. (1970) Oxidation of aqueous sulfide by O_2 : 1. General characteristics and catalytic influences. Presented at 5th International Water Poll. Res. Conf. July-Aug. 1970, Pergamon Press.
- Chen, K. Y., and Morris, J. C. (1972a) Oxidation of sulfide by O_2 : Catalysis and inhibition. J. Sanit. Eng. Div., Proc. Amer. Soc. Civ. Eng., Feb. 1972, 215.
- Chen, K. Y., and Morris, J. C. (1972b) Kinetics of oxidation of aqueous sulfide by O_2 . Env. Sci. and Tech. 6, 529.
- Chen, K. Y., and Gupta, S. K. (1973) Formation of polysulfides in aqueous solutions. Env. Letters 4(3), 187.
- Chizhikov, D. M. (1962) Cadmium, trans. by D. E. Hayler (1966), Pergamon Press, pp. 1-48.
- Clark, W. C., and Vondjidis, A. (1964) Changes in titanium dioxide-silver nitrate mixtures after ultra-violet irradiation. Nature 203, 635.
- Clark, W. C., and Vondjidis, A. G. (1968) The nature of the photolysis of silver at an oxide semiconductor surface. Can. J. Phys. 46, 1775.
- Cline, J. D., and Richards, F. A. (1969) Oxygenation of hydrogen sulfide in seawater at constant salinity, temperature, and pH. Env. Sci. and Tech. 3(9), 838.
- Cloke, P. L. (1963a) The geologic role of polysulfides--Part I: The distribution of ionic species in aqueous sodium polysulfide solutions. Geochim. Cosmochim. Acta 27, 1265.

- Cloke, P. L. (1963b) The geologic role of polysulfides -- Part II: The solubility of acanthite and covellite in sodium polysulfide solutions. *Geochim. Cosmochim. Acta* 27, 1299.
- Copenhagen, L., Ulrikson, G., Newman, L., and W. Fulkerson (1973) Cadmium in the environment--An annotated bibliography. ORNL-EIS-73-17, April, 1973.
- Cotton, F., and Wilkinson, G. (1972) Advanced Inorganic Chemistry, A Comprehensive Text, 3rd ed. Intersciences Publishers, 1972.
- Davis, J. A., and Leckie, J. O. (1977) Effect of complexing ligands on trace metal adsorption by hydrous oxides. In preparation.
- Dousma, J., and de Bruyn, P. L. (1976) Hydrolysis-precipitation studies of iron solutions. I. Model for hydrolysis and precipitation from Fe(III) nitrate solutions. *J. Coll. Int. Sci.* 56, 527.
- Doyle, R. W. (1968) Identification and solubility of iron sulfide in anaerobic lake sediment. *Amer. Jour. of Sci.* 266, 980-994.
- Dresher, W. H., Wadsworth, M. E., and Fassell, W. M. Jr. (1956) A kinetic study of the leaching of molybdenite. *Journal of Metals, Trans. AIME* 206, 794-800.
- Dugger, D. L., Stanton, J., Irby, B., McConnell, B., Cummings, W., and Maatman, R. (1964) The exchange of twenty metal ions with the weakly acid silanol groups of silica gel. *J. Phys. Chem.* 68, 757-760.
- Durst, R. A., and Duhart, B. T. (1970) Ion-selective electrode study of trace silver ion adsorption on selected surfaces. *Anal. Chem.* 42, 1002.
- Dyck, W. (1968) Adsorption and coprecipitation of silver on hydrous ferric oxide. *Can. J. Chem.* 46, 1441.
- Dyck, W. (1971) The adsorption and coprecipitation of silver on hydrous oxides of iron and manganese. *Geol. Survey of Canada, Paper 70-64*, Dept. of Energy, Mines, and Resources.
- Enea, O., and Berthon, G. (1973) Étude thermodynamique de la complexation de l'argent par la thiorée et certains de ses dérivés alkylsubstitués. *Thermochim. Acta* 6, 47.
- Eyring, E. M., and Wadsworth, M. E. (1956) Differential infrared spectra of adsorbed monolayers of N-hexanethiol of Zn minerals. *Trans. AIME* 205, 531.
- Feitknecht, von W., and Michaelis, W. (1962) Über die Hydrolyse von Eisen(III)-Perchlorat-Lösungen. *Helvetica Chimica Acta* 45(26), 212-224.
- Fleischauer, P. D., Kan, H. K. A., and Shepherd, J. R. (1972) Quantum yields of silver ion reduction on titanium dioxide and zinc oxide single crystals. *J. Am. Chem. Soc.* 94, 283.

- Fleischauer, P. D., and Shepherd, J. R. (1974) Kinetics of the reaction between Fe(II) and Ag(I) catalyzed by silver nuclei on TiO₂ surfaces. J. Phys. Chem. 78, 2580.
- Fleischer, M., Sarofim, A., Fassett, D., Hammond, P., Shacklette, H., Nisbet, I., and Epstein, S. (1974) Environmental impact of cadmium: A review by the panel on hazardous trace substances. Envir. Health Perspec., Experimental issue #7, 253-323.
- Framson, P., and Leckie, J. O. (1977) Limits of the co-precipitation of cadmium and ferrous sulfides. Accepted for publication (December 1977) by Environmental Science and Technology.
- Fulkerson, W., and Goeller, H. (1973) Cd, The Dissipated Element, ed. by W. Fulkerson and H. Goeller, ORNL-NSF-EP-21, 1973.
- Fulkerson, W. (1975) Cadmium, the dissipated element--revisited. Presented at the 2nd AIChE/EPA Conference on Complete Water Reuse, May 4-8, 1975, Chicago, Illinois.
- Gardiner, J. (1974a) The chemistry of cadmium in natural water--I: A study of cadmium complex formation using the Cd-specific ion electrode. Wat. Res. 8, 23-30.
- Gardiner, J. (1974b) The chemistry of cadmium in natural water--II: The adsorption of cadmium on river muds and naturally occurring solids. Wat. Res. 8, 157-164.
- Gardiner, L. R. (1974) Organic versus inorganic trace metal complexes in sulfidic marine waters--Some speculative calculations based on available stability constants. Geochim. Cosmochim. Acta 38, 1297-1302.
- Ghosh, M. M. (1974) Oxygenation of ferrous iron(II) in highly buffered waters, Ch. 5, 193-217, in: Aqueous-Environmental Chemistry of Metals, Alan J. Rubin, ed. Ann Arbor Sci. Publ. Inc., Ann Arbor, Mich.
- Glasstone, S., Laidlev, K. J., and Eyring, H. (1941) The Theory of Rate Processes, McGraw-Hill Book Co., New York.
- Goetz, A., and Inn, E. C. Y. (1948) Reversible photolysis of Ag sorbed on colloidal metal oxides. Rev. Mod. Phys. 20, 131.
- Goldhaber, M. B., and Kaplan, I. R. (1974) The sulfur cycle, Ch. 17 in: The Sea, Vol. 5, E. Goldberg, ed. Wiley-Interscience, New York, 1974.
- Goodman, B., and Cheshire, M. (1973) Electron paramagnetic resonance evidence that copper is complexed in humic acid by the nitrogen of porphyrin groups. Nature New Biol. 244, 158.
- Gottschalk, V. H., and Buehler, H. A. (1912) Oxidation of sulphides. Econ. Geol. 7, 15.
- Groenewegen, J. A., and Sachtler, W. M. H. (1974) Infrared spectra of some amino acids adsorbed on silica and on silica-supported nickel. J. Catal. 33, 176.

- Grønkvold, F., and Haraldsen, H. (1952) On the phase relations of synthetic and natural pyrrhotites. *Acta Chem. Scand.* 6, 1442-1469.
- Hahn, F. L., and Hertrich, M. (1923) Leicht filtrierbares Eisenhydroxyd durch Fällung mit Thiosulfaat und Jodat. *Ber. Dtsch. Chem. Gesellsch.* 56, 1729-1732.
- Han, K. N., Healy, T. W., and Fuerstenau, P. W. (1973) The mechanism of adsorption of fatty acids and other surfactants at the oxide-water interface. *J. Coll. Int. Sci.* 44, 407.
- Hem, J. D. (1972) Chemistry and occurrence of cadmium and zinc in surface water and groundwater. *Water Res. Res.* 8, 661-679.
- Hingston, F. J., Atkinson, R. J., et al. (1967) Specific adsorption of anions. *Nature* 215, 1459.
- Ho, T. L. (1975) The hard soft acids bases (HSAB) principle and organic chemistry, *Chem. Rev.* 75, 1.
- Hohl, H., and Stumm, W. (1976) Interaction of Pb^{2+} with hydrous $\gamma-Al_2O_3$. *J. Coll. Int. Sci.* 55, 281.
- Holmes, C., Slade, E., and McLerran, C. (1974) Migration and redistribution of zinc and cadmium in a marine estuary system. *Envir. Sci. and Tech.* 8, 255-259.
- Hsu, Pa Ho, and Ragone, S. E. (1972) Aging of hydrolyzed iron(III) solutions. *J. Soil Sci.* 23, 17.
- Huang, C. P. (1975) Adsorption of phosphate at the hydrous $\gamma-Al_2O_3$ - electrolyte interface. *J. Coll. Int. Sci.* 53, 178.
- Huang, C. P., Elliott, H. A., and Ashmead, R. M. (1975) Interfacial reactions and the fate of heavy metals in soil-water systems. Presented at Symposium on Solute Transport in Subsurface Water, American Geophysical Union, San Francisco, Dec. 1975.
- Huckabee, J., and Blaylock, B. (1973) Transfer of mercury and cadmium from terrestrial to aquatic ecosystems in: Metal Ions in Biological Systems, ed. by S. Dahr, Plenum Publishers, New York, 125-160.
- Israeli, M., and Pettit, L. D. (1975) Complex formation between unsaturated α -amino acids and silver(I) and some divalent transition metals. *J. Inorg. Nucl. Chem.* 37, 999.
- James, R. O., and Healy, T. W. (1972) Adsorption of hydrolyzable metal ions at the oxide/water interface. III. A thermodynamic model of adsorption. *J. Coll. Int. Sci.* 40, 65.
- James, R. O., and Parks, G. A. (1975) Adsorption of zinc(II) at the sulfide (HgS)/water interface. *AIChE* 71, 157.

- James, R. O., Stiglich, P. J., and Healy, T. W. (1975) Analysis of models of adsorption of metal ions at oxide/water interfaces. *Disc. Faraday Soc.* 59, 142.
- Jenne, E. A. (1968) Controls on Mn, Fe, Co, Ni, Cu and Zn concentrations in soils and water; the significant role of hydrous Mn and Fe oxides. *Adv. in Chem.* 73, 337.
- John, M. K. (1971) Influence of soil characteristics on adsorption and desorption of cadmium. *Envir. Letters* 2, 173.
- John, M. K. (1972) Cadmium adsorption maxima of soils as measured by the Langmuir isotherm. *Can. J. Soil Sci.* 52, 343.
- Kelly, D. P., Chambers, L. A., and Trudinger, P. A. (1969) Cyanolysis and spectrophotometric estimation of trithionate in mixtures with thiosulfate and tetrathionate. *Anal. Chem.* 41(7), 898-901.
- Knauer, G., and Martin, J. (1973) Seasonal variations of Cd, Cu, Mn, Pb, and Zn in water and phytoplankton in Monterey Bay, California. *Limnol. and Oceanog.* 18, 597-604.
- Kolthoff, I. M., and Belcher, R. (1957) *Volumetric Analysis, Vol. III. Titration Methods: Oxidation-Reduction Reactions.* Interscience Publ. Inc., New York, London.
- Kozawa, A. (1961) Ion-exchange adsorption of zinc and copper ions on silica. *J. Inorg. Nucl. Chem.* 21, 315.
- Kubota, J., Mills, E., and Oglesby, R. (1974) Lead, cadmium, zinc, copper, and cobalt in streams and lakes of Cayuga Lake Basin, New York. *Envir. Sci. & Tech.* 8, 243.
- Landa, Edward R., and Gast, R. G. (1973) Evaluation of crystallinity in hydrated ferric oxides. *Clays and Clay Minerals* 21, 121-130.
- Langmuir, D. (1969a) The Gibbs free energies of substances in the system Fe-O₂-H₂O-CO₂ at 25°C. USGS Prof. Paper 650-B, B180-B184.
- Langmuir, D. (1969b) Geochemistry of iron in a coastal plain ground water of the Camden, New Jersey area. USGS Prof. Paper 650-C, C224-C235.
- Lanza, P. (1968) An acidimetric criterion for evaluating the reliability of stability constants of complexes and the nature of the ligands. I. Introduction and application in the study of the Ag⁺-glycine system. *J. Electroanal. Chem.* 19, 275.
- Leckie, J. O., and James, R. O. (1975) Control mechanisms for trace metals in natural waters in: Aqueous-Environmental Chemistry of Metals, ed. by A. J. Rubin, Ann Arbor Science Pub., Ann Arbor, Mich., Chap. 1.
- Leckie, J. O., and Nelson, M. (1975) Role of natural heterogeneous sulfide systems in controlling the concentration of distribution of heavy metals. Presented at the 2nd International Symp. on Environmental Biogeochemistry, Burlington, Ontario, Canada.

- Lehman, G., and Wilson, L. (1971) Trace element removal from sewage effluent by soil filtration. *Water Res. Res.* 7, 90.
- Levenspiel, O. (1972) Chemical Reaction Engineering, John Wiley & Sons, New York.
- Li, H. C., and de Bruyn, P. L. (1966) Electrokinetic and adsorption studies on quartz. *Surf. Sci.* 5, 203.
- Little, L. H. (1966) Infrared Spectra of Adsorbed Species. Academic Press, London.
- Luckey, T., Venugopal, V., and Hutcheson, D. (1975) Heavy Metal Toxicity, Safety, and Hormology. Academic Press, 4-74.
- Mackenzie, R. C., Follett, E. A. G., and Meldav, R. (1971) The oxides of iron, aluminum and manganese, Ch. 11 in: *Mineralogical Soc. Monograph 3. The Electron-Optical Investigation of Clays*, ed. by J. A. Gard. Mineralog. Soc. Clay Minerals Group, 41 Queens Gate, London.
- MacNaughton, M. G. (1973) Adsorption of mercury(II) at the solid-water interface. Ph.D. thesis, Stanford University.
- MacNaughton, M. G., and James, R. O. (1974) Adsorption of aqueous Hg(II) complexes at oxide/water interface. *J. Coll. Int. Sci.* 47, 431.
- Mahlman, H. A., and Willmarth, T. E. (1964) Radiolytic and photolytic reduction of aqueous silver nitrate solutions. *Nature* 2-2, 590.
- Mallik, Tapas K. (1972) Opaque minerals from the shelf sediments off Mangalore, Western Coast, India. *Marine Geology* 12(3), 207-222.
- Marel, H. W. van der (1951) Gamma ferric oxide in sediments. *Journal of Sedimentary Petrology* 21(1), 12-21.
- Mathis, B., and Cummings, T. (1973) Selected metals in sediments, water, and biota in the Illinois River. *J. Wat. Poll. Cont. Fed.* 45, 1573.
- Matijevic, E., Sapieszko, R., and Melville, J. (1975) Ferric hydrous oxide sols. 1. Monodispersed basic iron(III) sulfate particles. *J. Coll. Int. Sci.* 50, 567.
- McLerran, C. J., and Holmes, C. W. (1974) Deposition of Zn and Cd by marine bacteria in estuarine sediments. *Limn. & Ocean.* 19, 998-1001.
- Mesmer, R. E., and Baes, C. F. (1976) The Hydrolysis of Cations. Wiley-Interscience Publ., New York, 1976.
- Misawa, T., Hashimoto, K., and Shimodaira, S. (1973) Formation of Fe(II)-Fe(III) intermediate green complex on oxidation of ferrous iron in neutral and slightly alkaline sulfate solutions. *J. Inorg. Nucl. Chem.* 35, 4167.

- Misra, D. N. (1968) Adsorption of silver ions on titanium dioxide. J. Coll. Int. Sci. 28, 24.
- Murphy, P. J., Posner, A. M., and Quirk, J. P. (1976) Characterization of partially neutralized ferric nitrate solutions. J. Coll. Int. Sci. 56, 270.
- Nagata, Shinji (1975) Mixing: Principles and Applications. John Wiley & Sons, New York.
- Nelson, M. B., Nordstrom, D. K., and Leckie, J. O. (1976) Modified ferrozine method for analysis of Fe(II) in presence of Fe(III). Submitted to Anal. Chem.
- Nickles,, G. (1968) Inorganic Sulfur Chemistry. Elsevier Publ. Co., Amsterdam, London, New York.
- Ol'Shanskii, Y. I., Ivanenko, V. V., and Khromov, A. V. (1959) The solubility of silver sulfide in aqueous solutions saturated with hydrogen sulfide. Akad. Nauk. SSSR, Dokl. Earth Sci. Secs., in English Trans. 124, 9.
- ORNL (1973) Ecology and analysis of trace contaminants. Progress Report 6172-1173, ORNL-NSF-EATC-1.
- Page, A. L., and Bingham, F. T. (1973) Cadmium residues in the environment. Residue Reviews 48, 1.
- Parks, G. A. (1965) The isoelectric points of solid oxides, solid hydroxides, and aqueous hydroxo complex systems. Chem. Reviews 65, 177.
- Pearson, R. G. (1968) Hard and soft acids and bases, HSAB, Part 1. J. Chem. Educ. 45, 581-587.
- Perhac, R. (1972) Distribution of Cd, Co, Cu, Fe, Mn, Ni, and Zn in dissolved and particulate solids from two streams in Tennessee. J. Hydrology 15, 177.
- Perhac, R. (1974) Heavy metal distribution in bottom sediment and water in the Tennessee River-Louden Lake Reservoir system. Research Report #40, Univ. of Tenn. Water Resources Research Center.
- Posselt, H. (1971) Environmental chemistry of cadmium in aqueous systems. University Microfilms, Ann Arbor, Michigan.
- Posselt, H. S., Anderson, F. J., and Weber, W. J. (1968) Cation sorption on colloidal hydrous manganese dioxide. Env. Sci. Tech. 2, 1087.
- Presley, B. J., Kolodny, Y., Nissenbaum, A., and Kaplan, I. R. (1972) Early diagenesis in a reducing fjord, Saanich Inlet British Columbia. II. Trace element distribution in interstit H₂O and sediments. Geochim. et Cosmochimica Acta 36, 1073-1090.

- Preston, A., Jeffries, D., Dutton, J., Harvey, B., and Steele, A. (1972) British Isles coastal waters: The concentrations of selected heavy metals in sea water, suspended matter, and biological indicators-- A pilot survey. *Envir. Poll.* 3, 69.
- Rebhun, M., and Manka, J. (1971) Classification of organics in secondary effluents. *Env. Sci. and Tech.* 5(7), 606-609.
- Ribbe, P. H. (1974) Sulfide mineralogy. Mineralogical Soc. of Amer. Short Course Notes, Vol. 1.
- Rickard, D. T. (1969) The chemistry of iron sulfide formation at low temperatures. *Stockholm Contr. Geol.* 20, 67-95.
- Riffaldi, R., and Levi-Minzi, R. (1975) Adsorption and desorption of Cd on humic acid fraction of soils. *Water, Air, and Soil Poll.* 5, 179.
- Robertson, D. E. (1968) The adsorption of trace elements in sea water on various container surfaces. *Anal. Chim. Acta* 42, 533.
- Sato, M. (1960) Oxidation of sulfide ore bodies. II. Oxidation mechanisms of sulfide minerals at 25°C. *Econ. Geol.* 55, 1202.
- Schickorr, von G. (1930) Über das beim Rostvorgang auftretende Eisen(III) Hydroxyd. *Z. Anorg. Allgem. Chem.* 191, 322-332.
- Schindler, P., Fürst, B., Dick, R., and Wolf, P. (1976) Ligand properties of surface silanol groups. 1. Surface complex formation with Fe^{3+} , Cu^{2+} , Cd^{2+} , and Pb^{2+} . *J. Coll. Int. Sci.* 55, 469.
- Schindler, P. W., and Gamajäger, H. (1972) Acid-base reactions of the TiO_2 (anatase)--water interface and point of zero charge of TiO_2 suspensions. *Kolloid Z. Z. Polym.* 250, 759.
- Schindler, P., and Kamber, H. R. (1968) Die Acidität von Silanolgruppen. *Helv. Chem. Acta* 51, 1781.
- Schnitzer, M., and Skinner, S. (1965) Organo-metallic interactions in soils: 4. Carboxyl and hydroxyl groups in organic matter and metal retention. *Soil Sci.* 99, 278.
- Schroeter, L. C. (1963) Potentiometric determination of sulfite oxidation rates. *J. Pharmaceutical Sci.* 52, 564.
- Schwertmann, U. (1959) Über die synthese definierter Eisenoxyde unter verschiedenen Bedingungen. *Z. Anorg. Allgem. Chem.* 298, 337-348.
- Schwertmann, U., and Taylor, R. M. (1972a) The transformation of lepidocrocite to goethite. *Clays and Clay Minerals* 20, 151-158.
- Schwertmann, U., and Taylor, R. M. (1972b) The influence of silicate on the transformation of lepidocrocite to goethite. *Clays and Clay Minerals* 20, 159-164.

- Schwertmann, U. (1966) Inhibitory effect of soil organic matter on the crystallization of amorphous ferric hydroxide. *Nature* 212(5062), 645-646.
- Schwertmann, U. (1973) Electron micrographs of soil lepidocrocites. *Clay Minerals* 10(1), 59-60.
- Sienko, M. J., and Plane, R. A. (1961) *Chemistry*, 2nd ed. McGraw-Hill Book Co., Inc., New York, Toronto, London.
- Sillen, L. G., and Martell, A. E. (1964) Stability constants of metal ion complexes. The Chemical Society, Special Publication #17.
- Sillen, L. G., and Martell, A. E. (1970) Stability constants of metal ion complexes: Supplement #1. The Chemical Society, Special Publication #25.
- Singer, P., and Stumm, W. (1970) Oxygenation of ferrous iron. *Water Poll. Res. Series* 14010-0669. Federal Water Quality Administration, Department of the Interior.
- Smith, H. G., and Rundle, R. E. (1958) The silver perchlorate-benzene complex, $C_6H_6 \cdot AgClO_4$, crystal structure and charge transfer energy. *J. Am. Chem. Soc.* 80, 5075.
- Snavely, E. S., and Blount, F. E. (1969) Rates of reaction of dissolved oxygen with scavengers in sweet and sour brines. *Corrosion* 25, 397.
- Spiro, T. G., Allerton, S. E., et al. (1966) The hydrolytic polymerization of iron(III). *J. Am. Chem. Soc.* 88, 2721.
- Sridharan, N., and Lee, G. F. (1972) Coprecipitation of organic compounds from lake water by iron salts. *Env. Sci. Tech.* 6, 1031.
- Stephen, W. I., and Townshend, A. (1966) The reaction of silver(I) ions with organic compounds containing the HN-C=S grouping. Part II. Some thiourea derivatives. *J. Chem. Soc. (A)*, 166.
- Struempfer, A. W. (1973) Adsorption characteristics of silver, lead, cadmium, zinc, and nickel on borosilicate glass, polyethylene, and polypropylene container surfaces. *Anal. Chem.* 45, 2251.
- Stumm, W., Huang, C. P., and Jenkins, S. R. (1970) Specific chemical interactions affecting the stability of dispersed systems. *Croat. Chem. Acta* 42, 223.
- Stumm, W., and Lee, G. F. (1961) Oxygenation of ferrous iron. *Ind. and Eng. Chemistry* 53(2), 143-146.
- Stumm, W., and Morgan, J. J. (1970) *Aquatic Chemistry*. Wiley Interscience, New York, London, Sydney, Toronto.
- Stumm, W., and Singer, P. C. (1966) Precipitation of iron in aerated ground waters. *J. Sanitary Eng. Div. (Proc. Am. Soc. Civ. Eng.)* 92, 120-124.

- Tadros, T. F., and Lyklema, J. (1968) Adsorption of potential-determining ions at the silica-aqueous electrolyte interface and the role of some cations. *J. Electroanal. Chem.* 17, 267.
- Taylor, D. (1974) Natural distribution of trace metals in sediments from a coastal environment, Tor Bay, England. *Estuarine and Coastal Mar. Sci.* 2, 417-424.
- Theis, T. L., and Singer, P. C. (1973) The stabilization of ferrous iron by organic compounds in natural waters, Ch. 10, 303-320, in: Trace Metals and Metal-Organic Interactions in Natural Waters, ed. by P. C. Singer. Ann Arbor Sci. Publishers, Ann Arbor, Mich.
- Theis, T. L., and Singer, P. C. (1974) Complexation of iron(II) by organic matter and its effect on iron(II) oxygenation. *Envir. Sci. and Tech.* 8(6), 569-573.
- Thompson, N. R. (1973) Silver, in: Comprehensive Inorganic Chemistry, ed. by Bailar. Pergamon Press, Oxford, p. 79.
- Troupe, B. N., Bricker, O. P., and Bray, J. T. (1974) Oxidation effect on the analysis of iron in the interstitial water of recent anoxic sediments. *Nature* 249, No. 5454, 237-239.
- Turekian, K. K., Harriss, R. C., and Johnson, D. G. (1967) The variations of Si, Cl, Na, Ca, Sr, Ba, Co, and Ag in the Neuse River, North Carolina. *Limn. Ocean.* 12, 702.
- Turekian, K. K., and Scott, M. R. (1967) Concentration of Cr, Ag, Mo, Ni, Co, and Mn in suspended matter in streams. *Env. Sci. Tech.* 1, 940.
- Urban, P. J. (1961a) Colorimetry of sulfur anions. I: An improved colorimetric method for the determination of thiosulfate. *Z. Anal. Chem.* 179, 415.
- Urban, P. J. (1961b) Colorimetry of sulfur anions. II: A specific colorimetric method for determination of trithionate. *Z. Anal. Chem.* 179, 422.
- Urban, P. J. (1961c) Colorimetry of sulfur anions. IV: Colorimetric evaluation of sulfur sols. *Z. Anal. Chem.* 180, 116-119.
- Van der Giessen, A. A. (1966) The structure of iron(III) oxide-hydrate gels. *J. Inorg. Nucl. Chem.* 28, 2155-2159.
- Van der Lier, J. A., de Bruyn, P. L., and Overbeek, J. T. G. (1960) The solubility of quartz. *J. Phys. Chem.* 64, 1675.
- Vuceta, J. (1976) Adsorption of Pb(II) and Cu(II) on α -quartz from aqueous solutions: Influence of pH, ionic strength, and complexing ligands. Ph.D. thesis, California Institute of Technology.

Weiss, J. (1935) Elektronenübergangsprozesse im Mechanismus von Oxydations- und Reduktions-Reaktionen in Lösungen. *Naturwissenschaften* 23, 64.

Welo, Lars A., and Baudisch, O. (1934) Relationships among the oxide hydrates and oxides of iron and some of their properties. *Chem. Reviews* 15, 45-97.

Yates, D. E. (1975) The structure of the oxide/aqueous electrolyte interface. Ph.D. thesis, Univ. of Melbourne.

Zasoki, R. J. (1974) Sorption and sorptive interaction of cadmium and zinc on hydrous manganese oxide. University Microfilms, University of California, Davis.

Zhitnikov, R. A., and Paugurt, A. P. (1966) FTT (*Soviet Phys. Solid State*), 6, 1796.

Zirino, R., and Yamamoto, S. (1972) A pH-dependent model for the chemical speciation of Cu, Zn, Cd, and Pb in seawater. *Limn. and Ocean.* 17, 661.

APPENDIX A

LIQUID SCINTILLATION COUNTING

Liquid scintillation counting is a method of detecting radioactivity by means of a solution of fluors and a multiplier phototube. The scintillation solution converts to light the energy of the primary particle emitted by the radioactive sample, and the phototube responds to this light energy by producing a charge pulse which can be amplified and counted by a scaling circuit. The widest application of liquid scintillation counting is the counting of low energy beta emitters. In any radiation detection method, the counting efficiency is greatest when the maximum number of emitted particles reaches the detector and interacts in the desired way. Beta rays lose their energy in passing through matter much more quickly than do x-rays or γ -rays of comparable energy, and thus have much shorter ranges. Absorption along their paths within the sample and between the sample and detector is most severe for low energy betas such as tritium. In order to avoid such losses and to count with high efficiency, these distances must be reduced as much as possible. This is the great advantage achieved in liquid scintillation counting.

In general, the radioactive substance is put into intimate contact with the scintillation solution by dissolving, suspending, or immersing the isotope in a liquid solution of fluors. Not only is unwanted absorption reduced by mixing the source material with the detecting solution, but escape of beta particles from the detector is minimized. Escape can occur only from a very thin surface layer.

Scintillation counting is a proportional counting method where the magnitude of the output signal from the detector is proportional to the energy given up to the detector by the primary particle. Specifically, if a particle is completely stopped in the scintillation solution, a condition fulfilled in the case of low energy beta emitters, the size of the voltage pulse produced by the photomultiplier tube should be proportional to the primary energy.

The ratio of the observed net counting rate (sample rate minus background rate) and the true disintegration rate of the sample is dependent on

all variables which affect pulse height, since losses in the system are cumulative and any pulses too far degraded in energy will not be counted. Some of these variables are system-dependent and some obey the laws of random fluctuations. The important variables which determine counting efficiency are: 1) fraction of primary particle energy absorbed in the scintillation solution, 2) conversion efficiency of the scintillation solution, 3) reabsorption of light by the scintillation solution, 4) spectral match between scintillator and phototubes, 5) quenching of light output by the radioactive sample solute, 6) the temperature of the sample, 7) the volume of the sample, 8) light collection efficiency, 9) conversion efficiency of the photocathode, 10) amplification factors, and 11) discriminator settings.

Quenching of light output may take place through color quenching or by a variety of mechanisms which interfere in some way with the scintillation process. The fluor molecules can be quenched if foreign molecules are present which absorb their excitation energy during the lifetime of the excited state before the energy is emitted as light. Solvent molecules can be quenched if their energy is transferred to solute molecules which are not fluors and which allow the energy to degrade to some form other than visible light. Non-fluorescent solute molecules are quenchers and vary tremendously in the degree of quenching they produce. Two of the more ubiquitous quenchers are dissolved oxygen and water.

It is obviously necessary that counting efficiency be constant or determinable for all samples to be compared. There are two purely instrumental methods of determining counting efficiency: the channels ratio method and the external standard method. Counting efficiency is determined by an indirect comparison of the unknown sample with a set of standard samples of the same isotope by means of a calibration curve.

In the channels ratio method, two counting channels are chosen so that together they include most of the pulse height distribution observed for the least quenched sample. As quenching increases, the ratio of the counting rates in the two channels changes monotonically with the counting efficiency. A calibration curve can be plotted with counting efficiency as a function of channels ratio for the particular isotope.

In the external standard method a calibration curve is established which relates counting efficiency for the isotope in the sample when it is

exposed to a gamma source placed nearby. The scintillator in the vial detects the gamma rays through Compton interactions. These produce high energy electrons which are detected in the same way as betas, with an efficiency depending on the degree of quenching. The net counting rate for the gamma source depends on several factors besides quenching such as the exact position of the source with respect to the vial, the vial wall thickness, the sample volume, and the electron density of the sample material. To minimize errors in preparing the calibration curve, the absolute counting rate of the gamma source may be replaced by the ratio of its counting rates in two channels. This ratio of external standard counts is sensitive to quenching as is the ratio of beta counts, but is less sensitive to most of the other factors. Two sample counts are required for external standardization: with and without exposure to the gamma source.

APPENDIX B

ADSORPTION OF SILVER BY FERROUS MONOSULFIDE

Two small experiments were conducted to determine the stability and capacity of silver uptake by the iron sulfide, mackinawite. Details of the preparation of the ferrous sulfide are presented elsewhere in this report. The experiments were conducted under a nitrogen atmosphere in a suspension of $\sim 10^{-2}$ M FeS at pH 9 with a slight excess of ferrous iron. The ionic strength was adjusted to 0.1M with sodium nitrate.

The experimental strategy was to titrate the surface of the solid with silver. It was hoped that a monolayer of adsorbed silver as silver sulfide would form on the particles. This point in the silver titration would be detected by an increase in the solution concentration of silver. Silver removal was greater than 99% for all total silver concentrations added, ranging from 5×10^{-5} M to $\sim 10^{-3}$ M. Samples were taken within five minutes after silver addition so the surface reactions are very rapid. At the end of the titration, the amount of silver removed was equivalent to 10% of the total sulfide present. The amount of silver removed is greater than expected by a simple surface reaction scheme. This suggests that silver is capable of diffusing rapidly into the ferrous sulfide lattice and may even replace ferrous ions in the solid. These results are consistent with the lower solubility of silver sulfide as compared to ferrous sulfide. When the adsorbing metal ion has a greater sulfide solubility than that of the lattice metal ion, adsorption may occur only by surface adsorption (James and Parks, 1974).

Additional experiments conducted in the presence of a large excess of thiosulfate yield identical results. Silver removal is greater than 99% despite the considerable complexing of thiosulfate (4×10^{-3} M).

APPENDIX C

KINETIC DATA FOR OXIDATION REACTIONS

Test Number	Age of FeS, days	Initial FeS, mole/l	pH	[O ₂], mg/l	T, °C	Ionic Media	Gas Mixture	Comments:
X-α-1	9	8.8 x 10 ⁻³	7	2	20	10 ⁻³ M Na ₂ SO ₄	Air	
2	9	"	7	4	20	"	Air	
3	9	"	7	8	20	"	Air	
4	10	"	7	6	20	"	Air	
9	15	"	7	6	20	"	Air/N ₂	
10	15	"	7	8	20	"	Air/N ₂	
11	16	"	7	3	20	"	Air/N ₂	
X-B-1	18	8.8 x 10 ⁻³	9	8	20	10 ⁻³ M Na ₂ SO ₄	Air/N ₂	40 ml FeS
2	22	"	9	16	20	"	Air/N ₂	40 ml FeS
3	24	1.76 x 10 ⁻²	9	16	20	"	Air/N ₂	80 ml FeS
4	28	1.32 x 10 ⁻²	9	16	20	"	Air/N ₂	60 ml FeS
5	29	4.4 x 10 ⁻³	9	16	20	"	Air/N ₂	20 ml FeS
6	38	8.8 x 10 ⁻³	9	16	20	"	Air/N ₂	40 ml FeS
X-C-1	23	8.6 x 10 ⁻³	9	16	20	10 ⁻³ M Na ₂ SO ₄	N ₂ /O ₂	
2	27	"	9	16	20	0.563N NaCl	N ₂ /O ₂	
4	72	"	7	8	20	10 ⁻³ M Na ₂ SO ₄	N ₂ /O ₂	40 ml FeS
5	72	"	7	8	20	"	N ₂ /O ₂	80 ml FeS
6	73	"	7.5	8	20	"	N ₂ /O ₂	
7	76	"	6.5	8	20	"	N ₂ /O ₂	
X-D-1	32	7.7 x 10 ⁻³	7	8	20-27	10 ⁻³ M Na ₂ SO ₄	N ₂ /O ₂	
2	32	"	7	4	20	0.1N NaCl	N ₂ /O ₂	
3	32	"	7-6.75	8	20	"	N ₂ /O ₂	
4	33	"	7	8	20	.033M Na ₂ SO ₄	N ₂ /O ₂	
5	34	"	7	8	20	0.1N NaCl	N ₂ /O ₂	
6	35	"	7	8	20	10 ⁻³ M Na ₂ SO ₄	N ₂ /O ₂	
7	39	"	7	8	20	.167M Na ₂ SO ₄	N ₂ /O ₂	
8	39	"	7	8	20	0.5M NaCl	N ₂ /O ₂	
9	41	"	9	16	20	.167M Na ₂ SO ₄	N ₂ /O ₂	

APPENDIX C (CONTINUED)

Test Number	Age of FeS, days	Initial FeS, mole/l	pH	[O ₂], mg/l	T, °C	Ionic Media	Gas Mixture	Comments:
X-E-1	20	9.0 x 10 ⁻³	9	16	20	10 ⁻³ M Na ₂ SO ₄	N ₂ /O ₂	10 ⁻⁴ M Cd <u>Adsorbed</u>
2	21	"	9	16	20	.10M NaCl	N ₂ /O ₂	
3	27	"	9	16	20	10 ⁻³ M Na ₂ SO ₄	N ₂ /O ₂	
X-Cd-1	14	9.0 x 10 ⁻³	9	16	20	10 ⁻³ M Na ₂ SO ₄	N ₂ /O ₂	1% Cd co-ppt with FeS
X-F-5	52	"	7	8	20	10 ⁻³ M Na ₂ SO ₄	N ₂ /O ₂	10 gm/l SiO ₂ 1.5 gm/l γ-FeCOH Pure O ₂ bubbled through solution Pure O ₂ bubbled through solution Pure O ₂ bubbled through solution 10 ⁻² M phenol Stirred with magnetic mixer Stirred violently with propeller
6	52	"	7	8	20	"	N ₂ /O ₂	
7	52	"	7	8	20	"	N ₂ /O ₂	
8	54	"	7	1 atm	10.5	"	1007 O ₂	
9	54	"	7	1 atm	10.5	"	1007 O ₂	
10	55	"	7	1 atm	10.5	"	1007 O ₂	
11	55	"	7	18	10.5	"	O ₂ /N ₂	
12	59	"	7	8	20	"	O ₂ /N ₂	
13	70	"	7	8	20	"	O ₂ /N ₂	
14	71	"	7	8	20	"	O ₂ /N ₂	
15	73	"	9	10	10	"	O ₂ /N ₂	
16	75	"	9	10	30	"	O ₂ /N ₂	
17	76	"	9	10	20	"	O ₂ /N ₂	
21	80	"	9	1 atm	20	"	O ₂ /N ₂	
22	83	"	9	10	44.2	"	O ₂ /N ₂	
23	84	"	10	10	20	"	N ₂ /O ₂	
24	90	"	9	16.6	20	"	N ₂ /O ₂	

APPENDIX C (CONTINUED)

Test Number	Age of FeS, days	Initial FeS, mole/l	pH	[O ₂], mg/l	T, °C	Ionic Media	Gas Mixture	Comments:
X-G-1	5	8.6×10^{-3}	9	10	35	10^{-3} M Na ₂ SO ₄	N ₂ /O ₂	
3	6	"	7	4	5	"	N ₂ /O ₂	
4	7	"	7	4	20	"	N ₂ /O ₂	
5	7	"	7	4	35	"	N ₂ /O ₂	
6	7	"	7	4	20	"	N ₂ /O ₂	10^{-4} M NiSO ₄
7	8	"	7	4	20	"	N ₂ /O ₂	10^{-5} M NiSO ₄
8	8	"	7	4	20	"	N ₂ /O ₂	"
9	8	"	7	4	20	"	N ₂ /O ₂	3×10^{-5} M NiSO ₄ (excess Fe)
10	8	"	7	4	20	"	N ₂ /O ₂	"
11	9	"	7	4	20	"	N ₂ /O ₂	3×10^{-5} M CuSO ₄
12	10	"	7	4	10	"	N ₂ /O ₂	
13	10	"	7	4	20	"	N ₂ /O ₂	10^{-4} M AgNO ₃
14	11	"	9	10	20	"	N ₂ /O ₂	5×10^{-4} M NiSO ₄
15	11	"	7	4	30	"	N ₂ /O ₂	
16	12	"	7	4	15	"	N ₂ /O ₂	
K-H-1	15	8.47×10^{-3}	9	10	20	10^{-3} M Na ₂ SO ₄	O ₂ /N ₂	
2	15	"	9	10	20	"	O ₂ /N ₂	1.13% (0.377M) formaldehyde present in reactor
K-I-1	65	8.9×10^{-3}	9	16	20	$10^{-3.7}$ M Na ₂ SO ₄	O ₂ /N ₂	
2	68	"	10	9	25	"	O ₂ /N ₂	
3	72	9.9×10^{-3}	7	11.1	10	"	O ₂ /N ₂	
4	72	"	7	21.6	10	"	O ₂ /N ₂	
5	73	"	7	31.4	10	"	O ₂ /N ₂	
6	73	"	7	36.8	10	"	O ₂ /N ₂	
7	73	"	7	47.6	10	"	O ₂ /N ₂	
8	74	"	7	10	15	"	O ₂ /N ₂	
9	74	"	7	19.5	15	"	O ₂ /N ₂	
10	74	"	7	29.3	15	"	O ₂ /N ₂	
11	75	"	7	4	20	"	O ₂ /N ₂	
12	75	"	7	16	20	"	O ₂ /N ₂	

APPENDIX C (CONCLUDED)

Test Number	Age of FeS, days,	Initial FeS, mole/l	pH	[O ₂], mg/l	T, °C	Ionic Media	Gas Mixture	Comments:
X-I-13	82	9.9×10^{-3}	7	4	20	0.167M Na ₂ SO ₄	O ₂ /N ₂	
14	82	"	7	4	20	0.5 M NaCl	O ₂ /N ₂	
15	82	"	7	4	20	0.1 M NaCl	O ₂ /N ₂	
16	82	"	7	4	20	0.033M Na ₂ SO ₄	O ₂ /N ₂	
17	84	"	7	16	20	0.5M NaCl	O ₂ /N ₂	
18	84	"	7	16	20	0.1 M NaCl	O ₂ /N ₂	
19	84	"	7	16	20	0.033M Na ₂ SO ₄	O ₂ /N ₂	
20	84	"	7	16	20	0.117M Na ₂ SO ₄	O ₂ /N ₂	

X-Q-1		X-Q-2		X-Q-3		X-Q-4	
Time of Oxi- dation min.	FeS Remaining moles/l	Time of Oxi- dation min.	FeS Remaining moles/l	Time of Oxi- dation min.	FeS Remaining moles/l	Time of Oxi- dation min.	FeS Remaining moles/l
0	7.17×10^{-3}	0	7.04×10^{-3}	0	6.46×10^{-3}	0	6.92×10^{-3}
15	6.62 "	5	6.74 "	5	6.0 "	5	6.65 "
30	6.19 "	10	6.62 "	10	5.42 "	10	6.09 "
45	5.67 "	15	6.34 "	15	4.87 "	15	5.67 "
60	5.02 "	20	6.00 "	20	4.26 "	20	5.05 "
75	4.35 "	30	5.33 "	25	3.77 "	25	4.56 "
90	3.71 "	40	4.69 "	30	3.19 "	30	4.04 "
105	3.09 "	50	4.04 "	35	2.57 "	40	3.06 "
120	2.45 "	60	3.37 "	40	1.90 "	50	2.11 "
135	1.93 "	70	2.70 "	45	1.35 "	60	0.64 "
150	1.41 "	80	2.02 "	50	1.01 "		
165	0.98 "	90	1.53 "				
		100	0.98 "				

X-α-9		X-α-10		X-α-11	
Time of Oxi- dation min.	FeS Remaining moles/l	Time of Oxi- dation min.	FeS Remaining moles/l	Time of Oxi- dation min.	FeS Remaining moles/l
0	7.4 x 10 ⁻³	0	6.83 x 10 ⁻³	0	7.56 x 10 ⁻³
5	6.75 "	5	6.18 "	10	6.99 "
10	6.43 "	10	5.37 "	15	6.87 "
15	5.82 "	15	4.64 "	20	6.67 "
20	5.12 "	20	3.9 "	30	6.22 "
25	4.51 "	25	3.13 "	40	5.53 "
30	3.82 "	30	2.48 "	50	4.8 "
35	3.17 "	35	1.87 "	60	4.23 "
40	2.52 "	40	1.30 "	70	3.42 "
45	1.95 "			80	2.60 "
50	1.42 "			90	1.93 "
55	0.98 "			100	1.06 "
60	0.57 "			110	0.49 "

X-B-1			X-B-2			X-B-3		
Time of Oxi- dation min.	FeS Remaining moles/l	Iodine Reactive Species eq/l	Time of Oxi- dation min.	FeS Remaining moles/l	Iodine Reactive Species eq/l	Time of Oxi- dation min.	FeS Remaining moles/l	Iodine Reactive Species eq/l
0	9.11×10^{-3}	0	0	8.95×10^{-3}	0.486×10^{-3}	0	1.57×10^{-2}	0.122×10^{-3}
0	8.14	0	0	7.57	0.486	15	1.29	0.78
20	7.21	0.324×10^{-3}	20	6.03	1.38	30	1.03	1.39
40	6.36	0.73	40	4.74	2.19	45	7.72×10^{-3}	2.11
60	5.59	0.972	60	3.56	3.0	60	5.77	2.72
80	4.90	1.30	80	2.63	3.73	75	4.13	3.21
100	4.21	1.54	100	1.86	4.37	90	2.67	3.69
120	3.65	1.78	120	1.42	4.86	105	1.76	4.06
140	3.12	2.11	140	0.97	5.27	120	1.07	4.30
210	1.86	2.67	160	0.73	5.59	135	0.67	4.42
240	1.62	2.75	180	0.61	5.67			
280	1.26	3.00	220	0.37	5.99			
320	0.96	3.24						
360	0.81	3.32						

X-B-4			X-B-5			X-B-6		
Time of Oxi- dation min.	FeS Remaining moles/l	Iodine Reactive Species eq/l	Time of Oxi- dation min.	FeS Remaining moles/l	Iodine Reactive Species eq/l	Time of Oxi- dation min.	FeS Remaining moles/l	Iodine Reactive Species eq/l
0	1.39×10^{-2}	0	0	4.28×10^{-3}	0	0	8.8×10^{-3}	0.172×10^{-3}
0	1.25	0	15	3.43	0.365×10^{-3}	20	7.17	0.97
10	1.06	0.85×10^{-3}	30	2.79	0.61	40	5.87	1.94
25	9.17×10^{-3}	1.22	45	2.13	0.972	60	4.56	2.79
45	6.93	2.55	60	1.55	1.34	80	3.22	4.01
60	5.65	3.40	75	1.12	1.58	100	2.23	4.62
75	4.13	4.01	90	0.85	1.82	120	1.56	5.22
90	3.04	4.62	105	0.64	1.94	140	1.05	5.59
105	2.07	5.10	120	0.486	2.07	160	0.71	5.95
120	1.52	5.35	135	0.365	2.19	180	0.57	6.08
135	1.09	5.47	150	0.27	2.25	250	0.30	6.44
150	0.73	5.71						

X-C-1

Time of Oxi- dation min.	FeS Oxidized moles/l	Iodine- Consuming Species eq/l	Hydrogen Ions Produced moles/l	Sulfur in Soluble Phase (moles/l as written)		
				$S_2O_3^{-2}$	$S_4O_6^{-2}$	Colloidal S^0
0	0.69×10^{-3}	0.49×10^{-3}				
20	2.70 "	0.97 "				
40	3.73 "	1.7 "		0.666×10^{-3}	0.072×10^{-3}	0.14×10^{-3}
60	4.95 "	2.56 "				
80	5.80 "	2.92 "		1.217 "	0.07 "	0.27 "
100	6.65 "	3.41 "				
120	7.50 "	4.14 "		1.487 "	0.14 "	0.35 "
140	7.81 "	4.14 "				
220	8.36 "	4.38 "		2.14 "	0.16 "	1.45 "

X-C-2

Time of Oxi- dation min.	FeS Oxidized moles/l	Iodine- Consuming Species eq/l	Hydrogen Ions Produced moles/l	Sulfur in Soluble Phase (moles/l as written)		
				$S_2O_3^{-2}$	$S_4O_6^{-2}$	Colloidal S^0
0	0.87×10^{-3}	0				
20	3.49 "	0.122×10^{-3}	0.164×10^{-3}			
40	5.03 "	0.122 "	0.275 "			
60	5.76 "	0.17 "	0.503 "			
80	6.41 "	0.122 "	0.621 "			
100	7.2 "	0.244 "	0.797 "			
140	7.81 "	0.365 "	1.16 "			
180	8.29 "	0.61 "	1.60 "	0.256×10^{-3}	0.048×10^{-3}	0.03×10^{-3}

X-C-4		X-C-5		X-C-6		X-C-7	
Time of Oxi- dation min.	FeS Remaining moles/l	Time of Oxi- dation min.	FeS Remaining moles/l	Time of Oxi- dation min.	FeS Remaining moles/l	Time of Oxi- dation min.	FeS Remaining moles/l
0	8.51×10^{-3}	0	1.648×10^{-2}	0	8.27×10^{-3}	0	9.8×10^{-3}
5	7.96	5	1.53	5	7.78	5	9.13
10	7.29	10	1.42	10	7.53	10	8.21
15	6.68	15	1.3	15	6.98	15	7.41
20	5.88	20	1.13	20	6.43	20	6.43
30	4.37	25	1.0	30	5.45	25	5.21
40	3.0	30	8.64×10^{-3}	40	4.59	30	4.04
50	1.72	35	7.04	50	3.61	35	3.12
60	0.86	40	5.76	60	2.88	40	2.14
70	0.43	50	3.49	75	1.78	45	1.47
		60	1.90	90	0.98	50	0.86
		70	0.98	105	0.55	55	0.61
						60	0.37
						65	0.18
						70	0.25

X-D-1		X-D-2		X-D-3		X-D-4	
Time of Oxi- dation min.	FeS Remaining moles/l	Time of Oxi- dation min.	FeS Remaining moles/l	Time of Oxi- dation min.	FeS Remaining moles/l	Time of Oxi- dation min.	FeS Remaining moles/l
0	7.29×10^{-3}	0	7.74×10^{-3}	0	7.7×10^{-3}	0	7.86×10^{-3}
5	6.84	0	7.25	0	7.17	0	7.25
10	6.23	5	6.96	5	6.84	5	6.91
15	5.46	10	6.76	10	6.6	10	6.43
20	4.68	15	6.56	15	6.31	15	6.07
25	3.79	20	6.35	20	6.0	20	5.37
30	2.93	31	5.86	30	5.17	25	4.72
35	2.16	40	5.20	35	4.76	30	3.99
40	1.36	50	4.52	40	4.32	35	3.18
45	0.814	60	3.79	50	3.5	40	2.44
50	0.407	70	3.18	60	2.65	45	1.71
55	0.163	80	2.61	70	1.87	50	1.10
		90	2.0	85	1.02	55	0.651
		100	1.55	100	0.49	60	0.407
						65	0.244
						70	0.122

X-D-5		X-D-6		X-D-7		X-D-8	
Time of Oxi- dation min.	FeS Remaining moles/l	Time of Oxi- dation min.	FeS Remaining moles/l	Time of Oxi- dation min.	FeS Remaining moles/l	Time of Oxi- dation min.	FeS Remaining moles/l
0	7.82 x 10 ⁻³	0	7.33 x 10 ⁻³	0	7.57 x 10 ⁻³	0	8.02 x 10 ⁻³
0	7.33 "	5	6.88 "	5	7.11 "	0	7.24 "
5	6.8 "	10	6.27 "	10	6.62 "	5	7.03 "
10	6.51 "	15	5.58 "	15	6.2 "	10	6.7 "
15	6.15 "	20	4.76 "	20	5.62 "	20	6.04 "
20	5.62 "	25	3.99 "	25	4.96 "	30	5.34 "
25	5.13 "	30	3.1 "	30	4.34 "	40	4.63 "
30	4.6 "	35	2.44 "	35	3.8 "	50	3.93 "
35	4.07 "	40	1.71 "	40	3.02 "	60	3.10 "
40	3.46 "	45	1.06 "	45	2.44 "	65	2.9 "
45	2.93 "	50	0.65 "	50	1.86 "	70	2.52 "
50	2.44 "	55	0.326 "	55	1.41 "	80	1.94 "
55	2.04 "	60	0.163 "	60	0.99 "	85	1.65 "
60	1.55 "	65	0.081 "	65	0.744 "	90	1.36 "
65	1.14 "			75	0.37 "	95	1.20 "
70	0.896 "			85	0.25 "	105	0.74 "
75	0.651 "					115	0.58 "
80	0.489 "						
85	0.407 "						
95	0.285 "						

Test X-D-9

Time of Oxi- dation min.	FeS Oxidized moles/l	Iodine- Consuming Species eq/l	Hydrogen Ions Produced moles/l	Sulfur in Soluble Phase (moles/l as written)		
				$S_2O_3^{-2}$	$S_4O_6^{-2}$	Colloidal S^0
0	0.49×10^{-3}	-				Samples Ruined
20	2.23 "	0.124×10^{-3}				
40	3.72 "	0.124 "	0.412×10^{-3}	0.105×10^{-3}	0.003×10^{-3}	
60	4.78 "	0.372 "	0.515 "			
80	5.64 "	0.372 "	0.841 "	0.162 "	0.018 "	
100	6.33 "	0.496 "	1.09 "			
120	6.80 "	0.571 "	1.23 "	0.244 "	0.010 "	
140	7.23 "	0.571 "	1.31 "			
160	7.63 "	0.62 "	1.43 "			
180	7.82 "	0.67 "	1.58 "	0.321 "	0.026 "	

X-E-1

Time of Oxi- dation min.	FeS Oxidized moles/l	Iodine- Consuming Species eq/l	Hydrogen Ions Produced moles/l	Sulfur in Soluble Phase (moles/l as written)		
				$S_2O_3^{-2}$	$S_4O_6^{-2}$	Colloidal S^0
0	1.12×10^{-3}					
20	2.96 "	0.735×10^{-3}	0.613×10^{-3}			
40	4.74 "	1.35 "	1.36 "	0.522×10^{-3}	0.046×10^{-3}	0.134×10^{-3}
60	6.58 "	2.21 "	-			
80	8.05 "	2.57 "	2.68 "	0.857 "	0.070 "	0.237 "
100	8.87 "	2.74 "	3.04 "			
120	9.39 "	3.06 "	3.39 "	1.24 "	0.10 "	0.18 "
160	9.58 "	2.94 "	3.75 "	1.18 "	0.085 "	0.267 "
220	9.7 "	2.84 "	4.36 "	1.47 "	0.050 "	0.195 "

X-E-2

Time of Oxi- dation min.	FeS Oxidized moles/l	Iodine- Consuming Species eq/l	Hydrogen Ions Produced moles/l	Sulfur in Soluble Phase (moles/l as written)		
				$S_2O_3^{-2}$	$S_4O_6^{-2}$	Colloidal S^0
0	0.94×10^{-3}	0.123×10^{-3}	0.054×10^{-3}			
20	3.33 "	0.245 "	0.145 "			
40	5.23 "	0.368 "	0.219 "	0.122×10^{-3}	0.027×10^{-3}	0.11×10^{-3}
60	6.27 "	0.368 "	0.298 "			
80	7.47 "	0.490 "	0.358 "	0.202 "	0.033 "	0.019 "
100	8.17 "	0.613 "	0.422 "			
120	8.97 "	0.735 "	0.488 "	0.313 "	0.029 "	0.030 "
160	9.39 "	0.858 "	0.65 "	0.371 "	0.047 "	0.038 "
220	9.7 "	0.98 "	0.75 "	0.406 "	0.062 "	0.041 "

X-E-3

Time of Oxi- dation min.	FeS Oxidized moles/l	Iodine- Consuming Species eq/l	Hydrogen Ions Produced moles/l	Sulfur in Soluble Phase (moles/l as written)		
				$S_2O_3^{-2}$	$S_4O_6^{-2}$	Colloidal S^0
0	0.27×10^{-3}					
20	1.74 "	0.613×10^{-3}	0.536×10^{-3}			
40	3.39 "	1.23 "	1.19 "			
60	4.92 "	1.84 "	1.90 "			
80	6.21 "	2.33 "	2.60 "			
100	7.37 "	2.82 "	3.29 "			
120	8.23 "	3.19 "	3.83 "			
160	9.09 "	3.31 "	4.67 "			
220	9.39 "	3.31 "	5.43 "			
320	9.61 "	3.14 "	6.14 "	3.23×10^{-3}	0	0

X-Cd-1

Time of Oxi- dation min.	FeS Oxidized moles/l	Iodine- Consuming Species eq/l	Hydrogen Ions Produced moles/l	Sulfur in Soluble Phase (moles/l as written)		
				$S_2O_3^{2-}$	$S_4O_6^{2-}$	Colloidal So
0	0.82×10^{-3}	0.49×10^{-3}				
20	3.08 "	1.35 "	0.65×10^{-3}			
40	4.62 "	2.21 "	1.11 "			
60	5.72 "	2.82 "	1.52 "			
80	6.39 "	3.19 "	1.8 "			
100	7.19 "	3.84 "	2.20 "			
120	7.80 "	4.04 "	2.44 "			
160	8.48 "	4.41 "	2.90 "	1.74×10^{-3}	0.125×10^{-3}	0.29×10^{-3}
200	8.48 "	4.41 "	3.16 "	2.09 "	0.090 "	-
250	8.72 "		3.29 "			

X-F-5			X-F-6			X-F-7			X-F-8		
Time of Oxi- dation min.	FeS Remaining moles/l		Time of Oxi- dation min.	FeS Remaining moles/l		Time of Oxi- dation min.	FeS Remaining moles/l		Time of Oxi- dation min.	FeS Remaining moles/l	
0	7.66×10^{-3}		0	7.66×10^{-3}		0	7.73×10^{-3}		0	7.6×10^{-3}	
0	7.41 "		0	7.29 "		0	7.41 "		0	7.29 "	
5	6.97 "		5	6.85 "		5	6.85 "		7	6.6 "	
10	6.62 "		10	6.47 "		10	6.35 "		8	5.84 "	
15	6.16 "		20	5.78 "		15	5.91 "		12	4.96 "	
20	5.84 "		30	4.84 "		20	5.53 "		16	3.9 "	
30	4.90 "		42	3.77 "		30	4.65 "		20	3.14 "	
40	3.90 "		50	2.95 "		40	3.64 "		24	2.64 "	
50	2.76 "		60	2.01 "		50	2.83 "		28	2.26 "	
60	1.95 "		70	1.26 "		60	1.88 "		32	1.76 "	
70	1.13 "					70	1.19 "		36	1.51 "	
						80	0.69 "		44	1.01 "	
						90	0.44 "		52	0.50 "	
						110	0.188 "				

X-F-9		X-F-10		X-F-11		X-F-12	
Time of Oxi- dation min.	FeS Remaining moles/l	Time of Oxi- dation min.	FeS Remaining moles/l	Time of Oxi- dation min.	FeS Remaining moles/l	Time of Oxi- dation min.	FeS Remaining moles/l
0	7.66×10^{-3}	0	7.60×10^{-3}	0	7.66×10^{-3}	0	7.66×10^{-3}
0	7.29 "	0	7.22 "	0	7.35 "	0	7.41 "
4	6.47 "	4	6.66 "	5	6.97 "	5	6.85 "
8	5.53 "	8	6.03 "	10	6.53 "	10	6.53 "
12	4.46 "	12	4.90 "	20	5.53 "	15	6.16 "
16	3.52 "	16	3.77 "	30	4.52 "	20	5.15 "
20	2.89 "	20	3.14 "	40	3.58 "	30	5.15 "
24	2.39 "	24	2.76 "	50	2.83 "	40	4.65 "
28	2.01 "	28	2.20 "	60	-	50	3.58 "
32.5	1.51 "	32	1.88 "	70	-	60	2.64 "
36	1.19 "	36	1.44 "	72	1.63 "	70	1.72 "
44	0.754 "	44	0.88 "	80	1.26 "	80	1.07 "
52	0.503 "	54	0.565 "	90	0.94 "	90	0.38 "
				100	0.565 "	90	0.13 "
				110	0.44 "		

X-F-13		X-F-14	
Time of Oxi- dation min.	FeS Remaining moles/l	Time of Oxi- dation min.	FeS Remaining moles/l
0	7.92×10^{-3}	0	7.66×10^{-3}
0	7.66 "	0	7.41 "
4.5	7.26 "	5	6.91 "
10	6.91 "	10	6.66 "
15	6.47 "	15	6.16 "
20	6.09 "	20	5.91 "
25	5.84 "	25	5.47 "
30	5.40 "	30	5.03 "
40	4.46 "	40	4.15 "
50	3.64 "	50	3.27 "
60	2.83 "	60	2.45 "
70	2.01 "	70	1.76 "
		80	1.13 "

X-F-15

Time of Oxi- dation min.	FeS Oxidized moles/l	Iodine- Consuming Species eq/l	Hydrogen Ions Produced moles/l	Sulfur in Soluble Phase (moles/l as written)		
				$S_2O_3^{-2}$	$S_4O_6^{-2}$	Colloidal SO
0	0.19×10^{-3}					
40	0.88 "	0.38×10^{-3}	0.19×10^{-3}			
80	1.38 "	0.63 "	0.38 "	0.071×10^{-3}	0.072×10^{-3}	0.044×10^{-3}
160	2.20 "	1.01 "	0.714 "			
240	3.20 "	1.76 "	1.21 "			
320	3.96 "	2.39 "	1.72 "			
400	4.84 "	2.89 "	-	0.576 "	0.115 "	0.26 "
475	5.34 "	3.27 "	2.7 "			
595	6.40 "	4.02 "	3.20 "	1.54 "	0.315 "	0.101 "
775	7.10 "	4.27 "	3.6 "	1.91 "	0.05 "	0.304 "
1285	7.60 "	3.02 "	-	2.20 "	0	0.18 "

X-F-16

Time of Oxidation min.	FeS Oxidized moles/l	Iodine-Consuming Species eq/l	Hydrogen Ions Produced moles/l	Sulfur in Soluble Phase (moles/l as written)		
				$S_2O_3^{-2}$	$S_4O_6^{-2}$	Colloidal S^0
0	0.44×10^{-3}	0.251×10^{-3}	0			
20	1.70 "	1.01 "	0.85×10^{-3}	0.46×10^{-3}	5×10^{-5}	0.066×10^{-3}
40	3.20 "	2.51 "	1.66 "			
60	3.96 "	3.52 "	2.61 "	1.22 "	0.12×10^{-3}	0.143 "
80	4.96 "	4.65 "	3.57 "			
100	5.78 "	5.4 "	4.36 "	1.94 "	0.26 "	0.387 "
140	6.85 "	6.53 "	5.41 "			
180	7.29 "	7.04 "	6.14 "	2.78 "	0.30 "	0.116 "
530	7.60 "	7.16 "	6.77 "	3.13 "	0.16 "	.41-.23 "

X-F-17

Time of Oxidation min.	FeS Oxidized moles/l	Iodine-Consuming Species eq/l	Hydrogen Ions Produced moles/l	Sulfur in Soluble Phase (moles/l as written)		
				$S_2O_3^{-2}$	$S_4O_6^{-2}$	Colloidal S^0
0	0.19×10^{-3}	0				
40	1.38 "	0.628×10^{-3}	0.379×10^{-3}			
80	2.32 "	1.26 "	0.925 "	0.531×10^{-3}	0.111×10^{-3}	0.055×10^{-3}
120	3.33 "	2.01 "	1.46 "			
160	4.21 "	2.76 "	2.04 "	1.17 "	0.111 "	0.192 "
240	5.59 "	4.02 "	3.16 "	1.76 "	0.111 "	0.282 "
360	6.59 "	5.03 "	4.3 "	2.69 "	0.180 "	0.42 "
560	7.41 "	5.91 "	5.1 "			
1370	7.6 "	3.52 "	5.32 "	3.42 "	4.0×10^{-5}	0.075 "

X-F-21

Time of Oxidation min.	FeS Oxidized moles/l	Iodine-Consuming Species eq/l	Hydrogen Ions Produced moles/l	Sulfur in Soluble Phase (moles/l as written)		
				$S_2O_3^{-2}$	$S_4O_6^{-2}$	Colloidal S^0
0	0.30×10^{-3}	0.124×10^{-3}				
10	0.92 "	0.619 "	0.301×10^{-3}			
20	2.4 "	0.99 "	0.750 "	0.525×10^{-3}	5.2×10^{-5}	3.1×10^{-5}
30	3.33 "	1.61 "	1.25 "			
40	4.38 "	2.23 "	1.57 "	0.909 "	1.52×10^{-4}	0.83×10^{-4}
50	5.25 "	2.72 "	1.92 "			
60	5.87 "	2.97 "	2.3 "	1.056 "	2.72 "	-
80	6.86 "	3.47 "	2.77 "			
100	7.29 "	3.84 "	3.04 "			
120	7.45 "	3.91 "	3.24 "	1.49 "	4.15 "	0.49 "
425	7.60 "	4.33 "	4.10 "	1.90 "	1.85 "	1.77 "

X-F-22

Time of Oxi-dation min.	FeS Oxidized moles/l	Iodine-Consuming Species eq/l	Hydrogen Ions Produced moles/l	Sulfur in Soluble Phase (moles/l as written)		
				$S_2O_3^{-2}$	$S_4O_6^{-2}$	Colloidal S^0
0	0.42×10^{-3}	0.371×10^{-3}				
5	1.35 "	0.99 "	0.686×10^{-3}			
10.5	2.28 "	2.23 "	1.50 "			
15.5	3.02 "	2.85 "	2.1 "			
21.5	3.89 "	3.71 "	2.85 "			
30	5.06 "	4.95 "	3.86 "			
40	6.05 "	6.06 "	4.9 "			
54.5	7.23 "	7.05 "	5.95 "			
70	7.6 "	7.3 "	6.35 "	4.12×10^{-3}	0	0.436×10^{-3}
188	7.60 "	6.93 "	6.91 "	4.11 "	0	0.353 "

X-F-23

Time of Oxi-dation min.	FeS Oxidized moles/l	Iodine-Consuming Species eq/l	Hydrogen Ions Produced moles/l	Sulfur in Soluble Phase (moles/l as written)		
				$S_2O_3^{-2}$	$S_4O_6^{-2}$	Colloidal S^0
0	-	0.126×10^{-3}				
40	1.32×10^{-3}	1.38 "	1.29×10^{-3}			
80	2.32 "	2.64 "	2.40 "	8.64×10^{-4}	1.42×10^{-4}	
120	3.08 "	3.39 "	3.44 "			
160	3.83 "	4.27 "	4.30 "			
240	5.09 "	6.16 "	5.45 "	1.78×10^{-3}	2.90 "	0.372×10^{-4}
320	6.16 "	7.04 "	6.27 "			
480	7.29 "	8.29 "	7.34 "	2.58 "	3.35 "	0.657×10^{-3}
1031	7.60 "	8.59 "	7.57 "	2.75 "	3.04 "	0.623 "

X-F-24

Time of Oxi-dation min.	FeS Oxidized moles/l	Iodine-Consuming Species eq/l	Hydrogen Ions Produced moles/l	Sulfur in Soluble Phase (moles/l as written)		
				$S_2O_3^{-2}$	$S_4O_6^{-2}$	Colloidal S^0
0	0	0.126×10^{-3}	-			
20	1.10×10^{-3}	0.754 "	0.39×10^{-3}			
40	2.11 "	1.38 "	0.83 "			
60	3.05 "	1.88 "	1.3 "			
80	3.93 "	2.39 "	1.83 "			
120	5.50 "	3.27 "	2.68 "			
160	6.57 "	4.02 "	3.22 "			
280	7.64 "	4.90 "	4.39 "			
320	-	-	4.68 "	2.43×10^{-3}	0.085×10^{-3}	0.22×10^{-3}

X-G-1

Time of Oxi- dation min.	FeS Oxidized moles/l	Iodine- Consuming Species eq/l	Hydrogen Ions Produced moles/l	Sulfur in Soluble Phase (moles/l as written)		
				$S_2O_3^{-2}$	$S_4O_6^{-2}$	Colloidal S ₀
0	0.02×10^{-3}					
10	1.91 "	0	0.803×10^{-3}			
20	3.48 "	2.01×10^{-3}	1.49 "			
30	4.52 "	2.76 "	2.20 "			
40	5.42 "	3.64 "	2.81 "			
50	6.18 "	4.27 "	3.44 "			
60	6.68 "	4.77 "	3.93 "			
70	7.12 "	5.03 "	4.33 "			
90	7.65 "	5.70 "	4.98 "	2.96×10^{-3}	0.18×10^{-3}	0.233×10^{-3}
120		6.03 "	5.55 "			

X-G-3			X-G-4			X-G-5			X-G-6		
Time of Oxi- dation min.	FeS Remaining moles/l		Time of Oxi- dation min.	FeS Remaining moles/l		Time of Oxi- dation min.	FeS Remaining moles/l		Time of Oxi- dation min.	FeS Remaining moles/l	
0	8.29 x 10 ⁻³		0	8.35 x 10 ⁻³		0	7.60 x 10 ⁻³		1	6.98 x 10 ⁻³	
30	7.41 "		5	7.22 "		5	6.73 "		6	2.62 "	
60	6.79 "		10	7.48 "		10	5.17 "		11	0.5 "	
90	6.16 "		15	7.16 "		15	3.86 "				
120	5.28 "		20	6.85 "		20	2.62 "				
150	4.52 "		30	6.17 "		25	1.68 "				
180	3.71 "		40	5.42 "		30	0.87 "				
210	3.02 "		50	4.73 "		35	0.37 "				
240	2.07 "		60	3.99 "							
270	1.51 "		80	2.68 "							
			100	1.50 "							
X-G-7			X-G-8			X-G-9			X-G-10		
Time of Oxi- dation min.	FeS Remaining moles/l		Time of Oxi- dation min.	FeS Remaining moles/l		Time of Oxi- dation min.	FeS Remaining moles/l		Time of Oxi- dation min.	FeS Remaining moles/l	
0	8.1 x 10 ⁻³		0	8.1 x 10 ⁻³		0	8.62 x 10 ⁻³		0	8.66 x 10 ⁻³	
5	7.6 "		5	7.6 "		0	8.22 "		0	7.97 "	
10	7.23 "		10	7.1 "		5	7.23 "		5	6.6 "	
15	6.98 "		15	6.73 "		10	6.6 "		10	5.48 "	
20	6.6 "		20	6.29 "		15	5.73 "		15	4.36 "	
30	5.92 "		30	5.54 "		20	4.3 "		20	2.8 "	
40	5.05 "		40	4.8 "		25	2.87 "		25	1.37 "	
50	4.24 "		50	4.05 "		30	1.43 "		30	0.5 "	
60	3.49 "		60	3.36 "		35	0.5 "		35	0.25 "	
70	2.3 "		70	2.55 "		40	0.125 "				
80	0.5 "		80	1.62 "							
			90	0.56 "							
			95	0.25 "							

X-G-11			X-G-12			X-G-13			X-G-15		
Time of Oxi- dation min.	FeS Remaining moles/l		Time of Oxi- dation min.	FeS Remaining moles/l		Time of Oxi- dation min.	FeS Remaining moles/l		Time of Oxi- dation min.	FeS Remaining moles/l	
0	8.6	$\times 10^{-3}$	0	8.72	$\times 10^{-3}$	0	8.54	$\times 10^{-3}$	0	8.78	$\times 10^{-3}$
0	7.97	"	0	8.35	"	0	8.04	"	0	8.04	"
5	7.66	"	20	7.41	"	5	7.48	"	5	7.41	"
10	7.35	"	40	6.85	"	10	7.23	"	10	6.67	"
20	6.85	"	60	6.23	"	20	6.67	"	15	5.79	"
30	6.23	"	80	5.54	"	30	5.92	"	20	4.98	"
40	5.61	"	100	4.86	"	40	5.17	"	25	4.24	"
50	4.98	"	120	4.11	"	50	4.55	"	30	3.61	"
60	4.36	"	140	3.43	"	60	3.74	"	35	2.87	"
70	3.74	"	162	2.68	"	70	2.93	"	40	2.37	"
80	3.11	"	180	1.99	"	80	2.31	"	50	1.19	"
90	2.62	"				90	1.74	"	60		
100	1.99	"									
110	1.62	"									

X-G-16

Time of Oxi- dation min.	FeS Remaining moles/l	
0	8.91	$\times 10^{-3}$
0	8.41	"
10	7.66	"
20	7.29	"
30	6.85	"
40	6.48	"
61	5.42	"
80	4.49	"
100	3.55	"
120	2.43	"

X-G-14

Time of Oxi- dation min.	FeS Oxidized moles/l	Iodine- Consuming Species eq/l	Hydrogen Ions Produced moles/l	Soluble Sulfur Species not measured
0	0.13 $\times 10^{-3}$	0.125 $\times 10^{-3}$	-	
10	1.68 "	0.374 "	0.328 $\times 10^{-3}$	
20	2.49 "	0.748 "	0.538 "	
30	3.30 "	1.12 "	0.795 "	
40	3.86 "	1.37 "	1.01 "	
50	4.42 "	1.62 "	1.28 "	
60	4.98 "	1.99 "	1.56 "	
*				
70	5.55 "	2.12 "	1.79 "	
80	6.11 "	2.24 "	1.94 "	

* Additional NiSO_4 added to increase concentration to 10^{-4} mole/l.

X-II-1

Time of Oxi- dation min.	FeS Oxidized moles/l	Iodine- Consuming Species eq/l	Hydrogen Ions Produced moles/l	Sulfur in Soluble Phase (moles/l as written)		
				$S_2O_3^{-2}$	$S_4O_6^{-2}$	Colloidal S^0
0	0.73×10^{-3}	0.122×10^{-3}	0			
16	1.46 "	0.488 "	0.325×10^{-3}			
31	2.07 "	0.854 "	0.583 "			
45	2.56 "	0.854 "	0.804 "			
77	3.90 "	1.34 "	1.16 "			
120	5.54 "	1.95 "	1.72 "			
180	7.37 "	2.80 "	2.34 "			
240	8.35 "	3.05 "	2.73 "			
280	8.47 "	2.93 "	2.83 "	$1.25-1.39 \times 10^{-3}$	0.07×10^{-3}	$0.33-0.59 \times 10^{-3}$

X-H-2

Time of Oxi- dation min.	FeS Oxidized moles/l	Iodine- Consuming Species eq/l	Hydrogen Ions Produced moles/l	Sulfur in Soluble Phase (moles/l as written)		
				$S_2O_3^{-2}$	$S_4O_6^{-2}$	Colloidal S^0
0	0.79×10^{-3}	0.244×10^{-3}	0			
15	1.58 "	0.488 "	0.375×10^{-3}			
30	2.07 "	0.732 "	0.561 "			
45	2.56 "	0.854 "	0.781 "			
75	3.59 "	1.10 "	1.15 "			
120	5.24 "	1.46 "	1.65 "			
185	7.01 "	1.95 "	2.43 "			
260	8.35 "	1.95 "	3.08 "	0.56×10^{-3}	Inter- ference	Inter- ference
380	8.47 "	2.07 "	3.20 "			

X-I-1

Time of Oxi- dation min.	FeS Oxidized moles/l	Iodine- Consuming Species eq/l	Hydrogen Ions Produced moles/l	Sulfur in Soluble Phase (moles/l as written)		
				$S_2O_3^{-2}$	$S_4O_6^{-2}$	Colloidal SO
0	0.82×10^{-3}	0.125×10^{-3}	0.08×10^{-3}			
30	3.89 "	1.00 "	0.65 "			
72	6.44 "	2.13 "	1.46 "			
105	8.07 "	2.63 "	2.01 "			
145	8.75 "	2.75 "	2.34 "	$1.33 \pm .036 \times 10^{-3}$	$0.312 \pm .105 \times 10^{-3}$	$0.147 \pm .123 \times 10^{-3}$

X-I-2

Time of Oxi- dation min.	FeS Oxidized moles/l	Iodine- Consuming Species eq/l	Hydrogen Ions Produced moles/l	Sulfur in Soluble Phase (moles/l as written)		
				S ₂ O ₃ ⁻²	S ₄ O ₆ ⁻²	Colloidal S ⁰
0	Not Measured as a Function of Time		-	3.16 ±.15 x 10 ⁻³	0.508 ±.11 x 10 ⁻³	1.14 ±.18 x 10 ⁻³
48			1.89 x 10 ⁻³			
76			3.00 "			
95			3.78 "			
126			4.76 "			
147			5.37 "			
183			6.26 "			
204			6.71 "			
250			7.40 "			
266			7.48 "			
600			7.52 "			

X-I-3		X-I-4		X-I-5		X-I-6	
Time of Oxi- dation min.	FeS Remaining moles/l	Time of Oxi- dation, min.	FeS Remaining moles/l	Time of Oxi- dation min.	FeS Remaining moles/l	Time of Oxi- dation min.	FeS Remaining moles/l
0	9.9×10^{-3}	0	9.65×10^{-3}	B	1.04×10^{-2}	0	8.69×10^{-3}
15	8.03 "	5	8.4 "	0	8.8×10^{-3}	5	7.0 "
30	6.90 "	10	7.4 "	10	6.31 "	10	5.56 "
45	5.59 "	20	5.78 "	14.5	5.25 "	15	4.56 "
60	4.28 "	32	4.21 "	20	4.50 "	20	3.75 "
75	3.03 "	40	3.28 "	25	3.69 "	25	2.94 "
90	1.84 "	50	2.15 "	30	2.94 "	30	2.25 "
105	1.09 "	60	1.36 "	40	1.75 "	40	1.19 "
				50	1.00 "	50	0.563 "
X-I-7		X-I-8		X-I-9		X-I-10	
Time of Oxi- dation min.	FeS Remaining moles/l	Time of Oxi- dation min.	FeS Remaining moles/l	Time of Oxi- dation min.	FeS Remaining moles/l	Time of Oxi- dation min.	FeS Remaining moles/l
0	-	0	9.78×10^{-3}	0	8.88×10^{-3}	0	9.38×10^{-3}
4	-	5	8.96 "	5	8.25 "	4	8.13 "
8	6.0×10^{-3}	10	8.40 "	10	6.81 "	8	6.75 "
12	4.88 "	20	7.09 "	15	5.63 "	12	5.63 "
16	4.0 "	30	5.90 "	20	4.88 "	16	4.63 "
20	3.13 "	40	4.71 "	30	3.25 "	20	3.75 "
24	2.50 "	50	3.46 "	40	1.88 "	24	3.0 "
28	1.88 "	60	2.34 "	50	0.94 "	28	2.19 "
32	1.44 "					32	1.63 "
36	0.938 "					36	1.13 "

X-I-11		X-I-12		X-I-13		X-I-14	
Time of Oxi- dation min.	FeS Remaining moles/l	Time of Oxi- dation min.	FeS Remaining moles/l	Time of Oxi- dation min.	FeS Remaining moles/l	Time of Oxi- dation min.	FeS Remaining moles/l
0	-	0	1.34×10^{-3}	0	0.43×10^{-3}	0	0.37×10^{-3}
10	-	5	2.84	10	1.32	10	1.26
20	1.59×10^{-3}	10	4.21	20	1.83	20	1.70
30	2.52	16	5.77	30	2.38	30	2.27
40	3.21	20	6.65	40	3.2	40	2.66
53	4.40	25	7.96	55	4.05	55	3.29
60	5.15	30	9.09	70	4.88	70	4.05
70	6.09	35	9.84	85	5.96	85	4.50
80	7.09	45	9.9	100	6.91	100	5.2
				118	7.93	120	6.15
						140	6.66
X-I-15		X-I-16		X-I-17		X-I-18	
Time of Oxi- dation min.	FeS Remaining moles/l	Time of Oxi- dation min.	FeS Remaining moles/l	Time of Oxi- dation min.	FeS Remaining moles/l	Time of Oxi- dation min.	FeS Remaining moles/l
0	0.49×10^{-3}	0	0.43×10^{-3}	0	1.40×10^{-3}	0	1.27×10^{-3}
10	1.38	10	1.32	5	2.34	5	2.21
20	1.83	20	-	10	3.09	10	3.15
30	2.53	30	2.4	15	3.71	15	4.09
40	3.16	40	3.04	20	4.21	20	4.84
55	4.05	55	3.93	30	5.34	25	5.59
70	4.94	75	5.58	40	6.34	30	6.27
85	6.21	85	6.40	50	7.09	35	7.15
100	6.96	100	7.74				

X-I-19		X-I-20	
Time of Oxi- dation min.	FeS Remaining moles/l	Time of Oxi- dation min.	FeS Remaining moles/l
0	1.40×10^{-3}	0	1.59×10^{-3}
5	2.40 "	5	2.46 "
10	3.52 "	10	2.96 "
15	4.27 "	15	3.15 "
20	5.21 "	20	3.46 "
25	6.09 "	26	4.15 "
30	7.15 "	35	5.21 "
35	8.04 "	40	5.84 "
		45	6.90 "
		50	7.46 "

APPENDIX D

SELECTED DATA FROM ADSORPTION EXPERIMENTS IN SILVER (I)/AMORPHOUS IRON OXIDE AND COPPER (II)/AMORPHOUS IRON OXIDE SYSTEMS

Experiment 1. $Ag_T = 4 \times 10^{-7} M$
 $Fe(OH)_3(s) = 10^{-4} M, 1.94 \text{ m}^2/l$
 $I = 10^{-1} M NaNO_3, 25^\circ C$

pH	Ag(I) remaining in solution ($\times 10^{-7} M$)	% Ag Adsorbed
7.10	3.39	15.3
7.24	3.20	20.0
8.72	2.07	48.2
9.07	1.56	61.1
9.43	1.62	59.4
10.05	1.25	68.8
10.85	0.71	82.3

Experiment 2. $Ag_T = 4 \times 10^{-7} M$
 $Fe(OH)_3(s) = 10^{-3} M, 19.4 \text{ m}^2/l$
 $I = 10^{-1} M NaNO_3, 25^\circ C$

3.98	4.00	0.0
4.77	3.84	4.0
5.63	3.55	11.2
6.03	3.37	15.8
6.50	2.96	26.0
6.81	2.38	40.5
6.95	2.16	46.0
7.20	1.79	55.2
7.34	1.60	60.1
7.40	1.40	64.9
7.42	1.35	66.1
7.56	1.11	72.3
7.71	1.01	74.8
8.04	0.50	87.5
8.19	0.45	88.7
8.44	0.38	90.4
9.85	0.32	92.1
9.36	0.35	91.2
9.63	0.32	92.1
10.22	0.31	92.2
11.82	0.51	87.3

<u>pH</u>	<u>Ag(I) remaining in solution ($\times 10^{-7}M$)</u>	<u>% Ag Adsorped</u>
<u>Experiment 3.</u> $Ag_T = 4 \times 10^{-7}M$		
$Fe(OH)_3(s) = 1.5 \times 10^{-2}M, 292 \text{ m}^2/1$		
$I = 10^{-1}M \text{ NaNO}_3, 25^\circ C$		
4.93	3.05	23.7
5.62	2.06	48.4
6.17	1.26	68.5
6.61	0.75	81.3
7.27	0.29	92.8

<u>Experiment 4.</u> $Ag_T = 4 \times 10^{-7}M$		
$S_2O_3^{2-} = 4 \times 10^{-7}M$		
$Fe(OH)_3(s) = 10^{-3}M, 19.4 \text{ m}^2/1$		
$I = 10^{-1}M \text{ NaNO}_3, 25^\circ C, \text{ darkroom experiment}$		
4.05	2.04	49
4.2	1.52	62
4.3	1.84	54
4.55	0.96	76
4.85	0.88	78
4.85	1.02	74.5
5.0	1.12	72
5.5	1.12	72
5.65	1.36	66
5.75	1.36	66
6.1	1.96	51
6.3	2.48	38
6.45	2.60	35
6.57	2.40	40
6.75	2.92	27
7.13	2.76	31
7.2	2.92	27
8.25	2.16	46
8.52	1.76	56
9.1	1.32	67
9.75	0.64	84
10.4	0.56	86
11.7	0.48	88

Experiment 5. $\text{Ag}_T = 4 \times 10^{-7} \text{M}$
 $\text{S}_2\text{O}_3^{2-} = 4 \times 10^{-6} \text{M}$
 $\text{Fe}(\text{OH})_3(\text{s}) = 10^{-3} \text{M}, 19.4 \text{ m}^2/\text{l}$
 $\text{I} = 10^{-1} \text{M NaNO}_3, 25^\circ\text{C}, \text{darkroom experiment}$

<u>pH</u>	<u>Ag(I) remaining in solution ($\times 10^{-7} \text{M}$)</u>	<u>% Ag Adsorbed</u>
4.05	0.10	97.4
4.45	0.12	97.1
4.85	0.22	94.6
5.25	0.40	90.0
5.95	1.80	55.1
6.67	3.28	18.0
6.80	3.55	11.2
7.11	3.48	13.1
7.45	3.76	6.0
9.2	3.45	13.7
10.1	3.09	23.3
11.0	2.40	40.1
11.7	1.97	50.8

Experiment 6. $\text{Cu}_T = 10^{-6} \text{M}$
 $\text{Fe}(\text{OH})_3(\text{s}) = 10^{-3} \text{M}, 19.4 \text{ m}^2/\text{l}$
 $\text{I} = 10^{-1} \text{M NaNO}_3, 25^\circ\text{C}$

<u>pH</u>	<u>Cu(II) remaining in solution ($\times 10^{-7} \text{M}$)</u>	<u>% Cu Adsorbed</u>
4.0	9.1	9
4.3	8.5	15
4.45	8.8	12
4.5	8.5	15
4.9	8.2	18
5.1	7.9	21
5.43	4.75	52.5
5.52	4.2	58
5.54	4.5	55
5.62	2.2	78
5.7	2.7	73
5.9	1.0	90
5.95	1.0	90
6.00	1.4	86
6.22	0.53	95
6.5	0.35	96.5
6.75	0.23	98

<u>pH</u>	<u>Cu(II) remaining in solution ($\times 10^{-7}\text{M}$)</u>	<u>% Cu Adsorbed</u>
<u>Experiment 7.</u> $\text{Cu}_T = 10^{-6}\text{M}$		
Picolinic Acid = $4 \times 10^{-5}\text{M}$		
$\text{Fe}(\text{OH})_3(\text{s}) = 10^{-3}\text{M}$, $19.4 \text{ m}^2/\text{l}$		
$\text{I} = 10^{-1}\text{M NaNO}_3$, 25°C		
4.03	9.8	2
4.42	9.75	2.5
4.85	9.7	3
5.43	9.5	5
5.80	9.4	6

<u>Experiment 8.</u> $\text{Cu}_T = 10^{-6}\text{M}$		
2,3-Pyrazinedicarboxylic Acid = $2 \times 10^{-5}\text{M}$		
$\text{Fe}(\text{OH})_3(\text{s}) = 10^{-3}\text{M}$, $19.4 \text{ m}^2/\text{l}$		
$\text{I} = 10^{-1}\text{M NaNO}_3$, 25°C		
4.02	9.0	10
4.45	8.35	16.5
4.84	7.2	28
4.98	5.7	43
5.60	3.3	67
5.62	2.5	75
5.91	1.5	85
6.60	1.2	88
7.60	0.80	92

INITIAL DISTRIBUTION

Hq USAF/IEEF	1 AFGL/XOI	1
Hq USAF/EDS	2 UAFSAB/LDE	2
Hq USAF/IAFPI	1 USAFSAB/VML	1
Hq USAF/IGIA	2 AFIP/Library	1
Hq USAF/PIV-1	1 PTD/IGH	1
Hq USAF/PIV-X	1 SAMTEC/SEH	1
Hq Comd USAF/DET	1 SAMSO/LEV	1
CINCAL/LIEN	1 SAMSO/SG	1
CINCAL/SGPAI	1 AMD/RDU	1
AFCS/DLEE	1 AMD/RDB	1
AFLC/SGE	1 ADTC/CSV	1
AFIC/DEPV	1 ADTC/DLODL	1
AFIC/MAUT	1 AFFTC/DE	1
AFIC/MMRF	1 AFETR/DER	1
AFSC/DE	1 1035 USAF Technical Ops Gp	1
AFSC/SD	1 1 Med Service Wg/SGB	1
AFSC/DEV	1 DDC/TCA	12
AFSC/SGB	1 ARPA	1
AFSC/DASR	1 Def Rsch & Engr/AD(E&IS)	1
AFSC/DLCAM	2 OASD/(I&L)ES	1
ATC/DEPV	1 USA Environ Hygrn Agcy	1
ATC/SGPAP	1 Dir, USA WW Exp Sta	1
AAC/SGB	1 USA CERL	1
MAC/SGPE	1 Dir, USA Eng R&D Lab/MERDC	1
MAC/DLEE	1 Dept of the Army/DARD-ARE-E	1
CINCPACAF/SGPE	1 NCEL, Code 25111	1
CINCSAC/DEPV	1 Naval Ship R&D Ctr (Code 3021)	1
CINCSAC/SGPA	1 Technology Transfer Staff (LFA)	2
TAC/DDEV	1 National Science Foundation	1
TAC/SGPB	1 US Army Med Bioengr R&D Lab/	
USAFSS/DEMM	1 SGRD-UBG	2
CINCUSAFE/Surgeon	1 Dept of Civil Engineering/	
CINCUSAFE/DEPV	1 Stanford Univ	10
AFISC/SGMS	1 Dept of Earth Sciences/	
AFISC/SES	2 Stanford Univ	2
AFRES/DLEE	1 Dept of Environmental Sciences/	
USAF/DEV	1 Cal Inst of Technology	1
USAF/Library	1 Dept of Civil Engr/	
AUL	1 Mass Inst of Technology	1
AU/Surgeon	1 Toxic Matls Info Ctr	1
AFOSR/NC	1 Southeast Environmental Rsch Lab	1
AFOSR/Life Sciences	1 Pacific Northwest Environ Rsch Lab	1
AMRL/DAL	1 CEEDO/PRT	1
AMRL/THE	1 CEEDO/WE	1
AFML/DO (Library)	1 CEEDO/CC	1
OEHL/CC	3 CEEDO/ECS	5
AFWL/SUL (Tech Library)	1 CEEDO/EC	1

INITIAL DISTRIBUTION (CONCLUDED)

CEEDO/ECE	4
Dept of Civil & Mineral Engr/ Univ of Minn	2
Dept of Civil Engineering/ Oregon State Univ	1
USGS Water Resources Div	1
USGS	1
Dept of Civil Engr/Univ of Wash	1
Scripps Inst of Oceanography	1
Water Chemistry Program/ Univ of Wisc	1
Dept of Chemistry/State Univ of New York	1
Dept of Oceanography/ Univ of Wash	1
Dept of Environ Sciences & Eng/ Univ of North Carolina	1
Dept of Oceanography/Texas A&M	1
Swiss Federal Inst of Tech	1